"FLUID FLOW AND MASS TRANSFER IN AN ANNULUS WITH THE INNER CYLINDER ROTATING"

by

ARTHUR PETER SHAHBENDERIAN, B.A., M.A.

Thesis submitted for the Degree of Ph.D.

August 1961

University of Edinburgh

Acknowledgements

The author wishes to thank Dr. N. Macleod, who originated and supervised this research project, for the constant encouragement and willing advice that he has given throughout the entire project.

The author is also grateful to Dr. D. M. Wilson for helpful comments on certain points concerning the design and operation of the mercury vapour transfer column described in Part II of this thesis.

The mercury vapour transfer column was largely built, with great precision, by the late Mr. A. W. Rodger and by Mr. C. McLeod. It is a tribute to their skill that the operation of the column has proved so successful.

CONTENTS - PART I

CONTENTS - PART I (continued)

PART I

DISTILLATION IN AN ANNULUS WITH THE INNER CYLINDER ROTATING OR STATIONARY

1. GENERAL INTRODUCTION

The principal purpose of this investigation was to gain greater insight into the mechanism of mass exchange and fluid flow in rotating concentric cylinder fractionating columns and to find an explanation for certain peculiarities in their observed behaviour. In such columns, the vapours from a still-pot rise up the annular space between a rotating inner cylinder and a fixed outer cylinder. Reflux from a condenser section at the top of the column flows down the wall of the outer cylinder and in some circumstances also down the wall of the rotating inner cylinder. For certain experimental conditions it has been shown directly (1, 2) that the resistance to mass exchange between the vapour and reflux streams resides predominantly in the vapour phase in such apparatus. For these conditions, at any rate, it would thus be expected that the performance of these columns would be affected by the appearance of Taylor vortices (4) in the vapour phase, since these regular vortices, by their nature, would be expected to promote radial diffusion and are indeed known to promote radial heat transfer. However, results obtained by previous investigators (1, 2, 3) have shown no significant increase in the number of theoretical plates at speeds of rotation of the inner cylinder at which the appearance of vortices might be expected.

In this investigation an attempt has been made to determine, theoretically and experimentally, how such a column behaves in the presence and absence of vortices. This also necessitated establishing the conditions for vortex

formation in order that the performance of the column could be compared with the appropriate theory. The performance of similar columns investigated by previous workers (3, 15, 17, 18, 19) was also compared with the relevant theory.

The experiments were performed on an existing rotary concentric cylinder fractionating column operating adiabatically under conditions of total reflux. Previous experiments on this column had been carried out by Macleod and Matterson (1, 2). Although the column was initially designed as a laboratory still, (rather than as an instrument for fundamental inquiry), it seemed from the high quality and regularity of its performance in previous investigations (1, 2) that it approximated well to an idealised concentric cylinder column. The results of these experiments were compared with the results of investigations on similar columns by previous workers (3). Experiments described in Part I of this thesis confirmed that the appearance of vortices did not significantly affect the overall column performance. It was, however, not clear whether this was due to a real lack of improvement in the radial mass transfer rate; for it was conceivable that the vortices were effective in promoting radial mass transfer but that they also increased the back-mixing of the vapours in an axial direction, so as to offset the effect of improved radial mass transfer on the column operation. This concept was suggested by the experiments of Croockewit et al (8) showing that vortices were very effective promoters of longitudinal mixing.

In order to investigate the effect of vortices in promoting both radial mass transfer and longitudinal mixing in an annulus, an apparatus was constructed in which these effects could be systematically studied. The apparatus used and experiments performed are described in Part II of this thesis. With this apparatus an experimental study was made of the evaporation

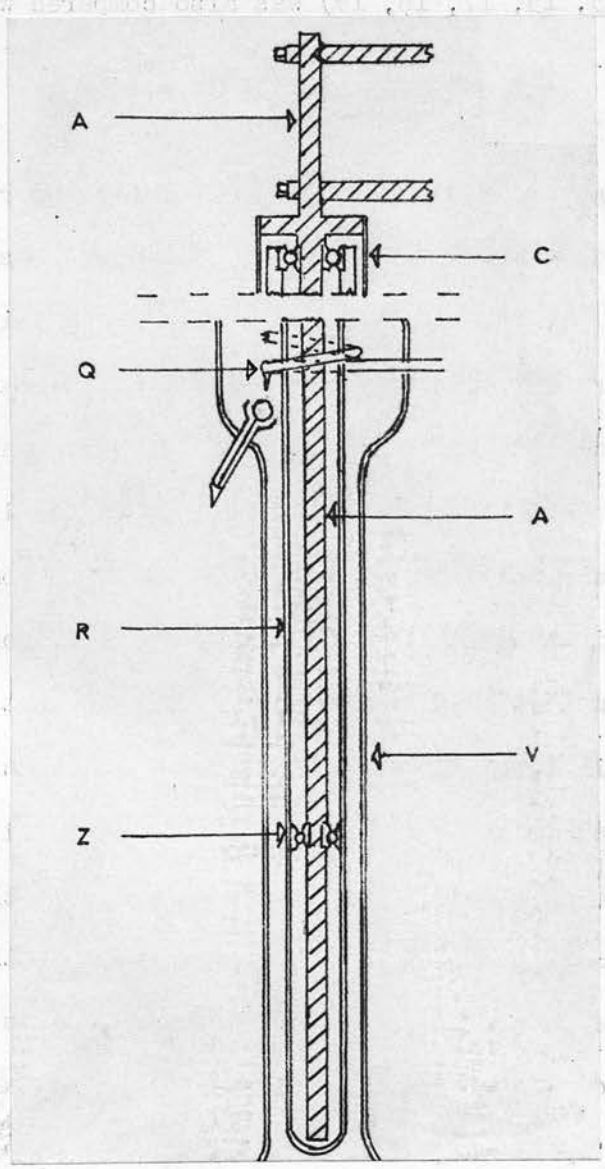

Key to figure 1

A Fixed central shaft

C Motor housing

Q Spiral water condense

R Rotating inner cylind

V Glass outer cylinder

Z Lower bearing assembl

Figure 1. General mechanical arrangement of rotating concentric cylinder fractionating column (2)
Schematic. Horizontal scale distorted and enlarged.

of mercury from the amalgamated surface of a narrow circumferential band into an air stream flowing in an annulus. The amalgamated band could be situated on either the inner or outer cylinder and the inner cylinder could be made to rotate. The fact that mercury vapour absorbs ultra-violet light in the 2537 Å wavelength region was used to determine the concentration of mercury vapour in the air leaving the annulus. Thus studies were made to determine whether the concentration of the mercury vapour in the air stream was significantly increased, due to increased radial mass transfer, by the presence of vortices in the annulus. Furthermore, the conditions of vortex formation were investigated and compared with other published results (4, 9, 10, 11, 13, 14, 28, 34), for varying axial flow rates and speeds of rotation of the inner cylinder. Longitudinal diffusion experiments were also performed in an attempt to determine the effect of vortices on back-mixing, in the hope that these experimental results, when analysed in conjunction with the radial mass transfer studies, would explain more clearly the behaviour of rotary concentric cylinder fractionating columns.

2. INTRODUCTION - DISTILLATION EXPERIMENTS

Experiments were performed on an existing rotary concentric cylinder fractionating column, the original design being due to Macleod and Matterson, (1, 2) who also studied the performance of this column. The general mechanical arrangement of the working section is shown in figure 1.

The column operated adiabatically under conditions of total reflux. The vapours rising from the still-pot, situated at the base of the column, did not come into contact with any bearings or shaft seals, the lower bearing being located entirely within the rotating inner cylinder. The vapours were condensed by a spiral water condenser at the top of the column. Condensation

could also take place on the condenser shell; in addition, it was found that condensate could form on the surface of the inner cylinder within the condenser section. Thus, when the inner cylinder was stationary or rotating slowly, it was a peculiar (and unintended) feature of the design of this column that both inner and outer cylinder surfaces might be wet with reflux. However, at high speeds of rotation the inner cylinder was found by experiment to be free from reflux due to removal of any liquid condensate by centrifugal force.

Samples could be taken from the still-pot and condenser section and by determining the refractive indices of these samples the number of theoretical plates could be found for a given boil-up rate and speed of rotation of the inner cylinder.

In the experimental study to be described the performance of this column was investigated for varying boil-up rates and varying speeds of rotation of the inner cylinder, for inner cylinders of three different diameters rotating inside the same fixed outer cylinder. Experiments were also conducted with the inner cylinders stationary. The main purpose of these experiments was to throw light on the effect of vortices (4) on the performance of this type of column.

The performance of such a column as this is of practical interest (1, 2, 3, 15, 16, 17, 18, 19) because, compared with other types of column of similar capacity, the Height of an Equivalent Theoretical Plate (H.E.T.P.) may be made very low. Furthermore the pressure drop and hold-up may be made small. This is a great advantage for low pressure batch distillation, the low hold-up enabling distillation to proceed to near completion.

The performance of this type of column should also prove amenable to theoretical treatment (2, 3) since the geometry of the fractionating section

is of a well-defined and simple nature and the effect of rotation of the inner cylinder predictable.

Accordingly a theoretical study, now to be presented, was made in which the performance of such columns was analysed under conditions of laminar, vortex and turbulent flow in the vapour phase. The results of this analysis were compared with the results obtained from experiments on the present column and also with the results of other investigators.

3. THEORY

Depending on the design of rotating concentric cylinder fractionating columns it is possible that either one or both cylinder walls are wetted by reflux. For the particular column investigated, when the speed of rotation of the inner cylinder was high any reflux condensing on the inner cylinder (within the condenser section) was rapidly removed at the top of the column by centrifugal force and thus, in this case, only the outer cylinder wall was wetted by a film of reflux. It was in fact a particular feature in the design of this column that this was the only way of ensuring dryness of the inner cylinder. When the inner cylinder was stationary or rotating at low speeds it is possible that both cylinder walls were wet with reflux.

The character of the vapour flow in such columns is also conditioned by the speed of rotation of the inner cylinder and it will be discussed in the course of this section how laminar, vortex or turbulent flow regimes may exist in the vapour phase.

The distribution of the liquid reflux phase and the flow condition of the vapour phase will naturally affect the performance of a concentric cylinder column and any theoretical analysis, applicable to all types of column design, must cover all the possible combinations of reflux and vapour

flow conditions. It is, therefore, convenient to discuss the theory for such columns under the following main headings:-

3.1 Laminar flow of ascending vapour with the inner cylinder free from reflux.

3.2 Laminar flow of ascending vapour with both inner and outer cylinders wetted by reflux.

3.3 Applicability of the theories derived in sections 3.1 and 3.2 to the particular rotating concentric cylinder column under investigation.

3.4 Turbulent flow of ascending vapour with the inner cylinder stationary.

3.5 Vortex and turbulent flow of vapour with the inner cylinder rotating.

3.6 Conditions for vortex formation and the onset of turbulence.

3.7 Longitudinal diffusion effects.

3.8 Summary of theory and use in practice.

3.9 Comparison of theory with previous work.

Wherever possible the results of other experiments in allied fields, e.g. heat transfer measurements in annuli or distillation in stationary annuli, are used to corroborate the validity of the theories presented. The question of the validity of the various theories in representing distillation in an annulus with the inner cylinder rotating is postponed until section 3.9, allowing a proper comparison to be made of theory and experiment, taking into account all possible combinations of vapour and liquid phase conditions.

3.1 Laminar flow of ascending vapour with the inner cylinder free from reflux

It is assumed throughout this analysis that the ratio of annular gap width to radius of the inner cylinder is very small. If this assumption is true and the column long then it may be considered that distillation takes place in the gap between parallel plates with fully developed flow of vapour

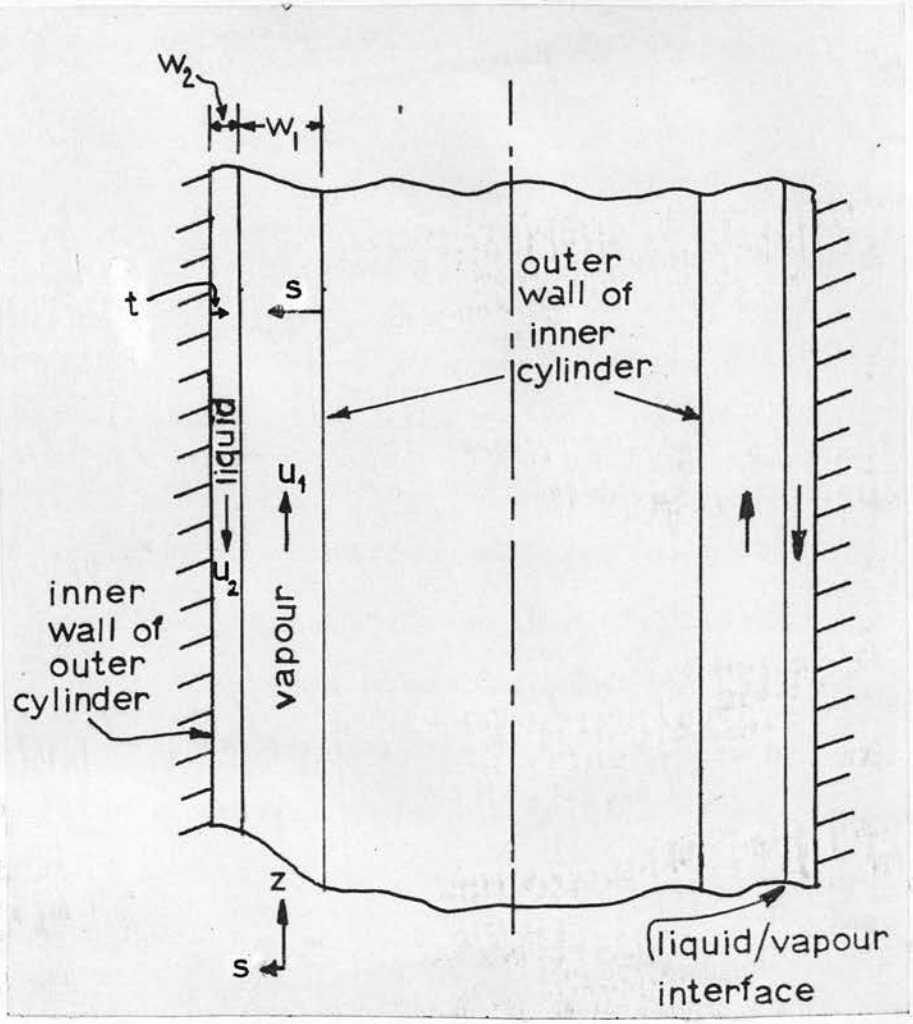

Figure 2. Distillation in an annulus (reflux down outer cylinder wall only).

and liquid phases.

In 1947 Willingham et al (3) published a paper in which a theoretical treatment was presented for this particular case, with one of the walls wetted by reflux. Equations were presented in integral form which enabled the H.E.T.P. to be calculated as the sum of two heights H_1 and H_2, where H_1 is the H.E.T.P. for the vapour phase and H_2 that for the liquid phase.

The number of theoretical plates, N, is then given by:-

$$N = \frac{l}{H_1 + H_2} \qquad \text{- - - (1)}$$

where l is the length of the fractionating section.

The integrals which evaluate H_1 and H_2 were stated to be as follows:-

$$H_1 = \frac{\int_0^{w_1} \frac{1}{D_1} \left[\int_0^s u_1 \, ds \right]^2 ds}{\bar{u}_1 \, w_1} \qquad \text{- - - (2)}$$

and

$$H_2 = \frac{\int_0^{w_2} \frac{1}{D_2} \left[\int_0^t u_2 \, dt \right]^2 dt}{\bar{u}_2 \, w_2} \qquad \text{- - - (3)}$$

Where $\bar{u}$ is the mean velocity, u the point velocity, w_1 the effective gap width for vapour flow, w_2 the reflux film thickness and D the molecular diffusion coefficient. The distance from a point in the vapour phase to the dry wall of the inner cylinder is s, and t is the distance from a point in the liquid reflux phase to the outer cylinder wall. Subscripts 1 and 2 refer to the vapour and liquid phases respectively. Figure 2 shows more clearly the meaning of this notation.

No formal proofs of the basic equations (2) and (3) were presented by Willingham et al (3). They are derived in Appendix A, following a method presented by Ruckenstein (20). The derivations in Appendix A were based on the following assumptions, some stated explicitly and others implied:-

(a) The column operates adiabatically under conditions of total reflux

(b) The vapour and liquid velocities are constant and independent of height

(c) The liquid reflux film flows uniformly over the wall surface concerned and has no surface transfer resistance

(d) There is no vapour drag by the liquid reflux film

(e) The diffusion coefficient of the more volatile component is independent of composition

(f) The axial change in composition of the vapour or liquid is independent of radial position

(g) Longitudinal diffusion is negligible

If laminar flow of vapour and reflux streams is assumed, then equations (2) and (3) may be integrated after the appropriate expressions for the laminar velocity profile have been substituted in them.

3.11 Integration of equation (2) for laminar flow of vapour

The equation for the vapour laminar velocity profile is given by:-

$$u_1 = \frac{6\bar{u}_1}{w_1^2} (w_1 s - s^2) \text{ - - - - } (4)$$

$$\therefore \quad \int_0^s u_1 \, ds = \int_0^s \frac{6\bar{u}_1}{w_1^2}(w_1 s - s^2)\, ds = \frac{6\bar{u}_1}{w_1^2}\left(w_1 \frac{s^2}{2} - \frac{s^3}{3}\right)$$

$$\therefore \quad \left(\int_0^s u_1 \, ds\right)^2 = \frac{36\bar{u}_1^2}{w_1^4}\left(w_1^2 \frac{s^4}{4} - \frac{w_1 s^5}{3} + \frac{s^6}{9}\right)$$

Substituting in (2):-

$$\therefore \quad H_1 = \frac{\frac{1}{D_1} \cdot \frac{36\bar{u}_1^2}{w_1^4}\left[\frac{w_1^2}{4}\cdot\frac{s^5}{5} - \frac{w_1 s^6}{18} + \frac{s^7}{63}\right]_0^{w_1}}{\bar{u}_1 w_1}$$

$$\text{or} \quad H_1 = \frac{52}{140} \cdot \frac{\bar{u}_1 w_1^2}{D_1} \qquad \text{------ (5)}$$

Thus equation (5) can be used to calculate the vapour phase H.E.T.P. (H_1) for the case where there is axial laminar flow of vapour in a narrow annulus with a film of reflux on the outer cylinder wall. It can only be used to predict the performance of <u>rotary</u> concentric cylinder columns under the conditions where rotation of the inner cylinder neither disturbs the laminar flow of vapour nor affects the mass transfer in the vapour phase. This point will be discussed further in section 3.3

Willingham et al (3) attempted to take into account the effect of liquid reflux surface velocity on the vapour laminar velocity profile. By postulating that the liquid reflux film drags down a layer of vapour adjacent to the surface of the film, they presented (without derivation) an equation for H_1 in the form:-

$$H_1' = \frac{\bar{u}_1 w_1^2}{140 D_1} \left[52 + \frac{22\bar{u}_2}{\bar{u}_1} + 3\left(\frac{\bar{u}_2}{\bar{u}_1}\right)^2 \right] \text{- - - - -} \quad (6)$$

where $\bar{u}_2$ is the mean liquid velocity. (6) may be seen to be an extension of (5), and a derivation is presented in Appendix B.

3.12 Integration of equation (3) for laminar flow of reflux

By substituting the equation for the liquid laminar velocity profile in (3) and integrating it is possible, in a manner identical to that shown in section 3.11, to derive an equation for H_2 in the form:-

$$H_2 = \frac{33}{140} \cdot \frac{\bar{u}_2 w_2^2}{D_2} \quad \text{- - - - -} \quad (7)$$

3.13 Total H.E.T.P., H, and number of theoretical plates, N

Hence the total H.E.T.P., H, when both phases are in laminar flow should be given by:-

$$H = H_1' + H_2 = \frac{\bar{u}_1 w_1^2}{140 D_1} \left[52 + \frac{22\bar{u}_2}{\bar{u}_1} + 3\left(\frac{\bar{u}_2}{\bar{u}_1}\right)^2 \right] + \frac{33}{140} \cdot \frac{\bar{u}_2 w_2^2}{D_2} \quad \text{- - -} \quad (8)$$

The number of theoretical plates, N, should then be given by:-

$$N = \frac{\text{length of rectifying section}}{H_1' + H_2} = \frac{1}{H_1' + H_2} \quad ----(9)$$

Macleod and Matterson (2) have shown by experiments on the existing column that, for mixtures of methylcyclohexane - n.heptane, (the mixture used in the present series of experiments), there was negligible resistance to diffusion in the liquid phase. This was established by two series of experiments. In the first, a pair of piano wires was mounted along the length of the rotating inner cylinder so that these wires wiped the reflux film but did not much disturb the vapour stream. It was found that the column performance was not improved by this technique. In the second set of experiments a pair of thick wires was soldered along the length of the rotating inner cylinder, the thickness of the wires being such that they stirred the vapour stream but did not touch the reflux film on the outer wall. This technique improved the column performance considerably. These experiments provided direct and conclusive evidence that for this system there was negligible liquid side resistance to diffusion.

If, in addition, the effect of liquid surface velocity drag on the vapour flow is negligible, the number of theoretical plates, N, may be calculated simply according to the equation:-

$$N = \frac{1}{H_1} = \frac{1}{\frac{52}{140}\frac{\bar{u}_1 w_1^2}{D_1}} \quad ------(10)$$

It has been assumed hitherto that distillation takes place between

parallel plates. This is not a reasonable approximation if the ratio of annular gap width to rotating cylinder radius becomes large. Although the parallel plate approximation should be sufficiently accurate for the cylinder sizes used in the present series of experiments, an analysis is presented in Appendix C for the case of laminar flow in a wide annulus. The form of the solution is cumbersome and evaluation of the final equation for the H.E.T.P. would probably necessitate the use of a computer.

3.2 Laminar flow of ascending vapour with both inner and outer cylinder wetted by reflux

When the inner cylinder is stationary or rotating slowly it is conceivable that any reflux formed on it in the condenser section will flow down the inner cylinder into the annular fractionating section. Assuming that the reflux spreads uniformly over the surfaces of both inner and outer cylinders, it is possible to derive an equation analogous to (5), for the vapour phase H.E.T.P., H_1. If the effective gap width for vapour flow is w_1, then it is possible to obtain in a manner identical with that expounded in Appendix A and section 3.11, the following expression for H_1 :-

$$H_1 = \frac{17}{140} \cdot \frac{\bar{u}_1 w_1^2}{D_1} \qquad \text{------ (11)}$$

This equation was also derived in a different manner by Westhaver (18) The number of theoretical plates, N, would then be given by:-

$$N = \frac{1}{\frac{17}{140} \cdot \frac{\bar{u}_1 w_1^2}{D_1}} \qquad \text{----- (12)}$$

Boil-up rate cc/hr	Number of theoretical plates N observed	Number of theoretical plates N theoretical (13)
76.8	84.8	66.3
91.8	76.2	55.4
106.8	62.2	48.5
123.6	52.5	42.3

Figure 3. Table of results obtained by Naragon and Lewis (5). Experiments conducted on a fixed concentric cylinder system.

neglecting liquid side resistance to diffusion and drag of vapour by liquid reflux.

3.21 Experimental verification

Naragon and Lewis (5) conducted experiments under conditions of total reflux with a concentric cylinder column, both cylinders being fixed. The liquid reflux was directed onto the surfaces of both the inner and outer cylinder. Figure 3 gives a table of their results using a 30.5 cm. long rectifying section, with the inner cylinder 0.64 cm. o/d. and the outer cylinder 0.8 cm. i/d. Methylcyclohexane - n . heptane was used as the test mixture and the theoretical values of the number of theoretical plates, N, shown in the third column, were calculated using an equation similar to (12), viz:-

$$N = \frac{1}{\frac{17}{140} \cdot \frac{\bar{u}_1 w_1^2}{D_1} + \frac{D_1}{\bar{u}_1}} \qquad - - - - - (13)$$

where the second term in the denominator takes into account the effect of longitudinal diffusion. Equation (13) may readily be derived from (12) if longitudinal diffusion is taken into consideration (see equation (A 13), Appendix A). In all practical cases the difference between equations (12) and (13) can be neglected.

The observed values of N were, for all boil-up rates, greater than the theoretical values. This has been attributed (5) to a systematic error in boil-up rate measurement. Nevertheless, the agreement between observed and theoretical values is quite good.

There is little other data available on the performance of concentric cylinder columns by which the validity of the theoretical equations given above can be tested. However, essentially the same theoretical treatment can be applied to the case of distillation in an open tube, for which there is a fair amount of experimental data. Open tube distillation experiments may thus be used to check the validity of the general assumptions of the concentric cylinder column theory.

Westhaver (21) and Kuhn (22) derived an equation for H_1 for the case of distillation in open tube, (wetted wall column), arriving at the result:-

$$H_1 = \frac{11}{48} \frac{\bar{u}_1 d^2}{4 D_1} = 0.057 \frac{\bar{u}_1 d^2}{D_1} \quad ---- (14)$$

where d is the tube diameter, $\bar{u}_1$ the mean vapour velocity and the reflux film thickness is ignored. This equation may also be derived using the method given in Appendix A.

Experimental results obtained by Rose (6) on a 0.6 cm. i/d column were shown by Westhaver (21) to agree with equation (14).

Experimental results obtained by Kuhn and Ryffel (7) on a 1.0 cm. i/d column were also in good agreement with equation (14).

Malyusov et al (23) showed theoretically and experimentally that the equation :-

$$H_1 = 0.068 \frac{\bar{u}_1 d^2}{D_1} \quad ----- (15)$$

was valid for open tubes over the range $0 < Re < 800$, where the Reynolds number, $Re = \rho_1 \bar{u}_1 d/\mu_1$, ρ_1 and μ_1 being the density and viscosity

respectively of the vapour phase.

Above a value of Re = 800, the experimentally determined values of H_1 fell below the theoretical values. Equation (15) is equivalent to (14) except for the value of the numerical constant.

The results of these experiments on open tubes, taken in conjunction with the results of Naragon and Lewis (5) for a concentric cylinder system, justify the use of the theoretical equation (12) in predicting, for the methylocyclohexane - n . heptane system, the number of theoretical plates, N, for the case when there is laminar flow of vapour and liquid streams in a narrow annulus, both cylinder surfaces being wetted by reflux. Equation (10) should be equally valid for those cases in which only one wall is wetted by reflux.

3. 3 Applicability of the theories derived in sections 3.1 and 3.2 to the particular rotating concentric cylinder column under investigation.

Equations such as (10) and (12) will be valid for the case of a rotating concentric cylinder column only under conditions where the motion of the inner cylinder has no effect (a) on the axial laminar vapour velocity profile and (b) on the rate of radial mass transfer, hitherto assumed to be solely due to radial molecular diffusion. With the axial flow laminar and the rotation of the inner cylinder giving rise only to a superimposed circumferentially laminar (Couette) flow it is reasonable to postulate that the axial and circumferential flows may be considered independent of each other and that equations (10) and (12) may be used to predict the performance of such columns, the choice of equation depending solely on reflux distribution. It is difficult to justify theoretically this postulate of the independence of laminar axial and

circumferential flows, but it can be considered that in this case an element of the vapour phase would be acted upon by two independent forces at right angles to each other, one force giving the element an axial velocity component and the other a circumferential component. The number of theoretical plates at a particular boil-up rate will then be independent of speed of rotation and will depend only on the liquid reflux distribution. The mercury vapour transfer experiments discussed in Part II of this thesis provide experimental verification of this postulate. The results of heat and mass transfer experiments by previous workers (28, 31, 32, 33, 34) which will be discussed later, also verify this postulate.

Providing, therefore, experiments can be conducted with both the circumferential and axial flows in a laminar condition, the results of such experiments should conform to equation (10) or (12), assuming longitudinal diffusion, liquid side resistance and vapour drag are negligible. The conformity with either equation (10) or (12) depends on the reflux distribution system of the column investigated. It was a feature particular to the existing fractionating column that dryness of the inner cylinder could be ensured only by rotating it fast enough to remove centrifugally any reflux falling onto it from the condenser section. However, at speeds of rotation sufficient to cause reflux removal the vapour flow regime was not generally purely laminar, since, as will be discussed later in section 3.5, regular toroidal vortices usually formed under these conditions. Thus it was rarely valid to use equation (10) as a standard with which to compare the experimental results obtained with the existing column.

Equation (12) can only be used when the inner cylinder is uniformly

wetted by reflux. The design of the existing column was such that, even with the inner cylinder stationary, it was by no means certain that this cylinder was wetted uniformly although visual observations on one of the inner cylinders used did indicate that condensation was taking place on its surface within the condenser section. If it is assumed that the inner cylinder was in fact wetted by reflux when it was stationary or rotating at low enough speeds, it is of interest to obtain an estimate of the speed of rotation necessary for reflux removal below which speed it may be postulated that equation (12) might hold providing that the motion of the inner cylinder has no effect on the axial laminar velocity profile or the rate of radial mass transfer in the vapour phase.

3.31 Estimation of speed of rotation of inner cylinder for reflux removal

By considering the forces acting on a circumferential element of a thin static film of reflux, thickness w_2 and unit height, a force balance gives:-

$$(\rho_2 \, r_1 \, d\theta . w_2 . 1) r_1 \, \Omega_1^2 = 2T \cos \left[\frac{\pi}{2} - \frac{d\theta}{2} \right] . 1$$

$$\doteqdot T . d\theta$$

ρ_2 is the density of reflux, r_1 the inner cylinder radius, T the surface tension of the liquid reflux and $d\theta$ is the small angle subtended at the cylinder axis by the circumferential element. Ω_1 is the angular velocity, of the inner cylinder, required to cause complete removal of the reflux film.

Simplifying the equation:-

$$w_2 \rho_2 \, r_1^2 \, \Omega_1^2 \doteqdot T \qquad - - - (16)$$

Example

The three inner cylinders used in the experimental study to be described had diameters of 2.60cm, 2.40cm and 2.14cms. For experiments with the

the 2.60cm diameter cylinder using a methyl cyclohexane - n.heptane test mixture equation (16) becomes:-

$$(0.004)\ (0.66)\ (1.3)^2\ \Omega_1^2 \quad \doteqdot \quad 13$$

where ρ_2 = 0.66 gm/cc (24) for the methyl cyclohexane - n.heptane mixture used and T = 13 dynes/cm (25) for this test mixture at its boiling point. The reflux film thickness, w_2, is taken to be approximately equal to 0.004cms (see Table IX) although its thickness is by no means certain. This value of the reflux film thickness corresponds to the lowest boil-up rate experimentally investigated and thus the value of Ω_1 arrived at by the use of (13) is in the nature of an upper limit.

$$\therefore \quad \Omega_1 \quad \doteqdot \quad \sqrt{\frac{13}{(0.66)\ (1.3)^2\ (0.004)}}$$

$$\doteqdot \quad 54 \text{ rad/sec.}$$

Therefore the speed of rotation of the cylinder necessary for reflux removal is given by:-

$$n_1 \quad \doteqdot \quad 54 \times \frac{60}{2\pi} \text{ rpm}$$

$$\therefore \quad n_1 \quad \doteqdot \quad 515 \text{ rpm}$$

Thus above speeds of the order of 500 rpm the 2.60cm diameter inner cylinder should be free of reflux. For the case of the 2.40cm and 2.14cm diameter cylinders used, this analysis gives values of n approximately equal to 550 and 600 rpm respectively.

It is assumed in this analysis that viscous effects are only important in determining the thickness of the reflux film, w_2 in equation (16) and that this quantity is not controlled by surface tension effects.

3.32 Numerical evaluation of equations (10) and (12)

In order to use equations (10) and (12) as a theoretical standard under the conditions for which they are applicable, it is necessary to calculate the values of $\bar{u}_1$ and w_1, the mean vapour velocity and the vapour gap width respectively, at various boil-up rates for the particular column under investigation. These values can then be substituted in the appropriate equation, (10) or (12) and the number of theoretical plates evaluated at a particular boil-up rate.

3.321 Evaluation of equation (10)

In order to calculate w_1, the effective gap width for vapour flow, the reflux film thickness, w_2, must be calculated and this value of w_2 subtracted from the actual annular gap width. w_2 can be calculated from the expression (26):-

$$w_2 = \left\{ \frac{Q \mu_2}{1200 \sigma_2 \rho_2 g} \right\}^{\frac{1}{3}} \quad - - - (17)$$

where μ_2 and ρ_2 are the liquid viscosity and density respectively and σ_2 is the mean circumference of the reflux film, all measured in c.g.s. units. Q is the boil-up rate measured in cc/hr. Since the reflux film is very thin:-

$$\sigma_2 \doteq 2\pi r_2 \quad - - - (18)$$

where r_2 = inside radius of outer cylinder.

Hence $$w_1 = (r_2 - r_1) - w_2$$

$$= b - w_2 \quad - - - (19)$$

where r_1 = outside radius of inner cylinder

and $b = r_2 - r_1$

Now $\bar{u}_1$ may be calculated from the equation:-

$$3600 \rho_1 \bar{u}_1 \psi = Q \rho_2 \quad - - - (20)$$

where ρ_1 is the density of the vapour in gm/cc and ψ is the cross-sectional flow area for vapour flow, in cm^2.

Hence $\bar{u}_1$ and w_1 may be calculated for a particular inner cylinder over a range of values of Q and thus equation (10) numerically evaluated for the range of boil-up rates experimentally investigated. Thus a "theoretical curve (one wall wetted)" of N versus boil-up rate may be compared with experimentally obtained values which are considered to conform to the conditions under which equation (10) was derived, viz:- purely axial laminar flow of vapour with the outer cylinder wall wetted by a laminar stream of reflux, the column operating adiabatically under conditions of total reflux with negligible liquid side resistance to diffusion and negligible longitudinal diffusion effects.

3.322 Evaluation of equation (12)

In evaluating equation (12) it is usually reasonable to assume that the total thickness of reflux film (i.e. the sum of the reflux film thicknesses on both cylinder walls), is equal to the value of w_2 used in evaluating equation (10). This approximation is valid for the existing column conditions because a calculation, based on the assumption that the reflux film thicknesses are the same on each cylinder wall, shows that the total reflux film thickness is not significantly different from the value of w_2 used in evaluating equation (10).

Thus, for each boil-up rate and inner cylinder diameter, $\bar{u}_1$ and w_1 may be assumed to have the same values as calculated for use in equation (10).

Thus a "theoretical curve (both walls wetted)" of N versus boil-up rate, may simply be calculated from points on a "theoretical curve (one wall wetted)" by multiplying the ordinate values of the latter curve by a factor of 52/17, as shown by comparing equations (12) and (10).

Tables IX, X and XI at the end of Part I of this report show details of such calculations for the 2.60 cm., 2.40 cm. and 2.14 cm. diameter inner cylinders respectively. The range of boil-up rates considered, 120-780 cc/hr, more than covered the range of experimentation. The axial Reynolds numbers ($Re_a = 2\rho \bar{u}_1{}^b/\mu_1$) corresponding to each boil-up rate, Q, is included in the tables. Note that in calculating the axial Reynolds numbers as $Re_a = 2\rho \bar{u}_1{}^b/\mu_1$, the reflux film thickness is ignored.

The question of the applicability of these calculated values, as a valid theoretical standard with which to compare the results obtained, will be discussed later in Section 7.

3.4 Turbulent flow of ascending vapour with the inner cylinder stationary

There is some doubt about the criterion for the onset of turbulence with purely axial flow in an annulus (36), but for the purposes of this discussion it will be supposed that when the axial Reynolds number ($Re_a = 2\bar{u}_1{}^b/\nu_1$) reaches a value in the region of 2000, the vapour phase becomes turbulent.

A tentative theoretical correlation will now be presented for the case when the boil-up rate is sufficiently high to cause the onset of axial turbulence in a parallel plate system.

3.41 Distillation between parallel plates with axial turbulence

With the inner cylinder stationary, the distribution of reflux on one or both cylinder surfaces depends primarily on the design of the column under investigation. For the existing column it was considered possible that

when the inner cylinder was stationary both cylinder surfaces were wetted by reflux. This will be assumed in the following analysis. For turbulent flow of vapour, by analogy with the Dittus-Boelter equation for heat transfer in a tube, a mass transfer coefficient, k_t, is given approximately by:-

$$\frac{k_t \cdot 2w_1}{D_1} = 0.023 \quad Re_a^{0.8} \quad Sc^{0.4} \quad \text{- - - - - (21)}$$

As shown in Appendix A, for <u>laminar</u> flow the H.E.T.P. is given by an equation of the form:-

$$(H_1)_{\text{laminar}} = \frac{V}{2K} = \frac{\bar{u}_1 \, w_1 \, c}{2K} \quad \text{- - - - - - - (22)}$$ analogous to

equation (A 13) in Appendix A, but for two walls wetted and neglecting longitudinal diffusion. In equation (22), V is the total vapour molal flow, c is the total molal concentration in the vapour phase and K is the mass transfer coefficient for laminar flow. It should be noted that equation (22) can be derived quite simply if it is assumed that the axial concentration gradient in the vapour phase is independent of radial position and longitudinal diffusion negligible. A mass balance on an elemental height dz, of the vapour phase then gives:-

$$V.d\bar{y} = 2Kdz \; (y_i - \bar{y})$$

for a parallel plate system of unit depth with two walls wetted, where $\bar{y}$ is the mean mole fraction of the more volatile component in the vapour phase and y_i the value of the mole fraction of the more volatile component at the vapour-

liquid interface. If this equation is integrated over the height, l, of the column then:

$$\frac{2K}{V} \cdot \int_{0}^{l} dz = \int_{\bar{y}_o}^{\bar{y}_l} \frac{d\bar{y}}{y_i - \bar{y}} \equiv \text{number of theoretical plates, N.}$$

where $\bar{y}_o$ and $\bar{y}_l$ are the values of $\bar{y}$ at the bottom and top of the column respectively. Thus the H.E.T.P. $\equiv \frac{V}{2K}$, which is identical with equation (22). For <u>turbulent</u> flow conditions an equation identical in form to (22) can be derived in a similar manner if it is again assumed that the axial concentration gradient in the vapour phase is independent of radial position and longitudinal diffusion negligible. Under these conditions an analysis identical to the one shown above leads to:-

$$(H_1)_{\text{turbulent}} = \frac{V}{2K}$$

where K is now the mass transfer coefficient for turbulent flow. The appropriate values of K may be obtained either on a tentative basis from equation (21) (since $K \equiv k_t c$) or, more directly from correlations of the results of experiments with concentric cylinder systems in which heat, mass or momentum transfer takes place, assuming that heat, mass and momentum transfer are analogous processes.

Thus, for a turbulent regime it is reasonable to write:-

$$(H_1)_{\text{turbulent}} = \frac{\bar{u}_1 w_1}{2 k_t} \quad \text{- - - - - - (23)}$$

$$= \frac{\bar{u}_1 w_1^2}{0.023 \, Re_a^{0.8} Sc^{0.4} D_1} \text{ using (21) as a source for } k_t$$

i.e. $(H_1)_{turbulent} = 21{\cdot}8\ w_1\ Re_a^{0.2}\ Sc^{0.6}$ - - - - (24)

assuming $Re_a = \frac{2\bar{u}_1 b}{\nu_1} \equiv \frac{2\bar{u}_1 w_1}{\nu_1}$, where ν_1 is the kinematic viscosity in the vapour phase.

Johnstone and Pigford (37) obtained experimentally a correlation equivalent to:-

$$(H_1)_{turbulent} = 7{\cdot}63\ d\ Re^{0.23}\ Sc^{0.63}$$

for distillation with turbulent flow of vapour in an open tube of diameter d. Malyusov et al (38) report the results of open tube distillation experiments, with turbulent flow of vapour, in the form:-

$$(H_1)_{turbulent} = 11{\cdot}1\ d^{0.64}\ Re^{0.23}\ Sc^{0.63}$$

for $1000 < Re < 15000$ where $Re = \bar{u}_1 d/\nu_1$

It is therefore reasonable to expect that the H.E.T.P. in the vapour phase, H_1, for turbulent flow distillation in a narrow annulus would be given by equation (24).

The theoretical equation (24) could not be verified experimentally since neither the results of the present investigation nor those of previous workers on similar columns furnished values of H_1 at Reynolds numbers greater than 2000.

In the mercury vapour transfer experiments, described in part II, axial Reynolds numbers slightly in excess of $Re_a = 2000$ were in fact realised but not over a sufficiently large range to arrive at a correlation similar to equation (21)

In order to produce a value of Re_a greater than 2000, using the system methylcyclohexane-n. heptane,

$$Re_a = \frac{2\bar{u}_1 w_1}{0{\cdot}0212} > 2000$$

where 0·0212 cm^2/sec is the approximate value of the kinematic viscosity of the vapour (24)

Thus $\bar{u}_1 w_1 > 21{\cdot}2 \ cm^2/sec$ ----- (25)

For the results of Willingham et al (3); $w_1 \doteqdot 0{\cdot}1$ and the maximum value of $\bar{u}_1$ (corresponding to a maximum experimental boil-up rate of 4,000 cc/hr) was 87·7 cm/sec.

Thus the left hand side of equation (25) is approximately 8.8 cm^2/sec in this case, indicating that a boil-up rate of about 10,000 cc/hr would be required to produce turbulence in the vapour phase.

Similarly, for the column under investigation, the maximum value of $\bar{u}_1$ (corresponding to a maximum experimental boil-up rate of 780 cc/hr) was 54·9 cm/sec using the 2.60 cm. diameter glass inner cylinder (see table IX). In

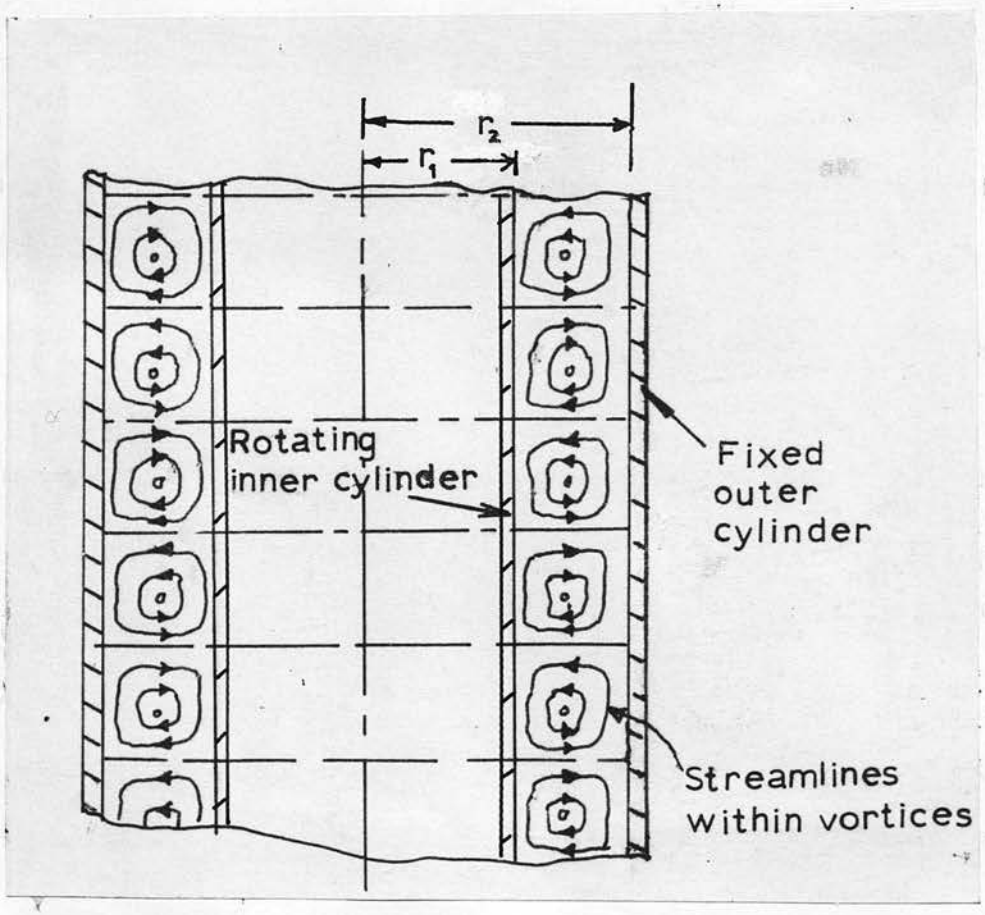

Figure 4. Taylor vortices.

this case, the left hand side of (25) is approximately $54.9 \times 0.1 = 5.5$ cm^2/sec, indicating that a boil-up rate of about 3,000 cc/hr would be required to produce turbulence in the vapour phase.

The analysis leading to equation (24) is therefore not of practical importance.

3.5 Vortex or turbulent flow of vapour with the inner cylinder rotating

It has been shown, both experimentally (9, 10, 11, 27, 28, 29, 33, 34) and theoretically, (13, 14) that when fluid flows through the annular gap between concentric cylinders, there exists a critical speed of rotation of the inner cylinder which marks the onset of instability in the fluid flow. The nature of this instability, for the special case of zero axial flow, was first investigated mathematically by Taylor (4) in 1923 and experimentally by Taylor (4) and in 1927 by Lewis (12) and subsequently by many other workers. Taylor showed that, at this critical speed of rotation, the laminar flow breaks down and vortices are formed occupying toroidal regions coaxial with the annulus, as shown in figure 4. These vortices are now often referred to as Taylor vortices. As indicated in figure 4, each vortex ring occupies, approximately, a square annular compartment.

Subsequently, it was shown experimentally (9, 10, 11, 27, 28, 29, 33, 34) and theoretically (13, 14) that similar vortices exist for finite axial flow rates in the annulus. Thus it would be expected that there should exist a critical rotational speed of the inner cylinder, for a particular column and boil-up rate, at which vortices are formed. These vortices would be expected

to increase radial diffusion in the vapour phase. Hence the appearance of vortices should be manifested by a sudden rise in the number of theoretical plates above a value which had previously remained constant over a range of lower rotational speeds.

The results of previous investigators (1, 2, 3), which will be discussed in more detail later, indicate that there is no change in column performance at speeds of rotation of the inner cylinder at which vortices would be expected to appear. These results show that:-

either (a) vortices are not formed at or near the predicted critical speeds in these columns

or (b) that vortices are formed but are not effective in promoting radial mass transfer

or, possibly (c) that vortices do improve radial mass transfer, but at the same time increase back-mixing so as to offset any improvement in column performance.

It is therefore of interest to establish, theoretically and experimentally, the conditions for vortex formation in concentric cylinder columns and also to determine the effect of these vortices on the process of distillation in such columns. This was in fact the purpose of further investigations described in Part II using a mercury vapour transfer column. The conditions for vortex formation are discussed in section 3.6, but theories of distillation will now be presented which assume the existence of vortices in the annulus

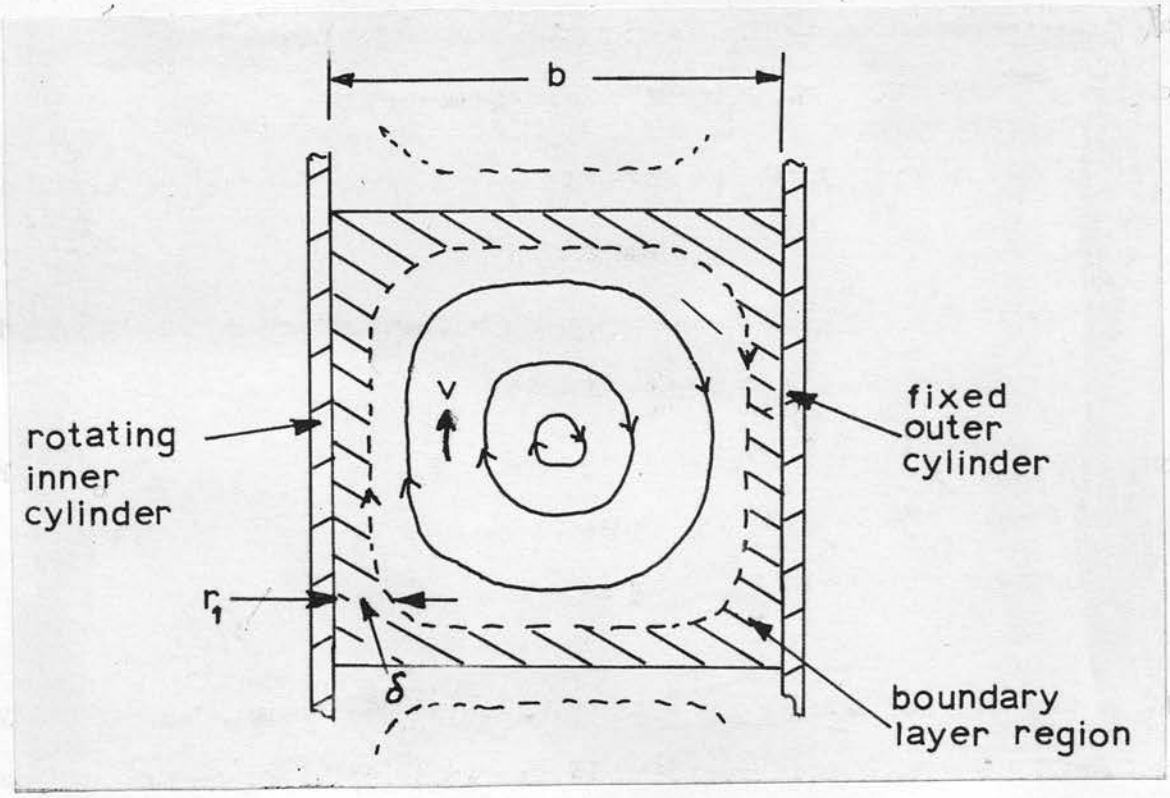

Figure 5. Single vortex in an annulus, showing boundary layer and inviscid core regions

of a rotating concentric cylinder fractionating column.

3.51 Distillation in an annulus when vortices are present

There appears to be no published theoretical derivation of the H.E.T.P. for distillation in an annulus when vortices are present. An approximate theory is recorded in this section, but should only be considered as the first step towards a more rigorous solution of the problem.

Batchelor (30) has shown, using an "inviscid core and boundary layer model" that it is possible to derive an approximate equation for momentum transfer in an annulus when vortices are present. Batchelor did not consider the case where an axial flow is superimposed on the system and assumed that the speed of rotation of the inner cylinder was well above the critical speed corresponding to vortex formation. A summary of Batchelor's treatment will now be given and a momentum-mass transfer analogy will then be used to derive an equation governing distillation in an annulus if and when vortices are present. It will be assumed that the boil-up rate is so low that it does not significantly disturb the well-established vortex pattern, with the inner cylinder rotating at speeds several times the critical value corresponding to vortex formation.

3.511 Batchelor's approximate analysis (30)

The sign $\sim$ is used throughout this discussion to signify that order of magnitude relationships are involved. Figure 5 shows a single vortex with an inviscid core rotating with velocity of the order v.

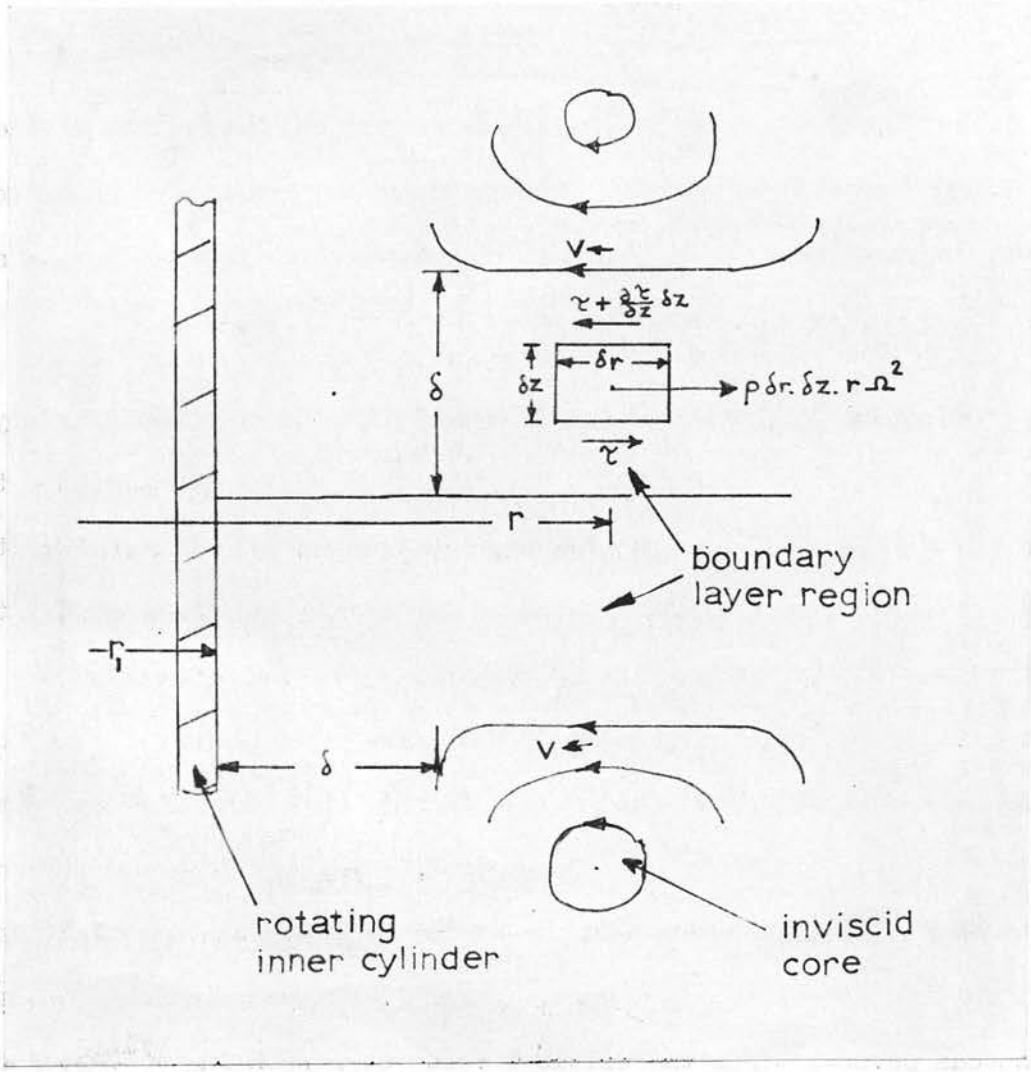

Figure 6. Forces acting on an element of fluid in boundary layer between two vortices

For parabolic growth of the boundary layer, between each vortex and also between a vortex and the cylinder wall

$$\frac{\delta}{b} \sim \left(\frac{b\,v}{\nu}\right)^{-\frac{1}{2}} \quad \text{- - - - (26)}$$

Where δ represents the thickness of the boundary layer, b the annular gap width and ν the kinematic viscosity of the fluid contained in the gap. As shown in figure 6, a balance between the centrifugal forces and viscous forces acting on an element of the boundary layer between two vortices gives:-

$$\rho.\delta r.\delta z.r.\Omega_1^2 = \frac{\partial \tau}{\partial z}\,\delta z.\,\delta r$$

where Ω_1 is the angular velocity of the rotating inner cylinder and τ the shear stress.

since: $\tau \sim \mu \frac{v}{\delta}$

then, $\frac{\partial \tau}{\partial z} \sim \mu \frac{v}{\delta^2}$

$$\therefore \quad \rho\, r\, \Omega_1^2 \sim \mu \frac{v}{\delta^2}$$

or $$\rho\, r_1\, \Omega_1^2 \sim \mu \frac{v}{\delta^2} \quad \text{- - - - (27)}$$

where r_1 is the radius of the rotating inner cylinder.

The torque on a length l of the inner cylinder is given by G, where

$$G \sim l r_1^2 \times \text{viscous stress at cylinder}$$

$$\sim l r_1^2 \left(\frac{\mu \Omega_1 r_1}{\delta}\right) \quad \text{- - - - - - (28)}$$

From (26) and (27) :-

$$\delta^2 \sim b^2 \left(\frac{b\,v}{\nu}\right)^{-1}$$

$$\sim \frac{\mu \cdot v}{\rho\, r_1\, \Omega_1^2}$$

$$\therefore \quad v \sim \Omega_1 (b r_1)^{\frac{1}{2}}$$

$$\therefore \quad \delta \sim \left(\frac{b}{r_1}\right)^{\frac{1}{4}} \cdot \left(\frac{\nu}{\Omega_1}\right)^{\frac{1}{2}} \qquad ----(29)$$

Substituting for δ from (29) in (28) :-

$$G \sim l r_1^2 \left(\frac{\mu\, \Omega_1 r_1 r_1^{\frac{1}{4}}\, \Omega_1^{\frac{1}{2}}}{b^{\frac{1}{4}}\, \nu^{\frac{1}{2}}}\right)$$

or $$G \sim l \rho r_1^4 \Omega_1^2 \left(\frac{\nu}{r_1 \Omega_1 b}\right)^{\frac{1}{2}} \left(\frac{b}{r_1}\right)^{\frac{1}{4}} \qquad ---(30)$$

If it is assumed that the thickness of the momentum boundary layer, δ, can be taken to be of the same order as the thickness of the fluid layer in which the whole of the mass transfer resistance is concentrated and through which the transfer is solely by molecular diffusion, then it is possible to write:-

$$N_m = k_v \cdot \Delta c \doteq \frac{D_1}{\delta} \Delta c \qquad ----------(31)$$

Where N_m is the mass transferred radially per unit area per unit time, k_v is a radial mass transfer coefficient for vortex flow, Δc represents the concentration change across the laminar boundary layer and D_1 is the vapour phase molecular diffusion coefficient. This equation may apply to mass transfer from the surface of the inner or outer cylinder, or both.

Defining the Sherwood number, $Sh \equiv \frac{k_v b}{D_1}$ then,

$$Sh \equiv \frac{k_v b}{D_1} = \frac{D_1}{\delta} \cdot \frac{b}{D_1} \quad \text{from (31)}$$

If an analogy between momentum and radial mass transfer holds, then from equation (29) in (31):-

$$Sh \sim \frac{b}{\left(\frac{b}{r_1}\right)^{\frac{1}{4}} \left(\frac{\nu}{\Omega_1}\right)^{\frac{1}{2}}}$$

$$\text{i.e.} \quad Sh \equiv \frac{k_v b}{D_1} \sim \left(\frac{r_1 \Omega_1 b}{\nu}\right)^{\frac{1}{2}} \left(\frac{b}{r_1}\right)^{\frac{1}{4}} \quad \text{-- (32)}$$

3.512 Distillation in an annulus - one wall wetted

Equation (32) is directly applicable to the case of distillation in an annulus once the vortex regime has been definitely established. It is assumed, by analogy with equation (A.13) in Appendix A, for one wall wetted that the H.E.T.P. in the vapour phase, H_1, is given by:-

$$H_1 = \frac{V}{k_v c} \sim \frac{V}{\frac{D_1}{w_1}\left(\frac{r_1 \Omega_1 w_1}{\nu_1}\right)^{\frac{1}{2}}\left(\frac{w_1}{r_1}\right)^{\frac{1}{4}} c} \quad \text{-- (33)}$$

using equation (32) and noting that for distillation $b = w_1$, (the effective

gap width for vapour flow) and that V is the total vapour molal flow rate, c the total molal concentration in the vapour phase and that the parallel plate approximation is used.

Longitudinal diffusion is neglected in this approximate analysis. This is justifiable since, despite the fact that the experiments of Croockewit et al (8) and the longitudinal diffusion experiments described in Part II of this investigation indicate that the apparent longitudinal diffusivity is greatly increased by the appearance of vortices, it will be shown in section 3.7 that the contribution, of even such an increased value of the diffusivity, to the value of H_1 is negligible.

$$\therefore \quad \text{if} \quad H_1 \sim \frac{w_1^2 \bar{u}_1 c}{D_1 \left(\frac{r_1 \Omega_1 w_1}{\nu_1}\right)^{\frac{1}{2}} \left(\frac{w_1}{r_1}\right)^{\frac{1}{4}} c}$$

$$\text{then} \qquad H_1 \sim \left\{w_1 \left(\frac{w_1}{r_1}\right)^{-\frac{1}{4}}\right\} \left(\frac{\bar{u}_1 w_1}{\nu_1}\right) \left(\frac{\nu_1}{D_1}\right) \left(\frac{r_1 \Omega_1 w_1}{\nu_1}\right)^{-\frac{1}{2}}$$

$$\text{or} \qquad H_1 \sim \left\{w_1 \left(\frac{w_1}{r_1}\right)^{-\frac{1}{4}}\right\} \left(Re_a\right) \left(Sc\right) \left(Re_c\right)^{-\frac{1}{2}} \qquad \text{---(34)}$$

where Re_a is the axial Reynolds number, Re_c is a circumferential Reynolds number and Sc the Schmidt number.

Thus, the number of theoretical plates, N, neglecting liquid side resistance, is given by:-

$$N \sim \frac{1}{\left\{w_1 \left(\frac{w_1}{r_1}\right)^{-\frac{1}{4}}\right\} \left(Re_a\right) . \left(Sc\right) . \left(Re_c\right)^{-\frac{1}{2}}} \qquad \text{---(35)}$$

It should be realised that this derivation of N is not dependent on the

form of the velocity profile in the vapour phase and can therefore be used for the case of vortex flow.

3.513 Previous experimental correlations

Bjorklund and Kays (31) obtained a correlation for heat transfer in an annulus with the inner cylinder rotating but without axial flow in the form:-

$$Nu = 0.175 \left[\frac{b/r_1}{\ln (1 + b/r_1)} \right] \left(\frac{r_1 \Omega_1 b}{\nu} \right)^{\frac{1}{2}} \left(\frac{b}{r_1} \right)^{\frac{1}{4}}$$

where Nu is the Nusselt number. This equation was valid in the range $90 < \left(\frac{r_1 \Omega_1 b}{\nu} \right) \left(\frac{b}{r_1} \right)^{\frac{1}{2}} < 2000$, in a region where vortices were presumed to exist.

The form of this heat transfer equation is very similar to equation (32) particularly when b/r_1 is small, since $\ln (1 + b/r_1) \rightarrow b/r_1$ for small b/r_1 and the equation then reduces to:-

$$Nu = 0.175 \times \left(\frac{r_1 \Omega_1 b}{\nu} \right)^{\frac{1}{2}} \left(\frac{b}{r_1} \right)^{\frac{1}{4}}$$

which is identical in form to (32).

Experiments by Gazley (32) and Becker (33) on similar systems confirmed the results obtained by Bjorklund and Kays.

A correlation of the results obtained from radial mass transfer experiments, with axial flow in the annulus, of the mercury vapour transfer column described in Part II, gives the expression:-

$$Sh = 0.45 \quad (Re_c)^{\frac{1}{2}} \quad (b/r_1)^{\frac{1}{4}} \qquad \text{- - - (95)}$$

$$\text{or} \qquad Sh = 0.45 \left(\frac{r_1 \Omega_1 b}{\nu} \right)^{\frac{1}{2}} \left(b/r_1 \right)^{\frac{1}{4}}$$

which is identical in form to the heat transfer equation of Bjorklund and Kays and also to the theoretical mass transfer equation (32). Equation (95) was found to be valid over a range $0 < Re_a < 300$ and $Re_c < 5000$. (The lower limit of this range of circumferential Reynolds number obviously depended on the axial flow rate). The correlation (95) was in fact obtained from results corresponding to a vortex flow regime in the annulus, the small axial flow rates having an insignificant effect on the stability of the vortex pattern.

It should be pointed out that the derivation of equation (32) from Batchelor's theoretical model is based on the assumption that the speed of rotation of the inner cylinder is many times the critical value corresponding to vortex formation. The experimental correlations just discussed which confirm the form of equation (32) were obtained from a wide range of results, some of which applied to the case where the inner cylinder was rotating at speeds only slightly greater than the critical speed. Torque measurements by Donnelly and Simon (30), for the case of

momentum transfer in an annulus with the inner cylinder rotating, do in fact only conform with Batchelor's theory at high speeds of rotation of the inner cylinder. It therefore appears that the relationship (30) is an assymptotic one for torque transmission but that the analogous relationships for heat and mass transfer are valid over a wider range of the vortex flow regime.

It should also be noted that the radial mass transfer experiments reported in Part II, involved the evaporation of mercury vapour from the surface of a short circumferential band on the outer or inner cylinder of the column. Thus the application of the correlation (95) to transfer processes occurring in a long annulus, e.g. the present distillation experiments, must be undertaken with caution. In general, the mass transfer coefficient, k_v, as calculated from equation (95) will have a higher value than the corresponding mass transfer coefficient for the distillation column, under dynamically similar conditions. This is because with a short circumferential diffusing band the mass transfer driving force is large, due to a large concentration gradient at the mass transfer surface. In the case of mass transfer from a long section, the local mass transfer coefficient at the leading edge of the section will be large, but the mass transfer coefficient averaged over the entire length of the annulus will be smaller than this local coefficient, due to the progressive saturation of the layers of the flowing stream near the wall. If it is assumed that the correlation (95) of results obtained from the mercury vapour transfer experiments, described in Part II, is applicable to the case of distillation in an annulus in which a vortex regime exists, the following analysis yields an equation for the number of theoretical plates, N, as a function of boil-up rate (i.e. axial Reynolds number, Re_a) and speed of rotation of the inner

cylinder (i.e. circumferential Reynolds number Re_c) for the case where the outer cylinder wall only is wetted by reflux.

3.52 Number of theoretical plates based on equation (95) for one wall wetted by reflux

From equation (A.13), Appendix A, neglecting longitudinal diffusion, the H.E.T.P. in the vapour phase, H_1 is given by:-

$$H_1 = \frac{V}{k_v c} = \frac{V}{0.45 \frac{D_1}{w_1} \cdot \left(\frac{r_1 \Omega_1 w_1}{\nu_1}\right)^{\frac{1}{2}} \left(\frac{w_1}{r_1}\right)^{\frac{1}{4}} \cdot c} \quad \text{using (95) with } b = w_1$$

$$\text{or} \quad N = \frac{1}{H_1} = \frac{0.45}{w_1 \bar{u}_1} \cdot \frac{D_1}{w_1} \cdot \left(\frac{r_1 \Omega_1 w_1}{\nu_1}\right)^{\frac{1}{2}} \left(\frac{w_1}{r_1}\right)^{\frac{1}{4}}$$

assuming that liquid side resistance to mass transfer is negligible.

$$\therefore \quad N = 0.9 \left(\frac{1}{w_1}\right) \left(\frac{w_1}{r_1}\right)^{\frac{1}{4}} \cdot \frac{Re_c^{\frac{1}{2}}}{Re_a \, Sc} \qquad \text{- - - - - - (36)}$$

where $Re_c = \frac{r_1 \Omega_1 w_1}{\nu_1}$; $Re_a = \frac{2\bar{u}_1 w_1}{\nu_1}$ and $Sc = \nu_1/D_1$

Equation (36) can therefore be used as a theoretical standard with which to compare the results of experiments on rotary concentric cylinder columns operating under the appropriate conditions i.e. with the outer cylinder wall wetted by reflux and a fully established vortex regime in the vapour phase.

An anonymous report written in 1948 describing work at the "Shell" Laboratories in Amsterdam (34) gives details of vapourisation experiments in a rotating concentric cylinder column. The rotating inner cylinder had an outside diameter of 8.5 cm. and the fixed outer cylinder had an inside diameter of 10 cm. N. butanol-2 was run down the inner wall of the fixed outer cylinder and evaporated into a counter-current flow of air through the annulus. The working section of the column was 30 cm. in length. For the conditions under which vortices should have existed in the vapour phase, the following correlation may be obtained from the results quoted:-

$$N.\,Re_a = 6.8\ (\Omega_1\, r_1\, 2b/\nu_1)^{0.52} \quad ------ (37)$$

(The correlation quoted in the report, $N.Re_a = 22.5\ (\Omega_1\, r_1\, 2b/\nu_1)^{0.52}$, is incorrect due to a graphical error)

Equation (37) reduces to:-

$$N = \frac{6.8 \times 2^{0.52}}{Re_a} (Re_c)^{0.52}$$

or $$N \doteq 9.72\ Re_c^{\frac{1}{2}} / Re_a \quad ---- (38)$$

The form of (38) is very similar to equation (36); hence assuming that the numerical constant 9.72 in (38) involves the dimensionless groups $\left(\frac{1}{w_1}\right)\left(\frac{w_1}{r_1}\right)^{\frac{1}{4}}$ and the Schmidt number, it is possible to write:-

$$N = 9.72\ \frac{Re_c^{\frac{1}{2}}}{Re_a} \equiv c \cdot \left(\frac{1}{w_1}\right)\left(\frac{w_1}{r_1}\right)^{\frac{1}{4}} \cdot \frac{Re_c^{\frac{1}{2}}}{Re_a \cdot Sc}$$

where c is a numerical constant equivalent to the value 0.9 in (36)

Now for the column used in Amsterdam, $l = 30$ cm., $w_1 = 0.75$ cm., $r_1 = 4.25$ cm., for n.butanol-2, $\nu_1 = 0.136$ cm^2/sec and $D_1 = 0.078$ cm^2/sec (34) $\therefore$ Sc = 1.75

Therefore:-

$$N = 9.72 \frac{Re_c^{\frac{1}{2}}}{Re_a} = c\left(\frac{30}{0.75}\right)\left(\frac{0.75}{4.25}\right)^{\frac{1}{4}} \frac{Re_c^{\frac{1}{2}}}{Re_a} \times 1.75$$

$$= c.\ 14.82 \frac{Re_c^{\frac{1}{2}}}{Re_a}$$

$$c = \frac{9.72}{14.82} = 0.66$$

Thus these vapourisation experiments yield a correlation:-

$$N = 0.66 \left(\frac{l}{w_1}\right)\left(\frac{w_1}{r_1}\right)^{\frac{1}{4}} \frac{Re_c^{\frac{1}{2}}}{Re_a \cdot Sc} \quad ---- \quad (39)$$

This is a very satisfactory confirmation of equation (36) in that the numerical constant of 0.66 would be expected to be less than the value 0.9, the latter value being obtained from a correlation of experimental results involving evaporation of mercury from a very narrow circumferential band. Equation (39) may therefore be more accurately applicable to the case of distillation in the annulus between rotating concentric cylinders.

From experiments involving the dissolution of a rotating inner cylinder, made of benzoic acid, in an annulus containing water, Eisenberg et al (35) obtained the following correlation in terms of the Colburn j-factor, j_D, for mass transfer:-

$$j_D = \frac{k_v}{r_1 \Omega_1} Sc^{0.644} = 0.079 \left(\frac{r_1 \Omega_1 b}{\nu}\right)^{-0.3} \left(\frac{b}{2r_1}\right)^{0.3} \quad ---- (40)$$

where Ω_1 was the angular velocity of the inner cylinder, radius r_1, and Sc the Schmidt number, ν/D. Several sizes of inner and outer cylinders were used and the speeds of rotation of the inner cylinder were such that vortices should have been present over the entire range of experimentation. There was no axial flow superimposed on the vortex regime.

Equation (40) may be put in the form:-

$$Sh = \frac{k_v b}{D} = \frac{0.079}{2^{0.3}} \left(\frac{r_1 \Omega_1 b}{\nu}\right)^{0.7} \left(\frac{b}{r_1}\right)^{0.3} (Sc)^{0.366} \quad ---- (41)$$

Equation (41) is dissimilar to equation (32), (the equation derived using Batchelor's analysis), in as much as the exponents of the groups are different and the Schmidt number is involved in (41). From (41), Eisenberg et al concluded that k_v, the mass transfer coefficient, was independent of annular gap width b, and that j_D was a function of a rotational Reynolds number based solely on the radius of the inner cylinder, i.e.

$$j_D = 0.079 \left(\frac{2r_1 \cdot r_1 \Omega_1}{\nu}\right)^{-0.3}$$

This conclusion was also supported by the experiments of Mawer and Wishart (41) for the dissolution of benzoic acid in water contained in an annulus with the inner cylinder rotating. Mass transfer took place from a narrow circumferential band of benzoic acid on the rotating inner cylinder. There was no axial flow

of water in the annulus.

This conclusion that k_v is independent of b disagrees with all the other correlations previously discussed.

It is clear therefore that more experimental and theoretical work is required before any definite correlation can be established for the influence of vortex motion on radial mass transfer.

If it is assumed that the correlation (40) of Eisenberg et al is applicable to the case of distillation in an annulus, in which a vortex regime exists, the following analysis yields an equation for the number of theoretical plates, N, as a function of boil-up rate (i.e. axial Reynolds number) and speed of rotation of the inner cylinder (i.e. circumferential Reynolds number) for one wall wetted by reflux.

3.53 Number of theoretical plates based on equation (40) for one wall wetted by reflux

From equation (A.13), Appendix A, neglecting longitudinal diffusion, the H.E.T.P., H_1, in the vapour phase is given by:-

$$H_1 = \frac{V}{k_v c} = \frac{w_1 \bar{u}_1}{k_v} \quad \text{since V, the vapour molal flow rate} = w_1 \bar{u}_1 c$$

where c is the total vapour molal concentration.

Now $N = \frac{1}{H_1}$, neglecting liquid side resistance to mass transfer

$$\therefore \quad N = \frac{1 \, k_v}{\bar{u}_1 w_1} \qquad - - - - - \quad (42)$$

Now From (40)

$$k_v = \frac{0.079}{2^{0.3}} \cdot \frac{r_1 \Omega_1}{Sc^{0.644}} \cdot \left(\frac{r_1^2 \Omega_1}{\nu_1}\right)^{-0.3}$$

$$\therefore N = \frac{1}{\bar{u}_1 w_1} \frac{0.079}{2^{0.3}} \frac{r_1 \Omega_1}{Sc^{0.644}} \left(\frac{r_1^2 \Omega_1}{\nu_1}\right)^{-0.3}$$

$$= (0.079) 2^{0.7} \left(\frac{r_1^2 \Omega_1}{\nu_1}\right)^{0.7} \frac{1}{Re_a} \cdot \left(\frac{1}{r_1}\right) \cdot \frac{1}{Sc^{0.644}}$$

where $Re_a = \frac{2 w_1 \bar{u}_1}{\nu_1}$ and ν_1 is the kinematic viscosity of the vapour in the annulus during distillation.

$$\therefore N = (0.1283) \left(\frac{1}{r_1}\right) \frac{1}{Re_a} \cdot \frac{1}{Sc^{0.644}} \cdot \left(\frac{r_1^2 \Omega_1}{\nu_1}\right)^{0.7} \text{ - - - (43)}$$

Equation (43), like equations (36) and (39) can be used as a theoretical standard with which to compare the results of experiments on rotary concentric cylinder columns operating under the appropriate conditions, i.e. with the outer cylinder wall wetted by reflux and a fully established vortex regime in the vapour phase. The question of the applicability of equations (36), (39) and (43) as valid theoretical standards is discussed in section 7 where a quantitative comparison is made between these theoretical correlations and results obtained from experiments on the existing column and results obtained by Willingham et al (3) on a similar column.

3.54 Turbulent flow with the inner cylinder rotating

Some workers (11, 28, 29, 31, 33) have observed the existence of a turbulent regime in the annulus when the speed of rotation of the inner cylinder is very high. It appears that vortices still persist at these

high circumferential Reynolds numbers but that the motion of a fluid element is of a much more random nature, corresponding to a turbulent motion superimposed on a vortex system.

If fully developed circumferential turbulence exists due to rapid rotation of the inner cylinder at very small axial flow rates, a correlation may be obtained of the form:-

$$(H_1)\ \text{turbulent} = \frac{1}{2m}\ \frac{w_1\ Re_a (Sc)^{0.6}}{(Re_c)^{0.8}} \qquad - - - (44)$$

where m is a numerical constant and the derivation is based on the assumption that shear flow is equivalent to pressure flow. This equation may be derived in a manner identical to that used in deriving equation (24) and is given in detail in Appendix D.

Unfortunately, equation (44) could not be tested in the present work, since, as will be discussed later, the conditions for turbulent flow due to rotation are ill-defined and experiments with the mercury vapour transfer column have indicated that turbulence would not exist even at the highest speeds of rotation used in the fractionating column experiments.

3.6 Conditions for vortex formation and the onset of turbulence

The derivation of equations (36), (39) and (43) for distillation in an annulus in which a vortex regime existed was based on the assumption that vortices were well established and that the axial flow superimposed on the vortex system had little effect on the stability of the vortex pattern. The conditions under which these assumptions are true will be discussed in the ensuing sections dealing with conditions for vortex flow, with and without an axial flow in the annulus of which the inner cylinder rotates. Brief references will also be made to the conditions for the onset of axial and circumferential turbulence, though, as mentioned previously in sections

3.41 and 3.54, a discussion of this possible flow regime appears to be of no practical significance in the present study.

3.61 Taylor vortex formation without axial flow in the annulus

For the particular case of no axial flow in the annulus, Taylor (4) obtained the following expression for the critical speed, Ω_c, at which vortices would appear:-

$$\Omega_c^2 = \frac{\pi^4 \nu^2 (r_1 + r_2)}{2P (r_2 - r_1)^3 r_1^2} \qquad \text{- - - (45)}$$

where $$P = 0.0571 \left[1 - 0.652 \left(\frac{r_2 - r_1}{r_1}\right)\right] + 0.00056 \left[1 - 0.652 \frac{(r_2 - r_1)}{r_1}\right]^{-1} \qquad \text{- - - (46)}$$

and ν is the kinematic viscosity of the fluid contained in the annulus, formed by a fixed outer cylinder of internal radius r_2 and a rotating inner cylinder of external radius r_1.

This equation was verified experimentally by Taylor (4) and also by Lewis (12) and many others (e.g. 10, 27, 31, 32)

3.62 Vortex formation with axial flow in the annulus

There is evidence that the vortex patterns obtained when an axial flow is superimposed on the rotation are complex and of several distinct kinds (27, 29). Shipp (27) has shown visually that vortices, similar to the Taylor vortices obtained without axial flow, can exist when an axial flow is superimposed on the system. When the axial flow is small a "flowing ring" system is observed in which the vortices travel along the annulus as a series of moving rings. When the axial flow is increased the vortex rings tilt and the motion becomes that of a "flowing spiral". The term

"Taylor vortices" will therefore be used solely to describe the vortex system without axial flow and when an axial flow is superimposed on the system the term "vortices" will be used to describe any of the possible vortex patterns existing in the annulus.

3.621 Critical conditions for vortex formation reported by previous investigators

In 1933 Cornish (9) investigated experimentally the case where there is an axial flow superimposed on the system. Cornish measured the axial pressure drop for flow of water in a very narrow annulus with the inner cylinder rotating. For an axial Reynolds number maintained as constant as possible experimentally determined plots of axial pressure drop versus speed of rotation showed that a marked rise in pressure drop occurred at a critical speed of rotation of the inner cylinder. In general it was observed that the higher the axial Reynolds number, the higher the speed of rotation necessary to produce the discontinuity in the plot of pressure drop versus speed of rotation. This discontinuity was assumed to represent the point at which the fluid flow changed from a purely laminar to a "special type of disturbance associated with rotation." No direct evidence was given to show that this discontinuity coincided with the formation of a vortex system.

Extrapolation of Cornish's results to zero axial Reynolds number in the plot of Reynolds number versus speed of rotation does not give a critical speed, corresponding to Taylor vortex formation, in agreement with equation (45).

Cornish was unable to maintain constant axial flow rates in his apparatus and the variation of axial Reynolds number may have been accentuated by the fact that a constant head tank was used to supply this axial flow of water. With a constant head tank the axial Reynolds number would have changed with changing speed of rotation of the inner cylinder, due to a variation of

pressure drop in the annulus. Furthermore, the pressure drop measurements were made by means of manometers connected to pressure chambers at either end of the annulus. This system must have introduced large entrance and exit losses. The clearances between the various inner and outer cylinders used were very small and thus, particularly at high speeds of rotation and low axial flow rates, hydro-dynamic heating effects were very important. Cornish states that under these conditions the rise in temperature was very rapid, the inner cylinder becoming much warmer than the outer, thus causing a reduction in the clearance by thermal expansion and introducing uncertainties in the values of the fluid properties.

The results obtained by Cornish indicate that the speed of rotation of the inner cylinder, at which the break point in the pressure drop versus speed of rotation curve occurs, is almost independent of the ratio of annular gap width, (b), to mean radius $\left(r_m = \frac{r_1 + r_2}{2}\right)$ for various combinations of cylinders used, covering a range $0.0036 < {}^{b}/_{r_m} < 0.0059$. In view of the subsequent theoretical and experimental investigations of other workers (2, 11, 14) and also in view of the results described in Part II, (in which the critical speed of rotation was found to be strongly dependent on both the value of ${}^{b}/_{r_m}$ and the axial Reynolds number), it is doubtful whether Cornish was in fact observing the onset of a vortex regime. The graphical results showing the critical conditions for vortex formation given in Cornish's paper, for the case where ${}^{b}/r_m = 0.0047$, must therefore be treated with great caution.

In 1938 Fage (10) used a method apparently more refined than that of

Cornish in which the pressure drop was measured over a small axial section of the annulus far removed from the entrance region. Fage also found that, as the speed of rotation of the inner cylinder was increased, the pressure drop suddenly changed at a critical speed of rotation of the inner cylinder for a fixed axial flow rate of water. These critical speeds, for very low axial flow rates, were very close to the critical speed calculated using equation (45), indicating that these critical speeds corresponded to vortex formation. The value of b/r_m was 0.209 for the apparatus used by Fage.

Kaye and Elgar (11) in 1957 reported the results of experiments in which air flowed through an annulus with the inner cylinder rotating. They showed that vortices could exist at finite axial flow rates. With the use of smoke, they detected visually the onset of vortices for varying axial flow rates and confirmed the critical speeds of rotation of the inner cylinder with hot wire anemometers placed in the annulus. Two sizes of annulus, (b/r_m = 0.198 and 0.307) were used in these investigations.

3.622 Definition of the Taylor Number and results of Kaye and Elgar (11)

Kaye and Elgar published their results in the form of a plot of axial Reynolds number, Re_a, versus the Taylor number, Ta; where the Taylor number is a dimensionless group given by:-

$$Ta = \frac{\Omega_1 \left(\frac{r_1 + r_2}{2}\right)^{\frac{1}{2}} (r_2 - r_1)^{\frac{3}{2}}}{\nu}$$

$$\text{or} \quad Ta = \frac{\Omega_1 r_m^{\frac{1}{2}} \cdot b^{\frac{3}{2}}}{\nu} \quad \text{------} \quad (47)$$

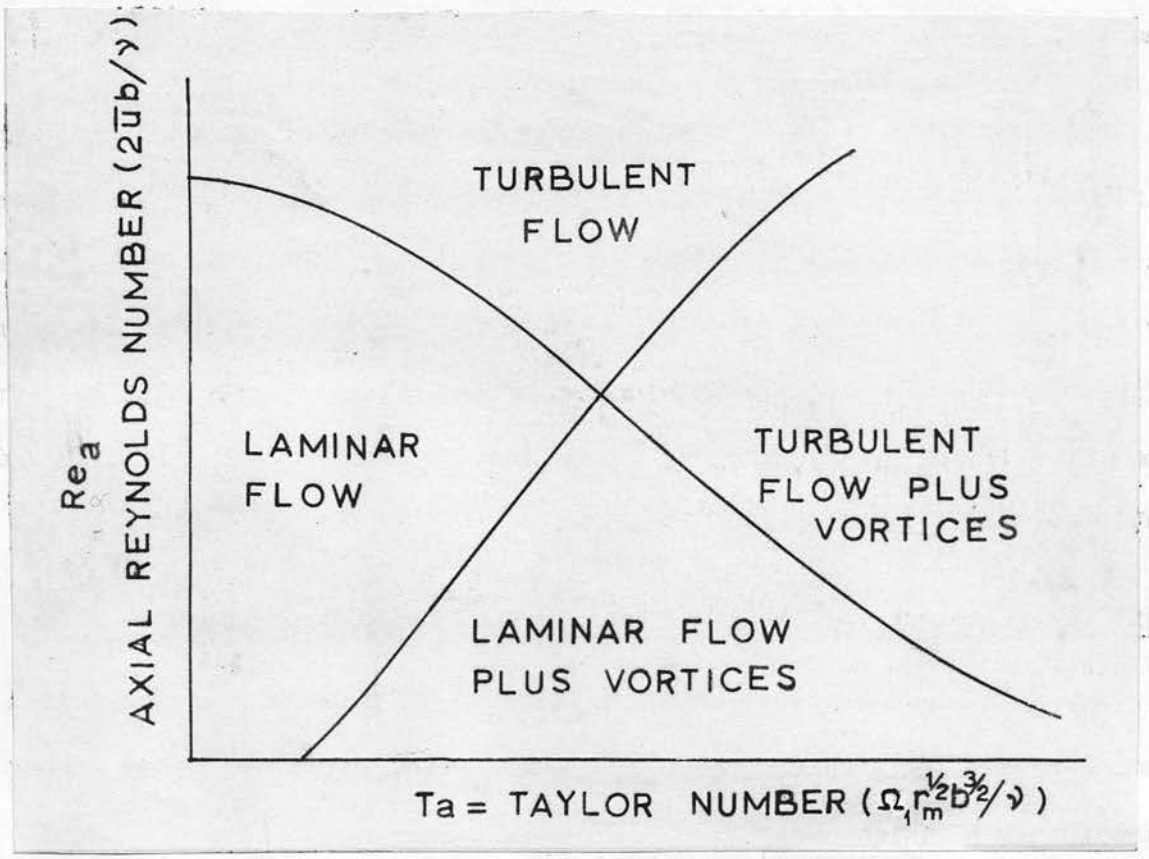

Figure 7. Possible flow regimes in an annulus with the inner cylinder rotating (11)

where $r_m = \frac{r_1 + r_2}{2}$ (mean radius) and $b = r_2 - r_1$ (gap width)

The Taylor number is, in effect a form of circumferential (or rotational) Reynolds number $\left(\frac{r_m \; b \, \Omega_1}{\nu}\right)$ multiplied by $\left(\frac{b}{r_m}\right)^{\frac{1}{2}}$

$$\text{i.e. } Ta = \frac{\Omega_1 r_m^{\frac{1}{2}} \; b^{\frac{3}{2}}}{\nu} \equiv \frac{r_m \; b \, \Omega_1}{\nu} \cdot \left(\frac{b}{r_m}\right)^{\frac{1}{2}}$$

and may therefore be used to characterise rotational flow.

The form of the plots of axial Reynolds number versus Taylor number obtained by Kaye and Elgar is shown in Figure 7. It was observed that four different flow regimes exist for air flowing in an annulus. For zero axial flow, the curve marking the transition between laminar and 'laminar plus vortex' flow was observed to cut the abscissa at a Taylor number which was in close agreement with that calculated using Taylor's equations (45) and (46) in equation (47)

3.623 Significance of the Taylor number for zero axial flow

The following consideration, due to Kaye and Elgar (11) indicates the significance of their choice of the Taylor number as the rotational parameter: For the limiting case $b/r_m \rightarrow 0$, the value of P = 0.0577 from (46) and therefore from (45) and (46) :-

$$c(Ta)_o = \frac{\Pi^2}{\sqrt{0.0577}} = 41.2$$

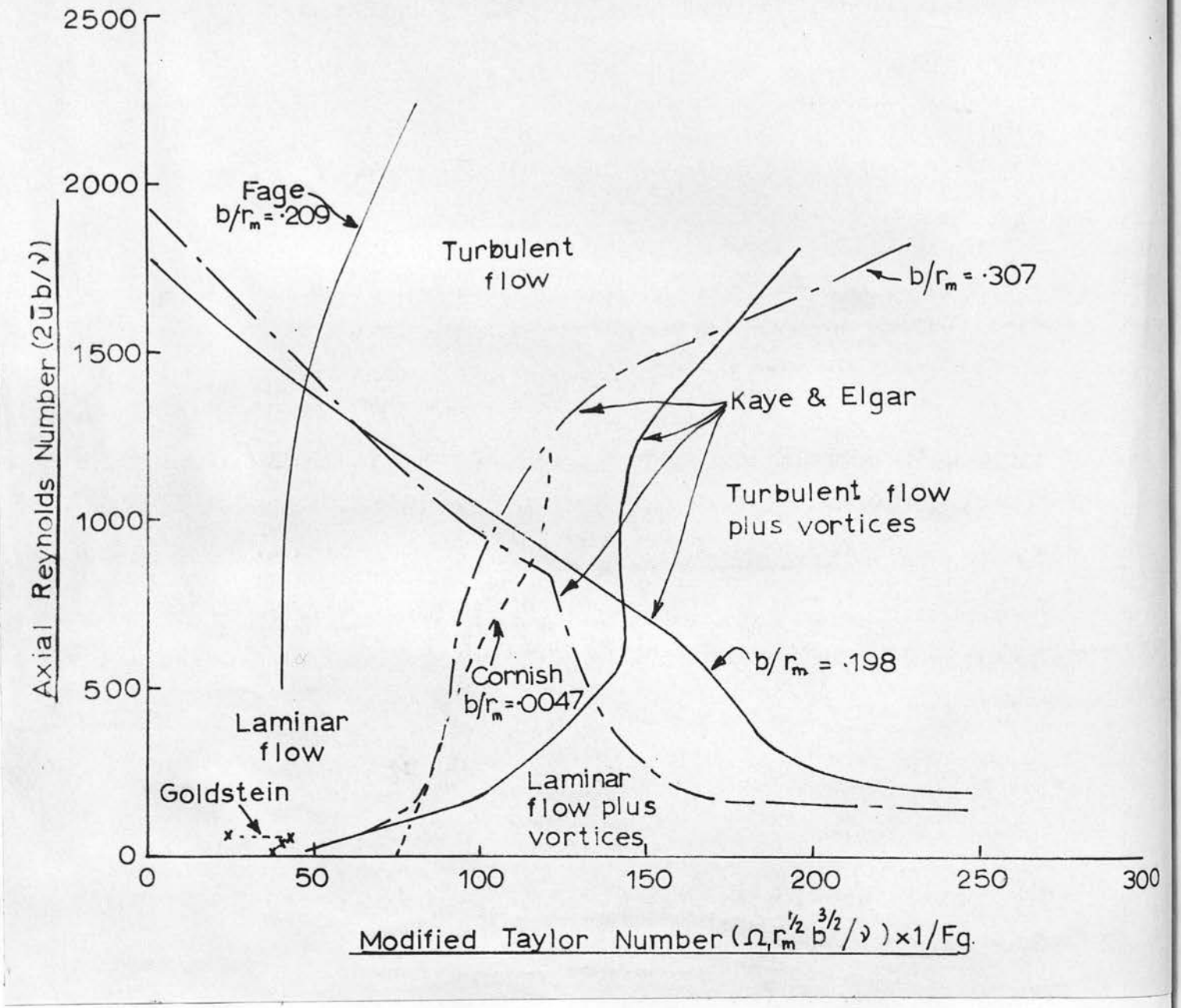

Figure 8. Plot of Re_a versus Ta/Fg showing flow regimes in an annulus with the inner cylinder rotating. Experimental and theoretical (9, 10, 11, 13)

where $^{c}(Ta)_{o}$ is the critical value of Ta at $^{b}/_{r_m} = 0$ with no axial flow.

For any finite value of $^{b}/_{r_m}$;

$$\Omega_c = (\Omega_c)_o \quad Fg$$

where $(\Omega_c)_o$ is the value of the critical angular velocity, Ω_c, at $^{b}/_{r_m} = 0$ with no axial flow. The geometrical factor, Fg, is a function only of $^{b}/_{r_m}$ and is given by:-

$$Fg = \frac{\pi^2}{41.2\,(1 - \frac{b}{2r_m})\;P^{\frac{1}{2}}} \qquad ----- (48)$$

Thus, as shown in Figure 8, Kaye and Elgar subsequently plotted the axial Reynolds number, ($Re_a = 2\bar{u}\, b/\nu$) against a "modified Taylor number; (Ta/Fg) assuming that these two parameters, Re_a and (Ta/Fg), were sufficient to characterise all flow regimes observed for any value of $^{b}/_{r_m}$. The experimental results of Cornish (9) ($^{b}/_{r_m} = 0.0047$) and Fage (10) are also shown in Figure 8. As indicated by Macleod and Matterson (2), whilst it is true that the group (Ta/Fg) characterises the transition from laminar to 'laminar plus vortex' motion, independently of $^{b}/_{r_m}$ in systems where there is no axial flow, there is no reason for assuming that it has a like significance in characterising transition to vortex or turbulent flow when axial flow is present. It is necessary, in the general case, to consider $^{b}/_{r_m}$ as a separate parameter and the flow regimes should be characterised by three-dimensional plots involving

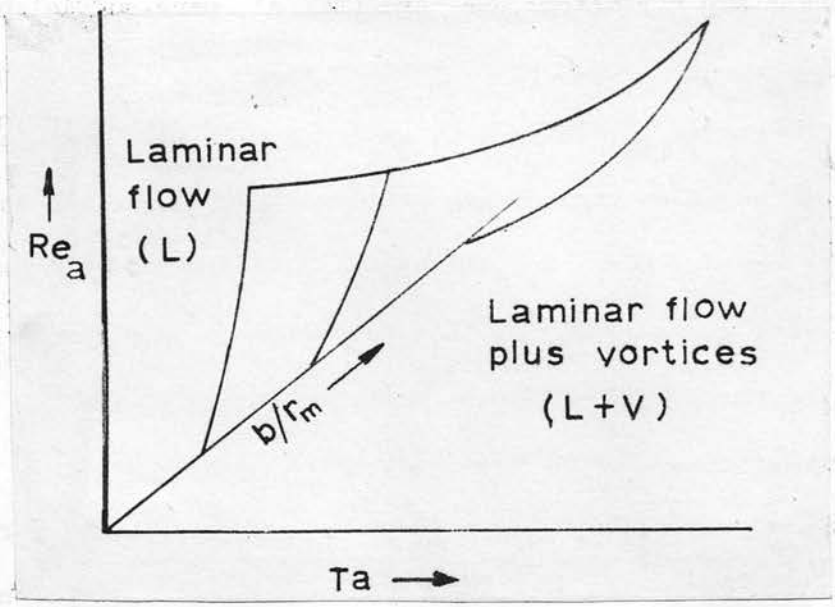

Figure 9. Possible type of three dimensional plot for transition from laminar to 'laminar plus vortex' flow.

the three dimensionless groups, Re_a, Ta and b/r_m. Figure 9 shows a possible type of plot that might be observed as b/r_m varies, for the transition laminar to 'laminar plus vortex' flow. Figure 9 indicates the possibility that, for a given axial Reynolds number, the critical Taylor number is greater the larger the value of b/r_m. This type of plot is indicated by experiments conducted with the mercury vapour transfer column, as described in Part II. Fage's apparatus, however, had a b/r_m very similar to one of those used by Kaye and Elgar, and his results (10) should therefore agree fairly closely with those of Kaye and Elgar (11) for the case where the b/r_m value was 0.198 (Fage's b/r_m value was 0.209). The fact that they do not agree is shown in Figure 8. This disagreement has been ascribed (11) to systematic errors in the experimental technique used by Fage. It is not clear why the results of Cornish (assuming they represent conditions for vortex formation) should coincide with the results of experiments by Kaye and Elgar on a column having a b/r_m value of 0.307, since the b/r_m value in Cornish's column was 0.0047. It is however possible that the transition curve laminar to 'laminar plus vortex' flow is in fact independent of or only weakly dependent on the value of b/r_m at these values of b/r_m.

As mentioned previously, an anonymous report received from the "Shell" laboratories in Amsterdam (34) gives details of vapourisation experiments in a rotating concentric cylinder column. It was found that with speeds of rotation of the inner cylinder below a certain critical speed, for a fixed axial flow rate, the value of the number of transfer units was independent of the speed of rotation of the inner cylinder and corresponded to the theoretical

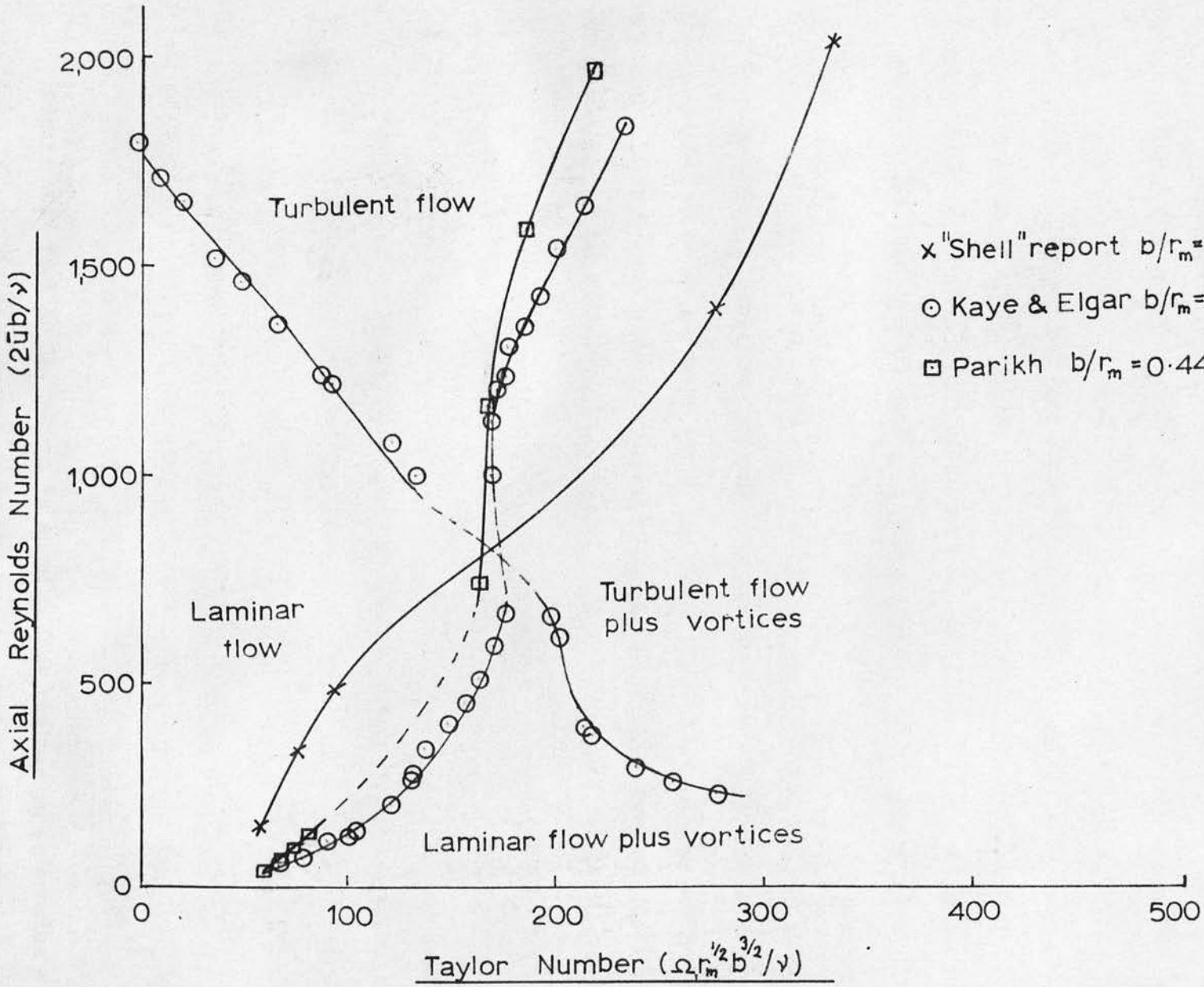

Figure 10 . Plot of Re_a versus Ta showing flow regimes in an annulus with the inner cylinder rotating. Experimental results (11, 28, 34).

value calculated on the basis of purely laminar axial flow in the annulus. At this critical speed the number of transfer units showed a sudden rise, and continued to increase as the speed of rotation of the inner cylinder was raised. Assuming that this critical speed corresponded to the onset of vortices for the particular axial flow rate, a curve of critical angular velocity of the inner cylinder versus axial Reynolds number, covering the entire range of experimentation, was plotted. This curve has been re-plotted in Figure 10 on the basis of axial Reynolds number, Re_a, versus Taylor number, Ta, and therefore gives a correlation of the critical conditions for transition from a laminar to a 'laminar plus vortex' regime which may be compared with the results obtained by Kaye and Elgar for a column having a b/r_m value of 0.198. The b/r_m value for the "Shell" column was 0.162 and results from it therefore should have agreed fairly closely with the curve due to Kaye and Elgar. The reasons for the divergence of results is not clear.

In the same figure, results due to Parikh (28) are given for the transition to a vortex regime. Parikh measured overall and film heat transfer coefficients for heat transfer across the outer cylinder of an annulus of which the inner cylinder rotated. Heat was transferred from a hot stream, (hot water circulated through a jacket on the outer cylinder) to a relatively cold test liquid, (water or oil), pumped through the annulus.

With water as the test liquid axial Reynolds numbers were obtained covering the range 700-2500. It was found that with speeds of rotation of the inner cylinder below a critical speed, assumed to correspond to vortex

formation the overall or water film coefficient was independent of the speed of rotation and these values of the heat transfer coefficient agreed with established correlations for streamline or turbulent flow in plain annuli, depending on the axial Reynolds number. The results also showed that axial turbulence existed for all values of the axial Reynolds number greater than 2000.

The critical inner cylinder speeds, corresponding to vortex formation, were found to be dependent on the rate of flow of water in the annulus and quite generally, the larger the flow rate the greater the speed required to produce vortices. This observation agrees with the results from the "Shell" laboratories in Amsterdam and also those of Becker (33).

With oil as the test liquid, axial Reynolds numbers were used in the range 20-120 and the same general dependence of critical speed on axial flow rate was observed.

Parikh plotted the critical conditions for vortex formation in the form of a plot of axial Reynolds number ($2\bar{u}b/\nu$) versus a "Reynolds group" ($4n_1 r_1^2/\nu$), where n_1 was the inner cylinder speed of rotation in r.p.m. and r_1 the radius of the inner cylinder. The diameter of the inner cylinder was 1" and that of the outer cylinder 1.566". Thus the value of b/r_m for this system was $0.283/0.6415 = 0.441$.

The critical data of Parikh, for experiments using both water and oil,

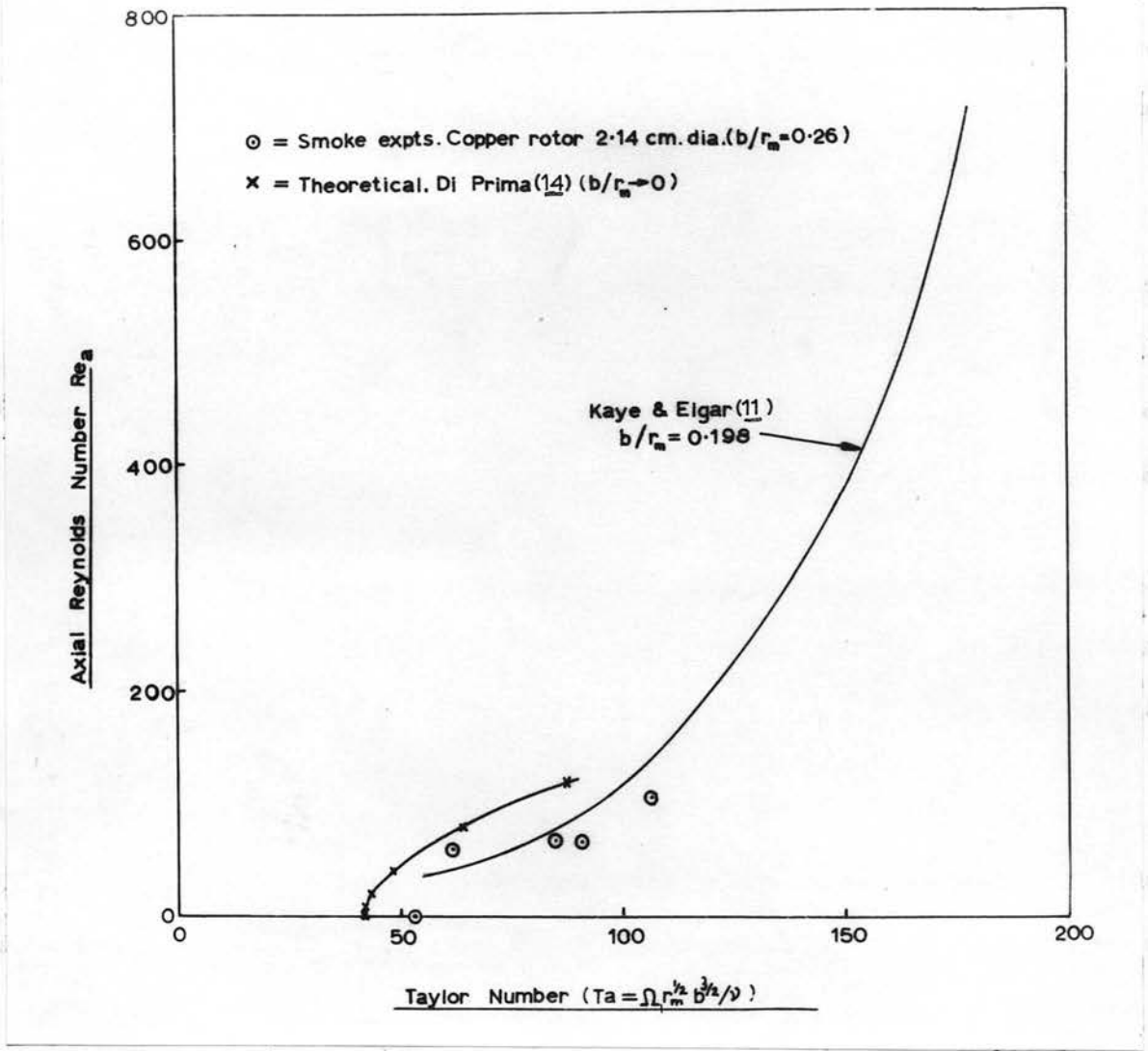

Figure 11. Critical values for the transition from laminar to 'laminar plus vortex' flow

have been replotted on a basis of Re_a versus Ta ($\Omega_1 r_m^{\frac{1}{2}} b^{\frac{3}{2}}/\nu$) in Figure 10. The agreement with the curve of Kaye and Elgar, $b/r_m = 0.198$ suggests that the transition from a laminar to a 'laminar plus vortex' region is in fact independent of or only weakly dependent on the value of b/r_m for these values of b/r_m over the region studied. This suggestion is contradicted by the results of experiments reported in Part II in which the conditions for vortex formation were investigated over a wide range of b/r_m values. Shipp (27) noted, visually, the critical conditions for vortex formation in an annulus through which oil flowed with the inner cylinder rotating. The critical conditions when plotted showed that the value of:- (inner cylinder speed/viscosity) increased monotonically with increasing oil velocity for a particular value of b/r_m. Unfortunately, Shipp does not disclose the density and viscosity data for the oil used and so it is impossible to compare Shipp's data, quantitatively, with the results previously discussed.

3.624 Theoretical conditions for vortex formation

Di Prima (14), in 1960, produced a theoretical derivation of the Re_a versus Ta curve for the limiting case, $b/r_m \rightarrow 0$, for very low Re_a. Di Prima showed that the theoretical curve fits reasonably well the results obtained by Kaye and Elgar. Figure 11 shows a plot of Di Prima's theoretical curve and Kaye and Elgar's curve for the experiments with a column having a b/r_m value equal to 0.198. Points obtained in the course of the present work from visual observations with smoke and air flowing in the annulus of the fractionating column are also shown. These experiments will be described later in Section 6.

Prior to the appearance of Di Prima's derivation, Goldstein (13) had also

calculated the form of the Re_a versus Ta vurve at very low Re_a and very small b/r_m. He found that the critical Taylor number increased initially, as the Reynolds number increased from 0 to 31 and then decreased quite rapidly as the Reynolds number increased from 31 to 52. Goldstein's calculated values are shown in Figure 8. Since the results of Di Prima's analysis, but not those of Goldstein's, are in qualitative agreement with the work of Kaye and Elgar and since Di Prima's theory also indicates that the critical Taylor number increases monotonically with increasing Reynolds number, it seems likely that the theoretical curve of Di Prima is a more accurate mathematical representation of the observed phenomena than the theoretical curve derived by Goldstein. Goldstein himself implies (13) that the error of his theoretical curve is large at any but the tiniest axial Reynolds number and that the error increases as the Reynolds number increases.

3.625 Results of present work

It is clear therefore that the conditions for vortex formation, with varying axial flow rates, varying speeds of rotation of the inner cylinder and varying b/r_m, are not well established. The need for further experimental and theoretical study is apparent. An attempt therefore was made, as described in Part II, to use the mercury vapour transfer column to find experimentally the conditions for vortex formation in annuli having four different b/r_m values. It was found, quite generally, that for a particular value of b/r_m the critical Taylor number required for vortex formation increased monotonically with increasing axial Reynolds number. It was also found that, at a particular value of the axial Reynolds number, the critical

Taylor number required for vortex formation was greater the larger the value of $^{b}/_{r_m}$. Thus, by cross-plotting, a graph was produced of $^{b}/_{r_m}$ versus axial Reynolds number with the critical Taylor number as a parameter. By interpolation on this graph, the critical conditions for vortex formation can now be determined for any concentric cylinder system with a $^{b}/_{r_m}$ value lying in the range $0.10 < {}^{b}/_{r_m} < 0.83$. The results obtained with the mercury vapour column also indicated a very strong dependence of the critical Taylor number, for a given axial Reynolds number, on the value of $^{b}/_{r_m}$. Thus if the results of Kaye and Elgar (11) Parikh (28), and the values obtained from the "Shell" report (34) are compared with the results from the mercury vapour column, the curves obtained by those investigators all lie close to the critical curve for $^{b}/_{r_m} = 0.104$, the smallest value of $^{b}/_{r_m}$ investigated with the vapour column. Despite the fact that, for example, the critical curve obtained by Parikh was for a $^{b}/_{r_m}$ value of 0.441, this curve lies very much closer to the curve for $^{b}/_{r_m} = 0.104$ than that for $^{b}/_{r_m} = 0.591$ also obtained with the mercury vapour transfer experiments. Possible reasons, for this stronger dependence of critical conditions on the value of $^{b}/_{r_m}$ in the mercury vapour transfer column, will be discussed later in Part II of this report.

3.7 Longitudinal diffusion effects

It has been assumed hitherto that, in deriving the theoretical correlations, longitudinal diffusion is negligible. The justification for this assumption, for the case of laminar and vortex flow, will now be given.

3.71 Laminar flow

If the vapour and liquid phases are in purely laminar flow then

calculations show that the effect of longitudinal (molecular) diffusion on the number of theoretical plates, N, is negligible for cases when one or both walls of the annulus are wet with reflux. For example, in the present work the lowest vapour velocity, $\bar{u}_1$, consistently obtained in practice was 2.63 cm/sec, (corresponding to a boil-up rate of 120cc/hour using the 2.14 cm. diameter glass inner cylinder). Since the value of the diffusion coefficient, D_1, was taken as 0.037 cm^2/sec (24), the maximum value of $D_1/\bar{u}_1$ was $0.037/2.63$ cm.

Now, if longitudinal diffusion is taken into account, the number of theoretical plates, N, for the case of both walls wetted, is given by:-

$$N = \frac{1}{\frac{17}{140}\,\frac{\bar{u}_1 w_1^2}{D_1} + \frac{D_1}{\bar{u}_1}} \qquad \text{- - - - -} \quad (13) \quad \text{(See section 3.2)}$$

Thus, for the experiments with the 2.14 cm. diameter inner cylinder, for which $w_1 = 0.3264$ at a flow rate of 120 cc/hr (see table XI) the value of N per 66 cm column length is given by:-

$$N = \frac{66}{\frac{17}{140} \times \frac{2.63 \times (0.3264)^2}{0.037} + \frac{0.037}{2.63}}$$

$$= \frac{66}{0.919 + 0.01406} = 70.7$$

If the longitudinal term, $0.037/2.63$ is neglected;

$$N = \frac{66}{0.919} = 71.8$$

Thus, if and when (13) is applicable, the contribution to the value of N of the longitudinal diffusion term, $D_1/\bar{u}_1$, is negligible under the most extreme conditions.

3.72 Vortex flow

Longitudinal diffusion experiments, performed on the mercury vapour transfer column as described in Part II, show that due to the existence of a vortex flow regime the apparent longitudinal diffusion coefficient, D_L, is increased considerably above that for purely laminar flow. The term 'apparent longitudinal diffusion coefficient' is used since the "spread" of material in the annulus is due to a combined molecular diffusion and velocity profile effect. The velocity profile effect gives rise to a different rate of travel of material between the centre and walls of the annulus and hence gives rise to an apparent diffusional effect. When vortices are present, the value of the apparent longitudinal diffusion coefficient will also depend on the combined effects of radial and longitudinal diffusion, together with a velocity profile effect.

In order to take into account longitudinal diffusion during distillation, it is possible to arrive at an equation for the H.E.T.P., H_1, in the form:-

$$H_1 = \frac{V}{k_v c} + \frac{D'}{\bar{u}_1} \quad ---- \quad (49)$$

using a method identical with the one used to arrive at equation (A.13), where k_v is now the mass transfer coefficient for vortex flow and D' is the diffusion coefficient for a homogeneous vortex regime analogous to the molecular diffusion coefficient, D_1, for laminar flow. Implied in this analogy is the assumption that the only effect of the vortex regime is to cause an identical increase in the value of both the longitudinal and radial diffusion coefficient from the molecular value, D_1, to the value D' and that in the analysis leading to equation (49) it may be assumed that second order terms involving longitudinal diffusion

are negligible compared with the corresponding radial diffusion terms. If this reasonable assumption is not made, the mathematics become intractable.

In order to obtain a value for D', at a particular boil-up rate and speed of rotation of the inner cylinder, it is assumed that:-

$$\frac{D'}{D_1} = \frac{\text{Apparent longitudinal diffusion coefficient for vortex flow}}{\text{Apparent longitudinal diffusion coefficient for purely laminar flow}} \quad --(50$$

where D_1 is the molecular diffusion coefficient in the vapour phase.

Thus if a value for D' is calculated from equation (50) (using experimental data to evaluate the right hand side of this equation) and substituted in equation (49), a value for H_1 and hence N, may be obtained at a particular boil-up rate and speed of rotation of the inner cylinder.

For example, in the distillation experiments to be described, the lowest vapour velocity used for experiments in which the inner cylinder was rotating at high speeds was in the region of 4.96 cm/sec (corresponding to a boil-up rate of 225 cc/hr using the 2.14 cm. diameter copper inner cylinder).

Using results obtained from experiments performed in Part II, it is easy to show that, if the 2.14 cm. diameter inner cylinder rotates at 2000 rpm, the maximum obtainable apparent longitudinal diffusion coefficient, D_L, is about seven times that corresponding to pure laminar flow (inner cylinder stationary), even when the boil-up rate is as low as about 100 cc/hr.

Thus, since D_1, the molecular diffusion coefficient was about 0.037 cm^2/sec

in these experiments,

$$\frac{D'}{0.037} \doteqdot 7 \quad \text{- - - - -} \quad (51)$$

By analogy with equation (13) it is assumed that equation (36) should be modified to take into account the effect of longitudinal diffusion according to the equation:-

$$N = \frac{1}{\frac{w_1 \, Re_a \, Sc}{0.9 \, (Re_c)^{\frac{1}{2}} \left(\frac{w_1}{r_1}\right)^{\frac{1}{4}}} + \frac{D'}{\bar{u}_1}} \quad \text{- - - - -} \quad (52)$$

Substituting the values, l = 66 cms, w_1 = 0.3255 cm, $\bar{u}_1$ = 4.96 cm/sec, r_1 = 1.07 cm, ν = 0.0212 cm^2/sec, D_1 = 0.037 cm^2/sec, which apply to the particular case of distillation with the 2.14 cm. diameter rotor, then (52) becomes:-

$$N = \frac{66}{\frac{(0.3255)\left(\frac{2x4.96 \times 0.3255}{0.0212}\right)\left(\frac{0.0212}{0.037}\right)}{0.9\left(\frac{1.07 \times 209.5 \times 0.3255}{0.0212}\right)^{\frac{1}{2}}\left(\frac{0.3255}{1.07}\right)^{\frac{1}{4}}} + \frac{D'}{4.96}}$$

for the case when the inner cylinder is rotating at 2000 rpm (Ω_1 = 209.5) and the boil-up rate is 225 cc/hr

If it is assumed that $D' \doteqdot 7D_1 \doteqdot 7 \times 0.037 \doteqdot 0.259$ cm^2/sec, then:-

$$N = \frac{66}{\frac{28.45}{0.9(3442)^{\frac{1}{2}}(0.3045)^{\frac{1}{4}}} + \frac{0.259}{4.96}} = \frac{66}{0.728 + 0.052}$$

$\therefore$ N = 84.6 theoretical plates

If longitudinal diffusion effects are completely neglected, then

$$N = \frac{66}{0.728}$$

or N = 90.6 theoretical plates

Thus, in the distillation experiments, even when the vapour flow is very small, the speed of rotation the highest attainable and the annulus wide, the longitudinal diffusion effect is such that the theoretical number of plates is reduced by about 7%.

If equation (43) is used instead of (36), the following calculated values of N are obtained under the corresponding conditions for which (36) was used, as shown above:

Taking into account longitudinal diffusion:-

$$N = \frac{1}{1.291 + 0.052} = 49.1$$

Ignoring longitudinal diffusion:-

$$N = \frac{1}{1.291} = 51.1$$

which corresponds to about a 4% reduction in the value of N.

Thus, using the theoretical correlations (36) or (43), under the most extreme practical conditions the effect of longitudinal diffusion hardly exceeds experimental error in the distillation experiments. The

apparent indifference of distillation column performance to the presumed appearance of a vortex regime cannot therefore be attributed to an increase in longitudinal diffusion masking a large influence of vortices on column performance; i.e. possibility (c) in section 3.5, that vortices do improve radial mass transfer but at the same time increase back-mixing so as to offset any improvement in column performance, is ruled out. Strictly, this conclusion applies only to the particular columns and test-mixture studied with the vapour phase in a 'laminar plus vortex' flow condition.

3.73 Turbulent flow.

The experiments conducted on the mercury vapour transfer column did not show up the existence of a 'turbulent plus vortex' regime in the range $0 < Re_a < 300$ for circumferential Reynolds numbers up to $Re_c = 5000$. Thus, it was not possible to establish criteria for the existence of circumferential turbulence nor, therefore, was it possible to predict the effect on longitudinal diffusion, if such turbulence existed.

3.8 Summary of theory and use in practice

For the case of distillation in an annulus, under adiabatic conditions and with total reflux, equations (10) and (12) are derived on the basis of laminar axial flow of vapour. Equation (10) is valid if the outer cylinder surface alone is wetted by reflux and equation (12) applies to the case where both inner and outer cylinder surfaces are wetted by reflux. Longitudinal diffusion is neglected in all cases. With the inner cylinder at rest, the applicability of either equation (10) or (12) depends on the design of the fractionating column.

With the apparatus used by Naragon and Lewis (5) equation (12) is definitely applicable since the reflux is distributed to both cylinder surfaces. It is also expected that equation (12) should predict the results obtained in the present work, with the inner cylinder at rest; since it is possible that both inner and outer cylinder are then wetted by reflux. With the inner cylinder rotating it is only rarely true that equation (10) will be applicable, since, when the inner cylinder is rotating fast enough to cause removal of any reflux condensed upon it, (see section 3.31), the vapour phase may no longer be laminar due to the onset of a vortex regime. The conditions under which either equations (10) or (12) are applicable in the present work will be discussed further in conjunction with the results obtained.

With high axial flow rates and the inner cylinder stationary, or rotating at very low speeds, the vapour phase may become axially turbulent. For these conditions an equation is derived (24), based on an analogy with the Dittus-Boelter equation. It is assumed that distillation takes place between infinite parallel plates, for which the total H.E.T.P. can be represented by the equation:

$$\text{Total H.E.T.P., } H = H_1 = \frac{V}{2k_t c} = \frac{w_1 \bar{u}_1}{2k_t}$$

in which longitudinal diffusion is neglected.

Equation (24) cannot be verified experimentally, since neither the results of the present investigations nor those of previous workers on similar columns furnish values of H_1 at Reynolds numbers greater than 2000, corresponding to the onset of axial turbulence in the annulus.

At speeds of rotation of the inner cylinder sufficient to cause the appearance of vortices, three equations, (36), (39) and (43) are derived

(based on two different correlations), giving the number of the theoretical plates, N, as a function of both boil-up rate and speed of rotation of the inner cylinder, with the inner cylinder free from reflux.

Equation (36) is based on a correlation of results obtained from experiments on the mercury vapour transfer column, described in Part II, the derivation of this correlation being suggested by a momentum-mass transfer analogy of the "inviscid core boundary layer model" put forward by Batchelor (30). Once again the assumption is made that distillation is taking place between infinitely long parallel plates for which the total H.E.T.P. can be represented by the equation:-

$$H_1 = \frac{V}{k_v c} = \frac{w_1 \bar{u}_1}{k_v}$$

Equation (39) is derived in a similar manner to (36) using the results of vapourisation studies (34) in a rotating concentric cylinder system.

Equation (43) is based on a correlation of results obtained by Eisenberg et al (35) and again the validity of the equation $H_1 = \frac{w_1 \bar{u}_1}{k_v}$ is assumed. Longitudinal diffusion is considered negligible. It is expected that these equations should give values which compare with experimental values for axial flow rates sufficiently low not to disturb the vortex pattern in the annulus. It is also expected that the theoretical values of N, (at a particular boil-up rate and speed of rotation of the inner cylinder), calculated using equation (43) should be smaller than the corresponding values calculated on the basis of equation (36). This is due to the fact that (36) is based on a correlation of results for mass transfer from a short circumferential band on the outer cylinder to a flowing axial stream, with the inner cylinder rotating; whereas (43) applies to mass transfer,

with no axial flow, from the complete surface of a rotating inner cylinder to a fluid contained in the annulus. As may be seen from the values of the numerical constants in (36) and (39), values of N calculated using equation (39) will lie below the corresponding values calculated from (36). At high rotational speeds the use of these equations (36), (39) and (43) may be incorrect due to the onset of a circumferential 'turbulent plus vortex' regime. Under such conditions (44) might be applicable, derived on the assumption that shear flow is equivalent to pressure flow as far as turbulent mass transfer is concerned. Unfortunately, this equation cannot be tested by the results of the present work since experiments with the mercury vapour transfer column do not show the existence of turbulent conditions with circumferential Reynolds numbers up to $Re_c = 5000$ and axial Reynolds numbers in the range $0 < Re_a < 300$, indicating that turbulence does not exist even at the highest speeds of rotation in the fractionating column experiments.

The conditions for vortex formation are then considered with and without an axial flow in the annulus. Concordance is not found between published results. This general disagreement between various investigators may be due to the possibility of obtaining several distinct vortex regimes with a superimposed axial flow, such as are mentioned by Appel (29) and Shipp (27). Under certain conditions Appel observed what appeared to be a secondary vortex motion adjacent to the wall of the rotating inner cylinder and Shipp showed that 'vortex rings' or 'vortex spirals' existed in the annulus, depending on the axial flow conditions and speed of rotation of the inner cylinder. The need for further experiments was apparent, and this was the reason for undertaking the experiments on vortex formation performed in Part II of this report. This work indicates that the conditions for vortex appearance are strongly dependent on the

value of b/r_m for the system used and that, in general, for a particular b/r_m, the critical Taylor number corresponding to vortex formation increases monotonically with axial Reynolds number.

Brief reference is also made to the conditions for turbulence in such annuli, and it is shown that these conditions are not obtained experimentally in the mercury vapour transfer studies.

Finally, calculations based on either of the two correlations (36) or (43) show that the effect of longitudinal diffusion is negligible in the distillation experiments under all practical operating conditions investigated.

3.9 Comparison of theory with previous work

The theoretical predictions and correlations developed so far, for the case of distillation in an annulus, with and without the inner cylinder rotating have been based on idealised conditions of operation. Apart from the fact that any or all of these idealised conditions may not exist in practice, the following conditions may also arise:-

(i) The cylinders are not circular in section and concentric with each other.

(ii) The inner cylinder "wobbles" or vibrates when in operation.

(iii) There may be rippling of the liquid reflux film.

(iv) There may be a fine spray of reflux in the vapour phase due to liquid reflux removal from the rotating inner cylinder by centrifugal force.

(v) Entrance effects may be important and laminar or vortex flow may only be fully developed at a point some way above the hemispherical base of the rotating inner cylinder, on which the vapours from the still-pot first impinge.

(vi) The surfaces may be contaminated with foreign material giving rise to channelling.

(vii) Hydrodynamic heating may occur in very narrow annuli with the inner cylinder rotating at very high speeds.

These possible defects, (i) to (vii) should constantly be borne in

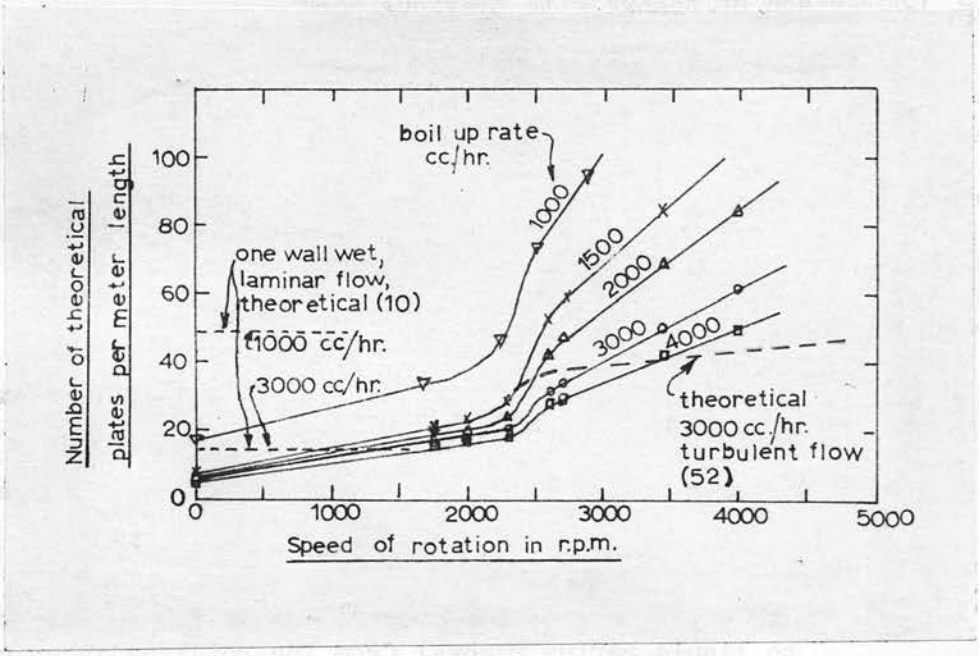

Figure 12. Experimental results obtained by Willingham et al (3) compared with values obtained from theoretical equations for laminar (10) and turbulent (52) flow. N versus rpm.

mind during the following comparison of the theories put forward in the past few sections with the results of previous investigators.

3.91 Results of Willingham et al (3)

In the paper by Willingham et al (3), an extensive series of experiments is described on a rotating concentric cylinder fractionating column, having an inner rotating cylinder 2.93" $^{o}/_{d}$ and 23" long. The annular gap was 0.043" (1.09 mm) wide, giving a value of $b/r_m = 0.027$.

With the inner cylinder stationary, the experimentally observed number of theoretical plates per meter length of column can be compared with the corresponding values calculated from equations (10) and (12). Table I gives details of such calculations, over a range of boil-up rates from 1000 to 4000 cc/hr, and the theoretical values for N, calculated using equation (10) only at boil-up rates of 1000 and 3000 cc/hr, are shown as horizontal dotted lines in Figure 12, in which figure the experimental results are also shown. The experimental results shown in Figure 12 were taken directly from the relevant plot in the paper by Willingham et al (3). It can be seen that with the inner cylinder stationary, or rotating at very low speeds, (corresponding to the conditions under which either equations (10) or (12) should be applicable), the observed values were about half those calculated by equation (10). If the theoretical values calculated from equation (12) were plotted (laminar flow, both walls wetted by reflux), the discrepancy would have been even greater. The disagreement between the laminar theory (10) and experiment was attributed, by Willingham et al, to rivulet channelling of the reflux film. In making this comparison of theory and experiment, liquid side resistance to diffusion and longitudinal

diffusion have been neglected. (Calculations of the terms H_2 and $D_1/\bar{u}_1$ from the data of Willingham et al have shown that the value of both these terms is much less than the value of H_1, the vapour phase H.E.T.P. at a particular boil-up rate).

As the speed of rotation of the inner cylinder was raised, the number of theoretical plates increased and beyond a critical speed of rotation of about 2300 rpm the number of theoretical plates rose sharply, for all boil-up rates investigated. This critical speed of rotation was assumed to correspond to the onset of turbulence in the vapour phase, resulting in increased radial diffusion. The circumferential Reynolds number, Re_c ($= r_1 \Omega_1 b/\nu_1$) for this column at 2300 rpm is about 3000. Willingham et al defined the Reynolds number as 0.84 x Re_c, (presumably attempting to account for the assumed turbulent circumferential velocity profile) and thus obtained a value of about 2500 for this critical Reynolds number. They then presented an equation, without proof, for the value of the turbulent H.E.T.P. in the vapour phase, $(H_1)_{turbulent}$, in the form:

$$(H_1)_{turbulent} = \left\{ \frac{150}{(0.84\ Re_c)^{0.8}} \right\} (H_1)_{laminar}$$

Now from equation (10), for one wall wetted by reflux, (since it was likely that only one wall was wetted at speeds of rotation $>$ 2300 rpm):-

$$(H_1)_{laminar} = \frac{52}{140} \cdot \frac{\bar{u}_1 w_1^2}{D_1} \equiv \frac{52}{140} \left(\frac{2\bar{u}_1 w_1}{\nu_1} \right) \left(\frac{\nu_1}{D_1} \right) \cdot \frac{w_1}{2}$$

$$\text{or } (H_1)_{laminar} = \frac{26}{140} \cdot w_1 \ (Re_a) \ (Sc)$$

The equation presented by Willingham et al for $(H_1)_{turbulent}$ therefore reduces to:-

$$(H_1)_{turbulent} = \frac{150}{(0.84)^{0.8} \ Re_c^{0.8}} \cdot \frac{26}{140} \cdot w_1 \ Re_a \ Sc$$

$$\text{or } (H_1)_{turbulent} = \frac{150 \times 26}{(0.84)^{0.8} \times 140} \cdot w_1 \cdot \frac{Re_a \cdot Sc}{Re_c^{0.8}} \quad ----- (52)$$

Now an equation (44) was also presented in section 3.54 of this report for the case of circumferential turbulence in the annulus, viz:-

$$(H_1)_{turbulent} = \frac{1}{2m} \cdot \frac{w_1 \ Re_a \ Sc^{0.6}}{Re_c^{0.8}} \quad ---- (44)$$ where m is a numerical constant

From the similarity of equations (44) and (52), it appears that Willingham et al derived equation (52) in a manner similar to that in which (44) was obtained.

The theoretical values of N versus rpm at a boil-up rate of 3000 cc/hr were obtained, using equation (52), by Willingham et al and plotted in Figure 12. As can be seen, there is not good agreement between theory and experiment at that boil-up rate.

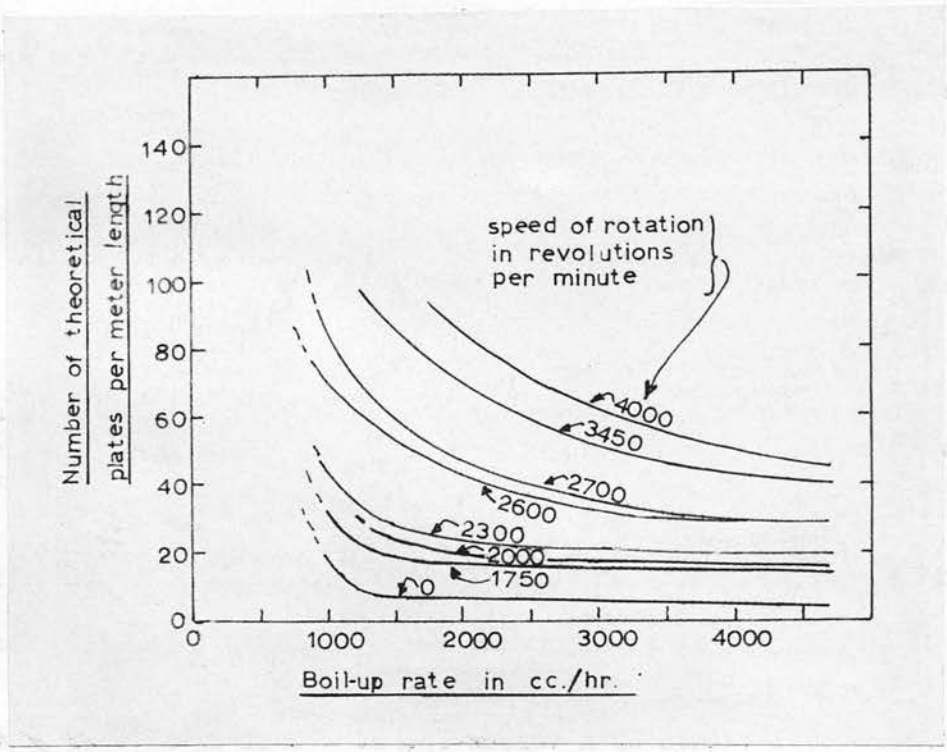

Figure 13. Cross-plot of experimental results shown in Figure 12 N versus boil-up rate

It is clear that if either equations (44) or (52) are to hold, N should be a function of $Re_c^{0.8}$ at a fixed boil-up rate (i.e. Re_a constant). At a fixed speed of rotation of the inner cylinder (i.e. Re_c constant), N should be inversely proportional to the axial Reynolds number (or boil-up rate).

Figure 12 shows that the first of these deductions is not borne out by experiment, since N appears to vary linearly with speed of rotation, the slope being a function of boil-up rate. The experimental results also do not conform to the second condition that N should be inversely proportional to boil-up rate for any constant value of the speed of rotation of the inner cylinder. This is shown more clearly in Figure 13 (a cross-plot of Figure 12). The results of Willingham et al do not therefore conform to either equation (44) or (52) and a value for m, the numerical constant in (44), cannot be obtained from their data.

3.911 Conditions for turbulent flow

It was assumed by Willingham et al that the circumferential flow in this system was analogous to flow between parallel plates and that the value of 2500 corresponded to the Reynolds number for transition from laminar to turbulent flow. Macleod and Matterson (2) have discussed in detail the experimental results of Willingham et al and have reached the conclusion, based on a consideration of the form of the Re_a versus Ta plot (see Figure 7) of Kaye and Elgar (11), that with systems having a very small b/r_m value, this simple turbulence criterion may be valid; for under ordinary operating conditions the axial vapour velocity is small compared with the circumferential velocity and therefore makes only

a small contribution to the vector sum of the two. It was also observed that for the large columns described by Mair et al (15) and Hawkins and Burris (17) this value of Re_c = 3000 corresponded to a critical speed of rotation of the inner cylinder, giving rise to an increase in the number of theoretical plates at a given boil-up rate.

For columns having a large b/r_m value this simple turbulence criterion will not be valid and the Re_a versus Ta curves marking the transition to turbulent or 'turbulent plus vortex' regimes will be a function of b/r_m.

3.912 Conditions for vortex formation

According to the equation derived by Taylor (45), vortices should have appeared in the column of Willingham et al for the hypothetical case of "zero" boil-up rate when the speed of rotation of the inner cylinder was about 130 r.p.m. The Re_a versus modified Taylor number curves of Kaye and Elgar (11)(see figure 8) cannot safely be used to predict the conditions for vortex formation at finite boil-up rates in the column used by Willingham et al, since the b/r_m value for that column was 0.027 and the results of Kaye and Elgar are for columns having b/r_m values of 0.198 and 0.307. However, results from the mercury vapour transfer experiments described in Part II and the theoretical curve of Di Prima (14), show that the curves marking the transition of regimes, laminar to 'laminar plus vortex', for b/r_m values varying from 0 to 0.2 are very similar in the range $0 < Re_a < 120$, and that in this range the Taylor number required for vortex formation increases to a value approximately twice that predicted by (45) for zero Re_a.

Now for example at a boil-up rate of 1500 cc/hr, in the distillation experiments of Willingham et al, the value of Re_a is about 300. Assuming

that the laminar/laminar plus vortex curve of Kaye and Elgar ($^{b}/_{r_m} = 0.198$) is valid up to $Re_a = 300$, vortices should have appeared in the distillation column at speeds of rotation about three times the value given by (45), i.e. at 3 x 130 or 390 rpm.

This speed of rotation is much lower than the critical speed for turbulence of 2300 rpm. The results of Willingham et al show that for all boil-up rates the number of theoretical plates is approximately doubled in the range of cylinder speeds 0 - 2300 rpm. If this rise is due solely to the increased radial diffusion promoted by the formation of vortices at about 390 rpm, the effect of vortex formation on column performance appears to be insignificant compared with the effect of a presumed turbulent regime. If it is assumed that a 'laminar plus vortex' regime did in fact exist in the range 390-2300 rpm, it is possible to compare the experimental results of Willingham et al with theoretical values of the number of theoretical plates, N, calculated from equations (36), (39) and (43), since these equations are applicable for the case of distillation in a vortex regime. These calculated values of N can only be compared with experimental values actually measured over a range of boil-up rates and rotational speeds for which vortices can be presumed to exist. This limited the range of comparison to 1750-2300 rpm for the rotational speed of the inner cylinder and 1000-2000 cc/hr for the boil-up rate. (Willingham et al show no experimental results in the range $0 < \text{rpm} < 1750$). The experiments conducted on the mercury vapour column showed that vortices should in fact have existed in such a column in the range considered.

Values of N were calculated for this range of values, using equations

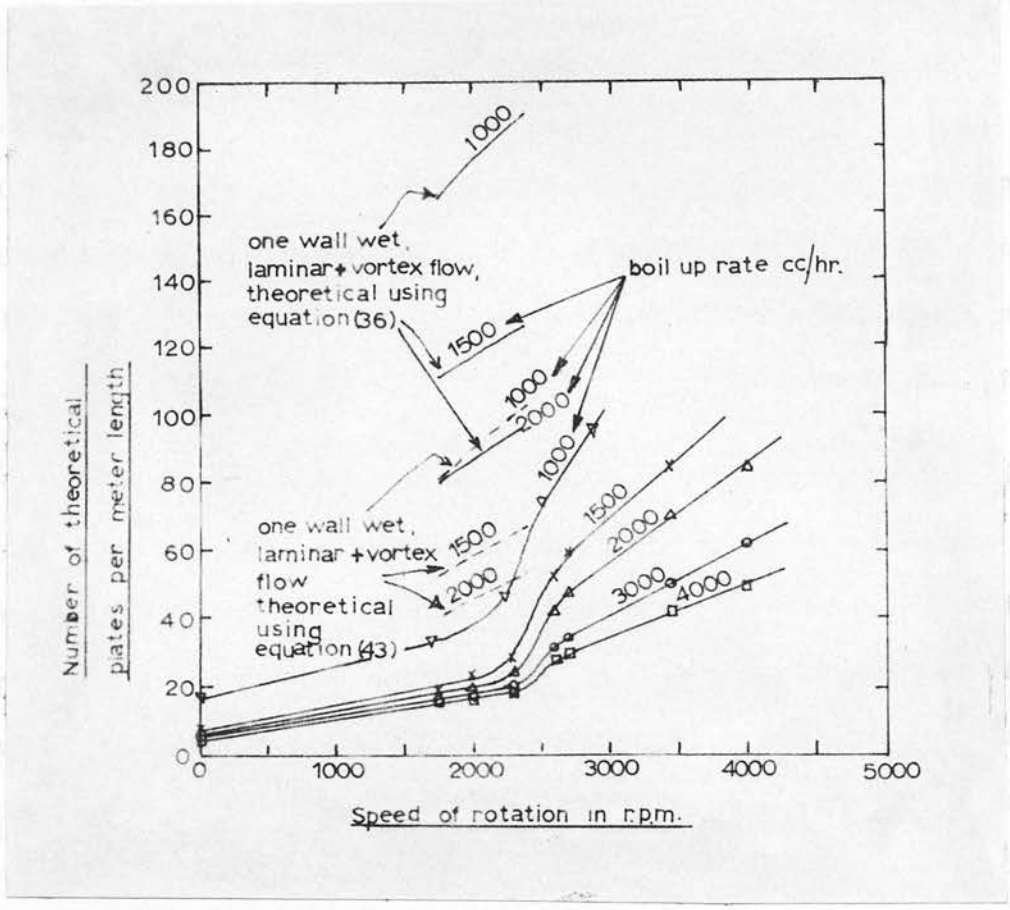

Figure 14. Comparison of theory and experiment for vortex flow N versus r.p.m.

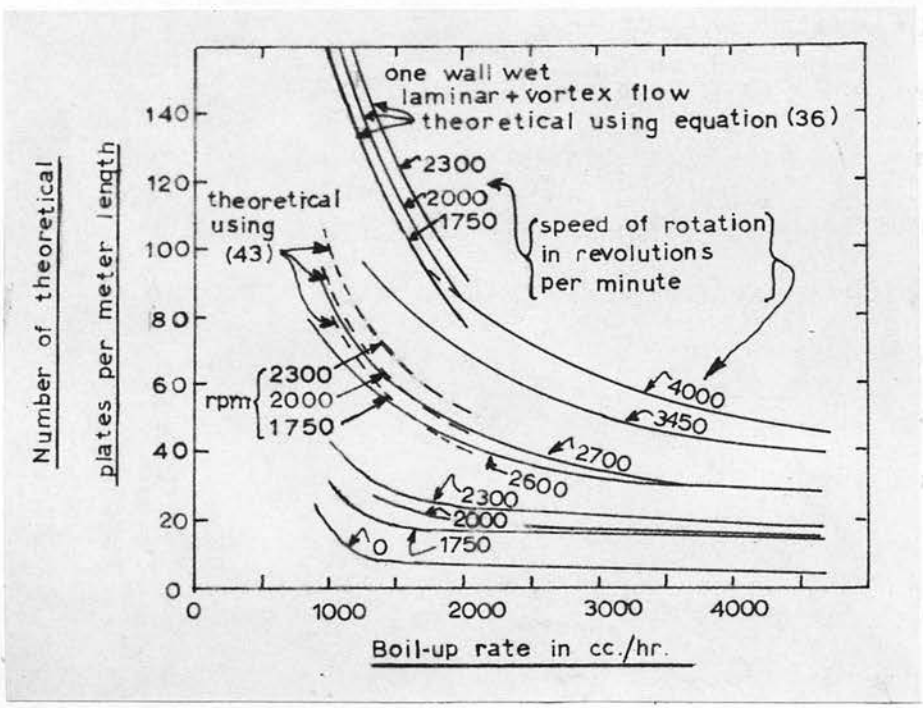

Figure 15. Cross plot of Figure 14. Comparison of theory and experiment for vortex flow. N versus boil-up rate

(36), (39) and (43) and the physical data supplied by Willingham et al (3). It was found in all cases that the theoretical values calculated using (39) fell in between the corresponding values calculated by equations (36) and (43). This was to be expected, since (36) and (43) should represent the upper and lower theoretical limits for values of N, and by comparison of (36) and (39), viz:-

$$N = 0.9 \left(\frac{1}{w_1}\right)\left(\frac{w_1}{r_1}\right)^{\frac{1}{4}} \times \frac{Re_c^{\frac{1}{2}}}{Re_a \cdot Sc} \quad \text{- - - - - - - - (36)}$$

$$N = 0.66 \left(\frac{1}{w_1}\right)\left(\frac{w_1}{r_1}\right)^{\frac{1}{4}} \times \frac{Re_c^{\frac{1}{2}}}{Re_a \cdot Sc} \quad \text{- - - - - - - - (39)}$$

it can be seen that the values of N, calculated by (39), are less than the corresponding values of N, calculated by (36), by a factor of 0.66/0.9.

The calculations involved in finding these values of N are shown in Tables II, III and IV, using the correlations (36), (39) and (43) respectively. However to avoid confusion only the theoretical values corresponding to the use of (36) and (43) were plotted, for comparison with the experimental data of Willingham et al, in Figures 14 and 15. Referring to these figures it will be seen the experimental values of N fall considerably below both the corresponding theoretical curves, calculated from equations (36) and (43). Although the theoretical curves based on equation (43) lie somewhat below the corresponding curves based on (36), the agreement between theory and experiment is not good.

As previously discussed, the experimental values of N lie considerably below the corresponding theoretical values of N, calculated by using equations (10) or (12), for the case where the inner cylinder is stationary or rotating

at speeds low enough to preserve laminar flow. In view of the fact that the theory leading to equations (10) and (12) has been confirmed in certain cases by previous workers (5, 6, 7, 23), it is reasonable to conclude that the results obtained by Willingham et al give very low values of N in the range considered, prior to the onset of a supposedly turbulent regime in the vapour phase. The existence of a turbulent regime is however open to question since the results with the mercury vapour column did not indicate the onset of turbulence even at circumferential Reynolds numbers as high as $Re_c = 5000$. Furthermore if the theoretical lines corresponding to the use of equation (43), as shown in Figure 14, are extrapolated to higher speeds of rotation (> 3500 rpm) the agreement between the theoretical curves (43) and experiment would be quite good. It is therefore possible that turbulence did not in fact set in at the speed of rotation of about 2300 rpm as suggested by Willingham et al. The fact that the performance of this column at low speeds of rotation was also well below the theoretical values predicted by the laminar flow theory suggests that this break point may not have marked the onset of turbulence but rather the removal of a cause associated with non-ideal operation of the column at low speeds of rotation of the inner cylinder, e.g. non-adiabatic conditions of operation. This suggestion, that the onset of turbulence may not have occurred at this speed, is further borne out by the disagreement between the experimental results at speeds above 2300 rpm and the form of the theoretical equation (44) for turbulent flow.

Thus, although the correlations (36), (39) and (43) do not agree with the results of Willingham et al they may in fact be valid correlations for columns operating under more nearly ideal conditions. It is clear that further experimental results are required to substantiate the applicability

of these correlations.

3.92 Results of Hawkins and Burris (17)

A column similar to that of Willingham et al, but capable of operating at higher speeds of rotation and at reduced pressures was built by Hawkins and Burris (17). The inner rotating cylinder had an outside diameter of 3.962" and was 50" long.

Since the operation of the column was under non-adiabatic conditions, a considerable amount of heat being released by mechanical effects at the bearings and by viscous effects, the results on this column cannot be compared quantitatively with equations (36), (39) or (43). However, the results obtained with operation at atmospheric pressure using a test mixture of methyl-cyclohexane-n.heptane are similar in form to the results obtained by Willingham et al. Their plot of N versus speed of rotation of the inner cylinder suggests the onset of turbulence at a value of Re_c of about 3000 (corresponding to a speed of 1725 rpm), where a marked increase in N occurs.

3.93 Results of Irlin and Brunce (18) and Sladecek (19)

A rotating concentric cylinder fractionating column investigated by Irlin and Brunce (18) operated with a glass inner cylinder 50 cms long and annular gap widths of 1 or 2 mms. The column could be operated up to speeds of 10,000 rpm. The test mixture used was a mixture of equal volumes of benzol and di-chloro-ethane. The main feature of the results is that reduction of the annular gap width from 2 to 1 mm had no effect on the efficiency of the column.

A paper by Sladecek (19) has recently appeared describing the performance of a rotary concentric cylinder fractionating column in which the fixed outer

cylinder had a diameter of 32.3 mm. and the annular clearances used were 2.75, 2.0 and 1.0 mm. A test mixture of n. heptane-methyl cyclohexane was used in the experiments. The column was capable of operation up to an inner cylinder speed of 10,000 rpm and numerical results were reported to be in very good agreement with those of Willingham et al (3). A linear relationship was found between the number of theoretical plates per meter length and the speed of rotation of the inner cylinder, in the range 3000-8000 rpm at a throughput of 600 cc/hr. The efficiency of the column was decreased by 15 to 20% when the gap width was increased from 1 mm. to 2 mm.

With the 1 mm. gap and the inner cylinder rotating at 8000 rpm, the circumferential Reynolds number, Re_c, is given by:-

$$Re_c = \frac{r_1 \, \Omega_1 b}{\nu} = \frac{1.515 \times \frac{(8000 \times 2\pi)}{60} \times 0.1}{0.0212}$$

$= 6000$, using a value of 0.0212 cm^2/sec for the kinematic viscosity of the vapour (24).

It is possible that the results quoted all lie in a turbulent region, based on the simple criterion for turbulence previously discussed, in that these results agree with those of Willingham et al whose results for a presumed turbulent regime show that a linear relationship exists between N and cylinder speed. However, the weak dependence of N on gap width disagrees with the form of equation (44), but appears to indicate the applicability of the vortex flow equation (43) even in a supposedly turbulent regime. (In

equation (43) N is less strongly dependent on w_1 than in equation (44)). This observation suggests that great care must be exercised in assuming that there must be turbulence at high speeds of rotation of the inner cylinder. As already discussed, the results from the present investigation with the mercury vapour column do not indicate turbulence even at values of the circumferential Reynolds number as high as 5000.

3.94 Results of Macleod and Matterson (1, 2)

The results obtained by Macleod and Matterson from experiments on the distillation column used in the present investigation have already been discussed in detail elsewhere (2). Macleod and Matterson were only able to operate this column with the inner cylinder stationary or rotating at a fixed speed of 1470 rpm. Inner cylinders of 2.60 and 2.14 cms diameter were used and the working section of the annulus was 61 cms long.

It can be shown that the results they obtained with the inner cylinder stationary do not very closely conform to either equations (10) or (12). Their experiments with the inner cylinders rotating at 1470 rpm indicate a marked improvement in column performance at this speed of operation. Since the performance of this column has also been investigated in the present project over a very wide range of cylinder speeds and boil-up rates, the results obtained by Macleod and Matterson are not analysed quantitatively in this report.

As discussed previously in section 3.13, a very important series of experiments were also conducted by Macleod and Matterson in which it was shown that for this column and the system methyl cyclohexane-n. heptane there was

negligible liquid side resistance to diffusion.

3.95 Conclusions

The following tentative conclusions may be drawn from the comparison of theory with previous investigations:-

The experimental results of Willingham et al (3), with the inner cylinder stationary or rotating at very low speeds, do not agree with equations (10) or (12), which were based on the assumption that the vapour phase was in laminar flow and liquid side resistance was negligible. This latter assumption was verified for the system studied by the experiments of Macleod and Matterson (1, 2). The disagreement with theory may be due to basic inaccuracies in the theoretical treatment or vitiation of the assumptions made by such features as reflux channelling or non-adiabatic operation.

The theory has shown that vortices should appear at comparatively low speeds of rotation of the inner cylinder, but the experimental results of Willingham et al show that if vortices do appear they have little effect on column performance. The correlations (36), (39) and (43), derived from results of mass transfer experiments, give values of N, as a function of boil-up rate, which are much greater than the experimental results of Willingham et al in a presumed 'laminar plus vortex' flow regime.

For columns having a very small value of b/r_m there is some indication that turbulence sets in when the circumferential Reynolds number, (based on the surface speed of the inner cylinder and width of the annular gap), reaches a value of about 3000. This presumed onset of a turbulent flow regime causes

a marked increase in the number of theoretical plates at a given boil-up rate and as the speed of rotation of the inner cylinder is raised a linear relationship is found to exist between the number of theoretical plates and speed of rotation of the inner cylinder. However, at these circumferential Reynolds numbers the performance of such columns is found to be relatively insensitive to changes in b/r_m values and this observation suggests that the equation for vortex flow (43) may be applicable in this supposedly turbulent regime. The possible applicability of equation (43) naturally casts some doubt on the justification for assuming that turbulence definitely sets in at high speeds of rotation. The experiments performed on the mercury vapour transfer column, described in Part II, show that such an assumption is not true for that column with circumferential Reynolds numbers as high as $Re_c = 5000$. Furthermore, the form of the theoretical equation (44) for distillation with a turbulent flow regime is not substantiated by the experiments of Willingham et al or other workers and at high rotor speeds the agreement between the results of Willingham et al and the theoretical equation (43) for vortex flow is quite good. Experiments which will now be described, were designed to investigate these matters further.

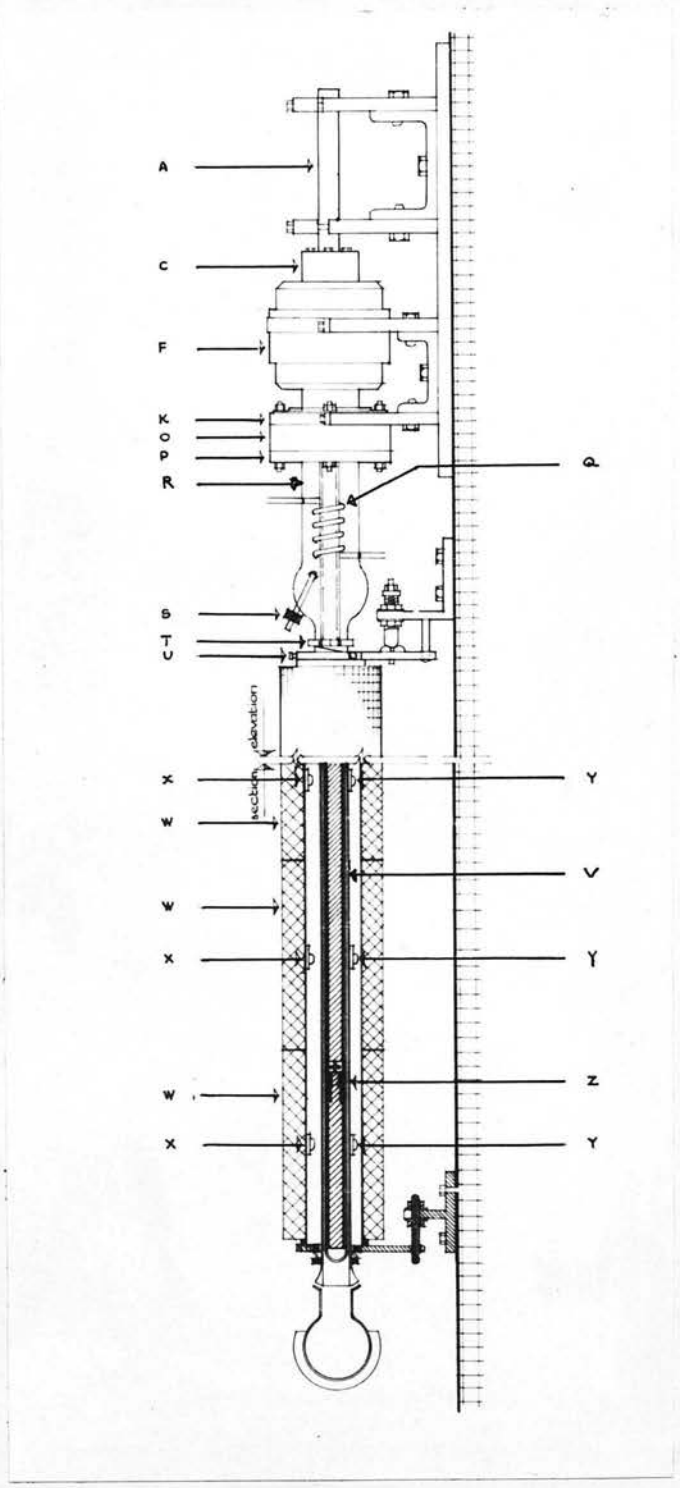

Figure 16 (a). Column Assembly. Approximately to scale

Key to Figures 16 (a) and 16 (b)

A Fixed central shaft

B Upper flange of motor housing

C Thin-walled stainless steel motor housing

D Upper ball-race of squirrel cage rotor

E Squirrel cage rotor

F Motor stator

G Lower ball-race of squirrel cage rotor

H Hollow shaft of squirrel cage motor

I Ball-race retainer and locking ring

J Drive pin

K Lower flange of motor housing

L Driving member of universal coupling

M Inner driven member of universal coupling

N Cork-lined clamping ring

O Body of glass-metal O-ring union

P O-ring sealing plate

Q Spiral water condenser

R Rotating glass inner cylinder

S Take-off valve

T Cork lined clamping ring supporting outer cylinder

U Centering screws

V Glass outer cylinder

W Compensating heaters

X Thermistors mounted on metal column jacket

Y Thermistors mounted on external wall of outer cylinder

Z Lower bearing assembly

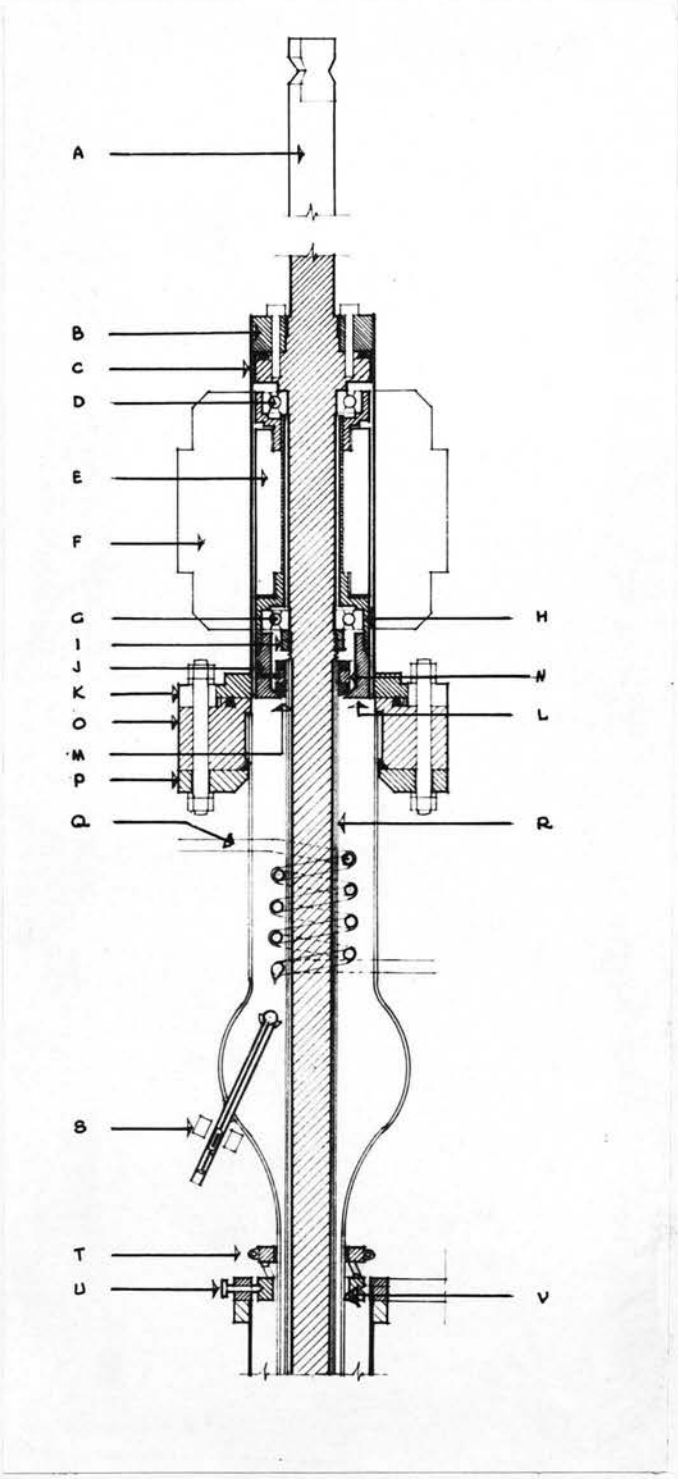

Figure 16 (b). Driving motor and condenser section

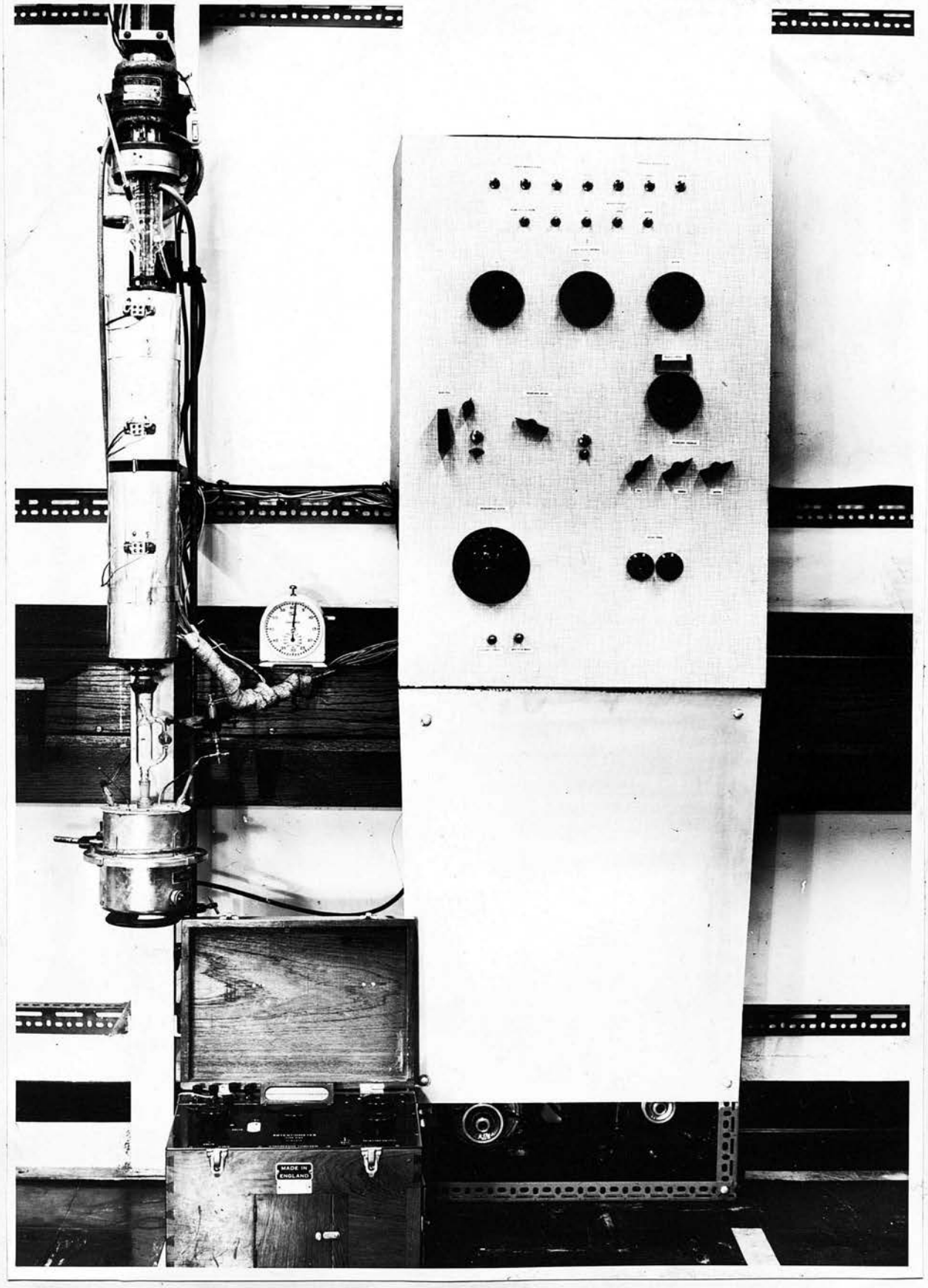

Figure 17 (a). General view of column and control panel

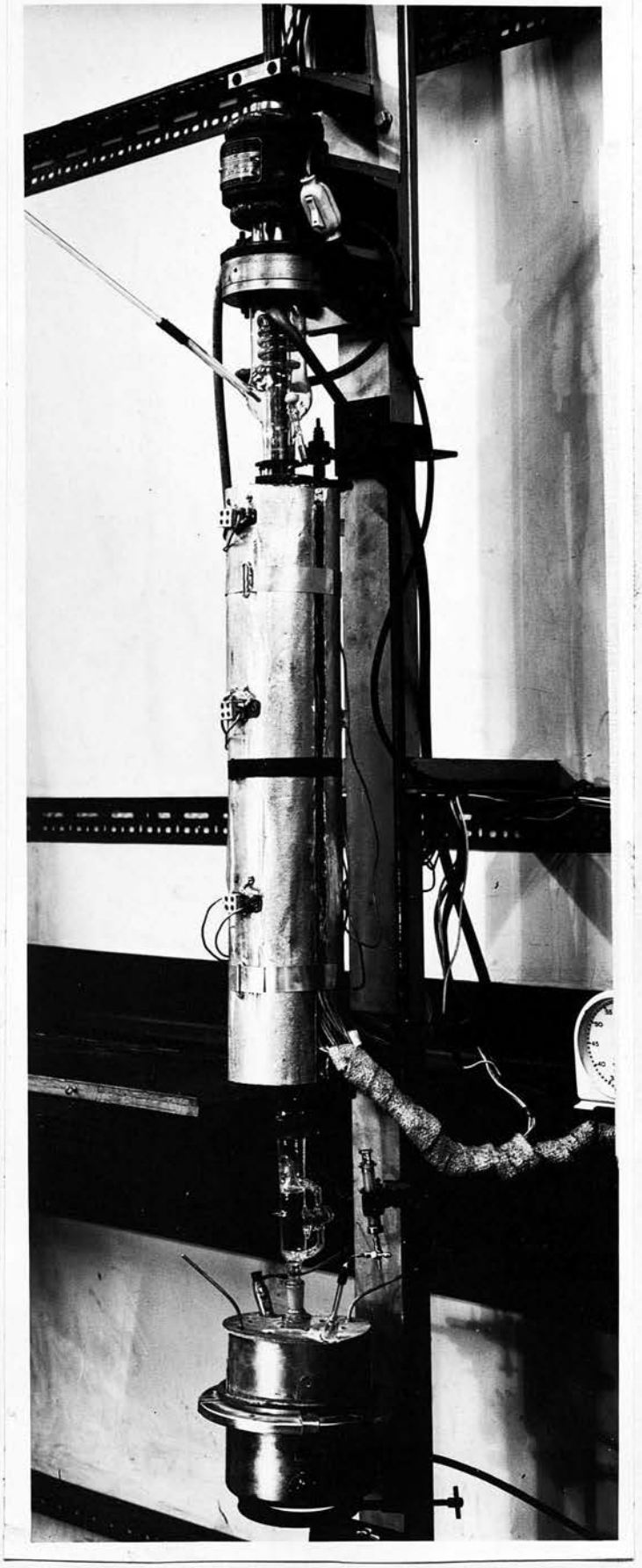

Figure 17 (b)

Oblique view of column

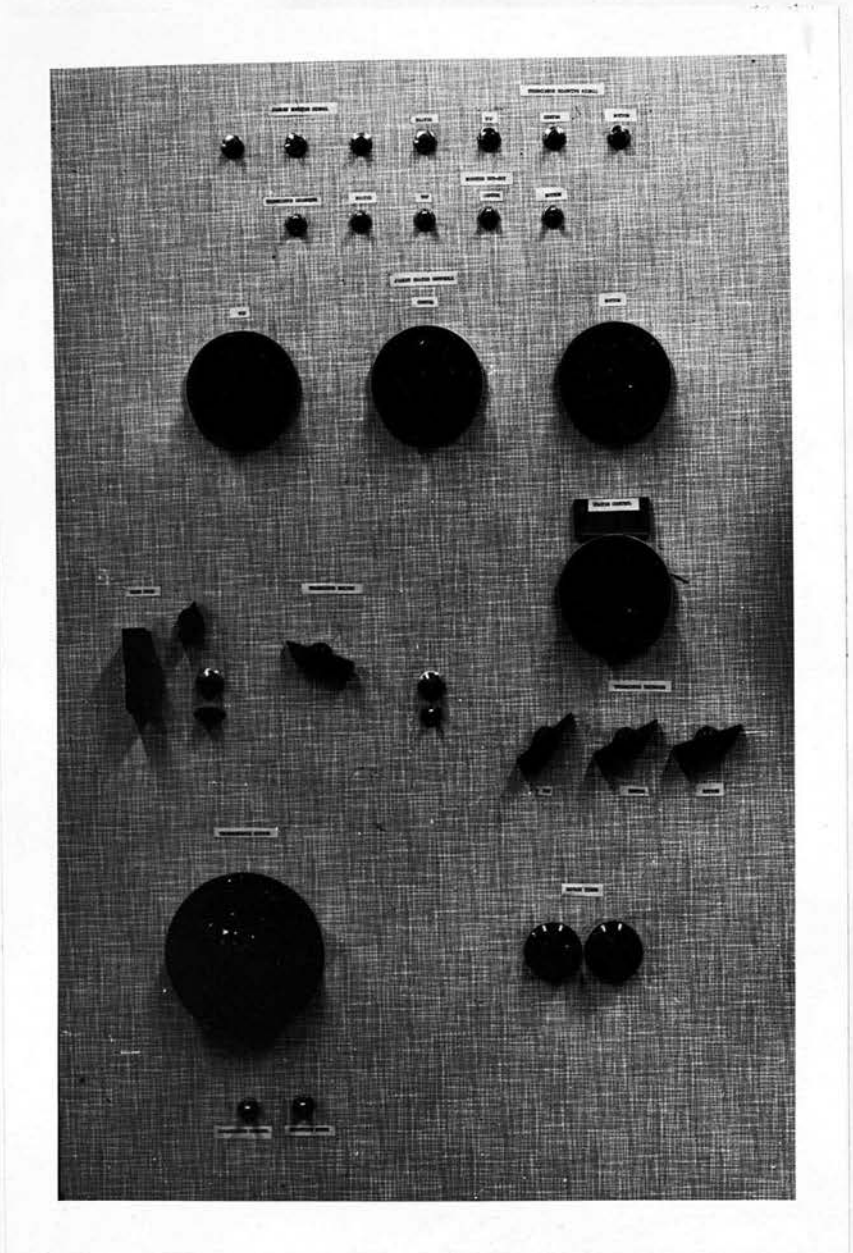

Figure 17 (c). View of control panel

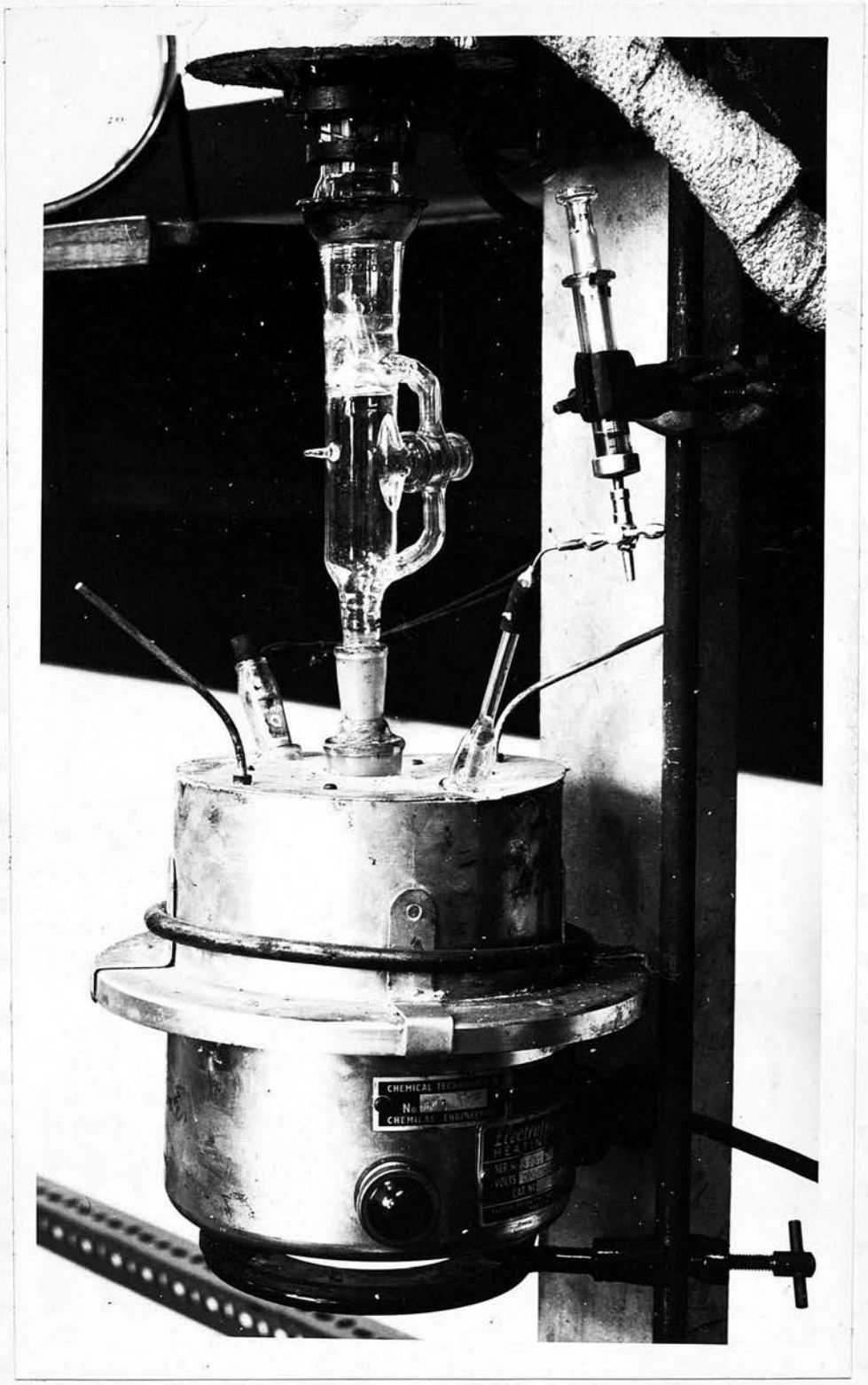

Figure 18. Details of boil-up rate meter and still-pot sampling device

4. Experimental - Apparatus

Figures 16 (a) and 16 (b) reproduced from the paper by Macleod and Matterson (2) give details of the column assembly. The key to these figures is given alongside Figure 16 (a) . Photographic views of the column and control panel are shown in Figures 17 (a), 17 (b) and 17 (c). The fixed outer cylinder had an internal diameter of 2.80 cm. Of the three alternative inner cylinders used the 2.60 and 2.40 cm. o.d cylinders were made of glass and the 2.14 cm. o.d cylinder made of copper. For the 2.60 and 2.40 cm. o.d glass cylinders the annular working section was 66 cms long but 61 cms long for the 2.14 cm. o.d copper cylinder. The still-pot was charged with a mixture of methyl cyclohexane and n-heptane, n-heptane being the more volatile component.

The boil-up rate was determined by a simple type of boil-up rate meter, interposed between the still-pot and column base, as shown in the photograph, Figure 18. All ground glass joints were sealed with Audco lubricant N°657. This grease had to be heated to about 60°F before it was soft enough to smear on the joints and once the seal was effected and the grease had cooled it proved very difficult to loosen the joints if for any reason the column had to be dismantled. Furthermore, after several hours use the Audco grease tended to cake and crack causing ineffective sealing. Unfortunately a better sealing compound could not be found. Silicone greases were scrupulously avoided since their use soon leads to contamination of the entire column with a fine layer of grease which is extremely difficult to remove. This contamination causes a serious reduction in column performance (42), due to uneven

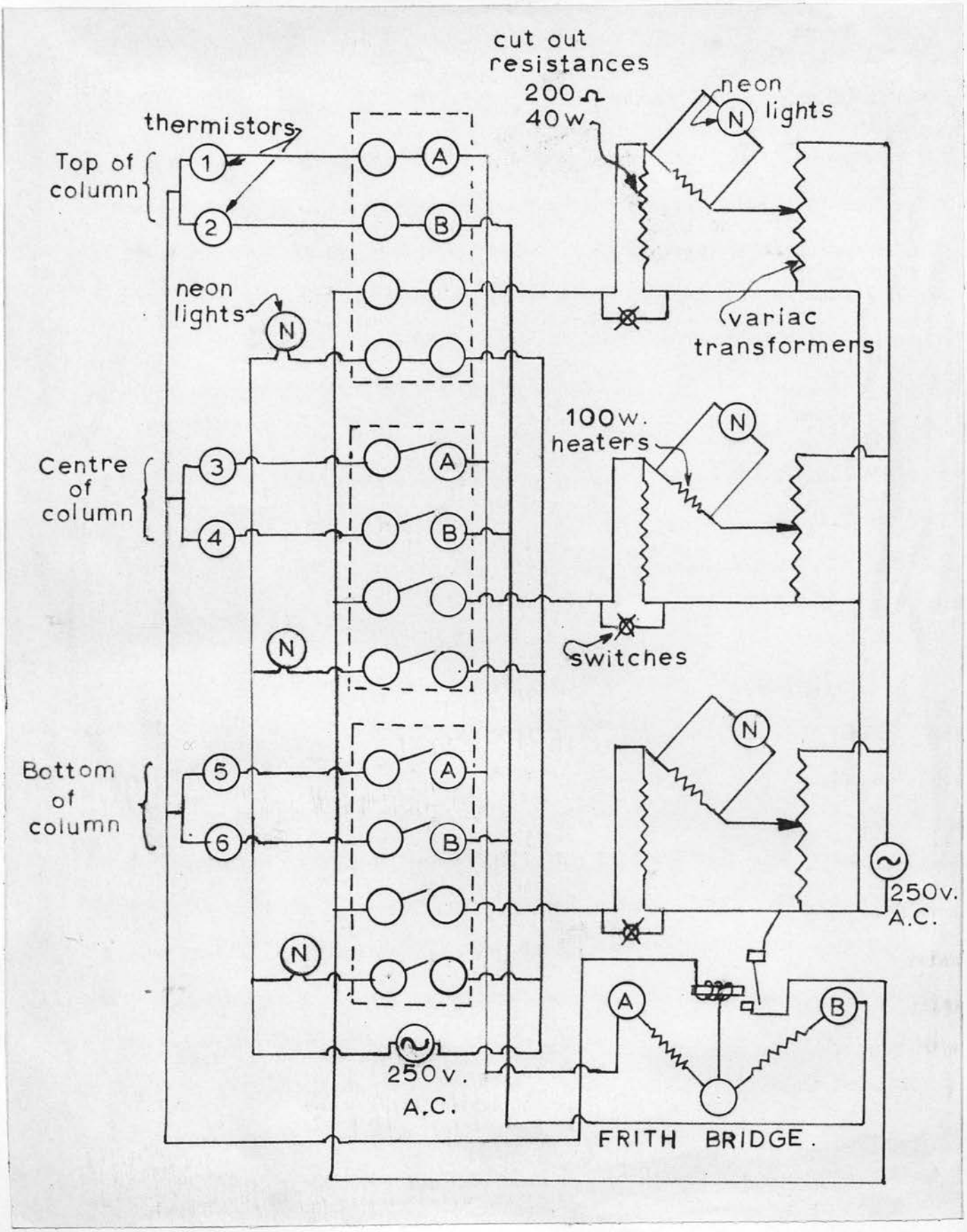

Figure 19. Circuit diagram used for automatic control of adiabatic conditions

wetting of the column walls by descending reflux.

The speed of rotation of the inner cylinder was measured by means of a stroboscopic lamp for speeds of rotation above 250 rpm. Below this speed, the time was taken for the inner cylinder to complete 100 revolutions and the speed of rotation calculated.

An automatic control system, (being a slightly modified form of the system described by Matterson (1)), incorporating thermistors, was used to maintain adiabatic operation of the column. Figure 19 shows details of the circuit used. Figure 16 (a) shows the positioning of the three thermistor pairs, and also details of the rectifying section of the column, which was surrounded by a metal jacket on which was mounted one thermistor of each pair (X in Figure 16 (a)). The other thermistors were mounted in corresponding positions on the external wall of the outer cylinder (Y). These thermistors had large, negative, temperature coefficients of resistance. A set of three compensating heaters, (W), receiving power from a 250 v. A.C. supply via "variac" transformers, manually preset to give approximately correct heating rates, surrounded the metal jacket. When the automatic control system was in operation, the electrical input to any one heater was controlled by the temperature difference of the corresponding thermistor pair. If, for example, the metal jacket temperature became too low at any point of the column, a temperature differential was set up between a particular thermistor pair. This produced an out of balance current in the Frith Bridge, (Wheatstone network), which operated the relay shown in Figure 19. The operation of the relay resulted in the short-circuiting of the 200 Ω resistance which was in series

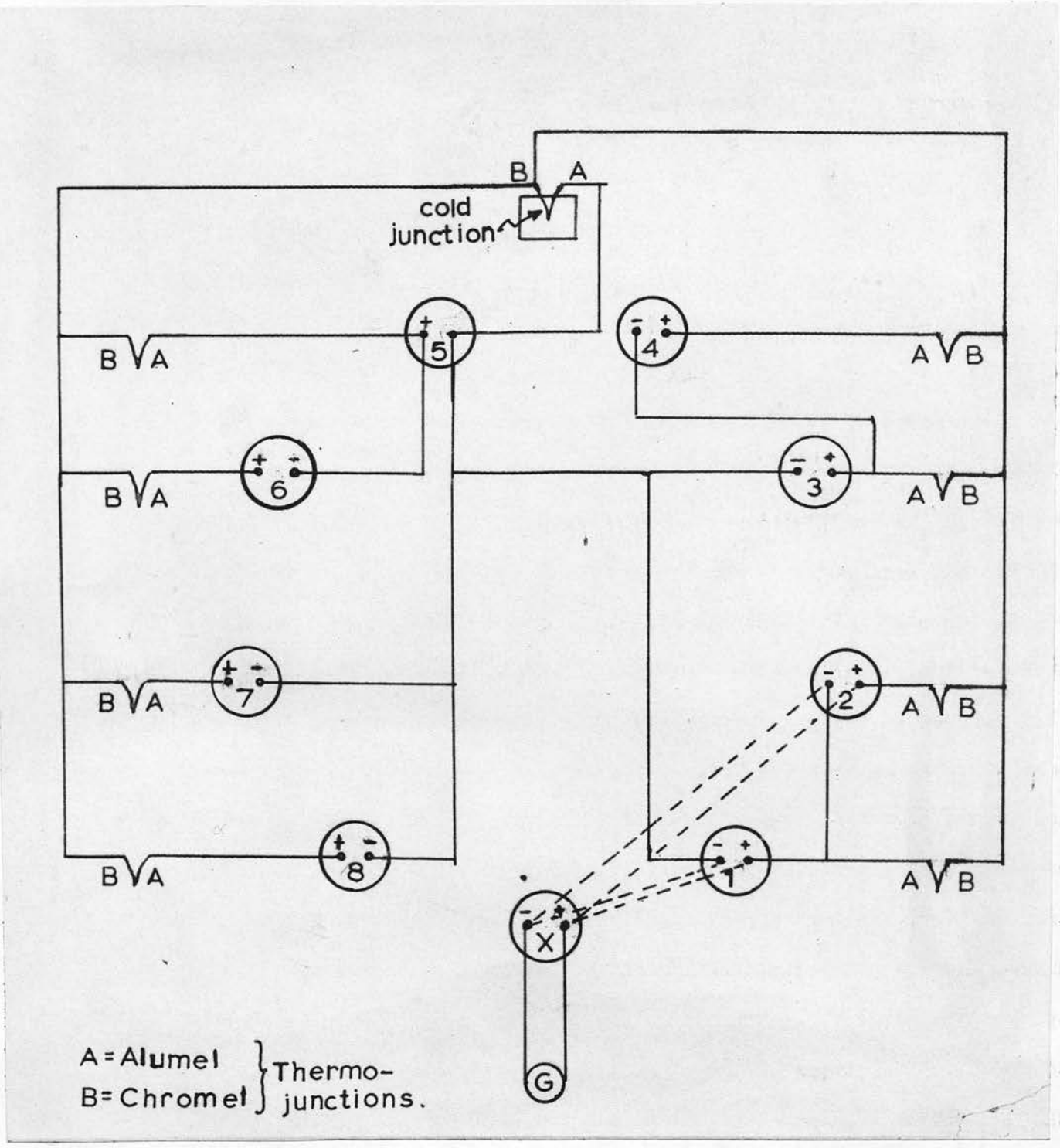

Figure 20. Thermocouple connections to galvanometer switch

with the compensating heater windings (100 watt capacity). The short-circuiting of this 200 Ω resistance boosted the heater current, causing the metal jacket temperature to rise once more. The threeby-pass switches shown in Figure 19 were normally open, except during start-up when they were closed to boost the heater current in order to speed up the heating of the column jacket. After approximately one hour's start-up period these switches were opened. The ratio arms of the Frith Bridge were then connected in sequence to the thermistor pairs by switching on a motor-driven rotary switch, and the column was allowed to reach adiabatic conditions. The thermistor pairs had to be well matched for the control system to function efficiently. Accordingly, a variable trimmer resistance of 500 Ω was placed in series with one of the thermistors of each pair. (These thermistor trimmers are not shown in Figure 19). By locating these thermistor rheostats on the control panel, small adjustments could be made where necessary to the balance position of the Frith Bridge.

Three thermocouple pairs were inserted in the column, adjacent to each of the three thermistor pairs. Figure 20 shows details of the thermocouple connections to the galvanometer switch, G, of the potentiometer. The thermocouples marked 1 to 6 correspond to the thermistors 1 to 6 in Figure 19. Chromel/alumel thermojunctions were used. When the galvanometer terminals were connected to the terminals of the thermocouple 1, the temperature at the top of the distillation column was measured, (since 1 was compared with the cold junction). When the galvanometer terminals were connected to the terminals of thermocouple 2, the temperature of thermocouple 2 was compared with the temperature of thermocouple 1. Thus the absolute and differential temperatures were measureable at the top, centre and bottom of the rectifying section and

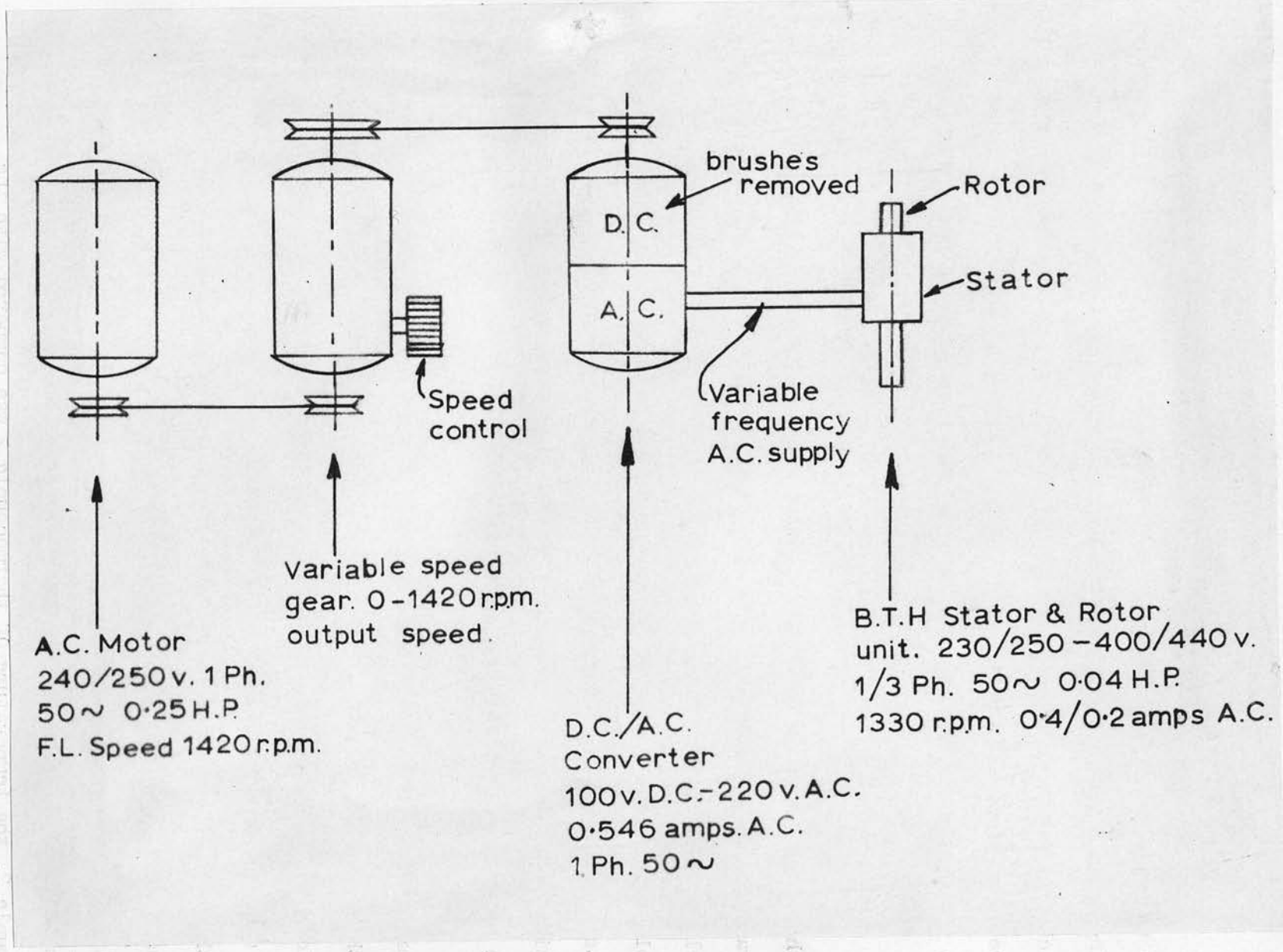

Figure 21. Variable speed control system

a check was thereby maintained on the adiabaticity of operation. Thermocouple 7 was inserted in the still-pot and thermocouple 8 could be used to measure the condensate temperature.

Certain other modifications and improvements were made to the column originally used by Macleod and Matterson (1, 2). The main improvement was the provision of a variable frequency A.C supply to the stator of the B.T.H. "canned" squirrel cage motor, allowing the rotor speed to be varied over a range of stable speeds from zero up to approximately 2200 rpm. (Hitherto, Macleod and Matterson had been able to operate the column with the inner cylinder either stationary or rotating at the fixed motor speed of 1470 rpm.) Figure 21 shows the means whereby this variable speed control was effected. As shown, an A.C. motor was used to drive a variable speed gear. The output shaft from this variable speed gear was connected to the shaft of a DC/AC converter with the brushes on the DC side removed. Thus an AC supply of variable frequency was generated which was fed to the stator of the B.T.H. motor. The manual speed control on the variable gear controlled the frequency of the A.C. supply and hence the speed of rotation of the inner cylinder. Figure 22 shows a photograph of the DC/AC converter situated vertically above the variable speed gear. The AC motor is shown to the left of the gear. The manual speed control knob is on the extreme right hand side of the gear

In the speed range 0-2200 rpm, each inner cylinder was observed to have two critical speeds at which the motion became unstable, manifested by "wobbling" of the inner cylinder. This instability was inevitable with the arrangement used, in which the inner cylinder turned about an internal bearing on a fixed shaft, the fixed shaft being cantilevered from a wall clamp above the column. Macleod and Matterson (1, 2) carried out extensive work on the dynamical

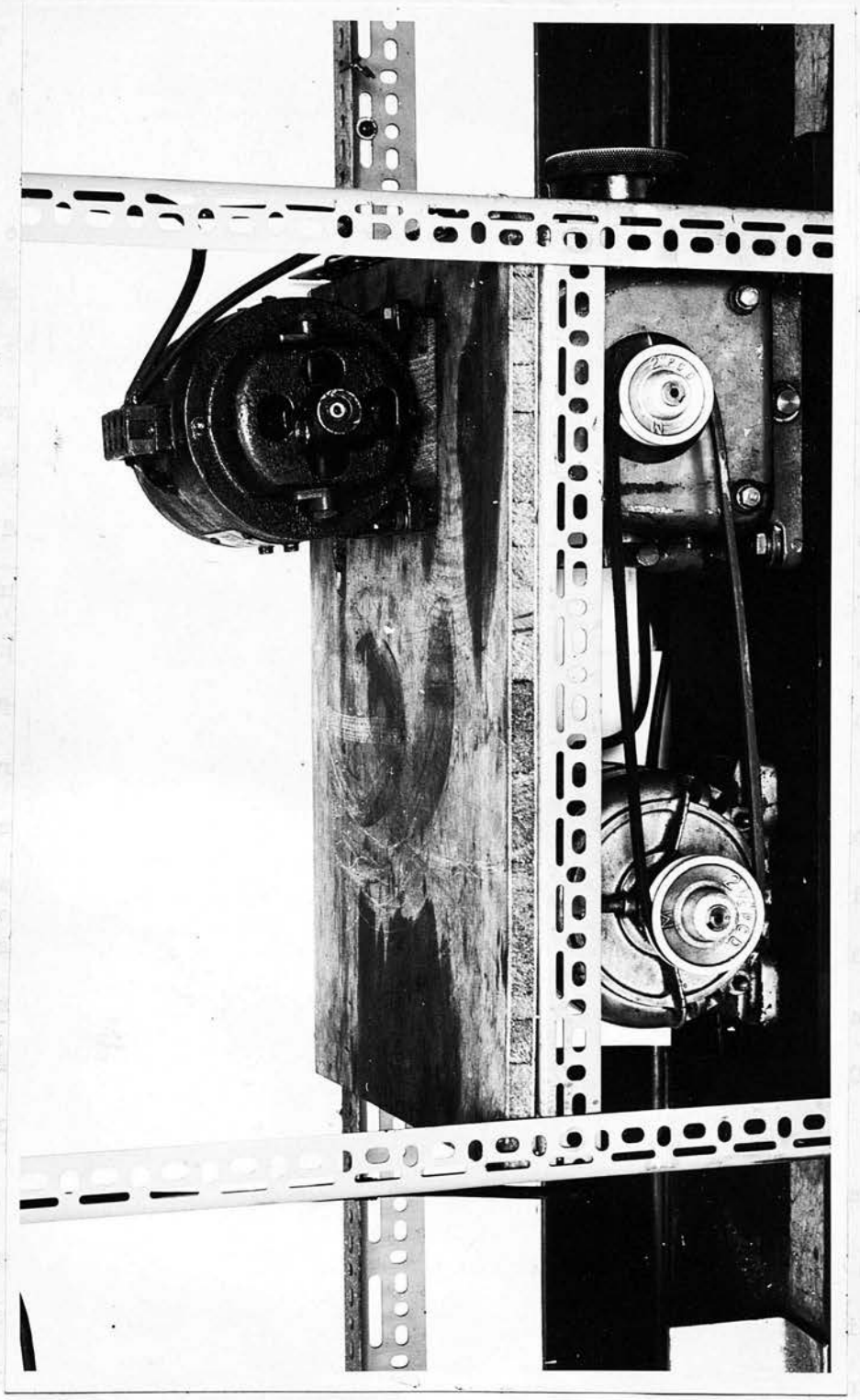

Figure 22. Photograph showing positioning of AC motor, variable speed gear and AC generator

characteristics of this arrangement of rotating cylinder and cantilevered shaft, and in accordance with their results the apparatus was finally designed with the lower bearing placed about a third of the way up the cantilevered shaft to secure maximum stability of the rotating inner cylinder. For each inner cylinder used the relative position of the lower bearing could be varied within small limits by screwing in different lengths of shaft below the lower bearing, until the most stable condition of operation were obtained. It was found possible in this way to reduce the range of instability to very narrow bands about the two critical speeds observed. Thus, for example, in the case of the 2.40 cm. diameter cylinder, the system was unstable in the ranges given (approximately) by :- 1200 $\pm$ 100 and 600 $\pm$ 50 rpm. No distillation experiments were undertaken with the inner cylinder speeds in such unstable ranges.

A further refinement was the use of a hypodermic syringe and three-way valve for the withdrawal of samples from the still-pot. One arm of the three-way valve was connected, via a stainless steel capillary tube, to a glass capillary tube which extended into the base of the still-pot. Figure 18 shows a close-up photograph of this arrangement.

Some months after the distillation experiments had been completed, a simple test was made to determine whether reflux could possibly remain on the 2.60 cm. diameter inner cylinder rotating at a speed of 1470 rpm. The column heaters, jacket and outer cylinder were removed and the test mixture was fed from a burette onto the rotating cylinder at a rate of about 6 cc/min (corresponding to a boil-up rate of 360 cc/hr). It was found that the reflux

was flung off the rotating cylinder before the reflux film had descended more than a few centimetres. This simple test was in agreement with the theoretical prediction of section 3.31, in which it was estimated that this inner cylinder would be free of reflux at speeds of rotation above about 515 rpm. Due to the fact that the variable speed gear was no longer available for use, the experiment could only be conducted with the cylinder rotating at this single speed of 1470 rpm, obtained by connecting directly the 250 v. AC main supply to the stator of the B.TH. motor at the top of the column.

5. Distillation experiments: procedure

The components of the column were cleaned and assembled, using one of the three available inner cylinders. The boil-up rate meter was calibrated at the outset by filling with water until the water level reached the top of a glass pointer within the instrument. The volume of water required was noted. This calibration was repeated several times and an average value taken. The electrically heated still-pot of 500 cc capacity was filled with approximately 200 cc of about 0.2 mole fraction n-heptane. The compensating heater "variac" transformers were preset, from previous experience, to provide approximately the necessary current to the heaters. The "variac" controlling the electrical input to the still-pot was set at a certain position, known from previous trial runs to give the required boil-up rate. The thermistor trimmer rheostats were also preset as the result of previous trial runs. The 250 v. AC supply and Frith Bridge switches were then turned on.

After about an hour, during which time the column had warmed up, the 200 Ω cut out resistances were switched into circuit, (see section 4 and Figure 19), and the motor driven rotary switch brought into operation. The inner cylinder was set in motion, the speed of rotation being set by the manual control on the variable speed gear (see section 4, Figures 21 and 22). The speed of rotation was measured and checked periodically using a stroboscopic lamp, or at low speeds, by timing one hundred revolutions. The column usually reached thermal equilibrium after a total time of about five hours operation.

The boil-up rate was determined by closing the by-pass line on the meter and finding the time required for the liquid level to reach the glass pointer.

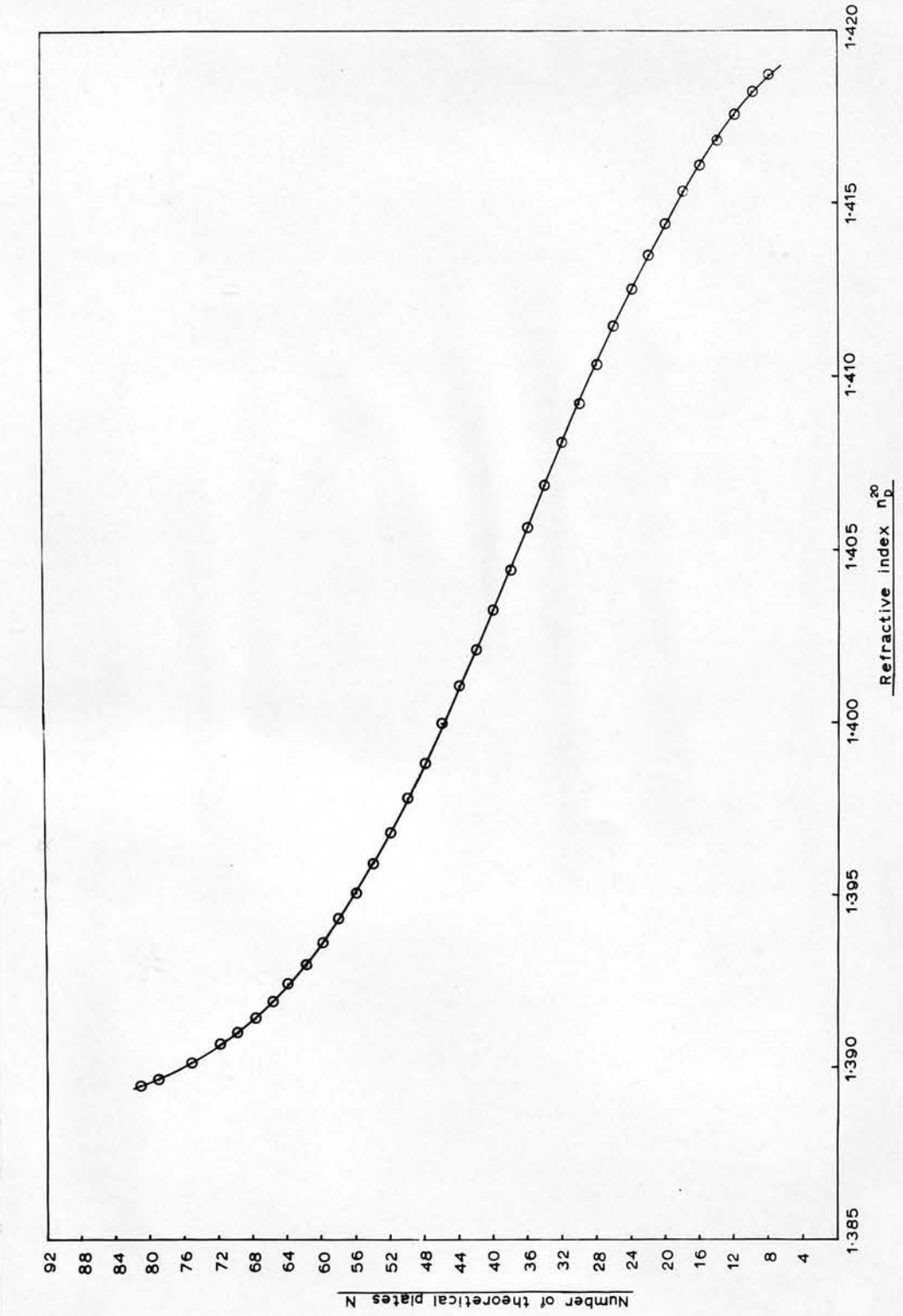

Figure 23. N versus refractive index. Lecky and Ewell (39)

A sample of the condensate was taken by raising the teflon sphere from its ground glass seating situated immediately below a drip point on the spiral condenser. The condensate dripped onto the teflon sphere and passed along the take-off tube into a small test-tube. The test-tube was subsequently removed and sealed, and the contents allowed to cool to room temperature. A sample from the still-pot was withdrawn by means of the hypodermic syringe (see photograph Figure 18), and also allowed to cool in a sealed tube. The refractive indices of these samples were measured at 20°C using an Abbé refractometer. It was assumed that equilibrium had been reached when two consecutive condensate samples, one taken not less than half an hour after the other, had the same refractive index. Lecky and Ewell (39) have published a curve of the number of theoretical plates versus refractive index for the methyl cyclohexane - n.heptane mixture used. The range of their curve was slightly extended, using the data of Bromiley and Quiggle (40) and is shown plotted in Figure 23. The difference in the ordinate readings, corresponding to the still-pot and condensate refractive indices, give the number of theoretical plates in the column for a particular boil-up rate and speed of rotation of the inner cylinder. The data of Bromiley and Quiggle (40) has also been plotted graphically in a convenient form in Figure 24. It is possible to use this graph to determine the number of plates in the conventional manner, by stepping off the number of theoretical plates between two liquid compositions corresponding to still-pot and condensate refractive indices. The two methods produce practically identical results but the former method is much more convenient to use, and all the results to be discussed have therefore been calculated with the use of Figure 23.

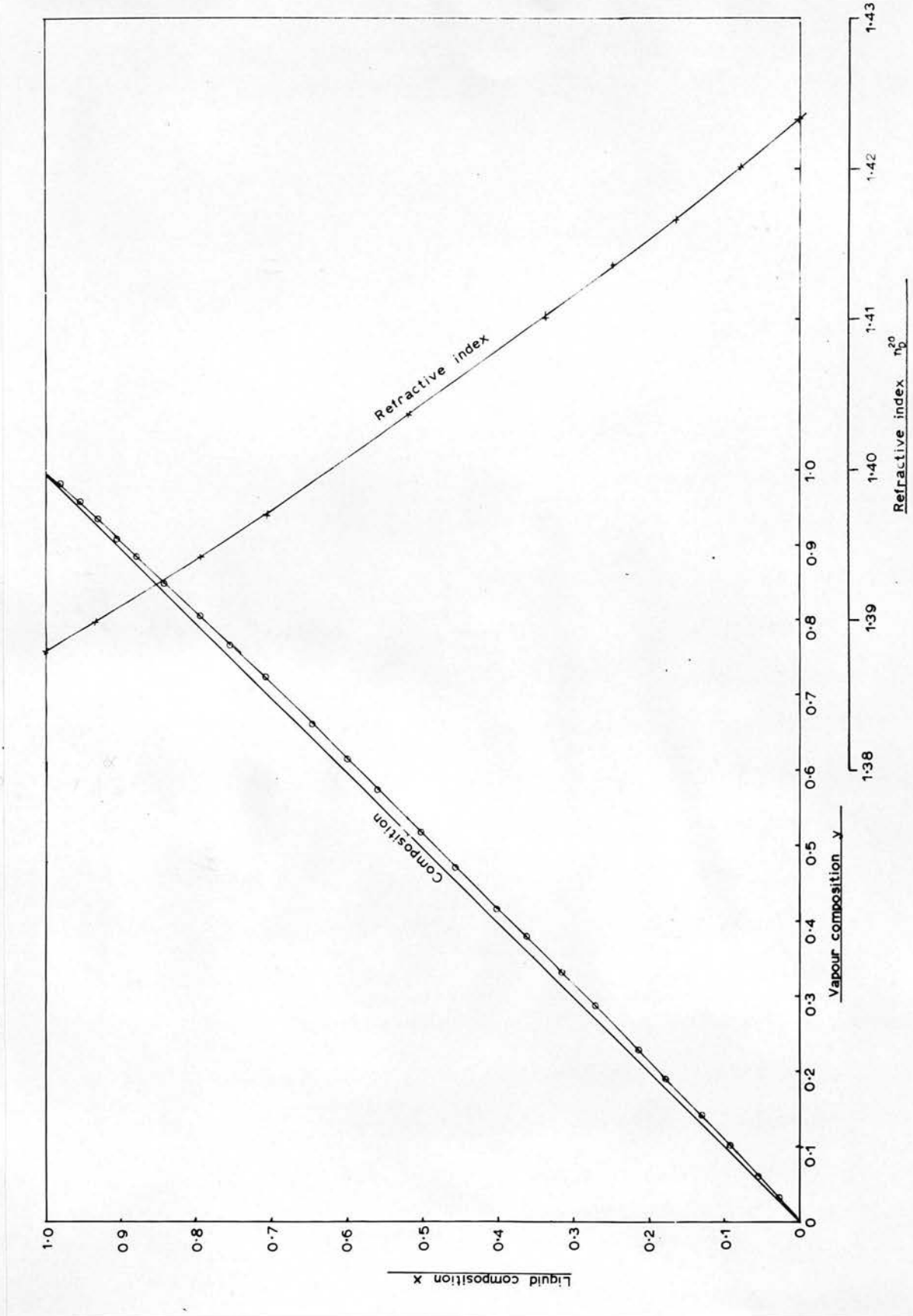

Figure 24. Data of Bromiley and Quiggle (40)

The same experimental procedure was adopted for different boil-up rates and speeds of rotation of the inner cylinder. Altering the boil-up rate or speed of rotation of the inner cylinder disturbed equilibrium conditions and it was necessary to wait three or four hours before samples for the new conditions could be taken. Consequently it was not usually possible to obtain, on any one day, satisfactory results for more than two sets of operating conditions.

Experiments at different boil-up rates were also conducted with the inner cylinder stationary.

After the entire range of boil-up rates and speeds of rotation had been covered, similar experiments were performed using the remaining two inner rotating cylinders.

During all the experiments it was noted that, at a fixed boil-up rate, the speed of rotation of the inner cylinder had a pronounced effect on the rate of condensation of the vapours on the spiral condenser at the top of the column. In all experiments, some of the vapour reaching the top of the column was condensed on this spiral, while the remainder condensed on the wall of the condenser shell. As can be seen from Figures 16 (a), 16 (b) and 17 (b), the clearance between the spiral condenser and the rotating cylinder was very small, and hence the heat transfer rate, between the cold water in the condenser spiral and the vapours in the column, was greatly affected by the rotation of the inner cylinder. As the speed of rotation was increased more warm vapour was brought into intimate contact with the condenser spiral and the heat transfer coefficient at its surface was increased, resulting in

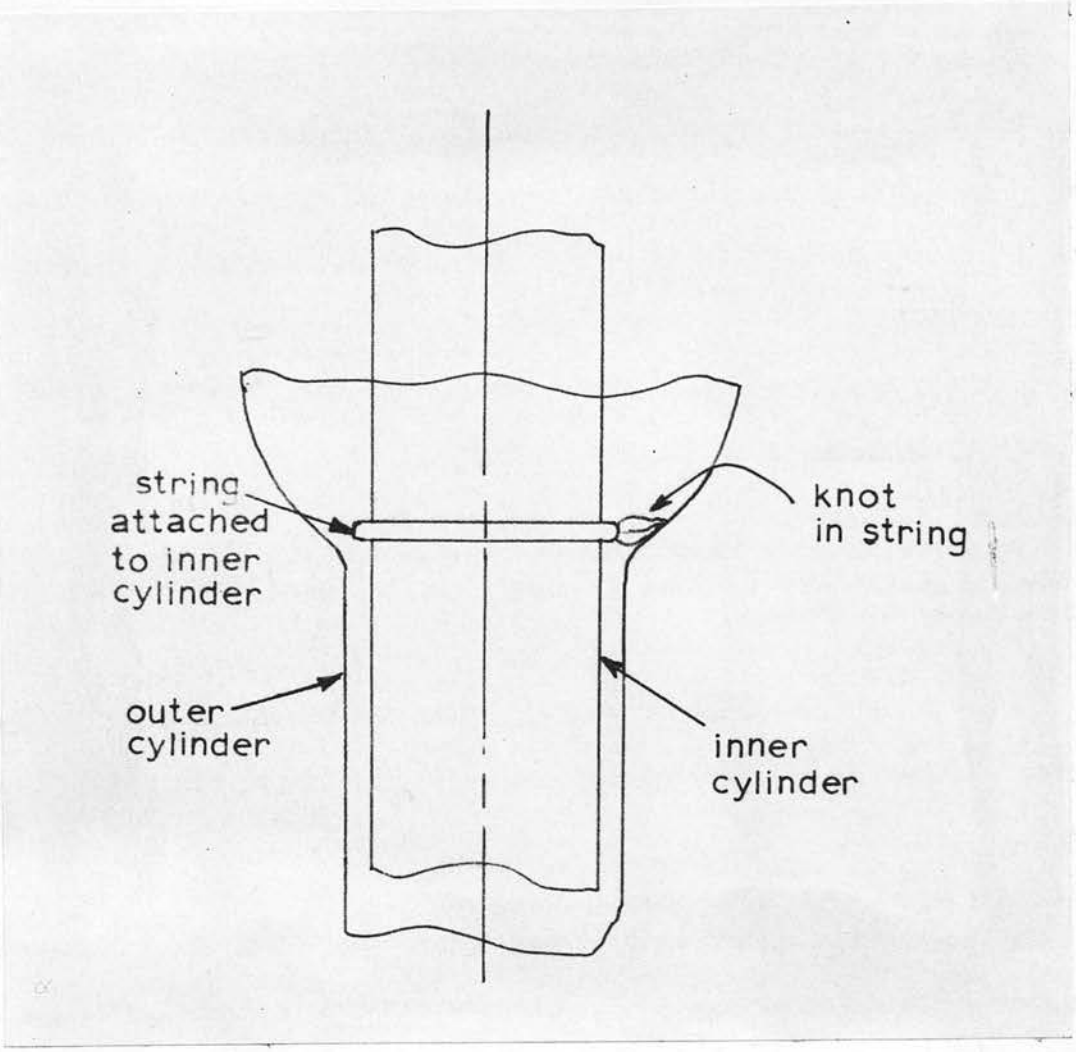

Figure 25. String wiper to distribute reflux around outer cylinder wall.

an increased drip-rate off the glas tip (see Figure 16 (b)). The drops of condensate from this glass tip fell onto the teflon sphere take-off valve and eventually channelled down the wall of the lower part of the condenser shell into the annulus. It was also observed that a stream of reflux channelled down from the joints where each arm of the condenser spiral passed through the condenser shell.

It was thought at the time of experimentation that such channelling, if it continued down the wall of the outer cylinder, would significantly affect the performance of the column, due to incomplete wetting of the surface of the annulus by reflux.

An attempt was made to remove the possibility of any such channelling. A length of string, tied once around the inner cylinder at the top of the rectifying section and carefully knotted, was found to be a simple and effective way of distributing, around the wall of the outer cylinder, any condensate dripping off the condenser glass tip. The knot on the string wiped the surface of the outer cylinder whilst vapour could continue to flow up through the gap between the circle of string and the outer cylinder. The arrangement is shown in Figure 25. Experiments were conducted with string attached to the 2.60 and 2.40 cm. diameter glass inner cylinders and readings taken over the entire range of speeds of rotation possible. During some of the experiments at low speeds of rotation of the inner cylinder performed with the 2.14 cm. diameter copper inner cylinder the visible section of that cylinder appeared to be wet with reflux. (See 'Remarks' column in Table VII). As this visible section was limited to a very short unlagged section between the top of the heater jacket and the bottom of the spiral condenser, there was no direct

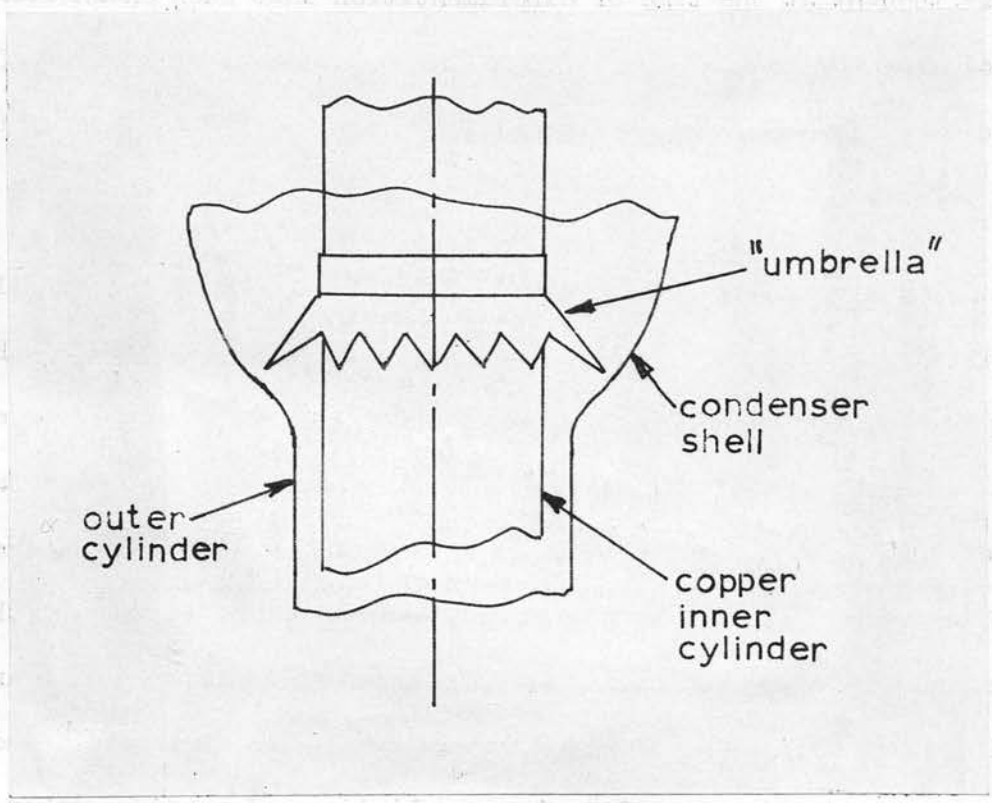

Figure 26. Copper "umbrella" fitted to 2.14 cm. diameter copper inner cylinder.

evidence that the copper cylinder was also wet in the adiabatic annular section. However, in an attempt to prevent reflux, which may have condensed on the inner cylinder, from flowing down the cylinder wall an "umbrella" made from thin copper sheet was fitted on the cylinder as shown in Figure 26. It was hoped that this 'saw-tooth' construction would divert any reflux from the inner to the outer cylinder but still allow the vapour to flow up into the condenser section. The majority of the experiments with this inner cylinder were conducted with this "umbrella" fitted to the cylinder.

The results obtained from experiments using all three sizes of inner cylinder are given in Tables V, VI and VII (at the end of Part I of this report) for the 2.60, 2.40 and 2.14 cm. diameter inner cylinders respectively.

6. Smoke experiments: procedure & discussion of results

6.1 Procedure

An attempt was made to verify more directly the existence of vortices during the distillation experiments at low boil-up rates and high speeds of rotation of the inner cylinder. It was obviously impossible in a distillation experiment to remove the heaters and metal jacket in order to make any kind of direct visual observation of the vapour flow, as this would have violated the equilibrium conditions of operation.

It was therefore decided to use air (containing smoke to make the motion visible) in place of the hydrocarbon test mixture, under dynamically similar conditions; the column heaters and metal jacket were removed so that the smoke patterns could be seen and photographed through the glass walls of the outer tube of the column. Air was blown up the annular gap and cigarette smoke was introduced as a tracer to determine whether vortices could be produced by slowly increasing the speed of rotation of the inner cylinder for a fixed flow rate of air in the annulus. Vortices were in fact made visible throughout the entire length of the annulus by the use of smoke. It was argued that if an experimental plot of axial Reynolds number, Re_a, versus Taylor number, Ta, could be obtained showing the critical conditions for vortex formation, then it would be possible to determine whether vortices would exist in the distillation experiments for the range of boil-up rates and inner cylinder speeds investigated.

By pouring both acetone and water down the outer cylinder wall, reflux

Direction of rotation

of inner cylinder

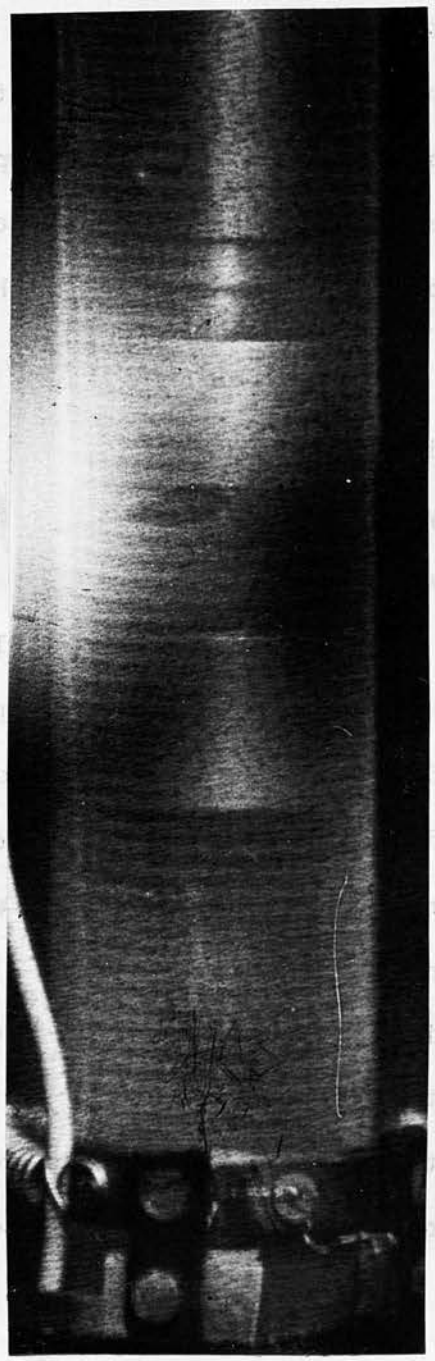

Figure 27. 2.60 cm. diameter glass inner cylinder. Speed of rotation 1000 rpm. Photograph of air and cigarette smoke in the annulus, without axial flow. Taylor vortices present

conditions were simulated in order to determine whether the reflux in the distillation experiments had any effect on the onset or physical appearance of vortices. No noticeable effect was found.

6.2 Discussion of results

Photographs were taken of the smoke vortices with the 2.60 cm. diameter glass inner cylinder rotating at about 1000 rpm. These photographs were difficult to obtain but Figure 27 does show the appearance of vortices, without axial flow of air, with the inner cylinder rotating well above the critical speed (241 rpm) calculated from Taylor's equation (45). When measurements of vortex spacing were attempted on the column, it was observed that smoke experiments allowed one to see the spacing between vortices rotating in the same direction and not counter-rotating ones, which were adjacent. Thus in Figure 27, the spacing of the white circumferential bands equals two vortex diameters, each band representing a single vortex.

As observed by Shipp (27), when the axial flow rate of air was increased the vortices began to move bodily up the column. (Shipp described this as a "flowing ring" system). As the axial flow rate was further increased the vortices tilted, as shown in Figure 28, and a "flowing spiral" motion was observed, as found by Shipp with experiments on liquid systems. As the flow rate increased the tilt of these flowing spirals increased until the spiral form eventually disappeared and an apparently purely axial flow regime existed once more. The angle of tilt of the vortex system, at a fixed axial flow rate, was observed to depend on the speed and direction of rotation of the inner cylinder (see Figure 28). Quantitative experiments were conducted with the

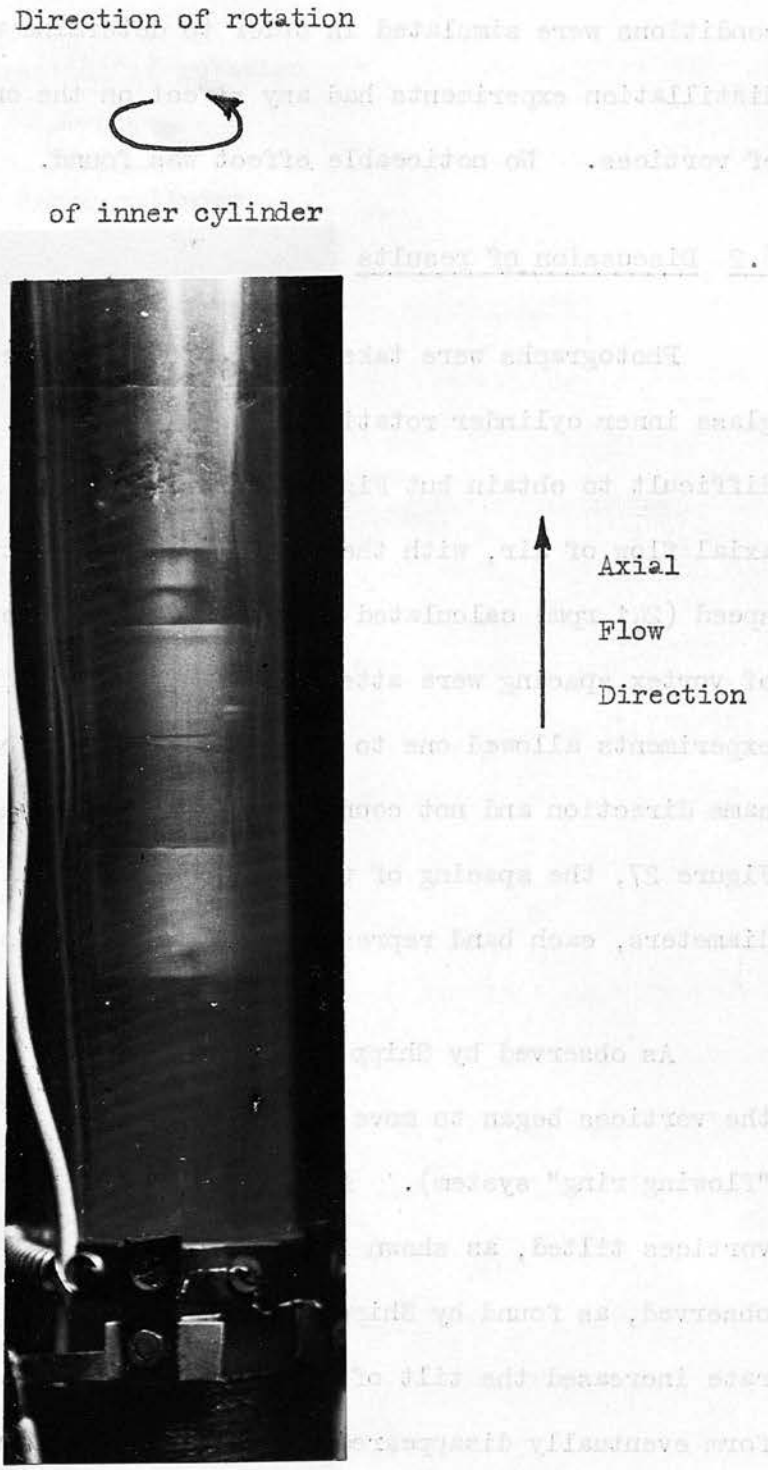

Figure 28. 2.60 cm. diameter glass inner cylinder. Speed of rotation 1000 rpm. Photograph of air and cigarette smoke in the annulus with axial flow. "Flowing spirals" just apparent.

2.14 cm. diameter copper inner cylinder, ($^{b}/_{r_m} = 0.267$), to determine values of the critical speeds of rotation for varying axial flow rates of air and smoke. Air and cigarette smoke were pumped, through a rotameter, metric size 7, through the annulus 0.26 cms. wide. The speed of rotation of the copper cylinder was fixed at a certain value and the air flow rate was increased until the vortices disappeared. These critical values of axial flow rate and cylinder speed are recorded in Table VIII. The axial Reynolds number, Re_a, and critical Taylor number, ^{c}Ta, were calculated and the results plotted in Figure 11 (see section 3.624). The results of Kaye and Elgar (11) ($^{b}/_{r_m} = 0.198$) and the theoretical curve due to Di Prima (14) ($^{b}/_{r_m} \rightarrow 0$) are also shown in Figure 11. Unfortunately the smoke experiments could not be conducted for axial Reynolds numbers greater than about $Re_a = 106$ and so a proper comparison could not be made with the results of Kaye and Elgar. However, the results obtained with the smoke experiments, although probably inaccurate and widely scattered, indicate a similar trend, in the plot of Re_a versus Ta, to the curves of Kaye and Elgar and Di Prima.

For an axial Reynolds number of 106, the boil-up rate during distillation with the copper cylinder is approximately 160 cc/hr. This very low boil-up rate was rarely attained in the distillation experiments; so, unfortunately, it cannot be claimed that the presence of vortices, under the ordinary conditions of still operation, was verified by these smoke experiments.

Another conclusion that can be drawn from these experiments is that entrance effects in this type of column are unimportant under the conditions

of the smoke tests. The use of smoke showed that vortices were produced throughout the entire length of the annulus, even in the entry region immediately above the hemi-spherical end of the rotating inner cylinder. It is therefore reasonable to expect that, if and when vortices appear in the fractionating column experiments, they would also appear over the whole length of the annulus, i.e. that the hydrodynamic entry length, necessary for the formation of a stable vortex flow, is extremely short. This conclusion contradicts a tentative suggestion in the "Shell" report from Amsterdam (34) that there is an entrance length, large compared with the total length of the apparatus, in which momentum transfer between the rotating inner cylinder and the vapour phase, is incomplete. This suggestion was put forward to explain the fact that the results obtained in Amsterdam, (from a system geometrically dissimilar from that used by Cornish (9)), did not agree with the results of Cornish. It is in fact more likely that the discrepancy observed between the results from Amsterdam and those of Cornish are in fact due to the large entry and exit effects in Cornish's apparatus (see section 3.621), and that Cornish was measuring changes in these entrance effects and not changes in the annulus pressure drop.

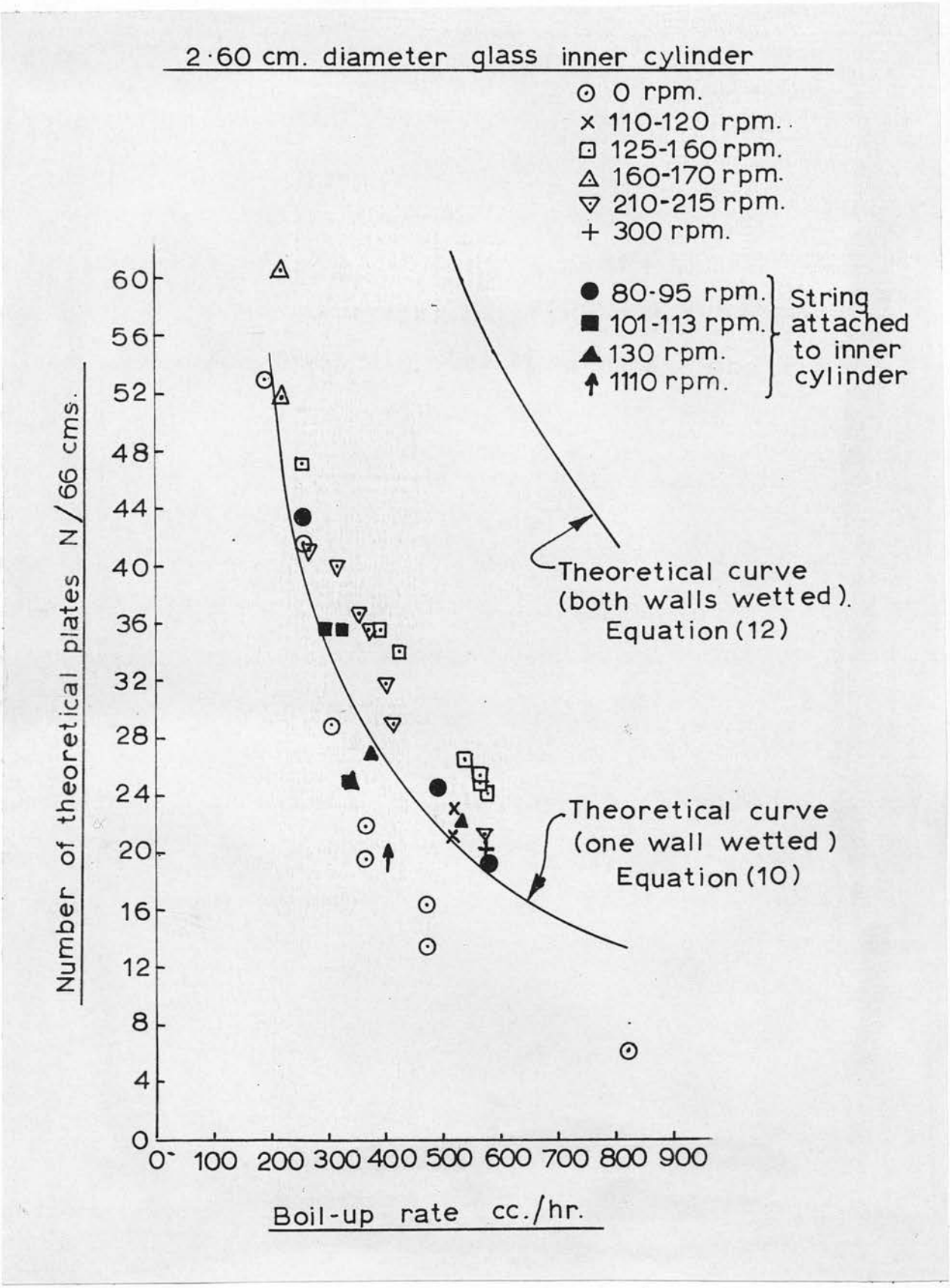

Figure 29. Experimental results together with theoretical curve for laminar flow (Equations (10) and (12)). 2.60 cms. diameter inner cylinder.

7. Discussion of results - distillation experiments

Sections 3.8 and 3.9 contain a summary of the theory of rotary concentric cylinder fractionating columns and a comparison of this theory with previous experimental data. It appears that this agreement is not very satisfactory and it was hoped that the present experimental investigation would throw light on the discrepancy.

7.1 Results obtained from experiments using the 2.60 cm. diameter glass inner cylinder

The experimental results obtained with this cylinder are shown in Figure 29, in which the number of theoretical plates, N, per 66 cms. is plotted as a function of boil-up rate. The experimental data from which Figure 29 was drawn is recorded in Table V. On the same plot are shown the theoretical curves for "one wall" and "both walls" wetted, calculated using equations (10) and (12) respectively. Table IX gives the calculated values of N at a particular boil-up rate used in plotting these two theoretical curves. The data given by Zuiderweg (24) for a methylcyclohexane - n.heptane test mixture was used in these calculations; the method of calculation being previously described in section 3.32.

The results obtained with the inner cylinder stationary (0 rpm) generally lie below the theoretical curve (one wall wetted) and indicate, somewhat surprisingly (see section 3.31) that for this particular case the outer cylinder only was wetted by reflux. If there was channelling of the reflux film down the wall of this outer cylinder the low performance of the column would be explained.

The performance of the column was investigated intensively over a small range of inner cylinder speeds, 80-310 rpm, in the hope of showing up the effect of vortex formation. Taylor's equations (45) and (46) predict a critical speed of about 241 rpm. for "zero" boil-up rate and thus it was thought at the time of experimentation that, for low boil-up rates, vortices should appear in the range 200-300 rpm. causing a marked rise in N. No such rise in N was noticed; in fact no significant trend would be indicated in a plot of N versus speed of rotation of the inner cylinder. The b/r_m value for this column is 0.074 and the experimental vurves of Re_a versus Ta due to Kaye and Elgar (11) ($b/r_m = 0.198$) may be assumed valid, (in agreement with the recent theory of Di Prima (14)), in predicting the approximate critical conditions for the onset of vortices, (but not turbulence), in this column with a finite boil-up rate. Using the curve of Kaye and Elgar, at a boil-up rate of 325 cc/hr, corresponding to an axial Reynolds number, Re_a, of 212 (see Table IX) the speed of rotation of the inner cylinder necessary for vortex formation is about 2.75 times the critical speed at "zero" boil-up rate, i.e. a speed of approximately $2.75 \times 241 \doteqdot 660$ rpm. Thus for the experimental data in the range 80-310 rpm the vapour was probably in laminar flow over the entire range of boil-up rates investigated and equation (10) or (12) should apply to these results. As shown in Figure 29 a single value of N was also obtained experimentally at 1110 rpm with a presumed vortex regime but the vibration of the inner cylinder was considerable at this speed and therefore this single value is unlikely to be accurate.

As shown in Figure 29 some of the results in the speed range 80-310 rpm

were obtained with the string wiper attached to the inner cylinder in order to remove the possibility of channelling of the reflux film. It appears that this wiper had no significant effect on column performance, indicating either that channelling did not occur with the inner cylinder rotating or that channelling did occur in any case/and that the wiper was inefficient. Since practically all the results in this speed range lie in a band close to but above the theoretical line (one wall wetted) it seems possible that the outer cylinder was in fact uniformly wetted by a reflux film and that the curve of equation (10) is an appropriate (though rough) theoretical standard for this case, in which the vapour phase is almost certainly in laminar flow, though agitated to a greater or less degree by small irregularities in the motion of the rotating inner cylinder.

If equation (10) is used as a theoretical standard with which to compare the performance of this column with the performance of the column investigated by Willingham et al (3), for similar conditions of laminar flow in the vapour phase, it is immediately seen that the agreement between theory and experiment is much closer for the present column than with the column of Willingham et al (see Figure 12). It may be concluded that the column under investigation was performing much more efficiently than the column of Willingham et al for the same conditions of vapour flow.

It is also of interest to note that the highest circumferential Reynolds number, Re_c, reached with experiments on this column was about 700, and the highest axial Reynolds number, Re_a, was about 500, (see Table IX). Since it is reasonable to assume that the simple turbulence criterion, $Re_c > 3000$, would

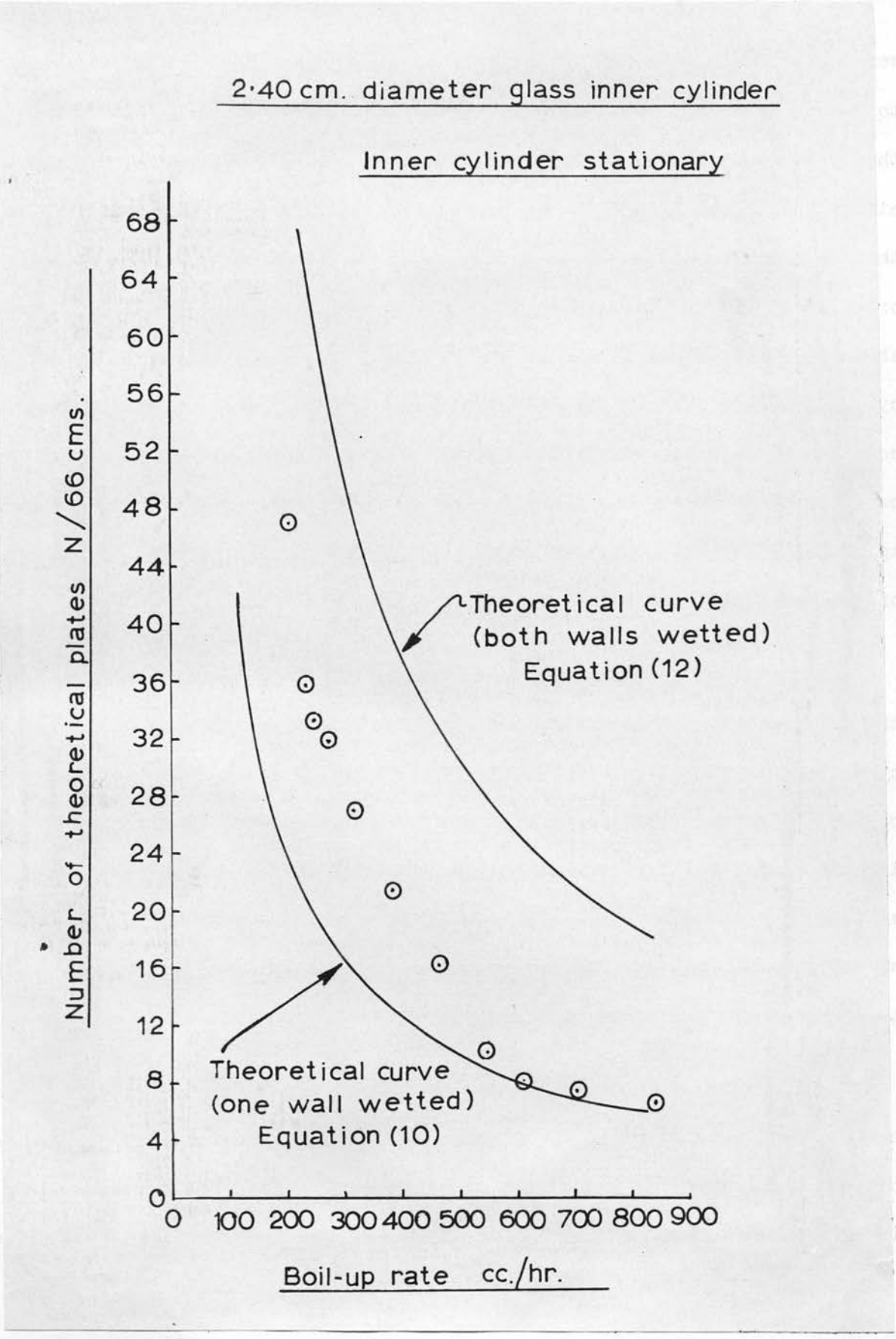

Figure 30. Experimental results together with theoretical curves for laminar flow. (Equations (10) and (12)). 2.40 cm. diameter inner cylinder.

be valid for this column having such a small value of b/r_m (0.074), it may be concluded that the vapour phase was never turbulent in these experiments.

7.2 Results obtained from experiments using the 2.40 cm. diameter glass inner cylinder

The experimental results obtained with this cylinder stationary are shown in Figure 30, the data being obtained from Table VI. On the same plot are shown the theoretical curves for "one wall" and "both walls" wetted, calculated using equations (10) and (12) respectively. Table X gives the calculated values of N used in plotting these two theoretical curves. The results with the cylinder stationary generally lie between the two theoretical curves corresponding to equations (10) and (12). These results suggest that both walls were partially wetted by reflux, although it is somewhat surprising that this should be so for this inner cylinder and not for the stationary 2.60 cm. diameter cylinder. However, if the experimental results with this cylinder are compared with the results obtained using the stationary 2.60 cm. diameter cylinder, it is observed that the experimental points are almost identical, suggesting that the theory leading to the curves of equation (10) and (12) shows too strong a dependence of N on annular gap width.

The experimental results with the inner cylinder rotating are given in Table VI and are shown plotted in Figure 31.

The calculated critical speed for Taylor vortex formation at "zero" boil-up rate in this column is about 93 rpm (using equations (45) and (46)); but

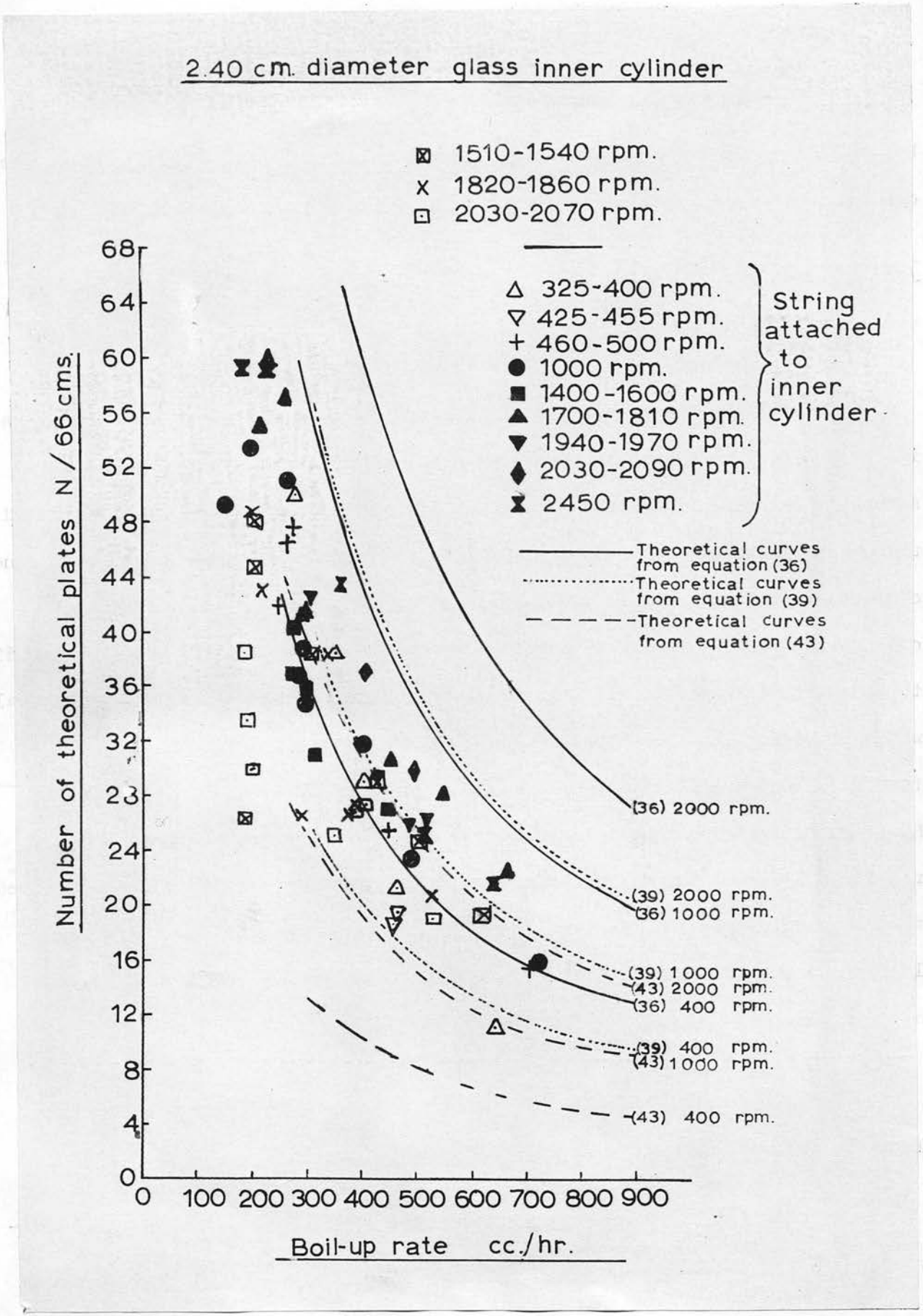

Figure 31. Experimental results together with theoretical curves for vortex flow. (Equations (36), (39) and (43)). 2.40 cm. diameter inner cylinder.

with a finite axial flow rate of vapour a higher speed of rotation of the inner cylinder would be required for the onset of vortices. The $^{b}/_{r_m}$ value for this column is 0.154; the experimental curve of Re_a versus Ta/Fg due to Kaye and Elgar (11) ($^{b}/_{r_m}$ = 0.198) shown in Figure 8 is assumed to apply in predicting approximate critical conditions for vortex formation in this column with a finite boil-up rate. Using the curve of Kaye and Elgar, at a boil-up rate of 325 cc/hr corresponding to an axial Reynolds number, Re_a of 214 (see Table X) the speed of rotation of the inner cylinder necessary for vortex formation is about 2.75 x 93 $\doteq$ 256 and at a boil-up rate of 640 cc/hr (Re_a = 425) the corresponding critical speed would be about 3.25 x 93 $\doteq$ 300 rpm. Thus it appears that at speeds of rotation of the inner cylinder greater than about 300 rpm vortices should have existed in the vapour phase for all boil-up rates investigated. Experiments performed with the mercury vapour transfer column, described in Part II of this report, confirmed these calculations and it was also found that even at the highest speeds attained with this fractionating column (2450 rpm) the vapour phase was probably still in a purely 'laminar plus vortex' regime. It should thus be noted that all the experimental results shown in Figure 31 may be assumed to fall within a vortex regime. Under these conditions it is possible to test the applicability of equations (36), (39) and (43) for distillation in a vortex regime with one wall wetted by reflux. Values of N, as a function of boil-up rate and speed of rotation of the inner cylinder, were calculated from these equations, as shown in Tables XII and XIII, and plotted in Figure 31 for three speeds of rotation, viz:- 400, 1000 and 2000 rpm. These speeds covered a range of experimentation in which vortices could be presumed to exist. It can be seen

that almost the whole of the experimental data with this inner cylinder lies in the relatively narrow band between the curves of equation (39) covering the appropriate speed range, (although equation (39) does predict rather too large a number of plates at 2000 rpm for this column). The exceptions are a few points at low boil-up rate and high speeds of rotation obtained without the string wiper attached to the inner cylinder. These points fall below the band of the remaining data presumably because of channelling. (Channelling probably occurred under these conditions because at high speeds of rotation it was observed that much condensation took place on the condenser spiral from which, without the wiper, the flow of reflux was badly distributed. Thus, with low boil-up rates and high speeds of rotation it is very likely that channelling occurred).

Although the experimental data fall generally within this narrow theoretical band corresponding to the use of equation (39), the scatter of the data is quite considerable. These results bring to light the very important fact that any change in column performance,(e.g. due to a change in speed of rotation of the inner cylinder at a particular boil-up rate), which occurs at those conditions for which the onset of vortices is believed to occur, is of no great significance and is small enough to be masked by other effects causing scatter in the experimental data. The theoretical curves corresponding to equation (36) lie considerably above the corresponding experimental data and the curves derived from equation (43) fall somewhat below the data. In view of the basis of derivation of equations (36) and (43) it is reasonable to assert that equations (36) and (43) represent upper and lower theoretical limits for the performance of this type of column, permitting the performance of this column

to be compared with the performance of the column investigated by Willingham et al (3). It is immediately seen (see Figures (14) and (15)) that the column under investigation was performing much more efficiently than the column of Willingham et al when vortices could be presumed to exist in the vapour phase in both columns.

It can be seen from Figure 31 that with the string wiper attached the performance of the column was rather better than without the wiper attached. This is particularly evident at low boil-up rates. As indicated previously the observation suggests that without the wiper attached channelling occurred in this column, particularly at low boil-up rates and high speeds of rotation of the inner cylinder. It was in fact noted that at high speeds of rotation the drip rate from the spiral condenser tip accounted for about a third of the reflux rate and without the wiper attached liquid reflux from this source was irregularly distributed as it flowed into the working section.

Another interesting observation is that at low boil-up rates with the wiper attached the values of N are very high compared with the vortex theory in the speed range 325-400 rpm. This might be explained by the fact that the inner cylinder was wet with reflux at these speeds and only became dry at speeds above 550 rpm (as indicated in section 3.31). There is some indication in Figure 31 that this is what occurred for this particular inner cylinder. At high boil-up rates the inner cylinder was probably dry at speeds in the range 325-400 rpm since the value of 550 rpm was calculated on the assumption that the reflux film thickness was about 0.004 cms, corresponding to a boil-up rate of about 200 cc/hr and this critical speed was therefore in the nature of an

upper limit. At higher boil-up rates the reflux film thickness would have been larger and therefore the critical speed for dryness somewhat smaller.

The maximum circumferential Reynolds number, Re_c, reached in the experiments with this 2.40 cm. diameter cylinder was 2900 (2450 rpm). The simple turbulence criterion (2, 3) previously discussed indicates that the vapour phase should have become turbulent in these experiments at about this inner cylinder speed of 2450 rpm. No marked rise in values of N is shown at this speed of rotation. It is however fairly certain that the simple turbulence criterion is not valid for a column with this relatively large value of b/r_m. In fact, as shown in Figure 8, the curve marking the transition from 'laminar plus vortex' to 'turbulent plus vortex' flow is nearly horizontal at high Taylor numbers for the b/r_m values of 0.198 and 0.307 investigated by Kaye and Elgar (11); this means that at high Taylor numbers, (i.e. high speeds of rotation) the vapour regime is critically dependent on axial flow rate rather than on circumferential speed.

If it is assumed that the curves of Kaye and Elgar, for $b/r_m = 0.198$ (see Figure 8), of Re_a versus Ta/F_g can be used to determine the conditions for turbulence or 'turbulence plus vortex' formation in the distillation column with the 2.40 cm. diameter inner cylinder, ($b/r_m = 0.154$), then it can be shown that 'turbulent plus vortex' conditions should have occurred when the speed of rotation of the inner cylinder was about 430 rpm at a boil-up rate of 640 cc/hr, ($Re_a = 425$) and that at a boil-up rate below 300 cc/hr, ($Re_a < 200$) 'turbulent plus vortex' conditions probably never occurred in the range of rotational speeds

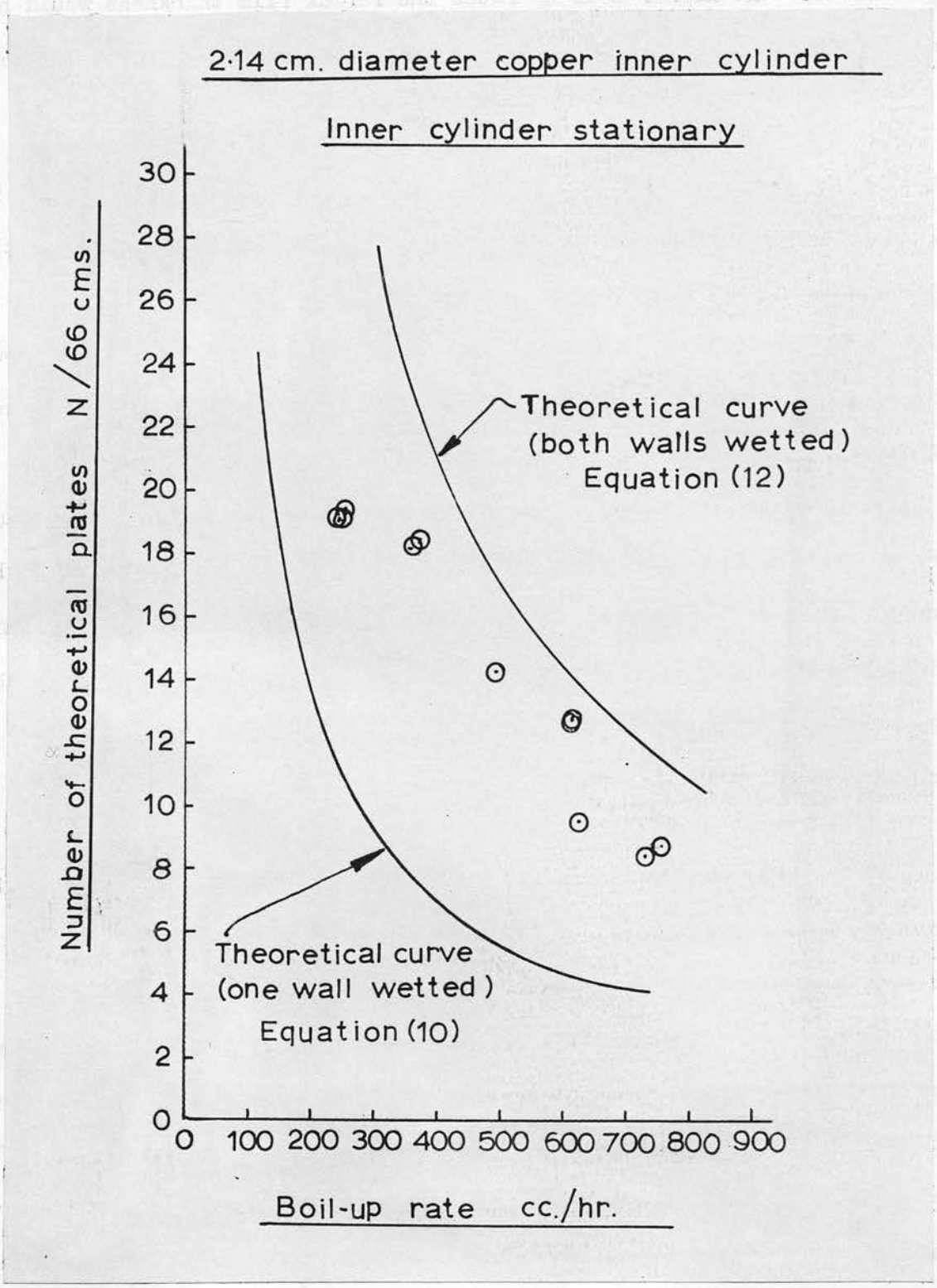

Figure 32. Experimental results together with theoretical curves for laminar flow (Equations (10) and (12)). 2.14 cm. diameter inner cylinder.

investigated. The distillation results plotted in Figure 31 do not show any marked increase in performance at a speed of rotation of about 430 rpm at a boil-up rate of 640 cc/hr. which would indicate a transition to a turbulent regime. It appears, therefore, that the curve given by Kaye and Elgar for the transition 'laminar plus vortex' to 'turbulent plus vortex' (Figure 8) for a $^{b}/_{r_m}$ value of 0.198 cannot be used to predict turbulent criteria in this distillation column having a $^{b}/_{r_m}$ value of 0.154.

7.3 Results obtained from experiments using the 2.14 cm. diameter copper inner cylinder

With this cylinder stationary the results shown in Figure 32 (obtained from Table VII) again lie between the two theoretical curves corresponding to equations (10) and (12) i.e. for one and both walls wetted respectively. It is possible that channelling of reflux occurred in this case with rivulet flow of reflux down both cylinder surfaces, giving rise to observed values of N lying between the two theoretical curves. However, it is difficult to explain why only one wall appeared to be wet for the case of the 2.60 cm. diameter cylinder and both walls partially wet for the 2.40 cm. and 2.14 diameter inner cylinders. It might well be that the laminar flow theory shows too strong a dependence of N on annular gap width, as suggested by a comparison of Figures 29, 30 and 32. The experimental results with the inner cylinder rotating are also given in Table VII and are shown plotted in Figure 33. The calculated critical speed of this inner cylinder for Taylor vortex formation ("zero" boil-up rate) is about 51 rpm, based on

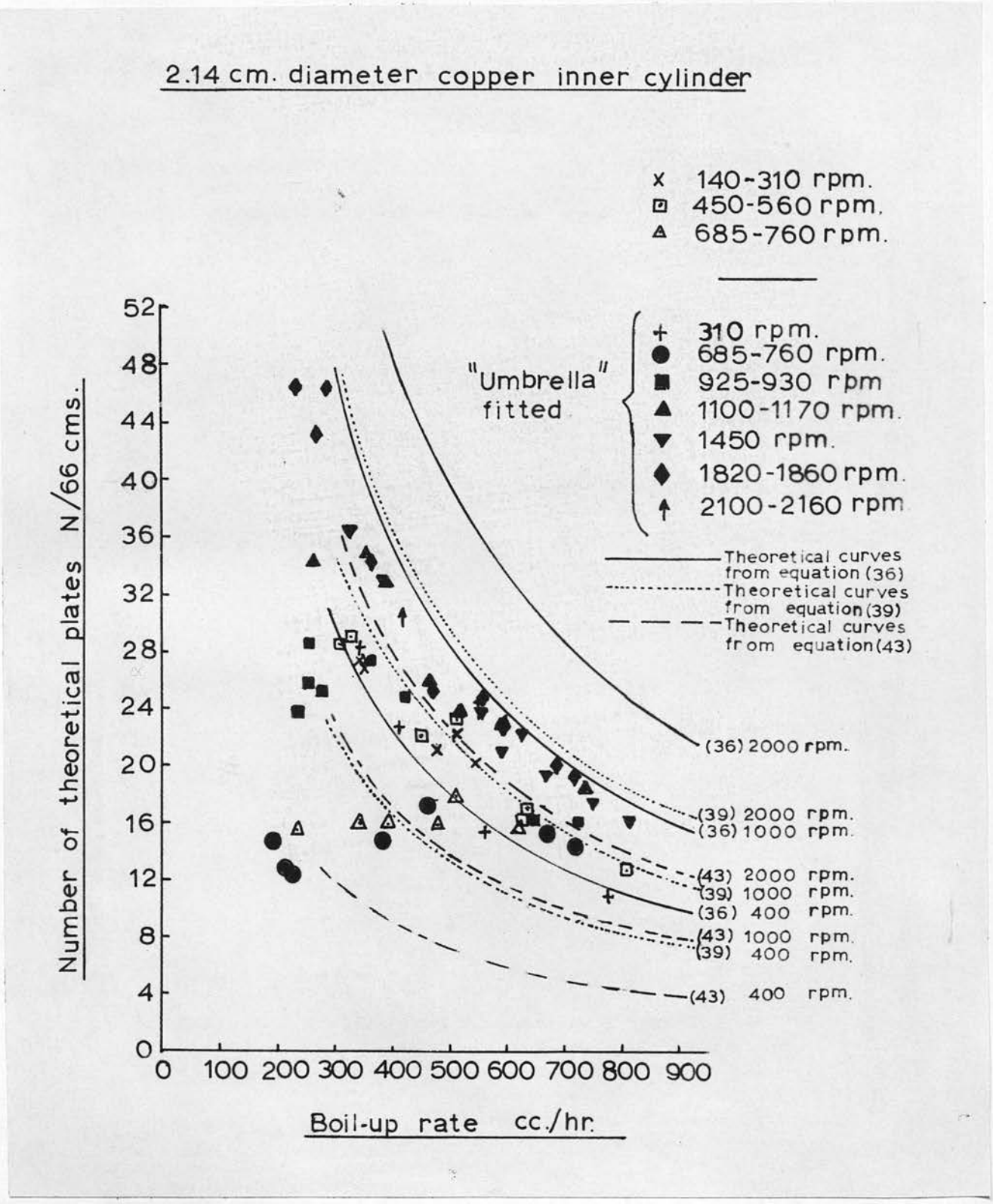

Figure 33. Experimental results together with theoretical curves for vortex flow (Equations (36), (39) and (43)). 2.14 cm. diameter inner cylinder.

Taylor's equations (45) and (46); but with a finite axial flow rate the critical speed for vortex formation is higher. It will be assumed that the experimental curve of Kaye and Elgar (11) with $^{b}/_{r_m} = 0.307$ (see Figure 8) is valid in predicting approximate critical conditions for this column having a $^{b}/_{r_m}$ value of 0.267. Thus at a boil-up rate of 325 cc/hr, corresponding to an axial Reynolds number of 223 (see Table XI), the speed of rotation of the inner cylinder necessary for vortex formation is about 2.0 x 51 = 102 rpm and at a boil-up rate of 640 cc/hr ($Re_a = 441$) the corresponding critical speed would probably be about 2.2 x 51 = 112 rpm. Thus it appears that at speeds of rotation of the inner cylinder greater than about 120 rpm vortices should have existed in the vapour phase for all boil-up rates investigated. It should thus be noted that vortices probably existed even at the lowest speeds of rotation of the inner cylinder recorded in Figure 33. Under these conditions it is possible to test the applicability of equations (36), (39) and (43) derived on the basis of a vortex regime in the vapour phase. Values of N, as a function of boil-up rate and speed of rotation of the inner cylinder, were calculated from these equations as shown in Tables XIV and XV and plotted in Figure 33 for three speeds of rotation:- 400, 1000 and 2000 rpm. (Experiments performed on the mercury vapour transfer column showed that these speeds covered a range of experimentation in which vortices could be presumed to exist.)

The results for the 2.14 cm. diameter inner cylinder resemble those for the 2.40 cm. diameter cylinder in that almost the whole of the experimental data for the 2.14 cm. diameter inner cylinder lies in the relatively narrow band between the curves of equation (39) covering the appropriate speed range of 400 to 2000 rpm. The exceptions are, as before, a few points at low boil-up

rates and high speeds of rotation (685-930 rpm) which fall below the band of the remaining data, probably because of channelling. Again it can be seen that, for the vortex regime, the effect of speed of rotation on number of theoretical plates at a given boil-up rate is small compared with the effect of un-reproducible factors causing the data to scatter. Once again the theoretical curves corresponding to equation (36) lie somewhat above the corresponding experimental data and the curves derived from equation (43) fall below the corresponding experimental data. In view of the basis of derivation of equations (36) and (43) it is once more reasonable to assert that (36) and (43) represent upper and lower theoretical limits for the performance of this type of column, permitting the performance of this column to be compared with the performance of the column investigated by Willingham et al (3). It is immediately seen that the column under investigation was performing much more efficiently than the column of Willingham et al when vortices could be presumed to exist in the vapour phase.

In an attempt to prevent reflux, which might have condensed on the rotating inner cylinder within the condenser section, from flowing down the inner cylinder, a "copper umbrella" (as described in section 5, see Figure 26) was fitted on the inner cylinder. The theoretical analysis given in section 3.31 shows that the inner cylinder would have probably been free from reflux at speeds above 600 rpm due to reflux removal by centrifugal force and that this value of the critical speed was in the nature of an upper limit. Thus only those results in the speed range 140-310 rpm could possibly apply to the case where the inner cylinder might have been wet with reflux. For these results the effect of the copper "umbrella" appears to be insignificant, but

the results are in general a little high compared with the theoretical curves shown, indicating that the inner cylinder might have been wet at speeds below 300 rpm, but that the "umbrella" was inefficient in removing reflux from the inner cylinder. Visual observations of this copper inner cylinder at low speeds of rotation did in fact show that condensation took place on the copper surface within the condenser section but it was impossible to tell whether reflux ran down the wall of the copper cylinder into the working section of the column. (With the other two inner cylinders, made of glass, it was impossible to tell whether condensation took place on the surface of these cylinders, since the wetting by the test mixture of a glass surface is not as easy to discern as wetting of a copper surface.)

As indicated previously, the anomalous results at low boil-up rates in the speed range 685-760 rpm (with and without the umbrella fitted) and 925-930 rpm are probably due to channelling down the wall of the outer cylinder. It was in fact observed that at these relatively high speeds and low boil-up rates a significant proportion of the vapour condensed on the spiral condenser. Reflux dripping off the glass tip of the spiral condenser resulted in maldistribution of the reflux in the working section. As a result the outer cylinder may have been incompletely wetted by reflux at low boil-up rates, resulting in a serious fall in column performance.

The speed of rotation of the copper inner cylinder corresponding to a circumferential Reynolds number of 3000 is about 1650 rpm and thus, if the simple turbulence criterion ($Re_c > 3000$) is valid for an annulus having a b/r_m value as large as 0.267, the vapour phase would be expected to become turbulent

at about 1650 rpm. Very little difference is in fact shown between the values of N, at a particular boil-up rate, in the speed range 1450-2160 rpm, indicating (as was expected) that this turbulence criterion does not hold for such large $^{b}/_{r_m}$ values. If it is assumed that the curve of Kaye and Elgar, for $^{b}/_{r_m} = 0.307$ (see Figure 8) of Re_a versus Ta/Fg can be used to determine the conditions for turbulence or turbulent plus vortex formation in the distillation column with this 2.14 cm. diameter cylinder ($^{b}/_{r_m} = 0.267$) then it can be shown that 'turbulence plus vortex' conditions should have occurred when the speed of rotation of the inner cylinder was about 145 rpm at a boil-up rate of 640 cc/hr ($Re_a = 441$) and that at a boil-up rate of 325 cc/hr ($Re_a = 223$) 'turbulent plus vortex' conditions should have occurred when the speed was about 180 rpm.

The experimental results plotted in Figure 33 do not show the existence of a 'turbulent plus vortex' regime at these speeds of rotation derived from Kaye and Elgar's curves. In fact the experimental data considerably above these speeds fit reasonably well a correlation (39) for purely 'laminar plus vortex' flow of vapour. The experiments with the mercury vapour transfer column, to be described in Part II of this report, also indicate that turbulence probably never existed in this distillation column in the range of cylinder speeds investigated. It must once again be concluded that the turbulence criterion, predicted by the use of Kaye and Elgar's curve, is not verified experimentally.

7.4 Conclusions

The experimental results may be summarised thus:

With the 2.60 cm. diameter inner cylinder stationary the results are found to lie somewhat below the theoretical curve (one wall wetted) predicted by equation (10) indicating that only the outer wall of the column was partially wetted by reflux. With the inner cylinder rotating over a range of speeds from 80-310 rpm it is shown that the vapour phase was in purely laminar flow and the results do in fact lie close to (but slightly above) the theoretical curve corresponding to equation (10). The agreement is good considering how difficult it is to obtain a laminar flow of vapour in the presence of moving parts. Using equation (10) as a theoretical standard it is found that the column under investigation was performing much more efficiently than the column of Willingham et al when the vapour phase could be assumed laminar in both columns.

With both the 2.40 cm. and 2.14 cm. diameter inner cylinders the results with the inner cylinder stationary fall between the theoretical curves corresponding to equations (10) and (12), i.e. one and both walls wetted respectively, suggesting that <u>both</u> walls were partially wetted by reflux. However, comparison of these results with the results for the stationary 2.60 cm. diameter cylinder suggests an alternative interpretation, viz. that the theory leading to equations (10) and (12) gives too strong a dependence of the number of theoretical plates, N, on annular gap width.

Over a range of rotational speeds for which a vortex regime may be presumed to exist the results for the 2.40 cm. diameter inner cylinder provide a reasonable vindication of equation (39) allowing for the considerable scatter of the experimental points and for the importance of channelling at low throughputs and high speeds of rotation of the inner cylinder (without the string

wiper attached). The fixing of a string wiper to this inner cylinder caused an improvement in column performance particularly at low boil-up rates due, presumably, to improved reflux distribution. The appropriate results for the 2.14 cm. diameter copper inner cylinder also fit equation (39) quite well if the same allowance is made for experimental scatter and channelling at high speeds of rotation and low boil-up rates. Equation (39) was derived from a correlation of results from vapourisation studies presented in the "Shell" report from Amsterdam (34); the form of the equation being suggested by the results of the mercury vapour transfer column described in Part II and also by Batchelor's theoretical model (30) for momentum transfer with a vortex regime. The experimental results and the closeness of fit with equation (39) bring to light the very important fact that, although the presence of a vortex regime can be shown theoretically and experimentally to promote an increase in column performance, this increase in column performance is of no great significance and is small enough to be masked by other effects causing scatter in the experimental points over the range of experimental conditions investigated.

For both the 2.40 and 2.14 cm. diameter inner cylinders the theoretical curves based on equation (36) generally fall above the relevant experimental data and the curves based on equation (43) generally fall below this data. Equation (36) is derived from results of experiments in which mass transfer took place into an air stream from a narrow circumferential band of mercury on the outer cylinder. These experiments are described in Part II of this report. Equation (43) is derived from the correlation of Eisenberg et al (35) obtained from experiments in which radial mass transfer took place from the entire length of a cylinder of benzoic acid rotating in water inside a fixed outer cylinder. There was no axial flow of

the water contained in the annulus. It is therefore reasonable to assert that equations (36) and (43) represent upper and lower theoretical limits respectively for the performance of this type of column with a vortex regime in the vapour phase. For the present column with the 2.40 cm. and 2.14 cm. diameter cylinders and for the column of Willingham et al, the theoretical curves derived from equation (39) do in fact lie in between the corresponding curves derived from equations (36) and (43). If the performance of the present column, with either the 2.40 cm. and 2.14 cm. diameter cylinders, is compared with the performance of the column of Willingham et al for conditions of operation in which vortices may be presumed to exist and therefore for which equations (36), (39) and (43) are valid, then it is found that the performance of Willingham et al's column falls considerably below the performance of the present column over a wide range of operating conditions. There is some indication that both the 2.40 cm. and 2.14 cm. diameter cylinders were wetted by reflux at sufficiently low speeds of rotation since values of the number of theoretical plates, N, are relatively high at these low speeds and in the case of the 2.14 cm. copper inner cylinder, a film of reflux was observed at low speeds of rotation on the inner cylinder surface within the condenser section. The fixing of an "umbrella" to the copper cylinder, designed to remove reflux from it, appears to have had no significant effect on column performance due, presumably, to inefficient operation of this "umbrella".

Finally, insofar as it is possible to test the turbulence criteria proposed by Willingham et al (3) and by Kaye and Elgar (11), it appears that they are not appropriate to the present column.

7.5 Recommendations for future work

It is clear that in any further investigations aimed at elucidating the mechanism of column operation the possibility of reflux channelling must be removed. This necessitates the design of a new condenser section incorporating a weir system, which would collect all condensate from the condenser shell and spiral and distribute it uniformly around the outer cylinder wall and, if possible, around the inner cylinder wall also. The use of this weir system and the consequent removal of the possibility of channelling would permit the theoretical equations, particularly equations (10) or (12), to be tested experimentally with greater rigour. The hold-up of the column would naturally be increased by such a modification, but for purposes of fundamental study this is not a disadvantage.

It has been shown that the appearance of vortices had little influence on fractionating column performance over the range of experimental conditions investigated. It will, however, be shown in Part II of this thesis that if further experiments are conducted at low boil-up rates and somewhat higher speeds of rotation of the inner cylinders, the existence of vortices should cause a discernible increase in column performance, particularly with columns having large b/r_m values. This would probably necessitate the use of shorter inner cylinders since the inner cylinders used in the present investigation became unstable at speeds higher than recorded in this thesis.

It would also be of great general interest to undertake experiments with the column operating under vacuum and also with finite reflux ratios.

APPENDIX A

Derivation of equations (2) and (3)

(i) Derivation of equation (2). Outer cylinder only wetted by reflux

Figure 2 (see section 3.1) shows the system under consideration, in which vapour flows up the annulus of effective width w_1, between a rotating inner cylinder and a fixed outer cylinder. Liquid reflux of uniform thickness w_2 returns down the inside of the outer cylinder. The ratio of annular gap width to rotating cylinder radius is assumed small and hence, for a long column, it may be considered that distillation takes place between parallel plates with a fully developed velocity profile.

A mass balance on an element of the vapour phase gives:-

$$D_1 \frac{\partial^2 cy}{\partial s^2} + D_1 \frac{\partial^2 cy}{\partial z^2} = \frac{\partial (u_1 cy)}{\partial z} \quad ----- \quad (A.1)$$

Where D_1 is the molecular diffusion coefficient in the vapour phase, assumed independent of composition, y the mole fraction of the more volatile component in the vapour phase, c the total molal concentration in the vapour phase, (assumed constant), and u_1 is the point vapour velocity. z represents distance measured in the direction of vapour flow.

A mass transfer coefficient, K, is now defined by the equation:-

$$K = \frac{D_1 \left(\frac{\partial cy}{\partial s} \right)_{s = w_1}}{y_i - \bar{y}} \quad ------ \quad (A.2)$$

where $\bar{y}$ is defined according to the equation:-

$$\bar{y} = \int_0^{w_1} \frac{u_1 y ds}{w_1 \bar{u}_1} \qquad ----- (A.3)$$

and y_i is the value of y at the liquid/vapour interface. If longitudinal diffusion in the vapour phase is assumed negligible (as in the treatment of Ruckenstein (20)) compared with lateral diffusion, then, ignoring the second term in equation (A.1) and integrating:-

$$D_1 \left(\frac{\partial cy}{\partial s} \right)_{s = w_1} = \int_0^{w_1} \frac{\partial (u_1 cy)}{\partial z} \, ds \qquad ---- (A.4)$$

assuming $\left(\frac{\partial cy}{\partial s} \right)_{s = 0} = 0$

Now V, the total vapour molal flow, is given by:-

$$V = w_1 \bar{u}_1 c \qquad ------- (A.5)$$ for unit depth of this parallel plate system

Using (A.3) and differentiating:-

$$\frac{dV\bar{y}}{dz} = \frac{1}{w_1 \bar{u}_1} \int_0^{w_1} \frac{\partial}{\partial z} (u_1 y \, ds . w_1 \bar{u}_1 c)$$

$$= \int_0^{w_1} \frac{\partial (u_1 cy) \, ds}{\partial z} \qquad ----- (A.6)$$

$\therefore$ Using (A.4) and (A.6)

$$D_1 \left(\frac{\partial cy}{\partial s} \right)_{s = w_1} = \frac{d\, V\bar{y}}{d\, z} \quad \text{- - - - - - - (A.7)}$$

$$\therefore \quad \frac{d\, V\bar{y}}{d\, z} = K (y_i - \bar{y}) \quad \text{- - - - - (A.8) from (A.2)}$$

An overall mass balance across any section of the column gives:-

$$V\bar{y} - w_1 D_1 \frac{dc\bar{y}'}{d\, z} = L\bar{x} \quad \text{- - - - (A.9)}$$

where $\bar{x}$ is the mean mole fraction of the more volatile component in the liquid phase and where $\bar{y}'$ is defined by the equation:-

$$\bar{y}' = \int_0^{w_1} \frac{y_1\, d\, s}{w_1} \quad \text{- - - - - (A.10)}$$

and is assumed equal to $\bar{y}$.

Differentiating (A.9) and assuming that the second order longitudinal diffusion term is negligible compared with other terms.

$$\frac{dV\bar{y}}{dz} = \frac{dL\bar{x}}{dz} = K (y_i - \bar{y}) \quad \text{- - - - - (A.11), using (A.8)}$$

$\therefore$ Using (A.9)

$$L \frac{d\bar{x}}{dz} \cdot \frac{1}{K} = y_i - \frac{L\bar{x}}{V} - \frac{w_1}{V} \cdot D_1 \frac{dc\bar{y}}{dz}, \quad \text{assuming } \bar{y} = \bar{y}'$$

$$= y_i - \frac{L\bar{x}}{V} - \frac{w_1}{V} \cdot D_1 c \cdot \frac{L}{V} \cdot \frac{d\bar{x}}{dz} \quad \text{from (A.11)}$$

$\therefore$

$$V \frac{d\bar{x}}{dz} \cdot \frac{1}{K} = \frac{V}{L} \cdot y_i - \bar{x} - w_1 D_1 \frac{c}{V} \cdot \frac{d\bar{x}}{dz}$$

$$= \frac{V}{L} y_i - \bar{x} - \frac{D_1}{\bar{u}_1 c} \cdot \frac{d\bar{x}}{dz}$$

$\therefore$

$$\left(\frac{V}{K} + \frac{D_1}{\bar{u}_1} \right) \int_{\bar{x}_o}^{\bar{x}_1} \frac{d\bar{x}}{\frac{V}{L} y_i - \bar{x}} = \int_o^1 dz = 1$$

where $\bar{x}_o$ and $\bar{x}_1$ are the values of $\bar{x}$ at the bottom and the top of the column respectively.

i.e. the height of the column (1) = H.E.T.P. $\left(\frac{V}{K} + \frac{D_1}{\bar{u}_1} \right)$ X Number of theoretical plates, N, $\left(\int_{\bar{x}_o}^{\bar{x}_1} \frac{d\bar{x}}{\frac{V}{L} y_i - \bar{x}} \right)$ - - (A.12)

Equation (A.12) indicates very clearly the relationship between the column height and the height, H_1, and number, N, of theoretical plates in the vapour

phase. It also shows the merit in using Ruckenstein's (20) method of analysis in that the H.E.T.P. is given in terms of a mass transfer coefficient, K, i.e.

$$\text{H.E.T.P.} = \frac{V}{K} + \frac{D_1}{\bar{u}_1} \quad \text{- - - -} \quad \text{(A.13)}$$

Thus when K is no longer definable by equation (A.2), for example when vortices exist in the vapour phase, the appropriate value of K, derived theoretically or experimentally for the particular flow regime, may be substituted in equation (A.13)

If the longitudinal diffusion term $\frac{D_1}{\bar{u}_1}$ is ignored in (A.13), ($\frac{D_1}{\bar{u}_1}$ is usually $\ll \frac{V}{K}$ in most practical cases) then:-

$$\text{H.E.T.P.} = H_1 = \frac{V}{K} = \frac{V}{\frac{d\bar{vy}}{dz}\left(\frac{1}{y_i - \bar{y}}\right)} \qquad \text{from (A.8)}$$

$$= \frac{V}{D_1} \frac{\left(y_i - \bar{y}\right)}{\left(\frac{\partial cy}{\partial s}\right)_{s = w_1}} \qquad \text{from (A.4)}$$

$$= \frac{w_1 \bar{u}_1 \left(y_i - \bar{y}\right)}{D_1 \left(\frac{\partial y}{\partial s}\right)_{s = w_1}} \quad \text{- - - -} \quad \text{(A.14) using (A.5)}$$

Now from (A.1) :-

$$D_1 \frac{\partial^2 cy}{\partial s^2} = \frac{\partial (u_1 cy)}{\partial z} \qquad \text{ignoring longitudinal diffusion}$$

Integrating $$D_1 \frac{\partial y}{\partial s} = \int_o^s \frac{\partial y}{\partial z} \cdot u_1 ds \quad ------ \text{(A.15)}$$

and integrating once more:-

$$y = \frac{1}{D_1} \int_o^s \int_o^s \frac{\partial y}{\partial z} \cdot u_1 ds.ds$$

Now, by definition, $$\bar{y} = \int_o^{w_1} \frac{u_1 y ds}{w_1 \bar{u}_1}$$

$$\therefore \quad \bar{y} = \frac{1}{w_1 \bar{u}_1} \cdot \frac{\partial y}{\partial z} - \frac{1}{D_1} \int_o^{w_1} \left[\int_o^s \int_o^s u_1 ds.ds \right] u_1 ds \qquad \text{--- (A.16)}$$

if it is assumed that $\frac{\partial y}{\partial z}$ is not a function of s, as Ruckenstein (20) and Willingham et al (3) also assume.

From (A.1) also by integration:-

$$y_i = \frac{1}{D_1} \int_o^{w_1} \int_o^s \frac{\partial y}{\partial z} \cdot u_1 ds.ds$$

$$= \frac{\partial y}{\partial z} \cdot \frac{1}{D_1} \int_o^{w_1} \int_o^s u_1 \, ds.ds \quad ------ \text{(A.17)}$$

again assuming $\frac{\partial y}{\partial z}$ is independent of s.

Subtracting (A.16) from (A.17), and integrating (A.16) by parts

$$y_i - \bar{y} = \frac{\partial y}{\partial z} \cdot \frac{1}{D_1} \int_0^{w_1} \int_0^{s} u_1 \, ds\,ds - \frac{1}{w_1 \bar{u}_1} \cdot \frac{\partial y}{\partial z} \cdot \frac{1}{D_1} \left[\int_0^{w_1} \int_0^{s} u_1 \, ds.ds \right] \int_0^{w_1} u_1 ds$$

$$+ \frac{1}{w_1 \bar{u}_1} \cdot \frac{\partial y}{\partial z} \cdot \frac{1}{D_1} \int_0^{w_1} \left[\int_0^{s} u_1 \, ds. \int_0^{s} u_1 \, ds \right] ds$$

$$= \frac{\partial y}{\partial z} \cdot \frac{1}{D_1} \int_0^{w_1} \int_0^{s} u_1 ds.ds - \frac{1}{w_1 \bar{u}_1} \cdot \frac{\partial y}{\partial z} \cdot \frac{1}{D_1} \left[\int_0^{w_1} \int_0^{s} u_1 ds.ds \right] \int_0^{w_1} u_1 ds$$

$$+ \frac{1}{w_1 \bar{u}_1} \cdot \frac{\partial y}{\partial z} \cdot \frac{1}{D_1} \int_0^{w_1} \left[\int_0^{s} u_1 ds \int_0^{s} u_1 ds \right] ds$$

$$= \frac{\partial y}{\partial z} \cdot \frac{1}{D_1} \int_0^{w_1} \int_0^{s} u_1 \, ds.ds - \frac{\partial y}{\partial z} \cdot \frac{1}{D_1} \int_0^{w_1} \int_0^{s} u_1 ds.ds$$

$$+ \frac{1}{w_1 \bar{u}_1} \cdot \frac{\partial y}{\partial z} \cdot \frac{1}{D_1} \int_0^{w_1} \left[\int_0^{s} u_1 \, ds \right]^2 ds \, ,$$

since $\int_0^{w_1} u ds = \bar{u}_1 w_1$

$$\therefore\ y_i - \bar{y} = \frac{1}{w_1\ \bar{u}_1\ D_1} \cdot \frac{\partial y}{\partial z} \int_0^{w_1} \left[\int_0^{s} u_1\, ds \right]^2 ds \quad ---- \text{(A.18)}$$

From A.(14)

$$\text{H.E.T.P.} = H_1 = \frac{w_1 \bar{u}_1 (y_i - \bar{y})}{D_1 \left(\frac{\partial y}{\partial s}\right)_{s = w_1}}$$

$$= \frac{w_1 \cdot \bar{u}_1 \cdot \frac{1}{w_1\ \bar{u}_1\ D_1} \int_0^{w_1} \left[\int_0^{s} u_1\, ds \right]^2 ds}{D_1 \left(\frac{\partial y}{\partial s}\right)_{s = w_1}}$$

$$= \frac{\int_0^{w_1} \frac{1}{D_1} \left[\int_0^{s} u_1\, ds \right]^2 ds}{\int_0^{w_1} u_1\, ds}$$

since $D_1 \left(\frac{\partial y}{\partial s}\right)_{s = w_1} = \int_0^{w_1} \frac{\partial u_1 y}{\partial z} \cdot ds$ from (A.4)

$$= \frac{\partial y}{\partial z} \int_0^{w_1} u_1\, ds$$

$$\therefore\ H_1 = \frac{\int_0^{w_1} \frac{1}{D_1} \left[\int_0^{s} u_1\, ds \right]^2 ds}{\bar{u}_1\ w_1} \quad ---- \text{(2)}$$

---

and this is equation (2) for the vapour phase H.E.T.P. given in section 3.1

By using an identical method for the liquid phase it is possible to derive the analogous equation (3) :-

$$H_2 = \frac{\int_0^{w_2} \frac{1}{D_2} \left[\int_0^{t} u_2 \, dt \right]^2 dt}{\bar{u}_2 \, w_2} \quad - - - \quad (3)$$

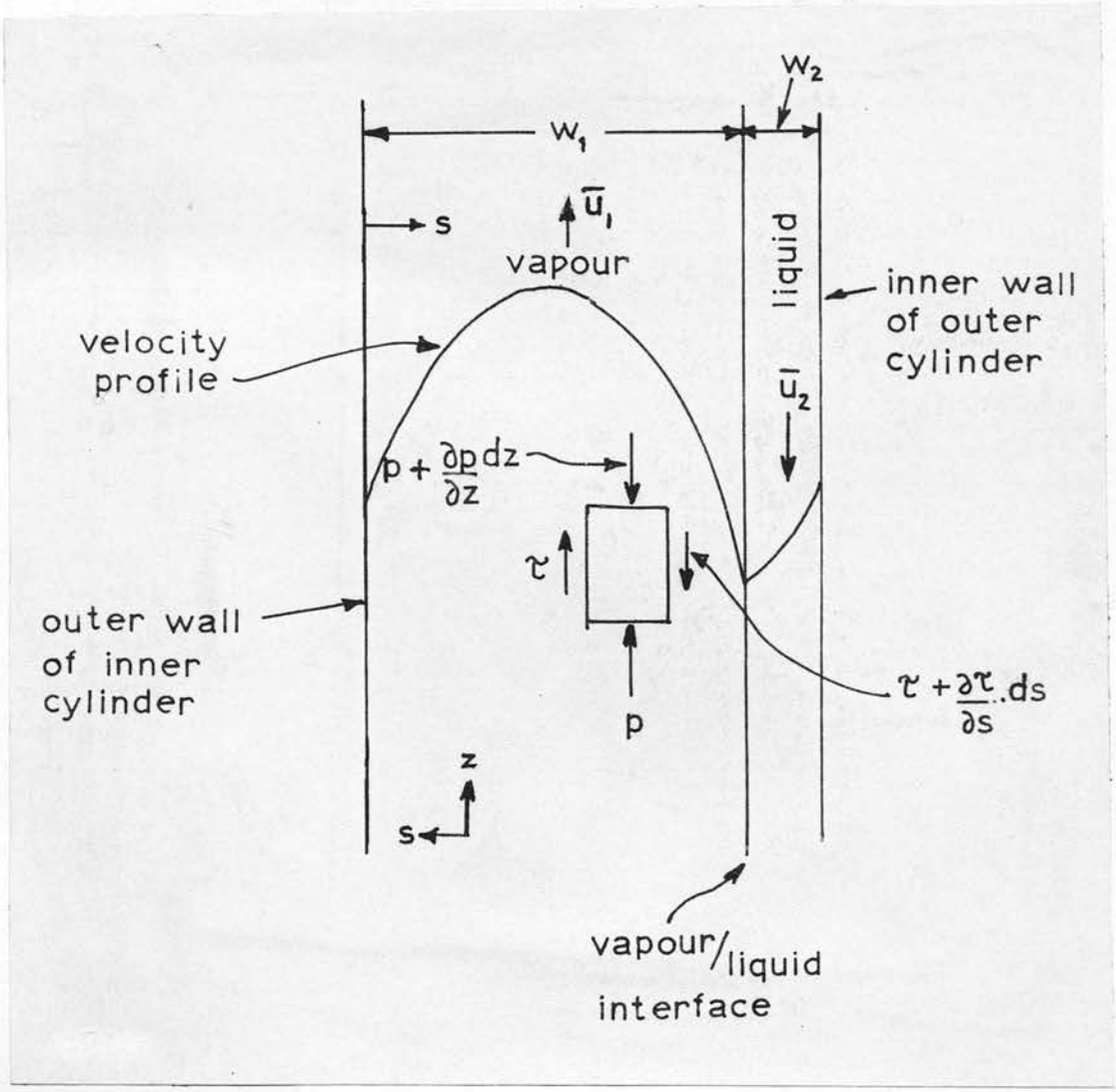

Figure 34. Forces acting on an element of the vapour phase

APPENDIX B

Derivation of H.E.T.P. for parallel plate system (laminar flow) allowing for vapour drag by reflux film

Equation (6) for the H.E.T.P. in the vapour phase will now be derived taking into account the effect of liquid surface velocity on vapour velocity profile, (but not vice-versa).

$$H_1 = \frac{\bar{u}_1 \, w_1^2}{140 \, D_1} \left[52 + 22\left(\frac{\bar{u}_2}{\bar{u}_1}\right) + 3\left(\frac{\bar{u}_2}{\bar{u}_1}\right)^2 \right] - - - \quad (6)$$

Figure 34 shows the forces acting on an element of the vapour phase.

τ represents shear stress and p pressure.

A momentum balance on the element gives, for unit depth:-

$$\frac{dp}{dz} \, dz.ds = \frac{\partial \tau}{\partial s} \, ds\,dz$$

$$\therefore \quad \tau = \int \frac{dp}{dz} \, ds + \gamma \qquad \text{where} \quad \gamma = \text{a constant}$$

$$= \frac{dp}{dz} \cdot s + \gamma$$

$$= -\frac{\mu_1 \partial u_1}{\partial s} \qquad \text{by definition}$$

Integrating

$$\therefore \quad -\mu_1 u_1 = \frac{dp}{dz} \cdot \frac{s^2}{2} + \gamma s + \beta \qquad - - - \text{(B.1)}$$

where β = constant

Boundary conditions

when $s = 0, u_1 = 0$

$s = w_1, u_1 = (u_2)_{w_2} = -\frac{3}{2}\bar{u}_2$, where $\bar{u}_2$ is the mean velocity of the falling reflux film, assumed to be laminar.

Using the first of these boundary conditions in (B.1)

$$-\mu_1 0 = \frac{dp}{dz} \cdot 0 + \gamma \cdot 0 + \beta$$

$$\therefore \beta = 0$$

Using the second boundary condition :-

$$+\frac{3}{2}\bar{u}_2\mu_1 = \frac{dp}{dz} \cdot \frac{w_1^2}{2} + \gamma \cdot w_1$$

$$\text{or} \quad \gamma = +\frac{3}{2}\frac{\mu_1 \bar{u}_2}{w_1} - \frac{dp}{dz} \cdot \frac{w_1}{2}$$

$$\therefore \mu_1 u_1 = -\frac{dp}{dz} \cdot \frac{s^2}{2} - \frac{3}{2}\frac{\mu_1 \bar{u}_2 s}{w_1} + \frac{dp}{dz} \cdot \frac{w_1 s}{2}$$

$$= \frac{dp}{dz}\left(\frac{w_1 s}{2} - \frac{s^2}{2}\right) - \frac{3}{2}\frac{\mu_1 \bar{u}_2 s}{w_1} \quad - - - \text{(B.2)}$$

But, by definition

$$\bar{u}_1 = \int_0^{w_1} \frac{u_1 ds}{w_1}$$

From (B.2)

$$\therefore\ \bar{u}_1 = \int_0^{w_1} \frac{1}{\mu_1} \frac{dp}{dz} \frac{1}{w_1} \left(\frac{w_1 s}{2} - \frac{s^2}{2} \right) ds - \int_0^{w_1} \frac{3}{2} \cdot \frac{\bar{u}_2}{w_1^2} \, s.ds$$

$$\therefore\ \bar{u}_1 = \frac{1}{\mu_1} \frac{dp}{dz} \left(\frac{w_1^2}{4} - \frac{w_1^2}{6} \right) - \frac{3}{4} \bar{u}_2$$

$$\text{or } \frac{dp}{dz} = \left(\bar{u}_1 + \frac{3}{4} \bar{u}_2 \right) \frac{\mu_1 . 12}{w_1^2} \quad \text{- - - - (B.3)}$$

Eliminating $\frac{dp}{dz}$ from (B.3) in (B.2)

$$\mu_1 u_1 = \left(\bar{u}_1 + \frac{3}{4} \bar{u}_2 \right) \left(\frac{12 \mu_1}{w_1^2} \right) \left(\frac{w_1 s}{2} - \frac{s^2}{2} \right) - \frac{3}{2} \frac{\mu_1 \bar{u}_2 s}{w_1}$$

$$\text{or } u_1 = \left(\bar{u}_1 + \frac{3}{4} \bar{u}_2 \right) \frac{6}{w_1^2} \left(w_1 s - s^2 \right) - \frac{3}{2} \frac{\bar{u}_2 s}{w_1} \quad \text{- - - (B.4)}$$

(B.4) is the equation for the velocity profile in the vapour phase, taking into account the reflux drag.

Now $H_1 = \dfrac{\displaystyle\int_0^{w_1} \frac{1}{D_1} \left[\int_0^{s} u_1 ds \right]^2 ds}{\bar{u}_1 w_1} \quad \text{- - - - (2)}$

Using (B.4)

$$\therefore H_1 = \frac{\int_0^{w_1} \frac{1}{D_1}\left[\int_0^{s}\left\{\left(\bar{u}_1 + \frac{3}{4}\bar{u}_2\right)\frac{6}{w_1^2}\left(w_1 s - s^2\right) - \frac{3}{2}\frac{\bar{u}_2 s}{w_1}\right\} ds\right]^2 ds}{\bar{u}_1 w_1}$$

$$= \frac{\int_0^{w_1} \frac{1}{D_1}\left[\left(\bar{u}_1 + \frac{3}{4}u_2\right)\frac{6}{w_1^2}\left(\frac{w_1 s^2}{2} - \frac{s^3}{3}\right) - \frac{3\bar{u}_2 s^2}{4 w_1}\right]^2 ds}{\bar{u}_1 w_1}$$

$$= \frac{\int_0^{w_1} \frac{1}{D_1}\left[\left(\bar{u}_1 + \frac{3}{4}\bar{u}_2\right)^2 \frac{36}{w_1^4}\left(\frac{w_1^2 s^4}{4} - \frac{w_1 s^5}{3} + \frac{s^6}{9}\right) - \frac{3}{2}\frac{\bar{u}_2 s^2}{w_1}\left(\bar{u}_1 + \frac{3}{4}\bar{u}_2\right)\frac{6}{w_1^2}\left(\frac{w_1 s^2}{2} - \frac{s^3}{3}\right) + \frac{9}{16}\frac{\bar{u}_2^2 s^4}{w_1^2}\right] ds}{\bar{u}_1 w_1}$$

$$= \frac{1}{D_1 \bar{u}_1 w_1}\left[\left(\bar{u}_1 + \frac{3}{4}\bar{u}_2\right)^2 \frac{36}{w_1^4}\left(\frac{w_1^7}{20} - \frac{w_1^7}{18} + \frac{w_1^7}{63}\right) - \frac{3\bar{u}_2}{2 w_1}\left(\bar{u}_1 + \frac{3}{4}\bar{u}_2\right)\frac{6}{w_1^2}\left(\frac{w_1^6}{10} - \frac{w_1^6}{18}\right) + \frac{9}{16}\frac{\bar{u}_2^2}{w_1^2}\cdot\frac{w^5}{5}\right]$$

$$\therefore H_1 = \frac{w_1^3}{D_1 \bar{u}_1 w_1} \left[\left(\bar{u}_1^2 + \frac{3}{2} \bar{u}_1 \bar{u}_2 + \frac{9}{16} \bar{u}_2^2 \right) \frac{52}{140} - \bar{u}_2 \left(\bar{u}_1 + \frac{3}{4} \bar{u}_2 \right) \frac{2}{5} + \frac{9}{80} \bar{u}_2^2 \right]$$

$$= \frac{w_1^2}{D_1 \bar{u}_1} \left[\frac{52}{140} \bar{u}_1^2 + \frac{22}{140} \bar{u}_1 \bar{u}_2 + \frac{3}{140} \bar{u}_2^2 \right]$$

Hence:-

$$H_1 = \frac{w_1^2 \bar{u}_1}{140 D_1} \left[52 + 22 \left(\frac{\bar{u}_2}{\bar{u}_1} \right) + 3 \left(\frac{\bar{u}_2}{\bar{u}_1} \right)^2 \right] \quad - - - - - (6)$$ which is

the form of H_1 given by Willingham et al (3)

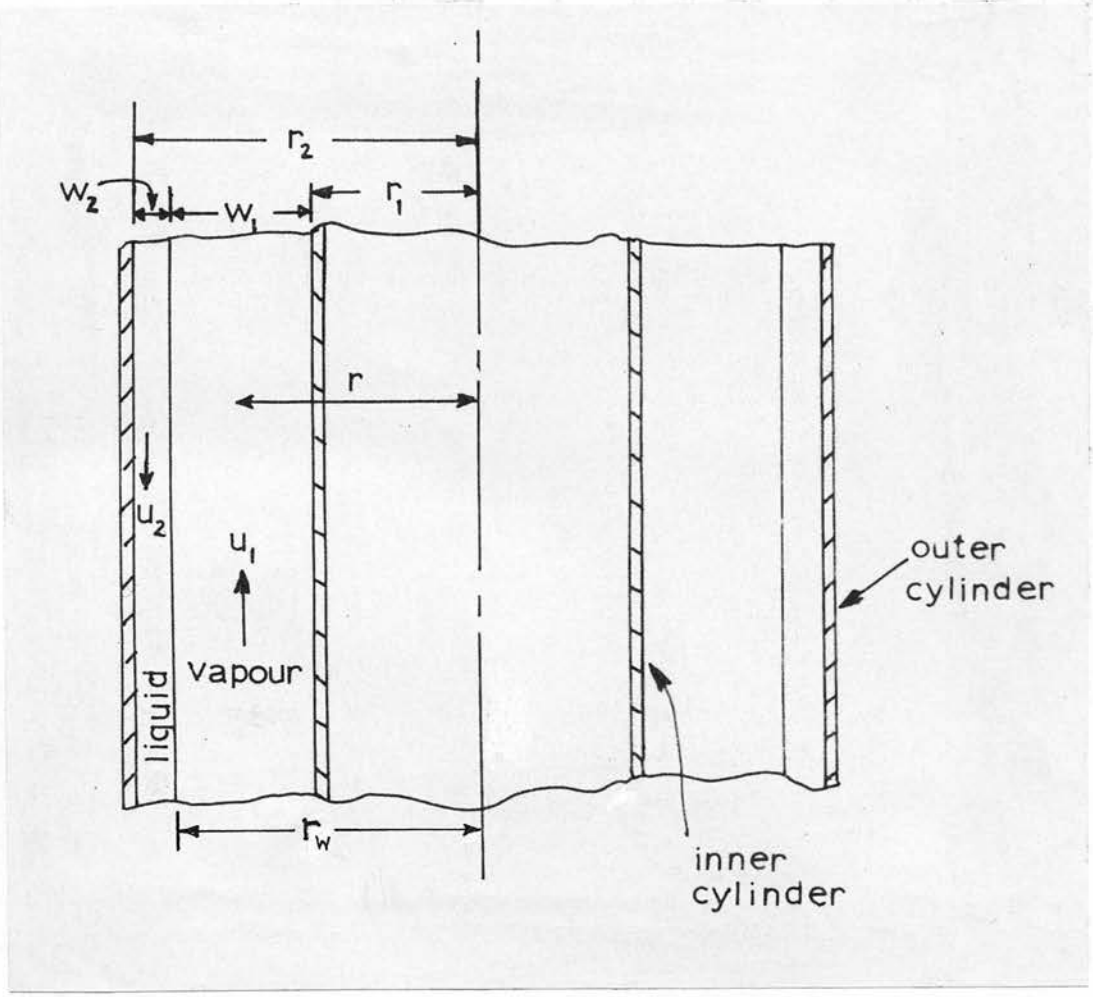

Figure 35. Concentric cylinder system

APPENDIX C

Derivation of H.E.T.P. for concentric tube column - laminar flow

An outline is given here of the derivation of the H.E.T.P. for a concentric tube column with the outer cylinder only wetted by reflux. This analysis applies to columns with annular gap widths large enough to invalidate the parallel plate approximations made in section 3.

Figure 35 shows the concentric cylinder system in which the rotating inner cylinder has radius r_1, the stationary outer cylinder radius r_2 and reflux of thickness w_2 flows down the outer cylinder wall. The remaining distances are measured as shown.

The vapour velocity profile used is given by Lamb (42)

$$u_1 = \frac{dp}{dz} \cdot \frac{1}{4\mu_1} \left[r_w^2 - r^2 + \frac{r_1^2 - r_w^2}{\ln \frac{r_1}{r_w}} \ln \frac{r}{r_w} \right]$$

where $\frac{dp}{dz}$ is the axial pressure gradient

Hence it is possible to obtain an equation for the point velocity, u_1, in the form

$$u_1 = U_1 \frac{\left\{ r_w^2 - r^2 + 2r_{max}^2 \ln \frac{r}{r_w} \right\}}{\left\{ r_w^2 - r_{max}^2 + 2r_{max}^2 \ln \frac{r_{max}}{r_w} \right\}}$$

where U_1 is the maximum point velocity which can be shown equal to:

$\frac{dp}{dz} \cdot \frac{1}{4\mu_1}\left\{ r_w^2 - r_{max}^2 + 2r_{max}^2 \ln \frac{r_{max}}{r_w} \right\}$ and r_{max} is the radius at

which the maximum velocity occurs and is given by:-

$$r_{max}^2 = \frac{r_1^2 - r_w^2}{2\ln \frac{r_1}{r_w}}$$

Proceeding exactly as in Appendix A and starting with a mass balance on an element of the vapour phase:-

$$D_1 \frac{\partial\left(\frac{r\ \partial cy}{\partial r}\right)}{\partial r} + rD_1 \frac{\partial^2 cy}{\partial z^2} = r\frac{\partial u_1 cy}{\partial z}$$

it is possible to derive an equation, similar to (A.12) of the form:-

$$l = \text{H.E.T.P.} \left[\frac{\bar{u}_1 c \left(r_w^2 - r_1^2 \right)}{2\ K\ r_w} + \frac{D_1}{\bar{u}_1} \right] \text{x Number of theoretical plates,} \left[\int_{\bar{x}_o}^{\bar{x}_1} \frac{d\bar{x}}{y_i - \bar{x}} \right] \text{- - -} \quad \text{(C.1)}$$

<u>N.B.</u> If $r_w \doteqdot r_1$ equation (C.1) reduces to (A.12)

i.e. $\frac{\bar{u}_1\ c\ (r_w^2 - r_1^2)}{2\ K\ r_w} \rightarrow \frac{\bar{u}_1\ c\ (r_w - r_1)\ 2\ r_w}{K.\ 2r_w} = \frac{V}{K}$

Proceeding again exactly as shown in Appendix A, it is finally possible to

obtain an expression for H_1 of the form

$$H_1 = \frac{\bar{u}_1 (r_w^2 - r_1^2) B}{2D_1 E^2} \quad ----- \quad (C.2)$$

where

$$B = \int_{r_1}^{r_w} \left\{ \frac{r_w^4 r^3}{4} - \frac{r_w^2 r^5}{16} + r_w^2 r . r_{max}^2 \left(\ln \frac{r}{r_w} . \frac{r^2}{2} - \frac{r^2}{4} \right) - r_w^2 . r_{max}^2 \frac{r^3}{4} - \right.$$

$$- r_w^2 r . (M) \ln r - r_w^2 . r . (J) - \frac{r_w^2 r^5}{4} + \frac{r^7}{16} - r^3 r_{max}^2 \left(\ln \frac{r}{r_w} . \frac{r^2}{2} - \frac{r^2}{4} \right)$$

$$+ \frac{r^5 . r_{max}^2}{4} + r^3 . (M) \ln r + (J) r^3 + 2r^3 r_{max}^2 \ln \frac{r}{r_w} . \frac{r_w^2}{4}$$

$$- \frac{2r^5}{16} . r_{max}^2 . \ln \frac{r}{r_w} + 2r . r_{max}^4 \ln \frac{r}{r_w} \left(\ln \frac{r}{r_w} . \frac{r^2}{2} - \frac{r^2}{4} \right) - \frac{r^3}{2} . r_{max}^4 \ln \frac{r}{r_w}$$

$$\left. - 2r . r_{max}^2 . \ln \frac{r}{r_w} . M \ln r - 2r . r_{max}^2 \ln \frac{r}{r_w} . (J) \right\} dr \quad ---- \quad (C.3)$$

and

$$J = \left\{ \frac{3}{16} r_w^4 - \frac{r_{max}^2 r_w^2}{2} - M \ln r_w \right\} \quad ---- \quad (C.4)$$

$$\text{and } M = \left\{ \frac{r_w^2 r_1^2}{2} - \frac{r_1^4}{4} + 2r_{max}^2 \left(\ln \frac{r_1}{r_w} \cdot \frac{r_1^2}{2} - \frac{r_1^2}{4} \right) \right\} \quad \text{(C.5)}$$

$$\text{and } E = \left\{ \frac{r_w^4}{4} - \frac{r_w^2 \cdot r_{max}^2}{2} - \frac{r_w^2 \cdot r_1^2}{2} + \frac{r_1^4}{4} - 2r_{max}^2 \ln \frac{r_1}{r_w} \cdot \frac{r_1^2}{2} + \frac{r_1^2 r_{max}^2}{2} \right\} \quad \text{(C.6)}$$

The evaluation of (C.2) is tedious and probably necessitates the use of a computer since the definite integral B is not easily evaluated.

APPENDIX D

Derivation of H.E.T.P. for circumferentially turbulent flow

Equation (44) will now be derived.

For circumferentially turbulent flow of vapour and very low axial flow rates, by analogy with the Dittus - Boelter equation for heat transfer in a tube, a mass transfer coefficient, k_t', is given approximately by:-

$$\frac{k_t' \cdot w_1}{D_1} \doteq m \times Re_c^{0.8} \cdot Sc^{0.4} \quad ---- (D.1)$$

assuming that shearing flow is the same as pressure flow as far as turbulent heat or mass transfer is concerned, and where m is a numerical constant.

As shown in Appendix A, for laminar flow, the H.E.T.P. is given by an equation of the form:-

$$(H_1)_{laminar} = \frac{\bar{u}_1 w_1 c}{K} \quad ----- (D.2)$$

for one wall wetted by reflux and neglecting longitudinal diffusion. For a turbulent regime it is reasonable to write:-

$$(H_1)_{turbulent} = \frac{\bar{u}_1 w_1}{k_t'}$$

$$= \frac{\bar{u}_1 w_1^2}{m. Re_c^{0.8} Sc^{0.4} D_1}$$

$$\therefore \quad (H_1)_{turbulent} = \frac{w_1 Re_a \cdot Sc^{0.6}}{2 m. Re_c^{0.8}} \quad ---- (44)$$

TABLE I

Calculated theoretical values - laminar flow equation (10)

Column of Willingham et al (3). Values of N per meter length. Annular gap width, 0.109 cm. Molecular diffusion coefficient in vapour phase $D_1 = 0.041$ cm^2/sec (3)

Q cc/hr	w_2 cm	w_1 cm	$\bar{u}_1$ cm/sec	N per meter length (10)
1000	0.0053	0.1037	21.29	48.2
1500	0.0060	0.1030	32.16	32.4
2000	0.0064	0.1026	43.04	24.4
2500	0.0071	0.1019	54.19	19.7
3000	0.0076	0.1014	65.33	16.5
3500	0.0080	0.1010	76.52	14.2
4000	0.0083	0.1007	87.74	12.4

TABLE II

Calculated theoretical values - vortex flow

Values of N per meter length and N per 66 cms according to equation (36)

$$N = 0.9\left(\frac{1}{w_1}\right)\left(\frac{w_1}{r_1}\right)^{\frac{1}{4}} \frac{Re_c^{\frac{1}{2}}}{Re_a \cdot Sc}$$

Column of Willingham et al (3)

$w_1 = 0.1$ cm; $\left(\frac{w_1}{r_1}\right)^{\frac{1}{4}} = 0.405$; Sc = 0.747, using data in (3)

Q cc/hr	Re_a	n rpm	Re_c	$Re_c^{\frac{1}{2}}$	Calculated N per meter (36)	Actual N per meter	Calculated N per 66 cms (36)	Actual N per 66 cms
1000	139.2	1750	2230	47.2	165.6	30	110.0	19.6
1500	210.3	1750	2230	47.2	109.8	20	72.5	13.2
2000	281.6	1750	2230	47.2	79.2	16	52.3	10.5
1000	139.2	2000	2545	50.4	176.9	40	116.7	27.7
1500	210.3	2000	2545	50.4	117.1	23	77.2	17.8
2000	281.6	2000	2545	50.4	87.6	20	57.8	14.5
1000	139.2	2300	2930	54.1	190.0	42	125.2	26.4
1500	210.3	2300	2930	54.1	125.8	27	82.8	15.2
2000	281.6	2300	2930	54.1	93.9	22	62.0	13.2

TABLE III

Calculated theoretical values - vortex flow

Values of N per meter length and N per 66 cms according to equation (39)

$$N = 0.66 \left(\frac{1}{w_1}\right)\left(\frac{w_1}{r_1}\right)^{\frac{1}{4}} \frac{Re_c^{\frac{1}{2}}}{Re_a \cdot Sc}$$

Column of Willingham et al (3)

Q cc/hr	Re_a	n rpm	Re_c	$Re_c^{\frac{1}{2}}$	Calculated N per meter (36)	Actual N per meter	Calculated N per 66 cms (39)	Actual N per 66 cms
1000	139.2	1750	2230	47.2	121.3	30	80.7	19.6
1500	210.3	1750	2230	47.2	80.6	20	53.2	13.2
2000	281.6	1750	2230	47.2	58.1	16	38.3	10.5
1000	139.2	2000	2545	50.4	129.8	40	85.6	27.7
1500	210.3	2000	2545	50.4	85.9	23	56.6	17.8
2000	281.6	2000	2545	50.4	64.2	20	42.4	14.5
1000	139.2	2300	2930	54.1	139.3	42	91.7	26.4
1500	210.3	2300	2930	54.1	92.3	27	60.7	15.2
2000	281.6	2300	2930	54.1	68.9	22	45.5	13.2

TABLE IV

Calculated theoretical values - vortex flow

Values of N calculated according to equation (43)

$$N = 0.1283 \left(\frac{1}{r_1}\right) \frac{1}{Re_a} \cdot \frac{1}{Sc^{0.644}} \left(\frac{r_1^2 \Omega_1}{\nu}\right)^{0.7}$$

Column of Willingham et al (3)

Q cc/hr	Re_a	n rpm	$r_1^2 \Omega_1/\nu$	$(r_1^2 \Omega_1/\nu)^{0.7}$	Calculated N per meter length	Actual N per meter length	Calculated N per 66 cms	Actual N per 66 cms
1000	139.2	1750	83000	2776	81.1	30	53.6	19.6
1500	210.3	1750	83000	2776	53.6	20	35.4	13.2
2000	281.6	1750	83000	2776	40.1	16	26.4	10.5
1000	139.2	2000	94700	3044	89.1	40	58.8	26.4
1500	210.3	2000	94700	3044	58.8	23	38.8	15.2
2000	281.6	2000	94700	3044	43.9	20	28.9	13.2
1000	139.2	2300	109000	3359	98.4	42	64.9	27.7
1500	210.3	2300	109000	3359	64.9	27	42.9	17.8
2000	281.6	2300	109000	3359	48.5	22	32.0	14.5

TABLE V

Experimental results - distillation

2.60 cm diameter glass inner cylinder. Height of fractionation section = 66.0 cms.

Annular gap width, b = 0.1 cm. b/r_m = 0.074

Boil-up rate cc/hr	Speed of rotation of inner cylinder r.p.m.	Still-pot refractive index at 20°C n_D^{20}	Condensate refractive index at 20°C n_D^{20}	Number of theoretical plates N in 66 cms.
190	0	1.4187	1.3934	53.0
257	0	1.4159	1.3939	42.7
305	0	1.4156	1.3999	28.9
364	0	1.4143	1.4021	21.8
366	0	1.4142	1.4034	19.5
477	0	1.4142	1.4070	13.6
477	0	1.4134	1.4042	16.3
821	0	1.4142	1.4113	6.1
518	111	1.4141	1.4022	21.2
520	120	1.4140	1.4009	23.3
565	127	1.4140	1.4002	24.6
566	133	1.4140	1.3998	25.2
539	135	1.4138	1.3989	26.6
253	140	1.4147	1.3917	47.1
424	142	1.4147	1.3963	34.0
390	142	1.4150	1.3959	35.5

Table V (continued)

2.60 cm. diameter glass inner cylinder. Height of fractionating section = 66.0 cms

Annular gap width b = 0.1 cm. b/r_m = 0.074

Boil-up rate cc/hr	Speed of rotation of inner cylinder r.p.m	Still-pot refractive index at 20°C n_D^{20}	Condensate refractive index at 20°C n_D^{20}	Number of theoretical plates N in 66 cms.	Remarks
578	150	1.4133	1.3997	24.1	
222	167	1.4147	1.3908	51.8	
222	167	1.4151	1.3896	60.6	
356	210	1.4163	1.3968	36.5	
578	210	1.4132	1.4011	21.4	
401	211	1.4133	1.3959	31.8	
415	214	1.4128	1.3967	28.9	
262	214	1.4132	1.3924	41.3	
317	215	1.4163	1.3953	40.0	
370	215	1.4160	1.3969	35.8	
576	300	1.4133	1.4019	20.1	
581	82	1.4131	1.4020	19.4	String attached
260	89	1.4148	1.3928	43.5	to inner
496	95	1.4120	1.3980	24.4	cylinder
336	101	1.4132	1.3992	24.9	
293	108	1.4156	1.3965	35.7	
321	113	1.4155	1.3964	35.7	
344	130	1.4131	1.3991	24.7	
373	130	1.4168	1.4029	26.8	
531	130	1.4111	1.3983	22.1	
403	1110	1.4161	1.4056	20.3	

TABLE VI

Experimental results - distillation

2.40 cm. diameter glass inner cylinder. Height of fractionation section = 66.0 cms.
Annular gap width, b = 0.2 cms. b/r_m = 0.154

Boil-up rate cc/hr	Speed of rotation of inner cylinder r.p.m	Still-pot refractive index at 20°C n_D^{20}	Condensate refractive index at 20°C n_D^{20}	Number of theoretical plates N in 66 cms	Remarks
203	0	1.4184	1.3950	47.0	
231	0	1.4171	1.3982	35.8	
248	0	1.4144	1.3963	33.3	
272	0	1.4156	1.3982	31.9	
319	0	1.4149	1.4001	26.9	
385	0	1.4149	1.4030	21.4	
465		1.4121	1.4027	16.1	
549	0	1.4139	1.4087	10.1	
704	0	1.4144	1.4108	7.5	
840	0	1.4139	1.4108	6.6	
207	1510	1.4163	1.3935	44.7	
309	1510	1.4158	1.3954	38.4	
432	1510	1.4149	1.3988	29.0	
504	1510	1.4149	1.4013	24.6	
617	1510	1.4157	1.4055	19.4	
185	1540	1.4171	1.4033	26.3	
206	1540	1.4168	1.3929	48.0	
531	1820	1.4130	1.4012	20.7	
339	1850	1.4156	1.3953	38.3	
200	1860	1.4188	1.3951	48.6	
216	1860	1.4146	1.3927	42.9	
291	1860	1.4147	1.4000	26.6	
373	1860	1.4122	1.3972	26.7	
383	1860	1.4133	1.3978	27.4	
530	2030	1.4111	1.4000	19.0	Noticed that
409	2050	1.4111	1.3959	27.4	drip rate from
351	2060	1.4106	1.3965	25.1	condenser tip
388	2060	1.4102	1.3955	26.6	was greater at these speeds of

Table VI continued

Boil-up rate cc/hr	Speed of rotation of inner cylinder r.p.m.	Still-pot refractive index at 20°C n_D^{20}	Condensate refractive index at 20°C n_D^{20}	Number of theoretical plates N in 66 cms	Remarks
187	2070	1.4163	1.3960	38.4	rotation than at
193	2070	1.4173	1.3998	33.5	lower speeds for
202	2070	1.4173	1.4018	29.8	similar boil-up rates
352	325	1.4163	1.3960	38.3	String attached
644	370	1.4128	1.4067	11.1	to inner cylinder
280	375	1.4140	1.3908	50.0	for all results
404	390	1.4136	1.3975	29.0	tabulated
466	400	1.4122	1.4000	21.2	hereafter
458	436	1.4137	1.4032	18.6	
466	455	1.4129	1.4017	19.6	
275	460	1.4121	1.3905	47.7	
452	460	1.4119	1.3975	25.4	
248	490	1.4142	1.3928	41.9	
704	490	1.4122	1.4032	15.4	
265	500	1.4157	1.3925	46.5	
153	1000	1.4150	1.3914	49.2	
200	1000	1.4145	1.3904	53.4	
263	1000	1.4122	1.3900	51.0	
283	1000	1.4121	1.3931	36.7	
297	1000	1.4114	1.3921	38.7	
297	1000	1.4112	1.3932	34.7	
404	1000	1.4121	1.3948	31.8	
492	1000	1.4132	1.4000	23.3	
720	1000	1.4122	1.4029	15.8	
275	1400	1.4115	1.3918	40.2	
451	1400	1.4109	1.3959	27.0	
270	1485	1.4118	1.3928	37.1	
297	1525	1.4099	1.3921	35.8	
312	1560	1.4149	1.3978	30.9	
297	1700	1.4117	1.3915	41.7	
215	1780	1.4140	1.3900	54.9	
452	1780	1.4130	1.3962	30.6	
666	1780	1.4129	1.4002	22.5	
291	1790	1.4129	1.3922	41.4	
550	1790	1.4135	1.3978	28.0	
231	1800	1.4129	1.3890	60.0	
259	1810	1.4129	1.3895	57.0	

Table VI continued

Boil-up rate cc/hr	Speed of rotation of inner cylinder r.p.m.	Still-pot refractive index n_{20}^{D}	Condensate refractive index n_{20}^{D}	Number of theoretical plates N in 66 cms.	Remarks
432	1940	1.4143	1.3980	29.2	
309	1960	1.4147	1.3930	42.6	
486	1970	1.4137	1.3992	25.8	
521	1970	1.4137	1.3990	26.2	
409	2030	1.4149	1.3951	37.0	
496	2030	1.4144	1.3978	29.9	
231	2090	1.4159	1.3900	59.4	
183	2450	1.4159	1.3900	59.4	
235	2450	1.4159	1.3900	59.4	
365	2450	1.4165	1.3941	43.7	
512	2450	1.4169	1.4042	24.5	
644	2450	1.4173	1.4068	21.5	

TABLE VII

Experimental results - distillation

2.14 cm. diameter copper inner cylinder. Height of fractionating section = 61.0 cms.

Annular gap width = 0.33 cms. $b/r_m = 0.267$

Boil-up rate cc/hr	Speed of rotation of inner cylinder r.p.m.	Still-pot refractive index at 20°C $n_{D\ 20}$	Condensate refractive index at 20°C $n_{D\ 20}$	Number of theoretical plates N in 66 cms.	Remarks
249	0	1.4140	1.4042	19.1	
251	0	1.4140	1.4042	19.0	
259	0	1.4135	1.4034	19.4	
361	0	1.4140	1.4048	18.1	
373	0	1.4135	1.4041	18.1	
375	0	1.4140	1.4046	18.4	
496	0	1.4151	1.4085	14.2	
618	0	1.4140	1.4078	12.7	
756	0	1.4135	1.4094	8.7	
627	0	1.4152	1.4110	9.5	
730	0	1.4158	1.4122	8.4	
549	143	1.4144	1.4037	20.9	Inner cylinder
356	158	1.4141	1.4002	26.8	appeared wet
345	167	1.4141	1.3998	27.5	" "
356	167	1.4141	1.3998	27.5	" "
480	300	1.4162	1.4061	21.3	" "
514	310	1.4150	1.4038	22.2	" "
811	452	1.4140	1.4078	12.7	
457	472	1.4146	1.4032	22.1	
514	472	1.4150	1.4031	23.4	
313	495	1.4141	1.3994	28.5	
333	495	1.4141	1.3992	28.9	
636	505	1.4150	1.4068	17.1	
627	560	1.4142	1.4062	16.1	
627	685	1.4139	1.4061	15.8	
514	690	1.4150	1.4063	17.9	
345	710	1.4142	1.4062	16.1	
351	716	1.4142	1.4062	16.1	
234	735	1.4140	1.4062	15.6	Inner cylinder
395	750	1.4140	1.4060	15.9	appeared dry
480	750	1.4140	1.4060	15.9	" "
"Umbrella" fitted for all results tabulated hereafter					
343	310	1.4139	1.3993	28.2	Inner cylinder
417	310	1.4141	1.4022	22.8	appeared wet
565	310	1.4139	1.4063	15.3	" "
778	310	1.4140	1.4088	10.9	" "
722	688	1.4142	1.4072	14.3	
465	690	1.4147	1.4062	17.3	
671	692	1.4146	1.4072	15.2	
217	750	1.4142	1.4080	12.8	
227	750	1.4141	1.4080	12.4	

Table VII continued

Boil-up rate cc/hr	Speed of rotation of inner cylinder r.p.m.	Still-pot refractive index at 20°C n^{D}_{20}	Condensate refractive index at 20°C n^{D}_{20}	Number of theoretical plates N in 66 cms.	Remarks
385	750	1.4142	1.4072	14.2	
192	760	1.4142	1.4069	14.8	
238	925	1.4139	1.4017	23.8	
252	925	1.4141	1.4008	25.8	
257	925	1.4141	1.3994	28.6	
279	925	1.4141	1.4010	25.3	
363	925	1.4141	1.3998	27.6	
426	925	1.4144	1.4018	24.8	
650	925	1.4141	1.4061	16.1	
724	930	1.4141	1.4061	16.1	
265	1100	1.4139	1.3966	34.3	
393	1110	1.4140	1.3972	32.8	
466	1130	1.4165	1.4039	25.9	
739	1130	1.4139	1.4044	18.5	
593	1140	1.4141	1.4022	22.9	
358	1160	1.4144	1.3968	34.8	
521	1170	1.4143	1.4021	23.8	
331	1450	1.4155	1.3974	36.4	
388	1450	1.4153	1.3987	32.8	
560	1450	1.4152	1.4033	23.7	
593	1450	1.4160	1.4060	21.1	
630	1450	1.4163	1.4056	22.3	
672	1450	1.4162	1.4071	19.4	
756	1450	1.4162	1.4081	17.4	
817	1450	1.4155	1.4079	16.1	
233	1820	1.4158	1.3938	46.3	
560	1830	1.4147	1.4020	24.8	
598	1830	1.4141	1.4022	22.9	
286	1840	1.4158	1.3938	46.3	
364	1840	1.4160	1.3990	34.2	
472	1840	1.4130	1.3997	25.3	
269	1860	1.4149	1.3941	43.1	
687	1860	1.4149	1.4049	19.8	
720	1860	1.4148	1.4052	19.3	
426	2110	1.4131	1.3972	30.6	
554	2150	1.4135	1.4008	24.4	

TABLE VIII

Critical Taylor numbers for finite axial flow rates

Smoke experiments with copper inner cylinder 2.14 cms. diameter. b/r_m for system equals 0.267. ^cTa = critical Taylor number for vortex formation

Copper cylinder speed r.p.m	Rotameter reading R 7	Air flow rate l/m	Air velocity $\bar{u}$ cm/sec	Ω_c	Re_a	^cTa
420	5.0	2.1	13.63	44.0	59.6	61.4
580	6.0	2.37	15.4	60.7	67.4	84.6
620	6.0	2.37	15.4	65.0	67.4	90.6
730	10.6	3.74	24.3	76.5	106.2	106.7

From Table VIII, shown above, at $Re_a = 106.2$; $^cTa = 106.7$

By definition, $$Ta = \frac{\Omega r_m^{\frac{1}{2}} b^{\frac{3}{2}}}{\nu}$$

$\therefore$ at a critical Taylor number given by $^cTa = 106.7$, for the distillation experiments with the copper inner cylinder :-

$$106.7 = \Omega_c \cdot \frac{(1.235)^{\frac{1}{2}} (0.33)^{\frac{3}{2}}}{(0.0212)},$$

where Ω_c = critical angular velocity for copper inner cylinder when distillation takes place with a boil-up rate giving a value for the axial Reynolds number, Re_a, of 106.2. Now the boil-up rate corresponding to $Re_a = 106.2$ is approximately 160 cc/hr (see Table XI).

$$\therefore \Omega_c \doteq \frac{106.7 \times 0.0212}{1.112 \times 0.19} \doteq 10.7$$

or critical rpm $\doteq 10.7 \times \frac{60}{2} \doteq 102$ rpm

Thus vortices should begin to form at speeds of rotation, of the inner copper cylinder, exceeding 100 rpm at a boil-up rate of approximately 160 cc/hr

TABLE IX

Calculated theoretical values - laminar flow equations (10) and (12)

2.60 cm. diameter glass inner cylinder. Height of fractionating section = 66.0 cms. Annular gap width = 0.1 cms. Molecular diffusion coefficient in vapour phase, D_1 = 0.037 cm^2/ sec.

Q cc/hr	Re_a	w_2 cm.	w_1 cm.	ψ cm^2	$\bar{u}_1$ cm/sec	N per 66 cms (10) "one wall wetted"	N per 66 cms (12) "both walls wetted"
120	77	0.0036	0.0964	0.817	8.17	86.6	265.0
225	146	0.0045	0.0955	0.809	15.45	46.6	142.4
325	212	0.0050	0.0950	0.805	22.41	32.5	99.3
430	276	0.0055	0.0945	0.801	29.30	25.1	76.7
530	349	0.0059	0.0941	0.796	37.01	20.1	61.4
640	423	0.0063	0.0937	0.793	44.85	16.7	51.1
700	464	0.0065	0.0935	0.791	49.20	15.8	48.3
780	519	0.0067	0.0933	0.790	54.90	13.8	42.2

TABLE X

Calculated theoretical values - laminar flow equations (10) and (12)

2.40 cm. diameter glass inner cylinder. Height of fractionating section = 66.0 cm. Annular gap width = 0.2 cm. Molecular diffusion coefficient in vapour phase, D_1 = 0.037 cm^2/sec

120	79	0.0036	0.1964	1.602	4.16	41.0	125.2
225	148	0.0045	0.1955	1.595	7.83	21.9	67.0
325	214	0.0050	0.1950	1.592	11.32	15.3	46.8
430	284	0.0055	0.1945	1.585	15.05	11.6	35.5
530	352	0.0059	0.1941	1.581	18.62	9.4	28.7
640	425	0.0063	0.1937	1.579	22.50	7.8	23.8
700	466	0.0065	0.1935	1.578	24.63	7.1	21.7
780	518	0.0067	0.1933	1.576	27.48	6.4	19.6

TABLE XI

Calculated theoretical values - laminar flow equations (10) and (12)

2.14 cm. diameter copper inner cylinder. Height of fractionating section = 61.0 cm. Annular gap width = 0.33 cm. Molecular diffusion coefficient, D_1 = 0.037 cm^2/sec.

120	82	0.0036	0.3264	2.529	2.63	23.5	71.8
225	154	0.0045	0.3255	2.521	4.96	12.6	38.3
325	223	0.0050	0.3250	2.519	7.17	8.7	26.6
430	296	0.0055	0.3245	2.511	9.51	6.6	20.1
530	366	0.0059	0.3241	2.509	11.73	5.3	16.3
640	441	0.0063	0.3237	2.508	14.14	4.4	13.6
700	482	0.0065	0.3235	2.505	15.50	4.1	12.4
780	539	0.0067	0.3233	2.502	17.30	3.7	11.2

TABLE XII

Calculated theoretical values - vortex flow

Values of N per 66 cms. calculated according to equations (36) and (39)

2.40 cm. diameter glass inner cylinder

$\left(\frac{1}{w_1}\right) = 338.5$; $\left(\frac{w_1}{r_1}\right)^{\frac{1}{4}} = 0.635$; Sc = 0.573 (24)

Q cc/hr	Re_a	n r.p.m	Re_c	$Re_c^{\frac{1}{2}}$	Calculated N per 66 cms (36)	Calculated N per 66 cms (39)
325	214	400	461	21.5	33.9	24.9
430	284	400	461	21.5	25.5	18.7
640	425	400	461	21.5	17.1	12.5
780	518	400	461	21.5	14.0	10.3
325	214	1000	1153	34.0	53.7	39.4
430	284	1000	1153	34.0	40.4	29.5
640	425	1000	1153	34.0	27.0	19.8
780	518	1000	1153	34.0	22.2	16.3
325	214	2000	2306	48.0	75.7	55.6
430	284	2000	2306	48.0	57.1	41.8
640	425	2000	2306	48.0	38.2	28.0
780	518	2000	2306	48.0	31.3	23.0

TABLE XIII

Calculated theoretical values - vortex flow

Values of N/66 cms. calculated according to equation (43)

2.40 cm. diameter glass inner cylinder.

Q cc/hr	Re_a	n r.p.m	$r_1^2 \Omega_{1/\gamma}$	$\left(r_1^2 \Omega_{1/\gamma}\right)^{0.7}$	Calculated N per 66 cm.
325	214	400	2840	267.5	12.6
430	284	400	2840	267.5	9.5
640	425	400	2840	267.5	6.4
780	518	400	2840	267.5	5.2
325	214	1000	7100	496.5	23.4
430	284	1000	7100	496.5	17.6
640	425	1000	7100	496.5	11.8
780	518	1000	7100	496.5	9.7
325	214	2000	14200	806.5	38.1
430	284	2000	14200	806.5	28.7
640	425	2000	14200	806.5	19.2
780	518	2000	14200	806.5	15.8

TABLE XIV

Calculated theoretical values - vortex flow

Values of N per 66 cms calculated according to equations (36) and (39).

2.14 cm. diameter copper inner cylinder.

$\left(\frac{1}{w_1}\right) = 203.0$, $\left(\frac{w_1}{r_1}\right)^{\frac{1}{4}} = 0.743$; Sc = 0.573 (24)

Q cc/hr	Re_a	n r.p.m	Re_c	$Re_c^{\frac{1}{2}}$	Calculated N per 66 cms (36)	Calculated N per 66 cm (39)
325	223	400	688	26.2	27.8	20.4
430	296	400	688	26.2	21.0	15.4
640	441	400	688	26.2	14.0	10.3
780	539	400	688	26.2	11.5	8.4
325	223	1000	1720	41.5	44.0	32.3
430	296	1000	1720	41.5	33.2	24.4
640	441	1000	1720	41.5	22.3	16.4
780	539	1000	1720	41.5	18.2	13.4
325	223	2000	3440	58.7	62.3	45.7
430	296	2000	3440	58.7	47.0	34.5
640	441	2000	3440	58.7	31.5	23.1
780	539	2000	3440	58.7	25.8	18.9

TABLE XV

Calculated theoretical values - vortex flow

Values of N/66 cms. calculated according to equation (43)

2.14 cm. diameter copper inner cylinder.

Q cc/hr	Re_a	n r.p.m	$r_1^2 \Omega_{1/\nu}$	$\left(r_1^2 \Omega_{1/\nu}\right)^{0.7}$	Calculated N per 66 cms.
325	223	400	2260	222.8	11.3
430	296	400	2260	222.8	8.5
640	441	400	2260	222.8	5.7
780	539	400	2260	222.8	4.7
325	223	1000	5640	422.6	21.5
430	296	1000	5640	422.6	16.2
640	441	1000	5640	422.6	10.9
780	539	1000	5640	422.6	8.9
325	223	2000	11280	686.4	34.9
430	296	2000	11280	686.4	26.3
640	441	2000	11280	686.4	17.6
780	539	2000	11280	686.4	14.4

NOTATION

B = value of definite integral in (C.3) (cm^8)

b = annular gap width (= $r_2 - r_1$) (cm)

c = total molal concentration in the vapour phase, assumed constant (moles/cc)

Δc = concentration change across boundary layer (moles/cc)

D = molecular diffusion coefficient (cm^2/sec). Subscripts 1 and 2 refer to vapour and liquid phases respectively.

D' = vapour diffusion coefficient for homogeneous vortex regime (cm^2/sec)

d = diameter of open tube distillation column (cm.)

E = value of function in (C.6) (cm^4)

F_g = geometrical factor defined in (48)

G = torque on length (l) of inner cylinder (dyne.cm.)

H = total H.E.T.P. (vapour and liquid phase) (cm)

H_1 = vapour phase H.E.T.P.; H_2 liquid phase H.E.T.P.; H_1' vapour phase H.E.T.P. taking into account reflux surface velocity. (cm)

J = value of function in (C.4) (cm^4)

j_D = Colburn j-factor for mass transfer

K = laminar flow lateral mass transfer coefficient, vapour phase (moles/cm^2.sec)

k_v = vortex flow lateral mass transfer coefficient, vapour or liquid phase (cm/sec)

k_t = turbulent axial flow lateral mass transfer coefficient, vapour phase (cm/sec)

k_t' = turbulent circumferential flow lateral mass transfer coefficient, vapour phase (cm/sec)

L = total liquid molal flow rate per unit depth (moles/sec)

l = height of annular fractionating column (cm.)

M = value of function in (C.5) (cm^4)

m = numerical constant in (44)

N = number of theoretical plates

N_m = radial mass transfer rate per unit area (moles/cm^2.sec)

NOTATION (continued)

Nu = Nusselt number for heat transfer in an annulus

n_1 = speed of rotation of inner cylinder (r.p.m.)

P = geometrical function defined by (46)

p = pressure (dynes/cm^2)

Q = boil-up rate (cc/hr)

r_1 = external radius of inner cylinder, r_2 internal radius of outer cylinder, r_m = mean radius of annulus $(r_1 + r_2)/2$, r_{max} = radius of maximum velocity, r_w = distance from surface of reflux to common axis of concentric tubes. (cm)

Re = Reynolds number for axial flow in an open tube

Re_a = Reynolds number for axial flow in an annulus $(2\bar{u}b/\nu)$

Re_c = circumferential (rotational) Reynolds number for annular column with inner cylinder rotating $(r_1 \Omega_1 w_1/\nu)$ or $(r_1 \Omega_1 b/\nu)$

Sc = Schmidt number (ν/D)

Sh = Sherwood number $\left(\frac{k_v b}{D}\right)$

s = distance from point in vapour phase to dry wall of rotating inner cylinder (cm)

T = surface tension of test mixture at boiling point (dynes/cm)

Ta = Taylor number $(\Omega_1 r_m^{\frac{1}{2}} b^{\frac{3}{2}}/\nu)$

c_{Ta} = Critical Taylor number for vortex formation

$c_{(Ta)_b}$ = Critical Taylor number for vortex formation for zero axial flow and zero b/r_m

t = distance from a point in liquid reflux phase to wall of fixed outer cylinder (cm)

u = point velocity, $\bar{u}$ = mean velocity (cm/sec). Subscripts 1 and 2 refer to vapour and liquid phases respectively

V = total vapour molal flow rate per unit depth (moles/sec.cm)

v = velocity of inviscid vortex core (cm/sec)

w_1 = effective gap width for vapour flow (cm)

w_2 = thickness of reflux film (cm)

x = mole fraction of more volatile component in liquid (reflux) phase

$\bar{x}$ = mean mole fraction of more volatile component in liquid (reflux) phase

$\bar{x}_o$ and $\bar{x}_1$ = $\bar{x}$ at bottom and top of fractionating column respectively

y = mole fraction of more volatile component in vapour phase

$\bar{y}$ = mean mole fraction of more volatile component in vapour phase defined in (A.3)

y_i = value of y at vapour-liquid interface

$\bar{y}'$ = mean mole fraction of more volatile component in vapour phase defined in (A.10)

z = distance measured parallel to common axis of concentric cylinder column (cm)

δ = boundary layer thickness (cm)

θ = angular measurement (radians)

μ = viscosity (gm/cm.sec)

ν = kinematic viscosity (cm^2/sec)

ρ = density (gm/cc)

σ_2 = mean circumference of reflux ($\doteq 2\pi r_2$) (cm)

τ = shear stress (dynes /cm^2)

ψ = cross-sectional area for vapour flow (cm^2)

Ω_1 = angular velocity of inner cylinder (rad/sec)

Ω_c = critical angular velocity of inner cylinder for vortex formation (rad/sec)

$(\Omega_c)_o$ = critical angular velocity of inner cylinder for vortex formation for zero axial flow and zero b/r_m (rad/sec)

1, 2 = subscripts used throughout to denote vapour and liquid phases respectively

REFERENCES

(1) Matterson K.J., M.Sc. Thesis, London 1957.

(2) Macleod N. and Matterson K.J. Chem. Engng. Sci. 1959, 10, 254

(3) Willingham C.B., Sedlak V.A., Rossini F.D. and Westhaver J.W. Industr. Engng. Chem. 1947, 39, 706

(4) Taylor G.I. Phil. Trans. 1923, A, 223, 289

(5) Naragon E.A. and Lewis C.J. Industr. Engng. Chem. (Analyt.) 1946, 18, 448

(6) Rose A. Industr. Engng. Chem. 1936, 28, 1210

(7) Kuhn W and Ryffel Helv. Chim. Acta. 1943, 26, 1693

(8) Croockewit P., Honig C.C. and Kramers H. Chem. Engng. Sci. 1955, 4, 111

(9) Cornish R.J. Proc. Roy. Soc. 1933, A. 140, 227

(10) Fage A. Proc. Roy. Soc. 1938, A 165, 501

(11) Kaye J. and Elgar E.C. Trans. Amer. Soc. Mech. Engrs. 1958, 80, 753

(12) Lewis J.W. Proc. Roy. Soc. 1927, A, 117, 388

(13) Goldstein S. Proc. Camb. Phil. Soc. 1937, 33, 41

(14) Di Prima R.C. J. Fluid Mech. 1960, 9, Pt. 4, 621

(15) Mair B.J., Krouskop N.C. and Rossini F.D. Report A.P.I. Project 6. Petroleum Research Laboratory, Carnegie Inst. of Technol. 29 Feb. 1956

(16) Golubyev I.F., Meshcheryakov I.V. and Olevsky V.M. Jred. Gos. Inst. Azot. Prom. 1956, 5, 316

(17) Hawkins J.E. and Burris W.A. Analyt. Chem. 1956, 28, 1715

(18) Irlin A.L. and Brunce B.P. Zh. Anal. Khim. 1950, 1, 44

(19) Sladecek J. Scientific papers Inst. Chem. Tech. Prague 1958, Fac. Technol. Fuel and Water, 2, Pt. 1

(20) Ruckenstein E. Comm. Acad. Rep. Populare Romîne 1956, 6, No 2, 263

(21) Westhaver J.W. Industr. Engng. Chem. 1942, 34, 126

(22) Kuhn W. Helv. Chim. Acta. 1946, 29, 26

(23) Malyusov V.A., Umnik N.N. and Zhavoronkov M.N. Dokl. Akad. Naouk SSSR 1955, 105, No 4, 779

(24) Zuiderweg F.J. Chem. Engng. Sci. 1951-52, 1, 174

(25) Zuiderweg F.J. and Harmens A. Chem. Engng. Sci. 1958-59, 9, 89

(26) Friedman S.J. and Miller C.O. Industr. Engng. Chem. 1941, 33, 885

(27) Shipp G.C. Ph.D. Thesis Imperial College, London 1953

(28) Parikh C.K. D.I.C. Thesis, London 1953

(29) Appel D.W. T.A.P.P.I. 1959, 42, 764

(30) Batchelor G.K. appendix to Donnelly R.J. and Simon N.J. J. Fluid Mech. 1960, 7. Pt. 3, 401

(31) Bjorklund I.S. and Kays W.M. Trans.Amer.Soc.Mech.Engrs. 1959, Aug.Series C,175

(32) Gazley C., Jr. Trans. Amer.Soc.Mech.Engrs. 1958, 80, 79

(33) Becker K.M. Sc.D. Thesis M.I.T. 1957, Aug. 28

(34) Anon. "Shell" report "Vapourisation Experiments in a rotary column" Amsterdam, 9th Jan. 1948

(35) Eisenberg M., Tobias C.W., Wilke, C.R. Chem. Engng. Prog. Symp. Series. 1955, 51, No. 16

(36) Lohrenz J. and Kurata F. Industr. Engng. Chem. 1960, 52, 703

(37) Johnstone H.F. and Pigford R.L. Trans. Amer. Inst. Chem. Engrs. 1942, 38, 25

(38) Malyusov V.A., Umnik N.N. and Zhavoronkov M.N. Dokl. Akad. Naouk. SSSR 1955, 105, No. 5, 1057

(39) Lecky H.S. and Ewell R.H. Industr. Engng. Chem. (Analyt.) 1940, 12, 544

(40) Bromiley E.G. and Quiggle D. Industr. Engng. Chem. 1933, 25, 1136

(41) Mawer D.J. and Wishart A.F. Research project report. Dept. of Chem. Tech. Edinburgh Univ. 1960

(42) Lamb H. "Hydrodynamics" 6th edition, P.586.

(42') Dawson S.H. Ph.D. Thesis, Leeds, 1950

CONTENTS PART II

CONTENTS PART II (continued)

PART II

Mercury vapour transfer column. Evaporation of mercury into air flowing in an annulus with the inner cylinder rotating or stationary.

8. INTRODUCTION

It was shown in Part I of this thesis that the experimentally observed performance of rotary concentric cylinder fractionating columns does not show any significant improvement at those rotor speeds at which vortices may be presumed to form in the vapour phase. Before the experiments described below were performed it appeared that:-

either (a) vortices were not formed in these fractionating columns at or near the critical speeds of rotation of the inner cylinder

or (b) that vortices were formed but were not effective in promoting radial mass transfer

or, possibly (c) that vortices did improve radial mass transfer, but at the same time increased back-mixing so as to off-set any improvement in column performance.

In order to distinguish between these alternatives it was considered necessary to determine, theoretically and experimentally, the conditions for vortex formation and the influence of vortices on radial and longitudinal mass transfer in an annulus with the inner cylinder rotating. This was the main purpose of the present investigation, using a mercury vapour transfer column.

The mechanical design of the mercury vapour transfer column was similar in principle to the rotary concentric cylinder fractionating column described in Part I of this thesis, although the scale of construction was much larger.

In this column a narrow band of silver foil amalgamated with mercury was fixed around the circumference of the outer cylinder and evaporation

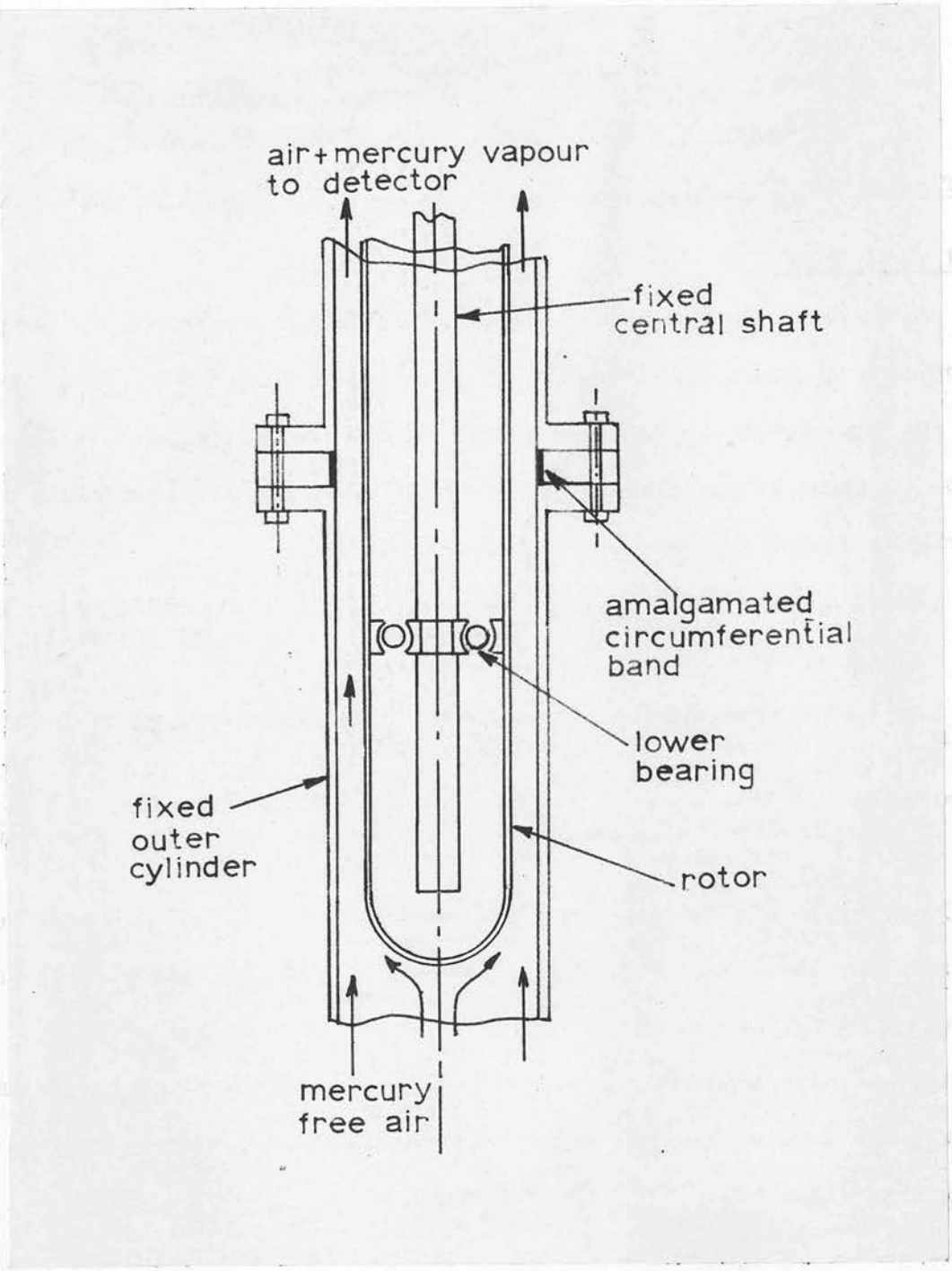

Figure 36. Working section of mercury vapour transfer column. Schematic.

took place from this surface to a stream of air flowing up a vertical annulus. The column was designed to yield results from experiments with inner cylinders (rotors) of four different diameters, either rotating or stationary. A few experiments were also performed with the amalgamated band fixed around the stationary inner cylinder. Figure 36 shows a schematic diagram of the relevant section of this column.

The concentration of mercury vapour in the air leaving the column was measured by means of a very sensitive Hanovia Mercury Vapour Detector, which operated on the principle that ultra-violet light of wavelength 2537Å is absorbed by mercury vapour. Maxwell and Storrow (43), using this technique, had previously determined local mass transfer rates from amalgamated portions of the surfaces of copper rods and spheres placed inside tubes through which air (or nitrogen) flowed. The advantage of this technique of measuring mass transfer rates is that mercury has on the one hand a low vapour pressure (44), giving low evaporation rates requiring low rates of energy transfer and thus ensuring effectively isothermal conditions during evaporation, while on the other hand, the measurement of ultra-violet absorption provides a sensitive and convenient means of determining the concentration of the vapour of the metal in the fluid stream.

In determining the conditions for vortex formation the axial flow rate was kept constant and the rotor speed was slowly increased from zero until, at a fairly well defined critical speed, the concentration of mercury vapour in the air leaving the annulus rose abruptly above a value which had previously remained constant. The observed critical speed depended on the value of the constant axial flow rate, and was assumed to represent the

speed of rotation corresponding to the onset of vortices in the annulus. This was a reasonable assumption, since such vortices would be expected to increase the rate of radial mass transfer of mercury vapour from the amalgamated circumferential band. It was found possible to determine these critical rotor speeds over a wide range of axial flow rates using rotors of four different diameters. These experimental results were compared with those obtained by other workers (11, 28, 34) and also with the theoretically predicted conditions (14) for vortex formation. From these results it was possible to establish the conditions under which it could be presumed that the fractionating columns, described in Part I of this report, operated with a vortex regime in the vapour phase.

Since the concentration of mercury vapour in the air leaving the annulus depended on the rate of radial diffusion from the amalgamated band, it was possible to determine the radial mass transfer coefficient, for a particular combination of rotor speed and axial flow rate, by measuring the steady state concentration of mercury vapour in the outlet air. By determining values of the radial mass transfer coefficient at rotor speeds above and below the critical speed corresponding to a particular axial flow rate, it was possible to determine the effect of vortex formation on radial mass transfer and hence throw light on the performance of fractionating columns operating with and without vortices in the annular vapour stream.

With the rotor stationary or revolving at speeds below the critical speed corresponding to vortex formation it was possible to compare the

experimentally derived values of the radial mass transfer coefficient with theoretical values derived on the basis of purely axial flow in the annulus. For rotor speeds above the critical value for each axial flow rate, a correlation was obtained from the experimental results between a dimensionless mass transfer coefficient (i.e. Sherwood number) and the other appropriate dimensionless groups, i.e. circumferential Reynolds number and a group involving the ratio of annular gap width to rotor radius. This correlation was derived from experimental results at low axial Reynolds numbers only (at which the axial flow would be expected to have little influence on the vortex pattern) and was found to agree with the form of analogous heat transfer correlations obtained by previous workers from heat transfer measurements on similar systems. The form of the correlation was also established theoretically.

The longitudinal diffusion of mercury vapour in the annulus was then measured as a function of both rotor speed and axial flow rate using a frequency response technique. Values of the longitudinal diffusion coefficient so determined were compared, where possible, with the appropriate theory. These experiments were designed to throw light on the effect of longitudinal diffusion in rotary concentric cylinder fractionating columns. As discussed in Part I, the results of these longitudinal diffusion experiments subsequently showed that longitudinal diffusion could be neglected in assessing the performance of the fractionating column studied in this project.

Finally, an attempt was made to prove, visually, that vortices could

exist in the annulus of the mercury vapour transfer column. By introducing finely divided talcum powder into the annulus, the presence of vortices was verified visually at high rotor speeds and very low axial flow rates.

9. THEORY

In this section the theory is discussed relating to radial diffusion of mercury vapour from the surface of a narrow amalgamated circumferential band into an air stream flowing in the annulus with the rotor stationary or rotating. Theories are also presented relating to the longitudinal mixing of mercury vapour in an air stream flowing axially in the annulus. It is convenient to present these theories under the following main headings, taking into account the various possible flow regimes in the annulus:-

9.1 Radial diffusion with the inner cylinder (rotor) stationary and laminar flow of air in the annulus.

9.2 Radial diffusion with the inner cylinder stationary and turbulent flow of air in the annulus.

9.3 Experimental investigation of conditions for vortex formation. Radial diffusion with the inner cylinder rotating and laminar or 'laminar plus vortex' flow in the annulus.

9.4 Radial diffusion with the inner cylinder rotating and turbulent or 'turbulent plus vortex' flow in the annulus.

9.5 Longitudinal diffusion in the annulus.

9.1 Radial diffusion with the inner cylinder (rotor) stationary and laminar flow of air in the annulus

9.11 Diffusing band on fixed outer cylinder - parallel plate approximation

A theoretical analysis will now be presented for the case where evaporation of mercury takes place, from the surface of a narrow amalgamated circumferential band on the outer cylinder, into a laminar air stream flowing in the annulus. If the ratio of annular gap width to rotor radius is very small, then it may be considered that mass transfer takes place from the surface of a narrow section placed transverse to a laminar air stream flowing

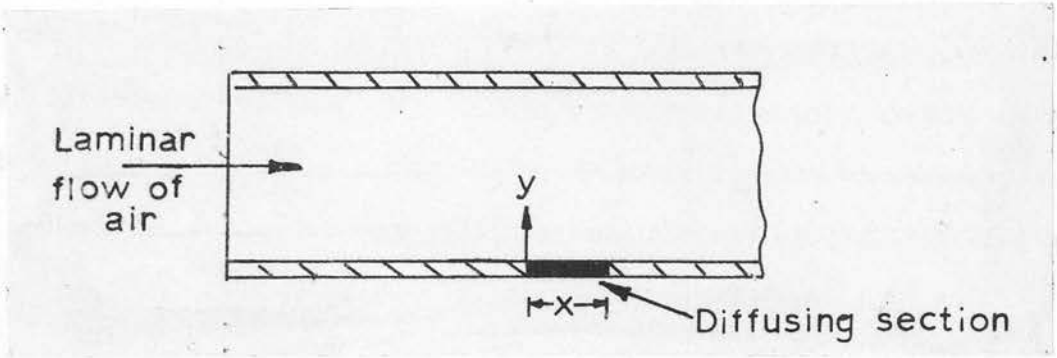

Figure 37. Mass transfer from narrow section to laminar air stream.

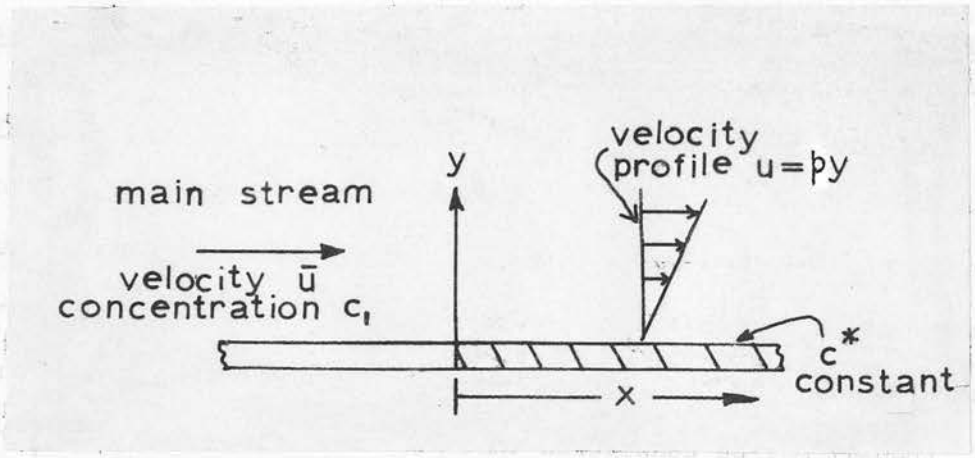

Figure 38. Mass transfer from amalgamated section.
Linear velocity profile in region close to wall.

between parallel plates. Figure 37 shows the narrow diffusing section of width x placed transverse to the air stream. The y - direction is measured normal to the section surface. In practice, this diffusing section corresponds to the narrow circumferential band of silver foil amalgamated with mercury.

The situation may be treated mathematically by developing a theory for mass transfer analogous to the Leveque (61) equation for heat transfer in the entrance region of a tube. The following assumptions are necessary:-

(a) The physical properties of the air remain constant in flowing over the amalgamated section.

(b) The surface concentration of the amalgamated section is constant at c^*, where c^* is the saturation concentration of mercury vapour in air at the temperature of the flowing air, i.e. it is assumed that the amalgamated surface behaves essentially as though it were pure liquid mercury.

(c) The temperature of the diffusing section is equal to that of the air flowing past that section.

(d) Mass transfer is due to molecular diffusion alone, and is considered to take place entirely within a region very close to the surface of the diffusing section; i.e. the distance of diffusional penetration is supposed very small. (This assumption will only be true for small values of x).

(e) The velocity of the air adjacent to the surface of the wall containing the diffusing section (outer cylinder) is given by:-

$$u = py \quad , \quad v = o \quad , \quad w = o$$

where p = a constant
u = velocity in x - direction
v = " " y - direction
w = " " direction perpendicular to both x and y directions.

Figure 38 represents the situation to be considered. $\bar{u}$ represents

the mean velocity of the main air stream. c_1 is the concentration of mercury vapour in this air steam, prior to reaching the amalgamated section, (shown shaded). The mercury vapour concentration of the air at a position well downstream from the diffusing section will be represented by c_2.

The general mass balance equation for mercury vapour in the three dimensional flow is:-

$$u\frac{\partial c}{\partial x} + v\frac{\partial c}{\partial y} + w\frac{\partial c}{\partial z} = D\left(\frac{\partial^2 c}{\partial x^2} + \frac{\partial^2 c}{\partial y^2} + \frac{\partial^2 c}{\partial z^2}\right) \quad - - - (53)$$

where c is the mercury vapour concentration at a point (x,y,z) and D is the molecular diffusion coefficient of mercury in air. u,v,w are the point velocities. Now u = 0, v = w and, for small values of y, $\frac{\partial^2 c}{\partial x^2} \ll \frac{\partial^2 c}{\partial y^2}$. Also $\frac{\partial^2 c}{\partial z^2}$ may be put = 0.

$\therefore$ Equation (53) reduces to:-

$$u\frac{\partial c}{\partial x} = D\frac{\partial^2 c}{\partial y^2} \quad - - - (54)$$

A solution to (54) is required with the following boundary conditions:-

$$\text{at } \begin{cases} x = 0 \\ y > 0 \\ c = c_1 \end{cases} \qquad \text{and} \qquad \text{at } \begin{cases} x > 0 \\ y = 0 \\ c = c^* \end{cases}$$

It is shown in Appendix E, at the end of this report, that a solution to equation (54), using these boundary conditions is given by:-

$$\frac{c - c^*}{c_1 - c^*} = \frac{1}{0.893} \cdot \int_0^X e^{-X^3}\, dX$$

where $X = y\left(\frac{p}{9Dx}\right)^{\frac{1}{3}}$

Thence, by stating mathematically that the mercury vapour lost by radial (molecular) diffusion from the amalgamated section is equal to that gained by the laminar air stream in flowing over the section, it is shown further that the fractional saturation of the air stream, $\frac{c_2 - c_1}{c^* - c_1}$, is given by:-

$$\frac{c_2 - c_1}{c^* - c_1} = 1.468 \cdot \left(\frac{Dx}{b^2 \bar{u}} \right)^{\frac{2}{3}} \qquad \text{- - - (55)}$$

where b is the distance between the parallel plates.

The symbol ϕ is henceforth used to represent the fractional saturation $\frac{c_2 - c_1}{c^* - c_1}$ and the symbol ψ is taken to represent the group $\left(\frac{Dx}{b^2 \bar{u}} \right)$.

$$\therefore \quad \phi = 1.468 \, \psi^{\frac{2}{3}} \qquad \text{- - - (56)}$$

Plewes et al (45) showed, for the evaporation of seven different volatile solids into a laminar air stream flowing in a square duct, that ϕ was proportional to $\psi^{\frac{2}{3}}$, as in (56), but that the constant was slightly different from the value 1.468, depending on the solid used. Evaporation took place from narrow strips of the solid of width x placed transverse to the air stream in one surface of the duct.

Similarly Linton and Sherwood (46) showed that for the dissolution of benzoic and cinnamic acid in water with streamline flow in a round tube the equation equivalent to (56) was verified, i.e.

$$\phi = 5.5 \left(\frac{Dx}{\bar{u} \pi R^2} \right)^{\frac{2}{3}} \qquad \text{- - - (57)}$$

where x is the length of the short cylindrical test section inserted in

the tube and R the internal radius of both tube and test section. These cylindrical test sections of cinnamic or benzoic acid were inserted several tube diameters downstream at a point where laminar flow was fully developed.

9.12 Diffusing band on fixed outer cylinder - concentric tube theory

In section 9.11 it is assumed that the ratio of annular gap width to rotor radius is sufficiently small for the parallel plate assumption to hold. This assumption is not likely to be valid for the annuli used in the present investigation and hence an equation equivalent to (56) is derived in Appendix F, which takes into account the shape of the velocity profile corresponding to laminar flow in an annulus. The equation equivalent to (56) for the fractional saturation of the air stream, ϕ, is shown to be:-

$$\phi \equiv \frac{c_2 - c_1}{c^{\infty} - c_1} = 2.565 \left\{ \frac{(r_2 - r^2_{max}/r_2)}{(r_1^2 + r_2^2 - 2r^2_{max})} \right\}^{\frac{1}{3}} \cdot \left(\frac{r_2}{r_2^2 - r_1^2} \right) \cdot \left(\frac{Dx}{\bar{u}} \right)^{\frac{2}{3}} \quad - - (58)$$

where r_1 is the outside radius of the rotor, r_2 the inside radius of the fixed outer cylinder and r_{max} the radius corresponding to the point of maximum velocity in the annulus. r_{max} is given by the equation:-

$$r_{max} = \frac{r_2^2 - r_1^2}{2 \ln r_2/r_1} \quad - - - (59)$$

It is then shown, in Appendix G, that equation (58) reduces to equation (56) when the ratio of annular gap width, b, to rotor radius, r_1, becomes very small.

9.13 Diffusing band on rotor - concentric tube theory

It is possible to derive an equation analogous to (58) for the case when the amalgamated band is on the stationary rotor. By finding the slope of the velocity profile at the surface of the rotor, an equation is obtained for ϕ given by:-

$$\phi = 2.565 \left\{ \frac{(r^2_{max}/r_1 - r_1)}{(r_1^2 + r_2^2 - 2r^2_{max})} \right\}^{\frac{1}{3}} \cdot \left(\frac{r_1}{r_2^2 - r_1^2} \right) \cdot \left(\frac{Dx}{\bar{u}} \right)^{\frac{2}{3}} \quad \text{--- (60)}$$

which is, in effect, equation (58) with r_1 interchanged with r_2.

Using the present column it was possible to test experimentally the validity of equations (58) and (60) for cylinders of different radii over a range of flow rates with an amalgamated section of variable width situated on the outer or inner cylinder. For any particular combination of concentric cylinders equations (58) and (60) reduce to an equation of the form:-

$$\phi = (\text{constant}) \cdot \left(\frac{Dx}{\bar{u}} \right)^{\frac{2}{3}}$$

Thus a plot of ϕ versus $\left(\frac{Dx}{\bar{u}}\right)$ on logarithmic graph paper (log./log. scales) gives a straight line of slope $\frac{2}{3}$. Experimentally obtained point values should lie along this curve.

In the present work it was assumed that the inlet air to the annulus was completely free of mercury vapour, i.e. $c_1 = 0$.

In this case :- $$\phi = \frac{c_2 - c_1}{c^* - c_1} = \frac{c_2}{c^*} \quad \text{- - - (61)}$$

c_2 was measured by the Hanovia mercury vapour detector and c^* corresponding

to the average air temperature in the column was obtained from a graph of c^{*} versus temperature constructed from published vapour pressure data (see figure 87 and Appendix L). x, the width of the amalgamated band, was known and the appropriate value of D was obtained from a curve of D versus temperature plotted from published data (see figure 88 and Appendix M).

The value of $\bar{u}$ was calculated from a knowledge of the volumetric flow rate in the annulus and the annulus cross-sectional flow area, A.

Hence ϕ could be evaluated and plotted as a function of $Dx/\bar{u}$ to check the validity of equations (58) or (60).

9.2 Radial diffusion with the inner cylinder stationary and turbulent flow of air in the annulus

When the flow of air in the annulus is turbulent it is assumed that there exists a laminar sub-layer adjacent to the surface of the amalgamated band and that all concentration changes take place entirely within this sub-layer. Based on these assumptions an equation is derived in Appendix H for the fractional saturation, ϕ, for the case where the amalgamated band is fixed around the inside of the outer cylinder. The parallel plate approximation is made. This equation takes the form:-

$$\phi = \frac{0.256\ (Dx)^{\frac{2}{3}}}{\bar{u}^{5/12} \cdot b^{13/12} \cdot \nu^{1/4}} \qquad - - - (62)$$

The conditions under which equation (62) may be assumed valid are derived in Appendix I and it is found that, providing:-

$$\left(\frac{x}{b}\right)^{\frac{1}{3}} (Sc)^{-\frac{1}{3}} \cdot Re_a^{\frac{7}{24}} < 5.22 \qquad - - - (63)$$

equation (62) may be assumed valid. Sc is the Schmidt number, (ν/D), and Re_a the axial Reynolds number ($Re_a = 2\bar{u}b/\nu$), ν being the kinematic viscosity of the air stream.

Thus knowing the physical dimensions of the apparatus, physical properties of the air stream and flow rate of air it is possible, using equation (63), to determine whether (62) can be used as a valid theoretical standard with which to compare the experimental results obtained with an axially turbulent flow of air.

9.3 Investigation of conditions for vortex formation. Radial diffusion with the inner cylinder rotating and laminar or 'laminar plus vortex' flow of air in the annulus. Amalgamated band on the outer cylinder.

As described in Part I section 3.5, the experiments of several workers (9, 10, 11, 27, 28, 29, 33, 34) show that for finite axial flow rates of air in the annulus vortices appear at a certain critical rotor speed. For a particular ratio of annular gap width to mean radius, b/r_m, Kaye and Elgar (11) found that the boundaries between the various flow regimes are as shown in Part I, figures 7 and 8.

With laminar flow of air in the annulus, (low axial flow rates and rotor speeds below the critical corresponding to vortex formation), the radial mass transfer rate from the amalgamated surface on the outer cylinder should be determined entirely by radial molecular diffusion into the laminar air stream. For a combined axial and circumferential flow, provided the flow is purely laminar, the velocity components may be resolved axially and circumferentially and, because of cylindrical symmetry, the circumferential velocity component has no effect on

radial mass transfer. Thus equation (58) should hold, at a particular flow rate, for a range of rotor speeds extending from zero to the critical speed for vortex formation. The validity of this argument and the applicability of equation (58) can be verified experimentally by noting if there is a range of rotor speeds, between zero and some critical speed, for which the concentration, c_2, of the mercury vapour in the air leaving the column (as measured by the Hanovia instrument) remained steady with the axial flow rate maintained at some constant value.

When vortices appear, at the critical rotor speed corresponding to a particular air flow rate, the radial mass transfer rate should increase due to improved radial mixing of mercury vapour and air. The appearance of vortices should thus be marked by a rise in the mercury vapour concentration in the air leaving the column, as detected by the Hanovia instrument. As the rotor speed is raised above this critical speed corresponding to vortex formation the outlet mercury vapour concentration, c_2, should continue to increase.

Experiments were, therefore, conducted to determine the form of the transition curves 'laminar' to 'laminar plus vortex' (see Part I, figure 7) for the four rotors available. The critical values of the Taylor number, Ta, $(\Omega r_m^{\frac{1}{2}} b^{\frac{3}{2}}/\nu)$, for various axial Reynolds numbers, Re_a, would be expected to be different for each rotor used and for the case of the largest diameter rotor ($b/r_m = 0.104$) these values should lie close to the theoretical curve of critical values of Re_a versus Ta due to Di Prima ($b/r_m \rightarrow 0$) (14).

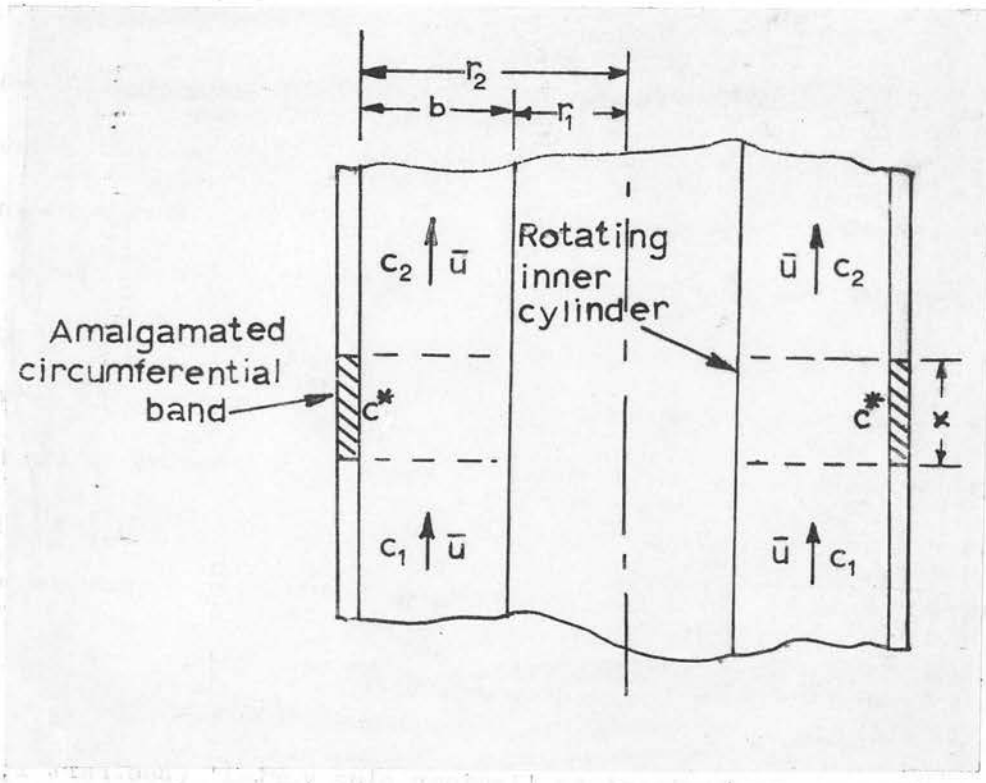

Figure 39. Radial diffusion from surface of amalgamated band on outer cylinder.

Experiments were also conducted to determine the variation in the rate of mass transfer from the surface of the amalgamated section as a function of rotor speed and axial flow rate. Values of a suitably defined radial mass transfer coefficient, K, were then obtained as a function of the circumferential (rotational) Reynolds number, Re_c, and the axial Reynolds number, Re_a. The circumferential Reynolds number, Re_c, is given by:-

$$Re_c = \frac{r_1 \Omega b}{\nu} \qquad - - - (64)$$

where Ω is the angular velocity of the rotor, radius r_1, b the annular gap width and ν the kinematic viscosity of the air.

The axial Reynolds number, Re_a, is given by $Re_a = \frac{2\bar{u}b}{\nu}$, where $\bar{u}$ is the mean air velocity. The radial mass transfer coefficient, K, will now be defined.

9.31 Definition of the radial mass transfer coefficient, K.

Figure 39 shows the amalgamated circumferential band, of width x, from the surface of which evaporation of mercury takes place. The annular gap width is b, r_2 is the inside radius of the fixed outer cylinder and r_1 is the outside radius of the rotor. The concentration of mercury vapour in the incoming air stream is c_1 and after passing the amalgamated section, the concentration is c_2. The concentration of mercury vapour at the mercury/air interface is c^*, the saturation vapour concentration at the average temperature of the air in the annulus.

A mass transfer coefficient, K, based on the logarithmic mean concentration difference may be defined according to the equation:-

$$K.S. \quad \frac{(c^{*} - c_1) - (c^{*} - c_2)}{\ln \frac{(c^{*} - c_1)}{(c^{*} - c_2)}} = \bar{u} \; A \; (c_2 - c_1) \qquad - - - (65)$$

where $\bar{u}$ is the mean air velocity and S is the surface area of the amalgamated band given by:-

$$S = 2\pi r_2 x \qquad - - - (66)$$

and A is the cross-sectional flow area, given by:-

$$A = \pi(r_2^2 - r_1^2) \qquad - - - (67)$$

Equation (65) is simply based on continuity, and expresses the fact that all the mercury vapour transferred from the surface of the amalgamated section is given up to the air stream; this equation serves as a definition of K whether the air flow is laminar, vortex or turbulent. In all the experiments conducted it was assumed that $c_1 = 0$, i.e. the air entering the annulus was free from mercury vapour.

$$\therefore \quad K = \bar{u} \; \frac{A}{S} \; \ln \frac{c^{*}}{c^{*} - c_2} \qquad - - - (68)$$

Since all the terms on the right hand side of (68) are capable of experimental determination, K may be evaluated and plotted as a function of the circumferential Reynolds number, Re_c, for varying axial Reynolds numbers, Re_a; Re_c and Re_a being calculated at the particular rotor speed and axial flow rate respectively at which K is evaluated.

N.B. Throughout these experiments the axial Reynolds number, Re_a, was evaluated on a "carrier gas" basis - i.e. using the physical properties of

mercury free air. For the small concentrations of mercury vapour present in the air stream at room temperature, the error introduced is negligible.

9.32 Relationship between K and ϕ

When the mercury vapour concentration, c_2, in the outlet stream is very small a relationship can be obtained between K and the parameter ϕ used in the previous sections.

From (68) $$K = \bar{u}\,\frac{A}{S}\,\ln\frac{c^*}{c^* - c_2}$$

$$= -\bar{u}\,\frac{A}{S}\,\ln(1-\phi)$$

$$\therefore\ K \doteqdot \bar{u}\,\frac{A}{S}\,\phi, \text{ if } \phi \ll 1$$

Since the axial Reynolds number, Re_a, is given by:-

$$Re_a = 2\bar{u}\,b/\nu$$

then, $$K = \frac{Re_a\,\nu}{2b} \cdot \frac{A}{S} \cdot \phi$$

Substituting the value of ϕ from (58) for the case of laminar flow radial mass transfer from an amalgamated band on the outer cylinder:

$$K = Re_a \cdot \frac{\nu}{2b} \cdot \frac{A}{S} \cdot 2.565 \left\{\frac{(r_2 - r_{max}^2/r_2)}{(r_1^2 + r_2^2 - 2r_{max}^2)}\right\}^{\frac{1}{3}} \cdot \left(\frac{r_2}{r_2^2 - r_1^2}\right) \cdot \left(\frac{Dx}{\bar{u}}\right)^{\frac{2}{3}}$$

$$K = Re_a^{\frac{1}{3}} \cdot \left(\frac{\nu}{2b}\right)^{\frac{1}{3}} \frac{A}{S}\,(Dx)^{\frac{2}{3}} \cdot 2.565 \left\{\frac{(r_2 - r_{max}^2/r_2)}{(r_1^2 + r_2^2 - 2r_{max}^2)}\right\}^{\frac{1}{3}} \cdot \left(\frac{r_2}{r_2^2 - r_1^2}\right) - - (6$$

Equation (69) shows that if the physical properties ν and D remain

constant for a particular geometrical system, K is proportional to $(Re_a)^{\frac{1}{3}}$. This result is in marked contrast to the case of fully developed laminar flow with mass transfer taking place from the surface of a long annulus. K in the latter case is independent of Re_a, as in the similar heat transfer case where the Nusselt number is independent of the Reynolds number.

9.33 Variation of the radial mass transfer coefficient, K, with rotor speed at constant axial flow rate.

As discussed in section 9.3, the value of K, for a particular flow rate in the annulus, should remain constant until the critical rotor speed is reached corresponding to the formation of vortices. Bjorklund and Kays (31) investigated an identical transition for the case of heat transfer across an annulus with the inner cylinder rotating but without axial flow in the annulus. As discussed in Part I, section 3.513, Bjorklund and Kays found that for several gap widths the Nusselt number, Nu, remained constant at a value corresponding to pure conduction across the annular gap until the known (calculable) speed of rotation for Taylor vortex formation was reached and then, as the rotor speed was increased, the Nusselt number began to rise according to the relationship:-

$$Nu = 0.175 \left\{ \frac{b/r_1}{\ln (1 + b/r_1)} \right\} N_{Ta}^{\frac{1}{2}} \qquad - - - (70)$$

for the range $90 < N_{Ta} < 2000$ and $0.054 < b/r_1 < 0.246$, where N_{Ta} is a form of the Taylor number, Ta, based on the inner cylinder and is given by:-

$$N_{Ta} = \left(\frac{r_1 \Omega b}{\nu} \right) \times \left(\frac{b}{r_1} \right)^{\frac{1}{2}} \equiv (Re_c) \cdot \left(\frac{b}{r_1} \right)^{\frac{1}{2}} \qquad - - - (71)$$

Above a value of $N_{Ta} = 2000$ equation (70) did not hold due to the

supposed existence of a 'turbulent plus vortex' regime.

As shown in Part I, section 3.513, equation (70) reduces to:-

$$Nu = 0.175 \left(\frac{r_1 \Omega b}{\nu}\right)^{\frac{1}{2}} \left(\frac{b}{r_1}\right)^{\frac{1}{4}} \quad - - - (72)$$

when b/r_1 is small.

Equation (72) is identical in form to the theoretical equation (36) for vortex mass transfer derived in Part I, section 3.511 on the basis of Batchelor's (30) "inviscid core and boundary layer" model, assuming that heat, mass and momentum transfer are analogous.

This identity provides indirect justification for the use of a form of equation (36) in correlating mass transfer data in similar systems.

The experiments by Gazley (32) on a system similar to that used by Bjorklund and Kays also showed that a critical value of the Taylor number exists at which the Nusselt number deviates from the constant value corresponding to pure conduction across the annular air gap (when there is no axial flow of air in the annulus).

Haas and Nissan (47) also investigated heat transfer across an annulus without axial flow and showed that the Nusselt number remained constant with increasing rotor speed until vortices appear in the annulus.

Heat transfer measurements by Becker (33) with axial flow of air in an annulus, having a b/r_m value of 0.214, showed a sharp rise in the Nusselt number at a critical rotor speed. This critical speed was taken to correspond to the appearance of vortices. The critical Taylor number corresponding to the onset of vortices increased monotonically with increasing axial Reynolds number. The plot of these critical values of Taylor number versus axial Reynolds number agreed with the similar plot

by Kaye and Elgar (11).

Becker also determined the variation of Nusselt number with Taylor number for a series of values of the axial Reynolds number. Becker's measurements were essentially of heat transfer in a purely radial direction (molecular or eddy transport) across the entire length of an annulus; longitudinal convective heat transfer being eliminated by arranging that the air entered and left the annulus at the same temperature. These measurements by Becker cannot be compared quantitatively with the results of the present investigation in which mass transfer took place, from a narrow amalgamated band on one wall of the annulus, into an axial air stream, the concentration of the air stream being different on either side of the amalgamated band. Nevertheless, certain general conclusions reached by Becker should be applicable to the present study. Becker concludes from the heat transfer measurements with a vortex regime that the axial flow in the annulus has a damping effect on the vortices and that it decreases the circulation within each vortex. If a boundary layer exists between the main vortex core and the wall of the annulus (Batchelor's model (30)), in which boundary layer the main resistance to heat or mass transfer lies, then a further conclusion of Becker's is also appropriate to the present study: this is that the mean tangential velocity of the air stream has a greater effect on the heat transfer coefficient than a purely axial velocity of the same magnitude. This last conclusion lends support to the theory that if the axial flow does not significantly alter the vortex pattern then the heat or mass transfer rate (at a constant and necessarily low axial flow rate) should be largely conditioned by the rotor speed. Thus it would be expected that the

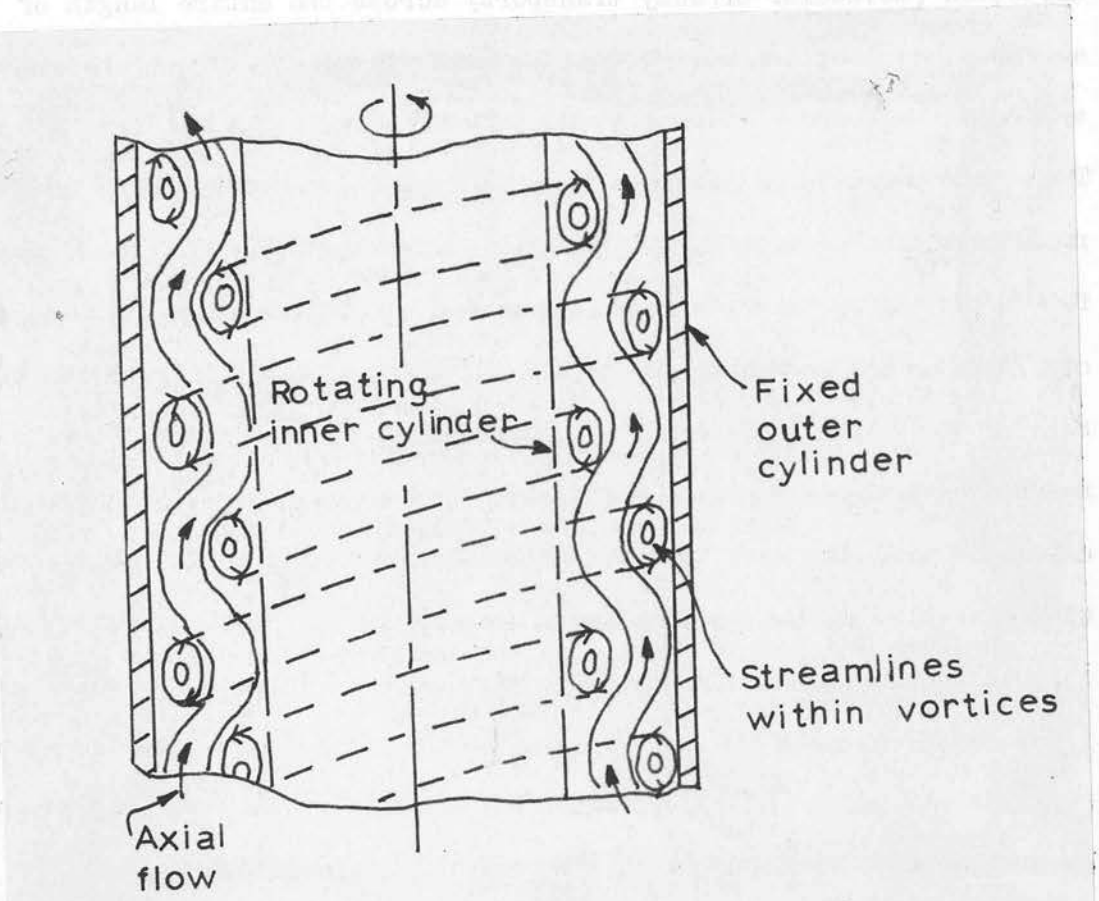

Figure 40 . Possible flow configuration of vortex system with a superimposed large axial flow rate.

correlation:-

$$Sh = \frac{K\,b}{D} \sim \left(\frac{r_1 \Omega b}{\nu}\right)^{\frac{1}{2}} \cdot \left(\frac{b}{r_1}\right)^{\frac{1}{4}} \qquad - - - (32)$$

should hold for this condition. This correlation would not be expected to hold when the axial flow rate is sufficiently large to disturb the vortex pattern producing, for example, a "flowing spiral" vortex pattern as reported by Shipp (27). With a large flow rate it is possible that the value of the mass transfer coefficient, K, at a fixed rotor speed is less than a value of K at a small axial flow rate; for the large axial flow rate may cause a distortion of the vortex flow as tentatively suggested in figure 40. (This flow configuration was suggested by the smoke photographs in the paper by Kaye and Elgar (11)). If the vortex flow is distorted in the manner shown, such that each vortex no longer occupies a square annular compartment, the influence of a vortex regime on radial mass transfer would probably be much reduced.

Mention was made in Part I, of the results of Eisenberg et al (35), for the dissolution of rotating inner cylinders of benzoic acid in annuli containing water. The following correlation, in terms of the Colburn j_D - factor, was obtained:-

$$j_D = \frac{K}{r_1 \Omega} \times Sc^{0.644} = 0.079 \left(\frac{r_1 \Omega b}{\nu}\right)^{-0.3} \cdot \left(\frac{b}{2r_1}\right)^{0.3}$$

$$= 0.079 \left(\frac{2r_1^2 \Omega}{\nu}\right)^{-0.3} \qquad - - - (40)$$

where Ω is the angular velocity of the inner cylinder of radius r_1 and Sc the Schmidt number. The form of this correlation is quite different

from those based on heat transfer measurements and also contradicts the theoretical expression of Batchelor (30) for momentum transfer. It was found in Part I that the performance of the rotary concentric cylinder fractionating column was somewhat better than the theoretically predicted performance based on this correlation, although the form of this correlation agrees with the observation that the performance of such columns is not strongly dependent on the ratio of annular gap width to rotor radius.

It is clear therefore that more experimental evidence is required before any definite correlation can be established for the influence of vortices on radial mass transfer. As described later in this thesis, experiments were undertaken with the mercury vapour column designed to yield results which would establish the nature of the correlation between the various dimensionless groups involved when radial mass transfer takes place in a vortex regime.

9.4 Radial diffusion with the inner cylinder rotating and turbulent or 'turbulent plus vortex' flow in the annulus

9.41 Turbulent flow in the annulus

At high axial flow rates and low rotor speeds, it is possible that axial turbulence of the air stream develops (see figure 7, Part I showing possible flow regimes). Under these conditions the arguments put forward in section 9.2 would still apply, since the small rotor speeds (insufficient to generate vortices) would have a negligible influence on the rate of radial mass transfer. Thus equation (62) can be used as a theoretical model providing the conditions laid down by equation (63) are satisfied.

Unfortunately no experimental results are known from previous

investigations which can be used to test the validity of equation (62).

9.42 'Turbulent plus vortex' flow

If the combined effect of rotor speed and axial flow rate is such that a 'turbulent plus vortex' regime exists in the annulus (see figure 7, Part I) and if the annulus is so narrow that its boundaries can be treated as parallel planes then, for very low axial flow rates, a relationship analogous to the Dittus-Boelter equation might be expected to hold, of the form:-

$$Sh \equiv \frac{Kb}{D} = g \; Re_c^{0.8} \; Sc^{0.4} \qquad - - - (73)$$

where g is a numerical constant. Implied in this relationship is the assumption that at very low axial flow rates the axial flow has no significant influence on radial mass transfer.

The validity of equation (73) could not be tested in the present investigation since the results obtained using all the rotors did not indicate the existence of a 'turbulent plus vortex' regime even with circumferential Reynolds numbers as high as 5000. Equation (73) is thus of little practical significance in the present investigation.

9.5 Longitudinal diffusion

In the theories of fractionation discussed in Part I of this thesis it is assumed that when the vapour and liquid phases are in laminar flow longitudinal diffusion effects can be neglected when calculating the number of theoretical plates. Under these conditions the number of theoretical plates, N, is calculated from the equation:-

$$N = \frac{1}{H_1} \qquad - - - (74)$$

where l is the length of the fractionating column and H_1 the vapour phase HETP, calculated on the basis of negligible longitudinal diffusion.

If longitudinal diffusion <u>is</u> taken into account, then it follows from the discussion in Part I, section 3.21, that the equation (74) for N should be modified to the form:-

$$N = \frac{l}{H_1 + \frac{D_1}{\bar{u}_1}} \qquad - - - (75)$$

where D_1 is the molecular diffusion coefficient of the more volatile component in the vapour phase and the term $\frac{D_1}{\bar{u}_1}$ represents the influence of longitudinal diffusion on the value of N. It is subsequently shown, in the example given in section 3.71, that under the most extreme conditions the term $\frac{D_1}{\bar{u}_1}$ has a negligible influence on the value of N for the particular column over the range of experimental conditions investigated. It was thus concluded that back-mixing effects were unimportant for purely laminar flow for the particular system studied.

With a 'laminar plus vortex' or 'turbulent plus vortex' flow regime in the annulus the term $\frac{D_1}{\bar{u}_1}$ in equation (75) should be replaced by a term $\frac{D'}{\bar{u}_1}$, where D' is now the diffusion coefficient for an assumed homogeneous vortex regime - i.e. a regime in which both the radial and longitudinal diffusion coefficients are assumed equal to D'. The value for H_1 should now be obtained from the appropriate equations (36), (39) or (43), derived on the basis of distillation in a vortex regime. [This was the method used in Part I, section 3.72 in which it was shown (using the results of the longitudinal diffusion experiments now to be described) that back-mixing due to vortices had

a negligible effect on fractionating column performance for the system and range of experimental conditions investigated].

In order to determine values of D', (and hence assess the influence of back-mixing on fractionating column performance), experiments were conducted on the mercury vapour transfer column to investigate the longitudinal diffusion of mercury vapour in air flowing through the annulus with the inner cylinder stationary and rotating. Now the experimental determination of longitudinal diffusion coefficients for fluid flow in tubes or annuli usually involves the injection of a tracer material at a convenient point in the system and an analysis of the "spread" of tracer material at another point downstream from the place of injection. For ease of mathematical analysis the injection of the tracer usually takes the form of a step change, pulse change or sinusoidal variation (8) in the quality (e.g. concentration) at the injection point of the flow system. A step change means an instantaneous and permanent change in the quality of the flowing stream at the injection point, whereas a pulse change involves the instantaneous introduction of a "slug" of tracer, the tracer in either case being injected uniformly across a plane perpendicular to the direction of flow at the point of injection. Similarly, the sinusoidal variation of tracer demands that the tracer be fed to the system in such a way that the quality (e.g. concentration) of fluid, uniformly injected across the system at the injection point, varies sinusoidally with time. When the fluid flow is laminar, the tracer will "spread" in a longitudinal direction due to the existence of a parabolic velocity profile superimposed on the effect of molecular

diffusion. The velocity profile effect is due to the fact that for flow in an annulus, tracer material near the centre of the annulus travels faster than material nearer the walls. When vortices are present the longitudinal "spread" will depend on the combined effects of radial and longitudinal diffusion (diffusion coefficient D') together with a velocity profile effect. Thus tracer experiments yield an apparent longitudinal diffusion coefficient which involves these combined effects. It will be shown later that for purely laminar flow it is also possible to calculate theoretically the value of this apparent longitudinal diffusion coefficient.

In order to obtain a value of D' from the results of the tracer experiments, it is assumed in the present investigation that:-

$$\frac{D'}{D_1} = \frac{\text{Apparent longitudinal diffusion coefficient for vortex flow}}{\text{Apparent longitudinal diffusion coefficient for laminar flow}} \quad - - - (50$$

where D_1 is the value of the molecular diffusion coefficient.

The value of D' obtained using this equation can then be used, under dynamically similar conditions, to determine the influence of longitudinal diffusion on the performance of fractionating columns operating with a vortex regime, using the analogous form of equation (75) for vortex flow.

It will now be shown how it is possible to obtain, both theoretically and experimentally, values of the apparent longitudinal diffusion coefficient for purely laminar flow in an annulus. Subsequently it is shown how the results of longitudinal diffusion experiments with a vortex regime may similarly be analysed to yield values of the apparent longitudinal diffusion coefficient, from which values of D' may be

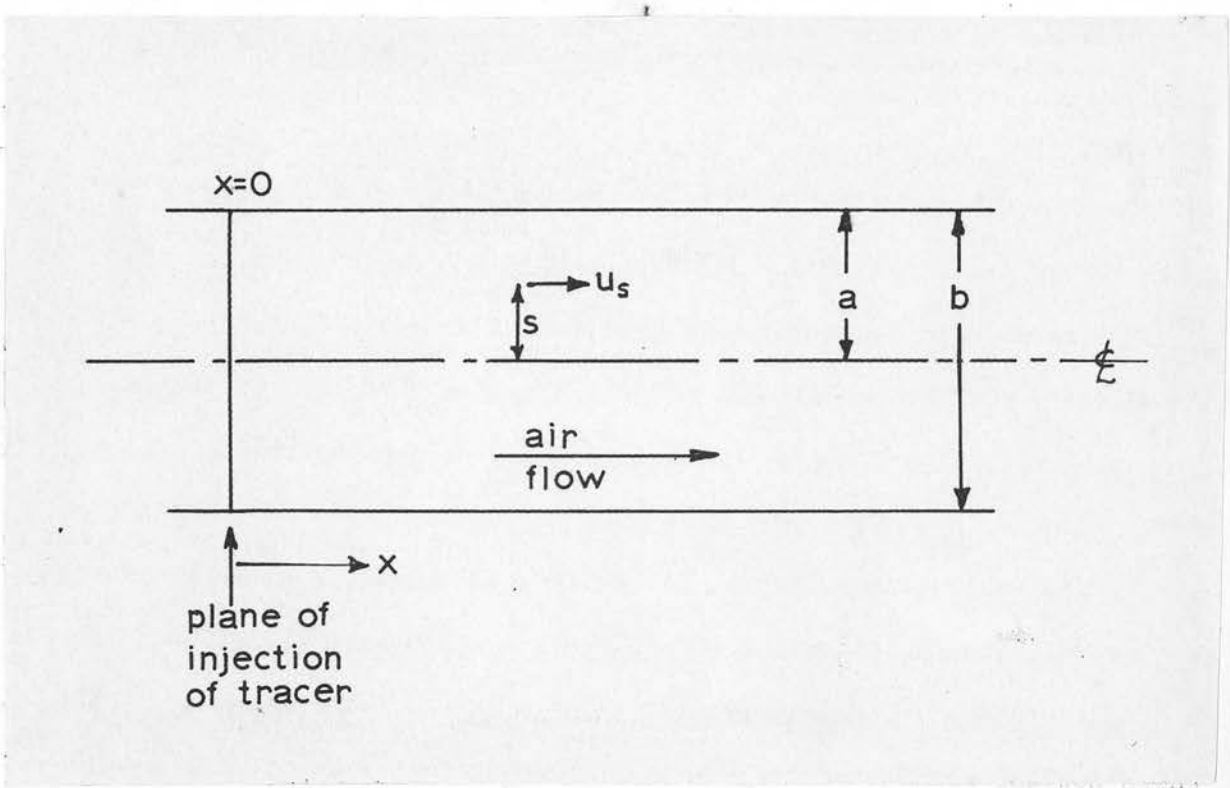

Figure 41. Longitudinal diffusion between parallel plates. Instantaneous uniform change in concentration of flowing fluid at plane x = 0

calculated on the basis of equation (50).

9.51 Longitudinal diffusion with laminar flow of air in an annulus. Parallel plate approximation. Pulse or step change.

Using a method identical with one developed by Taylor (48) an analysis is now presented for the case of longitudinal diffusion with laminar flow in the gap between parallel plates, it being assumed that the parallel plate theory is a sufficiently good approximation to that governing dispersion in a narrow annulus.

Figure 41 shows the system under consideration.

At the plane $x = 0$ and time $\theta = 0$ a change takes place in the concentration of the flowing stream, due to the injection of a tracer material (not necessarily a step or pulse change). It will be assumed that the concentration, c, of the tracer is symmetrical about the centre line of the system so that, in general, c is a function of s, x and θ only.

A mass balance on an element of the air stream at the point s, x, θ gives:-

$$D \frac{\partial^2 c}{\partial s^2} + D \frac{\partial^2 c}{\partial x^2} = \frac{\partial c}{\partial \theta} + u_s \frac{\partial c}{\partial x} \quad - - - (76)$$

where D is the coefficient of molecular diffusion of the tracer material in air, assumed independent of concentration, and u_s is the velocity of the air at a distance s from the centre line.

For flow between parallel plates, the velocity profile is given by:-

$$u_s = \frac{u_o}{a^2} (a^2 - s^2) \quad - - - (77)$$

where u_o is the maximum air velocity and a is half the gap width.

Assuming that $\frac{\partial^2 c}{\partial x^2} \ll \frac{\partial^2 c}{\partial s^2}$ and writing $z = \frac{s}{a}$, equation (76) becomes:-

$$\frac{D}{a^2}\frac{\partial^2 c}{\partial z^2} = \frac{\partial c}{\partial \theta} + \frac{u_o}{a^2}(a^2 - a^2 z^2)\frac{\partial c}{\partial x}$$

$$\text{or} \quad \frac{\partial^2 c}{\partial z^2} = \frac{a^2}{D}\frac{\partial c}{\partial \theta} + \frac{u_o a^2}{D}(1 - z^2)\frac{\partial c}{\partial x} \quad - - - (78)$$

The boundary condition expressing the fact that the wall is impermeable is:-

$$\frac{\partial c}{\partial z} = 0 \qquad \text{at} \qquad z = 1$$

It is difficult to find a complete solution of (78) giving the value of c for all values of s, x and θ when the distribution of c at time $\theta = 0$ is known. It is, however, possible to find approximate solutions which are valid in the following limiting conditions:-

(A) The changes in c due to convective transport along the system take place in a time which is so short that the effect of molecular diffusion may be neglected. (In this case, if for example a step change in concentration occurs, the boundary between tracer and air will in time distort into a parabola).

This condition (A) is of no practical significance in the present investigation since it is precisely the effects of molecular diffusion which are being investigated.

(B) "The time necessary for appreciable affects to appear, owing to convective transport, is long compared with the 'time of decay' during which radial variations of concentration are

reduced to a fraction of their initial value through the action of molecular diffusion" (quoting from Taylor (48)). Quoting again: "To find the conditions under which (B) may be expected to be valid it is necessary to calculate how rapidly a concentration which varies with s degenerates into a uniform concentration." The conditions under which this 'time of decay' is short are discussed separately in Appendix J.

Assuming that condition (B) is valid, an approximate solution to equation (78) will now be obtained.

Since molecular diffusion in the longitudinal direction has been neglected, $\frac{\partial^2 c}{\partial x^2} \ll \frac{\partial^2 c}{\partial s^2}$, the whole of the longitudinal transfer of c is supposed due to convection. Consider the convection of material across a plane which moves at a constant speed $\frac{2}{3}u_o$, i.e. with the mean speed of flow in the gap.

Let $x_1 = x - \frac{2}{3} u_o \theta$

Then $x = u_s \theta = u_o (1 - z^2) \theta$ from (77)

$$\therefore \quad x_1 = x - \frac{2}{3} \frac{x}{(1 - z^2)} = \frac{x \left(\frac{1}{3} - z^2\right)}{(1 - z^2)}$$

$$\therefore \quad (1 - z^2)\frac{\partial c}{\partial x} = \left(\frac{1}{3} - z^2\right)\frac{\partial c}{\partial x_1}$$

Thus equation (78) becomes:-

$$\frac{\partial^2 c}{\partial z^2} = \frac{a^2}{D} \cdot \frac{\partial c}{\partial \theta} + \frac{u_o a^2}{D} \left(\frac{1}{3} - z^2\right) \frac{\partial c}{\partial x_1} \qquad - - - (79)$$

Following Taylor's reasoning (48); since the mean velocity across planes for which x_1 is constant is zero, the transfer of c across such planes depends only on the radial variation of c. If c were independent of x and condition (B) satisfied, it is shown in Appendix J that any radial variation in c very rapidly disappears. The small radial variation in c can therefore be calculated from the equation:-

$$\frac{\partial^2 c}{\partial z^2} = \frac{a^2 u_o}{D} \left(\tfrac{1}{3} - z^2\right) \frac{\partial c}{\partial x_1} \qquad - - - (80)$$

in which calculation $\frac{\partial c}{\partial x_1}$ may be taken as independent of z.

A solution of (80) which satisfies the boundary condition $\frac{\partial c}{\partial z} = 0$ at z = 1, is given by:-

$$c = (c)_{x_1} + B\left(z^2 - \tfrac{1}{2}z^4\right) \qquad - - - (81)$$

where $(c)_{x_1}$ is the value of c at z = 0 and B is a constant.

From (81):-

$$\frac{\partial c}{\partial z} = 0 + 2Bz - 2Bz^3$$

$$\frac{\partial^2 c}{\partial z^2} = 2B - 6Bz^2$$

Substituting for $\frac{\partial^2 c}{\partial z^2}$ in (80):-

$$2B - 6Bz^2 = \frac{a^2 u_o}{D} \left(\tfrac{1}{3} - z^2\right) \frac{\partial c}{\partial x_1}$$

$$\therefore \quad B = \frac{a^2 u_o}{D} \cdot \frac{\left(\tfrac{1}{3} - z^2\right)}{2(1 - 3z^2)} \cdot \frac{\partial c}{\partial x_1} = \frac{a^2 u_o}{6D} \cdot \frac{\partial c}{\partial x_1} \qquad - - - (82)$$

The rate of transfer of c across the section at x_1 is given by Q, where:-

$$Q = -2 \int_0^a \frac{u_o}{a^2}(a^2 - s^2)c \,.\, ds \qquad \text{for unit depth}$$

$$= -2 \int_0^1 u_o \left(\tfrac{1}{3} - z^2\right)c \,.\, a \,.\, dz$$

$$= -2 \int_0^1 a u_o \left(\tfrac{1}{3} - z^2\right)\left[(c)_{x_1} + \frac{a^2 u_o}{6D}\frac{dc}{dx_1}\left(z^2 - \tfrac{1}{2}z^4\right)\right] dz$$

$$= -2\left[(c)_{x_1} \,.\, a u_o\left(\frac{z}{3} - \frac{z^2}{3}\right)\right]_0^1 + \frac{2a^3 u_o^2}{6D}\frac{\partial c}{\partial x_1}\int_0^1\left(\frac{z^2}{3} - \frac{7z^4}{6} + \frac{z^6}{2}\right) dz$$

$$= 0 - \frac{1}{3}\frac{a^3 u_o^2}{D}\frac{\partial c}{\partial x_1}\left(\frac{1}{9} - \frac{7}{30} + \frac{1}{14} - 0\right)$$

$$\text{or} \quad Q = \frac{16}{945} \cdot \frac{a^3 u_o^2}{D} \cdot \frac{\partial c}{\partial x_1} \qquad ---(83)$$

Following the method used by Taylor (48), the value of c from (81) and (82) is inserted in (83) giving:-

$$Q = \frac{16}{945} \cdot \frac{a^3 u_o^2}{D} \cdot \frac{\partial (c)_{x_1}}{\partial x_1}$$

Since the condition (B). is assumed to hold the radial variations in c are small compared with those in the longitudinal direction, and if c_m is the mean concentration over a cross-section, $\frac{\partial (c)_{x_1}}{\partial x_1}$ is indistinguishable from $\frac{\partial c_m}{\partial x_1}$, so that Q is given by:-

$$Q = \frac{16}{945} \cdot \frac{a^3 u_o^2}{D} \cdot \frac{\partial c_m}{\partial x_1} \qquad ---(84)$$

It may now be seen that c_m is dispersed relative to a plane which moves with the mean velocity, $\bar{u}(=\frac{2}{3}u_o)$, exactly as though it were being diffused by a process which obeys the same law as molecular diffusion, but with an apparent longitudinal diffusion coefficient, D_L, where:-

$$D_L = \frac{16}{945} \cdot \frac{a^3 u_o^2}{D} \cdot \frac{1}{2a} = \frac{8}{945} \cdot \frac{a^2 u_o^2}{D}$$

If $\bar{u} = \frac{2}{3}u_o$ and $b = 2a$;

$$D_L = \frac{8}{945} \cdot \frac{b^2}{4} \cdot \frac{9}{4}\frac{\bar{u}^2}{D} = \frac{1}{210} \cdot \frac{\bar{u}^2 b^2}{D}$$

$$\therefore \quad D_L = \frac{1}{210} \cdot \frac{\bar{u}^2 b^2}{D} \qquad \text{- - - (85)}$$

This value of D_L is identical to the value which may be obtained using a method suggested by Aris (49).

The fact that no material is lost in the process is expressed by the continuity equation for c_m, viz:-

$$\frac{\partial Q}{\partial x_1} = 2a \cdot \frac{\partial c_m}{\partial \theta}$$, where the symbol $\frac{\partial}{\partial \theta}$ here represents differentiation with respect to time at a point where x_1 is constant. Eliminating D from (84) and (85):-

$$Q = D_L \cdot 2a \cdot \frac{\partial c_m}{\partial x_1}$$

$$\frac{\partial Q}{\partial x_1} = D_L \cdot 2a \frac{\partial^2 c_m}{\partial x_1^2} = 2a \frac{\partial c_m}{\partial \theta}$$

$$\therefore \quad D_L \cdot \frac{\partial^2 c_m}{\partial x_1^2} = \frac{\partial c_m}{\partial \theta} \qquad \text{- - - (86)}$$ which is the equation governing longitudinal diffusion.

9.52 Calculation of apparent longitudinal diffusion coefficient, D_L, from experimental data. Step change in tracer concentration.

It was shown, in section 9.52, that in laminar flow the diffusing material is dispersed relative to a plane which moves with the mean velocity, $\bar{u}$, exactly as though it were being diffused by a process which obeys the same law as molecular diffusion, but with an apparent longitudinal diffusion coefficient, D_L, given by (85), viz:-

$$D_L = \frac{1}{210} \frac{\bar{u}^2 b^2}{D} \quad - - - (85)$$

where b is the gap width for a narrow annulus and D is the molecular diffusion coefficient.

The equation governing longitudinal diffusion is given by (86), viz:-

$$D_L \frac{\partial^2 c_m}{\partial x_1^2} = \frac{\partial c_m}{\partial \theta} \quad - - - (86)$$

where c_m is the mean concentration over a section and x_1 is the distance of that section from the plane moving with the mean velocity, $\bar{u}$.

It is now assumed that at time $\theta = 0$, the concentration of tracer in the air stream at $x_1 = 0$ is suddenly raised from $c_m' = 0$ to a value $c_m' = 1$, (i.e. step change in tracer concentration), where c_m' now represents a normalised (dimensionless) mean concentration of tracer material. Under these conditions the diffusion equation equivalent to (86) is:-

$$D_L \frac{\partial^2 c_m'}{\partial x_1^2} = \frac{\partial c_m'}{\partial \theta}$$

As assumed by Danckwerts (50) the following boundary conditions will represent the facts with sufficient precision:-

c_m'	= 0	at	$x_1 > 0$	for	$\theta =$	0
c_m'	= 1	at	$x_1 < 0$	for	$\theta =$	0
c_m'	= 0	at	$x_1 = \infty$	for	$\theta >$	0
c_m'	= 1	at	$x_1 = -\infty$	for	$\theta >$	0

As discussed by Danckwerts (50) these boundary conditions hold if

$\frac{4D_L}{Lu} \ll 1$ and in these circumstances, the solution to the equation

$D_L \frac{\partial^2 c'_m}{\partial x_1^2} = \frac{\partial c'_m}{\partial \theta}$ is given by:-

$$c'_m = \tfrac{1}{2}\left[1 - \operatorname{erf}\left(\frac{x_1}{2\sqrt{D_L\theta}}\right)\right] \qquad \text{---(87)}$$

where $\operatorname{erf}\left(\frac{x_1}{2\sqrt{D_L\theta}}\right) = \frac{2}{\sqrt{\pi}} \cdot \int_0^{x_1/2\sqrt{D_L\theta}} e^{-t^2}\,dt$ numerical values of which may be found in tables of the "error function".

Now at any time, θ, the plane which moves with the mean velocity $\bar{u}$ is at a distance $\bar{u}\theta$ from the entry to the column.

Thus at the column outlet $x_1 = L - \bar{u}\theta$, where L is the length of column over which diffusion is measured.

If $F(\theta)$ is the fractional change in the outlet tracer concentration at time θ, then from (87):

$$F(\theta) = \tfrac{1}{2}\left[1 - \operatorname{erf}\left(\frac{L - \bar{u}\theta}{2\sqrt{D_L\theta}}\right)\right] \qquad \text{---(88)}$$

Defining a mean residence time, θ_o, of tracer in the column as:

$$\theta_o = \frac{L}{\bar{u}} \qquad \text{---(120)}$$

then differentiating (88) with respect to θ/θ_o, and putting $\theta = \theta_o$, we obtain:-

$$\left[\frac{d\,F(\theta)}{d(\theta/\theta_o)}\right]_{\theta=\theta_o} = \theta_o \cdot \left[\frac{d\,F(\theta)}{d\theta}\right]_{\theta=\theta_o} = \tfrac{1}{2}\bar{u}\sqrt{\frac{\theta_o}{\pi D_L}} \qquad \text{---(89)}$$

Thus, if the fraction $F(\theta)$ of the tracer leaving the column at time θ is measured experimentally and plotted as a function of time, θ, the slope of the $F(\theta)$ versus θ curve at the point $\theta = \theta_o$ can be found and a value for D_L found from this value of the slope; θ_o and $\bar{u}$ being known

in equation (89). This value of D_L should agree with the theoretical value calculated using equation (85) when the flow is laminar. From (88), $F(\theta) = \frac{1}{2}$ when $\theta = \theta_o$; thus the curve of $F(\theta)$ versus θ should go through the point $F(\theta) = \frac{1}{2}$, $\theta = \theta_o$ and this condition can be used as another check on the correlation of experiment with theory.

It is assumed in this analysis for a step injection of tracer that D_L is independent of L for a given $\bar{u}$ and that the parallel plate assumption is valid for annuli with low values of the ratio of gap width to mean radius ($b:r_m$).

A similar analysis may be made for the case of a pulse injection of tracer material.

9.53 Concentric tube theory

If the ratio $b:r_m$ is not small then the parallel plate approximation is not valid. For this case a private communication from Aris (49) gives the value of the apparent longitudinal diffusivity for laminar flow in an annulus. If the radii of the inner and outer cylinders are represented by r_1 and r_2 respectively, then the relationship quoted by Aris is:-

$$D_L = \frac{\left\{\frac{1}{48}(1+\alpha^2)(1+8\alpha^2+\alpha^4) + \frac{1}{36}(5+32\alpha^2+5\alpha^4)E + \frac{1}{4}(1+\alpha^2)E^2 - \frac{\alpha^4}{4}E^{-1}\right\}\cdot\frac{\bar{u}^2 b^2}{D}}{(1-\alpha)^2 \quad (1+\alpha^2+2E)^2} \qquad -- (90)$$

where $E = \dfrac{1-\alpha^2}{\ln \alpha^2}$ and $r_2 - r_1 = b = r_2(1-\alpha)$

It is shown in Appendix K that equation (90) reduces to equation (85),

the equation for parallel plates when $\alpha \rightarrow 1$ i.e. $\frac{b}{r_2} \rightarrow 0$.

Equation (90) is rather cumbersome and although it should strictly be used to evaluate values of D_L for the rotors used in this study, equation (85) was in fact used. This was justifiable since even for the $2\frac{3}{8}$" diameter rotor ($\alpha = 0.4130$) the values of D_L calculated from both (90) and (85) were identical when the values of α^2, E, etc., were evaluated using four figure logarithmic tables.

9.54 Longitudinal diffusion in an annulus with turbulent axial flow and both cylinders stationary

Taylor has developed the theory (51) for turbulent flow longitudinal diffusion in a round pipe. A theory analogous to that given by Taylor could be developed for turbulent axial flow in an annulus, using the parallel plate approximation. This has not been done in this thesis because the mercury vapour transfer column, designed primarily for use with a 'laminar plus vortex' regime in the annulus, was not sufficiently long to permit longitudinal diffusion experiments to be undertaken under turbulent axial flow conditions.

9.55 Longitudinal diffusion with vortices present in the annulus

In section 9.51 the apparent longitudinal diffusion coefficient, D_L, was calculated for purely laminar flow and equation (86), viz:-

$$D_L \frac{\partial^2 c_m}{\partial x_1^2} = \frac{\partial c_m}{\partial \theta} \qquad \text{- - - (86)}$$

was established as the equation governing longitudinal diffusion. In section 9.52 equation (86) was integrated using the appropriate boundary conditions for a step change in concentration, (normalised).

For longitudinal diffusion in a vortex regime it will be assumed

that the presence of the vortices in the fluid stream merely affects the value of the apparent longitudinal diffusion coefficient, D_L, but that the form of the integrated solution of (86) is unaffected by the change of flow regime. This assumption permits values of D_L to be derived from the results of tracer experiments with a vortex regime present in the annulus.

At rotor speeds insufficient to cause the onset of vortices the value of the experimentally determined apparent longitudinal diffusion coefficient, D_L, should remain independent of rotor speed (with the axial flow rate kept constant) and should agree with the value calculated theoretically according to equation (85), i.e.:-

$$D_L = \frac{1}{210} \cdot \frac{\bar{u}^2 b^2}{D} \qquad - - - (85)$$

where $\bar{u}$ is the constant mean axial velocity, b the annular gap width and D the molecular diffusion coefficient of the tracer material.

When the rotor speed is increased beyond the point at which vortices appear equation (85) is no longer applicable. With vortices present it would be expected that D_L would rise with rising rotor speed; i.e. that there would be increased back-mixing. D_L may then be plotted as a function of the circumferential Reynolds number and experiments repeated with the axial velocity, $\bar{u}$, given a succession of constant values. In this manner the influence of vortices on back-mixing of the air stream could be determined for several sizes of annulus. It was hoped in this way to throw light on the influence of vortices on back-mixing in the annulus of rotating concentric cylinder fractionating columns in order to determine whether such back-mixing had a significant

effect on column performance.

Croockewit et al (8) undertook experiments with water flowing in the annulus to determine the apparent longitudinal diffusion coefficient with a 'laminar plus vortex' regime. Using a sinusoidally varying tracer input of ammonium chloride, they measured the diffusion coefficient D_L over a range of rotor speeds and annular gap widths. The axial flow rate was maintained at a very low value, it being assumed that there was negligible influence of the axial flow on the vortex pattern. In the region designated by Kaye and Elgar (11) as 'laminar plus vortex' (see figure 7, Part I), Croockewit et al found that D_L was very approximately proportional to rotor speed at the low axial flow rates used. The relationship obtained was of the form:-

$$\frac{D_L}{n_1' \, b r_1} = h \qquad \text{- - - (91)}$$

where n_1' was the rotor speed in rev/sec, b the annulus width in cms., r_1 the rotor radius in cms., and h a numerical constant.

About 70% of the experimental points for this regime fell in the range given by:-

$$0.14 \, n_1' b r_1 \leqslant D_L \leqslant 0.17 \, n_1' b r_1 \qquad \text{- - - (92)}$$

The large variation in h, from a value 0.14 to 0.19 was attributed to random errors in experimentation, since no systematic trend could be detected.

For high rotor speeds a transition was observed from the regular vortex pattern to a more general turbulence - presumably the 'turbulent

plus vortex' regime of Kaye and Elgar (see figure 7, Part I). The experimental results suggested the following approximate criterion for the appearance of turbulence:-

$$\frac{2\, n_1' \, b^2 \, r_1}{\nu_w (r_1 + r_2)} \doteq 1000 \quad - - - (93)$$

where r_2 was the radius of the fixed outer cylinder and ν_w the kinematic viscosity of the water in the annulus.

Once turbulence was established, it was observed that the value of the parameter $\frac{D_L}{n_1' b r_1}$ fell below the previously approximately constant value of h(0.14 - 0.19) as the rotor speed n_1', was increased.

These results indicate that the apparent longitudinal diffusion coefficient, D_L, should rise linearly with rotor speed until turbulence appears, after which D_L should continue to rise, as the rotor speed is increased, reaching a maximum and eventually falling in value. At rotor speeds below the critical value for vortex formation the value of D_L should be independent of rotor speed.

The suggested criterion for turbulence (93) can be written in terms of two dimensionless groups - a circumferential Reynolds number and the group b/r_m, viz:-

$$\left(\frac{r_1 \, n_1' \, b}{\nu_w} \right) \cdot \frac{b}{r_m} \doteq 1000$$

i.e., when b/r_m is large, this critical circumferential Reynolds number

$(r_1 n_1' b/\nu_w)$ is small. On the basis of the apparent absence of turbulence in experiments with the mercury vapour column this seems incorrect. It also disagrees with the simple turbulence criterion, discussed in section 3.91, Part I (i.e. $\frac{r_1 \Omega b}{\nu} = 3000$ as $b/r_m \longrightarrow 0$, where $\Omega = n_1'/2\pi$).

It was expected that, in the present experiments on longitudinal diffusion, the existence of a separate 'laminar plus vortex' and 'turbulent plus vortex' flow regime would be shown by a change in the form of the plots of D_L versus rotor speed at a critical speed corresponding to the transition from one regime to the other. Unfortunately no such transition was in fact observed, and so the results of the present investigation could not be compared with those of Croockewit et al as far as the transition to turbulence is concerned. It is in any case doubtful whether such a comparison is valid even for a purely 'laminar plus vortex' regime, since the experiments of Crookewit et al were conducted with extremely small axial flow rates.

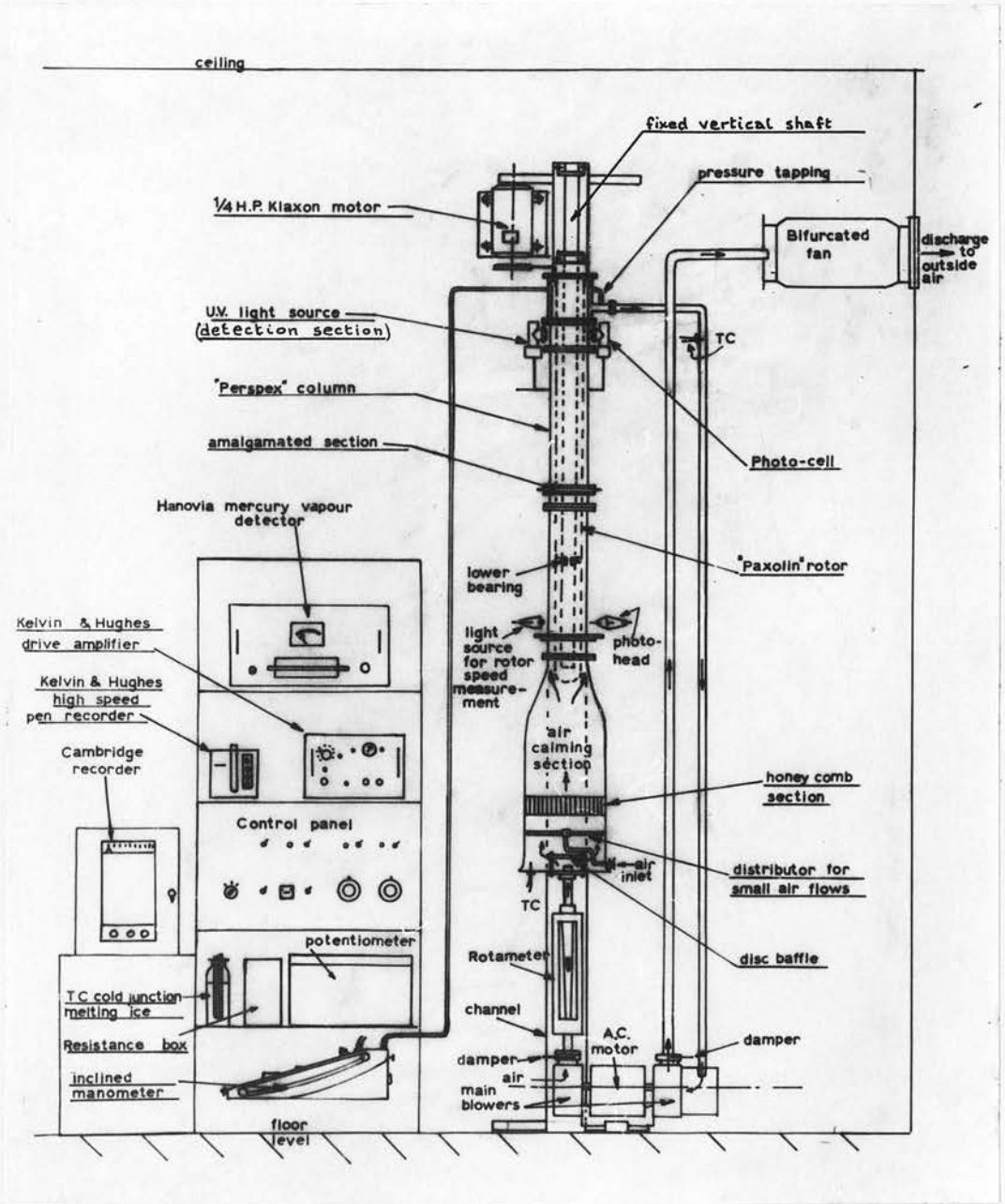

Figure 42. General layout diagram. Not to scale.

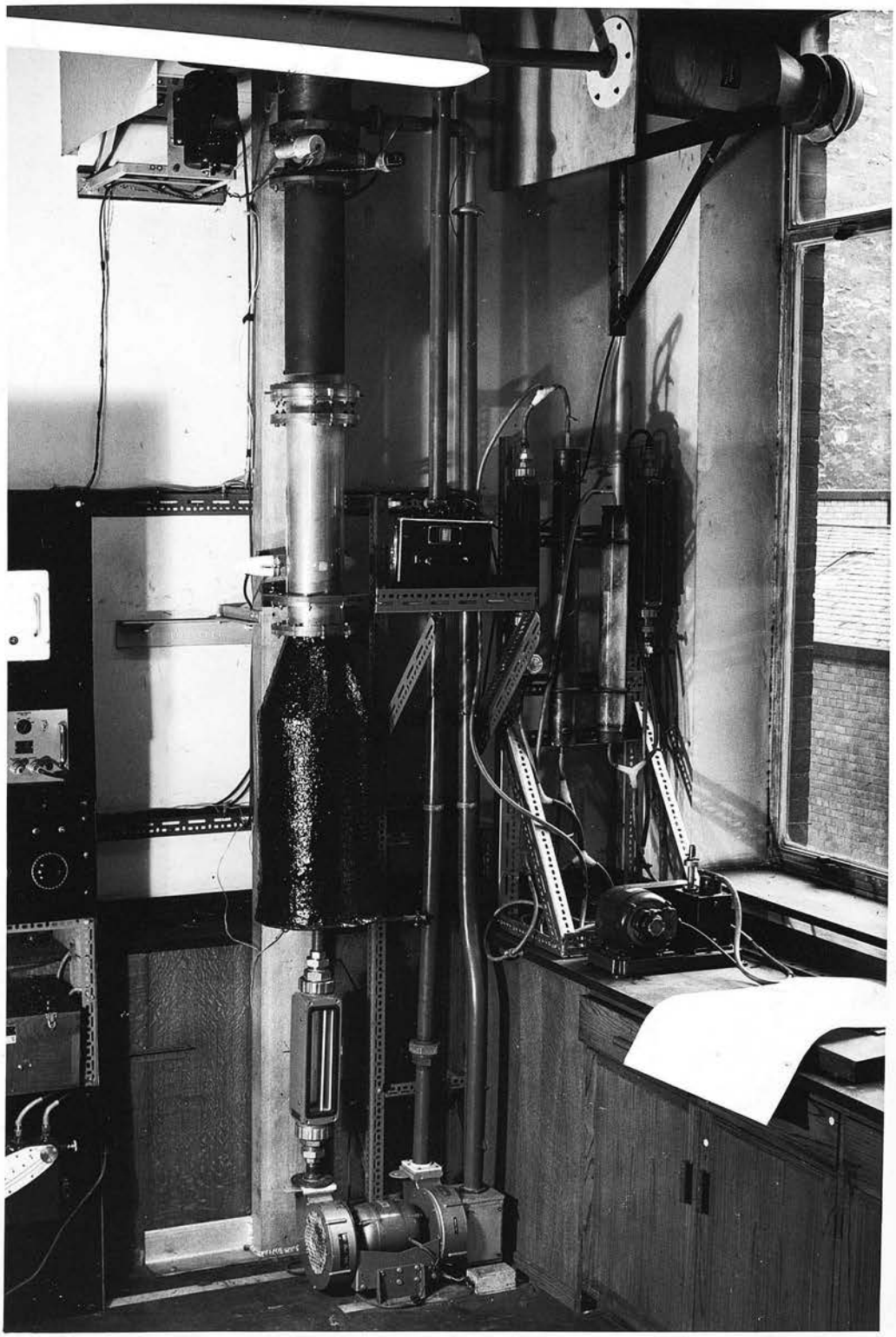

Figure 43a. Photograph of column.

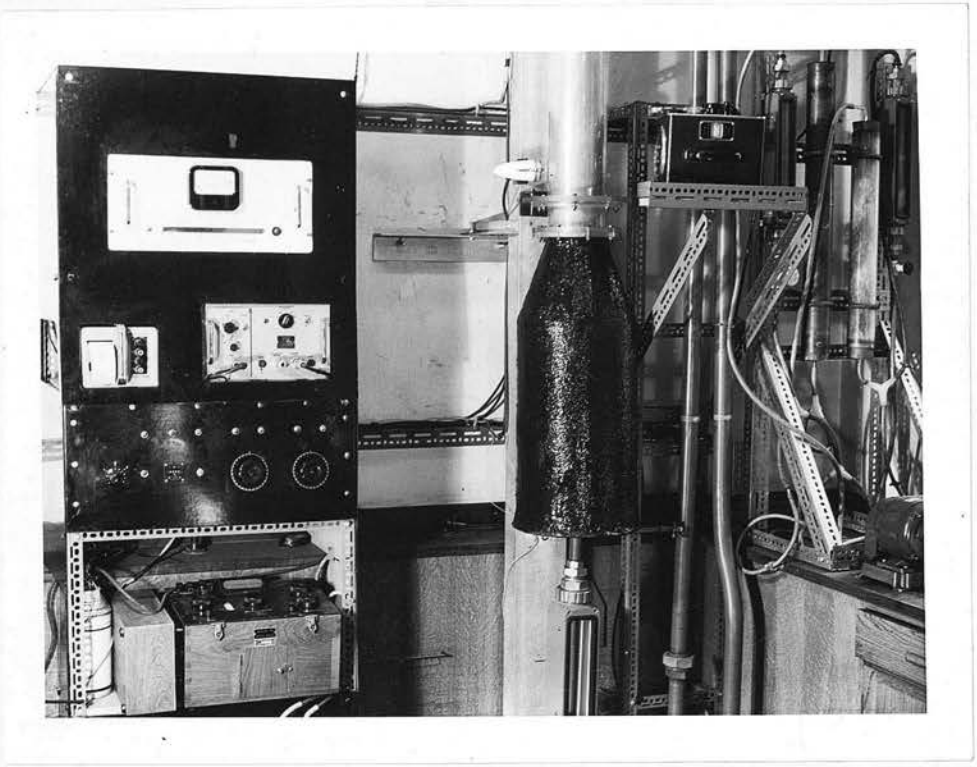

Figure 43b. Photograph of column.

Figure 44. Photograph of control panel and instruments used.

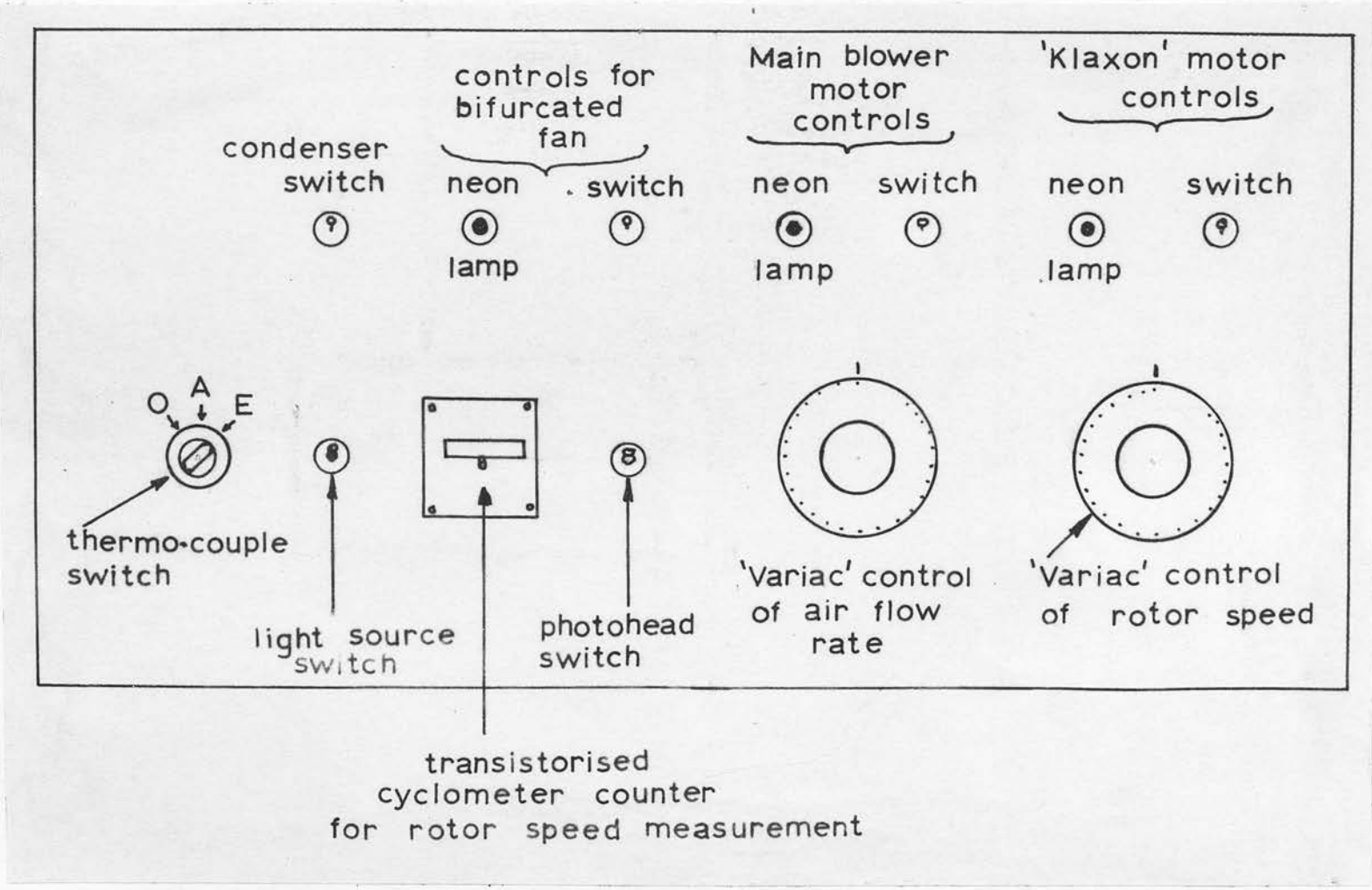

Figure 45. Details of controls on control panel.

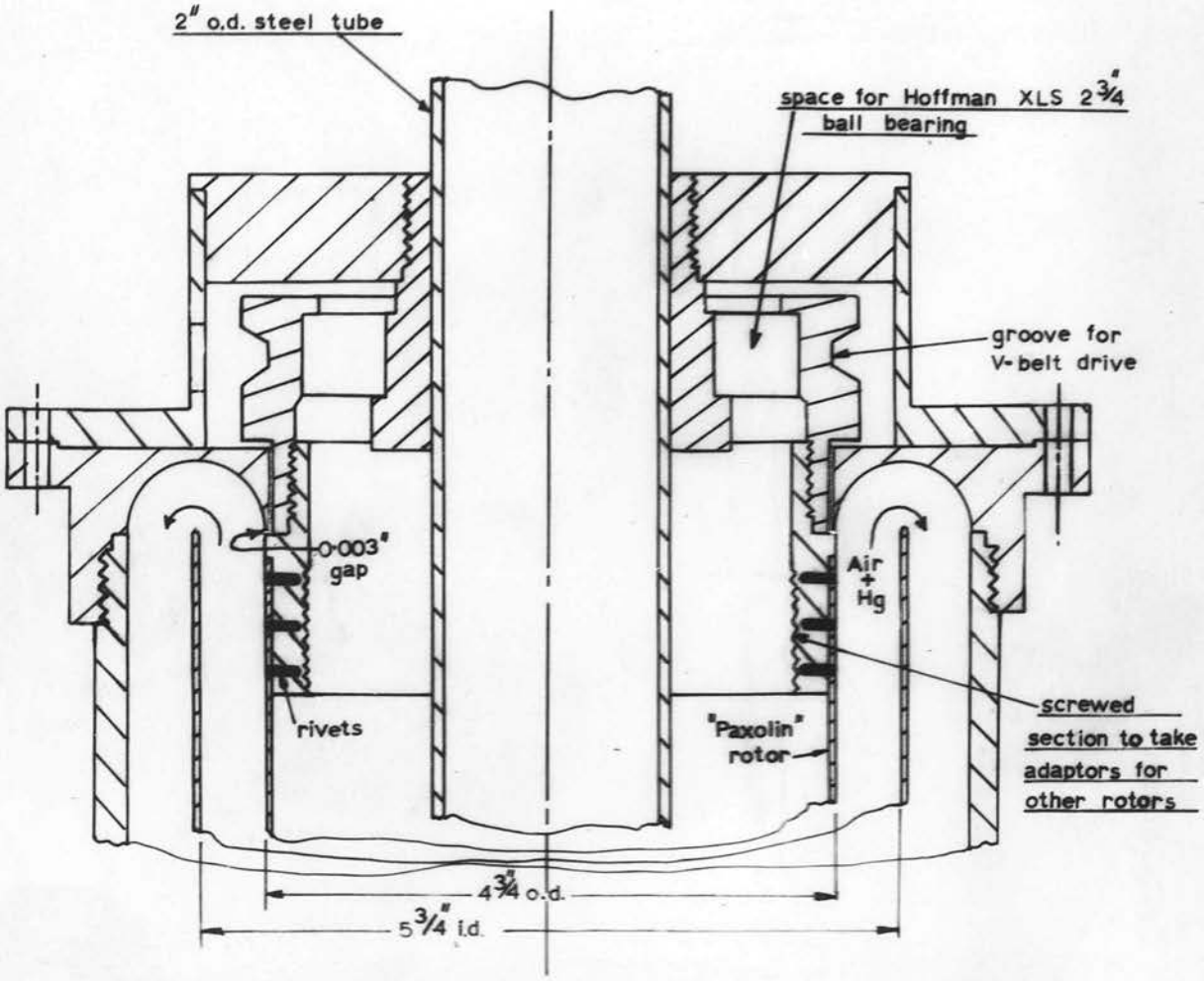

Figure 46. Details of upper bearing and rotor adaptor assembly.

10. EXPERIMENTAL

10.1 Description of Column

The mercury vapour transfer column was primarily designed to investigate the conditions of vortex formation and the effect of such vortex formation on radial and longitudinal mass transfer in an annulus with the inner cylinder rotating.

The general layout of the column assembly is shown in figure 42 and figures 43a, 43b and 44 show photographs of the column, control panel and instruments used. Figure 45 gives details of the controls situated on the control panel.

10.11 Mechanical arrangement

The mechanical design of this column is similar in principle to the design of the rotating concentric cylinder fractionating column described in Part I, in that the entire column assembly is centred around a fixed vertical shaft (see figures 36 and 42). This vertical shaft, made of 2"o.d steel tube, was rigidly clamped at its upper end to a vertical supporting girder. The girder was of channel section and was fixed to the wall of the laboratory and extended down to the floor. A rotor made of 'Paxolin' tube turned about the fixed vertical shaft, the upper bearing being situated near the top of the shaft and the lower bearing about two-thirds of the way down. The distance between bearings was about five feet.

The outer race of the upper bearing carried a pulley and rotor adaptor, as shown in figure 46. The 'Paxolin' rotor was fitted to

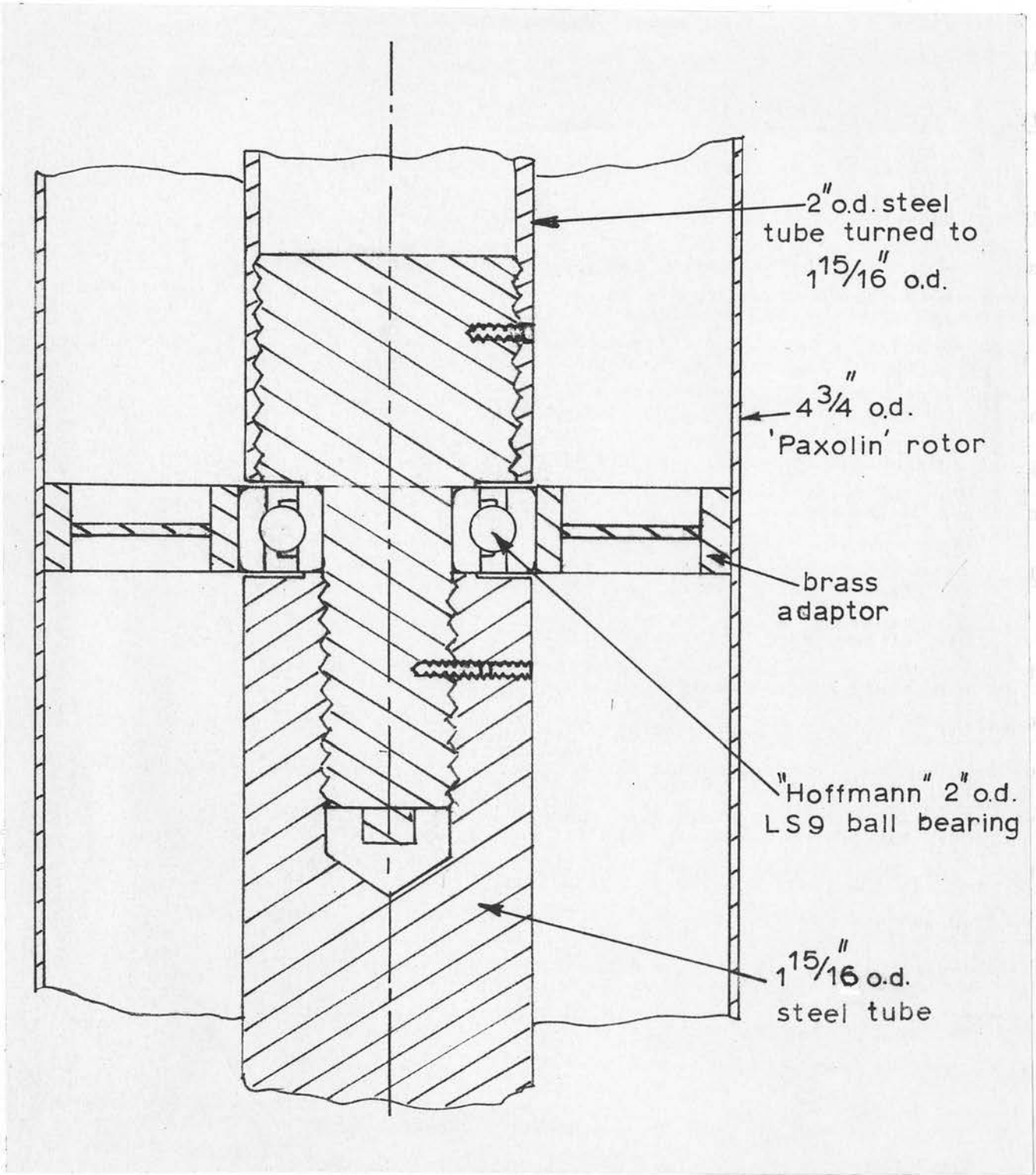

Figure 47. Details of lower bearing assembly for $4\frac{3}{4}$" o/d rotor. Brass adaptors of different sizes used for other rotors.

the adaptor and could be made to rotate about the central shaft by means of a V-belt drive from a $\frac{1}{4}$ H.P. series wound "Klaxon" motor mounted on a frame fixed to the laboratory wall. The speed of the "Klaxon" motor was controlled by means of a "variac" transformer mounted on the control panel (see figure 45). By fitting rotor adaptors of appropriate sizes to the pulley, it was possible to mount 'Paxolin' rotors of different diameters. Four different rotors were used, of outside diameters $2\frac{3}{8}$", $3\frac{1}{8}$", $4\frac{3}{4}$" and 5.18" respectively, in a fixed outer cylinder of $5\frac{3}{4}$" internal diameter. Figure 46 shows (for the sake of clarity) only one size of rotor adaptor.

The great advantage in using 'Paxolin' rotors (thin walled cylinders of cardboard impregnated with phenolic resin) was that they were rigid and extremely light in weight, and hence capable of rotation at high speeds without presenting a serious stability problem. As the design of the fractionating column investigated in Part I had proved extremely successful from the point of view of stablity the lower bearing in this mercury vapour transfer column was placed in a position similar to the lower bearing in the fractionating column, i.e. about two-thirds of the way down the fixed central shaft. Details of the lower bearing assembly are shown in figure 47.

The column was attached to the vertical support girder by the fixtures indicated in figures 48, 49a and 49b. These fixtures were made in accordance with Kinematic Design principles (52) and had the

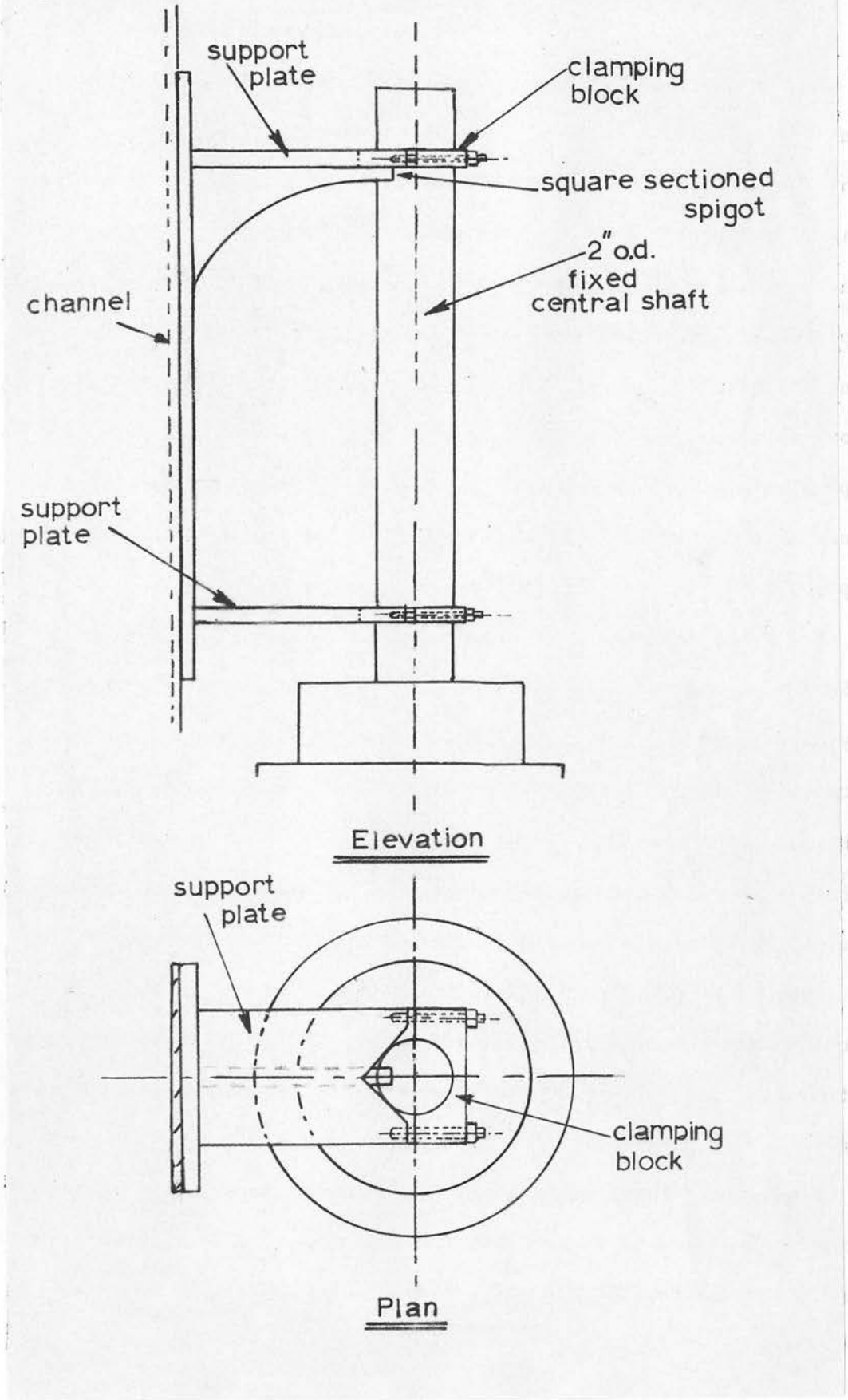

Figure 48. Upper fixture. Fixed central shaft clamped to channel.

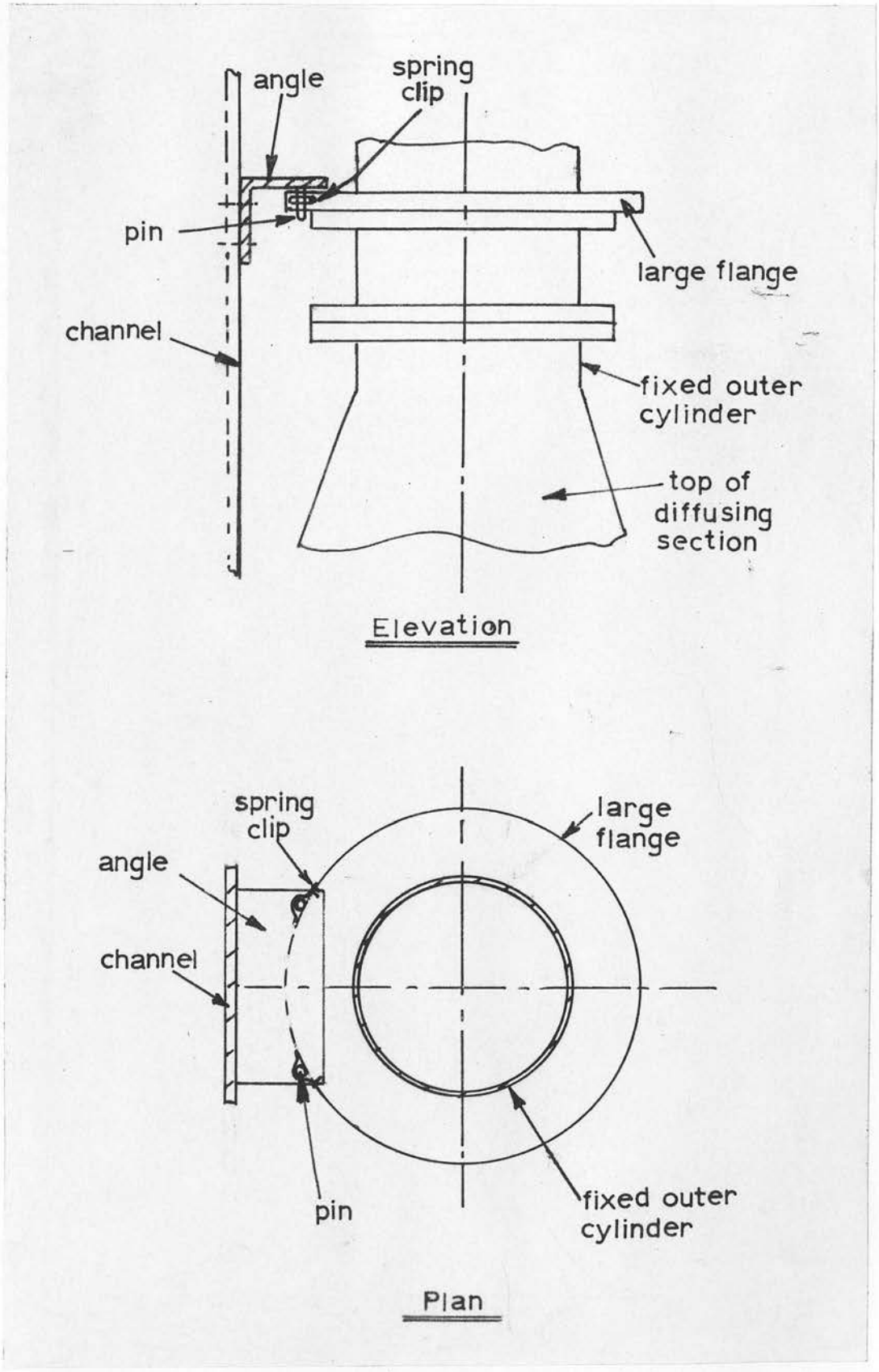

Figure 49a. Lower fixture. Large flange on outer cylinder located and fixed to channel.

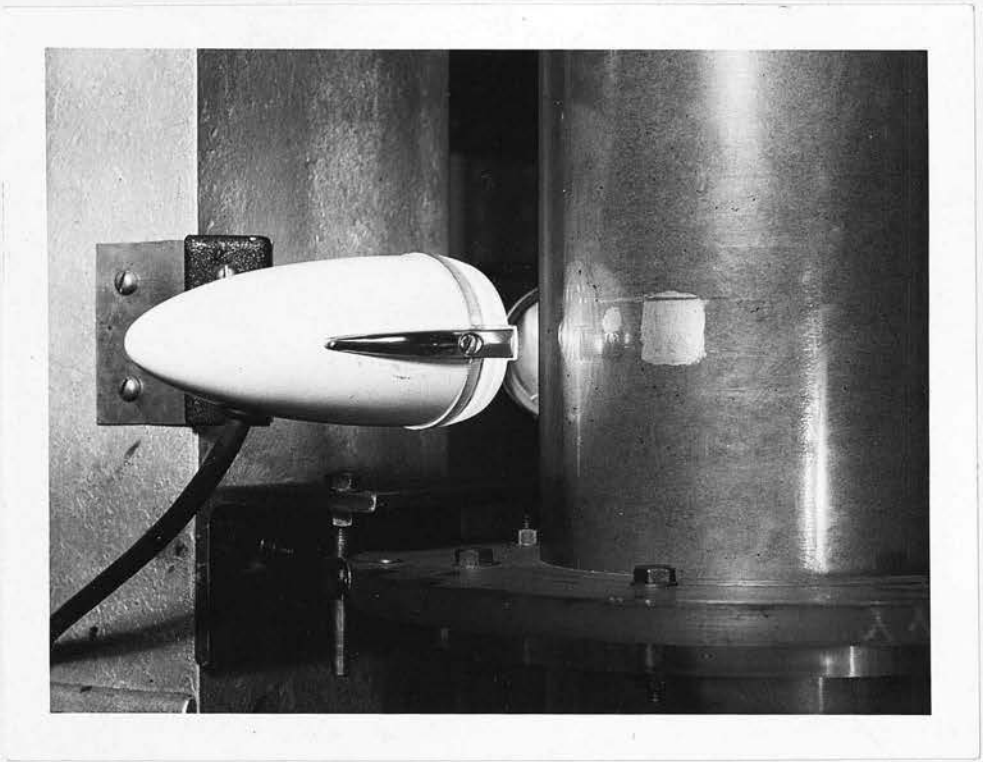

Figure 49b. Photograph of lower fixture and system for measuring rotor speed.

property that, once they were aligned, the column could be dismantled and re-assembled with ease without affecting the concentricity of the cylinders. As shown in figure 48 the 2" $^{o}/_{d}$ tubular central shaft was clamped at its upper end in V-notches cut in two support plates situated a foot apart. A horizontal square sectioned spigot, welded to the underside of the top plate, projected through a hole in the wall of the hollow shaft to provide positive support for its weight. The fixed central shaft could thus be securely clamped in a vertical position. Since both upper and lower bearings were located on this fixed shaft, rotation of the rotor about a vertical axis was ensured. The 'Perspex' outer cylinder was made of several flanged sections, as shown in figure 42. The top section was bolted to the flange of the outer cylinder shown in figure 46 (outer cylinder shown but flange at its lower end not shown). Any possible longitudinal movement of the outer cylinder at its lower end was allowed for by the fixture shown in figure 49a and the photograph in figure 49b, in which a flange, larger than the other column flanges was held against two fixed vertical pins by means of spring clips screwed to the edges of the flange. The pins kept the flange central, but allowed small vertical displacements. By loosening these clips and by removing the necessary boltsthe outer cylinder could easily be removed, allowing rotors of different diameter to be mounted on the fixed central shaft.

It was found with this mechanical arrangement, that for all the rotors used, speeds of rotation extending over the complete range from 0 to 2500 rpm were possible. Even greater speeds could be obtained with

some of the rotors used. For all these rotors it was observed that a critical speed existed at which considerable "wobbling" of the rotor occurred and above and below which the motion was stable; but this instability range was very narrow for all four rotors, and the impossibility of obtaining experimental results in these speed ranges was never a serious handicap.

10.12 Column operation

When the column was in operation, mercury-free air from the left-hand main blower (see figure 42) passed up through a rotameter (the capacity of which could be altered by using several sizes of tube) and then around a horizontal 'Perspex' disc baffle into the air-calming section. The main blower was situated at ground level vertically below the column and the speed of the blower motor was controlled by means of a "variac" transformer mounted on the control panel.

The bell-shaped air calming section, made of fibre glass and polished internally, had an internal diameter of 12" at the base tapering to $5\frac{3}{4}$" at the top where it joined onto the 'Perspex' fixed outer cylinder also of $5\frac{3}{4}$" inside diameter. A resin impregnated paper "honey-comb" section was inserted in the fibre-glass section to smooth the air flow.

On leaving the air-calming section the air entered the base of the annulus where the reduction in flow area caused additional smoothing of the air flow. The base of the rotor was sealed with a turned hemispherical wooden plug, which presented the minimum disturbance to the

flow of air into the annulus.

The air flowed up the annulus to the amalgamated section from which mercury vapour diffused into the air stream. The air and mercury vapour from the amalgamated section then flowed up the annulus to the mercury vapour detection section, across which passed a beam of ultra-violet light from the U.V. source mounted on the outside of the fixed outer cylinder. The part of the U.V. beam transmitted through the mercury vapour was detected by a suitably mounted photoelectric cell, the output from which was amplified and recorded on a D.C. microammeter in the Hanovia instrument. The microammeter was calibrated to give the concentration of mercury vapour in the air passing through the detection section. The method of calibration will be described later.

After flowing through the detection section, the air and mercury vapour mixture flowed over a weir, as shown in figure 46, and then out of the $1\frac{1}{2}$" N/B pipe into the suction side of the right-hand side main blower, which was located on a common shaft with the main blower supplying air to the column and powered by the same A.C. motor. The air and mercury vapour were finally discharged to atmosphere via the bifurcated fan at ceiling level.

10.13 Design of amalgamated section

This column was designed primarily to yield results with the amalgamated band of silver foil situated on the outer cylinder. Since the silver surface needed amalgamation prior to each experimental run, a design was required which permitted easy removal of the amalgamated section without dismantling the remainder of the column.

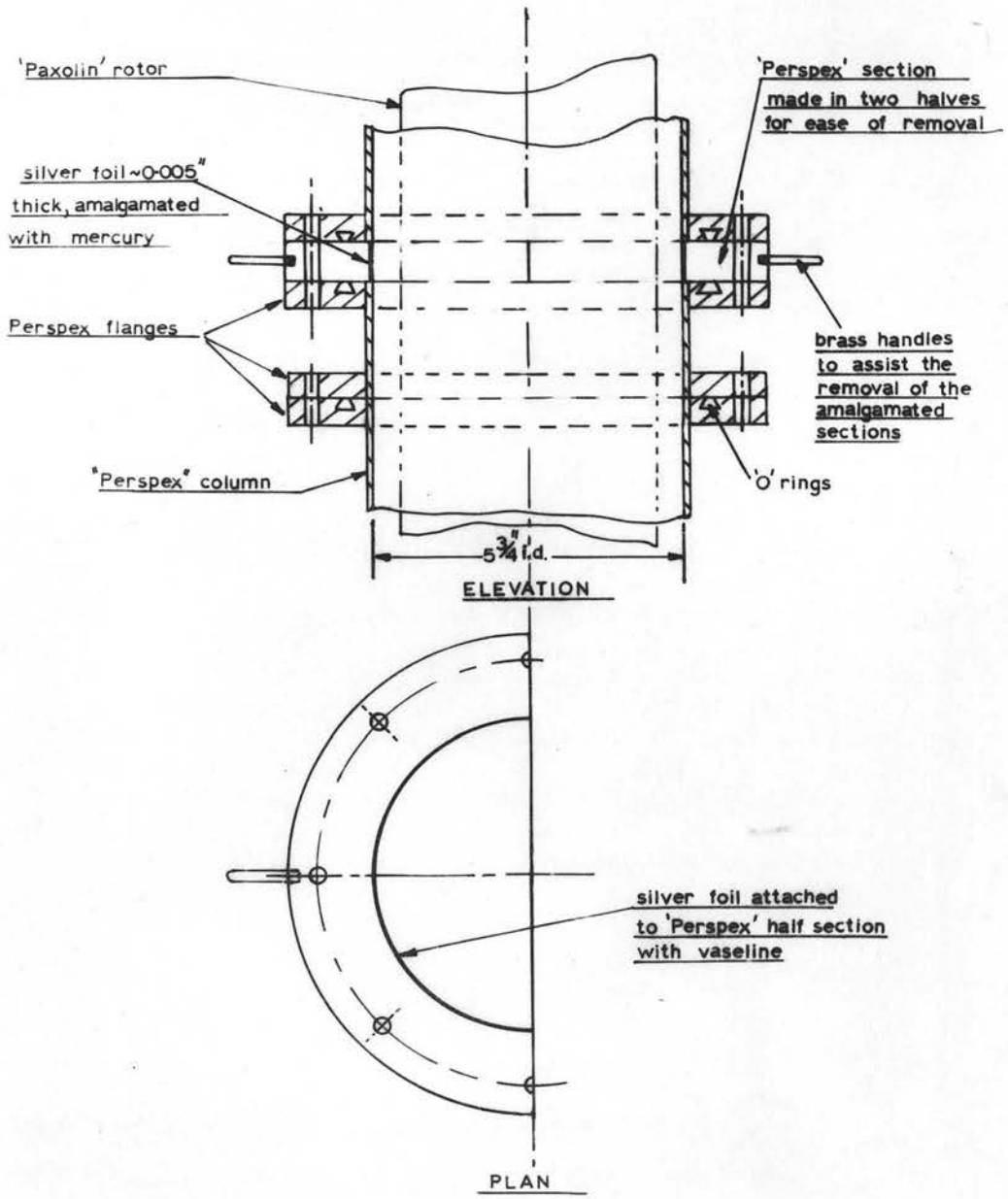

Figure 50. Amalgamation section made in two halves for ease of removal.

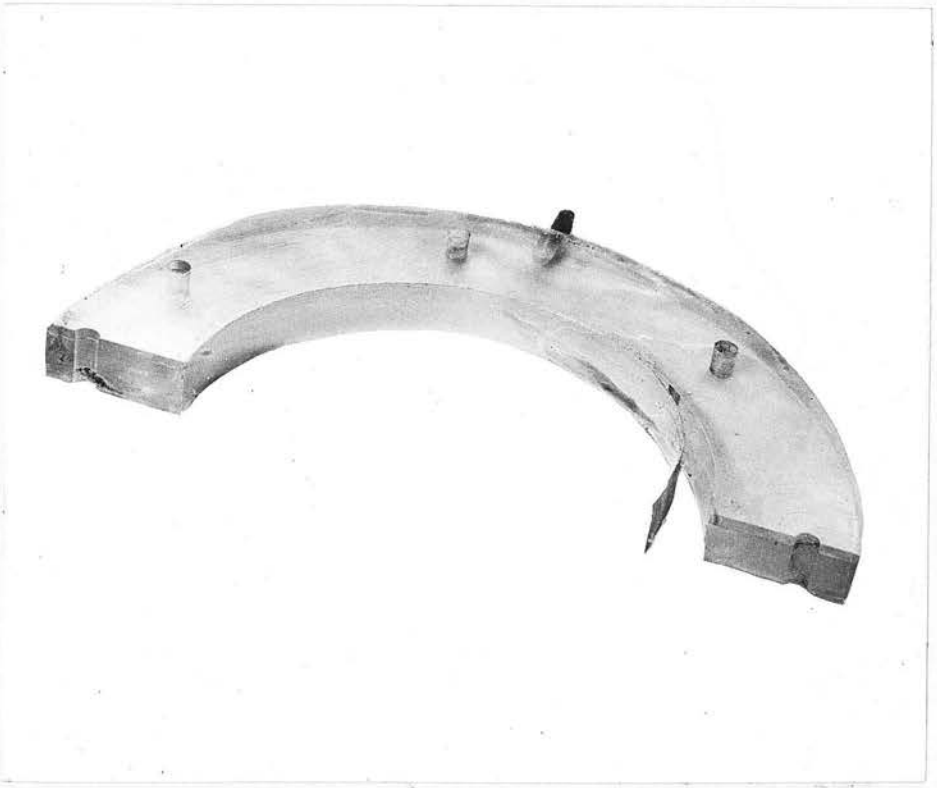

Figure 51. Photograph of half section with silver foil partly removed.

The design adopted is shown in figure 50. The 'Perspex' ring, carrying the amalgamated silver foil, was made in two half-sections with bolt holes drilled as shown. By removing the bolts which passed completely through each half-section and by loosening the two remaining bolts which passed through the split bolt-holes, it was possible to slide out the two halves of the 'Perspex' ring for re-amalgamation of the silver surface, without dismantling the rest of the column. Vaseline was used to fix 0.005" thick amalgamated silver foil to the two half-sections of the disc. The surface of the 'Perspex' was smeared with a layer of vaseline and the silver foil pressed into the vaseline, the excess being wiped away. Figure 51 shows the silver foil partly removed from the 'Perspex' half-section. Vaseline was found to be an excellent adhesive for this purpose since the bond required was essentially that between liquid mercury (which soon diffused through the silver foil) and a 'Perspex' surface; a quick-drying glue was of no use for this purpose.

The inside radii of the two half-sections were made greater than the inside radius of the outer cylinder by an amount equal to the thickness of silver foil plus the thickness of the layer of vaseline used for adhesion. Thus, when the amalgamated sections were inserted in the column, no discontinuity was presented to the air stream flowing past the amalgamated band of silver foil.

For the very few experiments in which the amalgamated band was situated on the rotor, the silver foil was merely wrapped around the rotor, soldered and amalgamated 'in situ'. This meant that the column

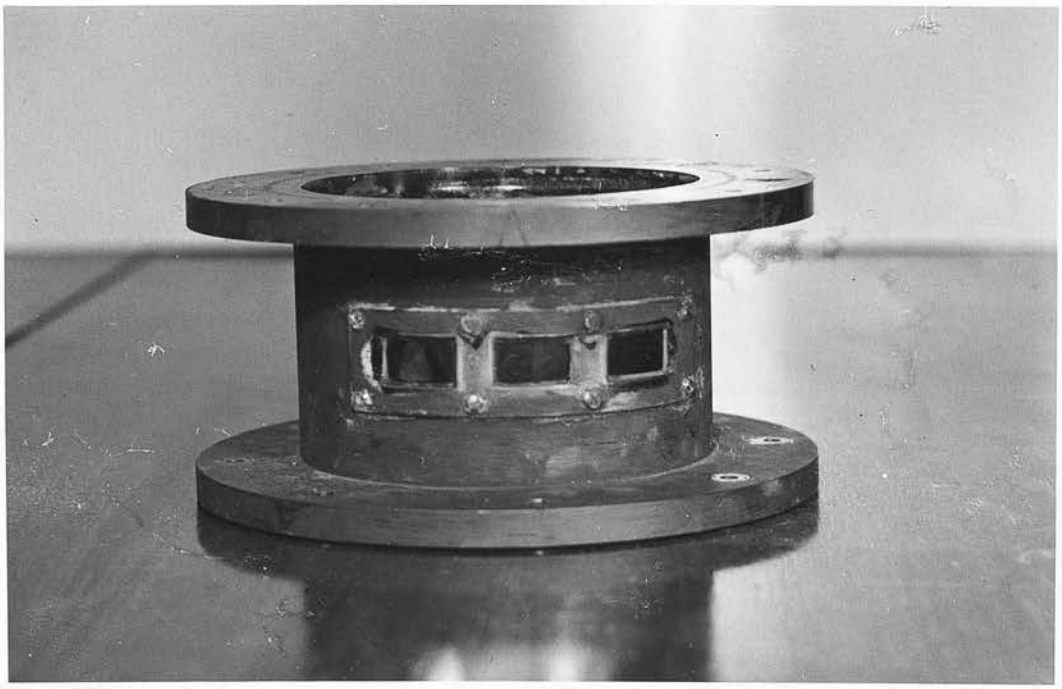

Figure 52. Photograph of detection section showing quartz 'windows'

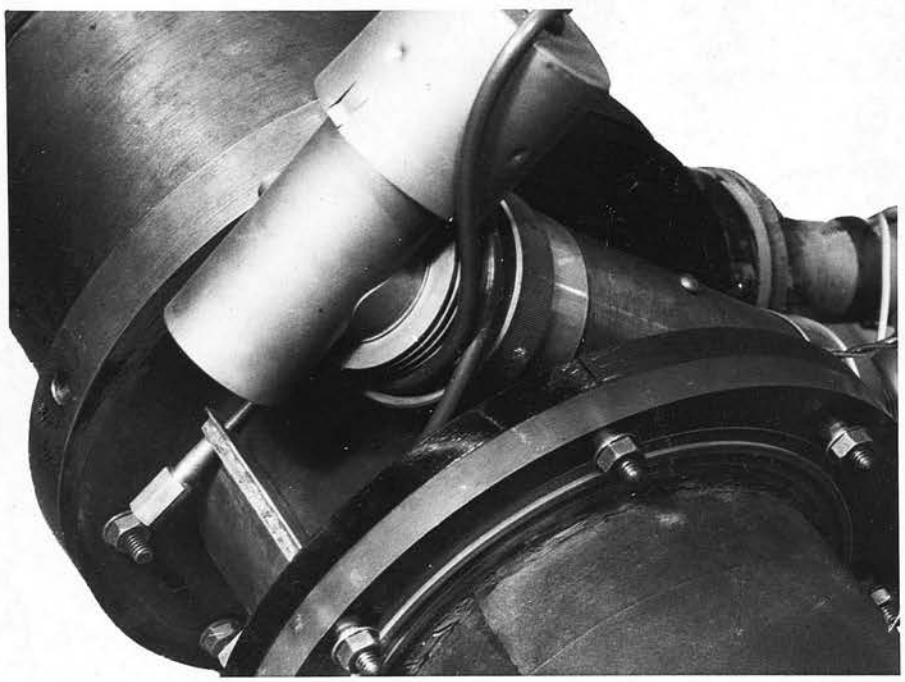

Figure 53. Photograph showing method of mounting the housing for the photoelectric cell and U.V. source. Photoelectric cell housing is shown in the foreground.

had to be completely dismantled to permit re-amalgamation of the silver foil prior to each experimental run.

10.14 Detection section for mercury vapour.

Because 'Perspex' is not transparent to ultra-violet light three quartz windows were fixed in the wall of the 'Perspex' outer cylinder in the detection section at the level of the U.V. source and photo-cell. These windows were inserted in such positions that no matter what size of rotor was used a beam of U.V. light could always pass tangentially across the annulus from source to photocell. Figure 52 is a photograph of the detection section indicating the manner in which the quartz windows were fitted. Figure 53 is a photograph of the housing (outside these windows) containing the photoelectric cell and ultra-violet source. The photoelectric cell holder is clearly visible in the foreground of this photograph. The purpose of the housing was to support both U.V. source and photoelectric cell and also to exclude daylight from the path of the U.V. light beam. In order to prevent stray light from entering the detection section the outside of the 'Perspex' outer cylinder in this region was painted black, and black paper was wrapped around the entire length of the outer cylinder between the detection section and amalgamated section, as shown in figure 43a.

10.15 Internal baffle.

For all experiments with the amalgamated band on the outer cylinder, except those conducted to determine longitudinal diffusion coefficients, a simple baffle was inserted between the amalgamated and detection section. This baffle (which is omitted from Figure 42) consisted of a thin 'Perspex'

circular disc, with its outside diameter machined so that it was a sliding fit inside the fixed outer cylinder. A hole was machined out of the disc having a diameter about a quarter of an inch greater than the outside diameter of the particular rotor being used. When inserted and held in place by plasticine (plasticine being used so that the baffle could easily be removed), the baffle prevented the possibility of mercury vapour streaming along the wall of the outer cylinder into the detection section without mixing with the rest of the air stream, causing a spurious value of mercury vapour concentration to be recorded. This value would be too high because the beam of U.V. light, passing tangentially across the annulus into the photoelectric cell, would then traverse a concentrated layer of mercury vapour adjacent to the wall of the outer cylinder. Previous trial runs had indicated that such streaming could occur and that this simple baffle arrangement caused effective mixing of the air and mercury vapour stream. It was found that this baffle was unnecessary for experiments with the 5.18" diameter rotor. Since the annular gap width in that case was 0.288", effective mixing of the mercury vapour and airstream would be expected by the time the detection section was reached.

10.16 Pumping system.

The need for the blower and bifurcated fan, at the column outlet is made clear by reference to Figure 46, showing details of the upper bearing and rotor assembly. It will be observed that no mechanical seal for the mercury vapour was provided at this bearing and that a small leak of air and mercury vapour could take place through the 0.003" wide

gap shown. Due to the highly toxic nature of mercury vapour (53,54) it was thought important to prevent any such leak by ensuring that the pressure inside the column, in the region of the 0.003" gap, was below atmospheric pressure, thus causing a very slight flow of air into the column through this gap. A pressure tapping on the 1½" N/B outlet pipe, connected to an inclined manometer on the control panel, was used to indicate the pressure in the column in the region of the gap. Throughout all experiments the manometer reading was kept at 0.1" water gauge, indicating that the pressure at the gap itself was probably very slightly less than 0.1" water below atmospheric pressure. Sliding "dampers", on the outlet from each main blower, were used for fine regulation of both air flow rate through the column and pressure differential at the 0.003" gap. Since this 0.003" gap was situated about 7" above the detection section, the slight flow of air into the column through it did not introduce any error in the determination of the mercury vapour concentration at the detection section. This was checked during the experimental runs by increasing the pressure differential at the gap. Quite large differentials (about 2") were required to cause sufficient introduction of air to significantly alter the microammeter reading on the Hanovia instrument.

When low air flow rates through the annulus were required, the main blowers were not used. In this case a small subsidiary pump, shown beneath the calibration apparatus in Figure 43a, was used to introduce air into the air-calming section by means of a tube connected to a

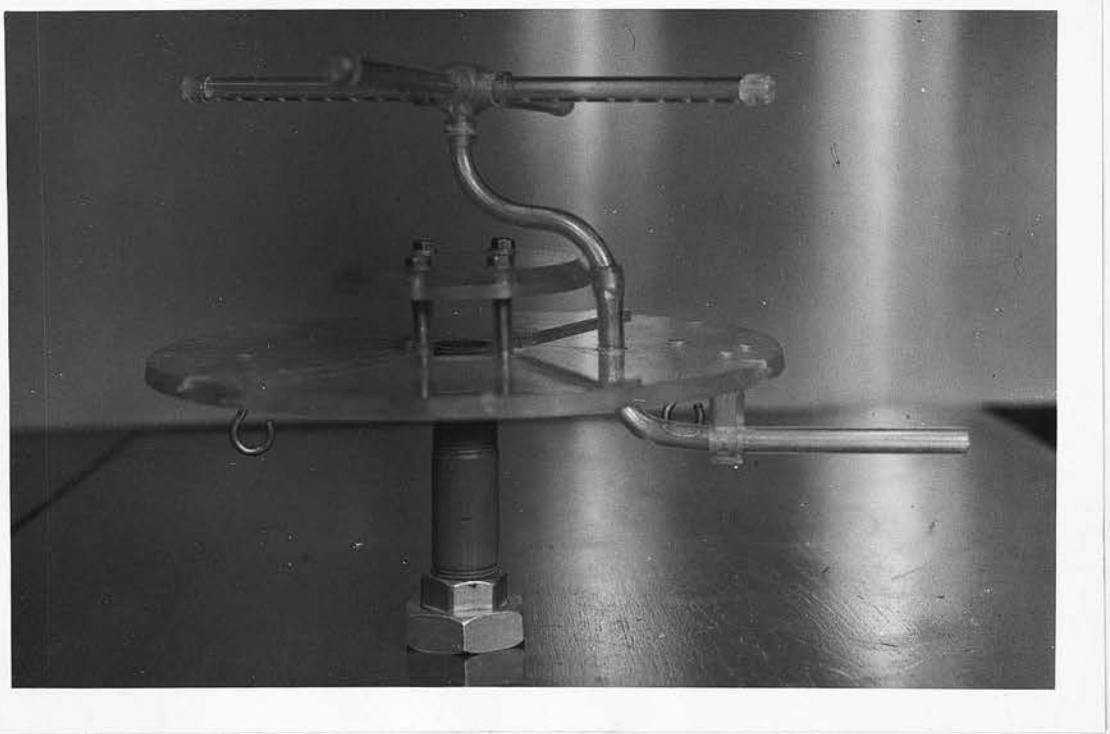

Figure 54. Photograph of cross distributor and disc baffle.

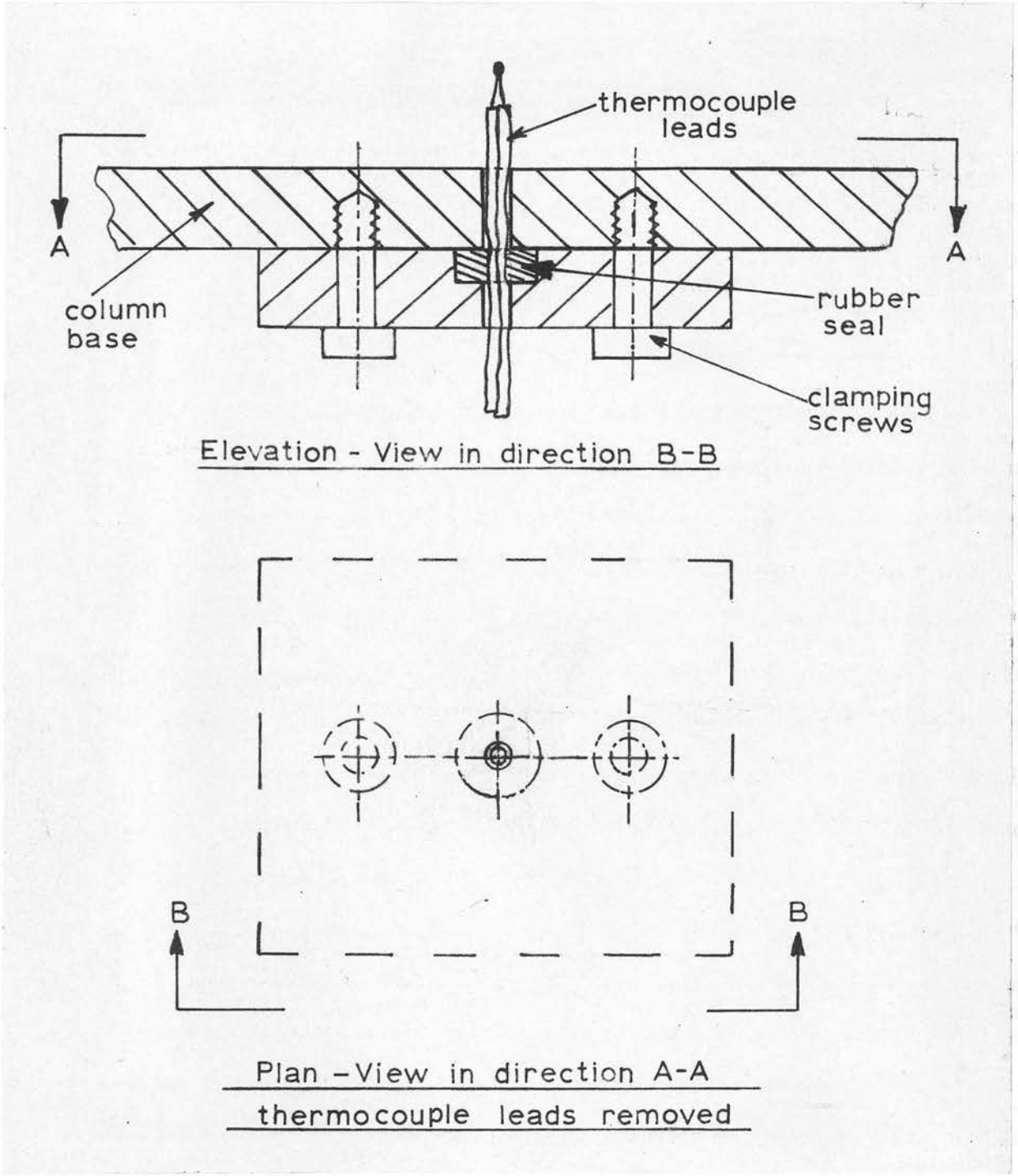

Figure 55. Details of thermocouple seal.

"Perspex" cross-shaped distributor.

A uniform flow of air across the calming section was ensured by the use of this "Perspex" distributor, shown in Figure 42. The air flowed out of several holes drilled in the walls of the "Perspex" tubes comprising this cross. Figure 54 shows a photograph of the distributor and also the disc baffle, the latter being used to distribute the air flow from the main blower when that blower was used.

When the subsidiary air inlet was used the bifurcated fan alone provided sufficient suction at the top of the column to ensure that there was no leak of mercury vapour through the 0.003" gap. The controls for the bifurcated fan were situated on the control panel as shown in Figure 45. 'O' ring seals, between the "Perspex" flanges on the column, ensured that there were no leaks of air or mercury vapour from the working section of the column. The temperature of the mercury-free air entering the air-calming section was measured by a chromel/alumel thermocouple inserted through a rubber seal into the base of the air calming section, as shown in Figure 55. A similar thermocouple inserted through the wall of the $1\frac{1}{2}$" N/B outlet at the top of the column, measured the temperature of the air and mercury vapour leaving the column. A third thermocouple was available for measuring the temperature of the air outside the column at the level of the amalgamated section. A thermocouple switch on the control panel (see Figure 45) connected any of these thermocouples to the galvanometer terminals of the potentiometer. (The potentiometer was situated under the control panel as shown in Figure 44). The positions O, A and E of the thermocouple switch corresponded to the thermocouples measuring the air outlet temperature (O), air temperature outside the annulus

(A), and the temperature of the air entering the column base (E), respectively. The system used for connecting the thermocouple junctions to the cold junctions and galvanometer terminals was identical to the system used for the thermojunctions of the fractionating column, described in Part I and shown in Figure 20.

10.17 Rotor speed measurement.

The speed of rotation of the 'Paxolin' rotor was measured by means of a stroboscopic lamp for speeds of rotation above about 350 r.p.m. Below these speeds a transistorised cyclometer counter, mounted on the control panel, was used for speed measurements. A light source and photohead were mounted on the channel behind the column, as shown in Figure 42 and the photograph Figure 49b. On each complete revolution of the rotor a patch of aluminium paint on the rotor reflected a beam of light from the source to the photohead. The output from the photohead was fed to the cyclometer counter which thus recorded the number of complete revolutions of the rotor from the time of switching on both light source and photohead during a time interval (normally one minute) determined by a stop clock. The cyclometer counter was capable of measuring speeds of rotation up to 360 r.p.m.

10.18 Recording devices.

For the longitudinal diffusion experiments a permanent record was required of the unsteady state variation of concentration with time after the step change had been introduced in the annulus. For this purpose both a Kelvin & Hughes high speed pen recorder and Cambridge pen recorder were provided, as shown in Figure 42. Although the

Cambridge instrument had a much slower response to concentration changes than the Kelvin and Hughes instrument, the pen deflection for a given concentration change was much greater. Thus, for those longitudinal diffusion experiments in which the concentration changes took place over a relatively long period of time, the Cambridge instrument was preferable. Furthermore, despite the provision of a mains voltage stabiliser, great difficulty was experienced in eliminating completely a 50 c/s vibration of the pen in the Kelvin and Hughes recorder. A 32 μF., 500 v. condenser (with switch shown on the control panel, see Figure 45) when inserted in the circuit of the Hanovia instrument reduced the amplitude of this vibration.

The Cambridge recorder could be connected via a potential divider (resistance box) to a D.C. amplifier, which in turn was connected to the photoelectric cell terminals of the Hanovia Mercury Vapour detector. The Kelvin and Hughes recorder could be connected directly to the D.C. amplifier. Thus the output signal from the photoelectric cell opposite the U.V. source was amplified by the D.C. amplifier and permanently recorded on the charts of either the Cambridge or Kelvin and Hughes recorders. At the same time the microammeter on the Hanovia instrument indicated the instantaneous output from the photoelectric cell and hence, from a calibration curve, the instantaneous concentration of mercury vapour in the air flowing through this detection section.

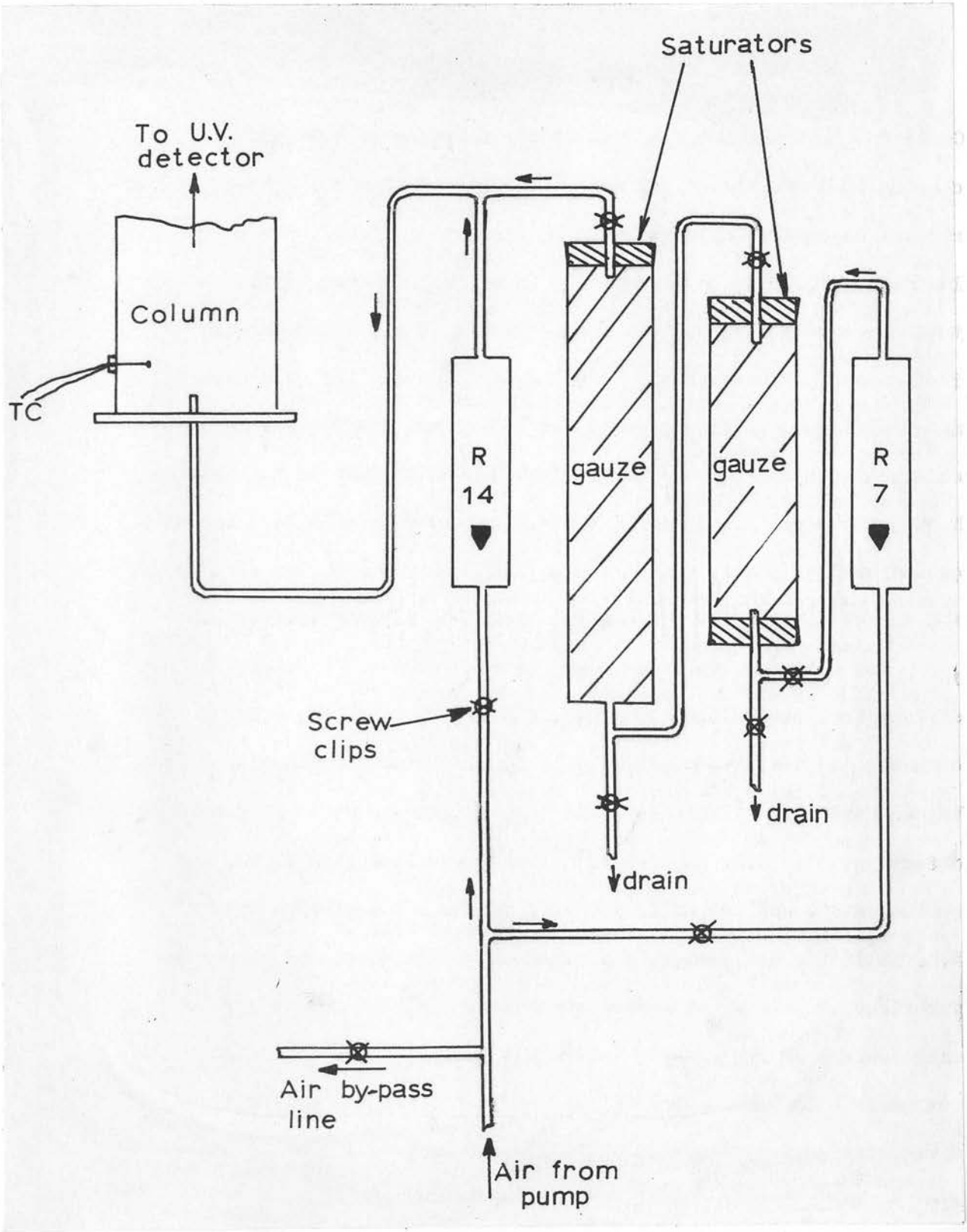

Figure 56. Calibration apparatus.

10.2 Calibration of the Hanovia Mercury Vapour Detector

The makers, when supplying this instrument (a modified version of the standard Hanovia mercury meter) expressed some doubt as to the reliability of the instrument if the U.V. source and photoelectric cell were used at such a great distance apart (approximately 11") as in the present system.

It was in fact found that the behaviour of the Hanovia instrument was erratic, the microammeter reading showing a "zero drift" after several hours use. This was possibly due to the large distance between source and photoelectric cell, in that the instrument was operating under maximum sensitivity under these conditions; but the defect was more likely due to ageing of the components within the instrument. On two occasions the instrument had to be completely overhauled and capacitances and rectifiers replaced. The erratic performance of the U.V. absorption system was a great handicap in this experimental project. It proved necessary to calibrate the microammeter prior to each experimental run with a particular rotor, since switching the instrument on and off also altered its calibration. A calibration method had therefore to be devised which was both reliable and easy to use.

The calibration method was based on a technique developed by Maxwell (55). The apparatus used is shown in figure 56 and photographed in figure 57. Air from a small subsidiary pump (shown in figure 57) flowed via a rotameter (metric size 7 (R7)) through two saturators placed in series, in which it was presumed that the air became saturated with mercury vapour. The mercury-laden air was then mixed with a stream of

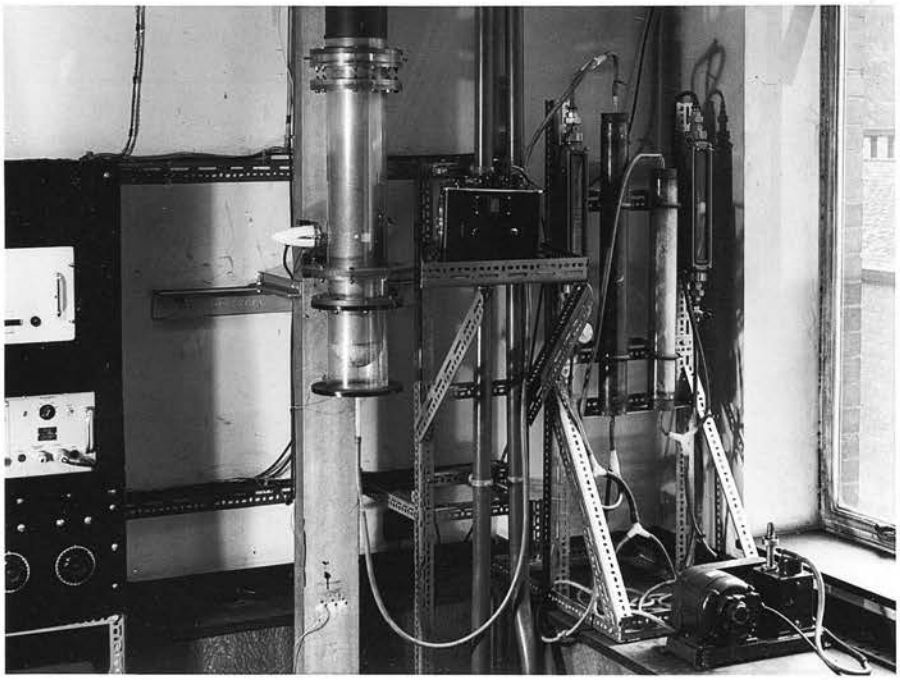

Figure 57. Photograph showing calibration apparatus and small section at column base for use in calibration runs.

mercury-free air flowing from the same subsidiary pump via the rotameter of metric size 14 (R14). The air and vapour mixture was passed into the base of the column where its temperature was measured by a thermocouple (TC). Prior to calibration the two half-sections carrying the amalgamated silver foil were removed from the column. The silver foil was stripped off these sections and the sections cleaned and replaced in the column. The air calming section at the base of the column was also removed and replaced by a short section, sealed at the end except for a small inlet, so that the air and mercury vapour mixture from the saturators could be introduced into the column. Figure 57 shows the arrangement used, the idea being to reduce the volume of air in the column and hence speed up the calibration procedure.

Thus a mixture of air and mercury vapour was obtained whose composition was uniform throughout the annulus and depended only on the relative flow rates of air through the rotameters R7 and R14.

With the rotor revolving at a speed of about 1000 rpm to ensure good mixing in the annulus the steady microammeter reading and corresponding float levels in the air rotameters R7 and R14 were noted, together with the temperature of the mixture entering the column. By means of the screw clips shown in figure 56, it was possible to alter the relative and absolute values of the flow rates through the rotameters R7 and R14 and thus calibrate the microammeter over its entire range. During the entire calibration procedure the reading on the inclined manometer was kept at 0.1" w.g. by adjusting the sliding damper above the right-hand blower.

The saturators consisted of two 3" diameter tubes, one made of copper 31" long and the other of "Perspex" 24" long, packed with amalgamated brass gauze. The brass gauze was amalgamated in situ by washing with acetone, draining (via the drain tubes shown in figures 56) and filling the tubes with saturated solutions of mercuric nitrate. The mercuric nitrate solution was drained from the tubes after it had been in contact with the gauze for about one hour. The saturators were then sealed off and left overnight, during which time any residual acetone or mercuric nitrate solution collected at the bottom of the saturator tubes, from where it was subsequently drained. The saturators were then ready for use.

The saturation concentration of mercury vapour in the air, at the temperature recorded by the thermocouple (TC) at the column inlet (assumed equal to the temperature of the air flowing through the saturators) was obtained from a curve of saturation concentration, c^{*}, versus temperature (^{o}C) shown in figure 87 after the Appendices to this report. This curve was obtained from values of the saturation vapour pressure, p^{*}, for mercury given in the International Critical Tables (44). Assuming that the ideal gas law held, these values of p^{*} were converted to saturation concentration values, c^{*}, as shown in Appendix L. Table 16 gives these calculated values of c^{*} as a function of temperature. The original values of p^{*} are also tabulated. The curve shown in figure 87 was drawn using this data.

If the float levels in the two rotameters R7 and R14 corresponded to flow rates, in litres/minute, of l_7 and l_{14} respectively, then the

concentration of mercury vapour, c_2, in the air at the detection section, was given by:-

$$c_2 = \frac{l_7}{l_7 + l_{14}} c^* \qquad - - - (94)$$

Values of c_2 corresponding to each microammeter reading could thus be calculated from equation (94) and plotted as a function of microammeter reading, giving the required calibration curve.

This technique was employed before each experimental run for all the rotors used. However, in some of the radial diffusion experiments using the $3\frac{1}{8}$" diameter rotor the microammeter readings obtained were very low and in this case the capacity of the small subsidiary pump was insufficient to permit calibration of these low meter readings. For these runs the calibration procedure was slightly modified: the air calming section was replaced at the column base and mercury free air was introduced via a rotameter R35 from the left-hand main blower. At the same time air was passed through the saturators, via the R7 rotameter, and also via the R14 rotameter on the saturation apparatus. This had the effect of diluting even further the mercury vapour saturated stream from the R7 rotameter and hence produced meter readings lower than could be obtained by mixing the streams from the R7 and R14 rotameters alone. As before the float positions on the R7, R14 and R35 rotameters were noted together with the microammeter reading and air temperature. By varying the relative and absolute values of the R7, R14 and R35 float levels the calibration of the Hanovia microammeter could be effected over the entire range required.

11. Experimental procedure

11.1 Radial diffusion experiments with the rotor stationary and an amalgamated band on the outer cylinder

Experiments were conducted using four different sizes of 'Paxolin' rotor to test the validity of equations (58), (60) and (62). The outside diameters of the rotors used were $2\frac{3}{8}$", $3\frac{1}{8}$", $4\frac{3}{4}$" and 5.18" respectively.

The column was assembled using one of these rotors and the Hanovia Mercury Vapour Detector was switched on. As recommended by the makers, this instrument was allowed to warm up for a period of about four hours prior to use. The microammeter pointer was then set to zero on the scale by means of the set zero adjustment provided on the panel of the instrument. Two sensitivity ranges were provided on the instrument and throughout these experiments the range corresponding to maximum sensitivity was used. The microammeter was then calibrated as described in section 10.2. When the calibration had been completed the air-calming section was replaced at the base of the column and a rotameter of suitable capacity was interposed between the base of the air-calming section and the left-hand main blower.

The two 'Perspex' half-sections, designed to carry the amalgamated silver bands, were then removed from the column in the manner previously described. The surface of each half-section was coated with a thin layer of vaseline and the two lengths of silver foil pressed into these half-sections. The silver surfaces of the two half-sections were then cleaned with cotton wool dipped in acetone and a drop of liquid mercury was then placed on each surface and gently rubbed over it until the

entire surface was amalgamated with mercury. A mirror finish was obtained and care was taken to ensure that a slight excess of liquid mercury was present on the amalgamated surfaces prior to replacement of the two half-sections in the column. In this manner a diffusing section on the inside surface of the outer cylinder was obtained which behaved virtually as a surface of pure liquid mercury. The amalgamated surfaces remained bright for periods up to about four hours and no falling off of mercury vapour concentration was noticed during this period of time.

Due to the highly toxic nature of mercury vapour, this amalgamation process was carried out in the open air outside the laboratory and rubber gloves were worn on all occasions. After amalgamation the two half-sections were replaced in the column as quickly as possible. The main blowers and bifurcated fan were then switched on by means of the "variac" control on the panel and the dampers above each blower were opened. The inclined manometer reading was set at 0.1" w.g. with a suitable flow rate recorded by the rotameter at the base of the column and the subsidiary air inlet to the cross-distributor (see figure 42) was closed.

With the rotor stationary, experiments were conducted in which the Hanovia microammeter reading and air temperatures at column inlet and outlet were recorded for varying values of the axial flow rate. By using rotameter tubes of metric sizes 7, 14, 18, 24 and 35 (with float calibrations supplied by the makers) (see figures 96 to 100 inclusive after the Appendices to this report), it was possible to take measurements over a wide range of axial Reynolds numbers. For

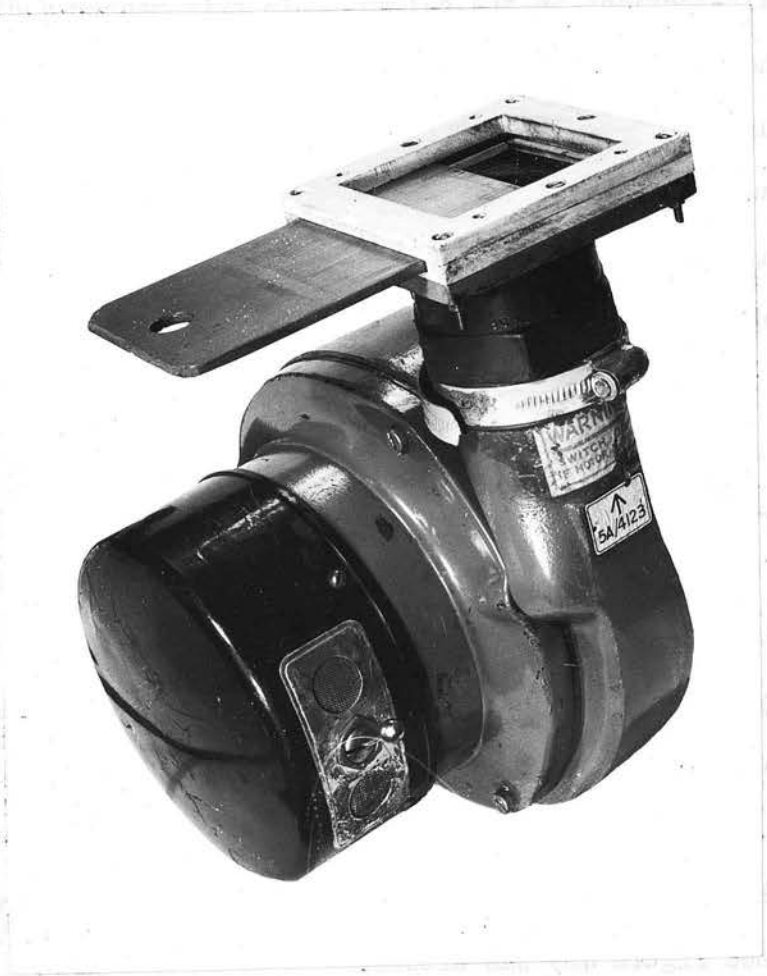

Figure 58. Photograph of large blower.

very small axial flow rates the cross-distributor was used to supply air to the annulus. In this case air from a small subsidiary pump flowed through the metric size 7 or 14 (R7 or R14) rotameter of the calibration apparatus and then into the distributor via the small air inlet projecting from the side of the air-calming section. In this manner the range of axial Reynolds numbers covered by the experiments was made to extend from about 0 - 1000.

At a much later date in this experimental project a centrifugal blower was obtained which had a much greater capacity than either main blower. The left-hand main blower was subsequently replaced by this larger blower and experiments performed at much higher flow rates with the $3\frac{1}{8}$" and 5.18" diameter rotors only. It was possible with this new blower, photographed in figure 58, to obtain axial Reynolds numbers up to values of about 2600. Figure 58 also shows clearly the construction of the damper which was used to regulate the air flow. The results for all these experiments are given in Tables 18, 19, 20 and 21 for all the rotors used.

11.2 Radial diffusion experiments with the rotor stationary and an amalgamated band on the rotor

In the case of the $3\frac{1}{8}$" and $4\frac{3}{4}$" diameter rotors, experiments were conducted with an amalgamated section fixed to the stationary rotor. The outside cylinder was removed and silver foil was wrapped around the rotor and soldered in situ at a level opposite the 'Perspex' half-sections. The silver foil was then amalgamated by rubbing the clean surface of the foil with another small piece of silver foil which had previously been dipped into liquid mercury. In this way it was

possible to amalgamate the silver foil on the rotor fairly quickly and the column was re-assembled.

Very few experiments were performed with silver foil situated on the rotor, due to the unsatisfactory nature of the technique involved in mounting and amalgamating the band. It was impossible to get a very close-fitting band on the rotor and the method of amalgamation did not produce a surface which was essentially saturated with liquid mercury, due to the difficulty involved in amalgamating a vertical surface in situ. Furthermore, reliable experiments could not be conducted with a revolving rotor, because as soon as rotation took place any excess liquid mercury on the amalgamated surface tended to spray off the rotor and became deposited eventually at the base of the column.

Thus only a few experiments were conducted with the rotor stationary in an attempt to verify equation (78) and none were conducted with a revolving rotor. The procedure involved was identical with the experimental procedure described in the last section and the results are presented in Tables 22 and 23 for the $3\frac{1}{8}$" and $4\frac{3}{4}$" diameter rotors respectively.

11.3 Radial diffusion experiments with the rotor revolving and an amalgamated band on the outer cylinder

Experiments were carried out with all the rotors to determine the variation of radial mass transfer coefficient with rotor speed. With the axial flow rate in the annulus kept constant and as low as possible the rotor speed was raised by small increments and the steady-state microammeter and thermocouple readings were recorded for each steady rotor speed. After the change to a new rotor speed the time required

for the microammeter reading to reach a steady state value was very small (less than one minute) for all experiments undertaken. Each steady rotor speed was measured either by the cyclometer counter or stroboscopic lamp as previously described. The axial flow rate was also noted from the rotameter reading.

The axial flow rate was then slightly increased, care being taken to ensure that the reading on the inclined manometer was re-adjusted to 0.1" w.g., and experiments repeated over the same range of rotor speeds used for the lower axial flow rate. This procedure was repeated until the entire range of possible axial flow rates had been investigated for rotor speeds varying from 0 to about 2500 rpm. The results from these experiments are given in Tables 24, 25, 26 and 27 for all rotors used.

11.4 Experiments to determine the conditions for vortex formation

It was observed, whilst performing the experiments described in section 11.3, that as the rotor speed was increased, with the axial flow rate kept constant, a critical rotor speed was reached at which the Hanovia microammeter reading increased above a value which had hitherto remained constant.* This critical speed was taken to represent that necessary for vortex formation at the particular constant value of the axial flow rate.

Experiments were therefore performed in which the axial flow rate of air in the annulus was kept constant and as low as possible whilst the rotor speed was gradually increased. The microammeter

* This observation confirms the validity of the argument put forward in section 9.3 that rotational and axial flows may be considered as independent variables in a purely laminar flow regime.

reading on the Hanovia instrument remained constant, at a value corresponding to purely laminar flow in the annulus until a critical rotor speed was reached causing a small rise in the microammeter reading.

In the experiments with the $2\frac{3}{8}$", $3\frac{1}{8}$" and $4\frac{3}{4}$" diameter rotors it was assumed that vortices appeared when the microammeter scale reading showed an increase of about half a division. As discussed later, this method led to considerable discrepancies between observed and expected critical values at low rotor speeds. Thus when experiments were conducted with the 5.18" diameter rotor, the critical rotor speed was taken to correspond to the first noticeable change in meter reading. When the rotor speed was increased above the critical value the meter reading increased, indicating improved radial mass transfer from the amalgamated band on the outer cylinder. The critical rotor speed and air flow rate were recorded together with the temperatures of the air entering and leaving the column.

In the experiments using the $2\frac{3}{8}$" diameter rotor the microammeter reading was very unsteady, particularly at low rotor speeds. This was possibly due to imperfect mixing of air and mercury vapour in such a wide annulus. At higher rotor speeds the pointer on the meter scale was much steadier. Thus the critical values recorded at low rotor speeds are rather suspect for this $2\frac{3}{8}$" diameter rotor.

Care was taken throughout these experiments to ensure that the reading on the inclined manometer was always at 0.1" w.g., no matter what axial flow rate was used.

Tables 28, 29, 30 and 31 record these critical conditions for

vortex formation for all rotors used. As it was unnecessary to calibrate the Hanovia microammeter for these experiments, values of Ta and Re_a only are calculated from the results recorded in Tables 28 to 31 inclusive.

11.5 Experiments to determine longitudinal diffusion coefficients

As discussed in the theoretical section, 9.5, the experimental determination of longitudinal diffusion coefficients for fluid flow in an annulus usually involves the injection of a tracer material at a convenient point in the system. An analysis of the "spread" of tracer material is then made at another point downstream from the place of injection. The injection of the tracer normally takes the form of a step change, pulse injection or sinusoidal variation of the tracer material.

In the present experiments mercury vapour was used as the tracer material. An abrupt change in the air flow rate produced approximately a step change in the concentration of mercury vapour in the annulus. The reason why the form of the step change was only approximate will be discussed later when the results are analysed. The experimental procedure will now be described.

11.51 Experimental procedure

The column was assembled with the amalgamated band of silver foil situated on the outer cylinder and the rotor was made to revolve at a constant speed. The small subsidiary pump, normally used for calibration purposes, was connected to the inlet of the cross-distributor projecting from the side of the calming section. In this way air was

introduced into the calming section and the rotameter (R14) situated on the calibration apparatus was used to meter this small air flow rate.

This air flow rate was maintained at a sufficiently small value by regulating the screw clip on the rubber air by-pass line, shown diagrammatically in figure 56. The Cambridge recorder was switched on and connected via a potential divider (resistance box) to the D.C. amplifier, which in turn was connected to the photoelectric cell terminals of the Hanovia instrument.

Using the 10 mv. scale on the Cambridge recorder a steady pen reading could be obtained on the recorder chart by suitable adjustment of the resistance values in the potential divider. Several chart speeds could be used on the instrument, but throughout the experiments the maximum chart speed of 10 inches/minute was used. Thus under steady state conditions, with both the rotor speed and axial flow rate constant, the mercury vapour concentration in the annulus remained constant at the value indicated on the chart of the Cambridge recorder and, simultaneously, on the microammeter of the Hanovia instrument.

The rotameter (R14) reading, rotor speed and air temperatures were recorded and it was arranged in all cases that the inclined manometer showed 0.1" w.g.

After conditions had been steady for some time the chart on the Cambridge recorder was set in motion and the air flow rate in the column was suddenly increased by sealing off the air by-pass line from the air pump. The sealing of the by-pass line was made to coincide

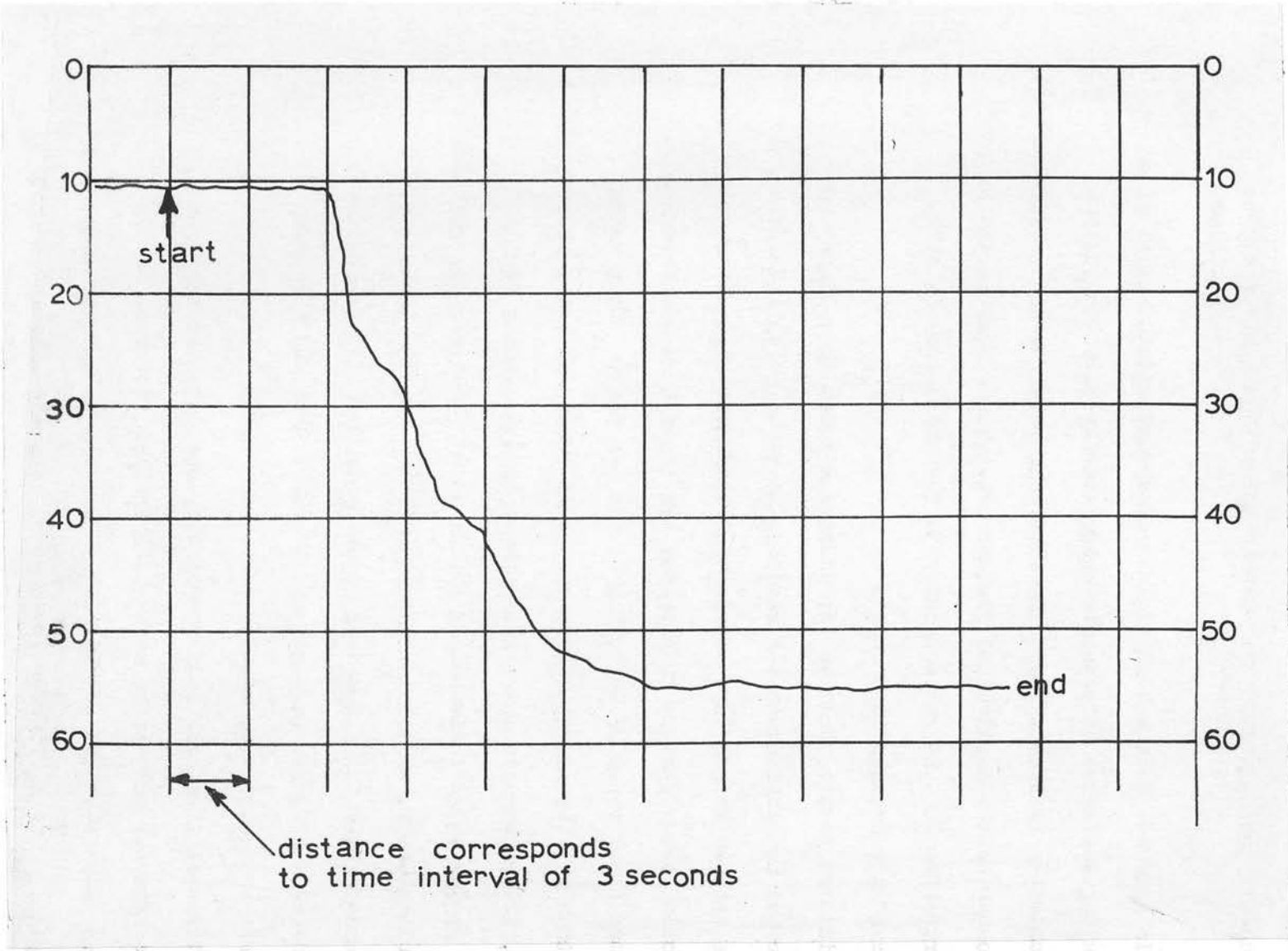

Figure 59. Longitudinal diffusion experiments. Typical 'sigmoidal' curve on chart of Cambridge recorder.

with the movement of a pre-selected line on the chart past the Cambridge recorder pen. The sudden increase in air flow rate caused an instantaneous decrease in the fractional saturation of the air stream at the amalgamated section and hence simulated approximately a step change in concentration of mercury vapour at that level. Subsequently the microammeter reading showed a gradual fall in value and simultaneously the Cambridge recorder showed a "sigmoidal" change in concentration of mercury vapour. The form of the curves obtained is shown in figure 59.

When steady state conditions had been reached again, indicated by steady pen and microammeter readings, the movement of the Cambridge chart was stopped and the new rotameter reading noted.

Similar experiments were repeated over a wide range of rotor speeds, for the same initial and final axial flow rates. The procedure was repeated for all the rotors available. For the case of the 5.18" diameter rotor the step change in concentration was simulated by suddenly decreasing the flow rate, rather than by increasing it. It was found that for this particular rotor this method gave somewhat improved reproducibility of results, particularly at high rotor speeds with a presumed vortex regime present in the annulus. This might be expected on the grounds that the vortex system would be stabilised by reduction in the flow rate at a fixed rotor speed. However, at low rotor speeds great difficulty was experienced in obtaining consistent results using the 5.18" diameter rotor. Since the annular gap was very small the concentration of mercury vapour in the annulus was very

high at the low axial flow rates used and it was found that the electronic system was not reliable at these high concentrations. The results for experiments on all rotors are given in Tables 37, 38, 39 and 40.

Previous experiments had indicated that the Cambridge recorder reading varied linearly with the Hanovia microammeter reading. The calibration curves of the Hanovia instrument could also be considered linear for a small change in concentration. It was therefore valid to assume that the "sigmoidal" curves of Cambridge recorder reading versus time were linearly related to mercury vapour concentration versus time curves, providing the change in Hanovia meter reading was small (less than about four divisions).

Since the technique used to determine longitudinal diffusion coefficients necessitated a reasonably large change in concentration, experiments had to be conducted at low values of the axial flow rate. At low axial flows a small change in the axial flow resulted in a relatively large change in concentration. Thus only the Cambridge Recorder was used to record the shape of the "sigmoidal" curves. It was not found possible with this technique to determine longitudinal diffusion coefficients at high axial flow rates (necessitating the use of the Kelvin and Hughes Recorder). This was because a very large step change in axial flow rate was required to produce a sufficiently large step change in concentration and this large change in axial flow rate resulted in oscillations in the flow regime due, presumably, to compressibility effects in the air stream.

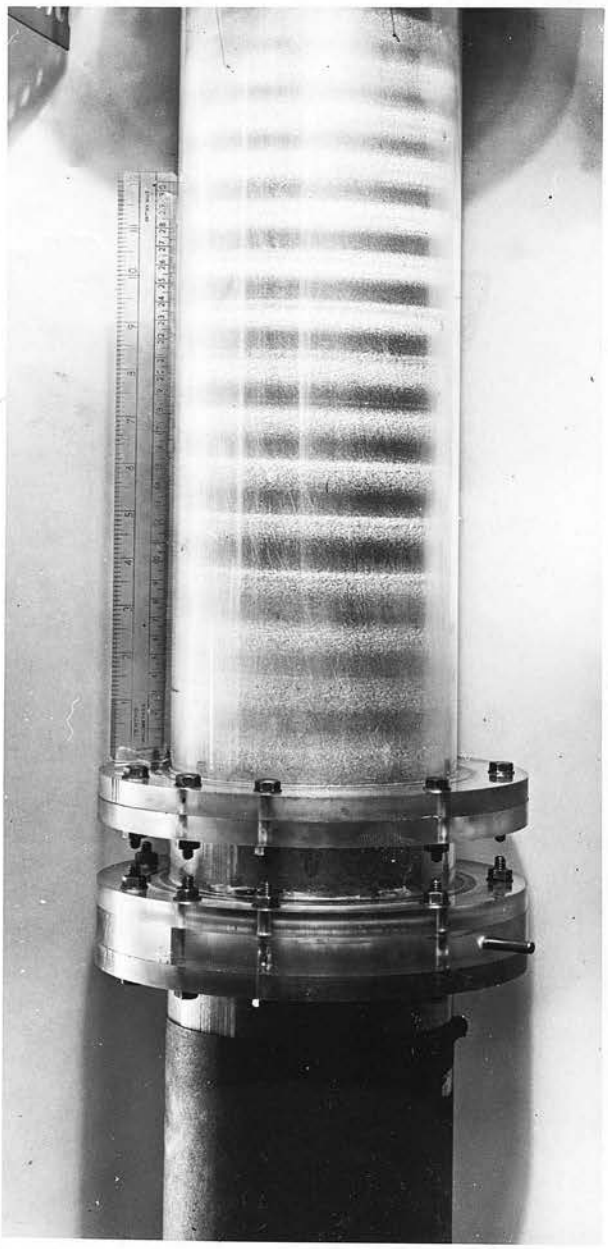

Figure 60. Photograph of Taylor vortices using talcum powder.

12. Visual studies - experimental procedure and discussion of results

An attempt was made to prove, visually, that vortices could in fact exist in the annulus of the mercury vapour transfer column. After removing the "Perspex" half-sections at the amalgamation section, talcum powder was blown into the annulus and was found to adhere to the surface of the fixed outer cylinder and rotor. The "Perspex" sections were replaced and the rotor set in motion without axial flow of air in the annulus. At a speed of rotation of about 2000 rpm, the momentum transfer from the rotor to the air and talc was sufficient to cause the segregation of the talcum powder into a series of equally spaced circumferential bands indicating the existence of a vortex regime in the annulus.

The photograph, figure 60, shows the appearance of the column under these conditions using the $4\frac{3}{4}$" diameter rotor. Using this rotor the annular gap was 1.27 cms. wide.

The scale placed alongside the column photographed in figure 60 shows that the height of each band of talcum powder was about 1.3 cms. and that the corresponding blank spaces were also about 1.3 cms. high. This observation agrees with the results of the smoke experiments described in Part I in that smoke (or talcum powder) enables one to see alternate vortices rotating in the same direction rather than adjacent, counter-rotating, vortices. The photographs also verify that each Taylor vortex occupies approximately a square annular compartment.

The density of talcum powder was too great for the critical

conditions for vortex formation to be verified in this manner since quite high rotor speeds were required to cause segregation of the powder on the wall surfaces and it was not possible to see the talcum powder suspended in the annular air gap.

With an axial flow superimposed on the system the talcum powder bands began to move up the column. This confirmed qualitatively the observations of Shipp (27) and also the smoke experiments described in Part I, that "flowing vortex" rings were possible.

An attempt was made to introduce smoke into the annulus in order to determine visually the conditions for the onset of vortices with and without axial flow in the annulus. Following a method described in Part I, cigarette smoke was introduced into the annulus but it was not dense enough to show up the existence of a vortex pattern. A paraffin "smoke generator" was also constructed which injected vapourised paraffin into the annulus, but again vortices could not be made apparent, even at quite high rotor speeds. It is probable that an optical viewing system similar to that used by Kaye and Elgar (11) is required to show up the existence of vortices with smoke in the annulus. In the experiments by Kaye and Elgar a collimated beam of light was passed through a transparent section of the outer cylinder and reflected by the cigarette smoke particles. The reflected light was observed visually or photographed.

13. Calculation and discussion of results - radial diffusion experiments

13.1 Calculation of results

The results obtained for each rotor with the rotor stationary or revolving, are given in the first six columns of Tables 18 to 27 inclusive. The first column, R, in each Table records the size of metric series rotameter used. The next two columns record the temperature of the air entering the base of the column (E) and leaving the column (O). The third column records the mean of these two temperatures. These temperatures were given by chromel/alumel thermo-junctions, connected to a potentiometer. The thermoelectric e.m.f.'s indicated were converted to degrees centigrade, using a conversion factor of 0.004 volts/^{o}C. This conversion factor was valid for the thermo-junction used over the range of temperatures involved in the experiments. The fifth column in the Tables records the microammeter reading and the sixth column the rotor speed in rpm.

The air flow rate, in litres/minute, was obtained from the calibration chart for the particular rotameter used. These calibration charts, supplied by the makers, are shown in figures 96 to 100 inclusive for the range of rotameters used. Unfortunately there were no facilities in the laboratory for an accurate check to be made of these calibration charts and so their degree of accuracy is unknown.

From a knowledge of the cross-sectional flow area in the annulus, the value of $\bar{u}$, the air velocity in cm/sec, was calculated and recorded in the eighth column.

The values of $c^{\ddagger}$ were obtained from the curve of $c^{\ddagger}$ versus

temperature shown in figure 87 (see Appendix L and Table 16) and the values of c_2 in the tenth column were obtained from calibration curves of microammeter reading versus mercury vapour concentration. These calibration curves are shown in figures 89 to 95 inclusive plotted from results of the calibration runs shown in Tables 32, 33, 34 and 35 and the particular calibration curve used is noted at the top of each table of results, together with the diameter of rotor used.

The values of ϕ recorded in the eleventh column of each table were obtained by dividing the corresponding values of c_2 by c^*. The values of D were obtained at the mean air temperature (fourth column) from figure 88. Figure 88 was obtained from data by Mullay and Jacques (56) for the diffusion of mercury vapour into nitrogen at a pressure of 3.52 mm.Hg. It was assumed that these values could be used to calculate values of the molecular diffusion coefficient, D, for mercury vapour into air at atmospheric pressure and temperatures varying from 15° to 25°C. These calculated values are given in Table 17 and the method whereby these values are calculated is shown in Appendix M.

Next the values of the kinematic viscosity of air, ν, at the values of the mean temperature shown in the fourth column, were obtained from a curve of ν versus temperature shown in figure (86). This curve was plotted from values of the viscosity and density of air at various temperatures given in Kaye and Laby (57). These values of ν were

tabulated in the thirteenth column. As shown, in the fourteenth and fifteenth columns, the values of $\frac{Dx}{u}$ and $\ln\left\{c^*/(c^* - c_2)\right\}$ were calculated and tabulated (x being the width of the amalgamated band of silver foil). The values of the radial mass transfer coefficient, K, were then calculated according to equation (68), i.e. $K = \frac{uA}{S} \ln \frac{c^*}{c^* - c_2}$.

The last two columns in Tables 18 to 27 inclusive show values of the axial and circumferential Reynolds numbers, Re_a and Re_c respectively. These values were calculated using the values of ν tabulated in the thirteenth column. Although mercury vapour was present in the air stream, the small quantities present had no significant effect on the physical properties of the air stream. This is made clear by the following simple analysis:-

From Table 16, the value of c^*, the saturation concentration of mercury vapour at 20°C is 13,187 μgm/m^3 or 13.187 x 10^{-9} gm/cc. Thus 1cc. of air saturated with mercury vapour at 20°C contains 13.187 x 10^{-9} gms. mercury. Now the density of air, at 20°C (57), is 0.001205 gm/cc. and hence the density of air is little affected by the presence of mercury vapour, even though the air is saturated with mercury vapour at this temperature. The effect of mercury vapour, present in these small quantities, on the viscosity of the air stream will also be negligible.

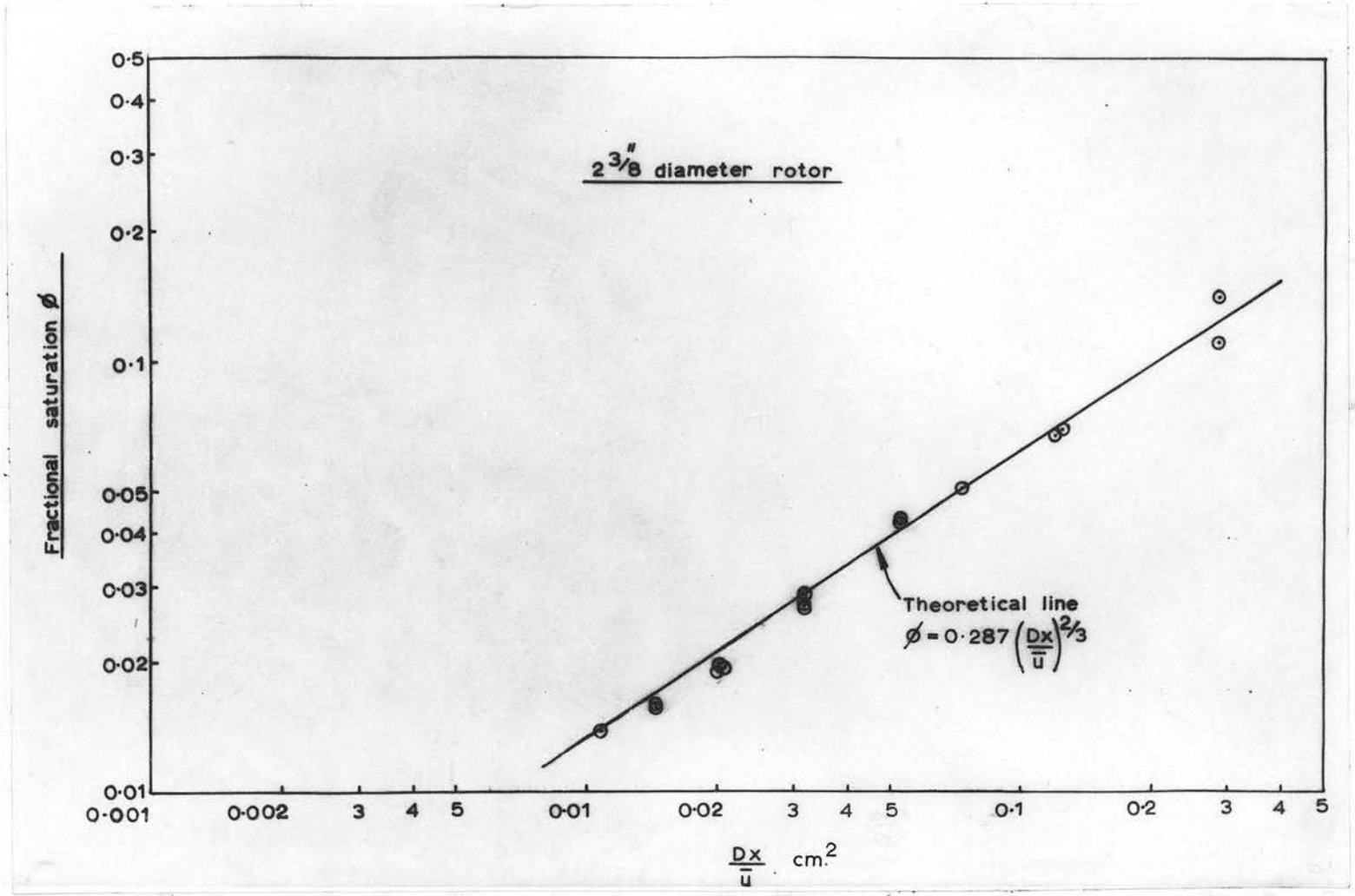

Figure 61. $2\frac{3}{8}$" diameter rotor. Fractional saturation, ϕ, of laminar air stream versus $(Dx/\bar{u})$. Transfer from wall (outer cylinder).

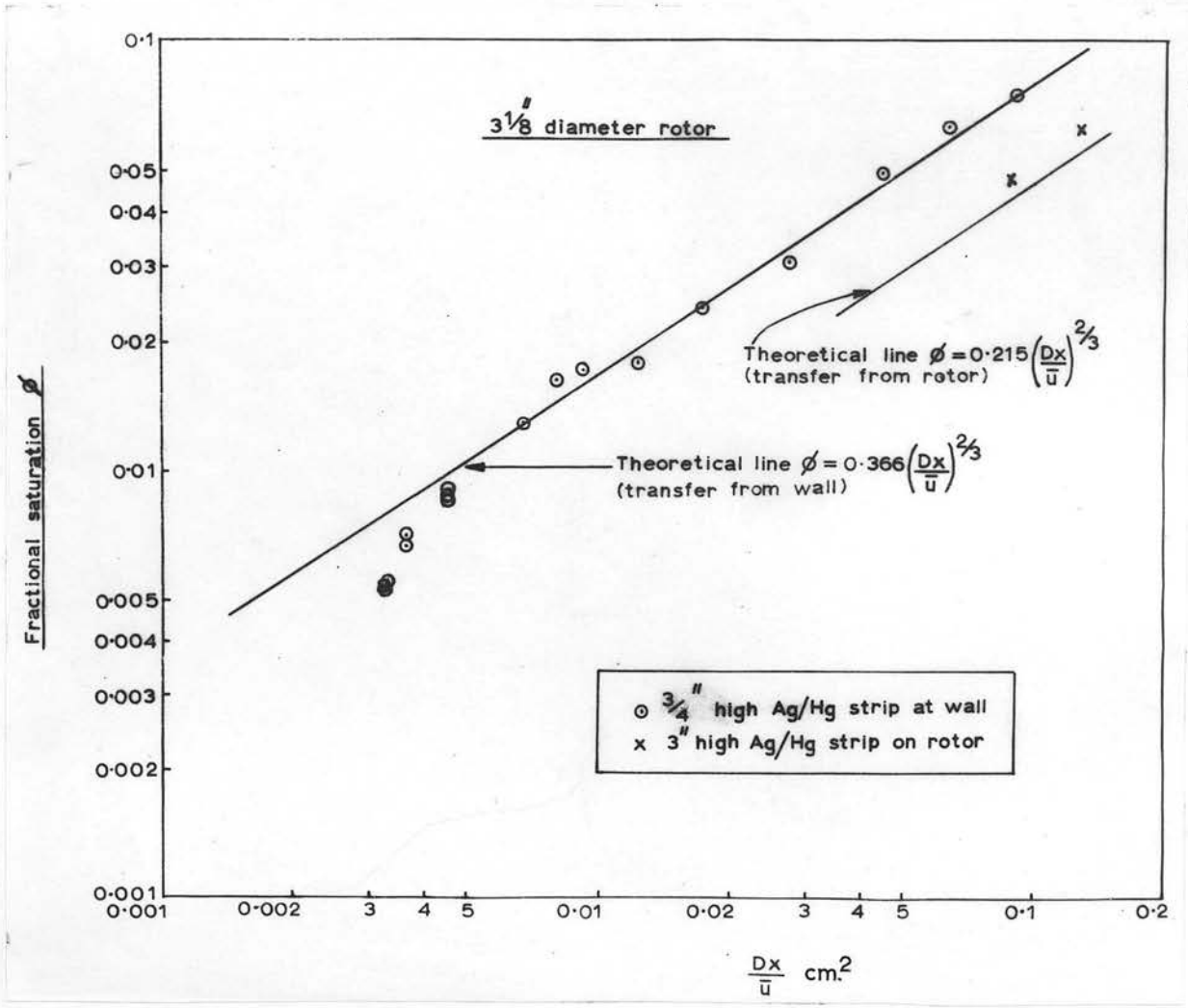

Figure 62. $3\frac{1}{8}$" diameter rotor. Fractional saturation, ϕ, of laminar air stream versus $(Dx/\bar{u})$. Transfer from both wall and rotor.

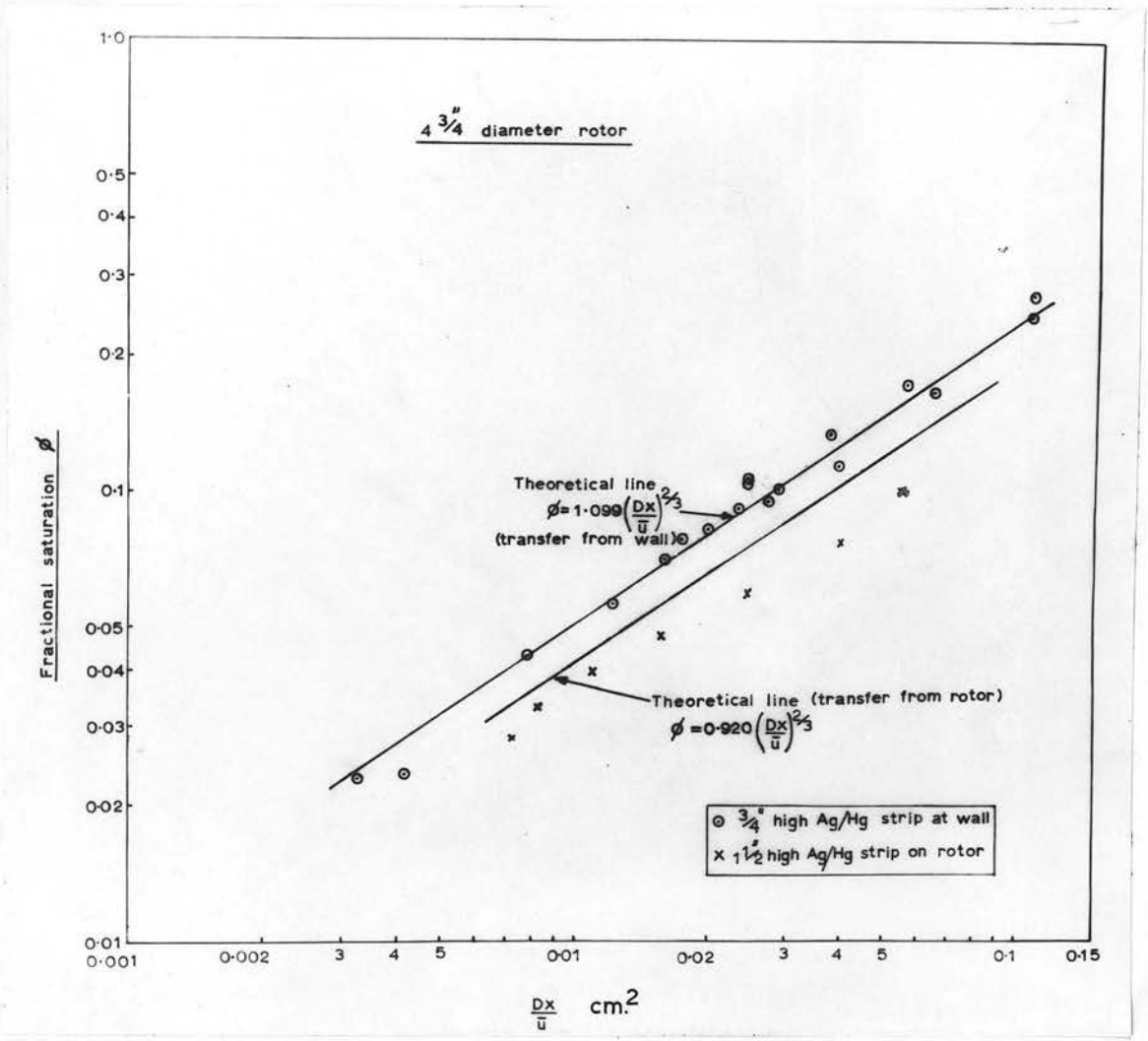

Figure 63. $4\frac{3}{4}$" diameter rotor. Fractional saturation, ϕ, of laminar air stream versus $(Dx/\bar{u})$. Transfer from both wall and rotor.

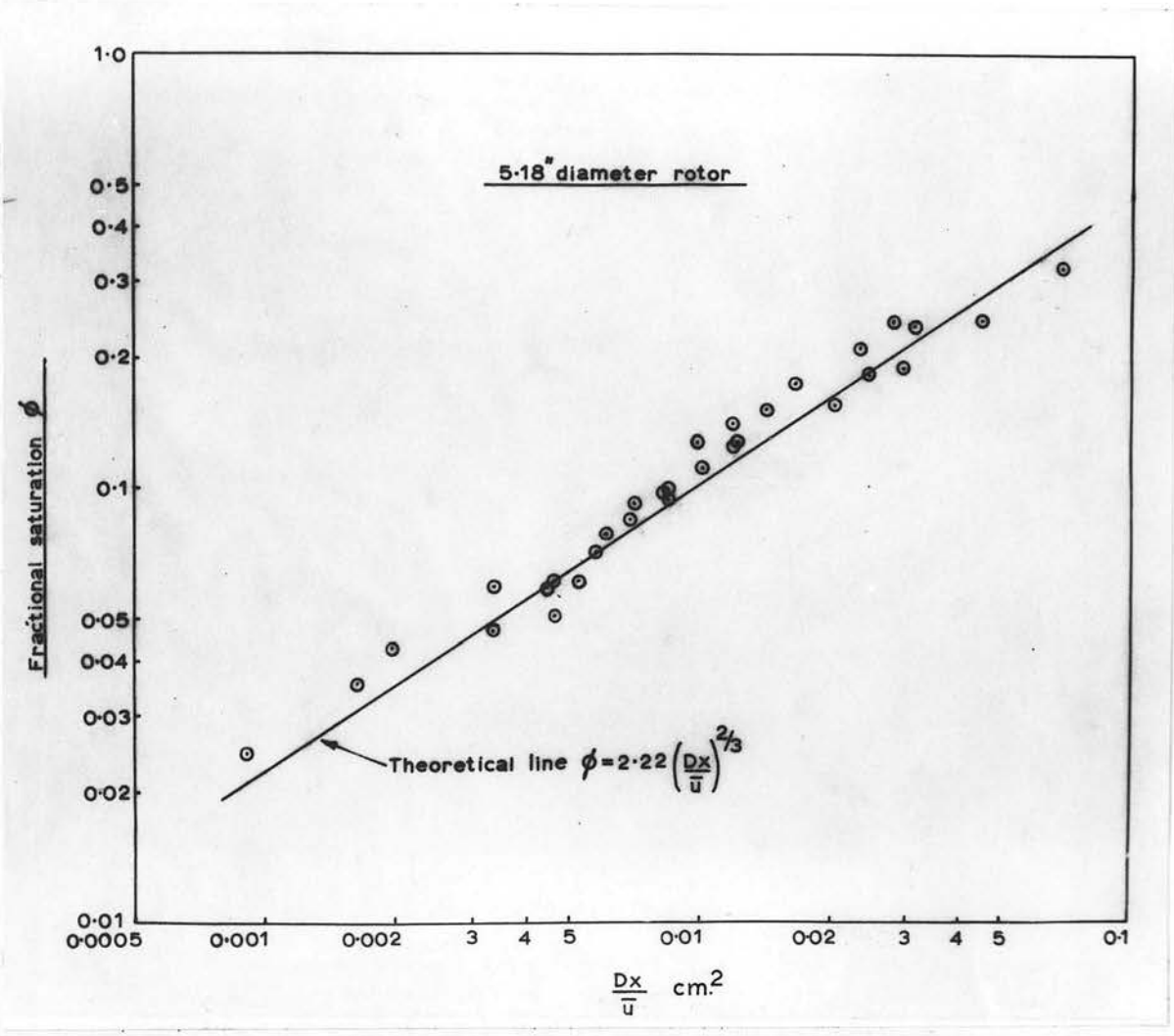

Figure 64. 5.18" diameter rotor. Fractional saturation, ϕ, of laminar air stream versus $(Dx/\bar{u})$. Transfer from wall (outer cylinder).

13.2 Comparison of results with theory

13.21 Radial diffusion into a laminar air stream

When the rotor is stationary (or revolving at speeds below the critical speed for vortex formation) equation (58) should apply to the case where the amalgamated band was situated on the wall of the outer cylinder. Values of ϕ, the fractional saturation, calculated from results of experiments with the rotor stationary are given in Tables 18 to 21 inclusive.

Figures 61, 62, 63 and 64 show, for the $2\frac{3}{8}$", $3\frac{1}{8}$", $4\frac{3}{4}$" and 5.18" diameter rotors respectively, these values of ϕ plotted against the corresponding values of $Dx/\bar{u}$, obtained from the fourteenth column in Tables 18 to 21 inclusive. Logarithmic scales are used. These values are compared with the theoretical line obtained by evaluating equation (58) using the appropriate values of r_1 and r_2, the rotor radius and outer cylinder radius respectively. In Appendix N the evaluation of (58) for the case of the 5.18" diameter rotor is given as an example.

Figures 62 and 63 also show, for the case of the $3\frac{1}{8}$" and $4\frac{3}{4}$" diameter rotors respectively, the few experimental results obtained with an amalgamated band situated on the rotor. These results are compared with the appropriate theoretical line obtained by evaluating equation (60).

The line obtained from equation (58) is referred to as the "Theoretical line (transfer from wall)" and the line obtained from equation (60) the "Theoretical line (transfer from rotor)".

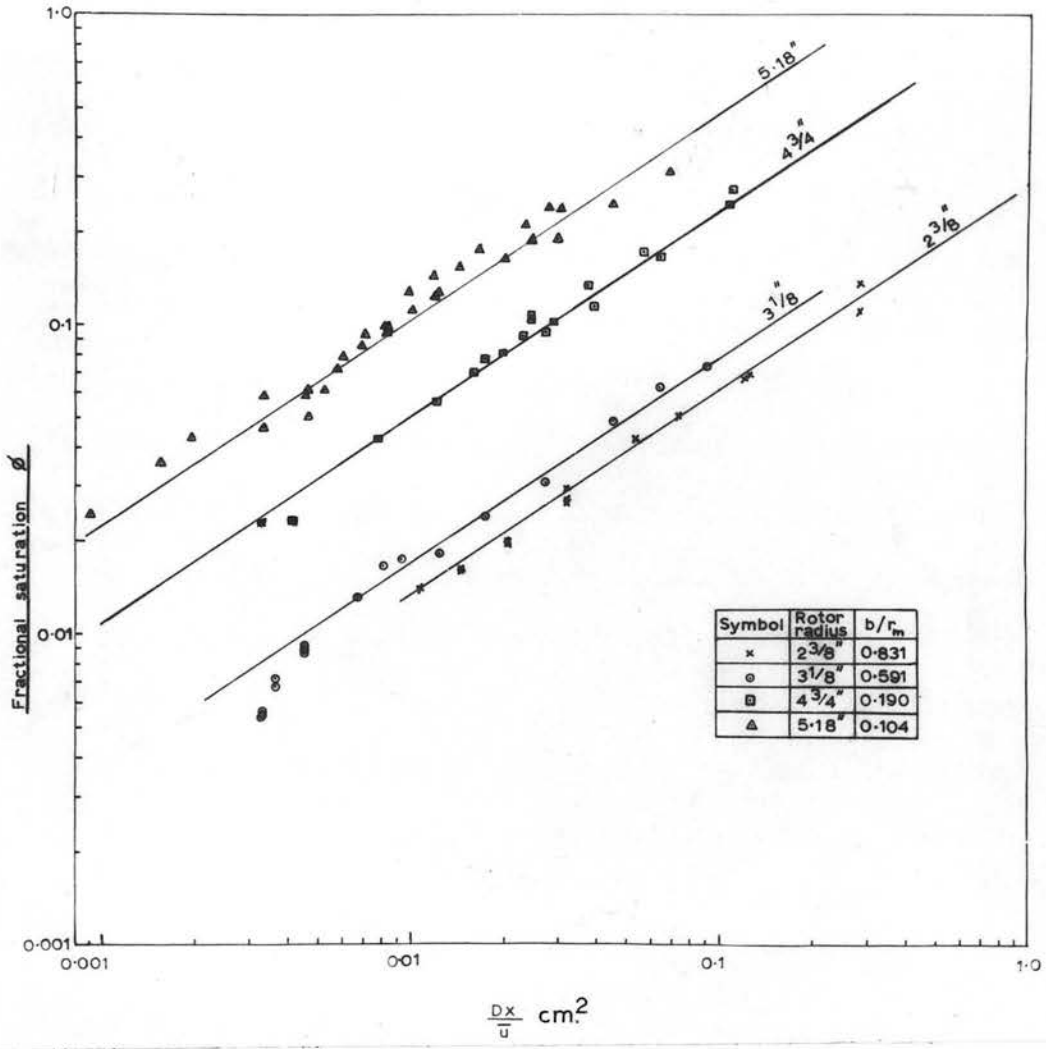

Figure 65. All rotors. Fractional saturation, ϕ, of laminar air stream versus $\frac{Dx}{\bar{u}}$. Transfer from wall (outer cylinder).

Figure 65 also shows a plot of experimental values of ϕ versus $Dx/\bar{u}$ with results for all the rotors used shown on one graph and compared with the appropriate theoretical lines. These values apply only to the case where the amalgamated band was situated on the fixed outer cylinder. From these figures it can be seen that the experimental points fit the theoretical equation (58) remarkably well, confirming the validity of that equation under the conditions of experimentation.

The results with an amalgamated band on the rotor do not correlate quite so well with the theoretical lines as shown in figures 62 and 63, but the reason for this probably lies in the unsatisfactory experimental technique used for the fixing and amalgamation of the silver foil on the rotor.

The results with the silver foil on the $4\frac{3}{4}$" diameter rotor given in figure 63 show that the value of ϕ is less than the theoretical. This indicates that if the theory is valid under the experimental conditions used, either the surface was incompletely amalgamated or the air and mercury vapour were not well mixed in the detection section due to a tendency for the more concentrated mercury vapour to remain near the rotor surface, despite the provision of a baffle in the annulus.

Only <u>two</u> results were obtained from experiments with the silver foil on the $3\frac{1}{8}$" diameter rotor as shown in figure 62 (in this case lying close to but above the theoretical line) and so it is impossible to attach any great significance to the results obtained from these experiments.

Returning to the experimental results with the amalgamated circumferential band on the outer cylinder it can be seen that at very low values of the variable $\frac{Dx}{\bar{u}}$, the experimental results with the $3\frac{1}{8}$" diameter rotor show that the values of ϕ tend to fall progressively below the theoretical line as $Dx/\bar{u}$ decreases, i.e. as

the velocity of the air stream, $\bar{u}$, increases. It is interesting to note that the fall away from the theoretical line starts when the value of $\bar{u}$ is such that the axial Reynolds number is about 2400, indicating that axial turbulence has probably set in and that the theoretical equation (58) is no longer a valid representation of the radial mass transfer process taking place. However, the values of c_2, the mercury vapour concentration in the annulus, are so low at these values of $Dx/\bar{u}$ (see Table 19) that the accuracy of the results is suspect. Figure 62 shows that the values of ϕ corresponding to these values of c_2 are the lowest obtained with any rotor and it is possible that the errors involved are very great when such low values of mercury vapour concentrations are estimated.

There is no rigorous way of estimating the errors involved, since the values of both variables ϕ and $(Dx/\bar{u})$ were calculated from experimentally obtained values, the individual errors of which were not readily determinable. For example, the error in the individual values of c_2, c^{*} and $\bar{u}$ are not easily estimated. Furthermore, even if these individual errors could be assessed, the derivation of confidence limits for a functional relationship between two variables $\{\phi$ and $(Dx/\bar{u})\}$, both of which are subject to error is a complex procedure and is usually (58) treated on an approximate basis.

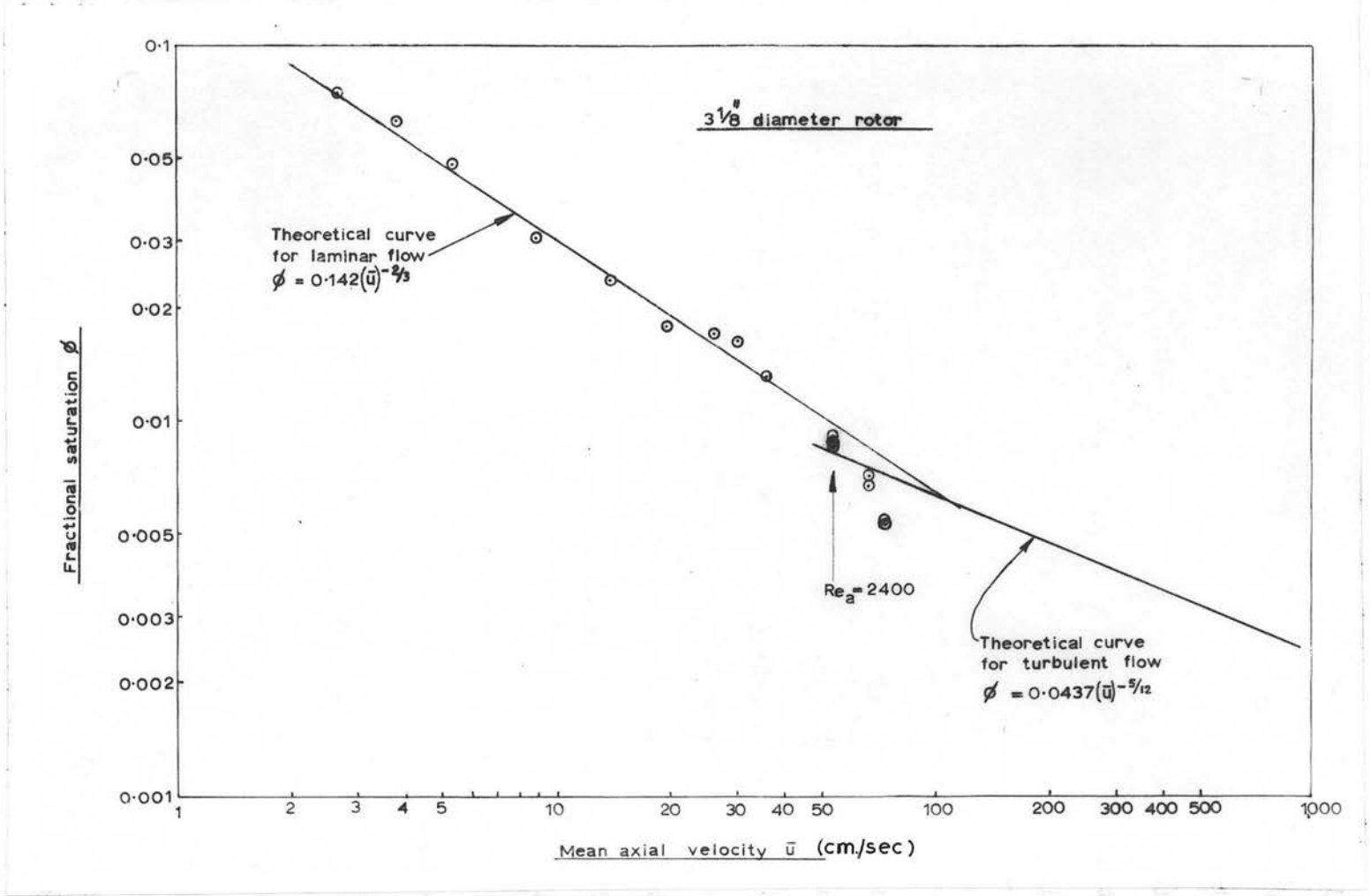

Figure 66. 3⅛" diameter rotor. Fractional saturation curves for laminar and turbulent flow. Transfer from wall (outer cylinder).

13.22 Radial diffusion into a turbulent air stream

Using the $3\frac{1}{8}$" diameter rotor, experiments were conducted with the rotor stationary and flow rates giving axial Reynolds numbers as high as 3300. It was expected that with the rotor stationary turbulent flow would appear in the annulus for values of the axial Reynolds number greater than about 2000 and that the results under these conditions would conform to equation (62), viz:-

$$\phi = \frac{0.256\ (Dx)^{\frac{2}{3}}}{\bar{u}^{5/12} b^{13/12} \nu^{1/4}}$$

which was derived in section 9.2 on the basis of turbulent flow between parallel plates. In order to test the validity of this equation, for the case of the $3\frac{1}{8}$" diameter rotor, equation (62) was reduced to the form:-

$$\phi = 0.0437\ (\bar{u})^{-5/12}$$

by inserting appropriate values of D and ν, (assumed constant throughout the experiments) together with values for x =1.905 cms and b = 3.334 cms.

Similarly, equation (58), for purely laminar flow, was reduced to the form:-

$$\phi = 0.142\ (\bar{u})^{-\frac{2}{3}}$$

These two equations are shown plotted on logarithmic co-ordinates in figure 66 in which the experimental results are also shown, the data being obtained from Table 19.

Unfortunately it cannot be verified from these experimental results whether the validity of equation (62) is established, since experimental results could not be obtained for higher values of $\bar{u}$ at which, theoretically, the values of ϕ should differ significantly from the theoretical line for laminar flow. Now the conditions for the general validity of equation (62), derived in Appendix I, are that:-

$$\left(\frac{x}{b}\right)^{\frac{1}{3}} (Sc)^{-\frac{1}{3}} Re_a^{\frac{7}{24}} < 5.22 \qquad \text{- - - (63)}$$

For mercury vapour in air, $Sc \doteq 1$ and taking $Re_a = 2500$, (63) becomes:-

$$\left(\frac{x}{b}\right)^{\frac{1}{3}} < \frac{5.22}{(2500)^{7/24}} < \frac{5.22}{9.8} < 0.53$$

Thus for equation (62) to be valid the max.m value of $\left(\frac{x}{b}\right)$ for $Re_a = 2500$ is given by:-

$$\left(\frac{x}{b}\right)_{max} = 0.53$$

For the experiments using the $3\frac{1}{8}$" diameter rotor with an amalgamated section $\frac{3}{4}$" high the value of (x/b) was 0.57. Thus equation (62) is not theoretically a valid representation of the results from these experiments with values of Re_a in the region of 2500. At higher values of Re_a the validity of equation (62) is even more doubtful; for example, at $Re_a = 5000$ equation (63) becomes:-

$$\left(\frac{x}{b}\right)_{max} < \frac{5.22}{(5000)^{7/24}} < \frac{5.22}{11.99} < 0.44$$

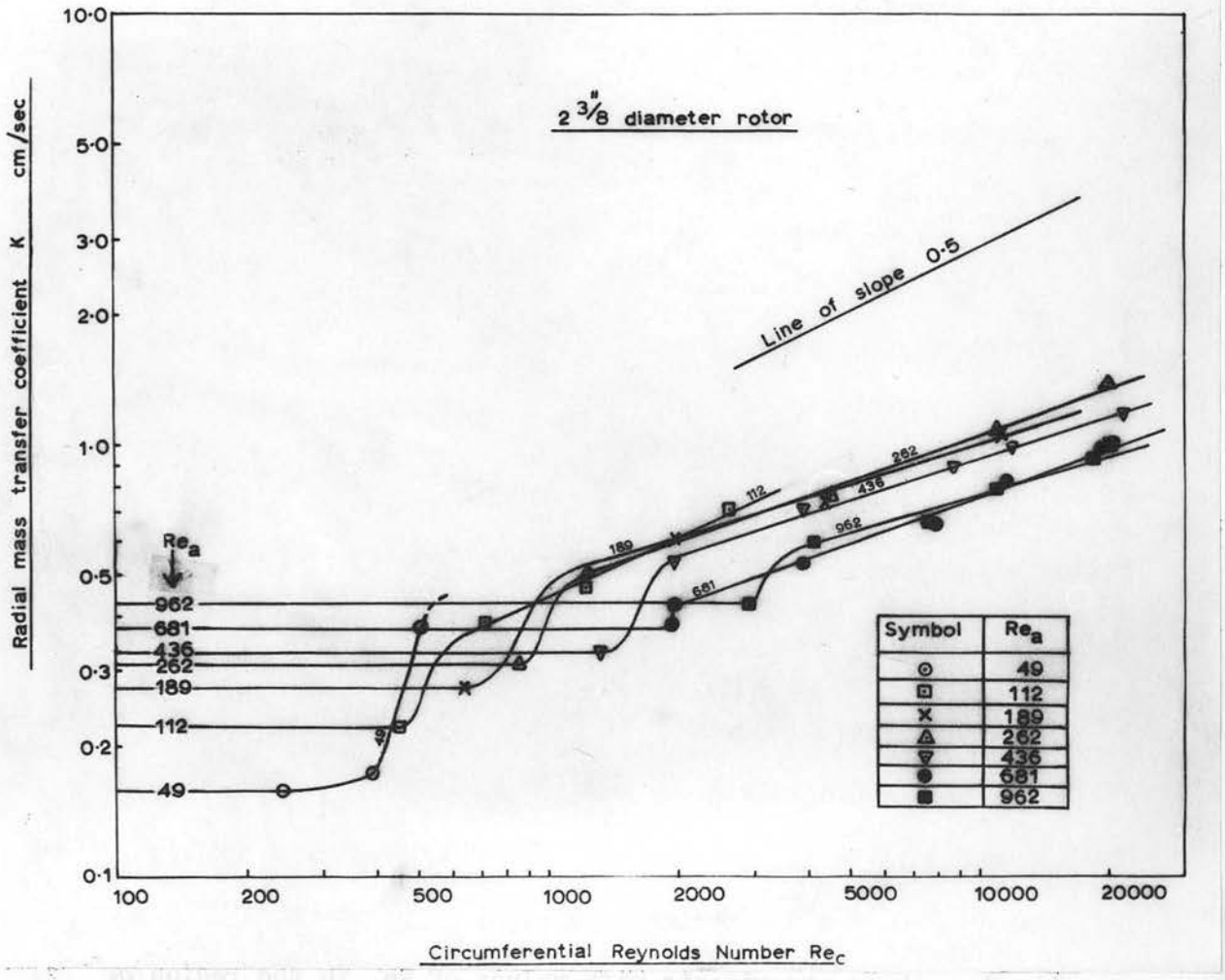

Figure 67. $2\frac{3}{8}$" diameter rotor. Radial mass transfer coefficient, K, versus Re_c. Transfer from wall (amalgamated band on outer cylinder).

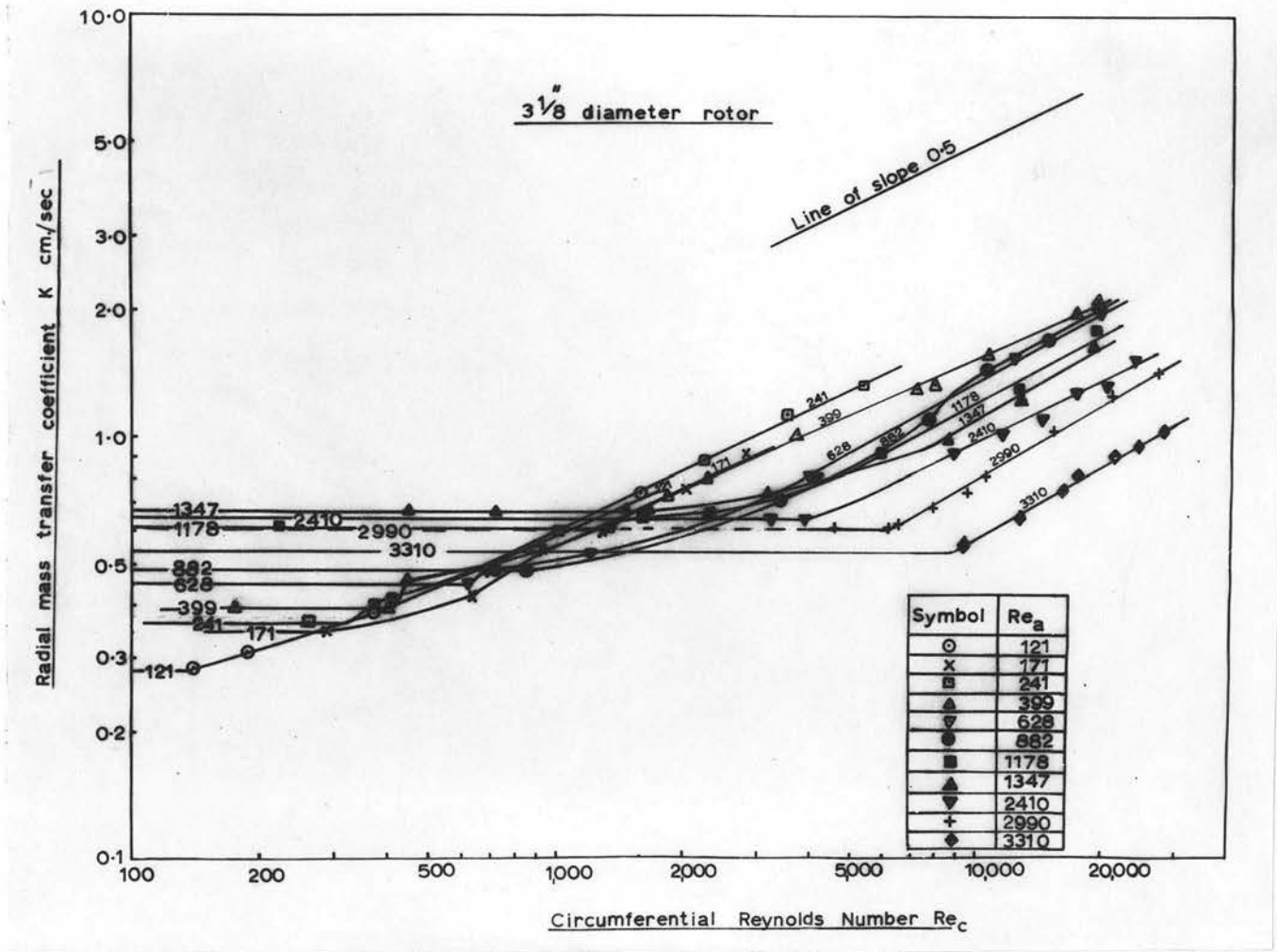

Figure 68. $3\frac{1}{8}$" diameter rotor. Radial mass transfer coefficient, K, versus Re_c. Transfer from wall (amalgamated band on outer cylinder).

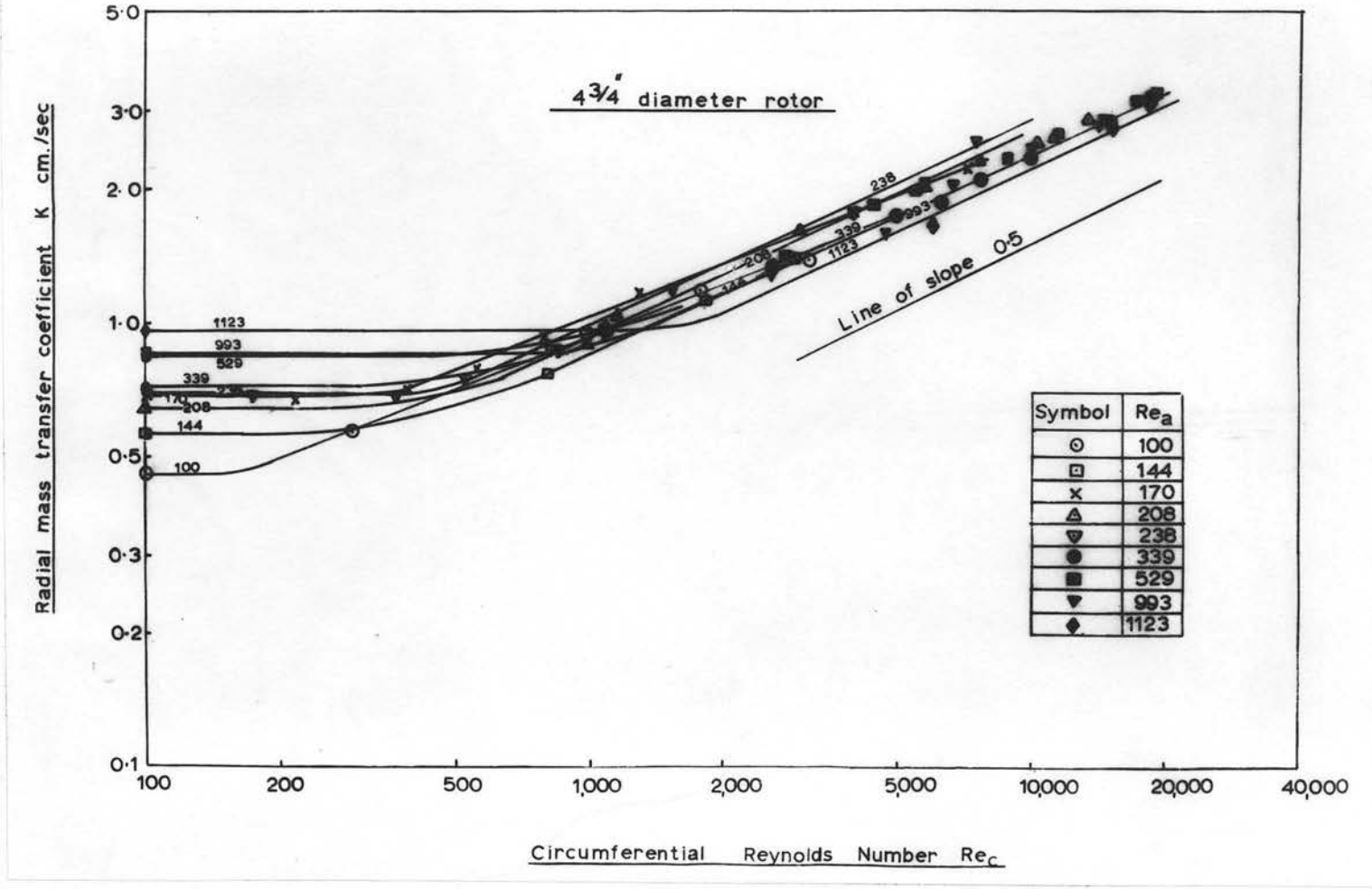

Figure 69. $4\frac{3}{4}$" diameter rotor. Radial mass transfer coefficient, K, versus Re_c. Transfer from wall (amalgamated band on outer cylinder).

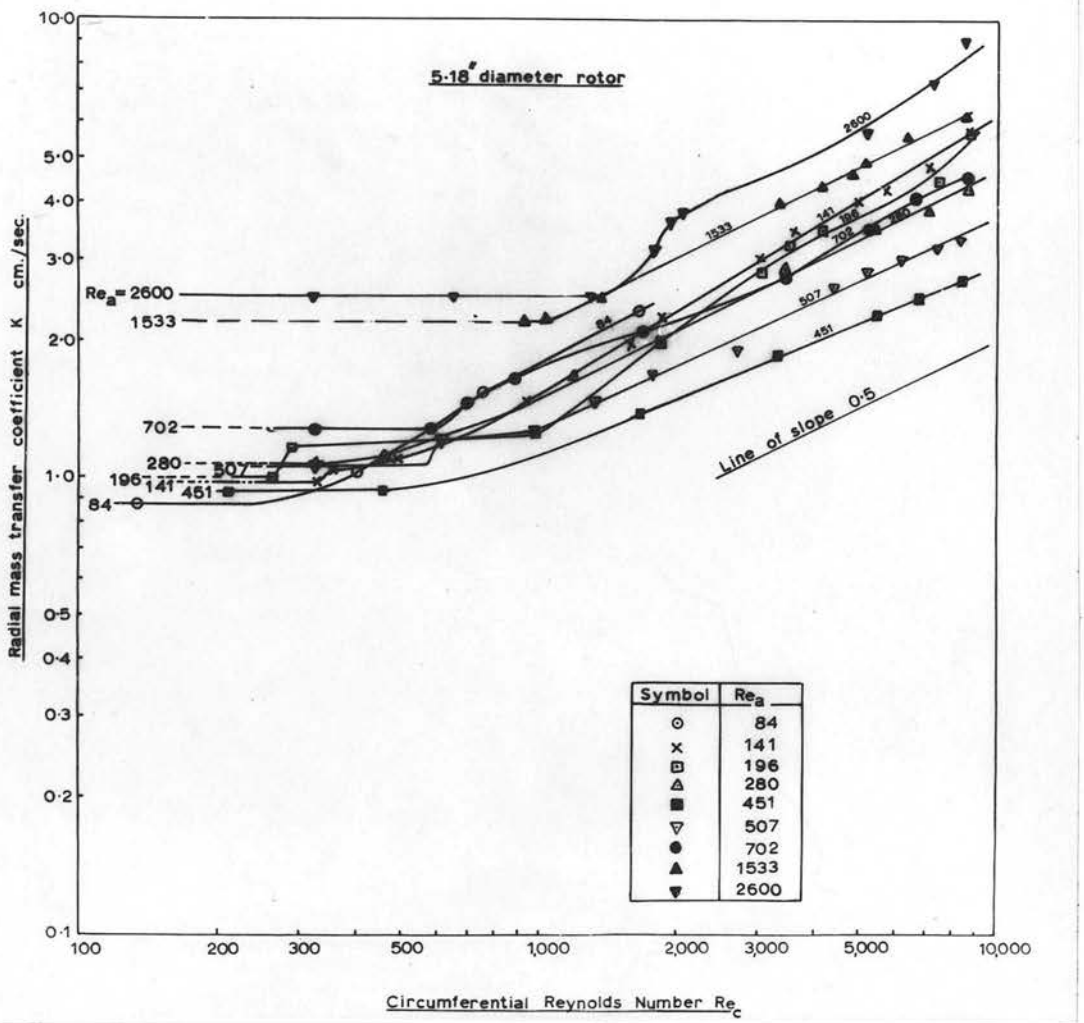

Figure 70. 5.18" diameter rotor. Radial mass transfer coefficient, K, versus Re_c. Transfer from wall (amalgamated band on outer cylinder).

Thus at large flow rates, when the flow is almost certainly turbulent, equation (62) is not theoretically valid for the particular system studied. Furthermore, equation (62) was derived on the basis of flow between parallel plates and so it is doubtful, in any case, whether it would be valid for experimental results with a $3\frac{1}{8}$" diameter rotor inside a $5\frac{3}{4}$" i.d. outer cylinder.

13.23 Radial diffusion into an air stream in which vortices are present

Tables 24, 25, 26 and 27 give values of the radial mass transfer coefficient K, calculated from the experimental results using the $2\frac{3}{8}$", $3\frac{1}{8}$", $4\frac{3}{4}$" and 5.18" diameter rotors respectively with the amalgamated band on the outer cylinder. Values of Re_a and Re_c have also been calculated and tabulated.

Figures 67, 68, 69 and 70 show, for the $2\frac{3}{8}$", $3\frac{1}{8}$", $4\frac{3}{4}$" and 5.18" diameter rotors respectively, plots of K versus Re_c for progressively increasing values of the axial Reynolds number, Re_a. K is plotted as a function of $Re_c \left(\frac{r_1 \Omega b}{\nu} \right)$, rather than as a function of the Taylor number, Ta.

The horizontal part of each curve extends down to a value of $Re_c = 0$, but points for values of $Re_c < 100$ are not shown since no change in K occurs in the range $0 < Re_c < 100$ for all rotors used over all values of Re_a investigated. Thus the range of the abscissa scale is conveniently reduced in length. The results for all rotors show that, with the axial Reynolds number maintained constant, the value of K remains independent of rotor speed until a certain critical speed is reached, at which the value of K shows a rise in value. At speeds

above this critical speed the value of K rises progressively with increasing rotor speed. As shown in figures 67 to 70 inclusive the value of the critical rotor speed depends on the axial Reynolds number. Quite generally, the higher the value of Re_a, the higher the rotor speed required to produce a change in the value of K. This critical rotor speed is assumed to correspond to the formation of vortices in the annulus, since the onset of such vortices would be expected to increase the rate of radial mass transfer between the surface of the amalgamated band and the air stream. This would cause the mass transfer coefficient, K, to rise above a value corresponding to purely laminar flow in the annulus.

The results from experiments conducted to determine the critical conditions for vortex formation are discussed in the next section, but critical values of Re_c at a particular Re_a were obtained from the results given in the next section to assist in the accurate plotting of the transition points for each curve shown in figures 67 to 70 inclusive.

Apart from some of the results with the smallest diameter rotor ($2\frac{3}{8}$" diameter) the results for all rotors for values of Re_a up to 3310 indicate that, once vortices are formed in the annulus, K appears to vary as a function of $(Re_c)^{\frac{1}{2}}$. This observation suggests that these experimental results might be correlated by an equation similar to (32) which was derived according to Batchelor's theory (30) for high rotor speeds and low axial Reynolds numbers. At low values of Re_a the vortex pattern should not be significantly disturbed by the axial flow and equation (32) should hold, i.e.:-

$$Sh = \frac{Kb}{D} \sim (Re_c)^{\frac{1}{2}} \left(\frac{b}{r_1}\right)^{\frac{1}{4}} \qquad - - - (32)$$

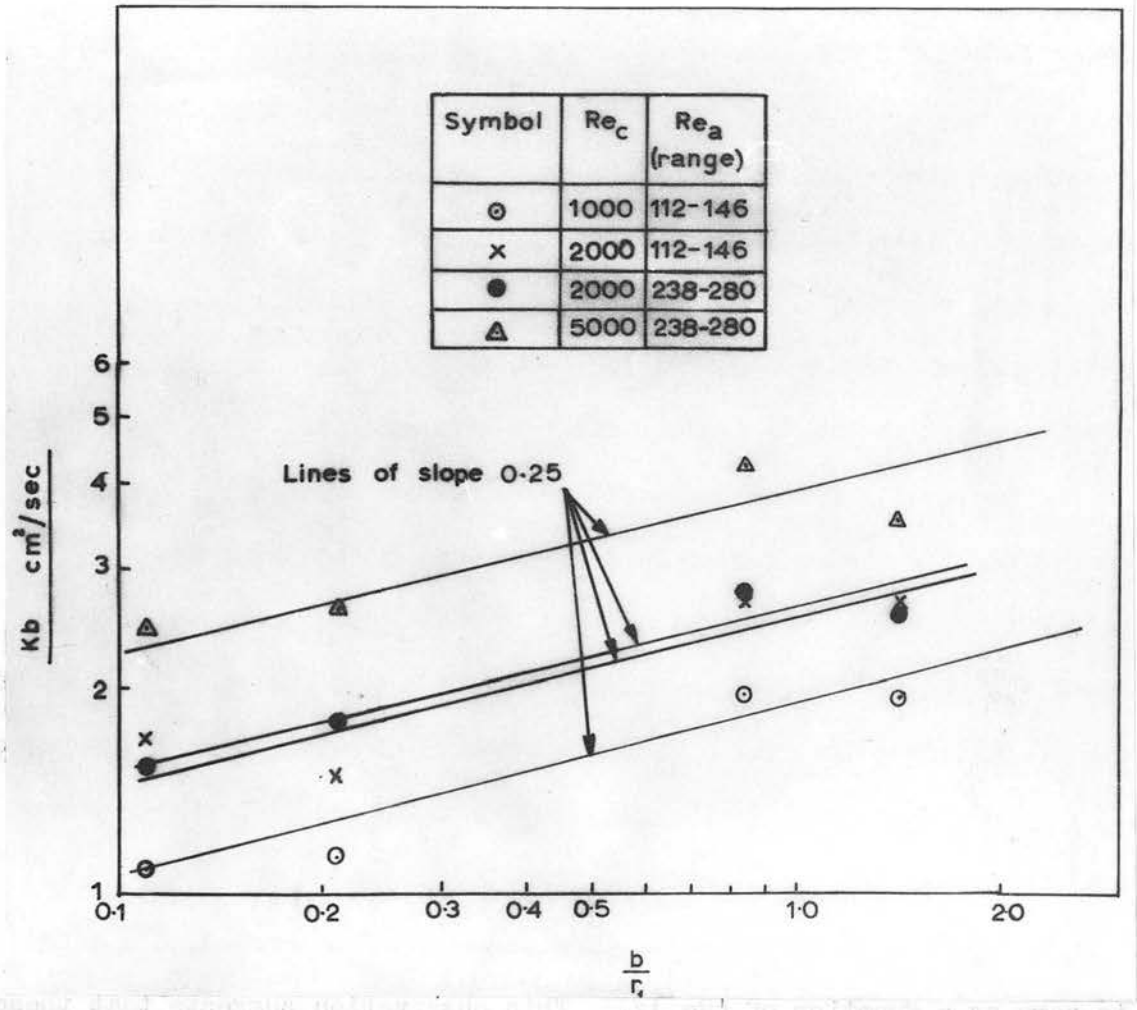

Figure 71. Plot of Kb versus b/r_1 for all rotors used. Values of K obtained from figures 67 to 70 inclusive.

where Sh = Sherwood number.

From figures 67 to 70 inclusive values of K were obtained and values of Kb were calculated and plotted as a function of b/r_1 as shown in figure 71 for all the rotors used. Table 36 shows the values of K and hence Kb obtained at values of Re_c of 1000, 2000 and 5000 for values of Re_a falling in the two narrow ranges $112 < Re_a < 146$, $238 < Re_a < 280$.

In figure 71 lines of slope 0.25 are drawn through corresponding sets of results and although the points are scattered it is reasonable to conclude tentatively that Kb varies as a function of $\left(\frac{b}{r_1}\right)^{\frac{1}{4}}$ at a constant value of Re_c, for the range $1000 < Re_c < 5000$, $112 < Re_a < 280$. Using an average value of the molecular diffusion coefficient, D, of 0.128 cm^2/sec, corresponding to an average air temperature of 19.6°C, figure 71 gives the correlation:-

$$Sh = \frac{Kb}{D} = 0.45 \ (Re_c)^{\frac{1}{2}} \left(\frac{b}{r_1}\right)^{\frac{1}{4}} \qquad - - - (95)$$

These experimental results therefore give a correlation which is identical in form to the correlation (32) suggested by Batchelor's momentum transfer theory but which applies to the entire vortex regime, not merely to rotor speeds several times the critical value corresponding to vortex formation. (Batchelor's "inviscid core and boundary layer model" applies only to this latter condition).

It is found that the values of K, calculated from equation (95) agree reasonably well with the values given in figures 71 over the complete range for which the correlation is assumed to hold. For

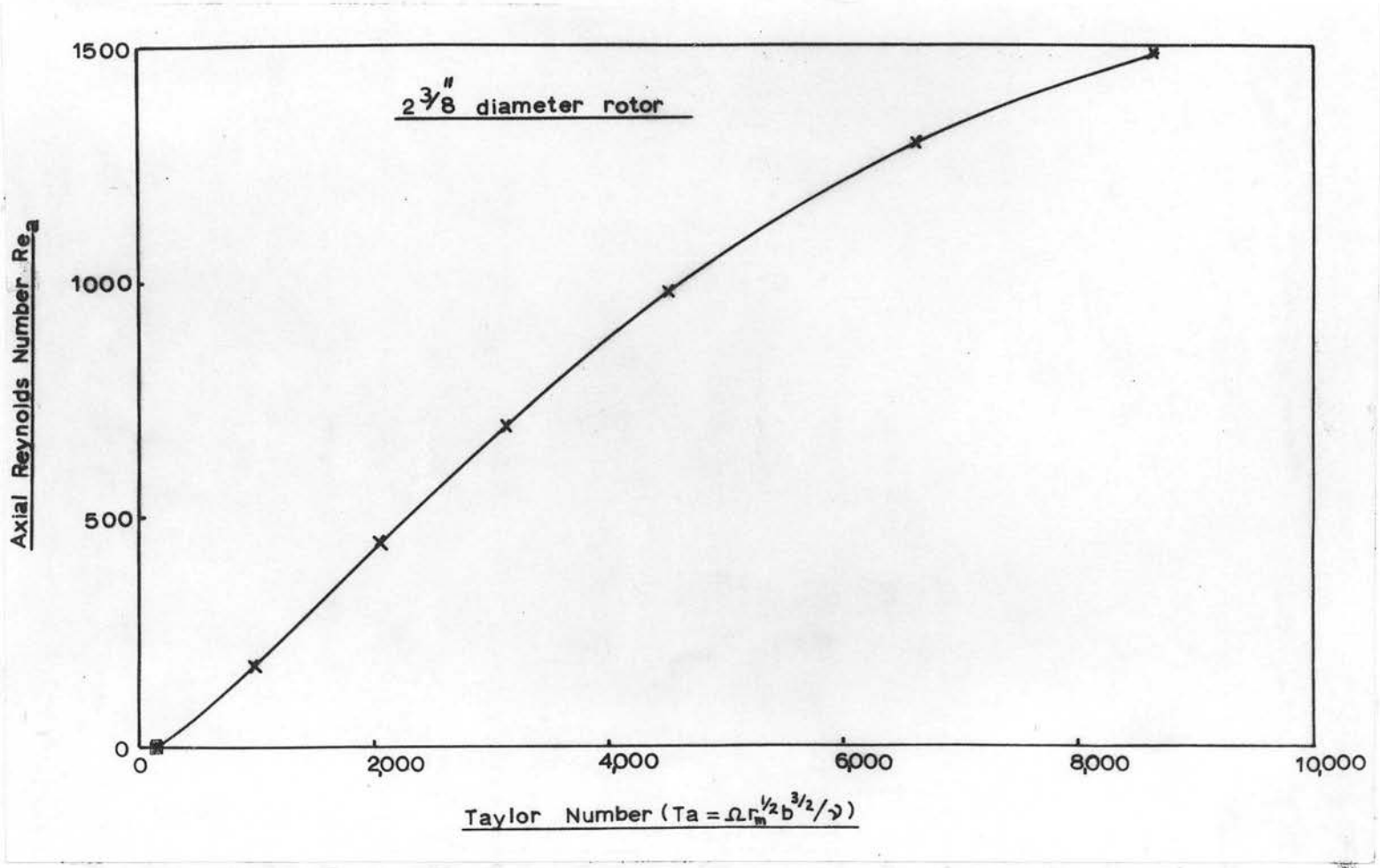

Figure 72. $2\frac{3}{8}$" diameter rotor. Critical curve for transition from laminar to 'laminar plus vortex' flow.

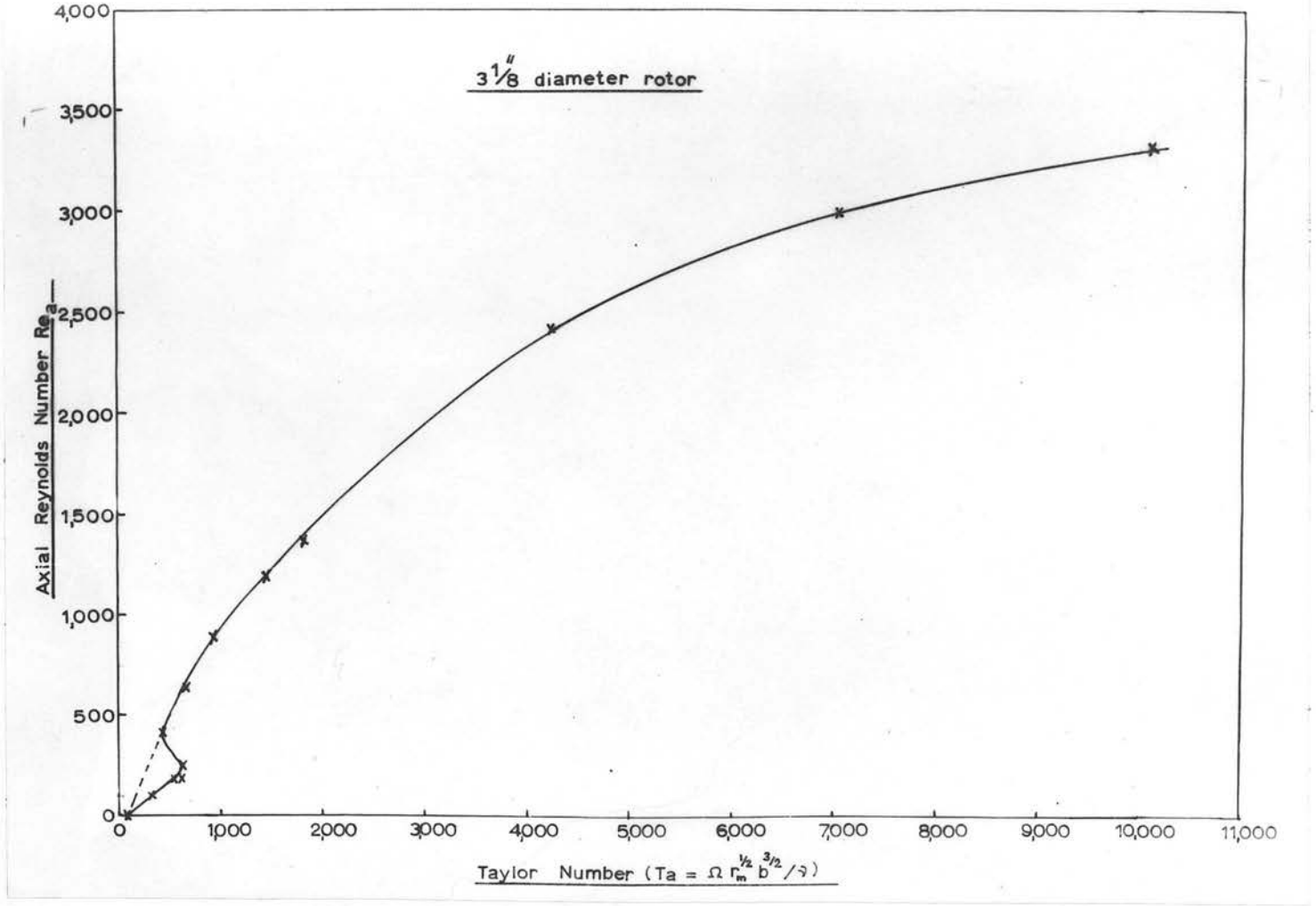

Figure 73. $3\frac{1}{8}$" diameter rotor. Critical curve for transition from laminar to 'laminar plus vortex' flow.

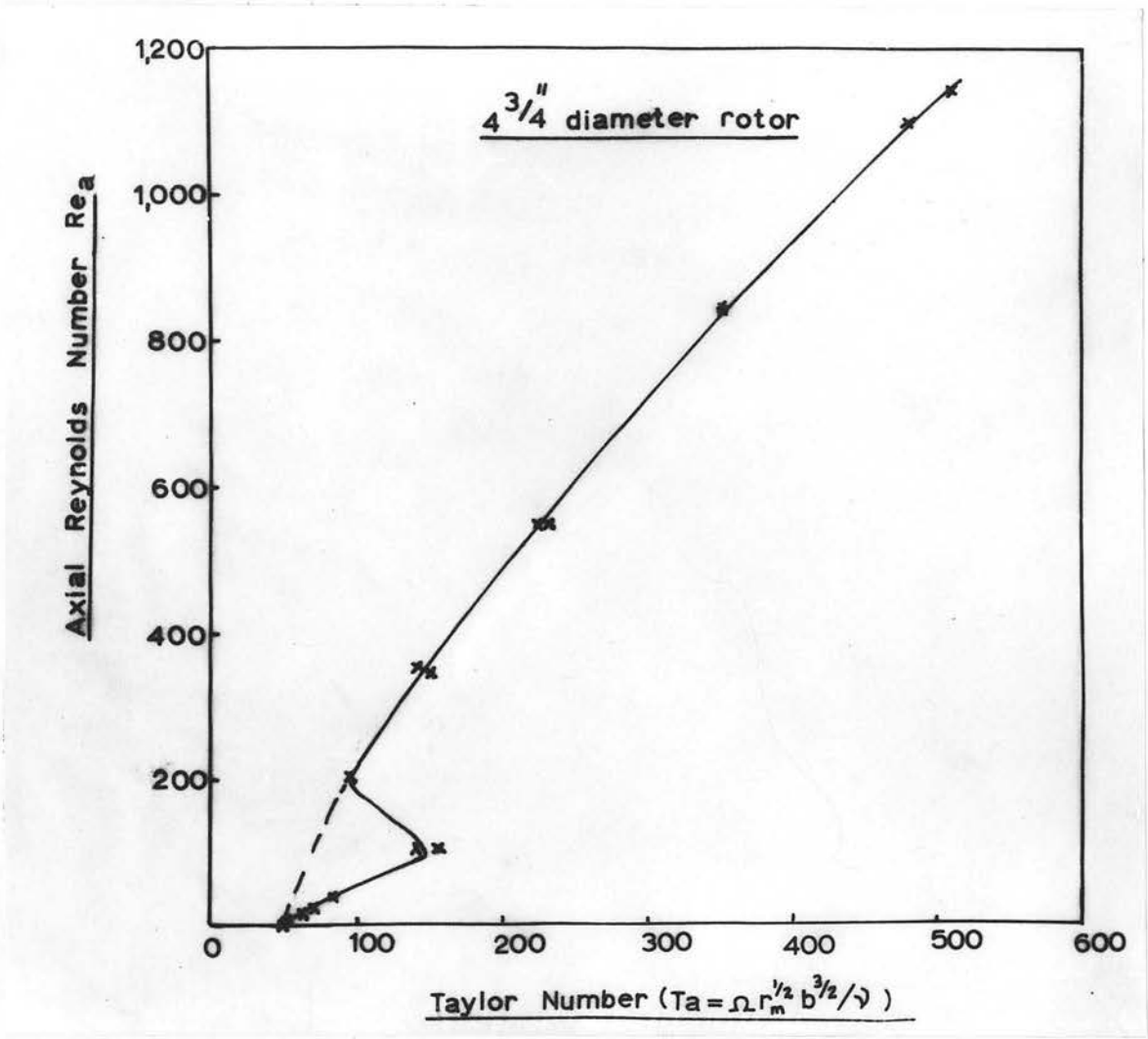

Figure 74. $4\frac{3}{4}$" diameter rotor. Critical curve for transition from laminar to 'laminar plus vortex' flow.

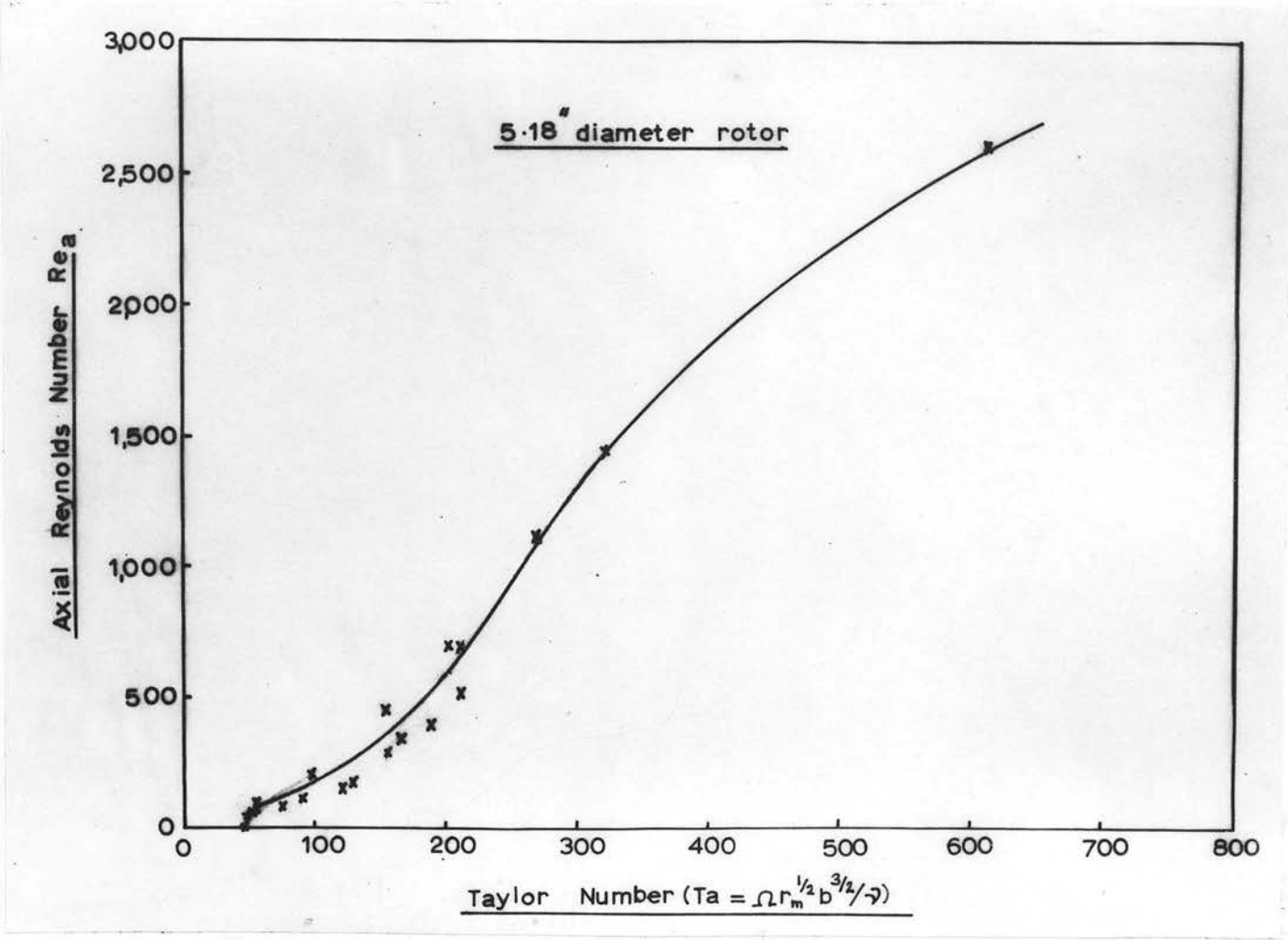

Figure 75. 5.18" diameter rotor. Critical curve for transition from laminar to 'laminar plus vortex' flow.

example, for the case of the $3\frac{1}{8}$" diameter rotor, b = 3.334 cms. and r_1 = 3.97 cms. Then taking D = 0.128 cm^2/sec and Re_c = 2000:-

$$K = \frac{0.128}{3.334} \cdot 0.45\ (2000)^{\frac{1}{2}} \left(\frac{3.334}{3.97}\right)^{\frac{1}{4}}$$

$$= 0.74$$

Now in figure 68, for a value of Re_c = 2000, K has the value $\div$ 0.78 for all values of Re_a in the range $120 < Re_a < 240$ in reasonable agreement with the value K = 0.74 calculated using equation (95).

13.3 Conditions for vortex formation - discussion of results.

Tables 28 to 31 inclusive record the critical conditions for vortex formation for all the rotors used in this investigation. From the data recorded critical values of Re_a versus Ta were plotted showing the transition from laminar to 'laminar plus vortex' flow. Figures 72, 73, 74 and 75 show these plots for the $2\frac{3}{8}$", $3\frac{1}{8}$", $4\frac{3}{4}$" and 5.18" diameter rotors respectively. The theoretical values of the critical Taylor number at zero Re_a, obtained from Taylor's equations (45) and (46) Part I, have also been plotted in these graphs and are also quoted at the top of each table of results, Tables 28 to 31 inclusive. In Appendix 0 the value of the critical Taylor number at Re_a = 0 is calculated for the $2\frac{3}{8}$" diameter rotor as an example. In general it is observed that the critical value of Re_a increases monotonically with the critical value of Ta, but in the case of both the $3\frac{1}{8}$" and $4\frac{3}{4}$" diameter rotors a peculiarity is observed in the shape of the curves in the region of low Re_a and Ta. From the theory due to Di Prima (14) and the results of previous investigators (9, 10, 11, 28, 34) discussed in Part I of this report, it would be expected that

for these rotors the critical conditions for vortex formation in this range would be more accurately represented by the smooth dotted curves (see figures 73 and 74) which are drawn to pass through the 'Taylor value' at zero Re_a. The experimental results in this region indicate that the observed critical speed of rotation was larger than the expected critical speed corresponding to vortex formation at a particular low value of Re_a. It is thought that this discrepancy is due to the rather insensitive behaviour of the Hanovia Mercury Vapour Detector at very low rotor speeds. In this region quite large changes in rotor speeds were required to produce an increase of about half a scale division in the microammeter reading and, as the rotor speeds were of the order of 30 - 80 rpm, it was quite possible to considerably over-estimate the critical rotor speed corresponding to such a small increase in scale reading. This "overshooting" of the estimated critical rotor speed at a particular low value of Re_a would explain the observed discrepancy in the graphs. This explanation was confirmed by experiments using the 5.18" diameter rotor in which several independent determinations were made, in the region of low Re_a and Ta, of the critical rotor speed corresponding to the first noticeable change in meter reading - and not to a change of about half a scale division, as for the other rotors. As seen from figure 75 a smooth curve can be drawn through the still slightly scattered data which does not exhibit the peculiarities of that for the other two rotors.

For the case of the $2\frac{3}{8}$" diameter rotor it is seen from figure 72

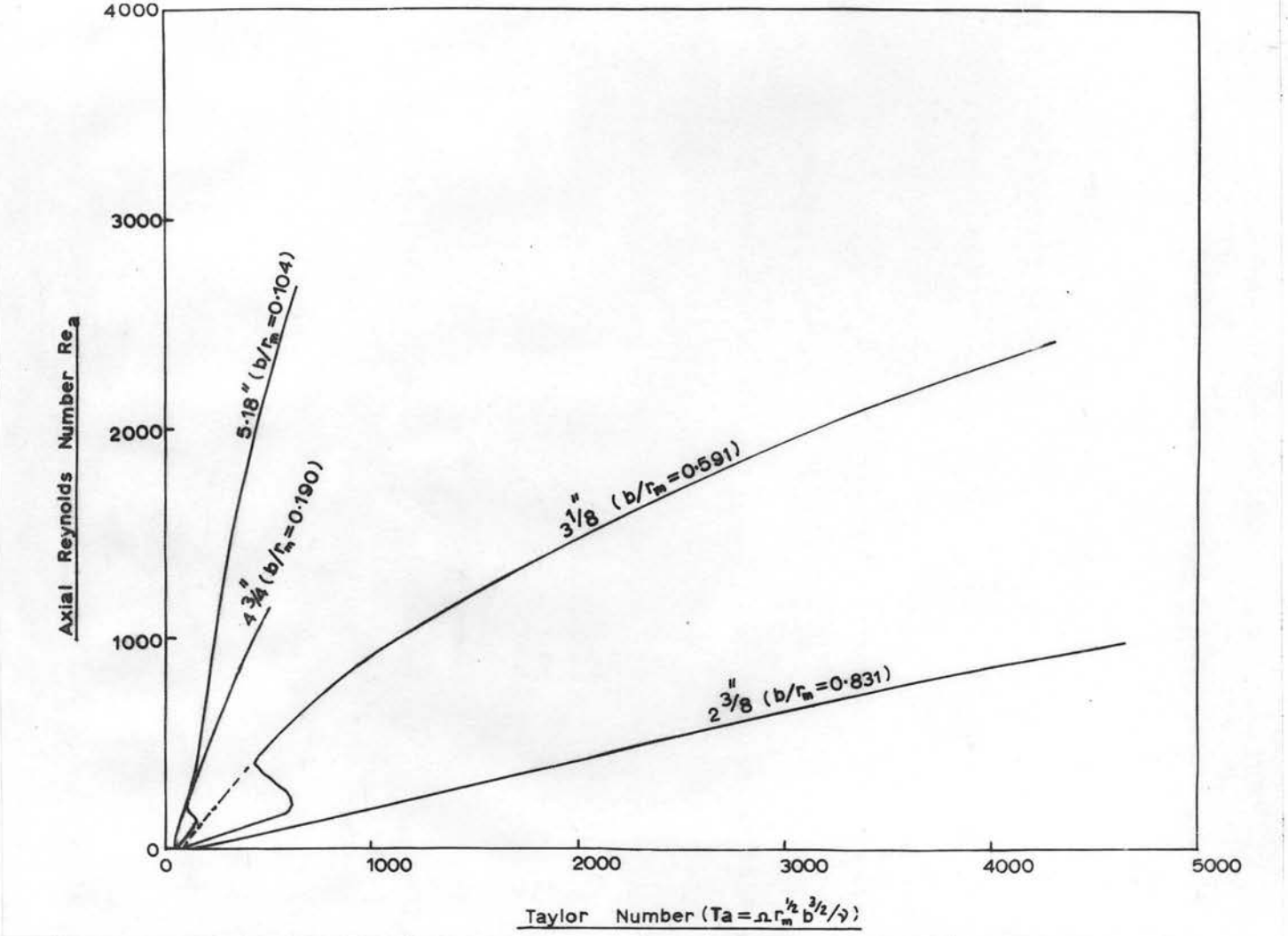

Figure 76. Critical curves for transition from laminar to 'laminar plus vortex' flow for all rotors investigated.

that a smooth curve may be drawn through the experimental data extrapolating to the 'Taylor value' at zero Re_a. No peculiarity is observed in the shape of this Re_a versus Ta curve. It is not entirely clear why this curve does not exhibit the same peculiar features as the corresponding curves for the $3\frac{1}{8}$" and $4\frac{3}{4}$" diameter rotors; it is perhaps possible that the experimentally determined critical values of Ta at a particular Re_a for the $2\frac{3}{8}$" diameter rotor are <u>all</u> slightly too large , particularly at low values of Re_a. This possibility is suggested by the observation that during an experimental run it was not possible to maintain a steady meter reading at a given low flow rate and low rotor speed. The pointer wavered about a mean value on the microammeter scale, probably due to ineffective mixing of mercury vapour and air in such a wide annulus. Thus, in assessing the critical rotor speed at a particular low value of Re_a, it is quite possible that the rotor speed had to be increased to a value somewhat in excess of the value corresponding to vortex formation before any definite change in the meter reading could be observed.

In figure 76 the critical conditions are plotted for all the rotors used. It is clear that the larger the value of b/r_m the nearer does the curve, marking the transition from a laminar to a 'laminar plus vortex' condition, lie to the Taylor number axis. Thus, for a column having a large value of b/r_m and in which vortices have just appeared, a small increase in the axial flow rate demands a considerable increase in rotor speed in order to maintain the vortex

regime. Conversely, for columns having a very small b/r_m value the conditions for vortex formation are relatively insensitive to axial flow rate.

It also appears from figure 76 that for b/r_m values less than 0.2 the curve marking the transition from laminar to 'laminar plus vortex' flow is almost independent of the value of b/r_m at values of Re_a less than about 350. This result was used in Part I, section 3.912 to determine the conditions for the onset of a vortex regime at low boil-up rates in the column studied by Willingham et al (3) ($b/r_m = 0.027$) using the experimental data of Kaye and Elgar (11) ($b/r_m = 0.198$).

It has hitherto been assumed that the critical rotor speed corresponding to a sudden increase in radial mass transfer corresponds also to the critical speed for vortex formation. The fact that the experimental data plotted in figures 72 to 75 inclusive extrapolate smoothly to the corresponding 'Taylor value' gives some indication that this assumption is valid. It is however fairly certain that an increase in radial mass transfer was not detected on the Hanovia instrument until vortices were definitely established and thus it is possible that the technique used to establish the conditions for vortex appearance tended to over-estimate the value of the critical rotor speed corresponding to a particular value of the axial flow rate in the annulus. It is therefore interesting to compare the experimental results obtained in this investigation with the theoretical (14) and experimental (11, 28, 34) results of other workers.

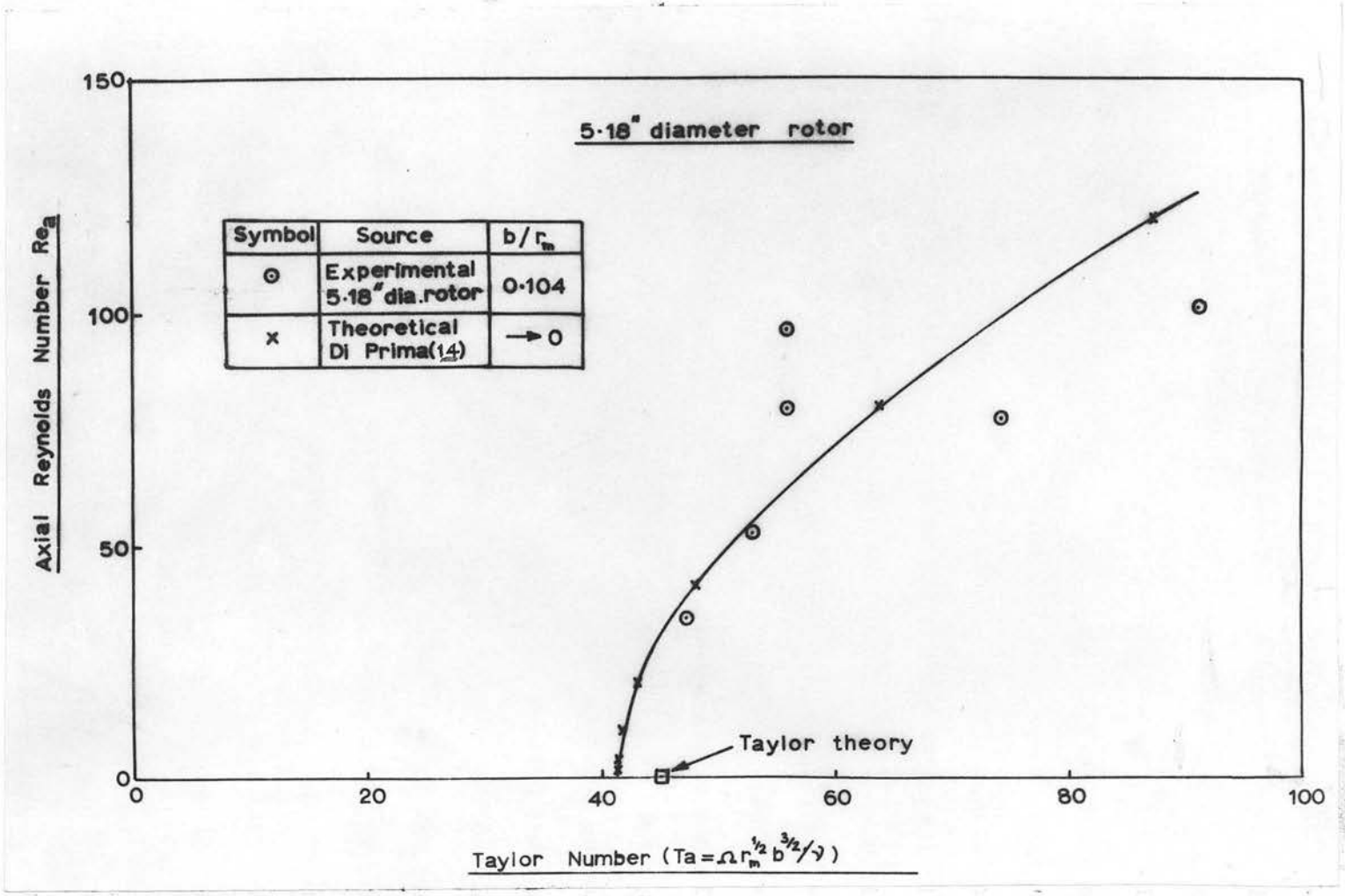

Figure 77. Comparison of experimental points for 5.18" diameter rotor with theoretical transition curve due to Di Prima (14)

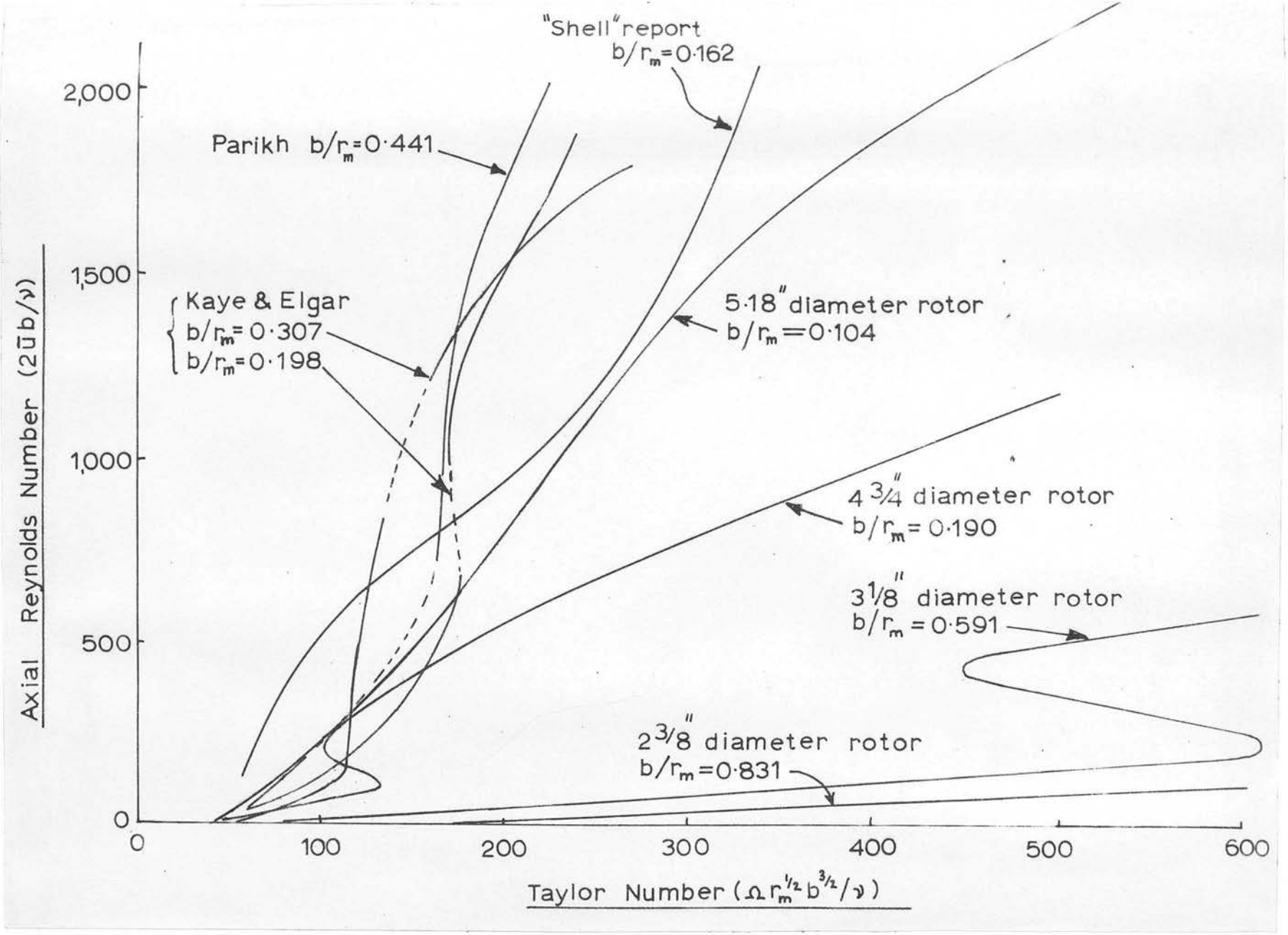

Figure 78. Critical curves for the transition from laminar to 'laminar plus vortex' flow. Comparison with previous work.

13.31 Comparison of results for critical conditions of vortex formation with previous work

In figure 77 the experimentally obtained critical values for the 5.18" diameter rotor ($b/r_m = 0.104$) are compared with the theoretical curve derived by Di Prima (14) for the limiting case $b/r_m \rightarrow 0$. The 'Taylor value' corresponding to $b/r_m = 0.104$ is also plotted in figure 77. Despite the considerable scatter of the experimental values when plotted on this scale there is good general agreement between the theoretical curve and the experimental data, indicating that the experimental values are a valid representation of the critical conditions for vortex appearance in this column using the 5.18" diameter rotor. In figure 78 the critical conditions found with the mercury vapour column are compared with the experimental data due to Kaye and Elgar (11) and Parikh (28) and also with the data obtained from the "Shell" report (34). It will be remembered that Kaye and Elgar's data was based on smoke experiments confirmed by hot wire measurements, whereas Parikh's results were based on heat transfer measurements. The "Shell" report gives values corresponding to a sudden change in the number of transfer units at a critical rotor speed for the vapourisation of n.butanol.

There is considerable discrepancy between the experimental curves of the present investigation and the curves obtained by these other workers. In general the data of these previous investigations show that the conditions for vortex formation are much less sensitive to the value of b/r_m than found in the present investigation. This is particularly evident at high axial flow rates at which, even with

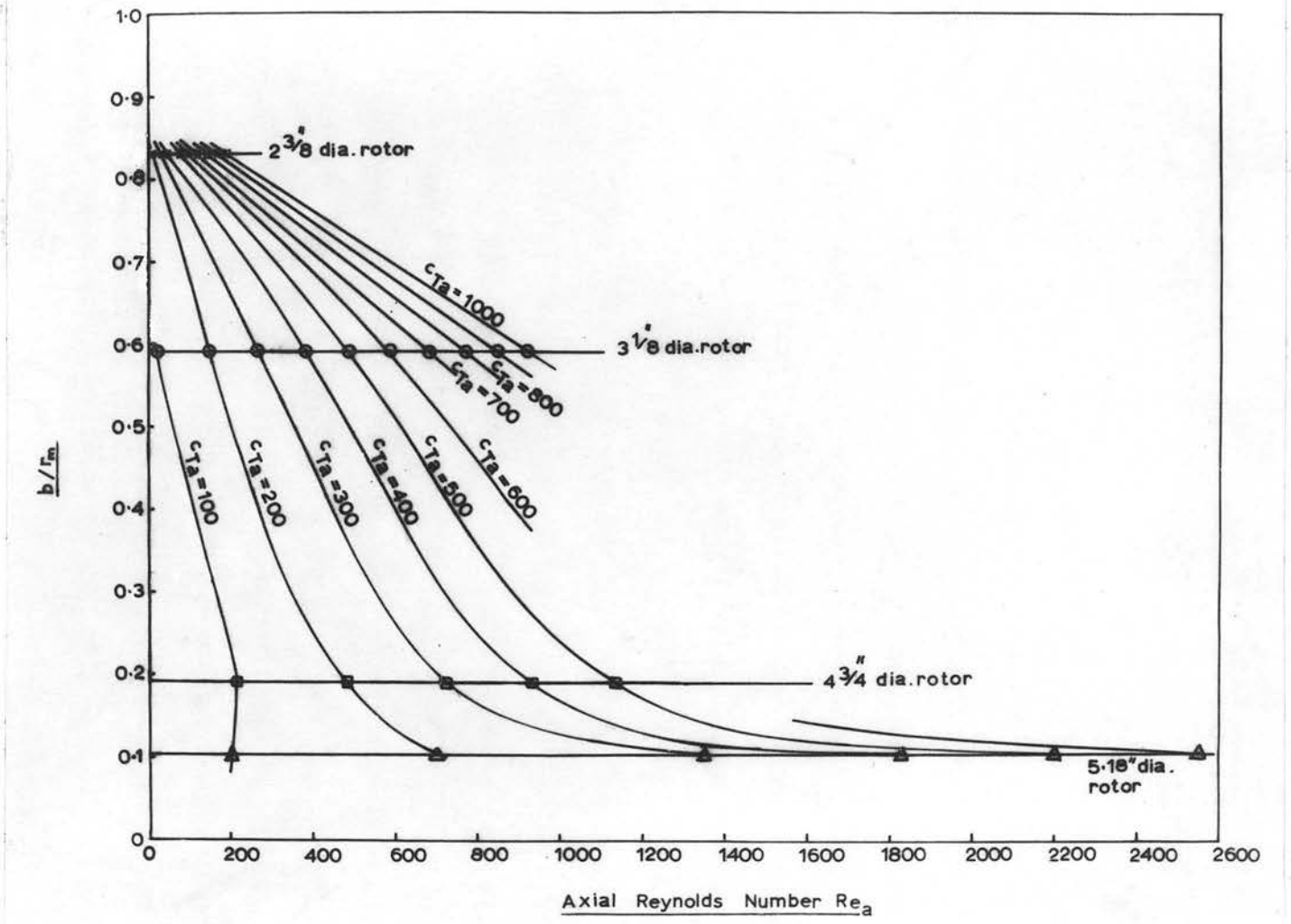

Figure 79. Critical values for transition from laminar to 'laminar plus vortex' flow for any system having a b/r_m value in the range $0.104 < b/r_m < 0.831$.

Parikh's column having a value of $b/r_m = 0.441$, the experimental critical values lie relatively near the data corresponding to the 5.18" diameter rotor, having a b/r_m of 0.104. Since there is a scarcity of such experimental data extending over the range of b/r_m values investigated in the present work it is difficult to conclude whether the results of previous investigations are erroneous or whether for columns with large values of b/r_m the method used in the present investigation gives unusually large values of the critical Taylor number for a particular value of Re_a. It should also be noticed that over most of the range investigated the curve for $b/r_m = 0.307$ obtained by Kaye and Elgar lies nearer the Re_a axis than the curve for $b/r_m = 0.198$ involving a similar transition. This result contradicts the trend of the results obtained in the present investigation.

If it is assumed that the conditions corresponding to vortex formation have been accurately determined in the present experimental investigation then it is possible to draw a series of curves, as shown in figure 79, which enable the critical conditions to be determined for any column having a b/r_m value lying within the range of values investigated in the present work. The curves in figure 79 were obtained from a cross-plot of figure 76. By interpolation on figure 79 it is possible to find values of the critical Taylor number (^cTa) at any value of Re_a for any value of b/r_m in the range $0.104 < b/r_m < 0.831$. The range of values of ^cTa and Re_a is obviously limited by the range of the experimental results obtained using each rotor.

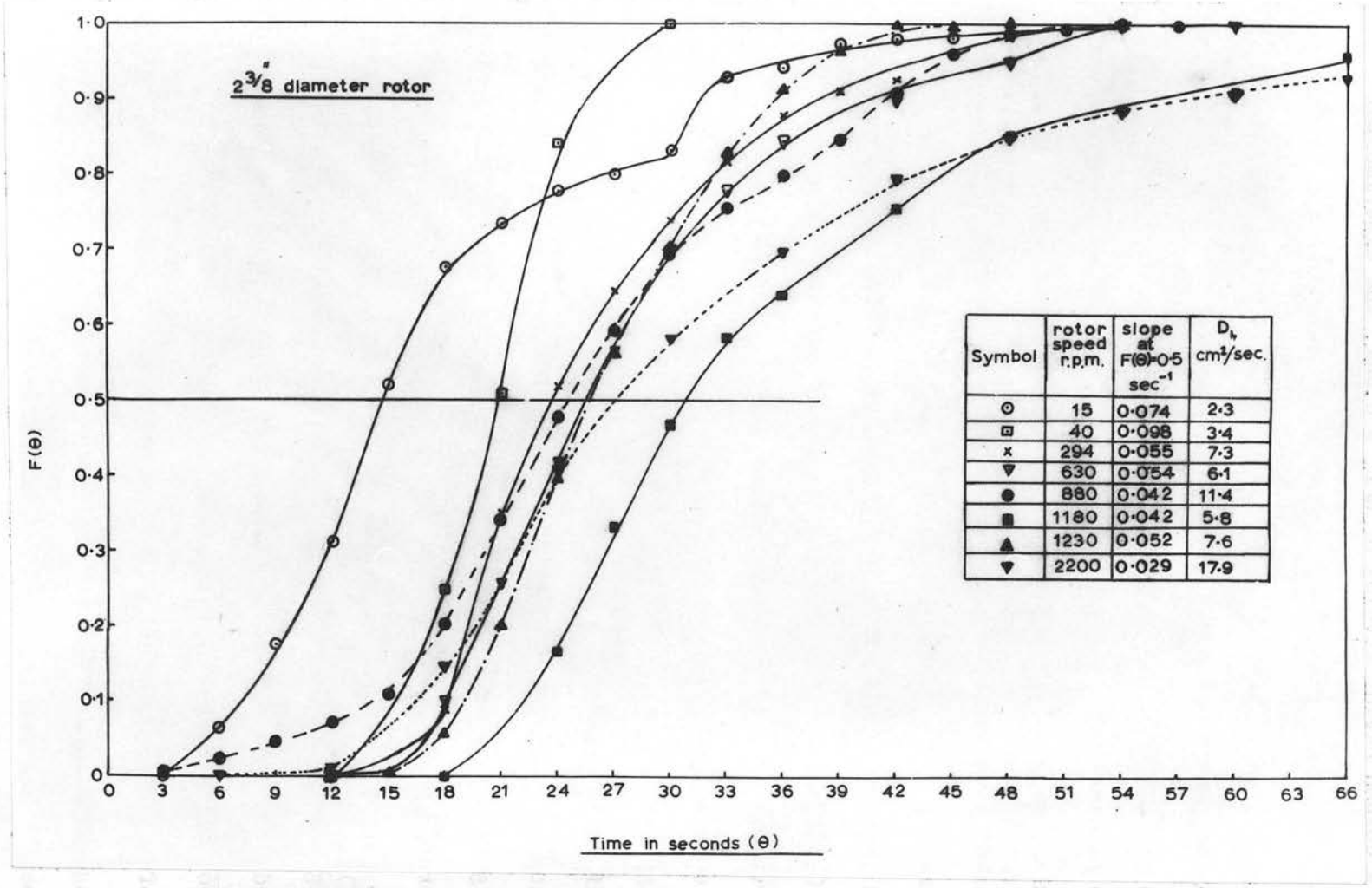

Figure 80. $2\frac{3}{8}$" diameter rotor. Plot of fractional change in concentration, $F(\theta)$, versus time, θ. Final $Re_a \doteqdot 158$.

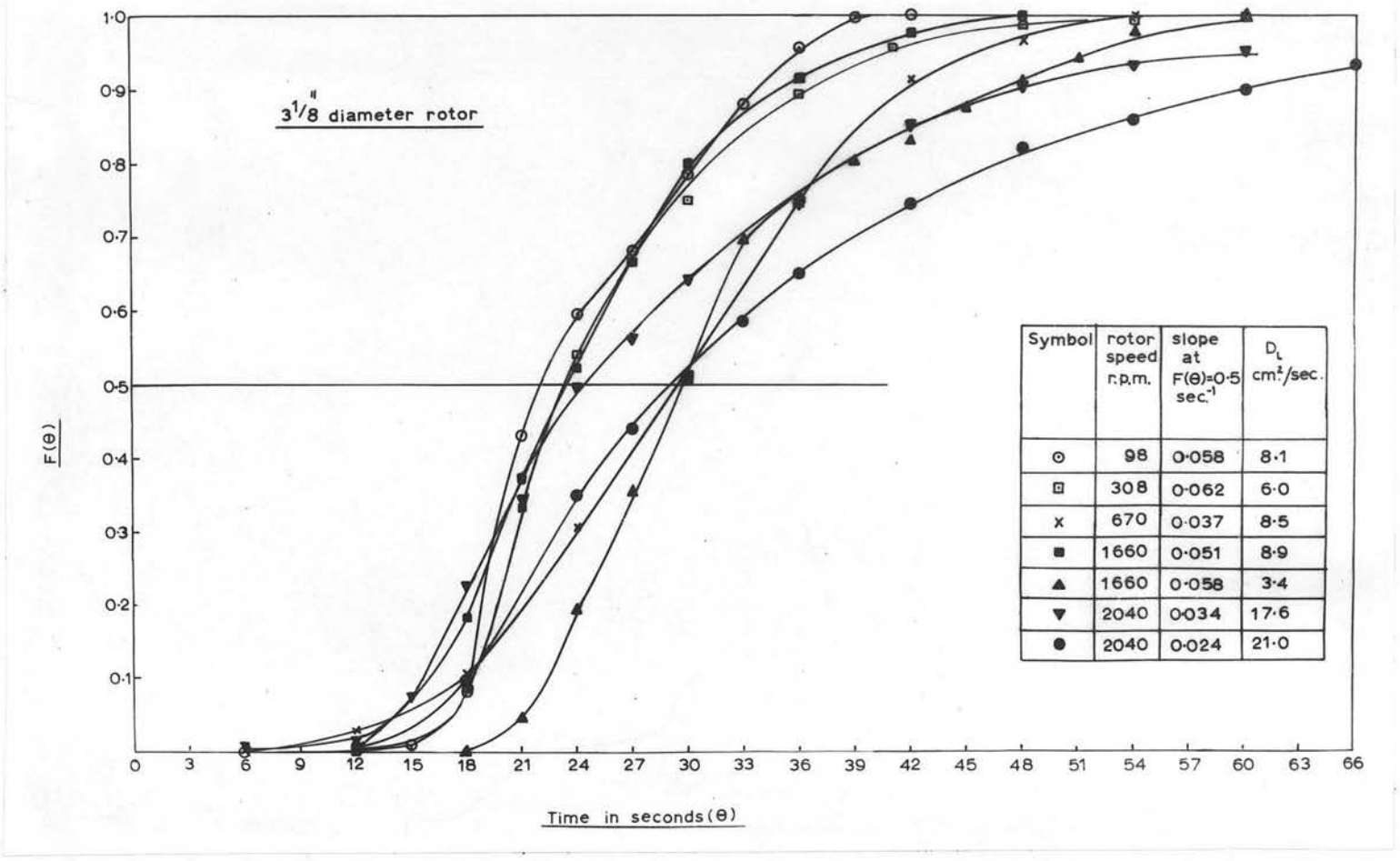

Figure 81a. $3\frac{1}{8}$" diameter rotor. Plot of fractional change in concentration, $F(\theta)$, versus time, θ. Final $Re_a \doteq 108$.

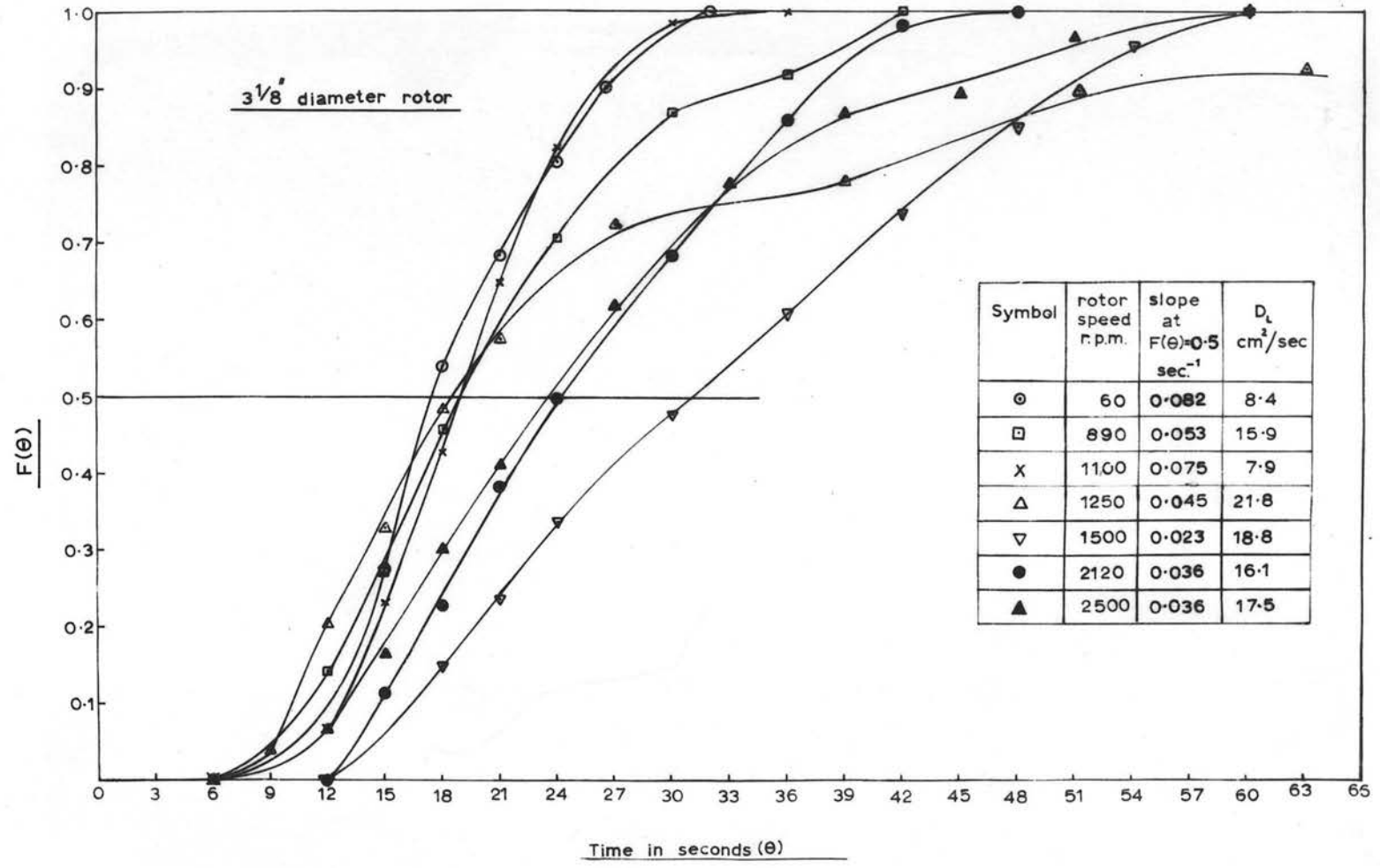

Figure 81b. $3\frac{1}{8}$" diameter rotor. Plot of fractional change in concentration, $F(\theta)$, versus time, θ. Final $Re_a \doteqdot 129$.

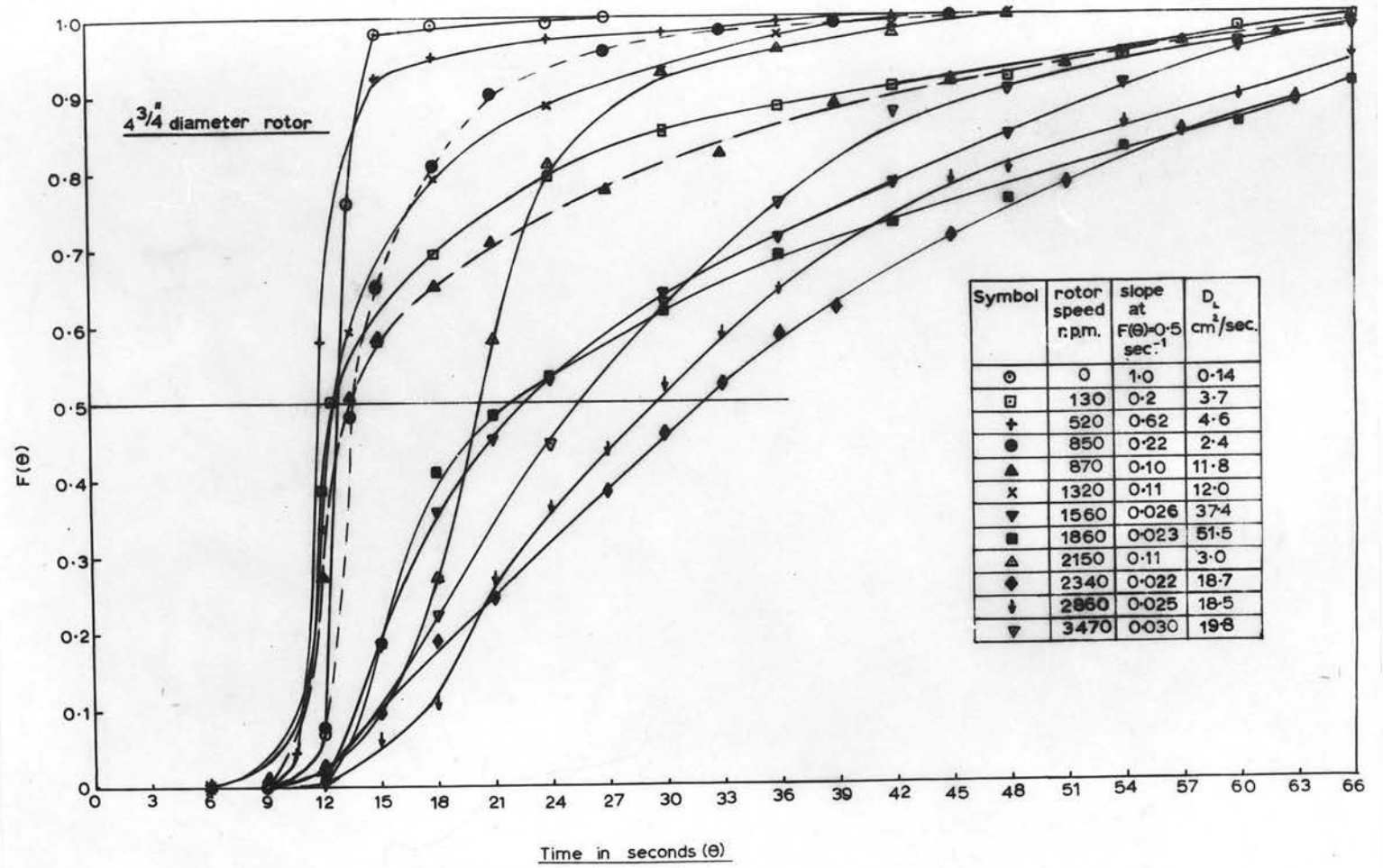

Figure 82. $4\frac{3}{4}$" diameter rotor. Plot of fractional change in concentration, $F(\theta)$, versus time, θ . Final $Re_a \doteqdot 64$.

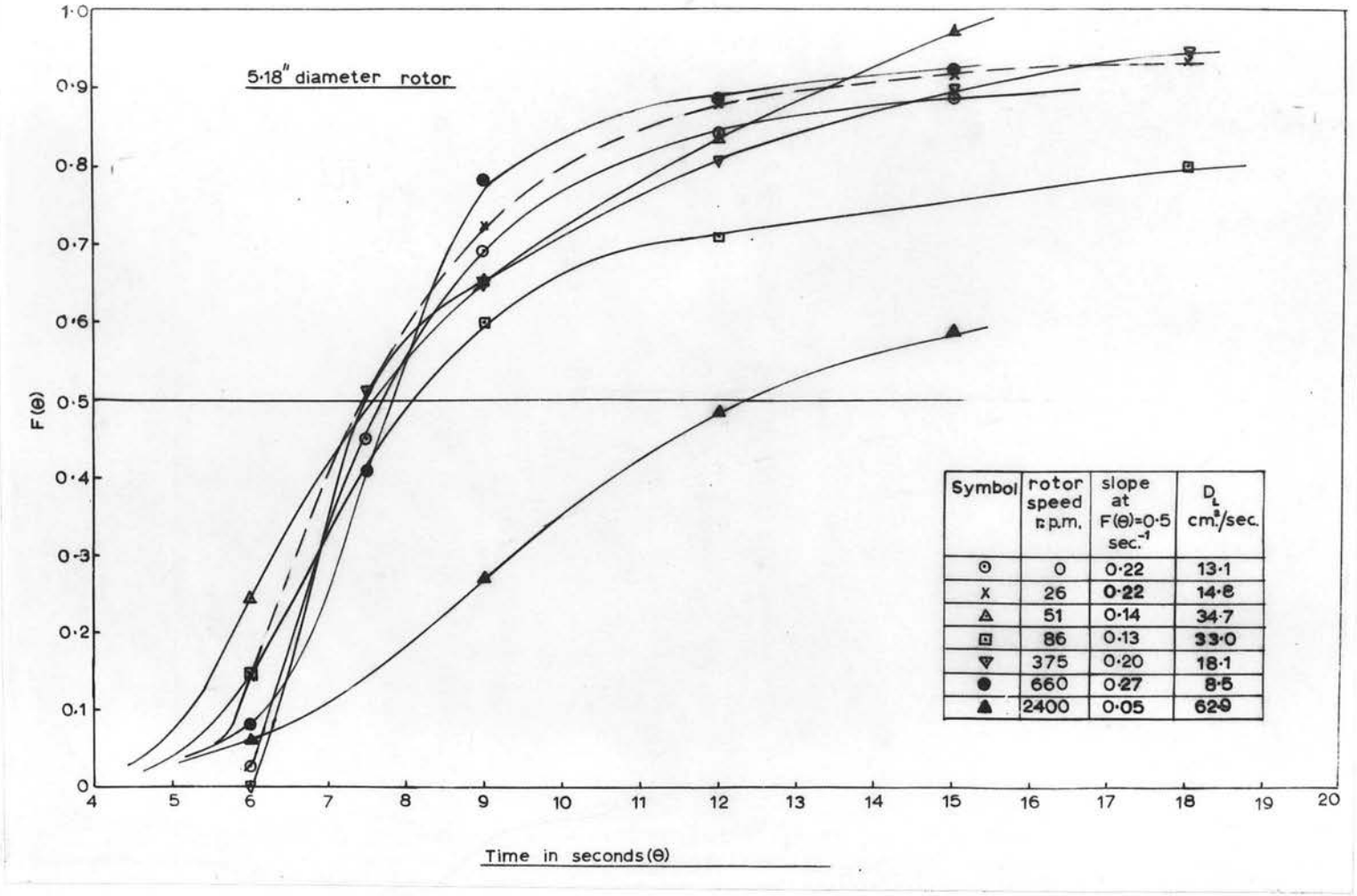

Figure 83. 5.18" diameter rotor. Plot of fractional change in concentration, $F(\theta)$, versus time, θ. Final $Re_a \doteqdot 72$.

13.4 Longitudinal diffusion experiments - calculation and discussion of results

The results for all the longitudinal diffusion experiments performed are given in Tables 37, 38, 39 and 40 inclusive for the $2\frac{3}{8}$", $3\frac{1}{8}$", $4\frac{3}{4}$" and 5.18" diameter rotors respectively. These results are plotted in figures 80 to 83 inclusive on the basis of $F(\theta)$ versus θ, where $F(\theta)$ is the fractional change in the outlet tracer concentration at time θ, the time being measured in seconds. In each figure curves of $F(\theta)$ versus θ are plotted for several values of the rotor speed with approximately the same final value throughout of the axial flow rate in the annulus. If the final axial flow rate had been the same in each experiment then according to theory (equation 88)) all the curves should pass through the point $F(\theta) = 0.5$, $\theta = \theta_o$ where θ_o is the "mean residence time" given by:-

$$\theta_o = \frac{L}{\bar{u}}$$

L being the length of the experimental section and $\bar{u}$ the average air velocity in the annulus. From figures 80 to 83 inclusive it is seen that the curves do not pass through one point. This may be due to several possible causes. One obvious cause is the possibility of a systemmatic error in setting the final flow rate; another is that oscillations appeared in the annulus after the sudden step change in flow rate and another possible cause is that the electronic system was unstable. It was occasionally noticed that the Cambridge Recorder pen "drifted" under apparently steady state conditions. This "drift" would have given rise to random errors in the form of the $F(\theta)$ versus θ curves. Since these $F(\theta)$ versus θ curves do not have a truly

"sigmoidal" shape as predicted by the error function equation (88) it must be concluded that these curves are only approximate. This was to be expected in any case since the method of simulating a step change in concentration did not really produce a uniform change in concentration across the entire annular gap. The sudden change in flow rate led to a sudden change in the rate of radial mass transferfrom the amalgamated section, which resulted in a change of concentration in the air flow only in the immediate neighbourhood of the amalgamated section. Although radial diffusion in the air stream was rapid, particularly in the presence of a vortex regime, it would be expected that the concentration of mercury vapour in the air stream would only be uniformly distributed across the annulus at some point downstream from the amalgamated section. Thus the theoretical equations developed in section 9.52 are not strictly valid for this case. However, at sufficiently high rotor speeds it is likely that radial mixing was very rapid immediately following the step change in flow rate and thus the results of experiments conducted at highrotor speeds should conform reasonably well to the theoretical conditions specified in section 9.52.

In calculating diffusion coefficients from the $F(\theta)$ versus θ curves it was assumed that the theory developed in section 9.52 was valid and that the slopes of the experimental curves at $F(\theta) = 0.5$ would furnish values of the apparent diffusion coefficient, D_L, by substitution in equation (89). The slopes at $F(\theta) = 0.5$ are tabulated in each figure. It was also assumed that the value of $F(\theta) = 0.5$ for each curve was reached after a time θ_o had elapsed. From equation (89):-

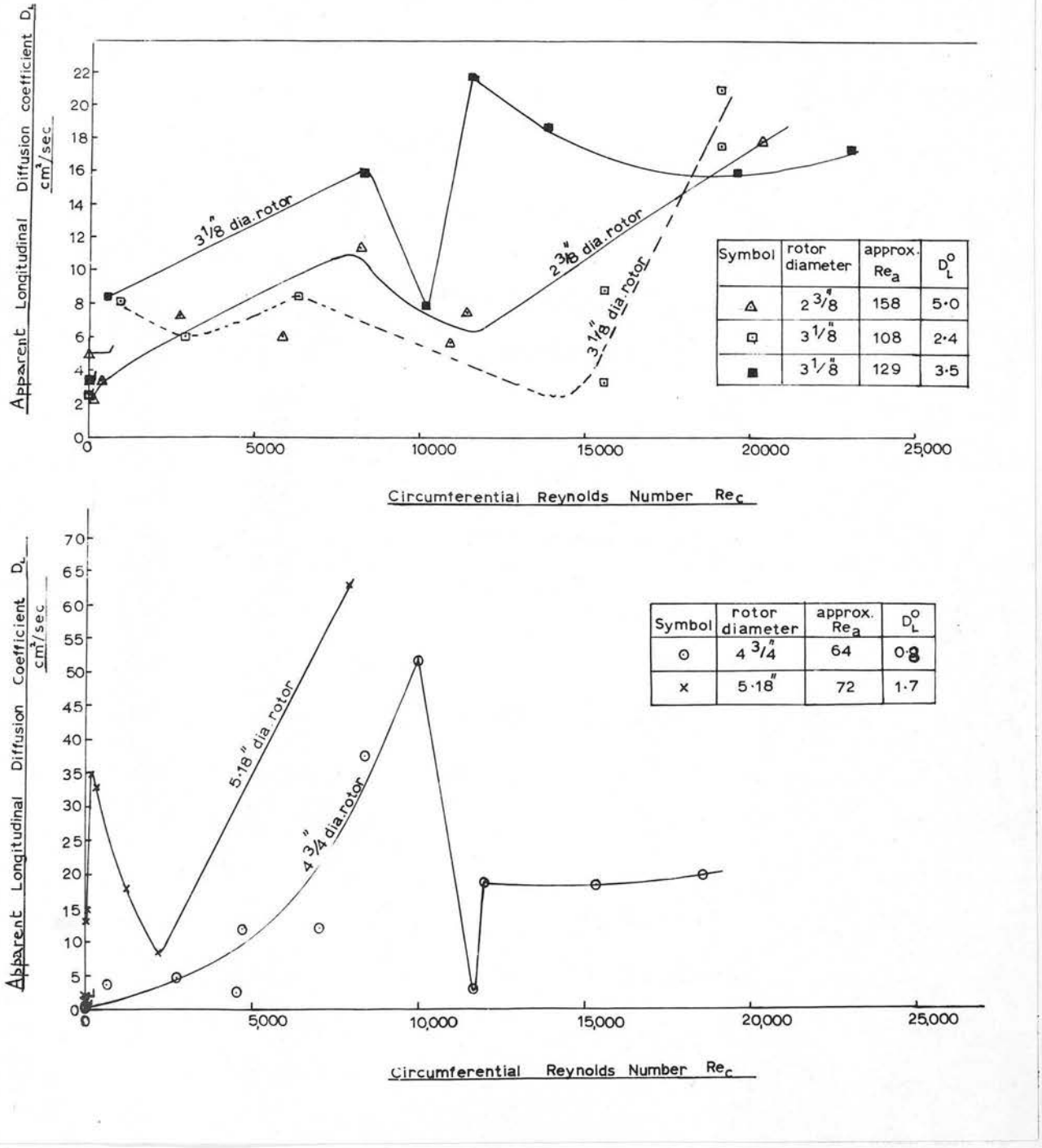

Figure 84. Results for all rotors. Plots of D_L versus Re_c at values of Re_a tabulated in figure.

$$\left[\frac{d\,F(\theta)}{d(\theta/\theta_o)}\right]_{\theta=\theta_o} = \frac{1}{2}\,\bar{u}\sqrt{\frac{\theta_o}{\pi D_L}} \qquad \text{- - - (89)}$$

$$\text{or } \left[\frac{d\,F(\theta)}{d\theta}\right]^2_{\theta=\theta_o} = \frac{\bar{u}^2\theta_o}{4\theta_o^2\pi D_L}$$

$$D_L = \frac{\bar{u}^2}{4\pi\,\theta_o\left[\frac{d\,F(\theta)}{d\theta}\right]^2_{\theta=\theta_o}} \qquad \text{- - - (96)}$$

where $\left[\frac{d\,F(\theta)}{d\theta}\right]_{\theta=\theta_o}$ is the slope of the $F(\theta)$ versus θ curve at $\theta = \theta_o$, i.e. at $F(\theta) = 0.5$ (from equation (88)).

Thus:-

$$D_L = \frac{\bar{u}^2}{4\pi\,\theta\,(\text{slope})^2_{F(\theta)\,=\,0.5}} \qquad \text{- - - (97)}$$

Values of D_L found from equation (97) are tabulated in figures 80 to 83 inclusive alongside the experimental curves for each rotor investigated.

It may be seen that in general with the axial flow rate maintained constant the value of D_L increases as the rotor speed is increased. In figure 84 the values of D_L are plotted against corresponding values of the circumferential Reynolds number, Re_c, for values of the axial Reynolds number, Re_a, corresponding to the final flow rate used for each experimental investigation with a particular rotor. In the case

of the $3\frac{1}{8}$" diameter rotor two series of experiments were conducted with two final values of the axial Reynolds number, $Re_a = 108$ and $Re_a = 129$ (see figures 81a and 81b respectively). Despite the fact that the two axial Reynolds numbers were close in value there is considerable disagreement between the results. This disagreement indicates that the experimental technique used was not very accurate and that this technique should only be used as a method of providing an approximate estimate of the variation of D_L with Re_c at a constant value of the axial Reynolds number.

The theoretical values of the apparent longitudinal diffusion coefficient for purely laminar flow in an annulus have been calculated according to the equation:-

$$D_L = \frac{1}{210} \frac{\bar{u}^2 b^2}{D} \qquad - - - (85)$$

where $\bar{u}$ is the constant average axial velocity, b the annular gap width and D the molecular diffusion coefficient. These values have been tabulated in figure 84 under the column heading D_L^o, where D_L^o represents the value of the theoretical apparent laminar longitudinal diffusion coefficient with the rotor stationary or rotating at speeds below the critical speed corresponding to vortex formation. These values of D_L^o have also been plotted along the ordinate scale in figure 84 for comparison with the experimental values derived from results with a moving rotor.

It is shown in Appendix J that values of D_L^o calculated from equation (85) should be valid for laminar flow experiments in columns satisfying the

condition:-

$$L \gg \frac{\bar{u}\, b^2}{4\pi^2 D} \qquad \text{- - - (J.5)}$$

Now for the longitudinal diffusion experiments with the $2\frac{3}{8}$" diameter rotor, (b = 4.287 cms), the value of $\bar{u}$ was 2.7 cm/sec (Re_a = 158) and L = 61 cms. With D = 0.128 cm^2/sec, the condition required for (85) to be valid is:-

$$61 \gg \frac{2.7\ (4.287)^2}{4\pi^2\ 0.128}$$

$$\text{i.e.} \quad 61 \gg 9.8$$

It can be shown similarly for the other experiments that L (= 61cms) was always greater than $\frac{\bar{u}\, b^2}{4\pi^2 D}$. Thus the values of D_L^o calculated from equation (85) represent the values of D_L^o expected in these experiments.

Horizontal lines have been drawn through these values of D_L^o and the limit of application of these values indicated by a small turn upwards in these lines at the critical value of Re_c corresponding to vortex formation. These critical values of Re_c at a particular Re_a were obtained from the results described in the previous section.

Except for the $2\frac{3}{8}$" diameter rotor the values of D_L^o at very low rotor speeds lie somewhat below the experimentally determined values of D_L. For $2\frac{3}{8}$" diameter rotor the value of D_L^o lies above the values of D_L obtained from experiments at very low rotor speeds, for which the air was probably still in a purely laminar condition. At very low rotor speeds

the experimental values of D_L should agree with the theoretically calculated values of D_L^o. The disagreement is probably due to experimental error coupled with the possibility that it may not be valid to use equation (89) in order to derive values of D_L from results of experiments at low rotor speeds, due to the technique of tracer injection used. Figure 84 shows that the curves of D_L versus Re_c exhibit the same general shape for all the rotors investigated: as the rotor speed is increased the value of D_L rises considerably above both the theoretical value, D_L^o, for purely laminar flow and the values of D_L obtained by experiments at low rotor speeds. A maximum is reached and the values of D_L then fall with increasing Re_c, finally rising again at higher values of Re_c. It has not been found possible to associate the maxima and minima on these curves with any change of regime of the air flow in the annulus and since the experimental technique used was one directed at giving only an approximate estimate of the dependence of D_L on Re_c, these results should not be scrutinised on too small a scale. Since considerable instability of the Hanovia microammeter pointer was observed during experiments with the 5.18" diameter rotor at very low speeds of rotation, it is highly probable that at these very low speeds the values of D_L are spurious. However, there is some indication in the results shown in figure 84 that the smaller the ratio of gap width to rotor radius the greater is the rate of increase of D_L with Re_c at a particular value of Re_a.

The results shown in figure 84 are not regular enough to enable

correlations to be made similar to equations (91) and (92) developed by Croockewit et al (8) for the longitudinal diffusion coefficient in a vortex regime (91) and the criterion for the transition to a turbulent regime (92) respectively. However, the results of Croockewit et al (8) when analysed indicate rises in D_L of the same order of magnitude over a similar range of circumferential Reynolds numbers, for columns having b/r_1 values similar to the mercury vapour transfer column.

It is reasonable to conclude from the results of the present investigation and those of Croockewit et al that the apparent longitudinal diffusion coefficient, D_L, is significantly increased by the appearance of vortices in the annulus.

Use has already been made in Part I, section 3.72 of the results of these longitudinal diffusion experiments in assessing the importance of back-mixing in rotary concentric cylinder fractionating columns. The performance of the column of Part I fitted with the 2.14 cm diameter copper inner cylinder was taken as an example. With the cylinder rotating at 2000 rpm in the fractionation experiments the circumferential Reynolds number is about 3400 (see Part I, Table XIV). The b/r_m value for this cylinder is 0.267 and thus it is reasonable to use the longitudinal diffusion results for the $4\frac{3}{4}$" diameter rotor ($b/r_m = 0.190$) shown in figure 84 to assess approximately the influence of longitudinal mixing in the fractionation experiments using the 2.14 cm diameter cylinder. It may be seen from figure 84 that for the $4\frac{3}{4}$" diameter rotor the maximum increase in the value of the apparent longitudinal diffusion

coefficient, D_L, is about seven-fold when the circumferential Reynolds number, Re_c, is increased from zero to a value of about 3400 with an axial Reynolds number of about 60 (corresponding to a boil-up rate of about 100 cc/hr in the fractionating column). Thus using equation (50), viz:-

$$\frac{D'}{D_1} = \frac{\text{apparent longitudinal diffusion coefficient for vortex flow}}{\text{apparent longitudinal diffusion coefficient for purely laminar flow}}$$

a value for D' is given by:-

$$\frac{D'}{0.037} \doteqdot 7$$

It is subsequently shown in section 3.72 that using this value of D', (the homogeneous vortex regime diffusion coefficient), the influence of back-mixing on the performance of the fractionating column is negligible even at extremely low boil-up rates of 100 cc/hr. This conclusion may also be reached for the other inner cylinders used in the distillation experiments.

This example shows that although these longitudinal diffusion experiments are only "order of magnitude" experiments they serve to dismiss the possibility (c), discussed in section 8, i.e. that vortices do improve radial mass transfer but at the same time increase back-mixing so as to offset any improvement in fractionating column performance in the system and experimental conditions investigated.

14. Application of results to fractionating column work

Before this research project was undertaken three suggestions were put forward to explain the apparent insensitivity of the performance of rotary concentric cylinder fractionating columns with respect to changes of rotor speed, in the speed range in which vortices would be expected to appear in the vapour phase. The suggested possibilities were:-

either (a) that vortices are not formed in these columns at or near the predicted (equation (45)) critical speeds of rotation of the inner cylinder.

or (b) that vortices are formed but are not effective in promoting radial mass transfer.

or (c) that vortices do improve radial mass transfer, but at the same time increase back-mixing so as to offset any improvement in column performance.

The possibility (c) has been discounted by arguments put forward in Part I, section 3.72 based on the results of the longitudinal diffusion experiments discussed in the last section, section 13.4. It is now clear that over the range of experimentation involved, longitudinal diffusion effects had negligible influence on the performance of the fractionating column investigated.

The results of the present investigation also show that it is imprecise to consider either of the two possibilities (a) or (b) to be generally and exclusively true. Although radial mass transfer experiments, described in Part II of this thesis, showed that vortices were probably formed at a certain critical speed of rotation of the inner cylinder in the fractionating column experiments, the value of the critical speed was markedly dependent on the boil-up rate and b/r_m value of the system. The critical speed of rotation of the inner cylinder was generally a good way above that predicted from Taylor's equation (45).

For the particular fractionating column investigated the results discussed in Part I, section 7 indicate that, when the 2.60 cm. diameter inner cylinder was used, no vortices were present under the operating conditions employed; so that the insensitivity of column performance to changes in the speed of rotation of the inner cylinder is explained for that case by possibility (a). When the other two inner cylinders were used, however, vortices were generally present, and the small effect of speed of rotation of the inner cylinder is explained by possibility (b), i.e. although the presence of a vortex regime does promote an increase in radial mass transfer the change in column performance in the neighbourhood of the transition speed is of no great significance and is small enough to be masked by other effects causing scatter in the experimental points. This conclusion was reached largely as a result of the radial mass transfer experiments on the mercury vapour transfer column. These results yielded directly a correlation from which equation (36) was derived and the form of equation (36) suggested the derivation of equation (39) which was obtained from the results of vapourisation experiments described in the "Shell" report (34). Both equations (36) and (39) were considered valid theoretical standards with which to compare the performance of rotary concentric cylinder fractionating columns operating with vortices present in the vapour phase. It was subsequently shown that equation (39) fitted fairly closely the results obtained from the fractionating column investigated in this project and that equation (36) could be taken to represent an upper theoretical limit for the performance of this column.*

* The connection between the fractionating column and mercury vapour transfer column lacks one link, because of the unknown effect of rippling on the mass transfer coefficient from the reflux film. The "Shell" data (equation (39)) is directly applicable and the nearness with which equations (39) and (36) tie up with the experimental results seems to indicate that the effect of rippling must be small.

It will now be shown that the radial mass transfer results from experiments on the mercury vapour column may be used to indicate directly and very clearly that, for the particular fractionating column experiments described in Part I of this thesis, if and when vortices do appear in the vapour phase the increase in the rate of radial mass transfer (and hence column performance) is not immediately significantly improved. It will, however, also be shown that this (possibility (b)) is only true for the particular column investigated over the range of operation actually studied and that if further experiments are undertaken, for example at higher speeds of rotation of the inner cylinder, and low boil-up rates, the presence of vortices in the vapour phase would cause a significant improvement in column performance. This becomes particularly clear if reference is made to figures 67 to 70 inclusive. These figures give the results of radial mass transfer experiments and show values of K plotted as a function of Re_c at several values of Re_a. From these curves it can be seen that, except for the $2\frac{3}{8}$" diameter rotor with low axial flow rates, the onset of a vortex regime for a particular value of Re_a does not give rise to a marked increase in the value of K. Furthermore, it is apparent that the subsequent rate and extent of increase of K with Re_c depends both on the b/r_m value of the system and the particular value of Re_a. The fractionating column experiments were performed using three different sizes of inner cylinder, corresponding to different values of b/r_m and different conditions of operation. The use of each cylinder must be discussed separately in order to establish the conditions and influence of vortex appearance.

14.1 The possible change in fractionating column performance due to the onset of vortices. 2.60 cm. diameter inner cylinder

For the 2.60 cm. diameter cylinder the b/r_m value of the column was 0.074. Thus it is reasonable to assume that the K versus Re_c curves for the 5.18" diameter rotor ($b/r_m = 0.104$), shown in figure 70, can be used to indicate whether vortices appeared and, if they did appear, the expected relative change in fractionating column performance using the 2.60 cm. diameter inner cylinder. Making this assumption, it will now be shown that, for the experiments performed with this cylinder, vortices probably never did appear; and that only if experiments are performed, for example, at much higher cylinder speeds and low boil-up rates would the subsequent appearance of vortices influence the performance of this particular column.

In the experiments described in Part I the range of boil-up rates was about 200-800 cc/hr (corresponding to axial Reynolds numbers, Re_a, in the range 130-530). The range of inner cylinder speeds was 0-300 rpm (corresponding to a variation of 0-190 in the values of Re_c). A single experiment was conducted with the inner cylinder rotating at 1110 rpm, but due to excessive vibration of the inner cylinder this one result was considered inaccurate and may be discarded.

It can be seen from figure 70 that for all values of Re_a in the range $130 < Re_a < 530$ vortices are definitely absent in the range $0 < Re_c < 190$. This confirms the conclusions reached in Part I of this thesis from consideration of Kaye and Elgar's (11) results and is consistent with the fact that the results with the 2.60 cm. diameter inner cylinder conform to a theoretical curve of N versus boil-up rate based on a

theoretical equation (10) for purely laminar flow in the annulus.

It is also obvious that even at a value of $Re_c = 700$ (corresponding to a cylinder speed of about 1100 rpm) the existence of a vortex regime over the entire range $130 < Re_a < 530$ would cause only a very small improvement - 10 to 15% at most - in the value of K and hence in N. Thus with this inner cylinder, the onset and appearance of vortices would have little influence on column performance over the range of boil-up rates investigated. However, if experiments were conducted at low boil-up rates and considerably higher speeds of rotation of the inner cylinder, figure 70 indicates that column performance would be significantly improved, e.g. at $Re_a = 141$ (a boil-up rate of approximately 220 cc/hr) figure 70 indicates that, if Re_c has a value of 3000 (necessitating a speed of rotation of the inner cylinder of about 5000 rpm) the performance of the fractionating column will increase by about a factor of three. (At 3000 rpm the number of theoretical plates should increase by a factor of two).

14.2 The possible change in fractionating column performance due to the onset of vortices. 2.40 cm. diameter inner cylinder.

For the 2.40 cm. diameter cylinder the b/r_m value of the column was 0.154. It is reasonable to assume that the K versus Re_c curves for the $4\frac{3}{4}$" diameter rotor ($b/r_m = 0.190$) shown in figure 69, can be used to indicate the expected relative change in fractionating column performance due to the possible appearance of vortices using this 2.40 cm. diameter inner cylinder. Making this assumption it will now be shown that vortices probably did appear but that the onset of a vortex regime had little influence on the number of theoretical plates over the range of boil-up rates

experimentally investigated compared with other factors causing scatter in the experimental results. It will also become apparent that if further experiments are undertaken, for example at low boil-up rates and higher speeds of rotation of the inner cylinder, the presence of vortices in the vapour phase would cause a significant and discernible improvement in column performance.

For this inner cylinder the range of boil-up rates was again about 200-800 cc/hr (corresponding approximately to the range $130 < Re_a < 530$). With the inner cylinder revolving the range of inner cylinder speeds was 325-2450 rpm (corresponding to the range $400 < Re_c < 2850$).

Figure 69 shows that vortices probably appeared over the entire range of operation of this column; a conclusion also reached on the basis of Kaye and Elgar's (11) results for the conditions of vortex formation. (Figure 69 shows that vortices exist for almost all possible combinations of Re_c and Re_a in the ranges $130 < Re_a < 530$, $400 < Re_c < 2850$). It can also be seen from figure 69 that, for each curve corresponding to a value of Re_a lying in the range $130 < Re_a < 530$, the appearance of a vortex regime is not marked by a sudden and appreciable increase in the value of K at the critical value of Re_c. Furthermore, over the range $400 < Re_c < 2850$, the increase in K is about two-fold for any particular value of Re_a in the range $130 < Re_a < 530$. The fractionating column results (see figure 31) did indicate such a rise in the number of theoretical plates over the range investigated but, due to un-reproducible factors causing scatter in the experimental results, it was not possible to obtain a plot of N versus rpm from these results. Such a plot would have given a direct indication of

vortex influence over the range investigated. It was therefore concluded that, compared with other systemmatic and random errors, the influence of vortex formation was not strongly marked.

In order to produce a discernible increase in column performance due to the action of vortices it is necessary to perform experiments at, for example, low boil-up rates and comparatively high speeds of rotation of the inner cylinder, e.g. at Re_a = 208 (a boil-up rate of approximately 300 cc/hr) figure 69 shows that, if Re_c has a value of 4000 (necessitating a speed of rotation of the inner cylinder of about 3400 rpm) the performance of the fractionating column will increase by about a factor of three.

14.3 The possible change in fractionating column performance due to the onset of vortices. 2.14 cm. diameter inner cylinder.

Using the 2.14 cm. diameter cylinder the b/r_m value of the column was 0.267. It is therefore hardly reasonable to assume that figure 69 may still be used to indicate whether vortices appeared and, if they did appear, the expected relative change in fractionating column performance using this 2.14 cm. diameter inner cylinder. However, if this assumption is made then it can be shown from figure 69 that vortices probably appeared over almost the entire range of operation of this column, a conclusion also reached on the basis of Kaye and Elgar's results for the conditions of vortex formation. (The range of operation of this column was approximately $130 < Re_a < 530$, $250 < Re_c < 3500$ and figure 69 shows that vortices should exist for almost all possible combinations of Re_c and Re_a in this range).

It can be seen from figure 69 that, for each curve corresponding to a

value of Re_a lying in the range $130 < Re_a < 530$, the appearance of a vortex regime is not marked by a sudden and appreciable increase in the value of K at the critical value of Re_c. Furthermore, over the range $250 < Re_c < 3500$, the increase in K is about two-fold for any particular value of Re_a in the range $130 < Re_a < 530$. The fractionating column results (see figure 33) did indicate such a rise in the number of theoretical plates over the range investigated but, due to un-reproducible factors causing scatter in the experimental results, it proved impossible to obtain a plot of N versus rpm from these results. It was therefore concluded that the influence of vortices was not strongly marked over the range of experimental conditions investigated.

In order to produce a discernible increase in column performance due to the action of vortices it is necessary to conduct experiments at, for example, low boil-up rates and somewhat higher speeds of rotation of the inner cylinder, e.g. at $Re_a = 208$ (a boil-up rate of approximately 300 cc/hr) figure 69 shows that, if Re_c has a value of 4000 (necessitating a speed of rotation of the inner cylinder of about 2350 rpm) the performance of the column will increase by about a factor of three. It should however be noted that if experiments are conducted at higher boil-up rates the speed of rotation of the inner cylinder, necessary to cause a three-fold increase in plate value, becomes very high, e.g. at $Re_a = 539$ (corresponding to a boil-up rate of approximately 490 cc/hr) figure 69 shows that, in order to increase the number of plates by a factor of three, Re_c must have a value of about 9000 (necessitating a speed of rotation of the inner cylinder of about 5200 rpm).

It emerges from the discussion in section 14.2 and 14.3 that the effect of vortices in the present column would be quite noticeable under some of the conditions of operation actually used if only column performance could be made more reproducible. It is possible for example that improved reflux distribution would lead to more reproducible results.

14.4 Dependence of vortex influence on ratio $b:r_m$

It is observed from figure 67 that for a column having a large value of b/r_m (0.831) the onset of a vortex regime causes a sudden and marked increase in the value of K at the critical speed. This effect is particularly noticeable at low values of Re_a.

Figures 68, 69 and 70 indicate that as the ratio $b:r_m$ decreases, the increase in K at the onset of a vortex regime becomes less and less significant in the immediate neighbourhood of the critical rotor speed.

This observation leads to the conclusion that in order to take advantage of the increase in radial mass transfer due to the onset of vortices, fractionating columns ought to be designed with large values of b/r_m and operated at low boil-up rates. Unfortunately, with large annular gaps the absolute value of the number of theoretical plates is likely to be very small and the low boil-up rates impose a considerable restriction on throughput. From the point of view of fundamental study, however, the results of experiments with columns having large b/r_m values operating at low boil-up rates would be of considerable interest and further experiments should be undertaken along these lines, as already suggested in Part I, section 7.5.

15. Conclusions and recommendations for further work

15.1 Conclusions

The mercury vapour transfer column described in Part II of this report has proved a useful tool in explaining the behaviour of rotary concentric cylinder fractionating columns.

The results from radial mass transfer experiments at rotor speeds well above the critical speed corresponding to vortex formation in the mercury vapour column have been correlated, for low values of the axial Reynolds number, in the form:-

$$Sh \equiv \frac{Kb}{D} = 0.45 \ (Re_c)^{\frac{1}{2}} \left(\frac{b}{r_1}\right)^{\frac{1}{4}} \qquad - - - (95)$$

This correlation was shown in Part I to represent an upper theoretical limit for the rate of radial mass transfer in fractionating columns of the type investigated; but assuming that the form of equation (95) was correct equation (39) was derived from the results of vapourisation experiments published in the "Shell" report (34). Equation (39) was found to represent remarkably well the performance of the fractionating column investigated in Part I for the case where a vortex regime could be presumed to exist, and also served to show that over the range of experimental conditions investigated the increase in fractionating column performance due to the appearance of a vortex regime was small enough to be masked by other un-reproducible effects, causing scatter in the experimental data. The results also showed that if further fractionating column experiments are performed at low boil-up rates and higher speeds of rotation of the inner cylinders, the existence of vortices

in the vapour phase should cause a discernible improvement in column performance. The conditions for vortex formation were established, for four different rotor sizes, by finding the critical rotor speed which gave a sudden small increase in the rate of radial mass transfer of mercury vapour at a particular value of the axial flow rate. This critical rotor speed was assumed to correspond to the critical speed for vortex formation, since at very low axial flow rates the value of the critical speed for a particular rotor approached the theoretical value calculated on the basis of Taylor's equations for the case of no axial flow in the annulus. From these results, curves were drawn which permit the critical conditions for vortex motion to be determined over a wide range of rotor speeds and axial flow rates for any column having a b/r_m value falling in the range $0.104 < b/r_m < 0.831$. The critical conditions for vortex formation established in this manner are found to differ from the results of previous workers. Notably, the present experimental results indicate a strong dependence of critical conditions on the b/r_m value of the column investigated for b/r_m values greater than about 0.2. Using talcum powder in the column, visual proof was provided of the existence of vortices at high rotor speeds and low axial flow rates.

With the rotor stationary (or revolving at speeds below the critical speed corresponding to vortex formation) it was found that for laminar flow of air in the annulus the results from radial mass transfer experiments agreed well with the theoretically predicted values for the fractional saturation of the air stream with mercury vapour.

When the air stream in the annulus could be presumed turbulent a

general theoretical equation, derived on the basis of turbulent flow mass transfer between parallel plates, was found to be invalid for the particular column and conditions investigated; thus, unfortunately, the experimental results for a presumed turbulent regime could not be compared with any known theoretical standard.

The longitudinal diffusion experiments at low axial flow rates provided an "order of magnitude" estimate of the variation of apparent longitudinal diffusivity with rotor speed. It was shown in general that the onset of a vortex regime caused a considerable increase in the value of the apparent longitudinal diffusion coefficient, but that this increase was insufficient to cause a significant change in fractionating column performance for the range of boil-up rates and speeds of rotation investigated. Thus the observed lack of improvement of fractionating column performance with the onset of a vortex regime was not due to increased longitudinal diffusion offsetting the effect of a significant improvement in radial transfer. As shown directly by the radial mass transfer experiments with the mercury vapour column the lack of improvement was due to only a small increase in radial mass transfer over the range of experimental conditions investigated; this increase being masked by considerable scatter in the experimental results. The ineffectual action of vortices in promoting a rapid and significant increase in radial transfer can be attributed to the existence of a laminar boundary layer between the reflux film and the main vortex core in the vapour phase, in which boundary layer the main resistance to mass transfer probably lies. The discovery that an equation (39), derived on the basis

of this boundary layer model, represents the fractionating column results remarkably well is strong evidence that such a model can be used as an approximate representation of the complex fluid flow and mass transfer processes occurring with vortices present in the annulus of rotating concentric cylinder columns.

15.2. Recommendations for further work

It would be of great interest to investigate further both experimentally and theoretically the problem of radial mass transfer with turbulent flow in the annulus. The general theoretical equation derived in the present work is only tentative and unfortunately could not be used as a theoretical standard for the particular results obtained with a presumed turbulent flow of air in the present column.

Further experiments should be undertaken with the amalgamated band fixed around the circumference of the rotor with laminar, vortex and turbulent flow of air. The results of such experiments would indicate whether there is any fundamental difference in radial mass transfer from the inner or outer cylinder surfaces.

Experiments should also be conducted with varying widths of the amalgamated circumferential band and, in order to investigate entrance effects, experiments should be performed with the circumferential band at various distances above the base of the annulus.

An attempt should be made to determine longitudinal diffusion coefficients over a wider range of axial flow rates using a more accurate technique. Instead of causing a sudden change in the axial flow rate in order to simulate a step change in mercury vapour concentration a device should be incorporated in the column which would enable an

amalgamated surface to be suddenly exposed, thus giving rise to an actual step change in concentration at a point near the base of the annulus. Such a device is in the course of manufacture. This method still suffers from the disadvantage that the tracer injection would not take place uniformly across the annulus cross-section. A more sophisticated method would be to inject into the annulus a sinusoidally varying mass of mercury vapour of known concentration, the diffusion coefficient being calculated by the determination of the phase shift and amplitude ratio between two points in the annulus (8). Recently a method was suggested privately (59) in which a step or pulse change might be effected by shining a strong beam of ultra violet light across the annulus at the point of injection. This beam of U.V. light would 'ozonise' the air in the path of the light beam and hence give rise to a pulse or step change of ozone tracer, depending, respectively, on whether the U.V. source was switched on momentarily or indefinitely. The ozone could be detected by the detection system of U.V. source and photoelectric cell at present in use. If all these further experiments and refinements are to be carried out the Hanovia Mercury Vapour Detector must be considerably modified to ensure stability and reliability over long periods of time without requiring calibration prior to each experimental run.

Furthermore, since the values of the mercury vapour molecular diffusion coefficient and also the physical properties of the air stream are sensitive to changes in air temperature, the accuracy of all these experiments would be even more improved if the temperature of the air

passing the amalgamated section were obtained more accurately. This could be done by inserting a thermocouple through a hole drilled in one of the 'Perspex' half-sections such that the thermo-junction comes into contact with the amalgamated silver foil.

Finally smoke experiments should be conducted similar to those described by Kaye and Elgar (11) in order to determine the conditions for vortex formation. It is hoped that these experiments would confirm the conditions established in the present investigation.

APPENDIX E

Solution of equation: $u \frac{\partial c}{\partial x} = D \frac{\partial^2 c}{\partial y^2}$ - - - - (54)

A solution to equation (54) is required under the following boundary conditions:-

at $\begin{cases} x = 0 \\ y > 0 \end{cases}$ and at $\begin{cases} x > 0 \\ y = 0 \end{cases}$

$c = c_1$ $\quad$ $c = c^*$

Equation (54) may be transformed to an ordinary differential equation by introducing a new variable X, where:-

$$X = y\left(\frac{p}{9Dx}\right)^{\frac{1}{3}} \quad \text{- - - - - - (E.1)}$$

Thus (54) becomes:-

$$\frac{d^2c}{dX^2} + 3X^2 \frac{dc}{dX} = 0 \quad \text{- - - - - (E.2)}$$

with the boundary conditions now given by:-

at $X = 0$ and at $X = \infty$

$c = c^*$ $\quad$ $c = c_1$

Using these boundary conditions, (E.2) has the following solution:-

$$\frac{c - c^*}{c_1 - c^*} = \frac{1}{0.893} \cdot \int_0^X e^{-X^3} dX \quad \text{- - - - - (E.3)}$$

Now at constant x:-

$$\frac{\partial c}{\partial y} = \frac{\partial c}{\partial X} \cdot \frac{\partial X}{\partial y} \quad \text{- - - - - (E.4)}$$

From (E.1) $$\frac{\partial X}{\partial y} = \left(\frac{p}{9Dx}\right)^{\frac{1}{3}} \quad \text{- - - - - (E.5)}$$

From (E.3), differentiating:-

$$\frac{\partial c}{\partial X} = \frac{(c_1 - c^*)}{0.893} e^{-X^3} \quad \text{- - - - (E.6)}$$

From (E.4) (E.5) and (E.6)

$$\therefore \quad \frac{\partial c}{\partial y} = \frac{(c_1 - c^*)}{0.893} \cdot e^{-X^3} \cdot \left(\frac{p}{9Dx}\right)^{\frac{1}{3}} \quad \text{- - - - (E.7)}$$

Now from (E.1) $X = 0$ when $y = 0$

$$\therefore \left(\frac{\partial c}{\partial y}\right)_{y=0} = \frac{c_1 - c^*}{0.893} \cdot \left(\frac{p}{9Dx}\right)^{\frac{1}{3}} \quad \text{- - - - (E.8)}$$

Now an expression for p is obtained by finding the slope of the velocity profile at the surface of the diffusing section, i.e. $p = \left(\frac{\partial u}{\partial y}\right)_{y=0}$ (see figure 38).

For flow between parallel plates:-

$$u = \frac{6\bar{u}}{b^2}(by - y^2)$$ where b is the distance between the parallel plates

$$\therefore \quad p = \left(\frac{\partial u}{\partial y}\right)_{y=0} = \frac{6\bar{u}}{b} \quad \text{- - - - (E.9)}$$

$\therefore$ Using (E.9) in (E.8)

$$\left(\frac{\partial c}{\partial y}\right)_{y=0} = \frac{c_1 - c^{*}}{0.893} \cdot \left(\frac{2\bar{u}}{3bDx}\right)^{\frac{1}{3}} \quad ---- \text{(E.10)}$$

Now the mass transferred per unit time, N, from a diffusing band length x and of unit width is given by:-

$$N = -\int_0^x D\left(\frac{\partial c}{\partial y}\right)_{y=0} \cdot dx \quad ----- \text{(E.11)}$$ if mass transfer is solely by molecular diffusion.

But $$N = \bar{u}b(c_2 - c_1) \quad --- \text{(E.12)}$$

Equation (E.11) and (E.12) may be combined in the statement that the mercury vapour lost by radial (molecular) diffusion from the amalgamated section (E.11) is equal to that gained by the laminar air stream in flowing over that section (E

$\therefore$ From (E.10), (E.11) and (E.12)

$$\bar{u}\ b(c_2 - c_1) = -\int_0^x D.\frac{(c_1 - c^{*})}{0.893} \cdot \left(\frac{2\bar{u}}{3\ bDx}\right)^{\frac{1}{3}} dx$$

$$\therefore \quad \frac{c_2 - c_1}{c^{*} - c_1} = \frac{D}{0.893\ b\ \bar{u}} \cdot \left(\frac{2\bar{u}}{3bD}\right)^{\frac{1}{3}} \cdot \left(\frac{3}{2}\ x^{2/3}\right)$$

$$\therefore \quad \frac{c_2 - c_1}{c^{*} - c_1} = 1.468 \cdot \left(\frac{Dx}{b^2\bar{u}}\right)^{2/3} \quad ----- \text{(55)}$$

---

where $\frac{c_2 - c_1}{c^{*} - c_1}$ is the fractional saturation of the air stream

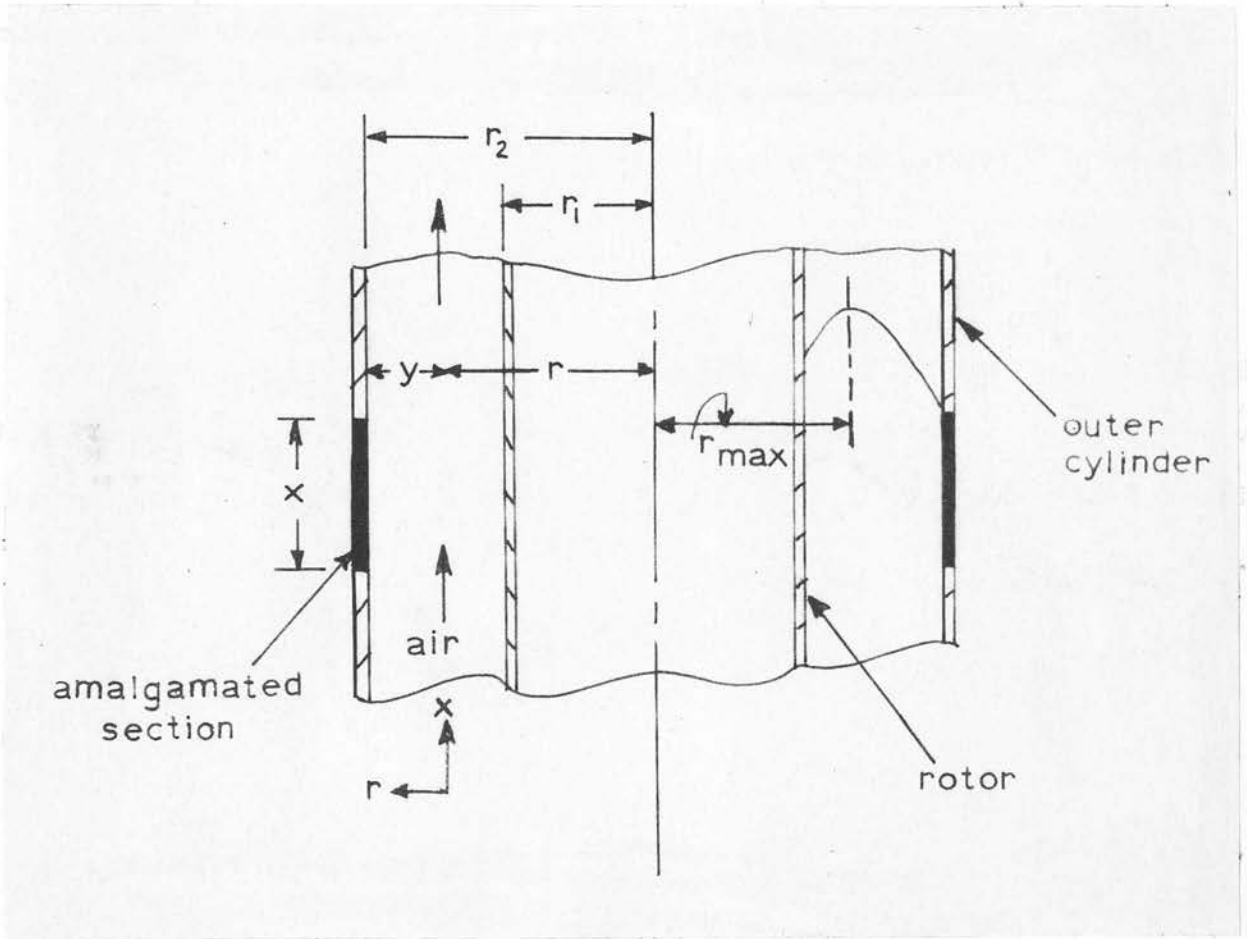

Figure 85. Concentric cylinder system. Radial diffusion from an amalgamated circumferential band on the outer cylinder.

APPENDIX F

Derivation of equation (58) - fractional saturation in an annulus

For laminar flow of fluid in a concentric cylinder system the velocity, u, at a radial distance r is given by Lamb (42) as:-

$$u = \frac{2\bar{u}\left(r_2^2 - r^2 - 2r_{max}^2 \cdot \ln {}^{r_2}/_{r}\right)}{\left(r_1^2 + r_2^2 - 2r_{max}^2\right)} \quad ---- \quad (F.1)$$

where r_1 is the outside radius of the rotor, r_2 the inside radius of the fixed outer cylinder, as shown in Figure 85, and r_{max} is the radius corresponding to the point of maximum velocity in the annulus, given by:-

$$r_{max} = \frac{r_2^2 - r_1^2}{2\ln {}^{r_2}/_{r_1}}$$

Following a method identical to that developed in Appendix E, the slope of the velocity profile at the surface of the amalgamated section is given by p where:-

$$p = \left(\frac{\partial u}{\partial y}\right)_{y=0} \equiv -\left(\frac{\partial u}{\partial r}\right)_{r=r_2}, \quad \text{since } y = (r_2 - r) \text{ from Figure 85.}$$

$$= -\frac{2\bar{u}}{\left(r_1^2 + r_2^2 - 2r_{max}^2\right)} \cdot \left[2r_{max}^2/r - 2r\right]_{r=r_2}$$

$$\therefore \quad p = +\frac{4\bar{u}\left(r_2 - r_{max}^2/r_2\right)}{\left(r_1^2 + r_2^2 - 2r_{max}^2\right)} \quad ------ \quad (F.2)$$

The equation corresponding to (E.8), for the concentration gradient at

the surface of the amalgamated section, is now given by:-

$$\left(\frac{\partial c}{\partial y}\right)_{y=0} \equiv -\left(\frac{\partial c}{\partial r}\right)_{r=r_2} = \frac{c_1 - c^{*}}{0.893} \cdot \left\{\frac{4\bar{u}\ (r_2 - r_{max}^2/r_2)}{(r_1^2 + r_2^2 - 2r_{max}^2)\ 9D\,x}\right\}^{\frac{1}{3}} \quad - - \text{(F.3)}$$

and the mass transfer rate, N, is now given by:-

$$N = \int_0^x D \left(\frac{\partial c}{\partial r}\right)_{r=r_2} 2\pi r_2\, dx = \pi(r_2^2 - r_1^2)\,\bar{u}\,(c_2 - c_1) \quad - - - - \text{(F.4)}$$

for the case where there is an amalgamated band on the outer cylinder as shown in Figure 85

From (F.4) and (F.3):-

$$\pi(r_2^2 - r_1^2)\,\bar{u}\,(c_2 - c_1) = -\frac{D\,(c_1 - c^{*})}{0.893} \cdot \left\{\frac{4\bar{u}\,(r_2 - r_{max}^2/r_2)}{(r_1^2 + r_2^2 - 2r_{max}^2)\ 9D}\right\}^{\frac{1}{3}} 2\pi r_2 \tfrac{3}{2} x^{\frac{2}{3}}$$

$$\text{or } \phi \equiv \frac{c_2 - c_1}{c^{*} - c_1} = 2.565 \left\{\frac{(r_2 - r_{max}^2/r_2)}{(r_1^2 + r_2^2 - 2r_{max}^2)}\right\}^{\frac{1}{3}} \cdot \left(\frac{r_2}{r_2^2 - r_1^2}\right) \cdot \left(\frac{Dx}{\bar{u}}\right)^{\frac{2}{3}} \quad - - - \text{(58)}$$

Equation (58) is the general equation for a concentric tube system with mass transfer taking place from a short diffusing section of length x into a laminar air stream flowing with mean velocity $\bar{u}$.

It will now be shown in Appendix G that equation (58) reduces to equation (56) if the ratio of annular gap width, b, to rotor radius, r_1, becomes very small.

APPENDIX G

Reduction of concentric tube mass transfer equation (58) to parallel plate equation (56)

Let $\dfrac{r_2 - r_1}{r_1} = e$ ------ (G.1) , where e is very small

Then $r^2_{max} = \dfrac{r_2^2 - r_1^2}{2\ln {}^{r_2}/_{r_1}} = \dfrac{r_1^2 (1 + e)^2 - r_1^2}{2 \ln (1 + e)} = \dfrac{r_1^2 (1 + 2e + e^2 - 1)}{2 \ln (1 + e)}$

$$r^2_{max} = \frac{r_1^2 \, e \, (e + 2)}{2 \ln (1 + e)} \quad \text{------ (G.2)}$$

$$\therefore \quad {}^{r^2_{max}}/_{r_1^2} = \frac{e \, (e + 2)}{2 \ln (1 + e)} = \frac{e \, ({}^{e}/_{2} + 1)}{e \, (1 - {}^{e}/_{2} + {}^{e^2}/_{3} - {}^{e^3}/_{4} - \text{------})}$$

$$\doteq (1 + {}^{e}/_{2}) \, (1 + {}^{e}/_{2} - {}^{e^2}/_{3} + {}^{e^3}/_{4}) \text{ neglecting higher terms in e}$$

$$\therefore \quad {}^{r^2_{max}}/_{r_1^2} \doteq 1 + e + {}^{e^2}/_{6} \quad \text{------ (G.3) neglecting higher terms in e}$$

From (G.1) and (G.3):-

$$(r_2 - {}^{r^2_{max}}/_{r_2}) = r_1 \, (1 + e) - \frac{r_1^2 \, (1 + e + {}^{e^2}/_{6})}{r_1 \, (1 + e)}$$

$$(r_2 - {}^{r^2_{max}}/_{r_2}) = r_1 \, \frac{\left(e + \frac{5}{6} \, e^2\right)}{(1 + e)} \quad \text{---------- (G.4)}$$

$$\therefore \quad r_1^2 + r_2^2 - 2r^2_{max} = r_1^2 \left\{1 + {}^{r_2^2}/_{r_1^2} - 2{}^{r^2_{max}}/_{r_1^2}\right\}$$

$$= r_1^2 \left\{1 + (1 + 2e + e^2) - (2 + 2e + {}^{e^2}/_{3})\right\} \text{ using (G.1) \& (G.3}$$

$$r_1^2 + r_2^2 - 2r^2_{max} = r_1^2 \left\{\frac{2}{3} \, e^2\right\} \quad \text{------ (G.5)}$$

From (G.4) and (G.5) :-

$$\left\{ \frac{\left(r_2 - r_{max}^2 / r_2 \right)}{\left(r_1^2 + r_2^2 - 2r_{max}^2 \right)} \right\}^{\frac{1}{3}} = \left\{ \frac{r_1 \left(e + \frac{5}{6} e^2 \right)}{(1 + e) r_1^2 \frac{2}{3} e^2} \right\}^{\frac{1}{3}}$$

$$\doteq \left\{ \frac{3}{2 e r_1} \right\}^{\frac{1}{3}}$$

Now $\dfrac{r_2}{r_2^2 - r_1^2} \doteq \dfrac{r_2}{2r_2 (r_2 - r_1)} \doteq \dfrac{1}{2 (r_2 - r_1)}$

$\therefore$ In equation (58) :-

$$\phi = 2.565 \left\{ \frac{3}{2 e r_1} \right\}^{\frac{1}{3}} \frac{1}{2 (r_2 - r_1)} \left(\frac{Dx}{\overline{u}} \right)^{\frac{2}{3}}$$

$$= 2.565 \cdot \frac{3^{\frac{1}{3}}}{2^{\frac{4}{3}}} \cdot \left\{ \frac{r_1}{(r_2 - r_1) r_1} \right\}^{\frac{1}{3}} \frac{1}{2 (r_2 - r_1)} \left(\frac{Dx}{\overline{u}} \right)^{\frac{2}{3}}$$

$$= 1.468 \left(\frac{Dx}{b^2 \overline{u}} \right)^{\frac{2}{3}} \quad \text{where } b = r_2 - r_1$$

$\therefore$ $\phi = 1.468 \, \psi^{\frac{2}{3}}$ ----- (56) where $\psi = \left(\dfrac{Dx}{b^2 \overline{u}} \right)$

This equation (56) is identical to that derived in Appendix E for the parallel plate system.

APPENDIX H

Derivation of equation (62) - fractional saturation with axially turbulent flow between parallel plates

It is assumed in this derivation that the amalgamated band of silver foil is fixed circumferentially around the inside of the outer cylinder. It will be assumed that, when the flow of air is turbulent, there exists a laminar sub-layer adjacent to either wall of the parallel plate system. The point velocity, u, varies linearly with distance, y, from the wall throughout this laminar sub-layer.

Thus $\tau = \frac{u}{y}$ ----- (H.1) where τ is the shear stress and μ the viscosity of air

Now the shear stress, τ, may be defined as:-

$$\tau = f \cdot \frac{1}{2} \rho \bar{u}^2 \quad \text{--- (H.2)}$$

where f is a friction factor at the wall and $\bar{u}$ is the mean air velocity in the annulus and ρ the air density.

Defining a Reynolds number, Re_a, as

$$Re_a = \frac{2 \bar{u} b}{\nu}$$

where ν is the kinematic viscosity (μ/ρ),

then from (H.1) and (H.2) :-

$$\mu \cdot \frac{u}{y} = f \frac{1}{2} \rho \frac{Re_a^2 \nu^2}{4 b^2}$$

or $$\frac{u}{y} = f \cdot \frac{Re_a^2 \nu}{8 b^2} \quad \text{----- (H.3)}$$

Thus the slope of the velocity profile at the wall, p , is given by:-

$$p = \left(\frac{\partial u}{\partial y}\right)_{y=0} \equiv \frac{u}{y} = f \cdot \frac{Re_a^2 \nu}{8 b^2} \quad ------ (H.4)$$

∴ The equation for the concentration gradient at the diffusing surface equivalent to (E.8) is given by :-

$$\left(\frac{\partial c}{\partial y}\right)_{y=0} = \left(\frac{c_1 - c^*}{0.893}\right) \cdot \left\{\frac{f \; Re_a^2 \nu}{72 D x b^2}\right\}^{\frac{1}{3}} \quad ---- (H.5)$$

This equation is based on the assumption that the physical properties of the air and mercury vapour may be taken to be the same as for mercury free air. For the small concentrations of mercury likely to be present at room temperature and for the high flow rates used this assumption introduces a negligible error in the theoretical derivation. Since the parallel plate approximation is being made, equations (E.11) and (E.12) hold, i.e.

$$\text{mass transfer rate, } N = \bar{u} b (c_2 - c_1) = - \int_0^x D \left(\frac{\partial c}{\partial y}\right)_{y=0} \cdot dx$$

$$\text{i.e. } \bar{u} b (c_2 - c_1) = - \frac{D (c_1 - c^*)}{0.893} \left\{\frac{f \, Re_a^2 \nu}{72 D b^2}\right\}^{\frac{1}{3}} \cdot \frac{3}{2} \cdot x^{\frac{2}{3}}$$

$$\text{or } \phi = \frac{c_2 - c_1}{c^* - c_1} = \frac{3 \cdot 4^{\frac{1}{3}} x^{\frac{2}{3}} D}{2 (0.893) (72)^{\frac{1}{3}} \bar{u} b} \cdot \left(\frac{f \bar{u}^2}{\nu D}\right)^{\frac{1}{3}} \text{ substituting for } Re_a$$

But for turbulent flow in narrow annuli the results of several investigators (62) give an approximate correlation of friction factor, f , with Re_a similar

to the Blasius equation for circular tubes, i.e.

$$f = 0.076\ Re_a^{-\frac{1}{4}} \quad ----(H.6) \quad \text{for } Re_a > 3000$$

substituting for f ,

$$\phi = \frac{0.641\ (Dx)^{\frac{2}{3}}}{b\ (\bar{u}\ \nu)^{\frac{1}{3}}} \cdot \frac{(0.076)^{\frac{1}{3}}}{1} \left(\frac{\nu}{2\ \bar{u}\ b} \right)^{\frac{1}{12}}$$

$$\phi = \frac{0.256\ (Dx)^{\frac{2}{3}}}{\bar{u}^{\frac{5}{12}} . b^{\frac{13}{12}} . \nu^{\frac{1}{4}}} \quad ----(62)$$

In deriving (62) it has been tacitly assumed that all concentration changes take place within this laminar sub-layer and therefore that these concentration changes depend only on the velocity profile in the sub-layer. The conditions under which this assumption is true will now be investigated in Appendix I.

APPENDIX I

Conditions under which equation (62) should be valid

From equation (E.3) in Appendix E

$$\frac{c^{*} - c}{c^{*} - c_1} = \frac{1}{0.893} \int_0^X e^{-X^3} dX \quad - - - (E.3)$$

where X is a function of x and y

If (62) is to be valid then concentration changes must take place entirely within the laminar sub-layer. Strictly, therefore, the concentration, c at the edge of the laminar sub-layer should equal the concentration, c_1 in the incoming turbulent air stream. This would mean that in (E.3), $\int_0^X \frac{e^{-X^3}}{0.893} dX$ should take the value unity. Now the values of the integral $\int_0^X e^{-X^3} dX$ are obtained from tabulated values (64) and for X = 1, this integral takes the value 0.8075. Thus (E.3) becomes:-

$$\frac{c^{*} - c}{c^{*} - c_1} = \frac{0.8075}{0.893} = 0.905 \quad - - - (I.1)$$

(i.e. approximately 90% concentration change within the sub-layer)

It is assumed that a 90% change of concentration within the laminar sub-layer is a sufficient criterion for equation (62) to be valid.

Thus from (E.1) :-

$$X = y\left\{\frac{p}{9 D x}\right\}^{\frac{1}{3}} \quad - - - (E.1)$$

If X = 1.0 and p is given by (H.4)

$$1.0 = y\left\{\frac{f\ Re_a^2\ \nu}{72\ b^2\ Dx}\right\}^{\frac{1}{3}}$$

$$\text{or } y = 1\left\{\frac{72\ b^2\ Dx}{f\ Re_a^2\ \nu}\right\}^{\frac{1}{3}} \quad - - - (I.2)$$

y is now the thickness of the laminar sub-layer such that at the edge of this sub-layer the concentration, c, equals the concentration of mercury vapour in the inlet stream; i.e. all concentration change takes place entirely within a laminar sub-layer of thickness y.

Now Laufer (63) has shown experimentally, for turbulent flow between parallel plates, that the laminar sub-layer extends a distance

$$y \frac{\bar{u}}{\nu}\sqrt{\frac{f}{2}} < 5 \quad \text{- - - - - (I.3)}$$

Thus:

$$y < \frac{5\nu}{\bar{u}} \cdot \frac{\sqrt{2}}{(0.076\ Re_a^{-\frac{1}{4}})^{\frac{1}{2}}} \quad \text{using (H.6)}$$

$$< \frac{5\sqrt{2} \cdot \nu \cdot 2b}{(0.076)^{\frac{1}{2}}\ 2b.\bar{u}\ Re_a^{-\frac{1}{8}}}$$

$$\therefore\ y < \frac{10\sqrt{2}\,b}{\sqrt{0.076}\ .\ Re_a^{\frac{7}{8}}} \quad \text{- - - - (I.4)}$$

Equating (I.2) and (I.4) to find the condition that all concentration change takes place within the laminar sub-layer:-

$$\left\{\frac{72\,b^2\,Dx}{f\ Re_a^2\ \nu}\right\}^{\frac{1}{3}} < \frac{10\sqrt{2}\,b}{\sqrt{0.076}\ Re_a^{\frac{7}{8}}}$$

$$\text{or}\quad 2\left\{\frac{9\,b^2\,Dx}{\nu\ Re_a^2}\right\}^{\frac{1}{3}} \cdot \frac{1}{(0.076)^{\frac{1}{3}}\ Re_a^{-\frac{1}{2}}} < \frac{10\sqrt{2}\ b}{\sqrt{0.076}\ Re_a^{\frac{7}{8}}}$$

$$\text{or}\quad \left(\frac{x}{b}\right)^{\frac{1}{3}} \cdot (Sc)^{\frac{1}{3}} \cdot Re_a^{\frac{7}{24}} < \frac{5\sqrt{2}}{(0.076)^{\frac{1}{6}} \cdot 9^{\frac{1}{3}}} < 5.22$$

---

where Sc is the Schmidt number ($\nu/_D$)

APPENDIX J

Conditions for short "time of decay" of radial variations in concentration

The conditions for this short time of decay may be obtained by putting $\frac{\partial c}{\partial x} = 0$ in (78) and solving

$$\frac{\partial^2 c}{\partial z^2} = \frac{a^2}{D} \frac{\partial c}{\partial \theta} \quad - - - (J.1) \quad \text{with } \frac{\partial c}{\partial z} = 0 \text{ at } z = 0 \text{ and } z = 1$$

assuming symmetry at the centre line of the parallel plates and impermeability at the walls.

The solution to (J.1) may be obtained in the usual manner by putting $c = Z(z)T(\theta)$

Then $\frac{T d^2 Z}{dz^2} = \frac{a^2}{D} Z \frac{dT}{d\theta}$

or $\frac{a^2}{DT} \cdot \frac{dT}{d\theta} = \frac{1}{Z} \cdot \frac{d^2 Z}{dz^2} = -\beta^2$ say (a constant)

Then $\frac{dT}{d\theta} + \frac{DT}{a^2}\beta^2 = 0 \quad - - - (J.2)$ and $\frac{d^2 Z}{dz^2} + \beta^2 Z = 0 \quad - - - (J.3)$

The solution to (J.2) is given by $T = J e^{-D\theta\beta^2/a^2}$ where J = a constant

The solution to (J.3) is given by $Z = M\cos\beta z + N \sin\beta z$ where M & N are constants

$$\therefore \quad c = Z(z)T(\theta) = (P\cos\beta z + U \sin\beta z)\, e^{-D\theta\beta^2/a^2}$$ where P and U are constants

The boundary condition $\frac{\partial c}{\partial z} = 0$ at $z = 0$ gives :-

$$U = 0$$

The boundary condition $\frac{\partial c}{\partial z} = 0$ at $z = 1$ gives:-

$$\sin\beta = n\pi, \text{ where } n = 1, 2, 3, - - - -$$

The general solution to (J.1) is $\therefore \quad c_n = P \cos n\pi z \, e^{-n^2\pi^2 D\theta/a^2} \quad - - (J.4)$

The value of c_n at time $\theta = 0$ is given by c_n^o, where :-

$$c_n^o = P \cos n\pi z$$

Thus, using the criterion suggested by Taylor (51), the time, θ, for the radial variation in c to fall to $\frac{1}{e}$ of its original value, c_n^o, is given by:-

$$\frac{c_n^o}{\frac{1}{e} c_n^o} = \frac{P \cos n\pi z}{P \cos n\pi z \; e^{-n^2 \pi^2 D \theta / a^2}}$$

$$\text{i.e.} \quad e = e^{n^2 \pi^2 D \theta / a^2}$$

$$\text{or} \quad \theta = \frac{a^2}{n^2 \pi^2 D}$$

The maximum value of θ is given by θ_{max} when $n = 1$, i.e.:-

$$\theta_{max} = \frac{a^2}{\pi^2 D}$$

If at any time the dispersing material is spread over a column length of order L, the time necessary for convection to make an appreciable change in c is of the order $\frac{L}{\bar{u}}$, so that in order that the condition of a long convection time may hold, compared with the "time of decay" of the radial variation in c; $L/\bar{u}$ must be much greater than θ_{max},

$$\text{i.e.} \quad \frac{L}{\bar{u}} \gg \frac{a^2}{\pi^2 D}$$

$$\text{or} \quad L \gg \frac{\bar{u} b^2}{4 \pi^2 D} \quad - - - \text{(J.5)}, \text{ where } b = 2a = \text{full gap width}$$

Thus, the column length, L, over which longitudinal diffusion measurements are to be made must be such that the condition represented by equation (J.5) is satisfied.

APPENDIX K

Reduction of concentric tube longitudinal diffusion equation (90) to parallel plate equation (85) (49)

$$D_L = \frac{\left[\frac{1}{48}(1+\alpha^2)(1+8\alpha^2+\alpha^4) + \frac{1}{36}(5+32\alpha^2+5\alpha^4)E + \frac{1}{4}(1+\alpha^2)E^2 - \frac{\alpha^4}{4}E^{-1}\right]\frac{\bar{u}^2 b^2}{D}}{(1-\alpha)^2\,(1+\alpha^2+2E)^2} \quad --(90)$$

where $E = \dfrac{1-\alpha^2}{\log \alpha^2}$ and $r_2 - r_1 = b = r_2(1-\alpha)$

Let $\alpha^2 = 1 - q$; then $E = \dfrac{q}{\log(1-q)}$

$$\text{Then } D_L = \frac{3F + 4G + 36H - 36I}{144\,(1-\sqrt{1-q})^2\left[(2-q)\log(1-q) + 2q\right]^2} \cdot \frac{\bar{u}^2 b^2}{D} \quad ---(K.1)$$

where $F = (20 - 30q + 12q^2 - q^3)\cdot\left\{\log(1-q)\right\}^2$

$G = (42 - 42q + 5q^2)\cdot q \cdot \log(1-q)$

$H = (2-q)\,q^2$

$I = (1 - 2q + q^2)\cdot\frac{1}{q}\cdot\left\{\log(1-q)\right\}^3$

Now $\log(1-q) = -q\left(1 + \frac{q}{2} + \frac{q^2}{3} + \frac{q^3}{4} + \frac{q^4}{5} + \frac{q^5}{6} + \frac{q^6}{7} + --\right)$

$$\log^2(1-q) = q^2\left(1 + q + \frac{11}{12}q^2 + \frac{5}{6}q^3 + \frac{137}{180}q^4 + \frac{7}{10}q^5 + \frac{363}{16.35}q^6 + --\right)$$

$$\log^3(1-q) = -q^3\left(1 + \frac{3}{2}q + \frac{7}{4}q^2 + \frac{15}{8}q^3 + \frac{29}{15}q^4 + \frac{469}{240}q^5 + \frac{29531}{16.27.35}q^6 + --\right)$$

$$\therefore \quad I = -q^2\left(1 - 2q + q^2\right)\left(1 + \frac{3}{2}q + \frac{7}{4}q^2 + \frac{15}{8}q^3 + \frac{29}{15}q^4 - - - -\right)$$

$$= -q^2\left(1 - \frac{1}{2}q - \frac{1}{4}q^2 - \frac{1}{8}q^3 - \frac{1}{15}q^4 - \frac{3}{80}q^5 - \frac{331}{16.2735}q^6\right)$$

$$H = q^2(2 - q)$$

$$H - I = q^2\left(3 - \frac{3}{2}q - \frac{1}{4}q^2 - \frac{1}{8}q^3 - \frac{1}{15}q^4 - - - - -\right)$$

$$36(H - I) = q^2\left(108 - 54q - 9q^2 - \frac{9}{2}q^3 - \frac{12}{5}q^4 - \frac{27}{20}q^5 - \frac{331}{4.3.35}q^6 - - - -\right)$$

$$G = -q^2\left(42 - 42q + 5q^2\right)\left(1 + \frac{q}{2} + \frac{q^2}{3} + \frac{q^3}{4} + \frac{q^4}{5} + \frac{q^5}{6} + \frac{q^6}{7}\right)$$

$$= -q^2\left(42 - 21q - 2q^2 - q^3 - \frac{13}{30}q^4 - \frac{3}{20}q^5 + 0.q^6\right)$$

$$4G = -q^2\left(168 - 84q - 8q^2 - 4q^3 - \frac{26}{15}q^4 - \frac{3}{5}q^5 + 0.q^6\right)$$

$$F = q^2\left(20 - 30q + 12q^2 - q^3\right)\left(1 + q + \frac{11}{12}q^2 + \frac{5}{6}q^3 + \frac{137}{180}q^4 + \frac{7}{10}q^5 + \frac{363}{16.35}q^6 + - -\right)$$

$$= q^2\left(20 - 10q + \frac{1}{3}q^2 + \frac{1}{6}q^3 + \frac{2}{9}q^4 + \frac{1}{4}q^5 + \frac{111}{420}q^6 - - - -\right)$$

$$\therefore \quad 3F = q^2\left(60 - 30q + q^2 + \frac{1}{2}q^3 + \frac{2}{3}q^4 + \frac{3}{4}q^5 + \frac{111}{140}q^6 - - - -\right)$$

adding up to terms including q^6 :-

$$\therefore\ 3F + 4G + 36(H - I) = q^2 \begin{bmatrix} 60 & -30 & 1 & 1/2 & 2/3 & 3/4 & 111/140 \\ -168 & +84q & 8q^2 & 4q^3 & 26/15\,q^4 & 3/5\,q^5 & 0q^6 \\ 108 & -54 & -9 & -9/2 & -12/5 & -27/20 & -331/12.35 \end{bmatrix}$$

$$= \frac{2}{3.140}q^6 = \frac{1}{210}q^6 - - - - \quad (K.2)$$

$$\text{Now } (2 - q)\log(1 - q) + 2q = q\left\{2 - (2 - q)\left(1 + \frac{q}{2} + \frac{q^2}{3} + \text{- - -}\right)\right\}$$

$$= q\left(2 - 2 + \frac{q^2}{2} - \frac{2}{3}q^2\right)$$

$$= -\frac{q^3}{6} \text{ - - - - -} \quad \text{(K.3)}$$

$$\text{and } \left(1 - \sqrt{1 - q}\right)^2 = 1 + (1 - q) - 2(1 - q)^{\frac{1}{2}}$$

$$= 2 - q - 2\left\{1 - \frac{q}{2} + \frac{\left(\frac{1}{2}\right)\left(-\frac{1}{2}\right)q^2}{2}\right\}$$

$$= \frac{q^2}{4} \text{ - - - - -} \quad \text{(K.4)}$$

$\therefore$ Substituting (K.2), (K.3) and (K.4) in (K.1) :-

$$D_L = \frac{\frac{1}{210}q^6}{144 \cdot \frac{q^2}{4} \cdot \left(-\frac{q^3}{6}\right)^2} \cdot \frac{b^2\bar{u}^2}{D} = \frac{q^6 \cdot 4 \cdot 36}{210 \cdot 144 \cdot q^2 \cdot q^6} \cdot \frac{b^2\bar{u}^2}{D}$$

$$D_L = \frac{1}{210\,q^2} \cdot \frac{b^2\bar{u}^2}{D}$$

As $q \rightarrow 1$; $\alpha \rightarrow 1$

$\therefore$ as $\alpha \rightarrow 1$:-

$$D_L \longrightarrow \frac{1}{210} \cdot \frac{\bar{u}^2 b^2}{D}$$ which is equation (85)

APPENDIX L

Conversion of values of saturation vapour pressure, p^*, to values of the saturation concentration c^* at a given temperature T.

If it is assumed that the ideal gas law holds for mercury vapour then the equation :-

$$c^* = \frac{200.61 \; p^* . \; 10^9}{760 \; R \; T} \; . \; \mu.gm./m^3 \quad - - - - \; (L.1)$$

may be used to calculate values of c^* in microgrammes per cubic meter from values of p^* at a certain absolute temperature T. In this equation 200.61 is the value of the atomic weight of mercury, 760 the number of mm. of mercury corresponding to 1 atmosphere pressure and R the gas constant expressed in litre.atmospheres/degree absolute (R = 0.08205 litre atmos/^oK). The values of p^*, obtained from the International Critical Tables (44) are given in Table 16 at various temperatures and the corresponding values of c^* calculated from equation (L.1) shown above are also tabulated. Figure 87 shows a plot of c^* versus temperature in ^oC

Sample calculation

At 20^oC the value of p^*, obtained from Table 16, (44), is given by

$p^* = 0.001201$. mm Hg

Thus in equation (L.1) :-

$$c^* = \frac{200.61 \; x \; 0.001201}{760 \; x \; 0.08205 \; x \; 293}$$

$$\therefore \quad c^* = 13,187 \; \mu gm/m^3$$

This is the value of c^* given in Table 16 corresponding to $p^* = 0.001201$ mm. Hg at a temperature of 20^oC.

APPENDIX M

Calculation of molecular diffusion coefficient, D, for mercury vapour into air using data of Mullay and Jacques (56)

The diffusion coefficient, D, for mercury into nitrogen has been determined by Mullay and Jacques (56), at 19.4°C and at a pressure of 3.5212 mm Hg. and the average value obtained from several experiments was D = 27.58 cm^2/sec. The diffusion coefficient for mercury vapour into air in the present work was assumed to be the same as that for mercury into nitrogen and the data of Mullay and Jacques have been corrected for the experimental conditions by the relationship (60) :-

$$D = D_o \cdot \left(\frac{T}{T_o}\right)^2 \frac{p_o'}{p'} \quad \text{- - - - -} \quad (M.1)$$

where D_o is the molecular diffusion coefficient at a pressure p_o' and absolute temperature T_o. Values of D calculated from (M.1) are given in Table 17 and a plot of D versus temperature in °C is shown in Figure 88

Sample calculation

At a temperature of 20°C and atmospheric pressure:

$$D = 27.58 \left(\frac{293}{292.4}\right)^2 \frac{3.5212}{760}$$

$$D = 0.1283 \ cm^2/sec$$

This was the value of D given in Table 17 at a temperature of 20°C. It was assumed that the air in the mercury vapour transfer column was at atmospheric pressure (760 mm Hg.)

APPENDIX N

Evaluation of equation (58) for 5.18" diameter rotor

The equation for the fractional saturation, ϕ, given by equation (58) is:-

$$\phi = 2.565 \left\{ \frac{\left(r_2 - \frac{r^2_{max}}{r_2} \right)}{\left(r_1^2 + r_2^2 - 2r^2_{max} \right)} \right\}^{\frac{1}{3}} \cdot \left(\frac{r_2}{r_2^2 - r_1^2} \right) \cdot \left(\frac{Dx}{\bar{u}} \right)^{\frac{2}{3}} \quad ---- (58)$$

For the 5.18" diameter rotor

$r_2 = 7.303$ cm. $\quad r_2^2 = 53.334$ cm^2 $\quad r_2 - r_1 = 0.724$ cm

$r_1 = 6.579$ cm. $\quad r_1^2 = 43.290$ cm^2 $\quad r_2^2 - r_1^2 = 10.044$ cm^2

$r_1 + r_2 = 13.88$ cm $\quad r_m^{\frac{1}{2}} = 2.635$ $\quad r^2_{max} = \frac{10.044}{2 \times 0.10436} = 48.10$

$r_m = \frac{r_1 + r_2}{2} = 6.941$ $\quad \ln r_2/r_1 = 0.10436$

In (58):-

$$\therefore \phi = 2.565 \left\{ \frac{\left(7.303 - \frac{48.10}{7.303} \right)}{(43.290 + 53.334 - 2 \times 48.10)} \right\}^{\frac{1}{3}} \cdot \left(\frac{7.303}{10.044} \right) \left(\frac{Dx}{\bar{u}} \right)^{\frac{2}{3}}$$

$$= 2.565 \left(\frac{0.717}{0.424} \right)^{\frac{1}{3}} \cdot (0.7272) \cdot \left(\frac{Dx}{\bar{u}} \right)^{\frac{2}{3}}$$

$$\therefore \phi = 2.22 \left(\frac{Dx}{\bar{u}} \right)^{\frac{2}{3}}$$

This theoretical line, $\phi = 2.22 \left(\frac{Dx}{\bar{u}} \right)^{\frac{2}{3}}$ has been plotted in Figure 64 for comparison with the experimental results using the 5.18" diameter rotor for the case where the rotor is stationary.

APPENDIX 0

Critical Taylor number at Re_a = 0 . $2\frac{3}{8}$" diameter rotor

Without axial flow in the annulus, Taylor's equations (45) and (46) (see Part I) may be used to find the critical Taylor number for a particular annulus.

For the case of the $2\frac{3}{8}$" diameter rotor:-

$r_2 = 7.303$ cm $\quad \therefore \; r_1 + r_2 = 10.319$ cm. $\quad r_2 - r_1 \equiv b = 4.287$ cm.

$r_1 = 3.016$ cm $\quad \therefore \; r_m = \dfrac{r_1 + r_2}{2} = 5.160$ cm

From equation (45); $\quad \Omega_c^2 = \dfrac{\pi^4 . \nu^2 (r_1 + r_2)}{2(r_2 - r_1)^3 \, b^2 \, P}$

where, from (46); $\quad P = 0.0571 \left\{ 1 - 0.652 \, \dfrac{b}{r_1} \right\} + 0.00056 \left\{ 1 - 0.652 \, \dfrac{b}{r_1} \right\}^{-1}$

$$= 0.0571 \left\{ 1 - 0.652 \times \frac{4.287}{3.016} \right\} + 0.00056 \left\{ 1 - 0.652 \times \frac{4.287}{3.016} \right\}^{-1}$$

or $\quad P = 0.0118$

$$\therefore \; \Omega_c^2 = \frac{\pi^4 . \nu^2 . (10.319)}{2(4.287)^3 (3.016)^2 (0.0118)}$$

$$= 59.44 \, \nu^2$$

$$\therefore \; \Omega_c = 7.71 \, \nu$$

$$\therefore \text{ critical Ta} = \frac{7.71 \, \nu \times r_m^{\frac{1}{2}} . (r_2 - r_1)^{\frac{3}{2}}}{\nu}$$

$$= 7.71 \times (5.160)^{\frac{1}{2}} (4.287)^{\frac{3}{2}}$$

$$\therefore \text{ critical Ta} = 155.7$$

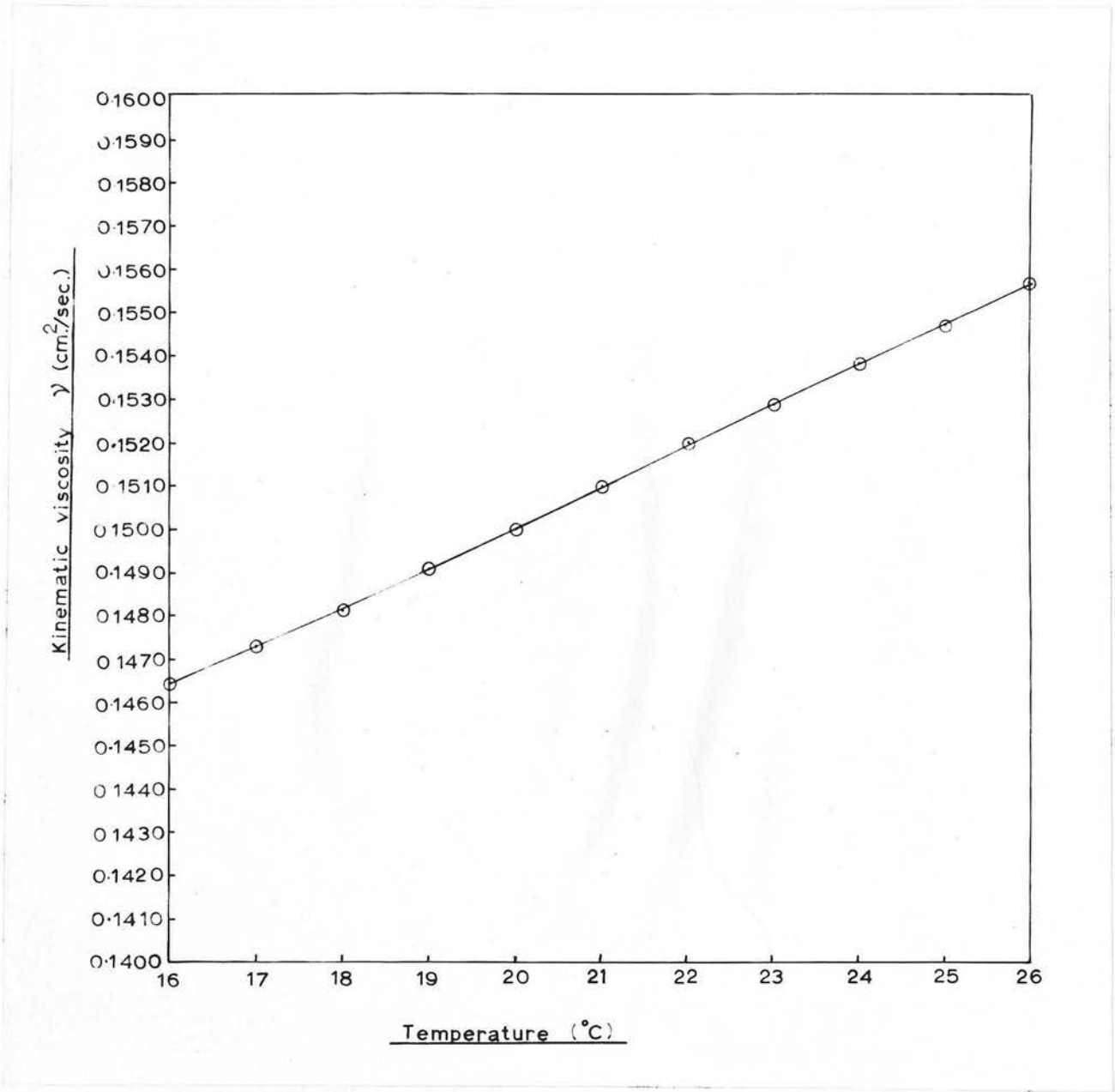

Figure 86. Kinematic viscosity of air, ν, as a function of temperature.

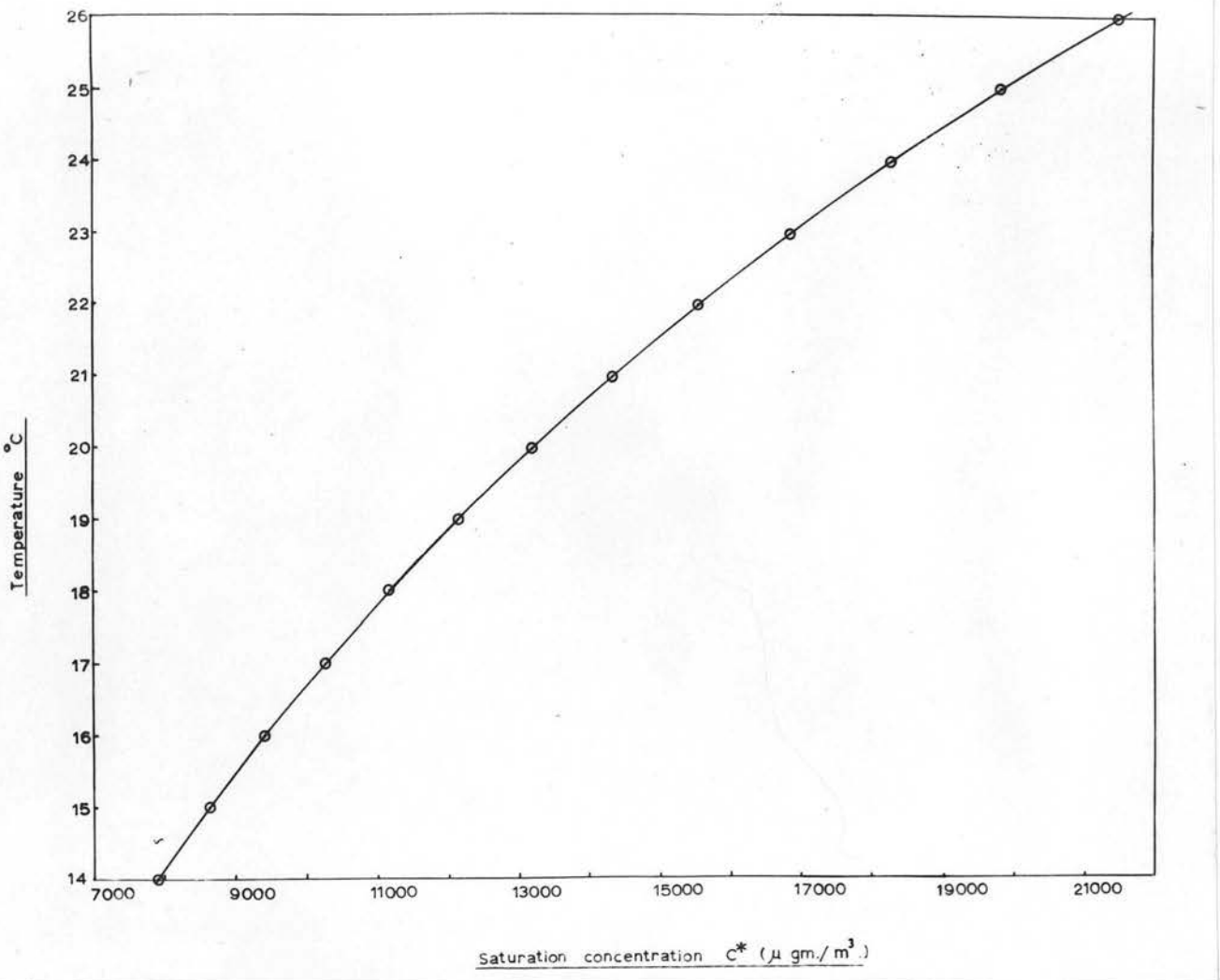

Figure 87. Saturation concentration of mercury vapour in air, c^{*}, as a function of temperature.

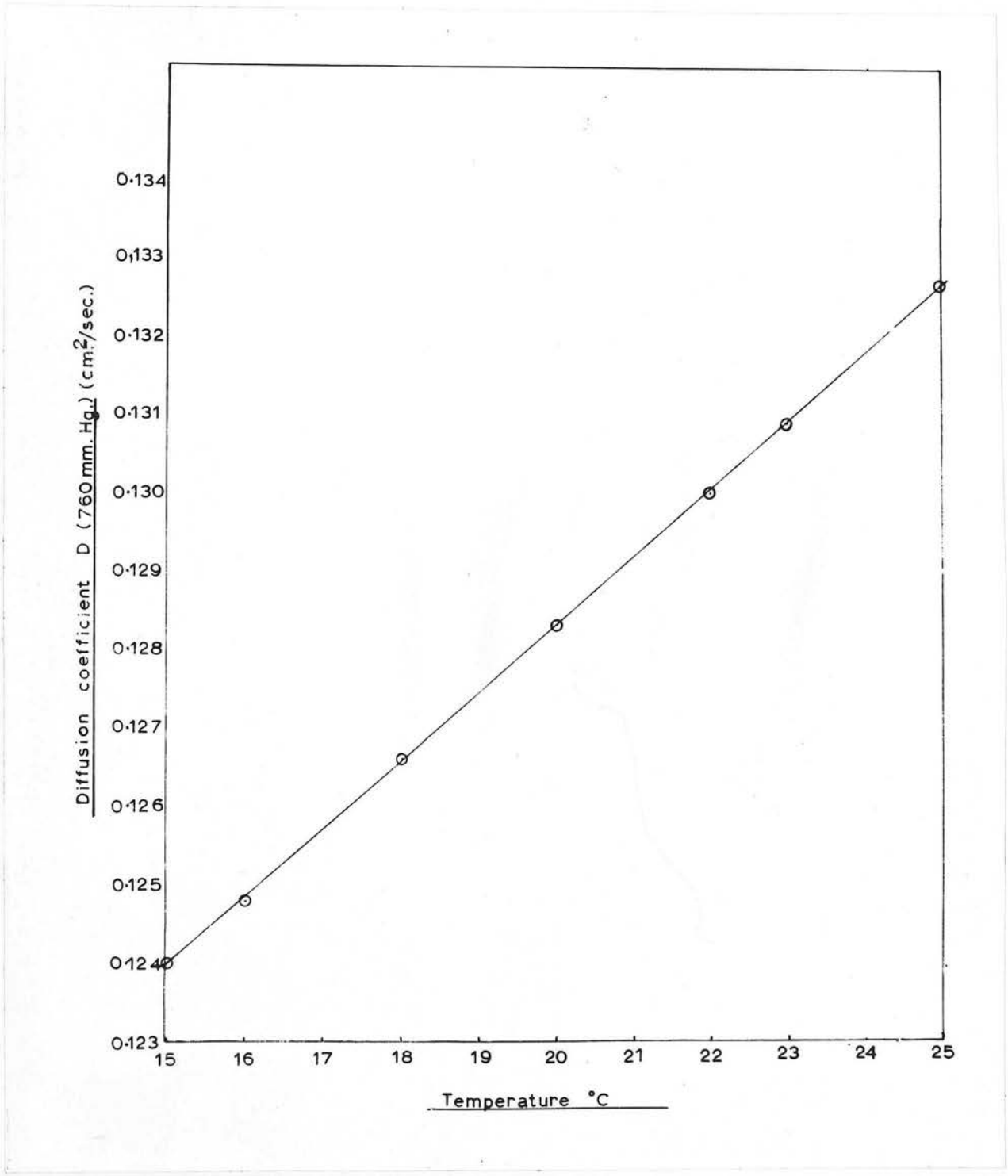

Figure 88. Molecular diffusion coefficient of mercury vapour in air, D, as a function of temperature.

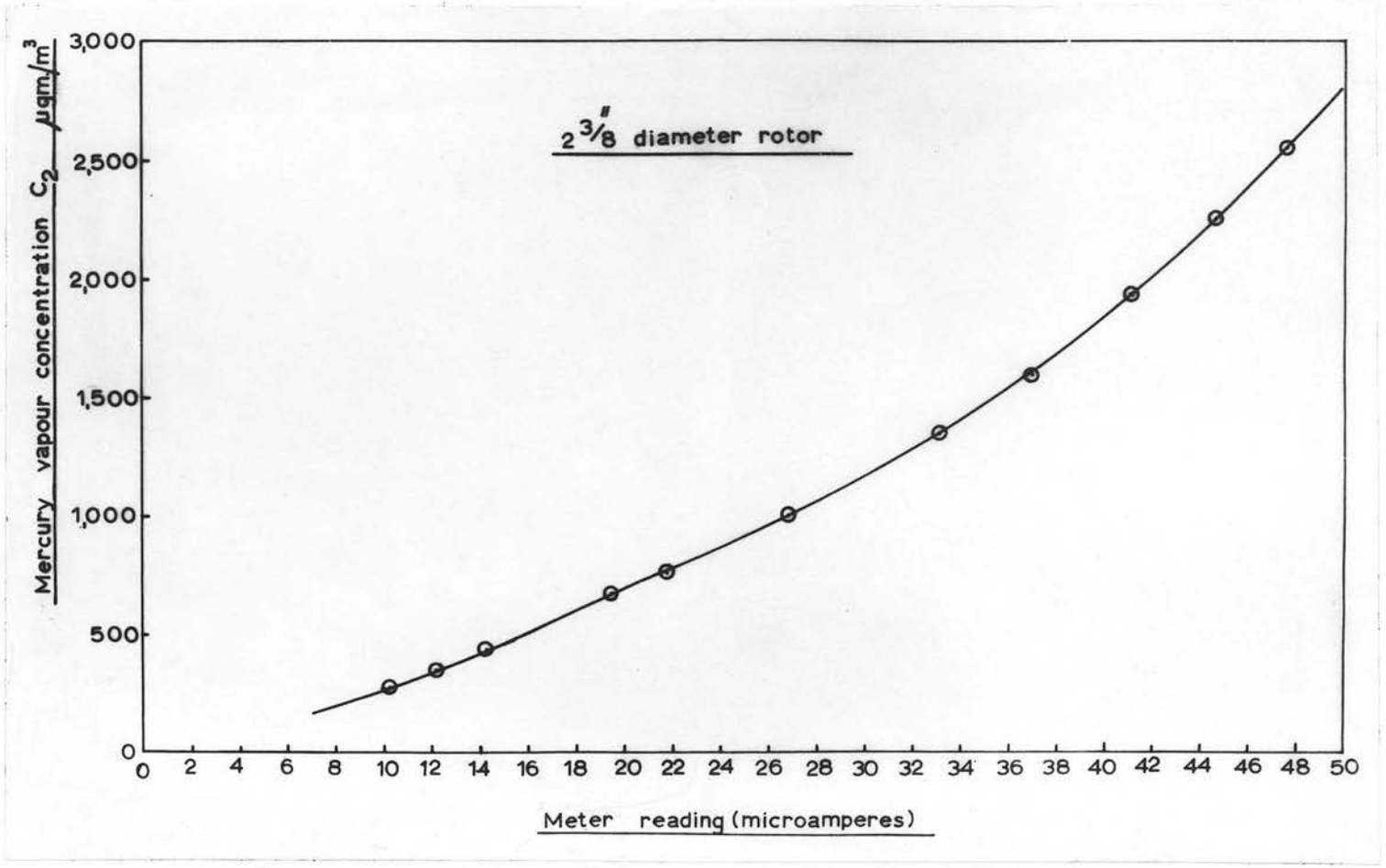

Figure 89. $2\frac{3}{8}$" diameter rotor. Calibration curve.

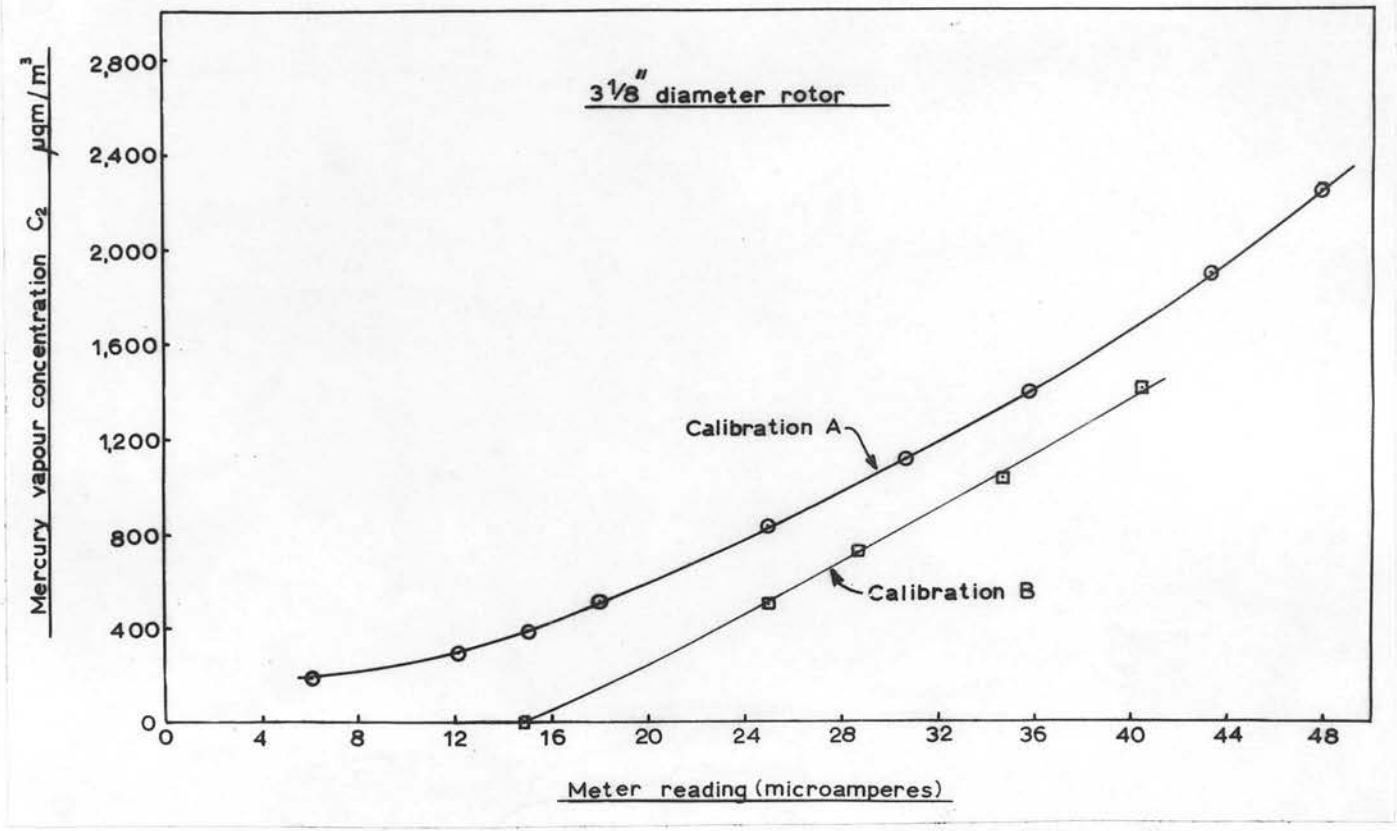

Figure 90. $3\frac{1}{8}$" diameter rotor. Calibration curves A and B.

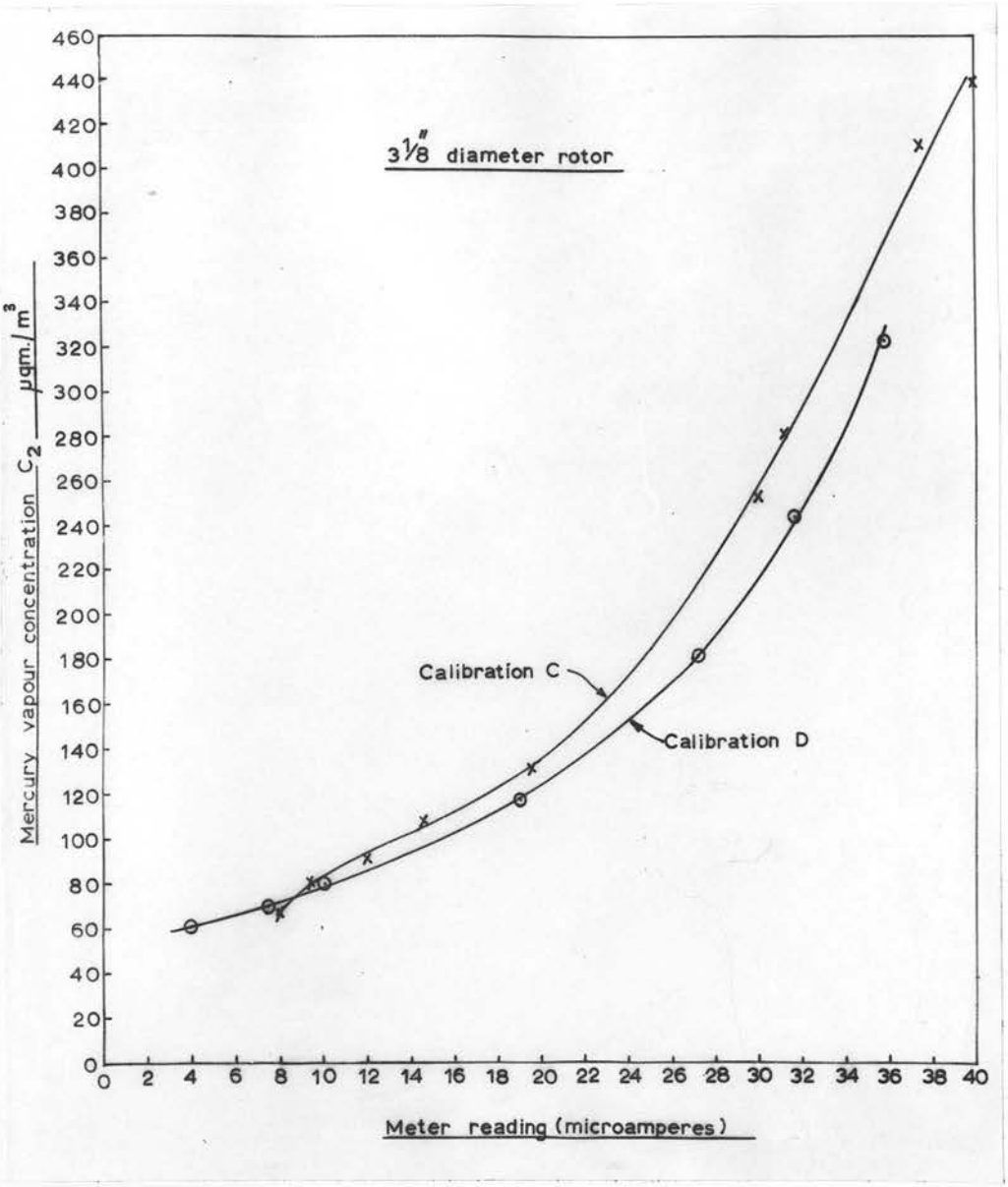

Figure 91. $3\frac{1}{8}$" diameter rotor. Calibration curves C and D.

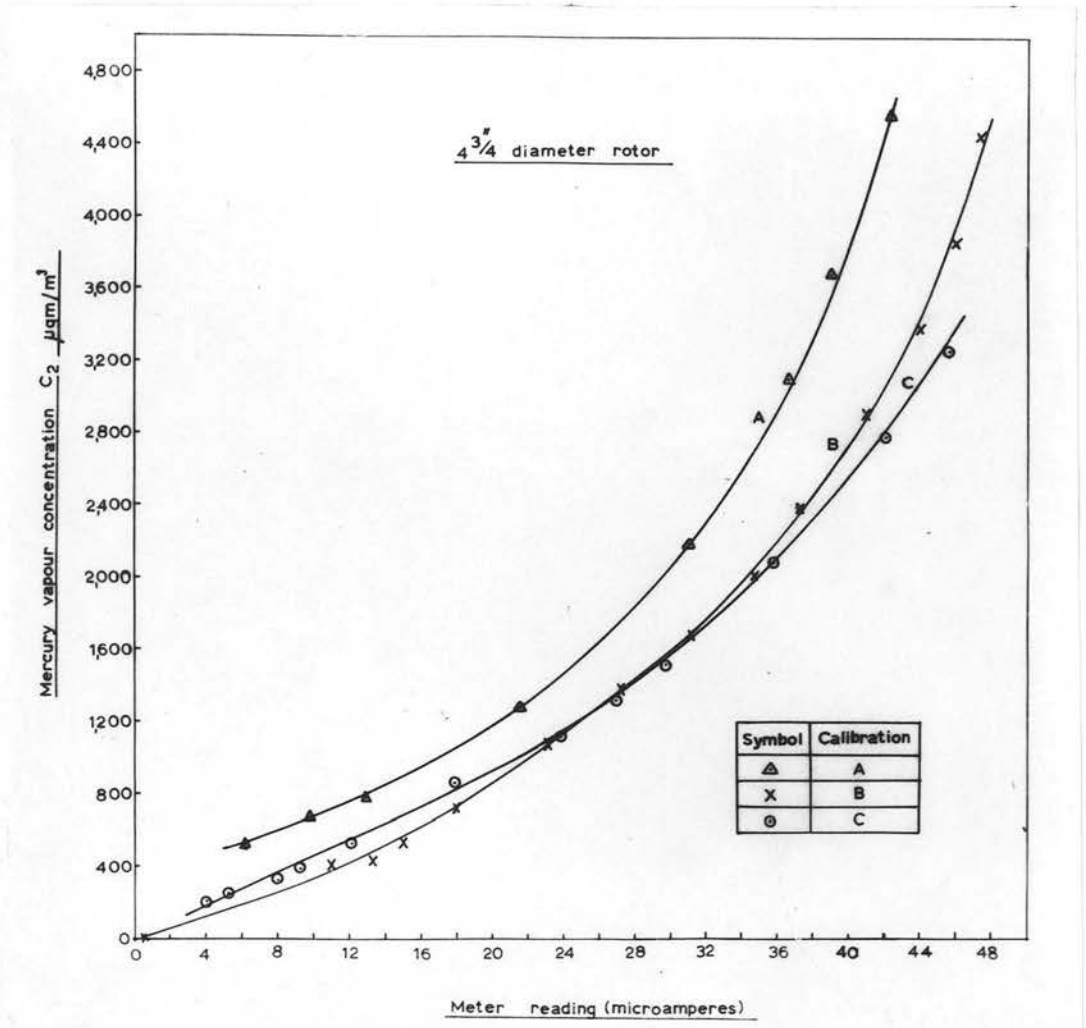

Figure 92. $4\frac{3}{4}$" diameter rotor. Calibration curves A, B and C.

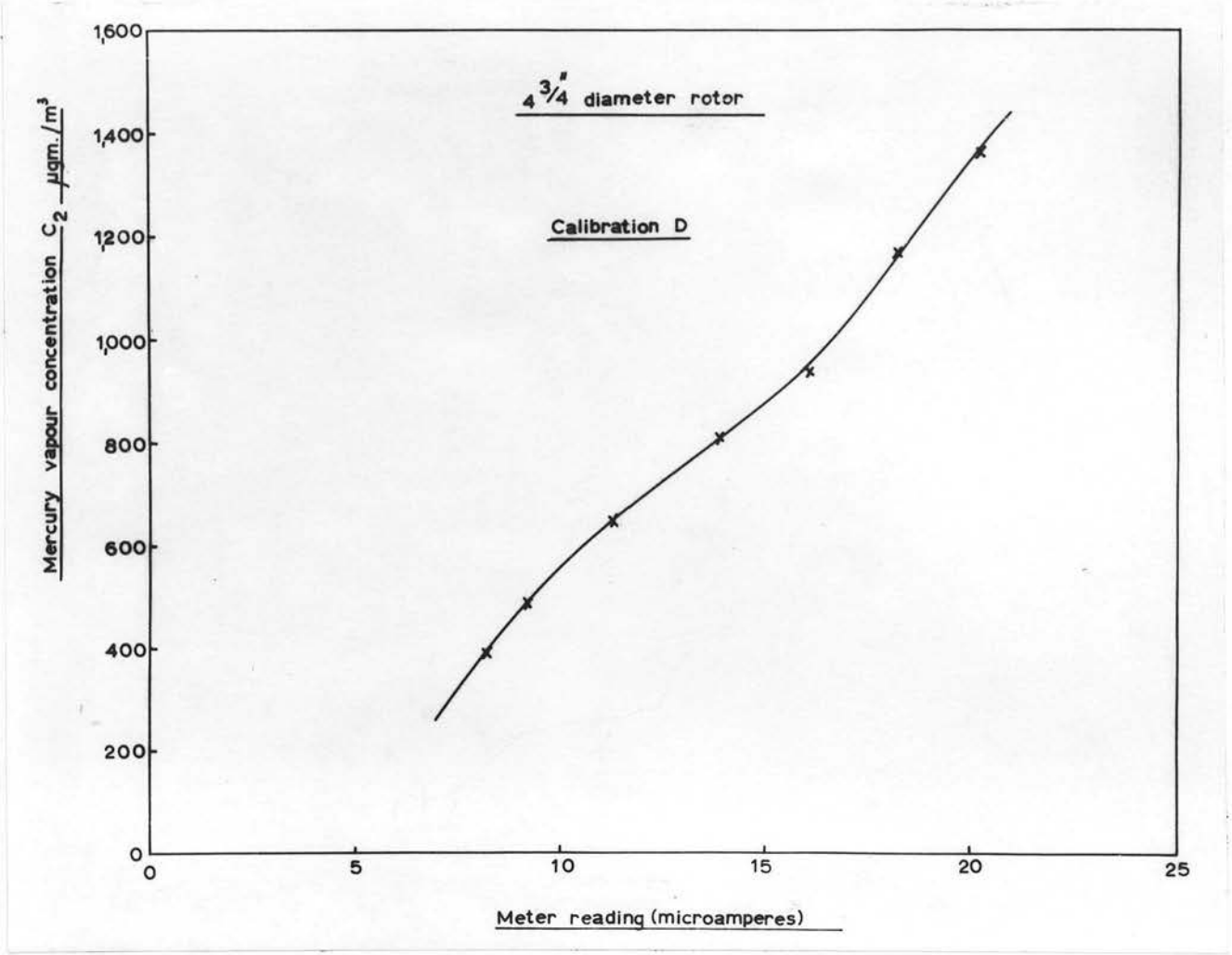

Figure 93. $4\frac{3}{4}$" diameter rotor. Calibration curve D.

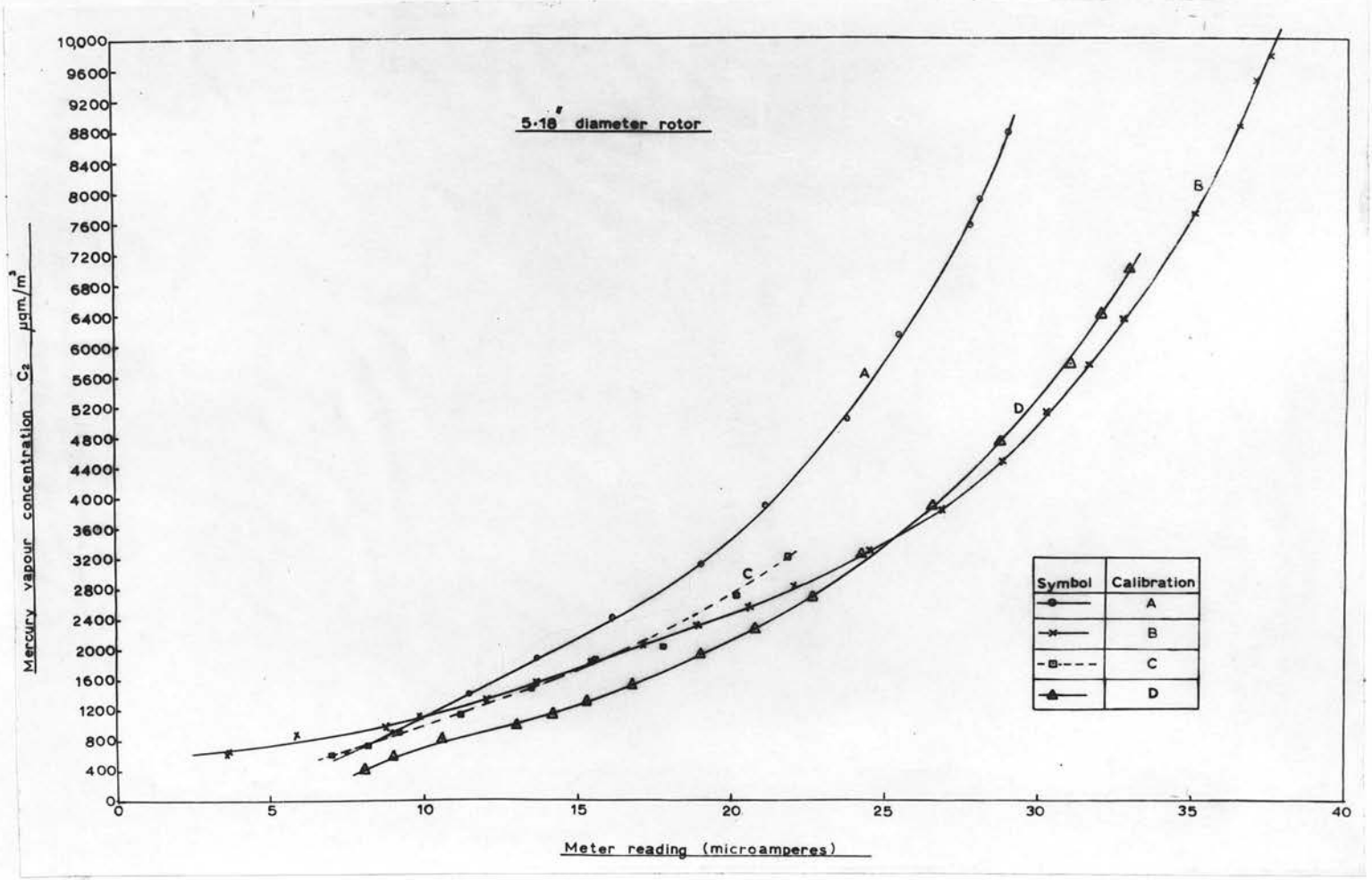

Figure 94. 5.18" diameter rotor. Calibration curves A, B, C and D.

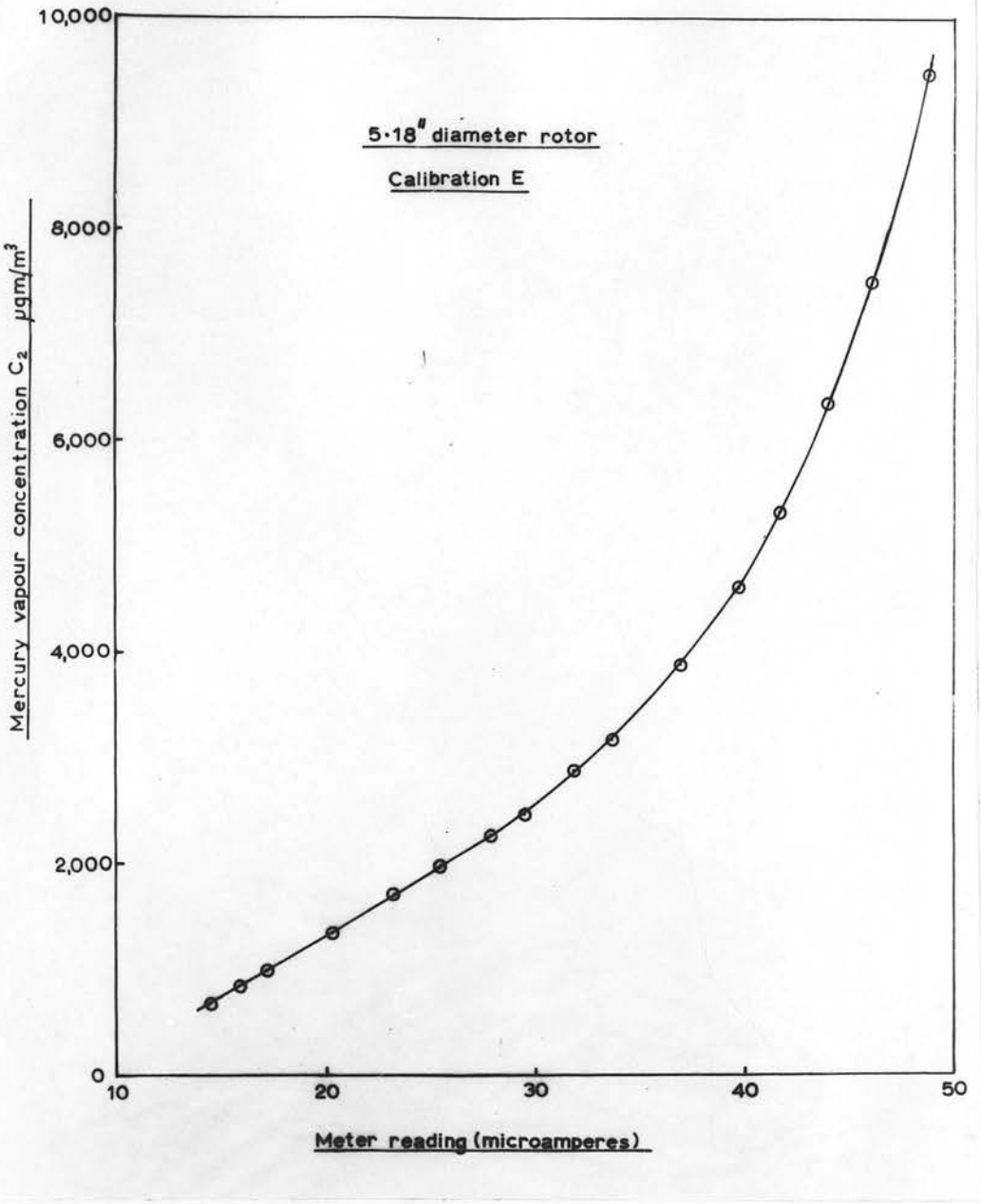

Figure 95. 5.18" diameter rotor. Calibration curve E.

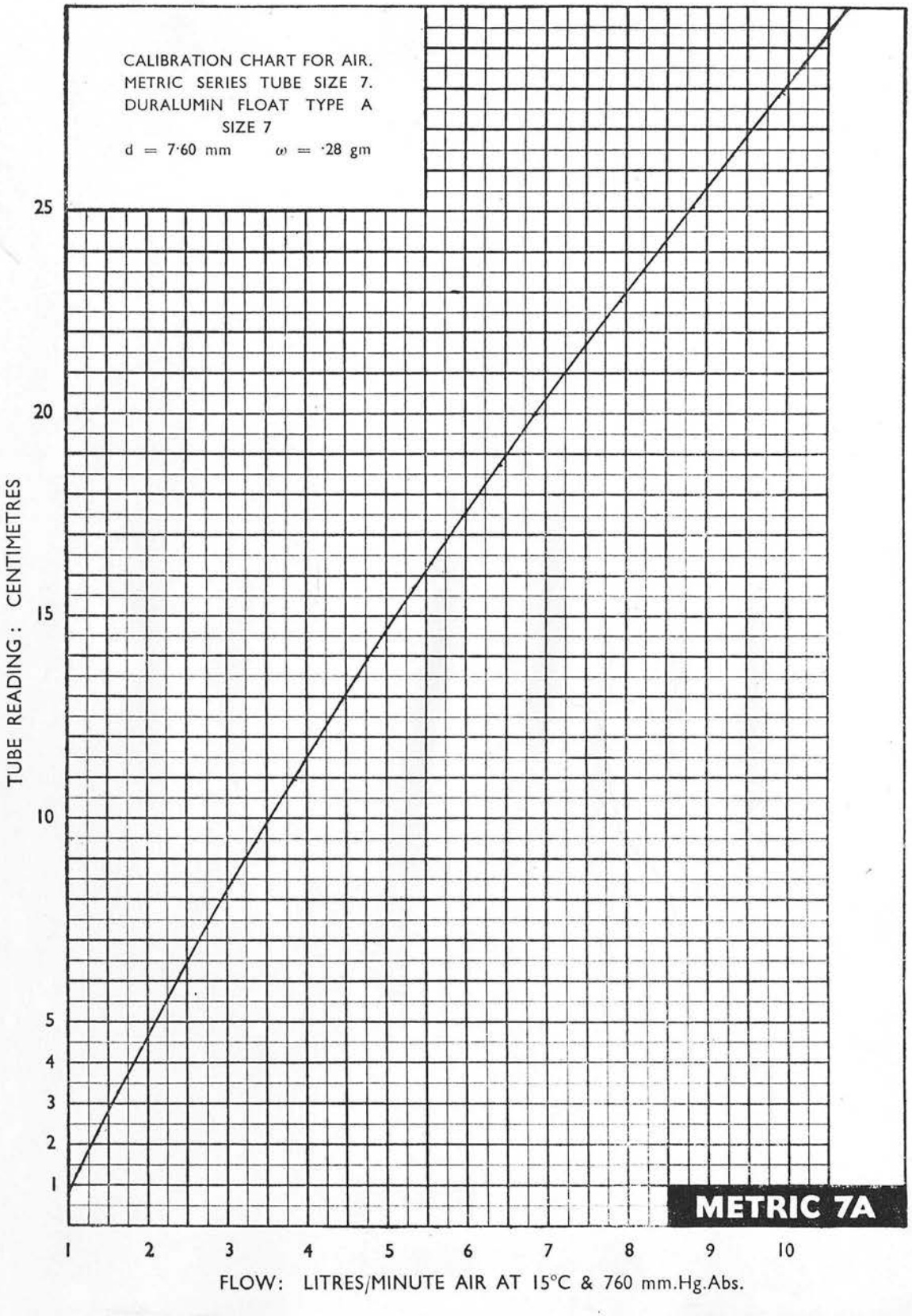

Figure 96. Rotameter metric size 7 (R7). Calibration curve.

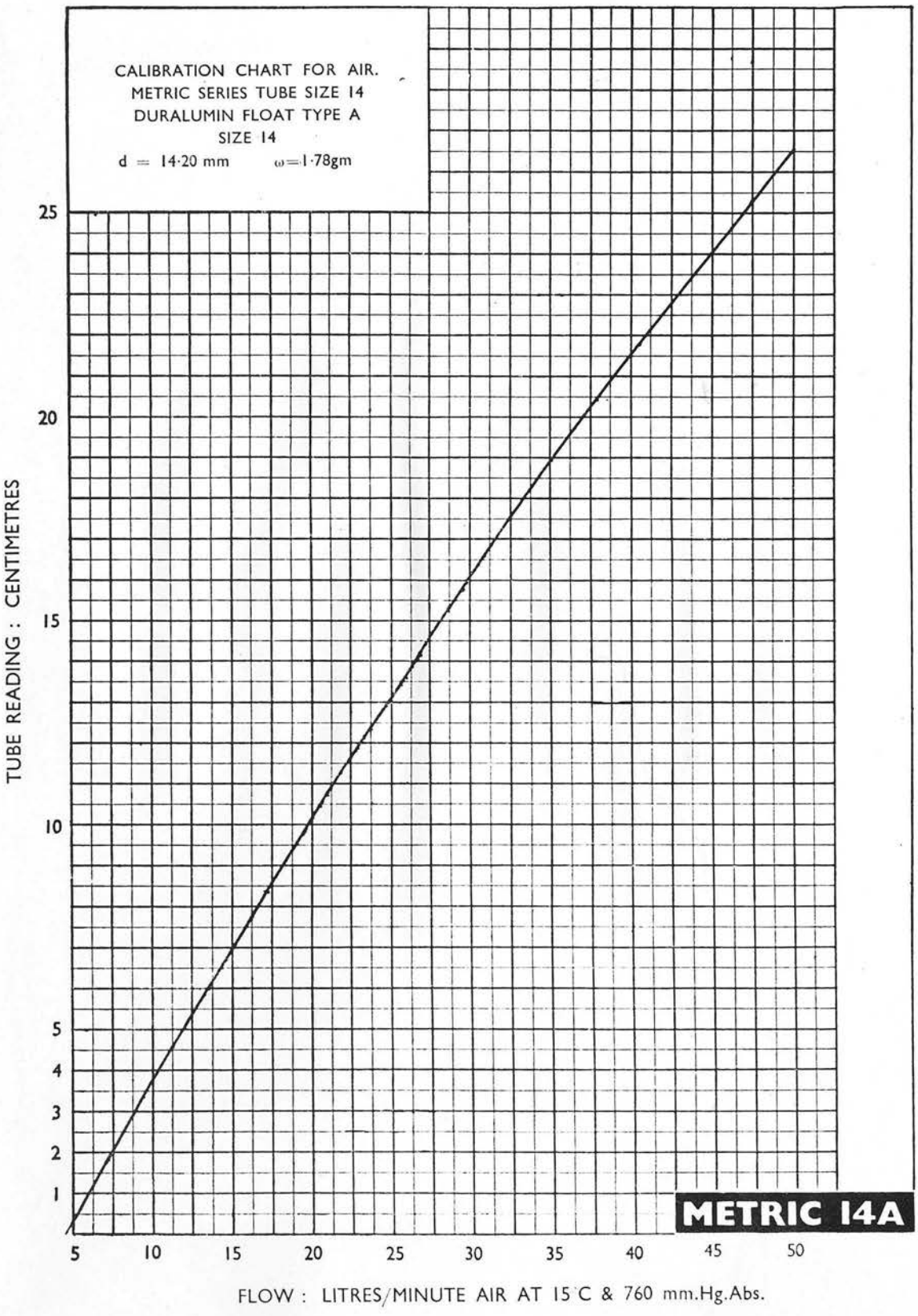

Figure 97. Rotameter metric size 14 (R14). Calibration curve.

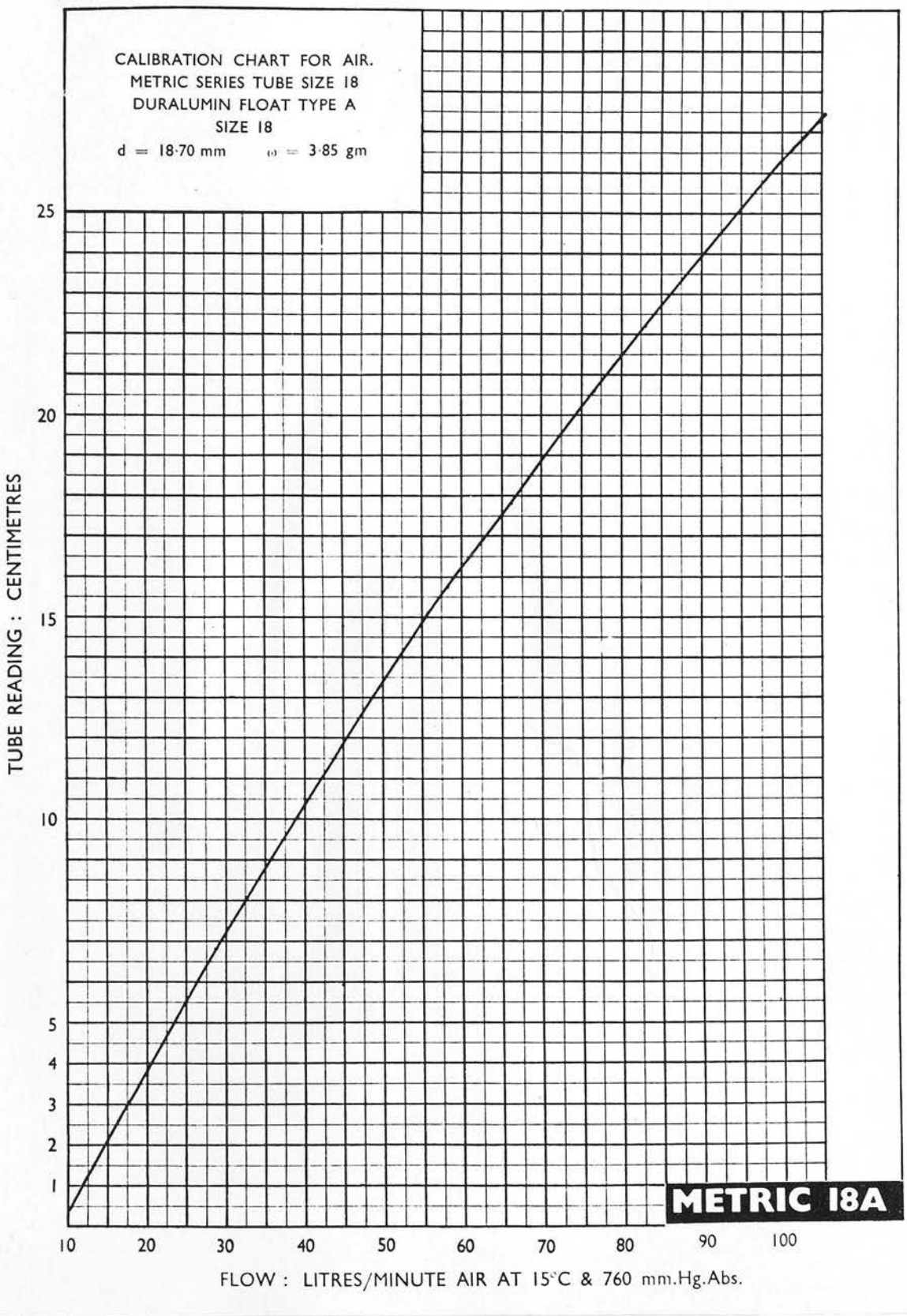

Figure 98. Rotameter metric size 18 (R18). Calibration curve.

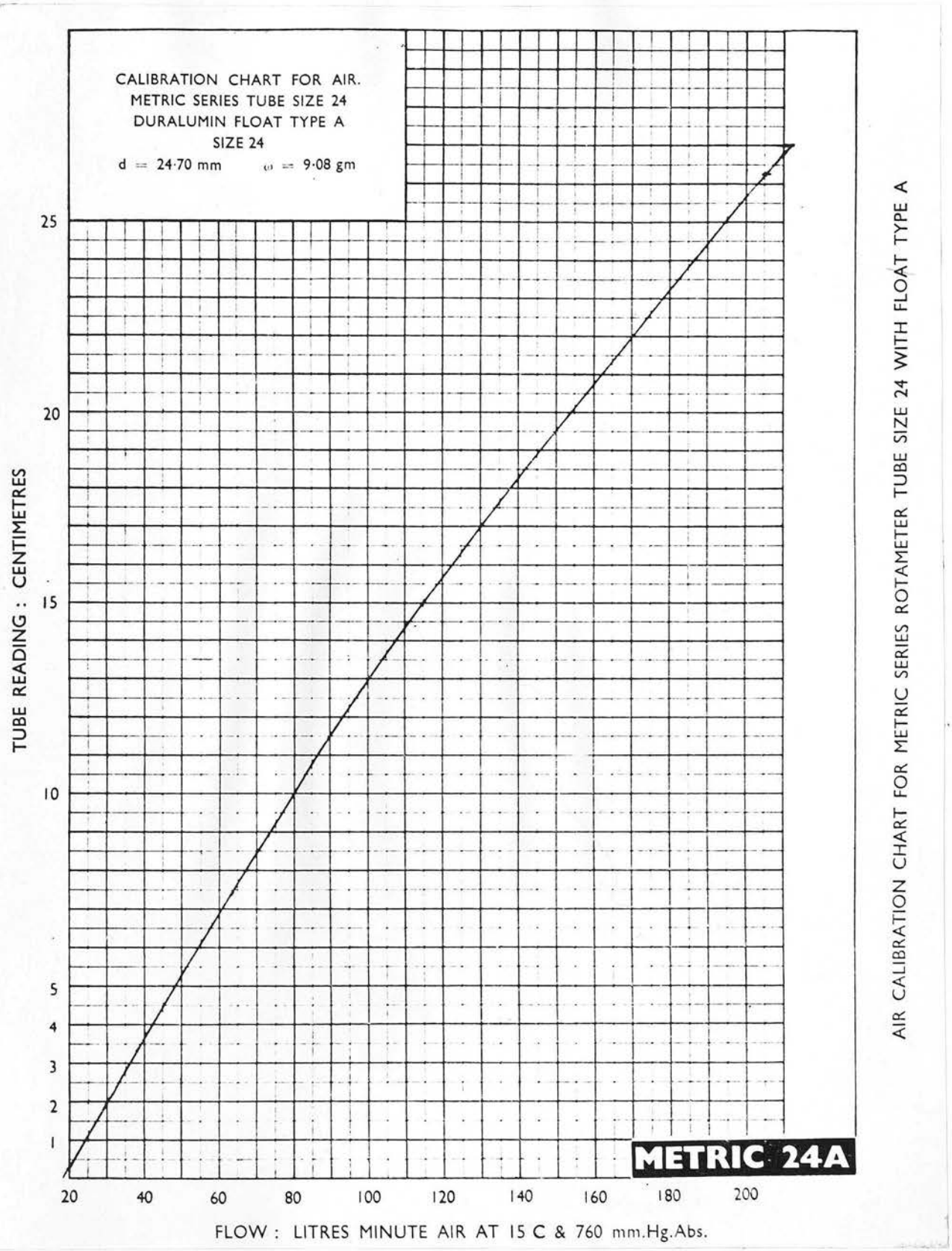

Figure 99. Rotameter metric size 24 (R24). Calibration curve.

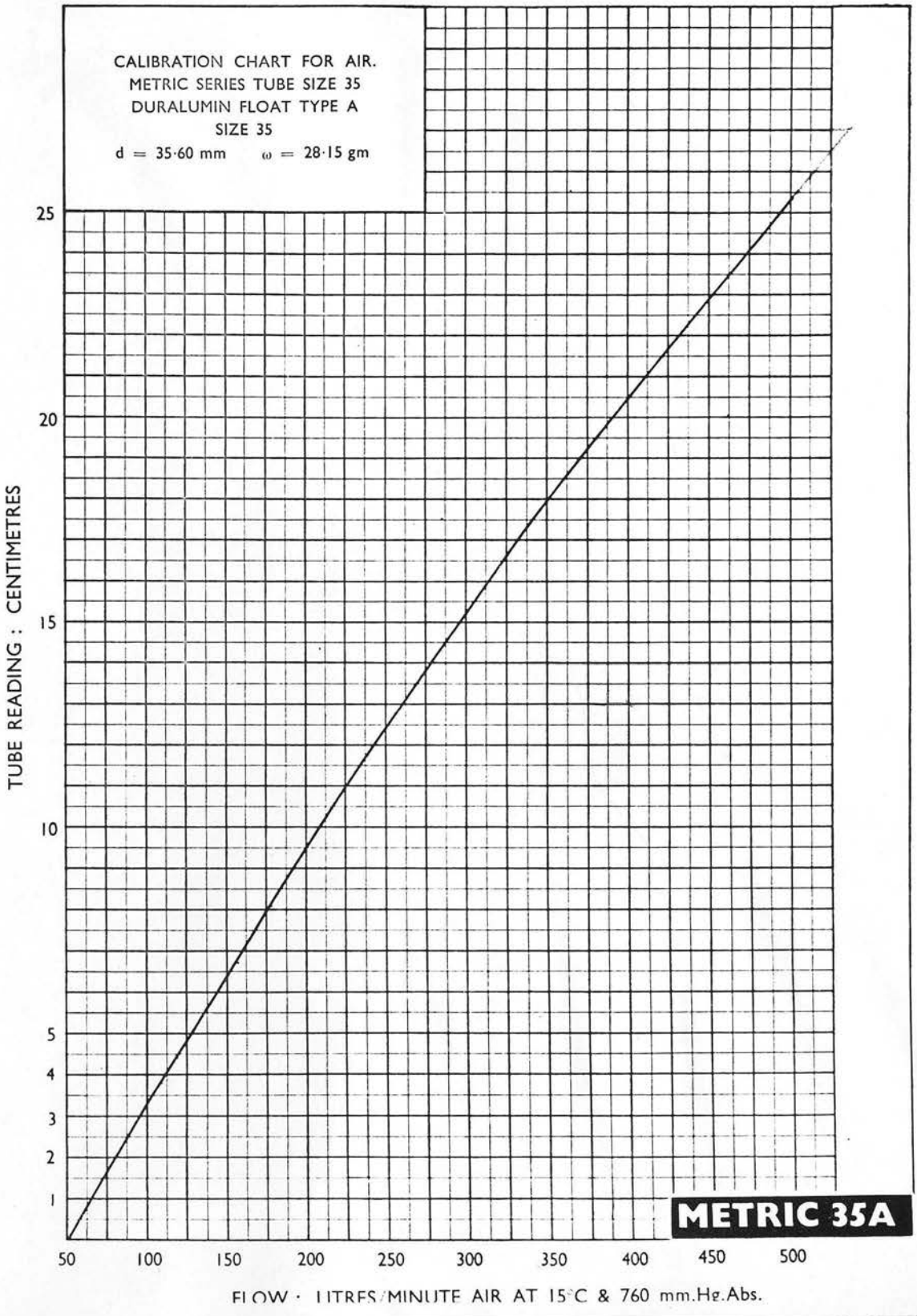

Figure 100. Rotameter metric size 35 (R35). Calibration curve.

TABLE XVI

Values of saturation concentration of mercury vapour, C^* as a function of temperature

The values of C^* given in the table below were calculated from values of the saturation vapour pressure of mercury, p^*, obtained from the International Critical Tables (44) at the temperatures shown. The method of calculation is shown in Appendix L. Figure 87 shows a plot of C^* versus temperature using the data given below.

Temperature ^oC	14	15	16	17	18	19	20	21	22	23	24	25	26
Saturation vapour pressure of mercury p^* mm.Hg	.000706	.000773	.000846	.000925	.001009	.001101	.001201	.001309	.001426	.001553	.001691	.001840	.0020000
saturation concentration of mercury vapour $c^* \mu gm/m^3$	7914	8635	9417	10261	11155	12130	13187	14324	15551	16879	18317	19863	21519

TABLE XVII

Values of molecular diffusion coefficient for mercury vapour into air

The values given below were calculated from the data of Mullay and Jacques (56) using the method shown in Appendix M Figure 88 shows a plot of D versus temperature using the data given below

Temperature ^oC	15	16	18	20	22	23	25
Diffusion coefficient D cm^2/sec	0.1240	0.1248	0.1266	0.1283	0.1300	0.1309	0.1327

TABLE XVIII

$2\frac{3}{8}$" diameter rotor. Radial diffusion experiments - stationary rotor. $\frac{3}{4}$" wide amalgamated band on outer cylinder

$A = 139.0\ cm^2$; $S = 87.4\ cm.^2$

Calibration - Figure 89

R 14	Temperature °c E	O	mean	micro ammeter reading μa.DC	Rotor speed rpm	Air flow rate l/m	$\bar{u}$ cm/sec	c^* μgm/m³	c_2 μgm/m³	ϕ	D cm^2/sec	ν cm^2/sec	$\frac{Dx}{\bar{u}}$ cm^2	$\ln\frac{c^*}{c^*-c_2}$	K cm/sec	Re_a	Re_c
1.8	17.85	18.05	17.95	36.0	0	7.1	0.851	11100	1533	0.1381	0.12648	0.1481	0.2831	0.14860	0.202	49.3	0
1.8	18.00	18.90	18.45	32.0	0	7.1	0.851	11570	1275	0.1102	0.12696	0.1486	0.2842	0.11676	0.158	49.0	0
7.8	18.35	19.35	18.85	23.0	0	16.3	1.953	11960	828	0.0692	0.12732	0.1490	0.1242	0.07175	0.224	112	0
8.0	17.85	18.05	17.95	21.0	0	16.7	1.996	11100	739	0.0666	0.12648	0.1481	0.1208	0.06890	0.213	116	0
14.6	18.25	19.35	18.80	18.0	0	27.5	3.300	11910	601	0.0504	0.12726	0.1489	0.0735	0.05178	0.273	189	0
R 24																	
3.3	18.65	18.38	18.52	15.8	0	38.0	4.56	11640	500	0.04296	0.12700	0.1486	0.0530	0.04391	0.320	269	0
3.3	18.10	18.10	18.10	15.5	0	38.0	4.56	11240	482	0.04290	0.12667	0.1482	0.0530	0.04411	0.321	265	0
7.4	18.50	18.50	18.50	12.2	0	63.1	7.56	11620	342	0.02940	0.12700	0.1486	0.0320	0.02987	0.360	436	0
7.4	18.63	18.35	18.49	11.5	0	63.1	7.56	11610	313	0.02700	0.12698	0.1486	0.0320	0.02733	0.330	436	0
7.4	18.10	18.10	18.10	11.0	0	63.1	7.56	11240	296	0.02632	0.12667	0.1482	0.0319	0.02669	0.322	438	0
12.8	18.60	18.50	18.55	9.1	0	98.5	11.80	11670	230	0.01973	0.12740	0.1487	0.0205	0.01991	0.375	681	0
12.8	18.10	18.10	18.10	8.9	0	98.5	11.80	11240	221	0.01965	0.12667	0.1482	0.0204	0.01980	0.373	682	0
12.8	18.50	18.50	18.50	9.0	0	98.5	11.80	11620	224	0.01926	0.12700	0.1486	0.0205	0.01947	0.367	681	0
18.2	18.10	18.10	18.10	7.8	0	139.5	16.72	11240	180	0.01605	0.12667	0.1482	0.0144	0.01614	0.431	968	0
18.2	18.85	19.23	19.04	7.9	0	139.5	16.72	12160	192	0.01578	0.12748	0.1491	0.0145	0.01592	0.425	962	0
24.0	18.63	19.00	18.81	6.9	0	186.0	22.29	11910	165	0.01383	0.12728	0.1489	0.0109	0.01395	0.496	1282	0

TABLE XIX

$3\frac{1}{8}$" diameter rotor. Radial diffusion experiments - stationary rotor. $\frac{3}{4}$" wide amalgamated band on outer cylinder

$A = 118.0\ cm^2$; $S = 87.4\ cm^2$ Calibration A - Figure 90

R 24	Temperature °c E	Temperature °c O	Temperature °c mean	micro ammeter reading μa.DC	Rotor speed rpm	Air Flow rate l/m	$\bar{u}$ cm/sec	c^* μgm/m³	c_2 μgm/m³	ϕ	D cm^2/sec	ν cm^2/sec	$\frac{Dx}{\bar{u}}$ cm^2	$\ln\frac{c^*}{c^*-c_2}$	K cm/sec	Re_a	Re_c
0.15	18.10	19.10	18.60	26.0	0	19.0	2.68	11720	870	0.0742	0.1271	0.1487	0.0902	0.0771	0.279	121	0
1.5	18.00	19.20	18.60	23.2	0	27.0	3.81	11720	740	0.0631	0.1271	0.1487	0.0636	0.0652	0.335	171	0
3.3	18.00	19.00	18.50	18.7	0	38.1	5.38	11620	539	0.0455	0.1270	0.1486	0.0450	0.0475	0.345	241	0
7.4	18.80	19.80	19.30	14.8	0	63.2	8.93	12415	382	0.0307	0.1277	0.1493	0.0272	0.0313	0.376	399	0
12.8	17.50	18.50	18.00	10.6	0	98.5	13.91	11155	265	0.0238	0.1266	0.1481	0.0173	0.0240	0.450	628	0
18.2	18.80	19.60	19.20	8.3	0	139.5	19.71	12320	222	0.0180	0.1276	0.1492	0.0123	0.0182	0.484	882	0
24.0	18.25	19.25	18.75	7.2	0	186.0	26.25	11860	205	0.0173	0.1272	0.1489	0.0092	0.0175	0.617	1178	0
27.0	18.60	19.40	19.00	6.5	0	213.0	30.08	12130	200	0.0165	0.1274	0.1491	0.0081	0.0166	0.674	1347	0
R 35							Calibration C - Figure 91										
12.7	19.25	20.25	19.75	23.6	0	256	36.2	12880	169	0.0131	0.1281	0.1498	0.00674	0.01321	0.646	1614	0
19.7	20.50	21.25	20.87	19.0	0	383	54.1	14170	129	0.0091	0.1291	0.1509	0.00455	0.00915	0.667	2399	0
19.7	19.25	20.25	19.75	15.8	0	383	54.1	12880	111	0.0086	0.1281	0.1498	0.00451	0.00866	0.632	2413	0
19.7	20.50	21.25	20.87	17.5	0	383	54.1	14170	120	0.0085	0.1291	0.1509	0.00455	0.00851	0.621	2399	0
24.1	19.25	20.25	19.75	11.4	0	475	67.1	12880	92	0.0072	0.1281	0.1498	0.00364	0.00717	0.650	2994	0
24.1	20.00	20.86	20.43	14.0	0	475	67.1	13650	104	0.0067	0.1287	0.1504	0.00366	0.00765	0.612	2990	0
26.5	20.25	20.87	20.56	9.0	0	525	74.2	13800	77	0.0056	0.1288	0.1506	0.00331	0.00560	0.560	3295	0
26.5	19.25	20.25	19.75	8.0	0	525	74.2	12880	68	0.0053	0.1281	0.1498	0.00329	0.00530	0.530	3314	0
R 35							Calibration D - Figure 91										
19.7	20.4	19.75	20.07	18.5	0	383	54.1	13250	116	0.0088	0.1284	0.1501	0.00452	0.00879	0.642	2410	0
26.5	20.4	19.75	20.07	7.8	0	525	74.2	13250	71	0.0054	0.1284	0.1501	0.00329	0.00537	0.539	3310	0

TABLE XX

$4\frac{3}{4}$" diameter rotor. Radial diffusion experiments - stationary rotor. $\frac{3}{4}$" wide amalgamated band on outer cylinder

$A = 53.3\ cm^2$; $S = 87.4\ cm^2$

R 14	Temperature °c E	Temperature °c O	Temperature °c mean	micro ammeter reading μa.DC	Rotor speed rpm	Air flow rate l/m	$\bar{u}$ cm/sec	C^* $\mu gm/m^3$	C_2 $\mu gm/m^3$	ϕ	D cm^2/sec	ν cm^2/sec	$\frac{Dx}{\bar{u}}$ cm^2	$\ln\frac{C^*}{C^* - C_2}$	K cm/sec	Re_a	Re_c
							Calibration C - Figure 92										
1.75	17.60	18.40	18.00	43.7	0	7.02	2.20	11150	3045	0.2730	0.1266	0.1481	0.1096	0.31896	0.427	38	0
6.16	17.60	18.40	18.00	34.2	0	13.71	4.30	11150	1935	0.1734	0.1266	0.1481	0.0562	0.19061	0.498	74	0
10.65	17.60	18.40	18.00	29.5	0	20.72	6.48	11150	1535	0.1377	0.1266	0.1481	0.0373	0.14812	0.587	111	0
16.90	17.60	18.40	18.00	25.0	0	31.45	9.85	11150	1210	0.1083	0.1266	0.1481	0.0245	0.11487	0.688	169	0
17.00	17.80	18.90	18.35	24.9	0	31.65	9.91	11480	1205	0.1050	0.1269	0.1485	0.0244	0.11089	0.669	170	0
23.80	18.00	19.10	18.55	19.8	0	44.40	13.90	11670	915	0.0785	0.1270	0.1487	0.0174	0.08165	0.691	238	0
25.50	17.60	18.40	18.00	17.2	0	48.50	15.18	11150	790	0.0709	0.1266	0.1481	0.0159	0.07349	0.679	260	0
							Calibration A - Figure 92										
1.80	17.50	16.80	17.15	33.5	0	7.10	2.22	10380	3080	0.2436	0.1258	0.1474	0.1081	0.29213	0.395	34	0
4.95	18.10	16.60	17.35	27.3	0	11.88	3.72	10650	1770	0.1675	0.1261	0.1476	0.0645	0.17966	0.407	51	0
9.95	18.20	16.60	17.40	20.7	0	19.62	6.14	10600	1220	0.1151	0.1261	0.1476	0.0391	0.11470	0.430	93	0
14.90	18.20	16.60	17.40	17.1	0	28.00	8.76	10600	1010	0.0953	0.1261	0.1476	0.0274	0.09256	0.494	132	0
17.70	18.00	16.60	17.30	16.5	0	32.75	10.25	10520	970	0.0922	0.1260	0.1475	0.0234	0.09674	0.605	155	0
R 24							Calibration B - Figure 92										
1.5	19.28	18.90	19.09	25.6	0	27.0	8.46	12200	1255	0.1029	0.1275	0.1492	0.02870	0.10856	0.561	144	0
3.5	19.15	18.75	18.95	22.0	0	39.0	12.20	12050	995	0.0825	0.1274	0.1491	0.01990	0.08619	0.641	208	0
7.4	18.35	18.14	18.24	16.5	0	63.2	19.80	11370	650	0.0571	0.1268	0.1483	0.01220	0.05887	0.709	339	0
12.8	18.22	17.50	17.86	13.3	0	98.5	30.85	11010	480	0.0436	0.1264	0.1480	0.00781	0.04458	0.839	529	0
24.0	19.75	19.37	19.56	9.0	0	186.5	58.40	12660	300	0.0237	0.1279	0.1496	0.00417	0.02398	0.853	993	0
30.0	17.63	17.63	17.63	7.8	0	241.0	75.50	10800	250	0.0232	0.1262	0.1478	0.00318	0.02247	0.915	1161	0

TABLE XXI

5.18" diameter rotor. Radial diffusion experiments - stationary rotor. $\frac{3}{4}$" wide amalgamated band on outer cylinder

$A = 31.6\ cm^2$; $S = 87.4\ cm^2$

Calibration A - Figure 94

R 18	Temperature °c E	Temperature °c O	Temperature °c mean	micro ammeter reading μa.DC	Rotor speed rpm	Air flow rate l/m	$\bar{u}$ cm/sec	C^* μgm/m³	C_2 μgm/m³	ϕ	D cm^2/sec	ν cm^2/sec	$\frac{Dx}{\bar{u}}$ cm^2	$\ln\frac{C^*}{C^*-C_2}$	K cm/sec	Re_a	Re_c
5.00	22.00	26.20	24.10	18.5	0	23.3	12.32	18430	2970	0.1611	0.1319	0.1539	0.0204	0.17572	0.781	116	0
10.20	22.00	26.20	24.10	16.0	0	39.0	20.60	18430	2340	0.1270	0.1319	0.1539	0.0122	0.13578	1.009	194	0
12.50	22.90	26.0	24.45	14.9	0	47.0	24.85	18960	2110	0.1112	0.1322	0.1543	0.0101	0.11798	1.067	233	0
15.70	22.90	26.0	24.45	13.6	0	58.1	30.70	18960	1860	0.0981	0.1322	0.1545	0.0082	0.10325	1.147	287	0
18.75	23.75	25.75	24.75	12.6	0	69.0	36.50	19410	1650	0.0850	0.1325	0.1545	0.0069	0.08884	1.171	342	0
22.20	25.00	25.00	25.00	11.5	0	83.0	43.90	19810	1410	0.0712	0.1327	0.1547	0.0058	0.07384	1.180	411	0
27.00	25.00	25.00	25.00	10.5	0	103.5	54.70	19810	1200	0.0606	0.1327	0.1547	0.0046	0.06429	1.268	512	0
R 35																	
6.0	25.10	25.52	25.31	10.5	0	143	75.60	20280	1200	0.0592	0.1329	0.1600	0.0034	0.06110	1.670	680	0

Calibration B - Figure 94

R 14																	
1.60	21.52	22.00	21.76	29.9	0	6.8	3.60	15230	4895	0.3210	0.1298	0.1518	0.0687	0.38772	0.504	34	0
4.00	21.52	22.00	21.76	26.4	0	10.4	5.50	15230	3690	0.2427	0.1298	0.1518	0.0450	0.27745	0.551	53	0
7.50	21.52	22.00	21.76	22.5	0	15.8	8.36	15230	2885	0.1894	0.1298	0.1518	0.0296	0.21002	0.633	80	0
9.60	21.52	22.00	21.76	21.1	0	19.1	10.09	15230	2635	0.1848	0.1298	0.1518	0.0245	0.18997	0.692	96	0
R 18																	
2.20	20.50	21.00	20.75	24.8	0	15.2	8.04	14020	3330	0.2371	0.1290	0.1508	0.0306	0.27118	0.787	77	0
3.75	20.50	21.00	20.75	22.9	0	19.9	10.52	14020	2950	0.2101	0.1290	0.1508	0.0233	0.23625	0.899	101	0
6.50	20.50	21.00	20.75	19.9	0	27.9	14.74	14020	2450	0.1745	0.1290	0.1508	0.0166	0.19207	1.022	142	0
8.00	20.75	21.00	20.88	17.9	0	32.5	17.18	14170	2150	0.1532	0.1291	0.1509	0.0143	0.16456	1.021	165	0
10.05	20.50	21.00	20.75	16.7	0	39.0	20.61	14020	1990	0.1418	0.1290	0.1508	0.0119	0.15308	1.138	198	0
12.50	20.75	21.00	20.88	15.5	0	47.0	24.86	14170	1815	0.1281	0.1291	0.1509	0.0099	0.13707	1.230	239	0
15.10	20.75	21.00	20.88	12.5	0	55.8	29.50	14170	1410	0.0994	0.1291	0.1509	0.0083	0.10410	1.110	283	0
17.80	20.75	21.00	20.88	11.6	0	66.3	35.10	14170	1310	0.0921	0.1291	0.1509	0.0070	0.09003	1.142	337	0
20.60	20.78	21.15	20.96	9.9	0	76.5	40.40	14260	1115	0.0782	0.1291	0.1510	0.0061	0.08143	1.188	388	0
26.60	20.78	21.15	20.96	6.8	0	101.2	53.55	14260	850	0.0596	0.1291	0.1510	0.0046	0.06145	1.188	514	0

TABLE XXI (continued)

Calibration B - Figure 94 (continued

R 18	Temperature °c E	O	mean	micro ammeter reading μa.DC	Rotor speed rpm	Air flow rate l/m	$\bar{u}$ cm/sec	C^* μgm/m^3	C_2 μgm/m^3	ϕ	D cm^2/sec	ν cm^2/sec	$\frac{Dx}{\bar{u}}$ cm^2	$\ln\frac{C^*}{C^*-C_2}$	K cm/sec	Re_a	Re_c
10.05	21.00	23.00	22.00	16.5	0	39.0	20.6	15550	1950	0.1253	0.1300	0.1520	0.0120	0.13366	0.994	196	0
15.10	21.70	23.50	22.60	13.5	0	55.8	29.5	16310	1550	0.0950	0.1306	0.1526	0.0084	0.09980	1.063	280	0
26.60	22.60	23.60	23.10	6.9	0	101.2	53.6	16980	855	0.0503	0.1310	0.1530	0.0047	0.05442	1.050	507	0
R 35																	
15.80	24.10	24.10	24.10	3.2	0	310.0	163.8	18420	660	0.0358	0.1319	0.1539	0.0015	0.03680	2.178	1530	0
2.90	20.13	21.87	21.00	7.2	0	89.0	47.0	14310	760	0.0607	0.1292	0.1510	0.0052	0.05457	0.925	451	0
R 35	Calibration C - Figure 94																
5.85	23.50	22.85	23.18	8.6	0	141.0	74.5	17100	795	0.0465	0.1310	0.1531	0.00335	0.04766	1.265	702	0
R 18	Calibration D - Figure 94																
2.60	19.00	21.16	20.08	24.5	0	16.5	8.73	13280	3190	0.2400	0.1283	0.1501	0.02800	0.27471	0.864	84	0
R 35	Calibration E - Figure 95																
12.10	25.00	23.80	24.40	15.6	0	244.0	129.0	18900	810	0.0429	0.1322	0.1542	0.00195	0.04380	1.204	1211	0
26.50	22.62	23.75	23.19	12.0	0	520.0	275.0	17110	420	0.0245	0.1311	0.1531	0.00090	0.02485	2.470	2600	0

TABLE XXII

$3\frac{1}{8}$" diameter rotor. Radial diffusion experiments - stationary rotor. 3" wide amalgamated band on rotor

Calibration B - Figure 90

R/24	Temperature °c E	Temperature °c O	Temperature °c mean	micro ammeter reading μa.DC	Rotor speed rpm	Air flow rate l/m	$\bar{u}$ cm/sec	C^* μgm/m³	C_2 μgm/m³	ϕ	D cm²/sec	$\frac{Dx}{\bar{u}}$ cm²
1.5	17.25	20.0	18.63	29.0	0	27.0	3.82	11750	730	0.0621	0.1271	0.1268
3.5	17.25	20.0	18.63	26.0	0	39.0	5.51	11750	565	0.0480	0.1271	0.0879

TABLE XXIII

$4\frac{3}{4}$" diameter rotor. Radial diffusion experiments - stationary rotor. $1\frac{1}{2}$" wide amalgamated band on rotor

Calibration D - Figure 93

R/24												
1.5	18.10	18.20	18.15	17.5	0	27.0	8.46	11290	1080	0.0957	0.1267	0.0571
3.5	18.10	18.20	18.15	15.2	0	39.2	12.20	11290	886	0.0783	0.1267	0.0396
7.4	18.10	18.20	18.15	11.6	0	63.2	19.80	11290	668	0.0592	0.1267	0.0244
12.8	18.10	18.20	18.15	9.8	0	98.5	30.85	11290	540	0.0478	0.1267	0.0156
18.2	18.10	18.20	18.15	8.8	0	140.0	43.80	11290	450	0.0399	0.1267	0.0110
24.0	18.10	18.20	18.15	8.0	0	186.5	58.50	11290	370	0.0328	0.1267	0.0083
27.0	18.10	18.20	18.15	7.5	0	241.0	66.70	11290	315	0.0279	0.1267	0.0072

TABLE XXIV

$2\frac{3}{8}$" diameter rotor. Radial diffusion experiments. $\frac{3}{4}$" wide amalgamated band on outer cylinder.

Calibration - Figure 89

R 14	Temperature °c E	O	mean	Micro ammeter reading μa.DC	Rotor speed rpm	Air flow rate l/m	$\bar{u}$ cm/sec	C^* μgm/m³	C_2 μgm/m³	ν cm²/sec	$\ln \frac{C^*}{C^* - C_2}$	K cm/sec	Re_a	Re_c
1.8	18.00	18.90	18.45	32.0	0	7.1	0.851	11570	1275	0.1486	0.11676	0.158	49	0
1.8	18.00	18.90	18.45	34.0	43	7.1	0.851	11570	1398	0.1486	0.12878	0.174	49	390
1.8	18.00	18.90	18.45	50.2	56	7.1	0.851	11570	2810	0.1486	0.27822	0.378	49	508
7.8	18.35	19.35	18.85	23.1	0	16.3	1.953	11960	828	0.1490	0.07175	0.224	112	0
7.8	18.15	19.25	18.70	32.1	78	16.3	1.953	10810	1281	0.1488	0.12613	0.394	112	709
7.8	18.35	19.35	18.85	37.5	134	16.3	1.953	11960	1640	0.1490	0.14748	0.465	112	1218
7.8	18.15	19.25	18.70	44.0	287	16.3	1.953	10810	2189	0.1488	0.22627	0.706	112	2610
14.6	18.25	19.35	18.80	18.0	0	27.5	3.300	11910	601	0.1489	0.05178	0.273	189	0
14.6	18.25	19.35	18.80	32.4	216	27.5	3.300	11910	1300	0.1489	0.11558	0.607	189	1965
14.6	18.25	19.35	18.80	36.2	482	27.5	3.300	11910	1550	0.1489	0.13943	0.735	189	4385
14.6	18.25	19.35	18.80	44.0	1240	27.5	3.300	11910	2189	0.1489	0.20309	1.070	189	11270
R 24														
3.3	18.60	19.28	18.94	15.9	0	38.0	4.56	12040	502	0.1490	0.04259	0.310	262	0
3.3	18.60	19.28	18.94	23.0	136	38.0	4.56	12040	821	0.1490	0.07045	0.513	262	1234
3.3	18.60	19.28	18.94	30.8	496	38.0	4.56	12040	1206	0.1490	0.10550	0.768	262	4508
3.3	18.60	19.28	18.94	38.0	1210	38.0	4.56	12040	1678	0.1490	0.15010	1.092	262	10980
3.3	18.60	19.28	18.94	43.2	2180	38.0	4.56	12040	2112	0.1490	0.19288	1.403	262	19810
7.4	18.63	18.35	18.49	11.5	0	63.1	7.56	11610	313	0.1486	0.02733	0.330	436	0
7.4	18.63	18.35	18.49	15.9	214	63.1	7.56	11610	502	0.1486	0.04421	0.534	436	1950
7.4	18.50	18.40	18.45	19.3	424	63.1	7.56	11570	660	0.1486	0.05874	0.708	436	3867
7.4	18.50	18.40	18.45	23.0	950	63.1	7.56	11570	820	0.1486	0.07351	0.886	436	8657
7.4	18.50	18.40	18.45	25.0	1290	63.1	7.56	11570	912	0.1486	0.08210	0.990	436	11760
7.4	18.50	18.40	18.45	28.3	2340	63.1	7.56	11570	1072	0.1486	0.09723	1.172	436	21310

TABLE XXIV (continued)

$2\frac{3}{8}$" diameter rotor. Radial diffusion experiments. $\frac{3}{4}$" wide amalgamated band on outer cylinder

Calibration - Figure 89

R 24	Temperature °c E	Temperature °c O	Temperature °c mean	Micro ammeter reading μa.DC	Rotor speed rpm	Air flow rate l/m	$\bar{u}$ cm/sec	c^* μgm/m³	c_2 μgm/m³	ν cm²/sec	$\ln \frac{c^*}{c^* - c_2}$	K cm/sec	Re_a	Re_c
12.8	18.60	18.50	18.55	9.1	0	98.5	11.80	11670	230	0.1487	0.01991	0.375	681	0
12.8	18.60	18.50	18.55	10.0	216	98.5	11.80	11670	260	0.1487	0.02253	0.424	681	1968
12.8	18.60	18.50	18.55	11.8	423	98.5	11.80	11670	324	0.1487	0.02816	0.530	681	3855
12.8	18.60	18.50	18.55	13.6	860	98.5	11.80	11670	400	0.1487	0.03488	0.656	681	7840
12.8	18.60	18.50	18.55	15.8	1260	98.5	11.80	11670	500	0.1487	0.04379	0.825	681	11480
12.8	18.60	18.50	18.55	17.9	2090	98.5	11.80	11670	599	0.1487	0.05269	0.992	681	19040
12.8	18.60	18.50	18.55	18.1	2200	98.5	11.80	11670	608	0.1487	0.05351	1.008	681	20010
18.2	18.85	19.23	19.04	7.9	0	139.5	16.72	12160	192	0.1491	0.01592	0.425	962	0
18.2	18.85	19.23	19.04	10.2	466	139.5	16.72	12160	268	0.1491	0.02229	0.595	962	4239
18.2	18.85	19.23	19.04	11.1	830	139.5	16.72	12160	299	0.1491	0.02490	0.665	962	7540
18.2	18.85	19.23	19.04	12.5	1190	139.5	16.72	12160	356	0.1491	0.02972	0.793	962	10800
18.2	18.85	19.23	19.04	14.0	1990	139.5	16.72	12160	418	0.1491	0.03498	0.933	962	18110
18.2	18.85	19.23	19.04	14.7	2200	139.5	16.72	12160	450	0.1491	0.03771	1.006	962	20000

TABLE XXV

$3\frac{1}{8}$" diameter rotor. Radial diffusion experiments. $\frac{3}{4}$" wide amalgamated band on outer cylinder

Calibration A - Figure 90

R/24	Temperature °c E	Temperature °c O	Temperature °c mean	Micro ammeter reading μa.DC	Rotor speed rpm	Air flow rate l/m	$\bar{u}$ cm/sec	C^* μgm/m³	C_2 μgm/m³	ν cm²/sec	$\ln \frac{c^*}{c^* - c_2}$	K cm/sec	Re_a	Re_c
0.15	18.10	19.10	18.60	26.0	0	19.0	2.68	11720	870	0.1487	0.0771	0.279	121	0
0.15	18.10	19.10	18.60	26.3	15	19.0	2.68	11720	883	0.1487	0.0783	0.284	121	140
0.15	18.10	19.10	18.60	27.1	20	19.0	2.68	11720	945	0.1487	0.0841	0.305	121	187
0.15	18.10	19.10	18.60	32.1	40	19.0	2.68	11720	1177	0.1487	0.1058	0.383	121	373
0.15	18.10	19.10	18.60	40.2	96	19.0	2.68	11720	1668	0.1487	0.1537	0.557	121	895
0.15	18.10	19.10	18.60	47.0	170	19.0	2.68	11720	2165	0.1487	0.2042	0.741	121	1584
1.5	18.00	19.20	18.60	23.2	0	27.0	3.81	11720	740	0.1487	0.0652	0.335	171	0
1.5	18.00	19.20	18.60	23.8	31	27.0	3.81	11720	767	0.1487	0.0677	0.348	171	289
1.5	18.00	19.20	18.60	26.9	68	27.0	3.81	11720	922	0.1487	0.0819	0.421	171	634
1.5	18.00	19.20	18.60	32.0	98	27.0	3.81	11720	1168	0.1487	0.1050	0.540	171	914
1.5	18.00	19.20	18.60	34.1	138	27.0	3.81	11720	1287	0.1487	0.1163	0.598	171	1286
1.5	18.00	19.20	18.60	39.3	217	27.0	3.81	11720	1608	0.1487	0.1476	0.758	171	2021
1.5	18.00	19.20	18.60	43.7	303	27.0	3.81	11720	1916	0.1487	0.1785	0.919	171	2826
3.3	18.00	19.00	18.50	18.7	0	38.1	5.38	11620	539	0.1486	0.0475	0.345	241	0
3.3	18.00	19.00	18.50	19.3	28	38.1	5.38	11620	564	0.1486	0.0498	0.362	241	261
3.3	18.00	19.00	18.50	20.5	40	38.1	5.38	11620	630	0.1486	0.0557	0.404	241	373
3.3	18.00	19.00	18.50	21.2	44	38.1	5.38	11620	649	0.1486	0.0575	0.417	241	410
3.3	18.00	19.04	18.52	27.3	108	38.1	5.38	11660	930	0.1486	0.0831	0.603	241	1006
3.3	18.00	19.04	18.52	34.9	240	38.1	5.38	11620	1335	0.1486	0.1220	0.885	241	2236
3.3	18.00	19.04	18.52	40.4	379	38.1	5.38	11620	1682	0.1486	0.1564	1.135	241	3536
3.3	18.00	19.04	18.52	44.2	573	38.1	5.38	11660	1953	0.1486	0.1833	1.330	241	5350
7.4	18.80	19.80	19.30	14.8	0	63.2	8.93	12415	382	0.1493	0.0313	0.376	399	0
7.4	18.80	19.80	19.30	15.3	20	63.2	8.93	12415	400	0.1493	0.0325	0.395	399	185
7.4	18.80	19.80	19.30	17.0	48	63.2	8.93	12415	465	0.1493	0.0382	0.460	399	445
7.4	18.80	19.80	19.30	23.0	198	63.2	8.93	12415	732	0.1493	0.0608	0.732	399	1836
7.4	18.80	19.80	19.30	24.5	231	63.2	8.93	12415	800	0.1493	0.0667	0.804	399	2142
7.4	18.80	19.80	19.30	29.0	401	63.2	8.93	12415	1014	0.1493	0.0852	1.028	399	3722

TABLE XXV (continued)

$3\frac{1}{8}$" diameter rotor. Radial diffusion experiments. $\frac{3}{4}$" wide amalgamated band on outer cylinder

Calibration A - Figure 90

R 24	Temperature °c E	Temperature °c O	Temperature °c mean	Micro ammeter reading μa.DC	Rotor speed rpm	Air flow rate l/m	$\bar{u}$ cm/sec	C^* μgm/m³	C_2 μgm/m³	ν cm²/sec	$\ln \frac{c^*}{c^* - c_2}$	K cm/sec	Re_a	Re_c
7.4	18.80	19.80	19.30	33.9	770	63.2	8.93	12415	1272	0.1493	0.1081	1.303	399	7150
7.4	18.80	19.80	19.30	34.4	850	63.2	8.93	12415	1305	0.1493	0.1111	1.340	399	7880
7.4	18.80	19.80	19.30	38.1	1140	63.2	8.93	12415	1530	0.1493	0.1315	1.583	399	10580
7.4	18.80	19.80	19.30	43.1	1840	63.2	8.93	12415	1875	0.1493	0.1637	1.969	399	17060
7.4	18.80	19.80	19.30	45.0	2080	63.2	8.93	12415	2015	0.1493	0.1771	2.134	399	19300
12.8	17.50	18.50	18.00	10.6	0	98.5	13.91	11155	265	0.1481	0.0240	0.450	628	0
12.8	17.50	18.50	18.00	11.5	73	98.5	13.91	11155	285	0.1481	0.0259	0.486	628	683
12.8	17.50	18.50	18.00	12.5	129	98.5	13.91	11155	312	0.1481	0.0283	0.531	628	1200
12.8	17.50	18.50	18.00	17.2	426	98.5	13.91	11155	475	0.1481	0.0435	0.816	628	3986
12.8	17.50	18.50	18.00	26.3	1300	98.5	13.91	11155	885	0.1481	0.0827	1.552	628	12170
12.8	17.50	18.50	18.00	31.1	2100	98.5	13.91	11155	1122	0.1481	0.1060	1.989	628	19670
18.2	18.80	19.60	19.20	8.3	0	139.5	19.71	12320	222	0.1492	0.0182	0.484	882	0
18.2	18.80	19.60	19.20	8.5	77	139.5	19.71	12320	224	0.1492	0.0184	0.489	882	715
18.2	18.80	19.60	19.20	12.9	364	139.5	19.71	12320	321	0.1492	0.0269	0.716	882	3381
18.2	18.90	19.70	19.30	18.1	825	139.5	19.71	12415	512	0.1493	0.0421	1.119	882	7660
18.2	18.90	19.70	19.30	21.6	1130	139.5	19.71	12415	666	0.1493	0.0551	1.468	882	10488
18.2	18.90	19.70	19.30	24.0	1570	139.5	19.71	12415	777	0.1493	0.0646	1.720	882	14580
18.2	18.90	19.70	19.30	26.8	2050	139.5	19.71	12415	909	0.1493	0.0760	2.022	882	19020
24.0	18.25	19.25	18.75	7.2	0	186.0	26.25	11860	205	0.1489	0.0175	0.617	1178	0
24.0	18.25	19.25	18.75	7.2	24	186.0	26.25	11860	205	0.1489	0.0175	0.617	1178	223
24.0	18.25	19.25	18.75	7.8	172	186.0	26.25	11860	215	0.1489	0.0183	0.647	1178	1600
24.0	18.25	19.25	18.75	8.3	248	186.0	26.25	11860	222	0.1489	0.0189	0.669	1178	2308
24.0	18.25	19.25	18.75	12.2	636	186.0	26.25	11860	303	0.1489	0.0259	0.918	1178	5920
24.0	18.25	19.25	18.75	16.2	1350	186.0	26.25	11860	435	0.1489	0.0373	1.320	1178	12570
24.0	18.25	19.25	18.75	20.0	2040	186.0	26.25	11860	595	0.1489	0.0515	1.822	1178	19000
27.0	18.60	19.40	19.00	6.5	0	213.0	30.08	12130	200	0.1491	0.0166	0.674	1347	0
27.0	18.60	19.40	19.00	6.5	48	213.0	30.08	12130	200	0.1491	0.0166	0.674	1347	447
27.0	18.60	19.40	19.00	6.2	77	213.0	30.08	12130	198	0.1491	0.0165	0.670	1347	717
27.0	18.60	19.40	19.00	6.8	158	213.0	30.08	12130	202	0.1491	0.0167	0.678	1347	1468
27.0	18.60	19.40	19.00	8.2	340	213.0	30.08	12130	221	0.1491	0.0183	0.743	1347	3160
27.0	18.76	19.60	19.20	11.8	910	213.0	30.08	12320	294	0.1492	0.0242	0.983	1347	8450
27.0	18.76	19.60	19.20	14.4	1350	213.0	30.08	12320	368	0.1492	0.0303	1.230	1347	12530
27.0	18.76	19.60	19.20	17.8	2020	213.0	30.08	12320	496	0.1492	0.0411	1.669	1347	18760

TABLE XXV (continued)

$3\frac{1}{8}$" diameter rotor. Radial diffusion experiments. $\frac{3}{4}$" wide amalgamated band on outer cylinder

Calibration C - Figure 91

R	Temperature °C E	Temperature °C O	Temperature °C mean	Micro ammeter reading μa.DC	Rotor speed rpm	Air flow rate l/m	$\bar{u}$ cm/sec	C^* μgm/m³	C_2 μgm/m³	ν cm²/sec	$\ln \frac{C^*}{C^* - C_2}$	K cm/sec	Re_a	Re_c
35														
24.1	20.00	20.86	20.43	11.4	0	475	67.1	13650	92	0.1504	0.00676	0.612	2990	0
24.1	20.00	20.86	20.43	11.4	500	475	67.1	13650	92	0.1504	0.00676	0.612	2990	4604
24.1	19.85	20.75	20.30	11.5	670	475	67.1	13500	92	0.1503	0.00684	0.619	2990	6180
24.1	20.00	20.86	20.43	12.0	700	475	67.1	13650	94	0.1504	0.00691	0.626	2990	6450
24.1	20.00	20.86	20.43	14.0	850	475	67.1	13650	104	0.1504	0.00765	0.682	2990	7834
24.1	19.85	20.75	20.30	15.5	1030	475	67.1	13500	110	0.1503	0.00818	0.741	2990	9480
24.1	19.85	20.75	20.30	17.7	1140	475	67.1	13500	121	0.1503	0.00902	0.817	2990	10510
24.1	19.85	20.75	20.30	22.2	1630	475	67.1	13500	154	0.1503	0.01147	1.039	2990	15020
24.1	19.50	20.50	20.00	24.9	2200	475	67.1	13180	184	0.1500	0.01406	1.273	2990	20340
24.1	19.50	20.50	20.00	26.5	2540	475	67.1	13180	206	0.1500	0.01575	1.427	2990	23450

Calibration D - Figure 91

19.7	20.40	19.75	20.07	18.5	0	383	54.1	13250	116	0.1501	0.00879	0.642	2410	0
19.7	20.40	19.75	20.07	18.5	350	383	54.1	13250	116	0.1501	0.00879	0.642	2410	3232
19.7	20.40	19.75	20.07	23.0	450	383	54.1	13250	145	0.1501	0.01101	0.804	2410	4160
19.7	20.40	19.75	20.07	25.5	950	383	54.1	13250	166	0.1501	0.01261	0.921	2410	8760
19.7	20.48	19.62	20.05	27.5	1240	383	54.1	13220	186	0.1501	0.01417	1.035	2410	11440
19.7	20.75	19.25	20.00	28.7	1530	383	54.1	13180	200	0.1500	0.01529	1.118	2410	14130
19.7	20.75	19.25	20.00	30.9	1860	383	54.1	13180	229	0.1500	0.01753	1.281	2410	17180
19.7	20.75	19.25	20.00	31.6	2180	383	54.1	13180	239	0.1500	0.01830	1.336	2410	20130
19.7	20.75	19.25	20.00	33.5	2550	383	54.1	13180	273	0.1500	0.02093	1.530	2410	23530
26.5	20.40	19.75	20.07	7.6	0	525	74.2	13250	71	0.1501	0.00537	0.539	3310	0
26.5	20.10	19.60	19.85	7.8	1000	525	74.2	12990	72	0.1499	0.00556	0.558	3310	9240
26.5	20.10	19.60	19.85	11.5	1360	525	74.2	12990	84	0.1499	0.00649	0.650	3310	12570
26.5	20.10	19.60	19.85	14.7	1710	525	74.2	12990	97	0.1499	0.00749	0.751	3310	15780
26.5	20.10	19.60	19.85	16.5	1880	525	74.2	12990	106	0.1499	0.00819	0.820	3310	17370
26.5	20.10	19.60	19.85	19.0	2230	525	74.2	12990	118	0.1499	0.00913	0.914	3310	20600
26.5	20.10	19.60	19.85	20.0	2390	525	74.2	12990	124	0.1499	0.00959	0.961	3310	22080
26.5	20.10	19.60	19.85	21.6	2560	525	74.2	12990	135	0.1499	0.01045	1.047	3310	23830

TABLE XXVI

$4\frac{3}{4}$" diameter rotor. Radial diffusion experiments. $\frac{3}{4}$" wide amalgamated band on outer cylinder

Calibration C - Figure 92

R 14	Temperature °c E	O	mean	Micro ammeter reading μa.DC	Rotor speed rpm	Air flow rate l/m	$\bar{u}$ cm/sec	C^* μgm/m³	C_2 μgm/m³	ν cm²/sec	$\ln \frac{C^*}{C^* - C_2}$	K cm/sec	Re_a	Re_c
9.45	18.00	19.00	18.50	31.6	54	18.80	58.80	11620	1704	0.1487	0.15858	0.568	100	291
9.45	18.00	19.00	18.50	41.2	183	18.80	58.80	11620	2700	0.1487	0.26443	0.946	100	988
9.45	18.00	19.00	18.50	45.2	328	18.80	58.80	11620	3265	0.1487	0.32987	1.180	100	1769
9.45	18.00	19.00	18.50	47.8	575	18.80	58.80	11620	3690	0.1487	0.38208	1.370	100	3107
17.0	17.80	18.90	18.35	24.9	0	31.65	9.91	11480	1205	0.1485	0.11089	0.669	170	216
17.0	17.80	18.90	18.35	25.7	72	31.65	9.91	11480	1265	0.1485	0.11675	0.704	170	389
17.0	17.80	18.90	18.35	27.8	103	31.65	9.91	11480	1410	0.1485	0.13105	0.791	170	556
17.0	17.80	18.90	18.35	30.9	147	31.65	9.91	11480	1645	0.1485	0.15466	0.934	170	794
17.0	17.80	18.90	18.35	35.1	236	31.65	9.91	11480	2022	0.1485	0.19375	1.168	170	1273
17.0	17.80	18.90	18.35	43.0	725	31.65	9.91	11480	2940	0.1485	0.29585	1.782	170	3920
17.0	17.80	18.90	18.35	46.8	1300	31.65	9.91	11480	3530	0.1485	0.36743	2.222	170	7020
23.8	18.00	19.10	18.55	19.8	0	44.40	13.90	11670	915	0.1487	0.08165	0.691	238	173
23.8	18.00	19.10	18.55	21.8	98	44.40	13.90	11670	980	0.1487	0.08771	0.743	238	529
23.8	18.00	19.10	18.55	24.0	152	44.40	13.90	11670	1140	0.1487	0.10279	0.870	238	821
23.8	18.00	19.00	18.50	29.5	289	44.40	13.90	11620	1535	0.1487	0.14103	1.194	238	1561
23.8	18.00	19.00	18.50	37.0	725	44.40	13.90	11620	2215	0.1487	0.21149	1.790	238	3915
23.8	18.00	19.00	18.50	39.5	1070	44.40	13.90	11620	2500	0.1487	0.24226	2.052	238	5770
23.8	18.00	19.00	18.50	43.4	1550	44.40	13.90	11620	3000	0.1487	0.29864	2.530	238	8380

Calibration B - Figure 92

R 24														
1.5	19.28	18.90	19.09	25.6	0	27.0	8.46	12200	1255	0.1492	0.10856	0.561	144	0
1.5	19.28	18.90	19.09	31.0	150	27.0	8.46	12200	1680	0.1492	0.14816	0.763	144	804
1.5	19.28	18.90	19.09	37.5	340	27.0	8.46	12200	2400	0.1492	0.21905	1.129	144	1828
1.5	19.28	18.90	19.09	41.0	540	27.0	8.46	12200	2890	0.1492	0.27035	1.394	144	2904
3.5	19.15	18.75	18.95	22.0	0	39.0	12.20	12050	995	0.1491	0.08619	0.641	208	0
3.5	19.15	18.75	18.95	26.8	184	39.0	12.20	12050	1350	0.1491	0.11882	0.889	208	988
3.5	19.15	18.75	18.95	29.5	214	39.0	12.20	12050	1560	0.1491	0.13864	1.030	208	1151
3.5	19.15	18.75	18.95	37.1	550	39.0	12.20	12050	2345	0.1491	0.21642	1.610	208	2965
3.5	19.25	18.88	19.06	41.0	1050	39.0	12.20	12170	2890	0.1491	0.27111	2.014	208	5640
3.5	19.25	18.88	19.06	43.0	1410	39.0	12.20	12170	3250	0.1491	0.31067	2.308	208	7565
3.5	19.25	18.88	19.06	44.2	1880	39.0	12.20	12170	3500	0.1491	0.33910	2.520	208	10110

TABLE XXVI (continued)

$4\frac{3}{4}$" diameter rotor. Radial diffusion experiments. $\frac{3}{4}$" wide amalgamated band on outer cylinder

Calibration B - Figure 92

R 24	Temperature °c E	O	mean	Micro ammeter reading μa.DC	Rotor speed rpm	Air flow rate l/m	$\bar{u}$ cm/sec	c^* μgm/m³	c_2 μgm/m³	γ cm²/sec	$\ln \frac{c^*}{c^* - c_2}$	K cm/sec	Re_a	Re_c
3.5	19.25	18.88	19.06	44.5	2060	39.0	12.20	12170	3570	0.1491	0.34721	2.580	208	11070
3.5	19.25	18.88	19.06	45.7	2650	39.0	12.20	12170	3880	0.1491	0.38392	2.853	208	14250
7.4	18.35	18.14	18.24	16.5	0	63.2	19.80	11370	650	0.1483	0.05887	0.709	339	0
7.4	19.10	18.62	18.86	25.5	480	63.2	19.80	11370	1250	0.1483	0.11039	1.330	339	2595
7.4	19.10	18.62	18.86	30.0	914	63.2	19.80	11370	1600	0.1483	0.14362	1.732	339	4940
7.4	18.75	18.25	18.50	31.3	1140	63.2	19.80	11370	1710	0.1483	0.15429	1.861	339	6175
7.4	18.75	18.25	18.50	32.7	1400	63.2	19.80	11370	1840	0.1483	0.17223	2.079	339	7560
7.4	18.75	18.25	18.50	33.9	1830	63.2	19.80	11370	1970	0.1483	0.18560	2.236	339	9880
7.4	18.35	18.14	18.24	36.9	2750	63.2	19.80	11370	2330	0.1483	0.22932	2.765	339	14880
7.4	18.35	18.14	18.24	38.7	3450	63.2	19.80	11370	2550	0.1483	0.25396	3.060	339	18650
12.8	18.22	17.50	17.86	13.3	0	98.5	30.85	11010	480	0.1480	0.04458	0.839	529	0
12.8	18.25	17.25	17.75	14.5	200	98.5	30.85	10920	540	0.1480	0.05072	0.953	529	1084
12.8	18.25	17.25	17.75	19.0	500	98.5	30.85	10920	790	0.1480	0.07510	1.410	529	2712
12.8	18.25	17.25	17.75	22.4	800	98.5	30.85	10920	1025	0.1480	0.09860	1.852	529	4340
12.8	18.25	17.25	17.75	23.4	1000	98.5	30.85	10920	1095	0.1480	0.10567	1.984	529	5420
12.8	18.25	17.25	17.75	25.8	1600	98.5	30.85	10920	1270	0.1480	0.12364	2.322	529	8670
12.8	18.22	17.50	17.86	28.3	2100	98.5	30.85	11010	1460	0.1480	0.14226	2.675	529	11380
12.8	18.22	17.50	17.86	30.0	2640	98.5	30.85	11010	1595	0.1480	0.15650	2.941	529	14290
12.8	18.22	17.50	17.86	31.0	3100	98.5	30.85	11010	1675	0.1480	0.16503	3.101	529	16810
12.8	18.22	17.50	17.86	31.7	3460	98.5	30.85	11010	1750	0.1480	0.17310	3.260	529	18730
24.0	19.75	19.37	19.56	9.0	0	186.5	58.40	12660	300	0.1496	0.02398	0.853	993	0
24.0	19.75	19.37	19.56	9.2	160	186.5	58.40	12660	305	0.1496	0.02439	0.867	993	857
24.0	19.90	19.75	19.83	13.0	475	186.5	58.40	12970	465	0.1496	0.03652	1.298	993	2550
24.0	19.90	19.75	19.83	15.0	870	186.5	58.40	12970	565	0.1496	0.04454	1.582	993	4660
24.0	19.85	19.68	19.76	17.6	1225	186.5	58.40	12880	710	0.1496	0.05670	2.017	993	6560
24.0	19.80	19.61	19.71	20.0	1850	186.5	58.40	12830	855	0.1496	0.06897	2.452	993	9910
24.0	19.75	19.58	19.66	21.6	2610	186.5	58.40	12780	965	0.1496	0.07851	2.790	993	14000
24.0	19.75	19.55	19.65	23.0	3400	186.5	58.40	12770	1070	0.1496	0.02439	3.114	993	18220
27.0	17.90	19.05	18.48	8.3	10	213.0	66.70	11600	270	0.1486	0.02355	0.958	1123	54
27.0	17.90	19.05	18.48	13.0	1100	213.0	66.70	11600	470	0.1486	0.04136	1.682	1123	5940
27.0	17.90	19.05	18.48	18.5	2800	213.0	66.70	11600	760	0.1486	0.06776	2.759	1123	15110
27.0	17.90	19.05	18.48	20.2	3430	213.0	66.70	11600	870	0.1486	0.07703	3.135	1123	18490

TABLE XXVII

5.18" diameter rotor. Radial diffusion experiments. $\frac{3}{4}$" wide amalgamated band on outer cylinder

Calibration D - Figure 94

R 18	Temperature E	Temperature O	o_c mean	Micro ammeter reading μa.DC	Rotor speed rpm	Air flow rate l/m	$\bar{u}$ cm/sec	C^* μgm/m³	C_2 μgm/m³	ν cm²/sec	$\ln \frac{C^*}{C^* - C_2}$	K cm/sec	Re_a	Re_c
2.60	19.00	21.16	20.08	24.5	22	16.5	8.73	13280	3190	0.1501	0.27471	0.864	84	73
2.60	19.00	21.16	20.08	24.5	44	16.5	8.73	13280	3190	0.1501	0.27471	0.864	84	133
2.60	19.25	21.25	20.25	26.2	121	16.5	8.73	13450	3710	0.1503	0.32270	1.014	84	402
2.60	19.25	21.25	20.25	29.8	228	16.5	8.73	13450	5175	0.1503	0.48570	1.528	84	758
2.60	19.25	21.25	20.25	33.0	490	16.5	8.73	13450	6980	0.1503	0.73180	2.304	84	1629

Calibration B - Figure 94

R 18														
6.5	20.90	22.90	21.90	29.5	490	27.9	14.75	15410	4730	0.1519	0.36664	1.955	141	1590
6.5	20.90	22.90	21.90	30.8	570	27.9	14.75	15410	5300	0.1519	0.42068	2.240	141	1852
6.5	20.90	22.90	21.90	33.4	920	27.9	14.75	15410	6650	0.1519	0.56531	3.014	141	3025
6.5	20.90	22.90	21.90	34.9	1100	27.9	14.75	15410	7580	0.1519	0.65180	3.474	141	3610
6.5	20.90	22.90	21.90	35.7	1510	27.9	14.75	15410	8170	0.1519	0.75565	4.029	141	4970
6.5	20.90	22.90	21.90	36.1	1740	27.9	14.75	15410	8500	0.1519	0.80200	4.270	141	5720
6.5	20.90	22.90	21.90	36.8	2160	27.9	14.75	15410	9150	0.1519	0.90016	4.800	141	7100
6.5	20.90	22.90	21.90	38.0	2650	27.9	14.75	15410	10200	0.1519	1.08519	5.780	141	8710
10.05	21.00	23.00	22.00	16.5	80	39.0	20.6	15550	1950	0.1520	0.13366	0.994	196	263
10.05	21.00	23.00	22.00	22.1	300	39.0	20.6	15550	2360	0.1520	0.16500	1.227	196	984
10.05	21.00	23.00	22.00	26.3	560	39.0	20.6	15550	3670	0.1520	0.26780	1.990	196	1840
10.05	21.60	23.20	22.40	29.9	930	39.0	20.6	15550	4895	0.1524	0.37803	2.812	196	3045
10.05	21.60	23.20	22.40	31.1	1070	39.0	20.6	15550	5440	0.1524	0.43015	3.201	196	3500
10.05	21.00	23.00	22.00	31.8	1270	39.0	20.6	15550	5780	0.1520	0.46460	3.454	196	4170
10.05	21.60	23.20	22.40	34.0	2210	39.0	20.6	15550	6990	0.1520	0.59690	4.440	196	7240
10.05	21.60	23.20	22.40	34.2	2700	39.0	20.6	15550	7180	0.1520	0.77288	5.750	196	8840
15.1	21.70	23.50	22.60	13.5	100	55.8	29.5	16310	1550	0.1526	0.09980	1.063	280	328
15.1	21.70	23.50	22.60	19.2	370	55.8	29.5	16310	2350	0.1526	0.15529	1.653	280	1196
15.1	21.70	23.50	22.60	22.0	560	55.8	29.5	16310	2790	0.1526	0.18648	1.985	280	1830
15.1	21.70	23.50	22.60	26.9	1050	55.8	29.5	16310	3825	0.1526	0.26697	2.842	280	3434
15.1	21.70	23.50	22.60	29.0	1670	55.8	29.5	16310	4530	0.1526	0.32498	3.460	280	5460
15.1	21.70	23.50	22.60	29.9	2180	55.8	29.5	16310	4900	0.1526	0.35630	3.798	280	7120
15.1	21.70	23.50	22.60	30.9	2650	55.8	29.5	16310	5345	0.1526	0.39778	4.235	280	8680

TABLE XXVII (continued)

5.18" diameter rotor. Radial diffusion experiments. $\frac{3}{4}$" wide amalgamated band on outer cylinder

Calibration B - Figure 94 (continued)

R 35	Temperature °c E	O	mean	Micro ammeter reading μa.DC	Rotor speed rpm	Air flow rate l/m	$\bar{u}$ cm/sec	C^* μgm/m³	C_2 μgm/m³	ν cm²/sec	$\ln \frac{C^*}{C^* - C_2}$	K cm/sec	Re_a	Re_c
2.9	20.13	21.87	21.00	7.2	64	89.0	47.0	14310	760	0.1292	0.05457	0.925	451	212
2.9	20.13	21.87	21.00	7.2	139	89.0	47.0	14310	760	0.1292	0.05457	0.925	451	459
2.9	20.13	21.87	21.00	9.9	500	89.0	47.0	14310	1110	0.1292	0.08074	1.370	451	1649
2.9	20.13	21.87	21.00	12.8	1100	89.0	47.0	14310	1460	0.1292	0.10762	1.826	451	3303
2.9	20.13	21.87	21.00	15.1	1650	89.0	47.0	14310	1765	0.1292	0.13164	2.232	451	5450
2.9	20.13	21.87	21.00	16.2	2050	89.0	47.0	14310	1910	0.1292	0.14326	2.430	451	6770
2.9	20.13	21.87	21.00	17.5	2550	89.0	47.0	14310	2100	0.1292	0.15870	2.692	451	8420
R 18														
26.6	22.60	23.60	23.10	6.9	100	101.2	53.6	16980	855	0.1530	0.05442	1.050	507	326
26.6	22.60	23.60	23.10	9.5	301	101.2	53.6	16980	1070	0.1530	0.06391	1.235	507	981
26.6	22.60	23.60	23.10	11.1	410	101.2	53.6	16980	1255	0.1530	0.07511	1.450	507	1322
26.6	22.60	23.60	23.10	12.4	550	101.2	53.6	16980	1405	0.1530	0.08710	1.682	507	1773
26.6	22.60	23.60	23.10	14.0	840	101.2	53.6	16980	1610	0.1530	0.09803	1.895	507	2710
26.6	22.60	23.60	23.10	18.0	1350	101.2	53.6	16980	2175	0.1530	0.12583	2.621	507	4400
26.6	22.60	23.60	23.10	19.0	1600	101.2	53.6	16980	2310	0.1530	0.14583	2.816	507	5215
26.6	22.60	23.60	23.10	19.9	1900	101.2	53.6	16980	2450	0.1530	0.15444	2.983	507	6190
26.6	22.60	23.60	23.10	20.7	2270	101.2	53.6	16980	2570	0.1530	0.16297	3.146	507	7400
26.6	22.60	23.60	23.10	21.3	2540	101.2	53.6	16980	2670	0.1530	0.17059	3.295	507	8280
R 35						Calibration C - Figure 94								
5.35	23.50	22.85	23.18	8.6	100	141.0	74.5	17100	795	0.1531	0.04766	1.265	702	326
5.35	23.62	22.85	23.24	9.3	215	141.0	74.5	17170	890	0.1531	0.05323	1.430	702	700
5.35	23.75	22.85	23.30	10.2	272	141.0	74.5	17260	1010	0.1532	0.06030	1.622	702	887
5.35	23.75	22.85	23.30	12.0	520	141.0	74.5	17260	1272	0.1532	0.07640	2.055	702	1694
5.35	24.05	22.85	23.45	14.8	1060	141.0	74.5	17480	1680	0.1533	0.10100	2.714	702	3450
5.35	24.05	22.85	23.45	17.2	1620	141.0	74.5	17480	2120	0.1533	0.12930	3.478	702	5270
5.35	24.05	22.85	23.45	18.9	2050	141.0	74.5	17480	2480	0.1533	0.15170	4.070	702	6690
5.35	24.35	23.00	23.68	20.2	2650	141.0	74.5	17820	2745	0.1536	0.16730	4.500	702	8620

TABLE XXVII (continued)

5.18" diameter rotor. Radial diffusion experiments. $\frac{3}{4}$" wide amalgamated band on outer cylinder

Calibration B - Figure 94

R 35	Temperature °c E	Temperature °c O	Temperature °c main	Micro ammeter reading μa.DC	Rotor speed rpm	Air flow rate l/m	$\bar{u}$ cm/sec	C^* μgm/m³	C_2 μgm/m³	ν cm²/sec	$\ln \frac{C^*}{C^* - C_2}$	K cm/sec	Re_a	Re_c
15.8	24.10	24.10	24.10	3.2	290	310	163.8	18420	660	0.1539	0.03680	2.178	1533	939
15.8	24.10	24.10	24.10	3.5	320	310	163.8	18420	675	0.1539	0.03730	2.204	1533	1038
15.8	24.10	24.10	24.10	5.1	420	310	163.8	18420	700	0.1539	0.04120	2.438	1533	1362

Calibration C - Figure 94

R 35														
15.8	25.75	24.00	24.88	11.9	1050	310	163.8	19620	1256	0.1547	0.06617	3.915	1533	3386
15.8	26.25	23.75	25.00	12.8	1290	310	163.8	19810	1388	0.1547	0.07260	4.290	1533	4164
15.8	25.75	24.00	24.88	13.2	1500	310	163.8	19620	1447	0.1547	0.07678	4.550	1533	4840
15.8	26.25	23.75	25.00	13.9	1610	310	163.8	19810	1554	0.1547	0.08170	4.830	1533	5199
15.8	26.25	23.75	25.00	15.2	1990	310	163.8	19810	1762	0.1547	0.09305	5.510	1533	6420
15.8	26.25	23.75	25.00	16.2	2650	310	163.8	19810	1933	0.1547	0.10270	6.065	1533	8560

Calibration E - Figure 95

R 35														
26.5	22.62	23.75	23.19	12.0	100	520	275.0	17110	420	0.1531	0.02485	2.470	2600	325
26.5	22.62	23.75	23.19	12.0	200	520	275.0	17110	420	0.1531	0.02485	2.470	2600	651
26.5	22.62	23.75	23.19	12.0	400	520	275.0	17110	420	0.1531	0.02485	2.470	2600	1300
26.5	22.62	23.75	23.19	13.0	550	520	275.0	17110	530	0.1531	0.03147	3.122	2600	1790
26.5	22.62	23.75	23.19	13.8	600	520	275.0	17110	610	0.1531	0.03630	3.604	2600	1951
26.5	22.62	23.75	23.19	14.0	650	520	275.0	17110	640	0.1531	0.03812	3.785	2600	2118
26.5	22.62	23.75	23.19	16.9	1610	520	275.0	17110	950	0.1531	0.05710	5.670	2600	5240
26.5	22.62	23.75	23.19	19.0	2230	520	275.0	17110	1200	0.1531	0.07272	7.225	2600	7270
26.5	22.62	23.75	23.19	21.3	2630	520	275.0	17110	1480	0.1531	0.09047	8.990	2600	8560

TABLE XXVIII

$2\frac{3}{8}$" diameter rotor. Conditions for vortex appearance.

At $Re_a = 0$, critical Ta = 155.7 (Taylor theory); $b/r_m = 0.831$

R 14	Temperature °c E	O	mean	Change in micro ammeter reading μa.DC	Critical rotor speed rpm	Air flow rate l/m	$\bar{u}$ cm/sec	ν cm^2/sec	Ta	Re_a
13.1	16.78	17.50	17.14	19.0/19.5	69	25.0	3.00	0.1474	988	175
R 24										
7.4	17.00	18.12	17.56	11.2/11.8	144	63.1	7.56	0.1477	2057	438
12.8	17.25	18.12	17.69	9.1/ 9.6	220	98.5	11.80	0.1478	3140	684
18.2	17.38	18.10	17.74	8.0/ 8.5	316	139.5	16.72	0.1478	4510	971
24.0	17.61	18.04	17.83	6.5/ 7.0	462	186.0	22.29	0.1479	6600	1292
27.0	17.38	17.90	17.64	5.9/ 6.2	604	213.0	25.50	0.1478	8630	1483

TABLE XXIX

$3\frac{1}{8}$" diameter rotor. Conditions for vortex appearance

At $Re_a = 0$, critical Ta = 85.3 (Taylor Theory). $^b/_{r_m} = 0.591$

R 14	Temperature °c E	Temperature °c O	Temperature °c mean	Change in micro ammeter reading μa.DC	Critical rotor speed rpm	Air flow rate l/m	$\bar{u}$ cm/sec	ν cm^2/sec	Ta	Re_a
6.7	17.5	18.5	18.0	33.8/34.2	32	14.3	2.01	0.1481	327	91
14.4	17.5	18.5	18.0	24.8/25.2	60	27.1	3.83	0.1481	614	173
R 24										
7.4	18.1	18.1	18.1	13.4/13.8	43	63.2	8.93	0.1482	440	403
1.5	18.1	18.1	18.1	23.8/24.2	54	27.0	3.81	0.1482	552	172
3.3	18.1	18.1	18.1	18.8/19.3	60	38.1	5.38	0.1482	614	243
12.8	18.0	18.0	18.0	10.5/11.0	66	98.5	13.91	0.1481	675	626
18.2	18.0	18.0	18.0	8.3/ 8.9	91	139.5	19.71	0.1481	930	889
24.0	18.0	18.0	18.0	7.6/ 8.0	141	186.0	26.25	0.1481	1441	1183
27.0	18.0	18.0	18.0	6.1/ 6.6	178	213.0	30.08	0.1481	1818	1358
R 35										
19.7	20.40	19.75	20.07	18.5/18.6	420	383.0	54.1	0.1501	4240	2410
24.1	20.00	20.86	20.43	12.0/12.1	700	475.0	67.1	0.1504	7050	2990
26.5	20.10	19.60	19.85	7.8/ 7.9	1000	525.0	74.2	0.1499	10110	3310

TABLE XXX

$4\frac{3}{4}$" diameter rotor. Conditions for vortex appearance

At $Re_a = 0$, critical Ta = 49.0 (Taylor theory); $b/r_m = 0.190$

	Temperature °c			Change in micro ammeter reading μa.DC	Critical rotor speed rpm	Air flow rate l/m	$\bar{u}$ cm/sec	ν cm^2/sec	Ta	Re_a
R 7	E	O	mean							
12.89	17.50	18.00	17.75	27.6/28.4	24	4.5	1.39	0.1479	62.7	23.9
17.75	17.80	18.00	17.90	24.6/25.2	28	6.1	1.89	0.1480	73.4	32.5
27.35	17.30	17.75	17.52	17.8/18.6	32	9.7	3.03	0.1477	83.8	41.0
R 24 off	17.00	17.45	17.42	25.0/25.5	13	0	0	0.1476	49.0	0
3.4	18.65	18.00	18.32	18.9/19.2	38	38.0	11.87	0.1484	98.6	203
0.3	18.65	18.00	18.32	25.0/25.5	54	20.0	6.26	0.1484	140.5	107
7.7	17.00	17.45	17.42	12.0/12.5	54	65.0	20.34	0.1476	141.2	350
7.7	18.90	17.85	18.40	12.3/12.9	58	65.0	20.34	0.1485	151.1	348
0.3	17.00	17.45	17.42	22.0/22.5	59	20.0	6.26	0.1476	154.2	108
13.5	18.90	17.85	18.40	10.9/11.5	86	103.0	32.20	0.1485	224.0	551
13.5	17.00	17.45	17.42	6.8/ 7.6	89	103.0	32.20	0.1476	233.0	554
20.5	18.00	18.35	18.17	5.8/ 6.5	135	158.0	49.40	0.1483	352.0	846
20.5	18.90	17.85	18.40	7.2/ 8.0	136	158.0	49.40	0.1485	354.0	846
26.2	18.90	17.85	18.40	6.8/ 7.4	185	205.0	64.10	0.1485	481.0	1100
27.0	18.00	18.35	18.17	5.5/ 6.2	190	213.0	66.60	0.1483	495.0	1140

TABLE XXXI

5.18" diameter rotor. Conditions for vortex appearance

At $Re_a = 0$, critical Ta = 45.0 (Taylor theory) ; $b/r_m = 0.104$

R 14	Temperature °c E	Temperature °c O	Temperature °c mean	Change in micro ammeter reading μa.DC	Critical rotor speed rpm	Air flow rate l/m	$\bar{u}$ cm/sec	ν cm^2/sec	Ta	Re_a
1.60	21.52	22.0	21.76	29.9 / 30.0	42	6.8	3.60	0.1518	47	34
4.00	21.52	22.0	21.76	26.4 / 26.5	47	10.4	5.50	0.1518	53	53
7.50	21.52	22.0	21.76	22.5 / 22.6	50	15.8	8.36	0.1518	56	80
9.60	21.52	22.0	21.76	21.1 / 21.2	50	19.1	10.09	0.1518	56	96
R 18										
2.20	20.50	21.00	20.75	24.8 / 24.9	66	15.2	8.04	0.1508	74	77
3.75	20.50	21.00	20.75	22.9 / 23.0	81	19.9	10.52	0.1508	91	101
6.50	20.50	21.00	20.75	19.9 / 20.0	108	27.9	14.74	0.1508	122	142
8.00	20.75	21.00	20.88	17.9 / 18.0	116	32.5	17.18	0.1509	130	165
10.05	20.50	21.00	20.75	16.7 / 16.8	88	30.9	20.61	0.1508	99	198
15.10	20.12	21.88	21.00	12.5 / 12.6	140	55.8	29.50	0.1510	157	283
17.80	20.12	21.88	21.00	11.6 / 11.7	148	66.3	35.10	0.1510	166	337
20.60	20.12	21.88	21.00	9.9 / 10.0	168	76.5	40.40	0.1510	187	388
26.60	22.60	23.60	23.10	6.9 / 7.0	188	101.2	53.55	0.1530	209	507
R 35										
2.90	20.12	21.88	21.00	7.2 / 7.3	139	89.0	47.00	**0.1510**	156	451
5.85	23.50	22.85	23.18	8.6 / 8.7	180	141.0	74.50	**0.1531**	200	702
5.85	23.63	23.63	23.63	5.8 / 5.9	192	141.0	74.50	0.1535	209	702
12.1	25.00	23.80	24.40	15.6 / 15.7	244	244.0	129.00	0.1542	268	1211
15.8	24.10	24.10	24.10	3.2 / 3.3	290	310.0	164.00	0.1539	320	1442
26.5	22.60	23.78	23.19	13.0 / 13.1	550	520.0	275.00	0.1531	609	2600

TABLE XXXII

$2\frac{3}{8}$" diameter rotor. Calibration (Figure 89)

Hg vapour R 7	Air R 14	$l/_m$ 7	$l/_m$ 14	^oc E	c^* $\mu gm/m^3$	c_2 $\mu gm/m^3$	micro ammeter $\mu a.DC$
0.05	14.20	0.78	26.70	16.25	9610	273	10.3
0.80	14.00	1.00	26.50	16.25	9610	349	12.2
1.80	13.80	1.25	26.25	16.22	9580	435	14.3
4.50	13.60	1.96	25.90	16.20	9570	673	19.5
5.40	13.40	2.23	25.60	16.15	9520	762	21.8
8.05	12.90	2.91	24.60	16.10	9480	1002	26.9
11.30	12.30	3.92	23.70	16.10	9480	1343	33.2
13.40	11.85	4.65	22.90	16.10	9480	1599	37.0
16.20	11.20	5.60	21.80	16.10	9480	1938	41.1
18.70	10.55	6.42	20.60	16.10	9480	2253	44.6
19.95	9.50	6.87	18.90	16.20	9570	2553	47.7

TABLE XXXIII

$3\frac{1}{8}$" diameter rotor. Calibration A (Figure 90)

0	23.80	0.75	44.4	18.30	11430	190	6.0
0	15.00	0.75	28.1	18.30	11430	297	12.1
0.95	14.60	1.01	27.5	17.15	10820	384	15.0
2.35	14.60	1.36	27.5	17.15	10820	510	18.0
5.50	14.30	2.24	27.0	17.15	10820	829	24.9
8.28	13.85	3.01	26.3	17.15	10820	1111	30.7
10.88	13.60	3.80	25.9	17.15	10820	1386	35.8
15.30	12.95	5.20	24.6	17.15	10820	1890	43.3
18.25	12.55	6.25	24.0	17.15	10820	2234	47.9

$3\frac{1}{8}$" diameter rotor. Calibration B (Figure 90)

closed	closed	0	0	16.00	9410	0	14.8
1.20	10.00	1.1	19.7	16.00	9410	497	25.0
3.00	9.80	1.6	19.4	16.00	9410	717	28.7
5.70	9.45	2.3	18.8	16.00	9410	1026	34.7
8.80	9.10	3.2	18.3	16.00	9410	1401	40.5

TABLE XXXIII (continued)

$3\frac{1}{8}$" diameter rotor. Calibration C (Figure 91)

Hg vapour R 7	Air R 14	Air R 35	$l/_m$ 7	$l/_m$ 14	$l/_m$ 35	o_c E	c^* $\mu gm/m^3$	c_2 $\mu gm/m^3$	Micro ammeter μa.DC
4.10	7.40	17.25	1.84	15.7	336	19.80	12940	67.4	8.0
4.15	7.40	14.10	1.85	15.7	279	19.78	12910	80.5	9.4
4.09	7.40	11.90	1.83	15.7	241	19.75	12880	91.0	12.0
4.04	7.35	9.37	1.82	15.6	198	19.70	12820	108.3	14.5
4.05	7.30	7.00	1.82	15.5	160	19.63	12750	130.9	19.5
4.10	7.15	1.20	1.84	15.3	68	18.63	11730	253.2	30.0
6.98	6.80	2.90	2.67	14.8	94	18.63	11730	281.0	31.2
11.00	5.95	2.90	3.85	13.4	94	18.65	11760	410.0	37.4
8.85	6.30	1.20	3.22	14.0	68	18.48	11590	437.8	40.0

$3\frac{1}{8}$" diameter rotor. Calibration D (Figure 91)

2.90	8.20	16.00	1.52	16.80	313	20.13	13300	61.1	4.0
3.05	8.40	13.50	1.54	16.95	268	20.13	13300	70.0	7.5
3.05	8.40	11.75	1.54	16.95	237	20.13	13300	80.1	10.0
3.52	8.75	7.30	1.69	17.70	164	19.63	12750	117.4	19.0
5.55	7.90	6.00	2.26	16.50	143	19.88	13040	182.2	27.2
8.25	7.35	6.00	3.03	15.60	143	19.88	13040	244.6	31.7
11.55	7.00	6.00	4.01	15.10	143	19.88	13040	323.0	35.8

TABLE XXXIV

$4\frac{3}{4}$" diameter rotor. Calibration A (Figure 92)

Hg vapour R 7	Air R 14	$l/_m$ 7	$l/_m$ 14	o_c E	c^* $\mu gm/m^3$	c_2 $\mu gm/m^3$	Micro ammeter μa. DC
5.3	23.1	2.18	42.9	17.75	10920	528	6.2
7.6	24.5	2.84	46.0	18.60	11720	682	9.8
5.6	16.5	2.27	30.8	18.20	11340	779	12.9
10.8	15.9	3.80	29.7	18.20	11340	1286	21.5
19.7	15.1	6.74	28.3	18.20	11340	2180	31.0
24.4	12.7	8.53	24.2	18.80	11910	3105	36.6
27.9	9.9	9.95	19.5	17.75	10920	3690	39.0
28.2	6.3	10.07	14.0	17.75	10920	4570	42.4

$4\frac{3}{4}$" diameter rotor. Calibration B (Figure 92)

closed	closed	0	0	18.45	11570	0	0.5
0	10.50	0.75	20.6	18.45	11570	406	11.0
0.2	11.00	0.82	21.3	18.45	11570	428	13.3
1.0	11.00	1.02	21.3	18.45	11570	529	15.0
2.55	10.75	1.39	21.0	18.45	11570	718	18.0
5.00	10.45	2.10	20.5	18.45	11570	1074	23.1
7.25	10.10	2.70	19.9	18.45	11570	1381	27.2
9.30	9.80	3.33	19.5	18.45	11570	1686	31.1
11.40	9.40	3.97	18.75	18.45	11570	2020	34.7
13.90	9.10	4.75	18.2	18.45	11570	2392	37.3
16.85	8.40	5.76	17.1	18.45	11570	2914	41.0
19.65	17.7	6.74	16.25	18.45	11570	3394	44.0
21.90	7.10	7.60	15.30	18.45	11570	3871	46.0
23.50	6.50	8.21	14.10	18.45	11570	4455	47.3

$4\frac{3}{4}$" diameter rotor. Calibration C (Figure 92)

0.32	25.3	0.90	48.00	18.30	11430	210	4.0
1.30	25.3	1.12	48.00	18.30	11430	260	5.2
0.45	16.8	0.92	31.30	18.30	11430	327	8.0
1.20	16.8	1.10	31.30	18.30	11430	388	9.2
2.78	16.55	1.48	30.84	18.30	11430	524	12.1
6.30	16.20	2.47	30.20	18.30	11430	866	17.8
9.0	15.95	3.27	29.81	18.20	11340	1120	23.8
11.10	15.75	3.90	29.46	18.20	11340	1325	26.9
13.25	15.80	4.56	29.54	18.20	11340	1518	29.7
18.70	14.85	6.46	27.90	18.10	11240	2084	35.8
25.05	13.95	8.70	26.41	18.10	11240	2786	42.1
26.35	11.75	9.31	22.70	18.10	11240	3266	45.7

$4\frac{3}{4}$" diameter rotor. Calibration D (Figure 93)

0.1	10.55	0.80	20.70	17.25	10470	389	8.2
0.9	10.50	1.00	20.50	17.25	10470	486	9.2
2.4	10.30	1.33	20.10	17.25	10470	648	11.3
3.4	10.20	1.68	20.00	17.25	10470	811	13.9
4.5	10.05	1.96	19.90	17.25	10470	937	16.1
6.35	9.85	2.45	19.46	17.25	10470	1171	18.2
7.95	9.60	2.96	19.08	17.25	10470	1403	20.2

TABLE XXXV

5.18" diameter rotor. Calibration A (Figure 94)

Hg vapour R 7	Air R 14	$1/_m$ 7	$1/_m$ 14	o_c E	c^* $\mu gm/m^3$	c_2 $\mu gm/m^3$	Micro ammeter μa.DC
1.2	10.0	1.10	19.70	18.75	11860	627	7.4
2.9	9.6	1.52	19.06	19.00	12120	896	8.9
5.8	9.3	2.33	18.58	19.25	12370	1378	11.4
8.3	8.7	3.05	17.60	19.50	12620	1865	13.6
11.4	8.2	3.98	16.95	19.55	12670	2411	16.1
14.8	7.4	5.08	15.70	19.63	12750	3118	19.0
18.2	6.6	6.22	14.45	19.80	12940	3896	21.1
22.6	5.3	7.82	12.47	19.90	13050	5030	23.8
25.8	4.2	9.08	10.60	20.10	13290	6130	25.5
29.4	2.5	10.60	8.10	20.18	13370	7580	27.8
29.1	1.3	10.47	6.35	20.25	13450	7890	28.1
29.3	0.8	10.55	5.60	20.25	13450	8790	29.0

5.18" diameter rotor. Calibration B (Figure 94)

0	8.30	0.75	16.9	20.8	14070	597	3.5
0.20	8.60	0.83	17.5	20.8	14070	637	3.6
1.35	8.40	1.13	17.2	20.8	14070	867	5.8
1.70	8.10	1.20	16.8	20.8	14070	937	8.7
2.45	7.95	1.40	16.6	20.8	14070	1096	9.8
3.60	7.90	1.70	16.5	20.8	14070	1313	12.0
4.70	7.70	2.00	16.2	20.8	14070	1546	13.6
5.90	7.40	2.35	15.7	20.8	14070	1831	15.4
6.80	7.20	2.63	15.4	20.8	14070	2048	17.1
7.90	7.00	2.94	15.1	20.8	14070	2292	18.9
9.00	6.80	3.27	14.8	20.8	14070	2545	20.6
10.10	6.52	3.60	14.3	20.8	14070	2822	22.1
11.90	6.05	4.15	13.6	20.8	14070	3291	24.6
14.00	5.60	4.81	12.9	20.8	14070	3820	26.9
16.50	5.10	5.63	12.1	20.8	14070	4465	28.9
18.40	4.45	6.27	11.0	20.8	14070	5110	30.3
20.20	3.85	6.93	10.1	20.8	14070	5730	31.7
22.00	3.30	7.63	9.3	20.8	14070	6340	32.8
25.70	2.00	9.01	7.4	20.8	14070	7715	35.1
28.50	1.05	10.20	6.0	20.8	14070	8850	36.5
29.70	0.50	10.66	5.2	20.8	14070	9460	37.0
30.00	0.20	10.90	4.8	20.8	14070	9770	37.5

TABLE XXXV (continued)

5.18" diameter rotor. Calibration C (Figure 94)

Hg vapour R 7	Air R 14	$1/_m$ 7	$1/_m$ 14	o_c E	c^* $\mu gm/m^3$	c_2 $\mu gm/m^3$	Micro ammeter $\mu a.DC$
0.10	8.00	0.76	16.67	20.60	13840	604	7.0
0.60	8.00	0.95	16.67	20.60	13840	746	8.2
1.40	7.85	1.13	16.42	20.65	13910	896	9.2
2.50	7.60	1.42	16.01	20.80	14070	1145	11.2
4.00	7.30	1.81	15.54	20.88	14170	1477	13.5
5.75	7.10	2.31	15.23	20.88	14170	1867	15.6
7.30	6.75	2.75	14.70	20.90	14190	2237	17.8
9.20	6.45	3.33	14.22	20.95	14270	2703	20.2
11.10	6.00	3.90	13.52	21.00	14320	3203	21.9

5.18 diameter rotor. Calibration D (Figure 94)

0.1	9.35	0.78	18.66	17.30	10520	421	8.1
1.2	9.10	1.10	18.30	17.25	10470	594	9.0
3.0	8.90	1.54	17.91	17.25	10470	829	10.6
4.0	8.65	1.81	17.55	17.40	10600	990	13.0
5.0	8.50	2.10	17.35	17.38	10590	1146	14.2
6.0	8.25	2.38	17.00	17.50	10690	1312	15.3
7.3	8.00	2.75	16.65	17.60	10790	1520	16.8
9.8	7.60	3.49	16.00	17.60	10790	1932	19.0
11.6	7.14	4.05	15.30	17.65	10820	2263	20.8
13.9	6.70	4.77	14.57	17.65	10820	2670	22.7
16.6	6.00	5.66	13.50	17.80	10970	3241	24.3
19.2	5.00	6.56	11.98	17.80	10970	3873	26.6
22.6	4.00	7.82	10.35	17.80	10970	4715	28.8
26.2	2.70	9.22	8.40	17.80	10970	5740	31.1
28.2	1.90	10.07	7.23	17.80	10970	6380	32.1
29.3	1.10	10.55	6.04	17.80	10970	6980	33.0

5.18" diameter rotor. Calibration E (Figure 95)

0.10	8.65	0.76	17.60	22.75	16520	684	14.5
0.70	8.60	0.95	17.52	22.75	16520	850	15.9
1.30	8.55	1.12	17.46	22.75	16520	996	17.2
2.80	8.20	1.49	16.80	22.75	16520	1347	20.3
4.40	8.00	1.93	16.68	22.75	16520	1714	23.2
5.40	7.80	2.22	16.31	22.75	16520	1977	25.4
6.45	7.55	2.53	15.90	22.80	16570	2270	27.8
7.35	7.45	2.77	15.78	22.75	16520	2465	29.4
8.80	7.10	3.21	15.25	22.80	16570	2880	31.8
9.95	6.85	3.55	14.90	22.80	16570	3186	33.6
12.25	6.25	4.25	13.90	22.80	16570	3880	36.9
14.80	5.85	5.07	13.30	22.88	16670	4604	39.7
17.30	5.40	5.90	12.59	22.88	16670	5320	41.7
20.10	4.52	6.90	11.20	22.88	16670	6350	44.0
23.20	3.70	8.08	9.89	22.88	16670	7492	46.1
27.70	2.10	9.87	7.52	22.88	16670	9465	48.8

TABLE XXXVI

Values of K obtained from Figures 67 to 70 inclusive. Values of Kb calculated from this data and plotted, as a function of b/r_1, in Figure 71.

Rotor diameter inches	$\frac{b}{r_1}$	Re_c	Re_a	K from plot cm/sec	Kb cm^2/sec
5.18	0.11	1000	141	1.51	1.09
5.18	0.11	2000	141	2.33	1.69
5.18	0.11	2000	280	2.11	1.53
5.18	0.11	5000	280	3.35	2.43
$4\frac{3}{4}$	0.21	1000	144	0.87	1.11
$4\frac{3}{4}$	0.21	2000	144	1.16	1.47
$4\frac{3}{4}$	0.21	2000	238	1.36	1.73
$4\frac{3}{4}$	0.21	5000	238	2.04	2.59
$3\frac{1}{8}$	0.84	1000	121	0.59	1.95
$3\frac{1}{8}$	0.84	2000	121	0.80	2.65
$3\frac{1}{8}$	0.84	2000	241	0.83	2.77
$3\frac{1}{8}$	0.84	5000	241	1.27	4.23
$2\frac{3}{8}$	1.42	1000	112	0.45	1.93
$2\frac{3}{8}$	1.42	2000	112	0.62	2.65
$2\frac{3}{8}$	1.42	2000	262	0.60	2.55
$2\frac{3}{8}$	1.42	5000	262	0.82	3.51

TABLE XXXVII

$2\frac{3}{8}$" diameter rotor. Longitudinal diffusion experiments (figure 80).

Experiment No.	R_{14} begin	R_{14} end	^{o}c E	^{o}c O	rotor rpm
1	9.75	13.9	15.25	16.00	15
2	"	14.0	"	"	40
3	"	13.3	15.48	16.20	294
4	"	14.3	16.50	17.45	630
5	"	13.3	15.48	16.00	880
6	"	13.1	15.50	16.40	1180
7	"	14.5	16.48	17.20	1230
8	"	13.3	15.48	16.00	2200

Results

Experiment No.	θ_o from figure 80 secs.	$\bar{u} = \frac{61}{\theta_o}$ cm/sec	$(\text{slope})^2 \times 10^4$ sec^{-2}	D_L cm^2/sec	Re_c
1	14.7	4.15	54.8	2.3	139
2	20.8	2.93	95.9	3.4	371
3	23.7	2.57	30.2	7.3	2,725
4	25.5	2.39	29.1	6.1	5,840
5	24.5	2.49	17.6	11.4	8,160
6	30.8	1.98	17.6	5.8	10,921
7	25.7	2.57	27.1	7.6	11,400
8	27.0	2.26	8.4	17.9	20,403
	$\Sigma\bar{u}$ =	21.34	Take mean $\bar{u}$ =	2.7 cm/sec	

TABLE XXXVII (continued)

Time θ secs	Expt. 1 Cambridge Recorder reading (mv)	F(θ)	Expt. 2 Cambridge Recorder reading (mv)	F(θ)	Expt. 3 Cambridge Recorder reading (mv)	F(θ)	Expt. 4 Cambridge Recorder reading (mv)	F(θ)	Expt. 5 Cambridge Recorder reading (mv)	F(θ)	Expt. 6 Cambridge Recorder reading (mv)	F(θ)	Expt. 7 Cambridge Recorder reading (mv)	F(θ)	Expt. 8 Cambridge Recorder reading (mv)	F(θ)
0	58.0	0	41.7	0	36.3	0	58.4	0	36.8	0	48.0	0	67.2	0	89.5	0
3	58.0	0							36.6	.006			67.2	0		
6	57.0	.065	41.7	0	36.3	0	58.4	0	36.0	.025			67.2	0	89.5	0
9	55.3	.175							35.3	.047			67.2	0		
12	53.2	.312	41.7	0	36.3	0	58.4	0	34.5	.073	48.0	0	67.2	0	89.1	.012
15	50.0	.520					58.3	.005	33.0	.110			67.1	.006		
18	47.6	.676	37.3	.249	34.1	.089	56.2	.101	30.0	.204	48.0	0	66.2	.058	84.8	.146
21	46.7	.734	32.7	.509	27.7	.351	52.8	.258	25.9	.344			63.7	.201		
24	46.1	.773	26.8	.841	23.6	.519	49.3	.419	21.6	.479	45.1	.166	60.3	.397	76.4	.406
27	45.1	.799			20.5	.645	46.1	.566	18.0	.593	42.2	.331	57.4	.564		
30	44.8	.857	24.0	1.000	18.2	.739	43.2	.701	14.9	.691	39.8	.469	55.0	.701	70.7	.582
33	43.7	.928			16.1	.825	41.5	.779	12.8	.757	37.8	.583	52.8	.828		
36	43.5	.941			14.8	.878	40.1	.844	11.5	.798	36.8	.640	51.3	.913	67.0	.697
39	43.0	.973			14.0	.910			10.0	.847			50.4	.965		
42	42.9	.980			13.6	.926	38.9	.899	8.0	.908	34.8	.755	50.0	.988	63.9	.793
45	42.9	.980							7.8	.915			49.9	.997		
48	42.8	.987			12.2	.984	37.8	.949	6.0	.983	33.1	.851	49.8	1.000	62.2	.845
51	42.7	.993							5.5	.987						
54	42.6	1.000			11.8	1.000	36.8	.995	5.1	1.000	32.5	.886			61.0	.882
60							36.7	1.000			32.1	.909			60.0	.912
66											31.2	.960			59.5	.928
72											30.8	.983			58.8	.951
78											30.8	.983			58.2	.969
84											30.5	1.000			57.8	.981
90															57.5	.990
96															57.2	1.000

TABLE XXXVIII

$3\frac{1}{8}$" diameter rotor. Longitudinal diffusion experiments (figure 81a).

Experiment No.	R 14 begin	R 14 end	$^{o}_{c}$ E	$^{o}_{c}$ O	rotor rpm
1	10.1	12.6	16.88	17.88	98
2	9.6	12.4	"	"	308
3	9.4	11.0	"	"	670
4	9.4	12.7	"	"	1660
5	9.4	12.6	"	"	1660
6	9.9	12.5	"	"	2040
7	9.8	12.5	"	"	2040

Results

Experiment No.	θ_o from figure 81a secs	$\bar{u} = \frac{61}{\theta_o}$ cm/sec	$(\text{slope})^2 \times 10^{-4}$ sec^{-2}	D_L cm^2/sec	Re_c
1	22.0	2.75	33.60	8.1	922
2	23.4	2.61	38.40	6.0	2,890
3	29.4	2.07	13.65	8.5	6,310
4	23.4	2.61	26.00	8.9	15,610
5	29.6	2.06	33.60	3.4	15,610
6	24.4	2.50	11.55	17.6	19,190
7	29.1	2.10	5.74	21.0	19,190
		$\Sigma\bar{u}$ = 16.70			

Take mean $\bar{u}$ = 2.4 cm/sec

TABLE XXXVIII

$3\frac{1}{8}$" diameter rotor. Longitudinal diffusion experiments (figure 81b).

Experiment No.	R 14 begin	R 14 end	$^{o}_{c}$ E	$^{o}_{c}$ O	rotor rpm
8	6.6	10.3	19.25	21.0	60
9	6.0	9.5	"	"	890
10	6.1	9.6	"	"	1100
11	"	"	"	"	1250
12	5.5	9.2	17.38	20.88	1500
13	5.9	9.3	19.50	21.75	2120
14	"	"	"	"	2500

Results

Experiment No.	θ_o from figure 81b secs	$\bar{u} = \frac{61}{\theta_o}$ cm/sec	$(\text{slope})^2 \times 10^4$ sec^{-2}	D_L cm^2/sec	Re_c
8	17.4	3.51	67.2	8.4	554
9	18.8	3.25	28.0	15.9	8230
10	18.8	3.25	56.2	7.9	10,170
11	18.5	3.29	20.2	21.8	11,530
12	31.0	1.97	5.3	18.8	13,870
13	24.2	2.52	13.0	16.1	19,640
14	23.5	2.59	13.0	17.5	23,100
		$\Sigma\bar{u}$ = 20.38		Take mean $\bar{u}$ = 2.9	

TABLE XXXVIII (continued)

Time θ secs	Expt. 1 Cambridge Recorder reading (mv)	F(θ)	Expt. 2 Cambridge Recorder reading (mv)	F(θ)	Expt. 3 Cambridge Recorder reading (mv)	F(θ)	Expt. 4 Cambridge Recorder reading (mv)	F(θ)	Expt. 5 Cambridge Recorder reading (mv)	F(θ)	Expt. 6 Cambridge Recorder reading (mv)	F(θ)	Expt. 7 Cambridge Recorder reading (mv)	F(θ)	Expt. 8 Cambridge Recorder reading (mv)	F(θ)
0	60.3	0	67.9	0	80.8	0	73.8	0	80.4	0	72.8	0	84.9	0	73.3	0
3	60.3	0							80.4	0					73.3	0
6	60.2	.002	67.9	0	80.8	0	73.8	0	80.4	0	72.5	.008	84.9	0		
9	60.1	.004							80.4	0						
12	60.0	.006	67.9	0	80.2	.029	73.5	.008	80.4	0	72.2	.016	84.9	0	73.3	0
15	59.9	.009							80.4	0	70.0	.075			71.0	.277
18	56.5	.081	65.4	.086	78.6	.105	66.5	.183	80.4	0	65.3	.227	82.3	.097	68.8	.542
21	40.0	.431	58.2	.332			60.0	.347	79.3	.046	60.0	.343			67.6	.687
24	32.3	.595	52.1	.541	74.4	.307	53.0	.523	75.8	.194	55.2	.497	75.5	.351	66.6	.807
27	28.2	.681					47.3	.666	72.0	.354	51.8	.561	73.1	.440	65.6	.928
30	23.3	.786	46.0	.750	70.1	.512	42.0	.799	68.3	.511	48.8	.642	71.1	.515		
33	18.8	.881							63.9	.696			69.2	.586	65.0	1.000
36	15.2	.957	41.8	.893	65.2	.746	37.4	.915	62.6	.751	44.8	.740	67.5	.650		
39	13.3	.998							61.4	.802						
42	13.2	1.000	40.0	.956	61.7	.913	34.9	.977	60.7	.830	41.0	.850	64.9	.746		
45									59.7	.874						
48			39.1	.986	60.6	.966	34.0	1.000	58.8	.911	38.9	.908	62.9	.821		
51									58.1	.941						
54			38.9	.982	59.9	1.000			57.2	.978	38.0	.931	61.9	.859		
57									57.0	.987						
60			38.7	1.000					56.7	1.000	37.2	.952	60.8	.900		
66											35.8	.990	59.8	.937		
72											35.4	1.000	59.1	.962		
78													58.7	.978		
84													58.2	.996		
90													58.1	1.000		

TABLE XXXVIII (continued)

Time θ secs	Expt. 9 Cambridge Recorder reading (mv)	F(θ)	Expt. 10 Cambridge Recorder reading (mv)	F(θ)	Expt. 11 Cambridge Recorder reading (mv)	F(θ)	Expt. 12 Cambridge Recorder reading (mv)	F(θ)	Expt. 13 Cambridge Recorder reading (mv)	F(θ)	Expt. 14 Cambridge Recorder reading (mv)	F(θ)
0	72.4	0	75.6	0	43.7	0	61.0	0	63.0	0	53.0	0
6	72.4	0	75.6	0	43.7	0	61.0	0	63.0	0	53.0	0
9	72.6	.145			43.0	.041						
12	71.0	.274	75.0	.070	40.1	.206	61.0	0	63.0	0	52.0	.069
15			73.6	.233	37.9	.331			61.5	.115	50.6	.166
18	68.7	.460	71.9	.430	35.2	.486	57.5	.152	60.0	.231	48.6	.303
21			70.0	.651	33.6	.577	55.1	.239	58.0	.385	47.0	.414
24	65.6	.710	68.5	.826			53.2	.339	56.5	.500		
27					31.0	.726					44.0	.620
30	63.6	.872	67.1	.988			50.0	.479	54.1	.685		
33											41.7	.780
36	63.0	.920	67.0	1.000			47.0	.609	51.8	.862		
39					30.0	.782					40.4	.869
42	62.0	1.000					44.0	.740	50.2	.984		
45											40.0	.897
48							41.4	.852	50.0	1.000		
51					28.0	.897					39.0	.965
54							39.0	.956				
60							38.5	.979			38.5	1.000
63					27.5	.926						
66							38.0	1.000				
75					26.2	1.000						

TABLE XXXIX

$4\frac{3}{4}$" diameter rotor. Longitudinal diffusion experiments (figure 82).

Experiment No.	R 14 begin	R 14 end	$^{o}_{c}$ E	$^{o}_{c}$ O	rotor rpm
1	6.0	9.5	18.81	20.61	0
2	"	"	19.00	21.13	130
3	"	"	17.88	21.13	520
4	"	"	"	"	850
5	"	"	"	"	870
6	"	"	19.00	21.13	1320
7	"	"	17.88	"	1560
8	"	"	"	"	1860
9	"	"	19.00	"	2150
10	"	"	17.88	"	2340
11	"	"	"	"	2860
12	"	"	"	"	2470

Results

Experiment No.	θ_o from figure 82 secs	$\bar{u} = \frac{61}{\theta_o}$ cm/sec	slope^2 x 10^4 sec^{-2}	D_L cm^2/sec	Re_c
1	13.2	4.6	10000.0	0.14	0
2	12.7	4.8	400.0	3.7	696
3	12.0	5.1	3840.0	4.6	2780
4	13.8	4.4	484.0	2.4	4550
5	13.6	4.5	100.0	11.8	4710
6	12.7	4.8	121.0	12.0	7060
7	22.8	2.7	6.8	37.4	8350
8	22.0	3.1	5.3	51.5	9950
9	20.5	3.0	121.0	3.0	11620
10	32.1	1.9	4.8	18.7	11980
11	29.7	2.1	6.3	16.5	15310
12	25.7	2.4	9.0	19.8	18580
		$\Sigma\bar{u}$ = 43.4	Take mean $\bar{u}$ = 3.6		

TABLE XXXIX (continued)

Time θ secs	Expt. 1 Cambridge Recorder reading (mv)	F(θ)	Expt. 2 Cambridge Recorder reading (mv)	F(θ)	Expt. 3 Cambridge Recorder reading (mv)	F(θ)	Expt. 4 Cambridge Recorder reading (mv)	F(θ)	Expt. 5 Cambridge Recorder reading (mv)	F(θ)	Expt. 6 Cambridge Recorder reading (mv)	F(θ)	Expt. 7 Cambridge Recorder reading (mv)	F(θ)
0	78.2	0	74.8	0	73.5	0	64.7	0	71.5	0	71.5	0	63.5	0
3	78.2	0												
6	78.2	0	74.8	0	73.5	0	64.7	0	71.5	0	71.5	0	63.5	0
9	78.2	0			73.5	0	64.7	0	71.0	.010	71.0	.010	58.8	.114
10.5					71.1	.044								
12	75.3	.069	60.5	.387	41.8	.579	61.8	.080	58.0	.274	58.0	.274	49.6	.337
13.5	46.1	.760	56.2	.502			47.2	.482	46.5	.508	46.5	.508	39.0	.593
15	36.8	.981	53.3	.581	22.9	.923	41.0	.653	42.7	.585	42.7	.585	34.0	.715
18	36.3	.992	49.1	.694	21.5	.949	35.3	.810	39.4	.652	39.4	.652	30.8	.792
21	36.2	.994					32.0	.901	36.5	.711	36.5	.711		
24	36.2	.994	45.4	.794	20.3	.972							26.9	.886
27	36.0	1.000					30.0	.956	33.3	.776	33.3	.776		
30			43.3	.851	19.8	.980							25.1	.930
33							29.0	.982	31.0	.823	31.0	.823		
36			42.1	.883	19.0	.993							23.3	.976
39							28.7	.991	27.9	.886	27.9	.886		
42			41.2	.907	18.7	1.000							22.7	.987
45							28.4	1.000	26.4	.917	26.4	.917		
48			40.8	.919									22.2	1.000
51									25.6	.934	25.6	.934		
54			39.9	.943										
57									24.2	.960	24.2	.960		
60			38.5	.981										
63									23.7	.970	23.7	.970		
66			38.0	.995										
69									22.9	.987	22.9	.987		
72			37.8	1.000										
75									22.8	.991	22.8	.991		
81									22.3	1.000	22.3	1.000		

TABLE XXXIX (continued)

Time θ secs	Expt. 8 Cambridge Recorder reading (mv)	F(θ)	Expt. 9 Cambridge Recorder reading (mv)	F(θ)	Expt. 10 Cambridge Recorder reading (mv)	F(θ)	Expt. 11 Cambridge Recorder reading (mv)	F(θ)	Expt. 12 Cambridge Recorder reading (mv)	F(θ)
0	65.0	0	65.6	0	72.6	0	60.7	0	62.2	0
6	65.0	0	65.6	0	72.6	0	60.7	0	62.2	0
9	65.0	0			72.6	0	60.7	0		
12	64.5	.014	65.0	.024	71.7	.028	60.5	.009	61.8	.020
15	58.3	.187			69.4	.098	59.5	.053		
18	50.3	.411	58.7	.272	67.0	.191	58.4	.101	57.7	.223
21	47.7	.484	45.0	.583	64.6	.245	54.7	.264		
24	45.9	.534	42.0	.811			52.6	.357	53.2	.446
27					60.0	.385	50.9	.432		
30	42.9	.618	41.3	.929	57.6	.459	49.0	.515	49.5	.628
33					55.5	.523	47.5	.581		
36	40.3	.690	40.8	.957	53.4	.587	46.2	.639	46.9	.758
39					52.3	.621				
42	38.8	.731	40.2	.977			44.1	.730	45.1	.847
45					49.3	.712	43.0	.779		
48	37.8	.760	40.2	1.000			48.0	.794	44.0	.901
51					47.1	.780				
54	35.4	.826					54.0	.851	43.0	.950
57					44.9	.847				
60	34.3	.857					60.0	.886	42.8	.960
63					43.6	.887				
66	32.5	.908					66.0	.940	42.4	.980
69					42.7	.914				
72	30.9	.952					72.0	.940	42.2	.990
75					41.3	.957				
78	29.8	.982					78.0	.951	42.1	.995
81					40.7	.976				
84	29.2	1.000					84.0	.986	42.0	1.000
87					39.9	1.000				
90							90.0	1.000		

TABLE XXXX

5.18" diameter rotor. Longitudinal diffusion experiments (figure 83).

Experiment No.	R 14 begin	R 14 end	$^{o}_{c}$ E	$^{o}_{c}$ 0	rotor rpm
1	2.0	8.8	21.50	23.25	0
2	"	"	"	"	26
3	"	"	"	"	51
4	1.9	8.7	"	"	86
5	1.8	8.6	"	"	375
6	"	"	"	"	660
7	1.9	8.7	"	"	2400

Results

Experiment No.	θ_o from figure 83 secs	$\bar{u} = \frac{61}{\theta_o}$ cm/sec	slope^2 x 10^4 sec^{-2}	D_L cm^2/sec	Re_c
1	7.70	7.92	484	13.1	0
2	7.45	8.19	484	14.8	85
3	7.58	8.06	196	34.7	166
4	8.10	7.53	169	33.0	288
5	7.42	8.22	400	18.1	1227
6	7.82	7.81	728	8.5	2160
7	12.34	4.94	25	62.9	7860
		Σu = 52.67	Take mean $\bar{u}$ = 7.5 cm/sec		

TABLE XXXX (continued)

Time θ secs	Expt. 1 Cambridge Recorder reading (mv)	F(θ)	Expt. 2 Cambridge Recorder reading (mv)	F(θ)	Expt. 3 Cambridge Recorder reading (mv)	F(θ)	Expt. 4 Cambridge Recorder reading (mv)	F(θ)	Expt. 5 Cambridge Recorder reading (mv)	F(θ)	Expt. 6 Cambridge Recorder reading (mv)	F(θ)	Expt. 7 Cambridge Recorder reading (mv)	F(θ)
0	30.1	0	30.3	0	12.3	0	22.0	0	22.2	0	17.2	0	46.6	0
3	30.1	0	30.3	0	12.3	0	22.0	0			17.2	0	46.6	0
6	31.0	.027	34.6	.143	23.0	.243	29.5	.144	22.2	0	19.5	.082	47.8	.062
7.5	45.0	.450							40.0	.512	32.0	.409		
9	53.0	.690	52.0	.723	41.0	.652	53.2	.600	44.9	.652	39.2	.780	51.9	.273
12	58.0	.840	56.6	.877	49.0	.834	58.9	.710	50.3	.807	42.1	.883	56.0	.485
15	59.5	.885	57.8	.916	55.0	.971			53.4	.897	43.2	.921	58.0	.588
18			58.3	.934			63.6	.801	54.9	.946				
21	61.3	.939			56.3	1.000			55.4	.954	45.0	.986	60.6	.722
24			59.0	.957					55.4	.954			61.3	.758
27	63.2	.998					67.2	.870			45.4	1.000		
30			59.5	.973			68.4	.892	55.4	.954			63.0	.846
33	63.3	1.000												
36			60.3	1.000			71.6	.954	56.0	.971			65.0	.948
42							73.0	.982	56.5	.985			66.0	1.000
48							74.0	1.000	57.0	1.000				

NOTATION FOR PART II

A = cross-sectional flow area of annulus (cm^2)

a = half gap width between parallel plates (cm)

B = numerical constant in equation (81)

b = annular gap width (cm)

c = concentration of mercury vapour in air ($\mu gm/m^3$)

c_1 = concentration of mercury vapour in air before reaching amalgamated section ($\mu gm/m^3$)

c_2 = concentration of mercury vapour in air at a point well downstream from amalgamated section ($\mu gm/m^3$)

c^* = saturation concentration of mercury vapour in air ($\mu gm/m^3$)

c_m = mean value of c over a cross-section ($\mu gm/m^3$)

c'_m = normalised (dimensionless) mean value of c over a cross-section

c_n = general value for c given in (J.4)

c_n^o = value of c_n at time $\theta = 0$

$(c)_{x_1}$ = value of c at $z = 0$

D = molecular diffusion coefficient of mercury vapour in air (cm^2/sec)

D_L = longitudinal diffusion coefficient of mercury vapour in air (cm^2/sec)

D_L^o = value of D_L for a stationary rotor with laminar flow of air in the annulus (cm^2/sec)

E = $(1 - \alpha^2) \Big/ \ln \alpha^2$

e = $\dfrac{r_2 - r_1}{r_1}$ for $r_1 \doteq r_2$

F = function of q in Appendix K

$F(\theta)$ = fractional change in outlet tracer concentration at time θ (equivalent to value of c'_m at the column outlet)

f = friction factor at wall

G = function of q in Appendix K

g = numerical constant in equation (73)

H = function of q in Appendix K

H_1 = H.E.T.P. in vapour phase of distillation column (cm)

h = numerical constant in equation (91)

NOTATION FOR PART II (continued)

I = function of q in Appendix K

j_D = Colburn j-factor for mass transfer

K = radial mass transfer coefficient (cm/sec)

L = length of annulus for longitudinal diffusion experiments (cm)

l_7, l_{14}, etc. = flow rate using rotameters metric size 7, 14 etc. (litres/min)

M = numerical constant defined in Appendix J

Nu = Nusselt number for heat transfer in an annulus

N = numerical constant defined in Appendix J

n_1' = rotor speed (rev/sec)

n = eigen values

N_{Ta} = value of Taylor number based on rotor radius = $(r_1\Omega b/\nu)(b/r_1)^{\frac{1}{2}}$

P = numerical constant defined in Appendix J

p' = pressure (mm.Hg)

p = u/y = velocity gradient in vicinity of wall (sec^{-1})

p^* = saturation vapour pressure of mercury in air (mm.Hg)

Q = rate of mass transfer across section at x_1 for unit depth of parallel plate system ($\mu gm/sec.cm$)

q = $1 - r_1^2/r_2^2$

R = radius of tube (cm)

R7, R14, etc. = rotameters metric size 7, 14, etc.

r = radial distance for concentric cylinder system (cm)

r_1 = outside radius of rotor (cm)

r_2 = inside radius of fixed outer cylinder (cm)

r_m = mean radius = $(r_1 + r_2)/2$ (cm)

r_{max} = radius corresponding to point of maximum velocity in annulus = $(r_2^2 - r_1^2)/2\ln\frac{r_2}{r_1}$ (cm)

Re_a = axial Reynolds number ($2\bar{u}b/\nu$)

Re_c = circumferential Reynolds number ($r_1\Omega b/\nu$)

S = surface area of amalgamated band (cm^2)

s = distance from centre line of parallel plate system (cm)

Sh = Sherwood number (Kb/D)

Sc = Schmidt number (ν/D)

T = absolute temperature (^oK)

$T(\theta)$ = function of time, θ.

Ta = Taylor number ($\Omega r_m^{\frac{1}{2}} b^{\frac{3}{2}} / \nu$)

^cTa = critical Taylor number corresponding to vortex formation

U = numerical constant defined in Appendix J

u = point velocity (cm/sec)

u_s = velocity at a distance s from centre line of parallel plate system (cm/sec)

$\bar{u}$ = mean velocity (cm/sec)

u_o = maximum velocity (cm/sec)

V = total vapour molal flow in distillation column (moles/sec.cm)

v = velocity in y-direction (cm/sec)

w = velocity perpendicular to both x and y-direction

$X = y\left(\frac{p}{9Dx}\right)^{\frac{1}{3}}$

x = axial distance (cm)

x_1 = distance from plane moving with mean velocity (cm)

y = distance measured perpendicular to wall (cm)

z = s/a

$Z(z)$ = function of z

α = r_1/r_2

β^2 = constant defined in Appendix J

θ = time (secs)

θ_o = mean residence time (secs)

NOTATION FOR PART II (continued)

μ = viscosity of air (gm/cm.sec)

ν = kinematic viscosity of air (cm^2/sec)

ν_w = kinematic viscosity of water (cm^2/sec)

ρ = density of air (gm/cm^3)

τ = shear stress ($dynes/cm^2$)

Ω = angular velocity of rotor (rad/sec)

Ω_c = critical angular velocity of rotor for Taylor vortex formation (no axial flow in the annulus) (rad/sec)

Additional References

(References (1) to (42) inclusive given at the end of Part I)

(43) Maxwell R.W. and Storrow J.A. Chem. Engng. Sci. 1957, 6, 204

(44) International Critical Tables, 1928, 3, 206

(45) Plewes A.C., Butler R.M. and Marshall H.E. Chem. Engng. Prog. 1954, 50, 77

(46) Linton W.H. and Sherwood T.K. Chem. Engng. Prog. 1950, 46, 258

(47) Haas F.C. and Nissan A.H. Proc. Roy. Soc. 1961, A, 261, 215

(48) Taylor G.I. Proc. Roy. Soc. 1953, A, 219, 186

(49) Aris R. Proc. Roy. Soc. 1956, A, 235, 67 followed by a private communication

(50) Danckwerts P.V. Chem. Engng. Sci. 1953, 2, 1

(51) Taylor G.I. Proc. Roy. Soc. 1954, A, 223, 446

(52) Pollard A.C.F. The Kinematic Design of Couplings in Instrument Mechanisms. Hilger. London 1929.

(53) Sax N.I. "Handbook of Dangerous Materials". Reinhold. 1951. p.236

(54) Jacobs M.B. Analytical Chemistry of Industrial Poisons. Inter Science 1950

(55) Maxwell R.W. Ph.D. Thesis, Manchester, 1956

(56) Mullay J.M. and Jacques H., Phil. Mag. 1924, 48, 1105

(57) Kaye G.W.C. and Laby T.H. "Tables of Physical and Chemical Constants". Longmans 1956

(58) Davies O.L. Statistical Methods in Research and Production. Oliver & Boyd. 1957, p.173

(59) Calderbank P.H. Private communication. Edinburgh University.

(60) International Critical Tables, 1929, 5, 62

(61) Leveque J. Ann. Mines. 1928, 13, 201, 305, 381

(62) Knudsen J.G. and Katz D.L. "Fluid Dynamics and Heat Transfer", McGraw-Hill. 1958, p.198

(63) Laufer J. N.A.C.A. Report 1951, 1053

(64) Knudsen J.G. and Katz D.L. "Fluid Dynamics and Heat Transfer" McGraw-Hill, 1958, p.365